2.5 GEOLOGY, SEISMOLOGY, AND GEOTECHNICAL ENGINEERING

{This section of the U.S. EPR FSAR is incorporated by reference with the following departure(s) and/or supplement(s).

This section presents information on the geological, seismological, and geotechnical engineering properties of the CCNPP3 site. Section 2.5.1 describes basic geological and seismologic data, focusing on those data developed since the publication of the Final Safety Analysis Report (FSAR) for licensing CCNPP Units 1 and 2. Section 2.5.2 describes the vibratory ground motion at the site, including an updated seismicity catalog, description of seismic sources, and development of the Safe Shutdown Earthquake and Operating Basis Earthquake ground motions. Section 2.5.3 describes the potential for surface faulting in the site area, and Section 2.5.4 and Section 2.5.5 describe the stability of surface materials at the site.

Appendix D of Regulatory Guide 1.165, "Geological, Seismological and Geophysical Investigations to Characterize Seismic Sources," (NRC, 1997) provides guidance for the recommended level of investigation at different distances from a proposed site for a nuclear facility.

- The site region is that area within 200 mi (322 km) of the site location (Figure 2.5-1).
- The site vicinity is that area within 25 mi (40 km) of the site location (Figure 2.5-2).
- The site area is that area within 5 mi (8 km) of the site location (Figure 2.5-3).
- The site is that area within 0.6 mi (1 km) of the site location (Figure 2.5-4).

These terms, site region, site vicinity, site area, and site, are used in Sections 2.5.1 through 2.5.3 to describe these specific areas of investigation. These terms are not applicable to other sections of the FSAR.

The geological and seismological information presented in this section was developed from a review of previous reports prepared for the existing units, published geologic literature, interpretation of aerial photography, and a subsurface investigation and field and aerial reconnaissance conducted for preparation of this application. Previous site-specific reports reviewed include the Preliminary Safety Analysis Report (BGE, 1968) and the Independent Spent Fuel Storage Installation Safety Analysis Report (CEG, 2005). A review of published geologic literature was used to supplement and update the existing geological and seismological information. In addition, relevant unpublished geologic literature, studies, and projects were identified by contacting the U.S. Geological Survey (USGS), State geological surveys and universities. The list of references used to compile the geological and seismological information is presented in the applicable section.

Field reconnaissance of the site and within a 25 mi (40 km) radius of the site was conducted by geologists in teams of two or more. Two field reconnaissance visits in late summer and autumn 2006 focused on exposed portions of the Calvert Cliffs, other cliff exposures along the west shore of Chesapeake Bay, and roads traversing the site and a 5 mi (8 km) radius of the CCNPP site. Key observations and discussion items were documented in field notebooks and photographs. Field locations were logged by hand on detailed topographic base maps and with hand-held Global Positioning System (GPS) receivers.

Aerial reconnaissance within a 25 mi (40 km) radius of the site was conducted by two geologists in a top-wing Cessna aircraft on January 3, 2007. The aerial reconnaissance

investigated the geomorphology of the Chesapeake Bay area and targeted numerous previously mapped geologic features and potential seismic sources within a 200 mi (322 km) radius of the CCNPP site (e.g., Mountain Run fault zone, Stafford fault system, Brandywine fault zone, Port Royal fault zone, and Skinkers Neck anticline). The flight crossed over the CCNPP site briefly but did not circle or approach the site closely in order to comply with restrictions imposed by the Federal Aviation Administration. Key observations and discussion items were documented in field notebooks and photographs. The flight path, photograph locations, and locations of key observations were logged with hand-held GPS receivers.

The investigations of regional and site physiographic provinces and geomorphic process, geologic history, and stratigraphy were conducted by Bechtel Power Corporation. The investigations of regional and site tectonics and structural geology were conducted by William Lettis and Associates.

This section is intended to demonstrate compliance with the requirements of paragraph c of 10 CFR 100.23, "Geologic and Seismic Siting Criteria" (CFR, 2007).}

2.5.1 Basic Geologic and Seismic Information

The U.S EPR FSAR includes the following COL Item in Section 2.5.1:

> A COL applicant that references the U.S. EPR design certification will use site-specific information to investigate and provide data concerning geological, seismic, geophysical, and geotechnical information.

This COL Item is addressed as follows:

{This section presents information on the geological and seismological characteristics of the site region (200 mi (322 km) radius), site vicinity (25 mi (40 km) radius), site area (5 mi (8 km) radius) and site (0.6 mi (1 km) radius). Section 2.5.1.1 describes the geologic and tectonic characteristics of the site region. Section 2.5.1.2 describes the geologic and tectonic characteristics of the site vicinity and location. The geological and seismological information was developed in accordance with the following NRC guidance documents:

- Regulatory Guide 1.70, Section 2.5.1, "Basic Geologic and Seismic Information," (NRC, 1978)
- Regulatory Guide 1.206, Section 2.5.1, "Basic Geologic and Seismic Information," (NRC, 2007) and
- Regulatory Guide 1.165, "Identification and Characterization of Seismic Sources and Determination of Safe Shutdown Earthquake Ground Motion," (NRC, 1997).

2.5.1.1 Regional Geology (200 mi (322 km) radius)

This section discusses the physiography, geologic history, stratigraphy, and tectonic setting within a 200 mi (322 km) radius of the site. The regional geologic map and explanation as shown in Figure 2.5-5 and Figure 2.5-6 contain information on the geology, stratigraphy, and tectonic setting of the region surrounding the CCNPP site (Schruben, 1994). Summaries of these aspects of regional geology are presented to provide the framework for evaluation of the geologic and seismologic hazards presented in the succeeding sections.

Sections 2.5.1.1.1 through 2.5.1.1.4 are added as a supplement to the U.S. EPR FSAR.

2.5.1.1.1 Regional Physiography and Geomorphology

The CCNPP site lies within the Coastal Plain Physiographic Province as shown in Figure 2.5-1 (Fenneman, 1946). The area within a 200 mi (322 km) radius of the site encompasses parts of five other physiographic provinces. These are the: Continental Shelf Physiographic Province, which is located east of the Coastal Plain Province, and the Piedmont, Blue Ridge, Valley and Ridge and Appalachian Plateau physiographic provinces, which are located successively west and northwest of the Piedmont Province (Thelin, 1991).

Each of these physiographic provinces is briefly described in the following sections. The physiographic provinces in the site region are shown on Figure 2.5-1 (Fenneman, 1946). A map showing the physiographic provinces of Maryland, as depicted by the Maryland Geological Survey (MGS), is shown on Figure 2.5-7.

2.5.1.1.1.1 Coastal Plain Physiographic Province

The Coastal Plain Physiographic Province extends eastward from the Fall Line (the physiographic and structural boundary between the Coastal Plain Province and the Piedmont Province) to the coastline as shown in Figure 2.5-1. The Coastal Plain Province is a low-lying, gently-rolling terrain developed on a wedge-shaped, eastward-dipping mass of Cretaceous, Tertiary, and Quaternary age as shown in Figure 2.5-5 and Figure 2.5-6, which are unconsolidated and semi-consolidated sediments (gravels, sands, silts, and clays), that thicken toward the coast. This wedge of sediments attains a thickness of more than 8,000 ft (2,430 m) along the coast of Maryland (MGS, 2007). In general, the Coastal Plain Province is an area of lower topographic relief than the Piedmont Province to the west. Elevations in the Coastal Plain Province of Maryland range from near sea level to 290 ft (88 m) above sea level near the District of Columbia - Prince Georges County line (Otton, 1955).

Four main periods of continental glaciation occurred in the site region during the Pleistocene. Glaciers advanced only as far south as northeastern Pennsylvania and central New Jersey as shown in Figure 2.5-5 and Figure 2.5-6. However, continental glaciation affected sea level and both coastal and fluvial geomorphic processes, resulting in the landforms that dominate the Coastal Plain Province.

In Maryland, the MGS subdivides the Coastal Plain Physiographic Province into the Western Shore Uplands and Lowlands regions, the Embayment occupied by the Chesapeake Estuary system, and the Delmarva Peninsula Region on the Eastern Shore of the Chesapeake Bay as shown in Figure 2.5-7. In the site region and vicinity, geomorphic surface expression is a useful criterion for mapping the contacts between Pliocene and Quaternary. These geomorphic features appear to be mappable only on the more detailed county (1:62500) or quadrangle (1:2400) scales. For example, geomorphic surface expression is one of the criteria used by McCartan (McCartan, 1989b) to map the contact between Pliocene and Quaternary units in St. Mary's County. Constructional surface deposits define the tops of estuarine and fluvial terraces and erosional scarps correspond with the sides of old estuaries (McCartan, 1989a) (McCartan, 1989b). In some areas, the physiographic expression of terraces that might have formed in response to alternate deposition and erosion during successive glacial stages is poorly defined (Glaser, 1994) (Glaser, 2003c). Sea levels were relatively lower during glacial stages than present-day, and relatively higher than present-day during interglacial stages. Deposition and erosion during periods of higher sea levels led to the formation of several discontinuous Quaternary-age stream terraces that are difficult to correlate (McCartan, 1989a). The distribution of Quaternary surficial deposits in the CCNPP site area and site location is discussed in Section 2.5.1.2. Northeast of the Chesapeake Bay, the Western Shore Uplands Region consists of extensive areas of relatively little topographic relief, less than 100 ft (30 m).

The Western Shore Lowlands Region located along the west shore of Chesapeake Bay and north of the Western Shore Uplands Region as shown in Figure 2.5-7 is underlain by interbedded quartz-rich gravels and sands of the Cretaceous Potomac Group and gravel, sand, silt and clay of the Quaternary Lowland deposits. During glacial retreats, large volumes of glacial melt-waters formed broad, high energy streams such as the ancestral Delaware, Susquehanna, and Potomac Rivers that incised deep canyons into the continental shelf. Southwest of the Chesapeake Bay, marine and fluvial terraces developed during the Pliocene and Pleistocene. As a result of post-Pleistocene sea level rise, the outline of the present day coastline is controlled by the configuration of drowned valleys, typified by the deeply recessed Chesapeake Bay and Delaware Bay. Exposed headlands and shorelines have been modified by the development of barrier islands and extensive lagoons (PSEG, 2002).

2.5.1.1.1.2 Continental Shelf Physiographic Province

The Continental Shelf Physiographic Province is the submerged continuation of the Coastal Plain Province and extends from the shoreline to the continental slope as shown in Figure 2.5-1. The shelf is characterized by a shallow gradient of approximately 10 ft/mi to the southeast (Schmidt, 1992) and many shallow water features that are relicts of lower sea levels. The shelf extends eastward for about 75 to 80 mi (121 to 129 km) , where sediments reach a maximum thickness of about 40,000 ft (12.2 km) (Edwards, 1981). The eastward margin of the continental shelf is marked by the distinct break in slope to the continental rise with a gradient of approximately 400 ft/mi (Schmidt, 1992).

2.5.1.1.1.3 Piedmont Physiographic Province

The Piedmont Physiographic Province extends southwest from New York to Alabama and lies west of, and adjacent to, the Coastal Plain Physiographic Province as shown in Figure 2.5-1. The Piedmont is a rolling to hilly province that extends from the Fall Line in the east to the foot of the Blue Ridge Mountains in the west as shown in Figure 2.5-1. The Fall Line is a low east-facing topographic scarp that separates crystalline rocks of the Piedmont Province to the west from less resistant sediments of the Coastal Plain Province to the east (Otton, 1955) (Vigil, 2000). The Piedmont Province is about 40 mi (64 km) wide in southern Maryland and narrows northward to about 10 mi (16 km) wide in southeastern New York.

Within the site region, the Piedmont Province is generally characterized by deeply weathered bedrock and a relative paucity of solid rock outcrop (Hunt, 1972). Residual soil (saprolite) covers the bedrock to varying depths. On hill slopes, the saprolite is capped locally by colluvium (Hunt, 1972).

In Maryland, the Piedmont Province is divided into the Piedmont Upland section to the east and the Piedmont Lowland section to the west, which is referred to as a sub-province in some publications as shown in Figure 2.5-7. The Piedmont Upland section is underlain by metamorphosed sedimentary and crystalline rocks of Precambrian to Paleozoic age. These lithologies are relatively resistant and their erosion has resulted in a moderately irregular surface. Topographically higher terrain is underlain by Precambrian crystalline rocks and Paleozoic quartzite and igneous intrusive rocks. The Piedmont Lowland section is a less rugged terrain containing fault-bounded basins filled with sedimentary and igneous rocks of Triassic and Early Jurassic age.

2.5.1.1.1.4 Blue Ridge Physiographic Province

The Blue Ridge Physiographic Province is bounded on the east by the Piedmont Province and on the west by the Valley and Ridge Province as shown in Figure 2.5-1. The Blue Ridge Province, aligned in a northeast-southwest direction, extends from Pennsylvania to northern

Georgia. It varies in approximate width from 5 mi (8 km) to more than 50 mi (80 km) (Hunt, 1967). This province corresponds with the core of the Appalachians and is underlain chiefly by more resistant granites and granitic gneisses, other crystalline rocks, metabasalts (greenstones), phyllites, and quartzite along its crest and eastern slopes.

2.5.1.1.1.5 Valley and Ridge Physiographic Province

The Valley and Ridge Physiographic Province lies west of the Blue Ridge Province and east of the Appalachian Plateau Province as shown in Figure 2.5-1. This is designated as the Valley and Ridge Province in Maryland as shown in Figure 2.5-7. Valleys and ridges are aligned in a northeast-southwest direction in this province, which is between 25 and 50 mi (40 and 80 km) wide. The sedimentary rocks underlying the Valley and Ridge Province are tightly folded and, in some locations, faulted. Sandstone units that are more resistant to weathering are the ridge formers. Less resistant shales and limestones underlie most of the valleys as shown in Figure 2.5-5 and Figure 2.5-6. The Great Valley Section of the province as shown in Figure 2.5-7, to the east, is divided into many distinct lowlands by ridges or knobs, the largest lowland being the Shenandoah Valley in Virginia. This broad valley is underlain by shales and by limestones that are prone to dissolution, resulting in the formation of sinkholes and caves. Elevations within the Shenandoah Valley typically range between 500 and 1,200 ft (152 and 366 m) msl. The western portion of the Valley and Ridge Province is characterized by a series of roughly parallel ridges and valleys, some of which are long and narrow (Lane, 1983). Elevations within the ridges and valleys range from about 1,000 to 4,500 ft (305 to 1,372 m) msl (Bailey, 1999).

2.5.1.1.1.6 Appalachian Plateau Physiographic Province

Located west of the Valley and Ridge Province, the Appalachian Plateau Physiographic Province includes the western part of the Appalachian Mountains, stretching from New York to Alabama as shown in Figure 2.5-1. The Allegheny Front is the topographic and structural boundary between the Appalachian Plateau and the Valley and Ridge Province (Clark, 1992). It is a bold, high escarpment, underlain primarily by clastic sedimentary rocks capped by sandstone and conglomerates. In eastern West Virginia, elevations along this escarpment reach 4,790 ft (1,460 m) (Hack, 1989). West of the Allegheny Front, the Appalachian Plateau's topographic surface slopes gently to the northwest and merges imperceptibly into the Interior Low Plateaus. Only a small portion of this province lies within 200 mi (322 km) of the CCNPP site as shown in Figure 2.5-1.

The Appalachian Plateau Physiographic Province is underlain by sedimentary rocks such as sandstone, shale, and coal of Cambrian to Permian age as shown in Figure 2.5-5 and Figure 2.5-6. These strata are generally subhorizontal to gently folded into broad synclines and anticlines and exhibit relatively little deformation. These sedimentary rocks differ significantly from each other with respect to resistance to weathering. Sandstone units tend to be more resistant to weathering and form topographic ridges. The relatively less resistant shales and siltstones weather preferentially and underlie most valleys. The Appalachian Plateau is deeply dissected by streams into a maze of deep, narrow valleys and high narrow ridges (Lane, 1983). Limestone dissolution and sinkholes occur where limestone units with high karst susceptibility occur at or near the ground surface.

2.5.1.1.2 Regional Geologic History

The geologic and tectonic setting of the CCNPP site region is the product of a long, complex history of continental and island arc collisions and rifting. The geologic history, as deduced from subsurface exploration, rock and rock / sediment exposures, structural and stratigraphic relationships, and geophysical evidence, spans a period of more than one billion years (1000

Ma). The geologic history includes the formation of the Grenville Mountains, the Appalachian Mountains, and associated island arc and microcontinental terranes that have been accreted to the existing mid-Atlantic continental margin. The top of the Grenville Mountains have been eroded and buried beneath younger rocks, but their bases underlie much of the eastern North America continental margin. Exposed remnants of the Grenville Mountains are found where overlying rocks have been worn away by erosion and the scraping action of glaciers. In the northeast, the Grenville rocks are exposed in the Adirondacks, the Hudson and Jersey Highlands, Manhattan and Westchester in New York, the Green Mountains of Vermont, the Reading Prong of Pennsylvania, and the Berkshire Hills of Massachusetts. The Appalachian Mountains include deformed rock of the Appalachian Plateau, Valley and Ridge, Blue Ridge, and rocks of the New England physiographic provinces, including Proterozoic through Paleozoic metamorphosed thrust sheets and plutons. The Appalachian Mountains are disrupted by subsequent development of Mesozoic (Late Triassic and Early Jurassic) rift basins filled with igneous and sedimentary rocks, and basalt dikes and sills that intruded both rift basins and surrounding Piedmont crystalline basement exposed in the hilly, subdued topography of the Piedmont physiographic province. The eastward dipping clastic wedge of Cenozoic sediments overlaps some of the Piedmont and New England physiographic provinces and covers the entire Coastal Plain province. This variation in lithologies results in varied terrane that is reflected in the physiographic provinces of the region, as shown in Figure 2.5-1.

This geologic history of the region is discussed within the context of tectonostratigraphic terranes shown in Figure 2.5-9. Episodes of continental collisions have produced a series of accreted terranes separated, in part, by low angle detachment faults or juxtaposed by higher-level normal faulting. Episodes of extension have reactivated many earlier structures and created new ones. The deformation of these terranes through time imparts a pre-existing structural grain in the crust that is important for understanding the current seismotectonic setting of the region.

Sources of seismicity may occur in the overlying, exposed terranes or along structures within the North American basement buried beneath the accreted terranes or overthrust plates. Therefore, regional seismicity may not be related to any known surface structure. Intervening episodes of continental rifting have produced high angle normal or transtensional faults that either sole downward into detachment faults or penetrate entirely through the accreted terranes and upper crust. Understanding the geologic history, including the evolution and the geometry of these crustal faults, is important for identifying potentially active faults and evaluating the distribution of historical seismicity within the tectonic context of the site region. Based on the geologic history presented here, the seismic implications of geologic structures and the current state of strain in the region are discussed in Sections 2.5.1.1.2.8, 2.5.1.1.3.2.1, and 2.5.2.2.

Major tectonic events recognized in the site region include five compressional orogenies (Grenville, Potomac, Taconic, Acadian and Alleghany) and two extensional episodes (Late Precambrian rifting to produce the Iapetus Ocean and Mesozoic rifting to produce the Atlantic Ocean)(Faill, 1997a). Extension probably occurred, perhaps of less scale and duration, between each of the compressional episodes (resulting in the opening of the Rheic and Theic oceans, for example). These compressional and extensional episodes began to be recognized in the 1970s through 1980s and are depicted in Figure 2.5-8, modified from Hatcher, 1987. While direct evidence of these deformational events is visible in the Appalachian Plateau, Valley and Ridge, Blue Ridge, Piedmont and New England physiographic provinces, other evidence is buried beneath the Coastal Plain sediments in the site region and is inferred based on

geophysical data, as described in Section 2.5.1.1.4.3, and borehole data as described in Section 2.5.1.1.3. The site region is located currently on the passive, trailing margin of the North American plate following the last episode of continental extension and rifting. The current stress regime of this region is discussed in Section 2.5.1.1.4.2. The history of orogenic events is described below.

2.5.1.1.2.1 Grenville Orogeny

The earliest compressional event (orogeny) recorded in the exposed rocks of the mid-Atlantic continental margin is the Grenville orogeny. Prior to the Grenville compressional event, a 'supercontinental' landmass known as Hudsonland (also known as Columbia) is postulated to have included the Laurentian craton (Pesonen, 2003). On the basis of purely paleomagnetic data, this supercontinent consisted of Laurentia, Baltica, Ukraine, Amazonia and Australia and perhaps also Siberia, North China and Kalahari. Hudsonland existed from 1830 Ma to ca. 1500–1250 Ma (Pesonen, 2003). The interior of the Laurentian craton experienced plutonism in the 1740 to 1504 Ma time frame and Hudsonland began to split apart and volcanic arcs were formed between 1300 and 1250 Ma. A composite arc belt or microcontinent was formed by about 1200 Ma in the Panthalassa-type ocean basin. (Carr, 2000; Murphy, 2004). This set the stage for the Grenville orogeny.

The Grenville orogeny occurred during Middle Proterozoic time, approximately one billion years ago (1000 Ma). Two phases of compression are recognized, from ca. 1080-1030 Ma and 1010-980 Ma (Carr, 2000). A composite arc or micro-continent was thrust over the eastern Laurentian margin. The uplifted terranes were dissected and exhumed by normal faulting before ca. 1040 Ma. Despite a long pre-Grenvillian tectonic and plutonic history, the present crustal architecture and much of the seismic reflectivity were acquired during the 1080-980 Ma phase of compression and extension (Carr, 2000).

The Grenville orogeny was the result of the convergence of the ancestral North American craton (Laurentia) with proto-African tectonic plates. During this orogeny, various terranes were accreted onto the edge of Laurentia, forming the Grenville Mountains (Faill, 1997a) and the supercontinent of Rodinia (Thomas, 2006). The Grenville Mountains were likely the size of the present day Himalayas (Carr, 2004). Convergence around the periphery of the Laurentian craton produced a series of mountain ranges offset by transform boundaries.

Intrusive Grenville rocks of the north-central Appalachians are exposed in the Piedmont physiographic province of central Maryland, southeastern Pennsylvania and northern New Jersey (Figure 2.5-212). In the north-central (Maryland and Pennsylvania) Appalachians, these massifs are separated by the Pleasant Grove-Huntingdon Valley shear zone (PGHV) into external and internal massifs (Figure 2.5-212)(Faill, 1997a). External massifs include the Reading Prong, Honey Brook Upland, Mine Ridge, and Trenton Prong. The stratigraphy of the external massifs is described in more detail in Section 2.5.1.1.3.1.1. Internal massifs include the Brandywine and Baltimore massifs (Figure 2.5-215). The stratigraphy of the internal massifs is described in more detail in Section 2.5.1.1.3.1.2. Other small external massifs are recognized throughout the area (Faill, 1997a).

External massifs are allochthonous massifs that were emplaced by Taconic or Alleghany age thrusts and are now surrounded by Paleozoic and Mesozoic age rocks. External basement massifs (closer to the foreland) in the central and northern Appalachians expose Mesoproterozoic rocks that are likely derived from the nearby craton and mark the eastern edge of Laurentia. They are important because they record the Neoproterozoic rifting of Rodinia (Figure 2.5-216) and the Paleozoic collisions of arcs and continents that eventually

formed the supercontinent of Pangea (Karabinos, 2008 and Hatcher, 2004). Internal basement massifs are located in the internal parts of an orogen and can be derived from a number of sources, not necessarily from the nearby craton (Hatcher, 2004).

The Grenville orogeny was followed by several hundred million years of tectonic quiescence, during which time the Grenville Mountains were eroded and their basement rocks exposed. The stratigraphy of Grenville remnants found within a 200-mile (322-kilometer) radius of the CCNPP site is described in more detail in Sections 2.5.1.1.3.1. Eventually, the supercontinent of Laurentia underwent a major rifting episode that led to the opening of the Iapetus Ocean (Figure 2.5-8) in late Precambrian time, 590–550 Ma (van Staal, 1998). Evidence of rifting can be found in the presence of metamorphosed mafic dikes (for example, the Chesnutt Hill Formation in the western New Jersey Highlands) (Gates, 2004) and the Catoctin and Swift Run formations in central Virginia (Bartholomew, 2004). Continued rifting produced a great basin off the Laurentian margin (the Theic or Rheic oceans) (Figure 2.5-214 and Figure 2.5-217) in which thousands of meters of quartz arenites and limestones/dolomites, including stromatolites, were deposited in shallow (e.g. Frederick Valley Chilhowee Group Weverton Formation) to deep waters (e.g. Great Valley Chilhowee Group Loudon Formation) on the continental slope and shelf platform (Cleaves, 1968) (Cecil, 2004). Further offshore in the deep water of the continental rise, fine-grained rocks (such as the Westminster terrane) were deposited as carbonates interspersed with turbidite deposits. Turbidites of the Potomac terrane were deposited even further offshore in a trench setting (Southworth, 2004). As discussed in Section 2.5.1.1.2.4, all of these units were metamorphosed, deformed, and intruded by plutons in the Ordovician Taconian orogeny (Drake, 1989) (Figure 2.5-9).

2.5.1.1.2.2 Late Precambrian Rifting

Following the Grenville orogeny, crustal extension and rifting began during Late Precambrian time, which caused the separation of the North America and African plates and created the proto-Atlantic Ocean (Iapetus Ocean). Rifting is interpreted to have occurred over a relatively large area, sub-parallel to the present day Appalachian mountain range (Faill, 1997a) (Wheeler, 1996). This period of crustal extension is documented by the metavolcanics of the Catoctin, Swift Run, and Sams Creek formations (Schmidt, 1992). During rifting, the newly formed continental margin began to subside and accumulate sediment. Initial sedimentation resulted in an eastward thickening wedge of clastic sediments consisting of graywackes, arkoses, and shales deposited unconformably on the Grenville basement rocks. In the Blue Ridge and western Piedmont, the Weverton and Sugarloaf Mountain quartzites represent late Precambrian to early Cambrian fluvial and beach deposits. Subsequent sedimentation included a transgressive sequence of additional clastic sediments followed by a thick and extensive sequence of carbonate sediments. Remnants of the rocks formed from these sediments can be found within the Valley and Ridge Province and Piedmont Province (Fichter, 2000). In the western Piedmont, the sandy Antietam Formation was deposited in a shallow sea. In the Valley and Ridge Province, a carbonate bank provided the environment of deposition for the thick carbonates ranging from the Cambrian Tomstown Dolomite through the Ordovician Chambersburg Formation. In the eastern Piedmont, the Setters Formation (quartzite and interbedded mica schist) and the Cockeysville Marble have been interpreted as metamorphosed beach and carbonate bank deposits that can be correlated from Connecticut to Virginia. Accumulation of this eastward thickening wedge of clastic and carbonate sediments is thought to have occurred from the Middle to Late Cambrian into Ordovician time (PSEG, 2002).

2.5.1.1.2.3 Late Precambrian to Early Cambrian Orogenies (Potomac/Penobscot Orogency)

The Potomac orogeny is the earliest Paleozoic age orogeny recorded in the north-central Appalachians. It is recognized along the western margin of the Piedmont province and is considered distinct from the Penobscot orogeny of the northern Appalachians and the Virgilian orogeny of Northern Carolina (Hibbard and Samson, 1995). The orogeny is dated from Late Cambrian to Early Ordovician and occurred a considerable distance from the North American continental margin, as the magmatic arc(s) in the Theic ocean (including the Jefferson and Smith River terranes) were obducted over the Brandywine microcontinent (Figure 2.5-218). The orogeny started with the magmatic arcs overriding the forearc sediments of the White Clay nappe and the Liberty Complex. The Wilmington Complex in Delaware and southeast Pennsylvania overrode the Glenarm Wissahickon Formation of the White Clay nappe (Figure 2.5-211, Figure 2.5-212 and Figure 2.5-213) and the Potomac-Philadelphia terrane. This obduction created the peak metamorphism of the Potomac orogeny in this part of the north-central Appalachians and possibly generated the Arden Pluton within the Wilmington Complex (Faill, 1997a).

This obduction of the combined Wilmington Complex (Figure 2.5-213), White Clay nappe and Philadelphia terrane over the Brandywine microcontinent continued for some time, although petrologic and microprobe evidence indicates that the schists of the White Clay nappe had cooled somewhat before the amalgamate was thrust over the Brandywine microcontinent on the Doe Run fault (Figure 2.5-211 and Figure 2.5-212). The weight of the obduction is considered to have caused the microcontinent to descend (Figure 2.5-218) raising temperatures and pressures in the massifs, especially in the West Chester massif, which occupied the lowest structural level in the amalgamation (Faill, 1997a).

Around the Baltimore microcontinent, a similar amalgamation was occurring. The westward advancing magmatic arc (James Run volcanics) and ophiolites (Baltimore Mafic Complex) produced a precursory mélange (Morgan Run Formation and the potentially equivalent Sykesville Formation) (Figure 2.5-211 and Figure 2.5-212) in the accretionary wedge to the west. The accretionary wedge and magmatic arc were obducted onto the eastern portion of the Baltimore microcontinent which subsequently became submerged (Figure 2.5-211 and Figure 2.5-212). During the thrusting, the Morgan Run Formation was elevated and provided a source of clasts for the associated Sykesville diamictite. The Ellicott City Granodiorite (west of Baltimore) was subsequently emplaced deep within the thickened crust between the Baltimore Mafic complex and metasediments (Faill, 1997a).

The southward extension of the Potomac Orogeny is represented by the Cambrian age Chopawamsic metavolcanics and associated mélanges of an accretionary / forearc complex. The one difference between the north-central and southern portions of the Appalachian orogeny is that microcontinents are not generally associated with the north-central Chopawamsic or Jefferson terranes (Figure 2.5-9). The Sauratown Mountains anticlinorium and the Goochland terrane of the eastern Piedmont may have a similar history to that of the north-central Appalachians. Lithic and metamorphic evidence of the Goochland gneisses indicate that the Goochland terrane was probably derived from the North American craton (Laurentian origin) and had an emplacement history quite different from that of the Baltimore and Brandywine internal massifs (Faill, 1997a).

2.5.1.1.2.4 Taconic Orogeny

The Taconic orogeny occurred during Middle to Late Ordovician time and was caused by continued collision of micro-continents and volcanic arcs with the eastern North America

margin along an eastward dipping subduction zone during progressive closure of the Iapetus Ocean (Figure 2.5-8). Taconic terranes are preserved today in the Piedmont in a series of belts representing island-arcs and micro-continents. They include the Chopawamsic terrane, the Carolina / Albemarle arc, the Goochland-Raleigh terrane, and the Sussex Terrane, directly west of the CCNPP site, as shown in Figure 2.5-9. These terranes are thought to have collided with, and accreted to, eastern North America craton at different times during the Taconic orogeny (Horton, 1991; Glover, 1997). Closer to the CCNPP site, the central Piedmont in Northern Virginia, Maryland, and Pennsylvania contains several belts of rocks whose age is unknown and/or whose relation to the pre- or synorogenic rocks of the Taconic orogen is uncertain (Drake, 1999). These stratigraphic units include the Wissahickon Formation, which is now recognized in the Potomac Valley as three distinct lithotectonic assemblages (Drake, 1999). Other stratigraphic units, whose ages range from Late Proterozoic to Late Ordovician and contain indications of Taconic deformation, include various units in the Ijamsville Belt, the Glenarm Group Belt, which includes the Baltimore Gneiss, the Potomac terrane that was thrust over the Glenarm Group belt, and the Baltimore mafic complex to the east as shown in Figure 2.5-9 (Horton, 1989) (Fichter, 2000). Additional details on the complex stratigraphy of the Taconic orogen in the Piedmont were described by Drake (Drake, 1999).

Accretion of the island-arcs and micro-continents to the eastern margin of North America created a mountain system, the Taconic Mountains, that became a major barrier between the Iapetus Ocean to the east and the carbonate platform to the west. The growth of this barrier transformed the area underlain by carbonate sediments to the west into a vast, elongate sedimentary basin, the Appalachian Basin. The present day Appalachian Basin extends from the Canadian Shield in southern Quebec and Ontario Provinces, Canada, southwestward to central Alabama, approximately parallel to the Atlantic coastline (Colton, 1970). The formation of the Appalachian Basin is one of the most significant consequences of the Taconic orogeny in the region defined by the Valley and Ridge Province and Appalachian Plateau Province. The Taconic mountain system was the source of most of the siliclastic sediment that accumulated in the Appalachian Basin during Late Ordovician and Early Silurian time. Many of these units are preserved closest to the CCNPP site in the Valley and Ridge Province. A continent-wide transgression in Early Silurian time brought marine shales and carbonate sedimentation eastward over much of the basin, and a series of transgressions and regressions thereafter repeatedly shifted the shoreline and shallow marine facies. Carbonate deposition continued in the eastern part of the basin into Early Devonian time (Faill, 1997b).

The type region of the Taconic orogeny in the northern Appalachians records the obduction of one or more volcanic arcs onto the eastward-dipping Ordovician Laurentian (Iapetan) margin. However, the southern Appalachians record late Cambrian initiation of a westward dipping subduction zone and Ordovician development of an arc-backarc system along the Laurentian margin, reflecting an extensional, not collisional, orogenesis. The limit of this Middle Ordovician extensional regime is currently unknown, but determining its northeastern extent is important in paleotectonic reconstructions of the Laurentian margin for the early Paleozoic (Barineau, 2008).

2.5.1.1.2.5 Acadian Orogeny

The Acadian orogeny began in early Devonian time and ended at the beginning of Mississippian time. Accretion of a composite Goochland-Avalonia terrane to Laurentia at c. 421 Ma and the subsequent accretion of Meguma between 400 and 390 Ma were probably responsible for the Acadian orogeny and continuing Devonian orogenesis (van Staal, 1998). The 1 billion year old (1000 Ma) Goochland terrane, possibly a displaced fragment of Laurentia

(Bartholomew and Tollo, 2004) had been sutured to the Avalonia terrane in the Taconian orogeny (Sheridan, 1993).

At its peak, the orogeny produced a continuous chain of mountains along the east coast of North America and brought with it associated volcanism and metamorphism. The Acadian orogeny ended the largely quiescent environment that dominated the Appalachian Basin during the Late Ordocician and into the Silurian, as vast amounts of terrigenous sediment from the Acadian Mountains were introduced into the basin and formed the Catskill clastic wedge in Pennsylvania and northeastern New York as shown in Figure 2.5-5, Figure 2.5-6, and Figure 2.5-8. Vast amounts of terrigenous sediment from the Acadian Mountains were introduced into the Catskill foreland basin during the Middle and Late Devonian and formed the Catskill clastic wedge sequence in Pennsylvania and New York. Thick accumulations of clastic sediments belonging to the Catskill Formation are spread throughout the Valley and Ridge Province (Faill, 1997b). The Catskill clastic wedge is representative of fluctuating shorelines and prograding alluvial environments along the western margin of the Acadian upland. This regressional sequence is represented in the sedimentary record with turbidites, slope deposits, alternating shallow marine and nonmarine sediments and alluvial plain fining-upward sequences (Walker, 1971, Faill, 1997b and USGS, 2008). The pebbles and sand grains of the Catskill Formation in New York, Pennsylvania and Maryland are mostly composed of metamorphic and granitic rock fragments, feldspar, mica and quartz. The red color is due to the presence of a small percentage of iron oxide between the grains (Dolt and Batten, 1988). The regressive sequence in the region is bounded above and below by marine transgressions which are represented by basal black shale overlain by gray shales and mudstones capped by small amounts of siltstone (Bridge, 1994; Huber, 2000). The Catskill clastic wedge was the site of the greatest accumulation of sediment in the region depositing as much as 7,000 feet of sediment (USGS, 2008). The sediments are the thickest in the east and grow progressively thinner westward and southward into the central Appalachian Basin region (Figure 2.5-211). In general, the Acadian Orogeny was superimposed upon terranes affected or formed by the Taconic Orogeny (Figure 2.5-211).

By Mississippian time, the Acadian Mountains had been denuded because the source material for the Catskill Delta was depleted and sedimentation ceased.

2.5.1.1.2.6 Allegheny Orogeny

The Allegheny orogeny occurred during the Late Carboniferous Period and extended into the Permian Period. The orogeny represents the final convergent phase in the closing of the Iapetus Ocean in the Paleozoic Era (Figure 2.5-8). Metamorphism and magmatism were significant events during the early part of the Allegheny orogeny. The Allegheny orogeny was caused by the collision of the North American and proto-African plates, and it produced the Allegheny Mountains. As the African continent was thrust westward over North America, the Taconic and Acadian terranes became detached and also were thrust westward over Grenville basement rocks (Mulley, 2004). The northwest movement of the displaced rock mass above the thrust was progressively converted into the deformation of the rock mass, primarily in the form of thrust faults and fold-and-thrust structures, as seen in the Blue Ridge and Piedmont Plateau Provinces. The youngest manifestation of the Allegheny orogeny was northeast-trending strike-slip faults and shear zones in the Piedmont Province. The extensive, thick, and undeformed Appalachian Basin and its underlying sequence of carbonate sediments were deformed and a fold-and-thrust array of structures, long considered the classic Appalachian structure, was impressed upon the basin. The tectonism produced the Allegheny Mountains and a vast alluvial plain to the northwest. The Allegheny Front along the eastern margin of the Appalachian Plateau Province is thought to represent the westernmost

extent of the Allegheny orogeny. Rocks throughout the Valley and Ridge Province are thrust faulted and folded up to this front, whereupon they become relatively flat and only slightly folded west of the Allegheny Front (Faill, 1998).

2.5.1.1.2.7 Early Mesozoic Extensional Episode (Triassic Rifting)

Crustal extension during Early Mesozoic time (Late Triassic and Early Jurassic) marked the opening of the Atlantic Ocean (Figure 2.5-8). This extensional episode produced numerous local, closed basins ("Triassic basins") along eastern North America continental margin (Figure 2.5-9) (Faill, 1998). The elongate basins generally trend northeast, parallel to the pre-existing Paleozoic structures (Figure 2.5-10). The basins range in length from less than 20 mi (32 km) to over 100 mi (161 km) and in width from less than 5 mi (8 km) to over 50 mi (80 km) . The basins are exposed in the Piedmont Lowland of Maryland and Northern Virginia and are also buried beneath sediments of the Coastal Plain and the continental shelf. The exposed and buried Mesozoic basins identified in Figure 2.5-9are described more fully in FSAR Section 2.5.1.1.3.4.

Generally, the Mesozoic rift basins are asymmetric half-grabens with principal faults located along the western margin of the basins. Triassic and Jurassic rocks that fill the basins primarily consist of conglomerates, sandstones, and shales interbedded with basaltic lava flows. At several locations, these rocks are cross-cut by basaltic dikes. The basaltic rocks are generally more resistant to erosion and form local topographically higher landforms. The Mesozoic rift basins along the length of the North American Atlantic margin are related to one of the largest intrusive systems in the world, the Central Atlantic Magmatic Province (CAMP) (de Boer, 2003). The CAMP intrusives were emplaced before the breakup of Pangea, during the embryonic stage of continental rifting. Correlative dike swarms are found in the western and southeastern margins of the African continental margin and the northern part of the South American continental margin (representing the "Early Jurassic Circum-Atlantic Dike System") (de Boer, 2003). The dikes of the Circum-Atlantic swarm show a convergence pattern, with a focal point near the present-day Blake Plateau, near Florida (present coordinates).

Subsidence of the rift basins was initiated ca. 230 Ma prior to the magmatic event. Dike intrusion began in the northern (New England) section of the North American continental margin. Most of the dikes along the length of the CAMP were emplaced between 205 and 195 Ma. Similar ages are found for dike swarms in Iberia, Africa and South America. de Boer (2003) summarizes various models proposed for the production of the voluminous magma that created the dike swarms. One proposal has a single hotspot plume, located near Florida (present coordinates) beneath the Blake Plateau. Another model proposed two hot spots, one off Florida and the other in the Gulf of Maine. Another model proposes that magmas were derived from multiple, rather than localized, sources below the rift valleys. The results of de Boer (2003) analyses of the anisotropy of magnetic susceptibility across the CAMP suggest that the overall radiating pattern ofthe circum-Atlantic dikes support a plume source in the vicinity of the Blake Plateau (de Boer, 2003).

The episode of crustal extension that produced the Mesozoic rift basins of the mid-Atlantic region is believed to have ended and the Atlantic margin stabilized as a passive margin before Eocene time (see discussion in Section 2.5.1.1.4.1.2).

2.5.1.1.2.8 Cenozoic History

The Early Mesozoic extensional episode gave rise to the Cenozoic Mid-Atlantic spreading center. The Atlantic seaboard presently represents the trailing passive margin related to the spreading at the Mid-Atlantic ridge. Ridge push forces resulting from the Mid-Atlantic

spreading center are believed to be responsible for the northeast-southwest directed horizontal compressive stress presently observed along the Atlantic seaboard.

During Cenozoic time, as the Atlantic Ocean opened, the newly formed continental margin cooled and subsided, leading to the present day passive trailing divergent continental margin. As the continental margin developed, continued erosion of the Appalachian Mountains produced extensive sedimentation within the Coastal Plain. The Cenozoic history of the Atlantic continental margin, therefore, is preserved in the sediments of the Coastal Plain Province, and under water along the continental shelf. The geologic record consists of a gently east-dipping, seaward-thickening wedge of sediments, caused by both subsidence of the continental margin and fluctuations in sea level. Sediments of the Coastal Plain Province cover igneous and metamorphic basement rocks and Triassic basin rift deposits.

During the Quaternary Period much of the northern United States experienced multiple glaciations interspersed with warm interglacial episodes. The last (Wisconsinan) Laurentide ice sheet advanced over much of North America during the Pleistocene. The southern limit of glaciation extended into parts of northern Pennsylvania and New Jersey, but did not cover the CCNPP site vicinity (Figure 2.5-5). South of the ice sheet, periglacial environments persisted throughout the site region (Conners, 1986). Present-day Holocene landscapes, therefore, are partially the result of geomorphic processes, responding to isostatic uplift, eustatic sea level change, and alternating periglacial and humid to temperate climatic conditions (Cleaves, 2000).

Recent studies demonstrate that widespread uplift of the central Appalachian Piedmont and subsidence of the Salisbury Embayment represents first-order, flexural isostatic processes driven by continental denudation and offshore deposition. Studies indicate that the mid-Atlantic margin experiences an average, long-term denudation rate of approximately 10 m/m.y., and the Piedmont has been flexurally upwarped between 35 and 130 meters in the last 15 m.y. (Pazzaglia, 1994). This Piedmont upwarp and basin subsidence are accommodated primarily by a convex-up flexural hinge, physiographically represented by the Fall Zone. The current state of resulting stress on the Atlantic margin lithosphere is discussed more fully in Section 2.5.1.1.2.8 and 2.5.1.1. 4.4.

2.5.1.1.3 Regional Stratigraphy

This section contains information on the regional stratigraphy within a 200-mile (322-km) radius of the CCNPP site. The regional geology and generalized stratigraphy within this area is shown on Figure 2.5-5 and described in Figure 2.5-6. For an illustration of regional stratigraphy, see Figure 2.5-220 through Figure 2.5-224. In this FSAR section, the description of pre-Silurian (pre-Taconian) stratigraphic units is organized by tectonostratigraphic affinity to Laurentian continental characteristics or by affinity to oceanic, island arc, or exotic microcontinent terranes. Figure 2.5-9 provides one interpretation of these tectonostratigraphic terranes within a 200-mile radius of the CCNPP site. The pre-Silurian terranes are described in FSAR sections 2.5.1.1.3.1, The Laurentian Realm, 2.5.1.1.3.2, The Iapetan Realm, and 2.5.1.1.3.3, The Peri- Gondwanan Realm. Silurian through Jurassic stratigraphic units are described in FSAR Section 2.5.1.1.3.4, The Pangean Realm. Finally, post-rifting Cretaceous, Tertiary and Quaternary sediments that drape the basement rocks across the Piedmont, Coastal Plains, and continental shelf of the mid-Atlantic margin are described in FSAR Section 2.5.1.1.3.5, Post-Pangean Sediments.

FSAR Sections 2.5.1.1.3.1 through 2.5.1.1.3.5 are supported by corresponding stratigraphic columns that correlate regional stratigraphic names across the 200-mile (322 kilometer) radius

of the CCNPP site. The stratigraphic units that comprise the Laurentian, Iapetan, and Peri-Gondwanan realms are correlated in Figure 2.5-220 and Figure 2.5-221. The description of stratigraphic units in FSAR Sections 2.5.1.1.3.1 through 2.5.1.1.3.3 refer to the map symbols on Figure 2.5-9. The post-Silurian through Jurassic stratigraphic units described in FSAR Section 2.5.1.1.3.4 are regionally correlated in Figure 2.5-222. The Cretaceous through Holocene stratigraphic units described in FSAR Section 2.5.1.1.3.5 are regional correlated in Figure 2.5-224.

A tectonostratigraphic map such as Figure 2.5-9 is by definition interpretive; both of the nature of boundaries, and in terms of the nature of tectonostratigraphic units. Some of the affinities depicted in Figure 2.5-9, which was based on work through 1991, have subsequently been questioned (Glover 1997, for example). According to Hibbard, the pre-Silurian Appalachian orogen is composed of three realms: Laurentian, Iapetan, and peri-Gondwanan (Hibbard, 2007). The three realms acquired their defining geologic character before the Late Ordovician. The Laurentian realm is composed of all rocks deposited either on or immediately adjacent to ancient proto-North America supercontinent known as Rodinia (see discussion in FSAR Section 2.5.1.1.2.1) at the close of the Grenville orogeny. The Laurentian realm formed the western flank of the Appalachian orogen. The Iapetan realm is a collection of terranes of oceanic and volcanic arc affinity that were caught between the Laurentian and peri-Gondwanan realm during Appalachian orogenesis. The peri-Gondwanan realm along the southeastern flank of the orogen formed near the supercontinent Gondwana and is exotic with respect to Laurentian elements. Only one terrane within a 200-mile (322-kilometer radius of the CCNPP site, the Raleigh-Goochland terrane, defies easy classification into this scheme. For the present discussion, it will be placed in the Iapetan realm.

According to Hibbard (2006), the Laurentian realm is represented by terranes found west of the Pleasant Grove-Huntington Valley fault system (Figure 2.5-23) (incorrectly referred to as the Pleasant Valley shear zone on the Hibbard 2006 map). Peri-Laurentian and Iapetan realm terranes are found west of the Central Piedmont- shear zone (including the Spotsylvania fault). The Peri-Gondwanan realm (Carolina and related terranes) is found east of the Central Piedmont shear zone (Figure 2.5-23). See FSAR Section 2.5.1.1.4.4.2.1, Appalachian Structures, for a description of these two regional structures.

2.5.1.1.3.1 The Laurentian Realm

The stratigraphic units within a 200-mile (322-kilometer) radius of the CCNPP site provide a history of the growth of the proto-North American continental margin within the past billion years. It is a history of recycling and redistribution of Mesoproterozoic crust of Laurentia, accretion and subsequent deformation of oceanic crust, volcanic arcs and microcontinents related to ancient oceans, and probable capture and subsequent deformation of portions of other supercontinents (such as the Pan-African Avalon terrane in the northern Appalachians and Suwannee terrane in the southern Appalachians, for example) by the North American continental margin.

Precambrian-age Grenville rocks of the north-central Appalachians outcrop in central Maryland, southeastern Pennsylvania and northern New Jersey (Figure 2.5-220 and Figure 2.5-221). These exposures are metamorphic massifs that were emplaced on Taconic or Allegheny orogenic thrusts and are now surrounded by Paleozoic and Mesozoic age rocks. In the north-central Appalachians these massifs are separated by the Pleasant Grove-Huntingdon Valley shear zone (Figure 2.5-23) into external and internal massifs (Figure 2.5-212) (Faill 1997a). External basement massifs are blocks of older crust that are

incorporated into the more external (foreland-ward) parts of an orogen, whereas internal basement massifs are blocks of older crust that are located in the internal parts of an orogen (Hatcher, 1983). External massifs are more likely to be derived from the nearby craton, but internal massifs can be derived from a variety of locales, not necessarily from the nearby craton, so they can be either proximally derived or parts of exotic terranes, such as the remains of the microcontinent that originated from the South America craton (Gondwana) (Faill, 1997a) (Figure 2.5-214).

Laurentian terrane (undivided): Tectonostratigraphic map (Figure 2.5-9) unit "L"

Almost half of the exposed landmass within a 200-mile (322-kilometer) radius of the CCNPP site is composed of ancestral North America, or Laurentia terrane together with probable related terranes deformed during the Grenville orogeny (see Section 2.4.1.1.2.1). The undifferentiated Laurentia terrane shown in Figure 2.5-9 includes a number of Mesoproterozoic massifs, rift-related Late Proterozoic clastic sedimentary and volcanic sequences, and deformed Paleozoic shelf and platform strata.

Chesapeake terrane: Tectonostratigraphic map (Figure 2.5-9) unit "ch"

The character of the Chesapeake terrane and its position at the outer limits of the mid-Atlantic continental margin has raised a great deal of interest regarding its affinities. The detected presence of the Chesapeake terrane in boreholes along the central Atlantic Coast implies some relationship to the broad gravity low [tectonostratigraphic map (Figure 2.5-9) unit "g3"] known as the Salisbury gravity anomaly (Faill 1998). Gravity and magnetic data, seismic reflection profiles, and drill hole data are interpreted to indicate that Laurentian crust of Grenville age underlies the New Jersey Coastal Plain as far south as Cape May (Maguire 2003). The tectonostratigraphic map (Figure 2.5-9) indicates that this terrane continues south beneath the coast of Virginia to about the Virginia-North Carolina line. Rb/Sr age dates indicate that the basement terrane was created 1025±0.035 Ma. Basement lithologies are similar to exposed Grenville-age rocks of the Appalachians and perhaps most importantly, the TiO_2 and Zr/P_2O_5 composition of metagabbro in the Chesapeake terrane overlap those of Proterozoic mafic dikes in the New Jersey Highlands. These new findings support the interpretation that Laurentian basement extends southeast as far as the continental shelf in the U.S. mid-Atlantic region. The subcrop of Laurentian crust under the mid-Atlantic Coastal Plain implies unroofing by erosion of the younger Carolina (Avalon) supracrustal terrane. Dextral-transpression fault duplexes may have caused excessive uplift in the Salisbury Embayment area during the Alleghanian orogeny (Sheridan 1998).

2.5.1.1.3.1.1 External Massifs

Grenville basement rocks are exposed in the cores of en echelon massifs which are interpreted to be allochthonous (Rankin, 1989) or para-autochthonous (Drake, 1989) and have been carried westward (current coordinates) by Taconian thrusting.

The external massifs include the Reading Prong, Honey Brook Upland, Mine Ridge, Trenton Prong and Blue Ridge massifs (Figure 2.5-212 and Figure 2.5-213). Following are brief descriptions of these massifs from Faill (1997a).

Reading Prong: Tectonostratigraphic map (Figure 2.5-9) unit "L," located immediately east of the Hamburg terrane

The Reading Prong extends from western New England southwestward across southern New York, northern New Jersey, and terminates in the vicinity of Reading, Pennsylvania in the "Little" South Mountain (Figure 2.5-212). Rocks of the Reading Prong consist of a variety of metamorphic and igneous rocks including quartzofeldspathic and calcareous metasediments, sodium-rich gneisses and amphibolites, granites and mafic plutonic rocks. The terrane, extending from the New Jersey Highlands to Reading, Pennsylvania, is underlain by a Middle Proterozoic assemblage of intrusive plutonic rocks and migmatites, metasediments, rocks of probable volcaniclastic origin and charnockitic rocks of unknown origin (Drake, 1989).

The Hexenkopf complex is part of the Reading Prong in Pennsylvania. It apparently represents the oldest basement rocks of the Reading Prong and is overlain by the Losee Metamorphic Suite, a largely sodic plagioclase and quartz series of granofels, granitoid,and foliated rocks. The Losee Suite is overlain in turn by a sequence of quartzofeldspathic and calcareous metasedimentary rocks. The rocks in this part of the Reading Prong are considered to be a part of Laurentia, and resemble the rocks of the Honey Brook massif but not the rocks in the internal or other external massifs to the south.

Honey Brook Upland: Tectonostratigraphic map (Figure 2.5-9) unit "L," located immediately north of the Westminster terrane

The Honey Brook Upland consists mainly of amphibolite to granulite facies, felsic to mafic gneisses having sedimentary, volcanic and/or volcaniclastic protoliths. The graphitic metasediments are interlayered with felsic gneisses in some areas. These rocks are somewhat similar to the rocks of the Reading Prong and the Adirondacks in northern New York, but the lenticular ultramafites in both the Honey Brook Uplands and Mine Ridge are not present in the Reading Prong. The Honey Brook Upland, Mine Ridge and the Trenton Prong are the southeastern most external basement massifs in the central Appalachians (Drake,1989). The Honey Brook Upland overlies undated, but presumably Middle Proterozoic rocks.

Granulite gneisses appear to be the oldest rocks in the massif, and are associated with, and probably intruded by, the Honey Brook anorthosite. The layered gneiss has both light and dark phases which are interpreted to be metamorphosed volcanics (Rankin, 1989). The layered gneiss appears to be younger than the granulite gneiss and the anorthosite. Amphibolite is found within both the layered gneiss and in the Pickering Gneiss, a coarsely crystalline highly variable rock characterized by abundant graphite and pods of marble. The intrusive rocks that characterize the Reading Prong are missing from the Honey Brook Upland.

Mine Ridge: Tectonostratigraphic map unit "L," located immediately south and west of the Honey Brook Upland

The Mine Ridge consists of amphibolite-facies felsic to mafic gneisses mixed with sedimentary and volcaniclastic protoliths and is similar to parts of the Honey Brook Upland. The presence of ultramafites in both the Mine Ridge and Honey Brook is considered to indicate either a Precambrian age oceanic provenance or tectonic emplacement along offshore and continental margin rocks. There is no evidence in the literature that there are intrusives in the Mine Ridge Anticline.

Trenton Prong: Tectonostratigraphic map (Figure 2.5-9) unit "L" located just south of the Newark Basin near Trenton, Pennsylvania

The Trenton Prong (or Trenton massif) consists of Grenville-age graphitic schists and intermediate grade gneiss with some mafic gneiss and the lithologies are similar to the schists and gneiss of the Honey Brook. The Trenton Prong contains Mesoproterozoic metagabbro, charnockite, and metadacite/tonalite, unconformably overlain by biotitebearing quartzo-feldspathic gneiss, calc-silicate gneiss, and minor marble. (Maguire, 2003). The rocks are unconformably overlain on the south by the Cambrian Chickies quartzite (Figure 2.5-220 and Figure 2.5-221).

Blue Ridge Anticlinorium: Tectonostratigraphic map (Figure 2.5-9) unit "L," located immediately west of the Little North Mountain Fault (Figure 2.5-23).

The Blue Ridge Anticlinorium contains the largest area of exposed Laurentian crust in the Appalachians. The Grenville rocks south of Pennsylvania are dominantly derived from plutonic igneous rocks with locally stratified rock protoliths. The interpretation of these local protoliths is questionable as they could be strongly deformed dikes as well as metasedimentary rocks (Rankin, 1989). The northern-most exposure of Grenville rocks in the Blue Ridge complex occurs in northern Virginia and Maryland, north of the Potomac River.

Above the Grenville basement rocks of the Blue Ridge Anticlinorium terrane, a clastic wedge began to form in late Precambrian time. It was intruded by basalts, presumably still related to the Iapetan rifting. The resulting terrane consists of stratified metasedimentary rocks and meta-basalts of Late Precambrian and Early Paleozoic age. The earliest sediments were siliciclastic and quartzose deposits derived from the Laurentian craton to the northwest (current coordinates). These sediments include the Chilhowee Formation within the Catoctin rift basins, the Hardyston quartzite in the Reading Prong, the Chickies, Harpers and Araby formations in Maryland, and the Weverton, Loudon, Antietam, and Harpers formations in Virginia. Some of these clastic sediments were trapped on the continental margin but some were deposited on the continental slope and deeper water in the Theic Ocean (Faill, 1997a). The clastic wedge progressively overlapped the Grenville basement rocks exposed to the northwest. Siliciclastic sediments were eventually replaced by carbonate deposition during the Early Cambrian. The eastern (present coordinates) margin of the shelf spalled large fragments of carbonate shelf deposits downslope, forming a slope-facies Conestoga Limestone. The carbonate bank, with local influx of sand and silt from the northwest (present coordinates), persisted for the next 100 ma. The carbonates varied in thickness across the platform, reflecting the impact of epeirogenic structural arches and basins (Faill, 1997a). In addition, the shelf-to-bank transition appears to have migrated back and forth in the central Laurentian continental margin because of the superposition of shelf over bank (such as slope-facies Vintage Limestone over Chilhowee clastics in Pennsylvania and slope-facies Conestoga over shelf carbonates further to the northwest (Faill, 1997a).

Eventually, the carbonate bank began to subside at different rates across its area probably also due to epeirogenic movements of the crust and the proximity to the shelf edge. This disparate subsidence produced locally different depositional environments, where contrasting carbonate sequences accumulated. These differences are reflected in the character of the Cumberland Valley, Lebanon Valley, Schuylkill and Lehigh Valley sequences (Figure 2.5-220 and Figure 2.5-221).

The initial closing of the Theic Ocean began in Middle Cambrian but the approaching tectonism did not affect the carbonate shelf until Middle Ordovician. Initial shelf response to the closure of the Theic Ocean was the Knox unconformity (Figure 2.5-211 and Figure 2.5-212). The magnitude of the Knox unconformity decreases from northwest to southeast and may

non-existent from central Pennsylvania to northern Virginia because the stratigraphic section there appears to be uninterrupted (Faill, 1997a).

The Late Precambrian to Ordovician clastic wedge sediments and igneous intrusives were deformed during three successive orogenies (the Taconic, the Acadian and the Alleghanian (see FSAR Sections 2.5.1.1.2.4 through 2.5.1.1.2.6). Throughout those orogenic events, post-Silurian sediments were shed across the uplifted terranes and deposited in basins resulting from orogenic crustal flexure and faulting. These post-Silurian sediments are described in FSAR Sections 2.5.1.1.3.4.

The stratigraphic units of the Valley and Ridge physiographic province of the central Appalachians is composed of Grenvillian crystalline basement rocks overlain by pre-Silurian clastic and carbonate bank deposits similar to those of the Blue Ridge described above. The initial clastic and carbonate bank deposits may have eroded from the northern Valley and Ridge (represented by the Knox unconformity). Further south, in the Virginia and North Carolina portions of the Valley and Ridge, deposition was continuous (Faill, 1997a) through the Lower Devonian, as the effects of the closure of Iapetus moved progressively westward in the Taconic orogeny. The stratigraphy of these post-Silurian units is described in FSAR Section 2.5.1.1.3.3.1.

2.5.1.1.3.1.2 Internal Massifs or Peri-Laurentian Microcontinents

The Internal Massifs in the north-central Appalachians include the Brandywine massifs in southeastern Pennsylvania and the Baltimore massifs in central Maryland. Following are descriptions of these massifs from Faill (1997a).

Brandywine Massifs: Tectonostratigraphic map (Figure 2.5-9) unit "L" and (Figure 2.5-212) unit "2"

The Brandywine massifs include the West Chester, Avondale, and Woodville bodies and possibly the gneiss in the Mill Creek "dome" (Figure 2.5-213). These four massifs comprise the Brandywine terrane of southern Pennsylvania.

The West Chester massif consists predominantly of quartzofeldspathic granulites of variable composition and pyroxene granulites of dioritic to olivine-gabbroic composition, metamorphosed to granulite facies during the Grenville orogeny and later recrystallized to amphibolite facies. There is little information available on the gneisses of the Avondale, Woodville and Miller Creek massifs. The Brandywine gneisses of the internal massifs are quite different lithologically from the gneisses of the external massifs in that they lack large Precambrian age intrusions, charnockitic rocks are not present in the massifs and Late Precambrian dikes in the internal massifs do not have the Catoctin-affinity chemistry present in the dikes in the gneisses north of the Pleasant Grove-Huntingdon Valley shear zone (Figure 2.5-23). These differences are considered to infer that the massifs may not have been derived from the ancestral North America craton (Laurentia) but from the remains of a microcontinent that originated from the South America craton (West Gondwana) (Faill, 1997a) (Figure 2.5-214).

The gneisses of the Avondale, Woodville and Miller Creek massifs are unconformably overlain by a siliciclastic and carbonate sequence of the Setters and Cockeysville Formations, which constitute the lower part of the Glenarm Group. This group was originally defined to include the Wissahickon schist, Peters Creek Formation, Cardiff Conglomerate, and Peach Bottom Slate and underlie much of the Piedmont Province in Maryland, Delaware, Pennsylvania, and New

Jersey and under the Coastal Plain to the southeast. The age of the Glenarm Group remains indeterminate, although Late Precambrian to Early Paleozoic is now generally assumed for most of the group.

Baltimore Massifs Tectonostratigraphic map (Figure 2.5-9) unit "ib"

The Baltimore Massifs lie in central Maryland clustered around the city of Baltimore (Figure 2.5-212). Seven gneiss-cored anticlines compose the Baltimore gneisses, which consist largely of layered quartzofeldspathic gneiss of granitic to granodioritc composition and are considered to be metamorphosed felsic and intermediate to mafic volcaniclastic rocks. Subordinate lithologies include amphibolite, augen gneiss, biotitehornblende gneiss and massive granitic gneiss. These gneisses are thought to represent multiple episodes of deformation in recumbent folds. These rocks are typically surrounded by carbonate and perhaps the basal clastics, forming a link between the Mesoproterozoic basement and the Avondale anticline of the Brandywine massif to the north.

Like the Brandywine gneisses, the Baltimore gneisses are different lithologically from the gneisses of the external massifs in that they lack the large Precambrian-age intrusions and charnockitic characteristics, indicating that the Baltimore massifs may also have been derived from the remains of a microcontinent that originated from the South American craton (Figure 2.5-214).

The Baltimore massifs, like several of the Brandywine massifs, are overlain unconformably by the lower Glenarm, Setters and Cockeysville Formations. In Maryland, the Cockeysville Formation is overlain by the Loch Raven schist. The Baltimore massifs and their sedimentary cover comprise the Baltimore terrane (Figure 2.5-212).

2.5.1.1.3.1.3 Laurentian Rift Sequences

Catoctin Rift

The Catoctin rift (Figure 2.5-214, Figure 2.5-215, and Figure 2.5-217) is part of the Late Precambrian age intracontinental rift system sub-parallel to the eastern margin of the Laurentian craton. Rocks of the Catoctin rift are largely associated with the Blue Ridge massif, as mapped from Charlottesville, Virginia to south central Pennsylvania. The exposed rock of the Catoctin rift in Virginia, Maryland and Pennsylvania include the volcanic rocks of the Catoctin Formation (Schmidt, 1993) and the overlying sedimentary clastics of the Chilhowee Group. In Virginia and Maryland, the Catoctin volcanics are mostly basalts and are present on both flanks of the Blue Ridge anticlinorium (known in Maryland as the South Mountain). In Maryland, the volcanics overlie the Precambrian-age Grenville basement rocks whereas south of the Potomac River the Catoctin volcanics are underlain by 702-704 Ma rift-filling sediments of the Fauquier Group. Northward intoPennsylvania the volcanics are predominantly rhyolite and form the exposed core of South Mountain. Catoctin volcanics are not present above the gneisses of the Honey Brook, Reading Prong and Trenton Prong massifs, suggesting that these massifs were outside the Catoctin rift. Metabasalt dikes in these eastern massifs, however, are geochemically very similar to the Catoctin volcanics of South Mountain in Pennsylvania.

Rome Trough

The Rome Trough (Faill, 1997a) extends from eastern Kentucky northeastward through West Virginia and southwestern Pennsylvania and disappears in north central Pennsylvania (Figure 2.5-214, Figure 2.5-215, and Figure 2.5-217). It is the result of crustal extension that

occurred primarily during Middle and Late Cambrian time. The trough is bounded on the northwest and southeast by steep normal faults that become listric at depth where they merge with the thrusts that originated during the Grenville orogeny. In the northcentral Appalachians, the lithology of the sediments that fill the trough is unknown. Correlative rocks outside the trough, however, consist of dolomite, limestone, sandstone and shale.

2.5.1.1.3.1.4 Laurentian Continental and Shelf Sediments

Early Cambrian-Early Ordovician Passive Margin Sequences

The oldest deposits on the Laurentian continental margin are Late Precambrian to Early Cambrian age siliciclastic and quartzose sediments derived from the exposed craton to the northwest (current coordinates). Continued subsidence of the continental margin through the Cambrian caused the quartzose facies to transgress westward and a carbonate shelf to develop behind (Figure 2.5-217 and Figure 2.5-212). Once the carbonate shelf formed, supplies of siliciclastic sediment from the Laurentian craton slowed (Faill, 1997a).

In southern Virginia, the basal siliciclastic and quartzose sediments are Early Cambrian in age and become progressively younger to the northwest. In northwestern Pennsylvania the oldest of these rocks are Middle Cambrian in age and in southern Ohio they are Early Ordovician. The Chilhowee sequence which is thickest in the Catoctin rift becomes progressively thinner toward the shelf edge (Figure 2.5-217). The Hardyston quartzite in the Reading Prong and the Lowerre quartzite in the Manhattan Prong in southern New York are much thinner across the New Jersey arch and into southern New England (Cheshire Quartzite) and thicken again in west central Connecticut (Faill, 1997a).

In Maryland, the first sediments deposited were sands which later became the Weverton and Sugarloaf Mountain quartzites. These were deposited during the Late Precambrian or Early Cambrian time followed by the Harpers, Urbana and Ijamsville formations. Sands and thin mud of the Setters Formation were deposited on the shelf edge together with the sands of the Antietam Formation. Farther offshore, mud and silt deposits would later become the Araby and Cash Smith formations (Schmidt, 1993).

Siliciclastic deposition near the shelf edge of the north-central Appalachians was replaced by carbonate deposition during the Early Cambrian (Figure 2.5-217 and Figure 2.5-212), indicative of either a decreased volume of siliciclastic deposits and/or a northwestward migration of the shoreline. In Maryland and Virginia, the carbonate-rimmed continental shelf graded into a carbonate ramp. In Maryland, the thick accumulations of limestones and dolomites include all of the formations between the Tomstown Dolomite and the Chambersburg formations, with the exception of the Waynesboro Formation (Schmidt, 1993). In southern New York, the shelf edge in the Manhattan Prong is represented by the Inwood Marble, which is correlated with the Wappinger Limestone, north of the Manhattan Prong. The carbonate bank edge or rim presently lies roughly along a line from White Marsh Valley north of Philadelphia to Lancaster and southwestward through Hanover and then through Frederick, Maryland (Figure 2.5-212). The current location of the carbonate bank edge in the latter area is due to thrusting during the Taconic and Alleghany orogenies (Faill 1997a).

Late Ordovician Drowning Margin Sequences

Subsidence of the continental shelf was not uniform. In northwestern Pennsylvania, the clastic/carbonate sequence thickens considerably to the southwest (Figure 2.5-217). The sequence becomes thinner to the north in southeastern New York as well as to the west and

northwest and thickens again farther north in the Champlain Valley. Near the shelf edge, the sequence thins to the northeast over the New Jersey arch and to the southwest over the Virginia arch. These thinner sequences and the inferred arches have been related to the New York and Virginia promontories (Faill, 1997a).

An unconformity (Figure 2.5-212) extending from eastern Pennsylvania to western Massachusetts during the Early and Middle Cambrian produced locally different environments of deposition. The variations are shown in several stratigraphic sequences including the Cumberland Valley, Lebanon Valley, Schuylkill, and Lehigh Valley sequences (Figure 2.5-215 and Figure 2.5-212). While initial tectonic events in the Theic Ocean may have started in the Middle Cambrian, it was not until the Middle Ordovician that the carbonate shelf was significantly affected. The Knox unconformity (Figure 2.5-212) developed as a result of flexural bulge during the Middle Ordovician. Rocks as old as Late Cambrian were eroded and subsequently overlain by Chazyan carbonates. The magnitude of the unconformity decreases to the southeast and is possibly absent from central Pennsylvania to northern Virginia where the stratigraphic sequence is uninterrupted. The Blackriveran unconformity affected Llanvirn to Early Caradoc rocks along the shelf margin from south-central Pennsylvania into New Jersey. In west-central New York and southeastern Ontario it occurs as an east-west trending arch under Lake Ontario and into the southwestern Adirondacks where approximately 1 km of shelf sequence from the Upper Cambrian age Potsdam Formation to the top of the Beekmantown Group was eroded form the arch crest. The arch was then unconformably overlain by the widespread Lowville Formation (Blackriveran) and Trenton units (Faill, 1997a).

2.5.1.1.3.2 The Iapetan Realm

Based on a compilation of core and cuttings descriptions from wells that penetrated the buried basement complex in the Maryland Coastal Plain and on regional magnetic and gravity data, Hansen (1986) interprets three distinct belts of crystalline rock underlying Cretaceous sediments (Figure 2.5-11). The “Inner Belt” has lithologies and geophysical characteristics similar to the adjacent, exposed Piedmont. As such, this belt appears to be similar to rocks that had been mapped as part of the Wissahickon Group, Baltimore Mafic Complex and the James Run Formation. Rocks of the Middle Belt do not crop out in Maryland but, based on along-strike projections, appear to be similar to the Fredericksburg Complex and Petersburg Granite in Virginia. Although schist or phyllite was logged in borehole CH-BE 57 (Figure 2.5-11), and CH-DA 6-14 toward the southeast, this belt appears to consist of more gneissic and granitic rocks. The Middle Belt in Maryland appears to be characterized by a relatively smooth, anomaly-free, magnetic gradient. The Outer Belt contains diverse lithologies such as gneisses, schists, mafic intrusives and metavolcanics rocks. En echelon geophysical anomalies are truncated at the contact with the Middle Belt. Hansen (1986) interpret the geophysical data as indicating that the Outer Belt may have been accreted to the main North American plate subsequent to the Taconic Orogeny.

2.5.1.1.3.2.1 Iapetan Slope and Abyssal Deposits

2.5.1.1.3.2.1.1 Iapetan Continental Slope and Rise Deposits

Hamburg terrane: Tectonostratigraphic map (Figure 2.5-9) unit “ah”

The Hamburg terrane is an allochthonous continental slope and rise sequence of the Laurentian margin. The Hamburg terrane, located in southeastern Pennsylvania, is one of the southernmost of the Taconic klippen that are so prominent in the central and northern Appalachians (Figure 2.5-9) (Hatcher, 2007). Like the Westminster terrane, the rocks of the Hamburg terrane are Late Proterozoic to Early Cambrian in age. The Hamburg terrane has been tectonically thickened and has been inferred to represent an Early Paleozoic subduction

complex. The terrane is composed of alternating sequences of sandstone, siltstone, olive-green mudstone (~85%), and red, purple and light green mudstone, deep water limestone, and radiolaria-bearing siliceous mudstone and chert. Minor proportions of pebble and boulder conglomerate and mafic intrusive and extrusive igneous rocks are also present (Lash, 1989). The generally coarsening-upward sequence has been interpreted as reflecting a migration from an abyssal plain on oceanic crust to a trench (Lash, 1989). Later analyses of the pebble/boulder conglomerate and intrusive and extrusive igneous rocks suggest that minor portions of the Hamburg terrane are para-autochthonous, with deposition of Late Ordovician siliciclastics and igneous rocks produced and erupted during complex plate interactions with subduction of the Laurentian margin beneath the Taconic arc (Figure 2.5-220 and Figure 2.5-221, Middle Ordovician). The Hamburg terrane was emplaced into the foreland basin (Martinsburg formation) on the Yellow Breeches fault (Figure 2.5-23) early in the Taconic orogeny (Ganis, 2005).

During Early and Middle Cambrian the transition between continental shelf and slope shifted back and forth. This shifting is evident from the presence of Vintage Limestone over Chilhowee clastics in southern Lancaster County and the Conestoga Formation over shelf carbonates farther to the northwest (Figure 2.5-217). The presence of Upper Cambrian and Ordovician shelf carbonates in central Lancaster County, however, indicate that this slope edge did not shift any further to the north (Faill, 1997a).

In Maryland, the transition between continental shelf and slope is considered to be somewhat different. From Early Cambrian to Middle Ordovician the slope edge migrated eastward towards the Octoraro Sea. The change from deep to shallow water facies of the Upper Cambrian Frederick limestone suggests a carbonate ramp rather than a reef rim. To the northeast, the correlative transition during Late Cambrian to Middle Ordovician is hidden under Westminster terrane siliciclastics south of the Martic Line in Pennsylvania and under Mesozoic and/or Cenozoic age rocks farther east in New Jersey (Figure 2.5-212). This lack of exposure of shelf to slope deposits within the north-central Appalachians led to a decade long controversy over- whether the Martic Line represents a conformable contact or a thrust fault (Faill, 1997a).

The Martic Line, east of the Susquehanna River, is the surface trace of the contact between the Lower Paleozoic carbonates of Chester and Lancaster Valleys and the siliciclastic rocks to the south (Figure 2.5-212). West of the Susquehanna River, west of Long Level in York County and southwestward into Maryland, the Martic Line does not correspond to the siliciclastic-carbonate boundary but rather was mapped between two predominantly pelitic assemblages. It is now generally considered that the Martic Line along the south edge of Chester Valley represents an early Taconic thrust fault which carried the Lower Paleozoic Octoraro Formation over the Conestoga Formation and the other Lower Paleozoic carbonates (Figure 2.5-212) with superposed late Alleghany transpressional shear zones. Along the Martic Line trace southwest of Mine Ridge, the relations are complicated by multiple thrusts and repetitious stratigraphy. An apparent break in the Conestoga Formation supports the interpretation of a thrust fault. West of the Susquehanna River the southern edge of the carbonate shelf is hidden under the Alleghany-age Stoner thrust sheet. The Martic Line disappears farther southwestward under the southeastern portion of the Gettysburg basin. It reappears in central Maryland as a thrust fault between the slope shales and siltstones of the Cash Smith and Araby formations below and the slightly older Ijamsville and Urbana Formations above (Faill, 1997a).

2.5.1.1.3.2.1.2 Iapetan Abyssal Deposits

Octoraro Sea

Translational movement in the Theic Ocean positioned the Brandywine and Baltimore microcontinents east (present coordinates) of the Laurentian craton creating the Octoraro Sea (Figure 2.5-217), its size throughout the Cambrian mainly dependent on the positions of these microcontinents. The apparent absence of carbonate shelf deposits southeast of the Martic Line is considered to indicate that the Octoraro Sea had already formed by the Early Cambrian. The Peters Creek Formation occupied the southeastern part of the sea and suggests a continental source consisting of interlayered sequences of quartzites, psammites, and pelites. The Jonestown Basalt in the Hamburg klippe and the Sams Creek Metabasalt in the western Piedmont of Maryland (Schmidt, 1993) and Pennsylvania suggest either an oceanic or highly-attenuated transitional continental/oceanic source (Faill, 1997a).

The sediments and volcanics deposited in the Octoraro Sea now make up the Westminster terrane (Figure 2.5-212). It is comprised of three segments, the Martinsburg segment, the Octoraro segment, and the Peters Creek segment. The Martinsburg segment includes the Urbana, Ijamsville, and Marburg Formations. The Octoraro segment includes Sams Creek, Gillis, Pretty Boy, and the Octoraro formations and is separated from the Marburg segment in Maryland by the Linganore thrust. The Peters Creek segment includes the Peters Creek Formation only (Faill, 1997a; Schmidt, 1993).

Westminster terrane: Tectonostratigraphic map (Figure 2.5-9) unit “aw”

The Westminster terrane of Maryland and Pennsylvania includes rocks previously described as Ijamsville-Pretty Boy-Octoraro terrane (Horton, 1989). This terrane consists of pelitic schist or phyllite, characterized by albite porphyroblasts, and a green and purple phyllite unit.

The rocks of the Westminster terrane have been interpreted to be a slope-rise deep-water prism related to the initial rifting of the Theic Ocean. At some point during the initial rifting, the Brandywine and Baltimore microcontinents (Section 2.5.1.1.3.1.1.2) moved independently within the Theic Ocean between the eastern cratonic margin and developing magmatic arc(s) (Figure 2.5-214). The Octoraro Sea is a proposed arm of the Theic Ocean, between the Laurentian margin and the South American craton (Faill, 1997a). The sediments that accumulated in the sea, mostly from the microcontinents, now constitute the Westminster terrane (Figure 2.5-212).

The rocks are probably correlative with rocks in the Hamburg terrane of Pennsylvania (Drake, 1989; Horton, 1991). The Westminster terrane rocks were metamorphosed to greenschist facies, assembled as a thrust sheet, and finally folded and contractually inverted during the Taconic orogeny (Southworth, 2006).

The Westminster terrane is comprised of three segments, the Marburg segment, the Octoraro segment, and the Peters Creek segment (Figure 2.5-212). The Marburg includes the Urbana, Ijamsville, and Marburg formations. The Octoraro segment includes Sams Creek, Gillis, Pretty Boy, and the Octoraro formations and is separated from the Marburg segment in Maryland by the Linganore thrust. The Peters segment includes the Peters Creek Formation only (Figure 2.5-220 and Figure 2.5-221) (Faill, 1997a; Schmidt, 1993).

While the metamorphic overprint of Westminster terrane rocks shows evidence of Early Silurian and Middle Devonian thermal events, the highest temperature steps of the age

spectrum of these rocks record ages that are consistent with cooling from Grenvillian metamorphism (Mulvey, 2004). The Westminster terrane is thought to have been thrust over the unmetamorphosed, Cambro-Ordovician Frederick Valley Limestone along the Martic Line fault onto the Laurentian margin during the Ordovician Taconic orogeny. (Mulvey, 2004). Later, rocks of the Potomac terrane were transported westward onto rocks of the Westminster terrane along the Pleasant Grove fault (Figure 2.5-23). The Pleasant Grove fault is a ductile shear zone as much as 1 to 2 km wide that initially formed as a thrust fault during deformation associated with the Ordovician Taconian orogeny (Drake, 1989).

Theic Ocean

The Theic Ocean beyond the Brandywine and Baltimore microcontinents was an oceanic basin. Parts of several separate structural bodies that existed in the Theic Ocean were obducted onto the North American continental margin during the Taconic orogeny, some of which were assembled during the Potomac orogeny. These structural bodies each represent a different Theic component and include the Philadelphia terrane, the Wilmington Complex, White Clay nape and Cecil Amalgamate (Figure 2.5-213). Following are descriptions of these structural bodies from Faill (1997a).

Philadelphia terrane

The Philadelphia terrane in southeastern Pennsylvania (Figure 2.5-212 and Figure 2.5-213) consists mostly of the Wissahickon Formation, a group of schists and gneisses whose pelitic and psammitic layering indicate accumulation of siliciclastic sediments in a basin environment, possibly as turbidites. The general homogeneity of the Wissahickon throughout the Philadelphia terrane indicates that the part of the Theic Ocean from which the terrane came, was an open basin. The lack of true amphibolites in the terrane indicates that it developed at some distance from any magmatic source. The presence of Springfield Granodiorite and Lima Granite in the Wissahickon Formation suggest a possible affinity with the Ellicott City Granodiorite in Baltimore, Maryland. The present northern contact of the Philadelphia terrane is the Huntington Valley fault (Figure 2.5-212). Initial contacts of the Philadelphia terrane were considered to be thrust faults but the evidence to support this has either been obscured, covered or destroyed by later deformation. The southeastern boundary of the terrane is hidden under Coastal Plain sediments. The early contact between the terrane and the Brandywine terrane to the west was obscured by Taconic shearing along the Rosemont fault. The contact with the White Clay nappe farther south is hidden under the Wilmington Complex.

White Clay Nappe

The White Clay Nappe (Figure 2.5-212 and Figure 2.5-213) consists of pelitic and psammitic schists and gneisses of the "Glenarm Wissahickon," so named because in the past they have been related to the Wissahickon of the Philadelphia terrane and formed part of the Glenarm Series. The White Clay Nappe schists and gneisses are lithologically similar to the metasedimentary micaceous and quartzose schists and gneisses of the Wissahickon Formation of the Philadelphia terrane. However, they are separated from the Philadelphia terrane by the Rosemont fault and so associated with ultramafic bodies. On the northwest side, the nappe rocks are in fault contact with the Brandywine massifs, they overlie the Cockeysville and Setters Formations in the western part of the massifs and lie directly on massif gneisses in the east. Evidence suggests that the White Clay nappe was probably generated out of the accretionary wedge that accumulated in front of the northwestward moving magmatic arc.

The nappe rocks were subsequently carried on the Doe Run thrust over the massifs of the Brandywine terrane.

Cecil Amalgamate

The Cecil Amalgamate lies mostly in Maryland, southeast of the Westminster and Baltimore terranes and southwest of the White Clay nappe (Figure 2.5-213). A portion of it, the Liberty Complex, lies between the Westminster and Baltimore terranes (Figure 2.5-212). It occupies northern Cecil County, eastern and northern Harford County, and southern Baltimore County. The Liberty Complex crosses northern Baltimore County into Carroll County where it passes southward into the Potomac terrane, which is a complex of thrust sheets and sedimentary mélanges that extend southward into northern Virginia. The Cecil Amalgamate consists of five separate lithic assemblages, the Liberty Complex, the Baltimore Mafic Complex, a metasedimentary sequence, the James Run Formation and the Port Deposit Tonalite. All of these five separate assemblages, while quite distinct lithologically, all have characteristics that relate them to a magmatic arc origin.

The Liberty Complex is the northwestern-most assemblage of the Cecil Amalgamate and consists of the Morgan Run Formation and the younger Sykesville Formation. The assemblage is considered to represent an accretionary wedge accumulated in front of a westward advancing magmatic arc. Fragments of basalt, amphibolite and ultramafics from the magmatic arc were deposited in the Morgan Run schist, while blocks from the Morgan Run were incorporated into the Sykesville metadiamictitic mélange. The combined Morgan Run-Sykesville assemblage was thrust over the Baltimore terrane to its present location between Baltimore and Westminster terranes.

The Baltimore Mafic Complex lies southeast of the Baltimore and Westminster terranes and includes the Aberdeen block (Figure 2.5-212). It consists of a layered sequence of ultramafic, cumulate mafic and mafic intrusives, and volcanic rocks. It has many of the characteristics of an ophiolite sequence, but evidence suggests that it may not be derived from typical depleted oceanic crust as it contains contamination from continental material. The Baltimore Mafic Complex probably developed in a magmatic arc setting over a subduction zone with its contamination coming from subducted continental sediment from nearby microcontinents.

South of the main body of the Baltimore Complex (Figure 2.5-212) lies a belt of metasedimentary rocks which consist of pelitic schists, diamictites, and metagraywackes. The clasts in the diamictites are reported to match lithically the metavolcanics of the James Run Formation and the felsic rocks of the Port Deposit Tonalite indicating that they accumulated in close proximity to both. This metasedimentary belt is reportedly included within the Potomac terrane and Morgan Run Formation in a couple of publications.

The James Run Formation is the southeastern-most belt of the Cecil Amalgamate (Figure 2.5-212) and consists of a sequence of mostly felsic to intermediate rocks of bimodal volcanic, hypabyssal, and volcaniclastic origin. The rocks of the James Run Formation have been associated with the Chopawamsic terrane because of the lithological similarities between the James Run rocks and the rocks of the Chopawamsic terrane. However, an alternate interpretation is that the James Run Formation has a greater chemical affinity to the Baltimore Mafic Complex than to the Chopawamsic Formation (Faill, 1997a).

Within the metasedimentary belt and the James Run Formation is the Port Deposit Tonalite, a metamorphosed felsic pluton (Figure 2.5-212). It has a gradational contact with the James Run

Formation and is chemically similar to these volcanics. It is considered to be the extrusive equivalent of the James Run and pre-dates the Taconic orogeny; a post-Taconic shallow granodiorite/granite (the Basin Run Granitoid) reportedly lies to the northwest.

2.5.1.1.3.2.2 Iapetan Oceanic Crust Remnants

Variously sized bodies of ultramafic rocks are found within the Baltimore Gneiss, all parts of the Wissahickon Formation, and the Peters Creek Schist and variably tectonized schist. They are primarily serpentinite, ranging in color from dark green to yellow-green. Steatite, chlorite-talc schist, anthophyllite schist, pyroxenite, and norite are also present. The relationships between the ultramafic and surrounding rocks, and between the ultramafic bodies themselves, are unclear. The age of these rocks is also uncertain. The largest bodies lie along and near the Rosemont Fault. Other concentrations of ultramafic rocks are close to the boundary between the Avondale Anticline and West Chester Massif, and to the Cream Valley Fault. The remaining small bodies are scattered through the surrounding rocks with no apparent pattern. Examples of possible obducted oceanic crust include the Bel Air-Rising Sun terrane [Tectonostratigraphic map (Figure 2.5-9) unit "ob"] and the Sussex terrane [Tectonostratigraphic map (Figure 2.5-9) unit "os"].

A newly identified remnant of the Siluro-Devonian ocean crust is the Cat Square terrane (Merchat, 2007). The Cat Square terrane is located just south of the Virginia-North Carolina border southwest of the Milton terrane. It is bound on the west by the Brevard fault zone (southern extension of the Bowens Creek fault) and on the east by the central Piedmont suture (Figure 2.5-23). The terrane consists of metapsammite and pelitic schist that was intruded by Devonian anatectic granitoids. Rare mafic and ultramafic rocks occur in the eastern Cat Square terrane. The metapsammite and pelitic schist may represent turbidites derived from approaching highlands on both sides of the closing ocean.

2.5.1.1.3.2.3 Iapetan Volcanic Arc Terranes

The volcanic arcs accreted along the mid-Atlantic margin of North America consist of a collection of terranes that generally display first-order similarities with respect to lithic content and depositional-crystallization ages; however, each of these terranes records differences with respect to the proportions of different rock types, isotopic signatures of magmatic rocks, and tectonothermal histories that distinguish one terrane from another. The components of the zone can be crudely divided on the basis of tectonothermal imprint. Some elements have remained at upper crustal levels throughout their history, experiencing mainly low-grade metamorphism and simple structural imprints and thus are designated ''suprastructural'' terranes; primary structures are commonly preserved in these terranes, thus allowing for the establishment of stratigraphic sequences (Hibbard, 2003). Suprastructural terranes include the Wilmington, Chopawamsic, Milton, Carolina / Albemarle, Spring Hope, and Roanoke Rapids terranes (Figure 2.5-9). Locally some of these terranes display higher grade metamorphism and complex structural geometries. The accreted island arc terranes are described in the following paragraphs.

Wilmington terrane: Tectonostratigraphic map (Figure 2.5-9) unit "cw"

The Wilmington terrane consists of granulite grade felsic to mafic gneisses presently exposed in northern Delaware and adjacent Pennsylvania (Figure 2.5-212 and Figure 2.5-213). The complex is considered to have formed in the lower portion of a magmatic arch that developed over an eastward dipping subduction zone in the ocean basin as early as the Middle Cambrian. Its emplacement over the Philadelphia terrane, White Clay nappe, and Brandywine Avondale massif occurred during the Late Proterozoic-Early Cambrian Potomac orogeny (Faill, 1997a).

Chopawamsic and Milton terranes: Tectonostratigraphic map (Figure 2.5-9) unit "vcp" and "um," respectively

The Early Cambrian Chopawamsic terrane and its southeastward extensions, the Milton terrane, comprise a broad central part of the Piedmont Province extending from southeast Delaware to North Carolina. The Chopawamsic and Milton terranes consist predominantly of meta-sedimentary and meta-volcanic rocks. The Chopawamsic terrane includes the Ta River (Virginia) and James Run (Maryland) metamorphic suites (Figure 2.5-220 and Figure 2.5-221). The Ta River and James Run metamorphic suites consist of a sequence of amphibolites and amphibole-bearing gneisses with subordinate ferruginous quartzites and biotite gneiss. Rocks of the Ta River Metamorphic Suite are generally thought to be more mafic and to have experienced higher-grade regional metamorphism than the rocks of the Chopawamsic Formation (Spears, 2002).

The Chopawamsic and Milton terranes are interpreted to be vestiges of island-arc(s) that were accreted to ancestral North America during the Taconic orogeny (Figure 2.5-219). The terranes consist of sequences of felsic, intermediate and mafic meta-volcanic rocks with subordinate meta-sedimentary rocks. The Chopawamsic and Milton terranes (and others described later in this section) are regarded as exotic, or suspect, terrains that formed ocean-ward from the Laurentian continental margin. Recent U-Pb studies consistently yield Ordovician ages for Chopawamsic volcanic rocks. Rb-Sr and U-Pb dating of granite plutons give late Ordovician ages (Spears, 2002). Detrital zircon ages for the Arvonia and Quantico overlap sequences indicate deposition in early Devonian/late Silurian.

Figure 2.5-9, based on the Horton map (1991) correctly shows the regional extent of the Milton terrane as a southern extension of the Chopawamsic terrane. However, the map legend indicates that the Milton terrane represents an accreted portion of continental crust, distinct from the volcanic arc affinity of the Chopawamsic terrane. Subsequent analytical work shows conclusively that the Milton terrane rocks are isotopically, geochemically, and geochronologically equivalent to the Chopawamsic terrane in the central Virginia Piedmont (Henika, 2006).

Within the 200-mile (322-kilometer) radius of the CCNPP site, the Chopawamsic transitions to the Milton terrane south-southeast of Richmond, Virginia (Figure 2.5-9). The Chopawamsic and Milton terranes are bounded on the west by the Brookneal northeast-trending dextral shear zone (Figure 2.5-23) and its northern extension, the Chopawamsic thrust fault (Figure 2.5-23). Further south, the Milton terrane is overlain on the east by sediments of the Mesozoic Dan River-Danville Basin (tectonostratigraphic map unit "Mz_3"), bounded to the west by a down-to-the-east normal fault. To the east, the Goochland terrane overrides the Chopawamsic and Milton terranes along the Spotsylvania thrust fault. The Chopawamsic and Milton terranes, as well as the contiguous Potomac terrane on the east, are intruded by the Ordovician Occoquan pluton (tectonostratigraphic map unit "p_1"), the Ellisville pluton (tectonostratigraphic map unit "p_2"), and Tanyard Branch pluton (tectonostratigraphic map unit "p_3"). These are "stitching" plutons whose age dates provide a maximum age of terrane assembly (Howell, 1995) (see discussion of Paleozoic plutons in Section 2.5.1.1.3.2.2). Unconformably overlying the Chopawamsic and Milton terranes and their intruded plutons are in-folded remnants of a Paleozoic overlap sequences, the Arvonia Formation (tectonostratigraphic map unit "O_1") and Quantico Formation (tectonostratigraphic map unit "O_2"), consisting of slates, phyllites, schists, and quartzites (see description of Paleozoic overlap sequences in Section 2.5.1.1.3.2.1)

2.5.1.1.3.2.4 Iapetan Disrupted (Infrastructural) Terranes

Some terranes have been subjected to either middle or lower crustal conditions at some time(s) during their history and are thus considered as ''infrastructural'' terranes; most of these terranes are imprinted by both amphibolite facies or higher metamorphism and complex deformational geometries; primary structures have generally been obliterated in these terranes, thus precluding the establishment of any stratigraphy (Hibbard, 2003). Terranes with infrastructural character within a 200-mile (322-kilometer) radius of the CCNPP site include Potomac composite terrane, the Jefferson terrane, the Smith River terrane, the Falls Lake, and Raleigh - Goochland, terranes.

Potomac composite terrane: Tectonostratigraphic map (Figure 2.5-9) unit "dp"

The Potomac terrane is characterized by a stack of mainly metaclastic thrust sheets and intervening mélanges with ophiolitic remnants (Horton, 1989). The Potomac terrane has been divided into Mather Gorge, Sykesville, and Laurel formations. The protoliths of the three formations were interpreted to be Neoproterozoic to Early Cambrian distal slope deposits and olistostromes (Drake, 1989). The three formations are separated by major north-northeast–striking faults (Drake, 1989). Multiple foliations are common and composite foliations are strongest in phyllonitic rocks close to these fault zones.

The relationship between the Smith River allochthon and the Potomac terrane is unknown, although it is likely that the north end of the Smith River allochthon structurally overlies the Potomac terrane. Slices of the Potomac Terrane from central Virginia to the New York Bight appear to have been dextrally transposed along the Brookneal shear zone in Virginia (Figure 2.5-23) and its continuation northeastward.

Jefferson terrane: Tectonostratigraphic map (Figure 2.5-9) unit "dje"

The Jefferson terrane contains mainly metaclastic rocks with subordinate amphibolite and meta-ultramafic rocks that structurally underlie the allochthon. The age of rocks in the Jefferson terrane is unknown, although traditionally they have been viewed to be Neoproterozoic to early Paleozoic (Faill, 1997a). The terrane has been thrust over the Laurentia cover sequence on the Creek Fault and was, in turn, overthrust by the Smith River terrane by the Chatham Fault (Figure 2.5-9).

Smith River terrane: Tectonostratigraphic map (Figure 2.5-9) unit "ds"

The Smith River allochthon is in a southern Appalachian belt of metaclastic rocks that has traditionally been considered to be of peri-Laurentian origin. New Th-U-Pb monzonite ages confirm that the allochthon was involved in an Early Cambrian tectonothermal event. and The presence of ca. 1000 Ma Detrital zircons indicate that the terrane is exotic with respect to adjacent Laurentian rocks and could have a Gondwanan source, because Detrital and xenocrystic zircons of this age are also found in Appalachian peri-Gondwanan crustal elements (Hibbard, 2003). The allochthon may form a new link between the Appalachians and the Pampean terrane of western South America; in addition, its position in the orogen has implications for recent models of the opening of the Iapetus (Hibbard, 2003).

The Smith River terrane includes the structurally underlying Bassett Formation and the structurally overlying Fork Mountain Formation; the contact between the units appears to be conformable, although there is no evidence preserved that indicates their stratigraphic sequence (Conley, 1973). Both units are dominated by biotite paragneiss; the Fork Mountain

Formation also includes matrix-supported breccias that have been favorably compared to some of the mélanges in the Potomac terrane (Horton, 1989). The only age constraint for these units is that they are intruded by the Martinsville intrusive suite. (Hibbard, 2003)

Falls Lake terrane: Tectonostratigraphic map (Figure 2.5-9) unit "df"

The Falls Lake terrane is a small allochthonous unit found in Grenville County, North Carolina, just at the limit of the 200-mile (322-kilometer) radius of the CCNPP site. The western boundary of the Falls Lake terrane is thrust over the eastern edge of the upper greenschist facies Carolina/Albemarle arc along the ductile normal Upper Barton Creek fault while western boundary of the Spring Hope terrane is thrust over the eastern boundary of the Falls Lake terrane along the Nutbush Creek Fault (Figure 2.5-9 and Figure 2.5-23). In Grenville County, a greenschist facies pluton of the Carolina / Albemarle terrane contains a variety of relict igneous features including greenstone, metagabbro, and meta-ultramafic blocks similar to the amphibolite facies Falls Lake terrane.

Goochland or Raleigh / Goochland terrane: Tectonostratigraphic map (Figure 2.5-9) unit "cg"

The Goochland terrane (also known as the Raleigh-Goochland terrane of Hibbard,2003) stretches southward from Fredericksburg, Virginia, to the North Carolina state line east of the Spotsylvania fault (discussed in Section 2.5.1.1.4.4.2) (Frye, 1986) (Figure 2.5-9). The Goochland belt (Virginia) is composed predominantly of granulite facies (high grade) metamorphic rocks and the Raleigh belt (North Carolina) is composed of sillimanite (very high grade) metamorphic rocks (Hibbard, 2007). The Goochland-Raleigh terrane is interpreted to be a microcontinent that was accreted to ancestral North America during the Taconic orogeny. Some geologists believe that the micro-continent was rifted from ancestral North America during the proto-Atlantic rifting while others believe that it formed outboard of ancestral North America (exotic or suspect terrane). Rocks of the Goochland-Raleigh belt are considered to be the oldest rocks of the Piedmont Province and bear many similarities to the Grenville age rocks of the Blue Ridge Province (Spears, 2002).

The Po River Metamorphic Suite and the Goochland terrane, that lie southeast of the Spotsylvania fault, make up the easternmost part of the Goochland-Raleigh terrane. The Po River Metamorphic Suite was named after the Po River in the Fredericksburg area and comprises amphibolite grade (high grade) metamorphic rocks, predominantly biotite gneiss and lesser amounts of hornblende gneiss and amphibolite (Pavlides, 1989). The age of this unit is uncertain, but it has been assigned a provisional age of Precambrian to Early Paleozoic (Pavlides, 1980). The Goochland terrane was first studied along the James River west of Richmond, Virginia, and contains the only dated Precambrian rocks east of the Spotsylvania fault. It is a Precambrian granulite facies (high grade) metamorphic terrane.

2.5.1.1.3.3 The Peri-Gondwanan Realm

2.5.1.1.3.3.1 Peri-Gondwanan Microcontinents

Avalonia or the Avalon terrane has been identified as a microcontinent of peri-Gondwanan affinity (Faill, 1998). Remnants of Avalonian continental crust are not found within the 200-mile (322-kilometer) radius of the CCNPP site. However, exposures in the northern Appalachians indicate that the Carolina volcanic arc terrane was accreted to the Avalonia terrane before the amalgamated microcontinent impinged of the North Atlantic continental margin. The impingement of the amalgamated microcontinent added to the intensity of the collision during the Alleghanian orogeny. Only southeastward (current coordinates) translated portions of the Carolina arc are found within the 200-mile radius of the CCNPP site. Therefore,

the discussion of this terrane is limited to the volcanic arc terranes described in the next section FSAR Section 2.5.1.1.3.3.2. The other identified peri-Gondwanan microcontinent, the Suwannee terrane of the southern Appalachians, is only found outside the 200-mile radius of the CCNPP site and is not discussed further.

2.5.1.1.3.3.2 Peri-Gondwanan Volcanic Arcs

Carolina terrane: Tectonostratigraphic map (Figure 2.5-9) unit "vca"

The Carolina terrane extends southward from southern Virginia to central Georgia, while the Eastern Slate belt is located predominantly in North Carolina, east of the Goochland-Raleigh belt (Figure 2.5-9). Both the Carolina and Eastern Slate belts are composed of greenschist facies (low grade) metamorphic rocks (Hackley, 2007), including metagraywacke, tuffaceous argillites, quartzites, and meta-siltstones (Glover, 1997). The Carolina and Eastern Slate belts are interpreted to be island-arcs that were accreted to ancestral North America during the Taconic orogeny. The island-arcs are interpreted to have been transported from somewhere in the proto-Atlantic Ocean, and are therefore considered to be exotic or suspect terranes. Rocks of the Carolina and Eastern Slate belts generally are considered to be Early Paleozoic in age. Granitic and gabbro-rich plutons that intrude the belts generally are considered to be Middle to Late Paleozoic in age).

New analytical work shows that the Milton terrane and Carolina terrane are distinct and unrelated crustal blocks, separated by a significant shear zone, the Hyco shear zone, a segment of the central Piedmont shear zone (Henika, 2006).

Hatteras terrane: Tectonostratigraphic map (Figure 2.5-9) unit "uh"

The Hatteras terrane is a pluton-rich belt of amphibolite metamorphic grade metaigneous rocks that range in composition from tonalite gneiss with mafic amphibolite layers through quartz monzonite to granite to cordierite-bearing granite. The rocks have a compositional range appropriate for magmatic arcs on continental crust. The western boundary is an abrupt transition to greenschist facies volcaniclastic rocks and may be a fault. Rb/Sr whole-rock ages of 583±46 Ma for the granite and 633±61 Ma for the quartz monzonite. Except for the younger age, the Hatteras terrane is compositionally similar to the eastern high-grade continental basement of the mid-Atlantic states. The plutonic and sub-volcanic to volcanic nature and age span of the Hatteras terrane rocks is consistent with those of the Carolinian terrane (Glover, 1997).

In the Carolinas, magmatic arc rocks are continuous across the Piedmont and under the coastal plain from west of Charlotte, North Carolina, to Cape Hatteras. In Virginia the Piedmont nappes of Goochland Grenville basement are warped into an antiformal structure that plunges southward beneath the Carolinian terrane magmatic arc rocks near Raleigh North Carolina (Glover, 1997). Glover (1997) goes on to state that "The Carolinian terrane is broken by faults and interrupted by Mesozoic basins (Keppie, 1989), but there is little evidence to suggest that it comprises more than a single exotic terrane. Recent maps of the Atlantic Coastal Plain basement (Thomas, 1989; Keppie; 1989) generally agree. Horton (1991), however, split Carolinia into five terranes but consider several to be possible extensions of adjacent volcanic 'terranes.'" Based on the Glover (1997) analysis, this FSAR section groups the Chopawamsic and Milton terranes, the Carolina / Albemarle arcs, and the Hatteras terrane together as possibly correlative accreted volcanic arc terranes built on continental crust.

2.5.1.1.3.4 The Pangean Realm

2.5.1.1.3.4.1 Paleozoic Pangean Sediments

The Paleozoic orogenies eventually led to the formation of the Pangean supercontinent by Late Paleozoic time. The closure of the Iapetus/Theic oceans beginning in the Middle Ordovician was accompanied by the loading onto the Rodinian (see discussion in FSAR Sections 2.5.1.1.3 and 2.5.1.1.2.1) continental margin of thrust sheets. These thrust sheets included microcontinental, abyssal and volcanic arc terranes. This loading likely led to a crustal bulge that uplifted the cratonward portion of carbonate platform in the northern Appalachians causing erosion (the Knox unconformity) of carbonate platform sediments that were shed westward into a foreland basin. On the opposite side of the bulge, subsidence was occurring. Twenty-plus ash falls that thickened southwestward were deposited across the carbonate shelf of the orogenic belt during the Upper Ordovician (the Millbrig K-bentonite, for example). Based on thicknesses of these units, the source of these volcanic deposits is believed to have been off the coast of South Carolina (present coordinates), from a magmatic arc or the Baltica continent colliding with Laurentia (Faill, 1997a).

As the Taconic orogeny reached greater intensity in the central Appalachians, the Brandywine and Baltimore microcontinents began to impinge on the Laurentian margin, leading to subsidence along the continental shelf. Carbonate shelf deposition was replaced by pelitic sedimentation (Martinsburg and Reedville formations (Figure 2.5-220 and Figure 2.5-221). Pelitic units were soon replaced by coarser siliciclastic sediments (Bald Eagle, Juniata and Tuscarora formations) derived from uplifted terranes to the southeast (Figure 2.5-222) (Faill, 1997a). The start of regional deposition of these coarse siliciclastics ended the 100 ma of carbonate shelf deposition on the Laurentian margin. The area of subsidence widened during the Taconic orogeny, spreading northwestward with deposition of the Reedsville shale, for example. Deposition of these marine units spread as far westward (current coordinates) as far north as Ontario and as far west as the Mid-continent (Faill, 1997a). As the Octoraro Sea continued to close, crustal fragments and supracrustal rocks were thrust onto the Laurentian margin, generating several nappes and producing widespread metamorphism. Events associated with the collapse of the Octoraro basin included the development of the Martic thrust, emplacement of the Hamburg klippe, creation of the Reading meganappe system, and the obduction onto the Laurentian margin of microcontinent/magmatic arc packages, previously assembled within the Octoraro basin (Faill, 1997a).

East of the Susquehanna river, oceanic basin sediments were thrust over the Conestoga slope and carbonate shelf sediments. Further south, in south-central Pennsylvania and central Maryland, equivalent Octoraro and related sediments were thrust over pelitic and carbonate slope deposits along the Linganore thrust fault. A deeper thrust, probably still affecting Octoraro basin sediments but not oceanic crust, provided the mechanism by which the Reading meganappe system was emplaced. (Faill,1997a). The depth limit of this thrust is based on the lack of ophiolitic material in the resulting nappe. This lower thrust fault, however, was probably responsible for the inclusion of slivers of Laurentian continental basement into the interleaved and stacked thrust sheets.

The Appalachian basin developed as a consequence of the Taconic orogeny, which produced a crustal downwarp cratonward of new highlands to the west (present coordinates) uplifted as a result of crustal bulging. The initial deposits in the basin included molasse deposits of conglomerate, sandstone, siltstone, and shales of the Shagawunk Formation and its lateral facies, the Bloomsburg delta. A series of transgressions and regressions repeatedly shifted the shore zone and shallow marine facies. The lagoonal-tidal Wills Creek and laminated limestones

of the Tonolway formations (Figure 2.5-222) accumulated in the Late Silurian. The Appalachian basin continued to receive sediments nearly uninterrupted through the remainder of the Paleozoic. Sedimentation in the basin accelerated as a result of Silurian through Permian orogenies.

The Acadian orogeny (Figure 2.5-8) was caused by the collision of the microcontinent Avalon with eastern North America during the Middle to Late Devonian Period. At its peak, the orogeny produced a continuous chain of mountains along the east coast of North America and brought with it associated volcanism and metamorphism. The Acadian orogeny ended the largely quiescent environment that dominated the Appalachian Basin during the Late Ordovician and into the Silurian, as vast amounts of terrigenous sediment from the Acadian Mountains were introduced into the basin and formed the Catskill clastic wedge in central Pennsylvania and northeastern New York (Figure 2.5-211). Vast amounts of terrigenous sediment from the Acadian Mountains were introduced into the Catskill foreland basin during the Middle and Late Devonian and formed the Catskill clastic wedge sequence in Pennsylvania and New York. Thick accumulations of clastic sediments belonging to the Catskill Formation are spread throughout the Valley and Ridge Province (Faill, 1997b). The Catskill clastic wedge is representative of fluctuating shorelines and prograding alluvial environments along the western margin of the Acadian upland. This regressional sequence is represented in the sedimentary record with turbidites, slope deposits, alternating shallow marine and non-marine sediments and alluvial plain fining-upward sequences (Walker, 1971, Faill, 1997b and USGS, 2008). The pebbles and sand grains of the Catskill Formation in New York, Pennsylvania and Maryland are mostly composed of metamorphic and granitic rock fragments, feldspar, mica and quartz. The red color is due to the presence of a small percentage of iron oxide between the grains (Dolt, 1988). The regressive sequence in the region is bounded above and below by marine transgressions which are represented by basal black shale overlain by gray shales and mudstones capped by small amounts of siltstone (Bridge, 1994 and Huber, 2000). The Catskill clastic wedge was the site of the greatest accumulation of sediment in the region, depositing as much as 7,000 feet of sediment (USGS, 2008). The sediments are the thickest in the east and grow progressively thinner westward and southward into the central Appalachian Basin region (Figure 2.5-211). In general, the Acadian Orogeny was superimposed upon terranes affected or formed by the Taconic Orogeny (Dolt, 1988) (Figure 2.5-211).

The Catskill clastic wedge in the central Appalachians is overlain by cyclothems of the Mississippian Pocono Group (Figure 2.5-222), consisting predominantly hard gray massive sandstones, with some shale. In the Eastern Panhandle of Maryland, the Pocono Group has been divided into the Hedges, Purslane, and Rockwell formations unconformably overlain by the Greenbrier and Mauch Chunk formations. The Mississippian stratigraphic units in northern Virginia and West Virginia, and western Maryland/Delaware includes the Rockville and Burgoon/Purslane Sandstone unconformably overlain by the Greenbrier and Mauch Chunk formations.

Sediments of the Mississippian Pocono Group are overlain by cyclothems in the Pennsylvanian Pottsville Group (Figure 2.5-222). The Pottsville Group consists predominantly of sandstones, some of which are conglomeratic, interbedded with thin shales and coals. In eastern Pennsylvania, the Pennsylvanian stratigraphic units include the Pottsville Group and overlying Allegheny, Glenshaw, Casselman, and Monongahela formations. In Maryland and Delaware, the Pennsylvanian stratigraphic units consist of the Pottsville Group and overlying Allegheny, Conemaugh and Monongahela formations. The Pottsville Group is known only from the southwestern portion of Virginia and the southeastern portion of West Virginia (outside the

200-mile (322-kilometer) radius of the CCNPP site). There, the Pottsville is known as the Pocahontas, New River, and Kanawha formations (Stewart 2002). Interestingly, the Late Mississippian Mauch Chunk Group north of Bluefield, Virginia at the state border with West Virginia, evidence is found of a paleoseismite, including clastic sand dikes and slumps, probably associated with the Alleghany orogeny (Stewart 2002).

2.5.1.1.3.4.2 Late Paleozoic Plutons

Late Paleozoic plutons were the result of the final orogeny (the Alleghany orogeny) that contributed to the formation of the Pangean supercontinent. Plutonism was widespread across the Appalachian orogen. Some of the plutons were intruded into paraautochthonous and allochthonous terranes that had been accreted during previous orogenies and provide a means of dating the minimum age of emplacement of the thrusted units. These plutons are termed "stitching" plutons. Some of the major "stitching" plutons and the terranes they affected are described below.

Occoquan pluton: Tectonostratigraphic map (Figure 2.5-9) unit "p_1"

The Occoquan pluton is a granite-granodiorite-tonalite body that is medium- to coarsegrained with rare xenoliths and exhibits moderate to strong metamorphic foliation and mineral lineation by quartz rods and mica layers. The pluton intrudes the upper part of the Wissahickon Schist and the Chopawamsic Formation.

Ellisville pluton: Tectonostratigraphic map (Figure 2.5-9) unit "p_2"

The Ellisville pluton is a large granodiorite body that intrudes the high metamorphic grade rocks of the Hatcher Complex and the lower-grade rocks of the Chopawamsic Formation. Most of the pluton is porphyritic granodiorite with minor foliation, but the body is sheared along the southern margin along the James River.

2.5.1.1.3.4.3 Mesozoic Rift Sequences

The Mesozoic rift basins within a 200-mile (322-kilometer) radius of the CCNPP site are identified collectively in Figure 2.5-9 as map unit "Mz_3" and individually in Figure 2.5-10 with numerical designators.

As described in the subsection on Cenozoic History (Section 2.5.1.1.2.8), early Mesozoic rifting and opening of the Atlantic Ocean was followed by sea floor spreading and the continued opening of the Atlantic Ocean during Cenozoic time. Continued erosion of the Appalachian Mountains and the exposed Piedmont produced extensive sedimentation within the Coastal Plain Province that includes the CCNPP site region.

The non-marine and marine sediments deposited in the Coastal Plain Physiographic Province overlie what are most likely foliated metamorphic or granitic rocks, similar to those cropping out in the Piedmont approximately 50 mi (80 km) to the northwest (Figure 2.5-5 and Figure 2.5-6). A combination of erosion, downwarping, and faulting resulted in an undulatory, east-dipping basement surface with local slope variations that underlies the Coastal Plan Province. The Pre-Cretaceous basement bedrock is only encountered in the Coastal Plain Province by borings designed to characterize deep aquifers above the underlying basement rock. Hansen (Hansen, 1986) indicates that most of the borings that penetrate coastal plain sediments and extend to the underlying basement have encountered metamorphic or igneous rocks. For example, well DO-CE 88 in Dorchester, County located approximately 24 mi (39 km) east of the CCNPP site was drilled into gneissic basement rock at 3,304 ft (1,007 m) in

depth (Figure 2.5-11). Based on the characteristics summarized in FSAR Section 2.5.1.1.3.2.1, this lithology is within the Outer Belt of the terranes underlying the Coastal Plain sequence. Well QA-EB 110, in Queen Anne's County, located 38 mi (61 km) north of the CCNPP site, was drilled to explore for deep freshwater aquifers. This well was drilled into basement at a depth of 2,518 ft (767 m). The basement rock was only sampled in the drill cuttings and suggests a gneiss/schist from the mineralogy present, (i.e., biotite, chlorite, and clear quartz). This crystalline sample lies within the Middle Belt terrane.

Regional geophysical and scattered borehole data indicate that a Mesozoic basin might be present in the site vicinity, buried beneath Coastal Plain sediments. Triassic clastic deposits, indicative of a possible rift basin, were penetrated in Charles County (well CH-CE 37), located over 20 mi (32 km) west of the site, for an interval of 99 ft (30 m), returning samples of weathered brick red clay and shale. Hansen (1986) reports the occurrence of siltstones, sandstones, and clays in several borings north of this well within Prince Georges County. These samples appear to represent continental deposits within the buried Taylorsville Basin. The Inner Belt as defined by Hansen (Hansen, 1986) may contain portions of a buried Mesozoic basin or basins similar to the Neward-Gettysburg terrane to the Northwest (Figure 2.5-9). FSAR Section 2.5.1.1.4.4.3 contains further discussions of potential Mesozoic extensional (rift) basins buried beneath coastal plain sediments.

Diabase was cored in the closest deep boring (SM-DF 84) to the CCNPP site that penetrated the Pre-Cretaceous basement. The boring is located in Lexington Park, St. Mary's County, about 13 mi (21 km) south of the CCNPP site (Hansen, 1984) (Figure 2.5-11). Hansen (Hansen, 1984) states:

As no other basement lithologies were encountered, it is presently not known whether the diabase is from a sill or dike associated with the rift-basin sediments or whether it is cross-cutting the crystalline rocks. The diabase is apparently a one-pyroxene (augite) rock, which Fisher (1964) suggests is evidence of rapid, undifferentiated crystallization in a relatively thin intrusive body, such as a dike.

The occurrence of Mesozoic rift-basin rocks in St. Mary's and Prince George's County are further discussed (Hansen, 1986): "The basins that occur in Maryland are all half-grabens with near-vertical border faults along the western sides. The strata generally strike north-easterly, but, in places, particularly in the vicinity of cross-faults, strike may diverge greatly from the average."

Exposed Mesozoic rift basins found within a 200-mile (322-kilometer) radius of the CCNPP site include the Culpepper Basin, the Deep River Basin, the Gettysburg Basin, the Newark Basin, the Oatlands-Studley Basin, the Richmond Basin, and the Taylorsville Basin. Buried Mesozoic rift basins, inferred from geophysical studies or borehole drilling within a 200-mile radius of the CCNPP site, include New York Bight Basin, the Queen Anne Basin, the Delmarva Basin, the Norfolk Basin, and other unnamed basins identified in Figure 2.5-9 and Figure 2.5-10. All of the exposed rift basins identified above belong to the Newark Supergroup. Instead of describing individual stratigraphic units within each basin, the following is a brief description of the rift basin formation associated with the Eastern North America Magmatic Province (discussion in Section 2.5.1.1.2.7), and a more specific discussion of the Newark Basin Supergroup lithologies.

The Newark Supergroup consists largely of poorly-sorted non-marine sediments deposited within rift basins along the mid-Atlantic margin. The typical lithologies are conglomerate, arkosic sandstone, siltstone, and shale. Most of the strata are red beds that feature ripple

marks, mud cracks, and rain drop imprints; dinosaur footprints are common, though actual body fossils are very rare. Some of the strata are detailed to the level of varves, with indications of Milankovitch cycles. The Triassic stratigraphy of a typical Newark Group basin consists of a basal fluvial unit overlain by lacustrine strata. The deepest lakes occur near the base of the lacustrine succession and then gradually shoal upward. This Triassic sequence is referred to as the "tripartite stratigraphy" (Schlische, 2003). The tripartite stratigraphy is generally overlain by an Early Jurassic age sequence of lava flows and intercalated lacustrine (commonly deep-water) strata overlain in turn by shallow lacustrine strata and, in some cases, by fluvial strata (Schlische, 2003). Based on basin geometry, onlap geometry, and major stratigraphic transitions, the basins grow wider, longer, and deeper through time. Sediment supply appears to keep pace with basin subsidence. Transition from fluvial to lacustrine appears to be a consequence of gradual growth of basin length and width (Schlische, 2003).

The Mesozoic rift basins along the length of the North American Atlantic margin are related to the Eastern North America Magmatic Province (de Boer, 2003). Subsidence of the rift basins was initiated ca. 230 Ma. The orientation of the rift basin follows the general axis of deformation of the Appalachian orogen, including changes along strike related to promontories and recesses. This likely indicates that crustal thinning took advantage of pre-existing deep crustal features such as a major translithospheric suture zone, possibly related to the edge of the Grenvillian basement.

2.5.1.1.3.5 Post-Pangean Sediments

2.5.1.1.3.5.1 Upper Mesozoic Stratigraphic Units

Regionally, coastal plain deposits lap onto portions of the eastern Piedmont. (Mixon, 2000). East of the Fall Line, the Coastal Plain sediments range from Early Cretaceous to Quaternary in age and consist of interbedded silty clays, sands, and gravels that were deposited in both marine and non-marine environments. These sediments dip and thicken toward the southeast. Whereas the basement surface dips southeast at about 100 ft/mi in Charles County, west of the CCNPP site, a marker bed in the middle of the Cretaceous Potomac Group dips southeast at about 50 ft per mile (McCartan, 1989a). This wedge of unlithified sediments consists of Early Cretaceous terrestrial sediments and an overlying sequence of well-defined, Late Cretaceous, marine stratigraphic units. These units from oldest to youngest are summarized in the following paragraphs.

The Lower Cretaceous strata of the Potomac Group consists of a thick succession of variegated red, brown, maroon, yellow, and gray silts and clays with interstratified beds of fine to coarse gray and tan sand. The Potomac Group occurs on Proterozoic to Cambrian metamorphic and igneous rocks in the Washington DC area (McCartan,1990) In the Baltimore-Washington area, the Potomac Group is subdivided from oldest to youngest into the Patuxent, Arundel, and Patapsco Formations. This subdivision is recognizable in the greater Washington-Baltimore area where the clayey Arundel Formation is easily recognized and separates the two dominantly sandy formations (Hansen, 1984). This distinction is less pronounced to the east and southeast where the Potomac Group is divided into the Arundel/Patuxent formations (undivided) and the overlying Patapsco Formation. At Lexington Park, Maryland, the clayey beds that dominate the formation below a depth of 1,797 ft (548 m) are assigned to the Arundel/Patuxent Formations (undivided) (Hansen, 1984).

At the Lexington Park well, located about 13 mi (21 km) south of the CCNPP site (Figure 2.5-11), about 30 ft (9 m) of a denser, acoustically faster, light gray, fine to medium clayey sand occurs at the base of the Potomac Group and might represent an early

Cretaceous, pre-Patuxent Formation. These sediments might correlate with the Waste Gate Formation encountered east of Chesapeake Bay in the DOE Crisfield No. 1 well (Hansen, 1984).

The Patapsco Formation contains interbedded sands, silts, and clays, but it contains more sand than the overlying Arundel/Patuxent Formations (undivided). The contact is marked by an interval dominated by thicker clay deposits. The Arundel/Patuxent Formations (undivided) are marked by the absence of marine deposits. The Mattaponi Formation was proposed (Cederstrom, 1957) for the stratigraphic interval immediately above the Patapsco Formation. An identified interval (Hansen, 1984) as the Mattaponi (?) is now recognized as part of the upper Patapsco Formation.

The Upper Cretaceous Magothy Formation (Figure 2.5-224) is approximately 200 ft (61 m) thick in northern Calvert County but becomes considerably thinner southward at the CCNPP site and pinches out south of the site and north of wells in Solomons and Lexington Park, Maryland (Hansen, 1996) (Achmad, 1997) (Figure 2.5-13). This pattern also appears to reflect thicker deposition in the Salisbury Embayment. The Magothy Formation is intermittently exposed near Severna Park, Maryland, and in the interstream area between the Severn and Magothy Rivers. This outcrop belt becomes thinner to the south in Prince Georges County. The Magothy consists mainly of lignitic or carbonaceous light gray to yellowish quartz sand interbedded with clay layers. The sand is commonly coarse and arkosic and in many places is cross bedded or laminar. Pyrite and glauconite occur locally (Otton, 1955).

The upper Cretaceous Matawan and Monmouth formations (Figure 2.5-224) are exposed in Anne Arundel County, Maryland. While the Matawan is absent in Prince Georges County, the Monmouth crops out in a narrow belt near Bowie, Maryland. Exposures of these formations have not been identified in Charles County. These formations are inseparable in sample cuttings and drillers' logs and are undifferentiated in southern Maryland (Otton 1955) (Hansen, 1996). They consist mainly of gray to grayish-black micaceous sandy clay and weather to a grayish brown. Glauconite is common in both formations and fossils include fish remains, gastropods, pelecypods, foraminifera, and ostracods. The presence of glauconite and this fossil fauna indicate that the Matawan and Monmouth are the oldest in a sequence of marine formations. These formations range in thickness from a few feet or less in their outcrop area to more than 130 ft (40 m) at the Annapolis Water Works (Otton, 1955). The formations thin to the west and average about 45 ft (14 m) in Prince Georges County. The combined formations along with the Brightseat Formation form the Lower Confining Beds (Section 2.4.12) that become progressively thinner from southern Anne Arundel County through Calvert County to St. Mary's County where this hydrostratigraphic unit appears to consist mainly of the Brightseat Formation (Hansen, 1996).

2.5.1.1.3.5.2 Tertiary Stratigraphic Units

The Brightseat Formation is exposed in a few localities in Prince Georges County and contains foraminifera of Paleocene age (Figure 2.5-224). This unit is relatively thin [up to about 25 ft (8m)] but occurs widely in Calvert and St. Mary's counties. It is generally medium and olive gray to black, clayey, very fine to fine sand that is commonly micaceous and / or phosphatic (Otton, 1955; Hansen, 1996). It can be distinguished from the overlying Aquia Formation by the absence or sparse occurrence of glauconite. It generally contains less fragmental carbonaceous material than the underlying Cretaceous sediments (Otton, 1955). The Brightseat Formation is bounded by unconformities with a distinct gamma log signature that is useful for stratigraphic correlation (Hansen, 1996). The Late Paleocene Aquia Formation (Figure 2.5-224) was formerly identified as a greensand due to the ubiquitous occurrence of glauconite. This formation is a poorly to well sorted, variably shelly, and glauconitic quartz

sand that contains calcareous cemented sandstone and shell beds. The Aquia Formation was deposited on a shoaling marine shelf that resulted in a coarsening upward lithology. This unit has been identified in the Virginia Coastal Plain and underlies all of Calvert County and most of St. Mary's County, Maryland (Hansen, 1996). The Aquia Formation forms an important aquifer as discussed in Section 2.4.12. The Late Paleocene Marlboro Clay (Figure 2.5-224) was formerly considered to be a lower part of the early Eocene Nanjemoy Formation but is now recognized as a widely distributed formation. The Marlboro Clay extends approximately 120 mi (193 km) in a northeast-southwest direction from the Chesapeake Bay near Annapolis, Maryland to the James River in Virginia. Micropaleontological data indicate a late Paleocene age although the Eocene-Paleocene boundary may occur within the unit (Hansen, 1996). The Marlboro Clay is one of the most distinctive stratigraphic markers of the Coastal Plain in Maryland and Virginia. It consists chiefly of reddish brown or pink soft clay that changes to a gray color in the subsurface of southern St. Mary's and Calvert Counties. Its thickness ranges from 40 ft (12 m) in Charles County to about 2 ft (60 cm) in St. Mary's County (Otton, 1955). However, the thickness is relatively constant from Anne Arundel County south through the CCNPP site to Solomons and Lexington Park, Maryland (Figure 2.5-13). The apparent localized thickening in Charles County might represent a local depocenter rather than a broader downwarping of the Salisbury Embayment relative to the Norfolk Arch (Figure 2.5-12).

The lower part of the overlying Early Eocene Nanjemoy Formation (Figure 2.5-224) is predominantly a pale-gray to greenish gray, glauconitic very fine muddy sand to sandy clay. This formation becomes coarser upward from dominantly sandy silts and clays to dominantly clayey sands. The gradational contact between the two parts of the Nanjemoy is defined on the basis of geophysical log correlations (Hansen, 1996). In southern Maryland the Nanjemoy Formation ranges in thickness from several ft in its outcrop belt to as much as 240 ft (73 m) in the subsurface in St Mary's County (Otton, 1955) (Figure 2.5-13).

The Middle Eocene Piney Point Formation (Figure 2.5-224) was recognized (Otton, 1955) as a sequence of shelly glauconitic sands underlying the Calvert Formation in southern Calvert County. The contact with the underlying Nanjemoy Formation is relatively sharp on geophysical logs, implying a depositional hiatus or unconformity (Hansen, 1996). The Piney Point Formation ranges in thickness from 0 ft (0 m) in central Calvert County to about 90 ft (27 m) at Point Lookout at the confluence of the Potomac River and Chesapeake Bay (Hansen, 1996). The Piney Point Formation contains distinctive carbonate-cemented interbeds of sand and shelly sand that range up to about 5 ft (1.5 m) in thickness (Hansen, 1996) and a characteristic fauna belonging to the Middle Eocene Jackson Stage (Otton, 1955). This unit is recognizable in the subsurface in Charles, Calvert, St. Marys, Dorchester, and Somerset Counties in Maryland and in Northumberland and Westmoreland Counties in Virginia but has not been recognized at the surface (Otton,1955). The work of several investigators were summarized (Hansen, 1996) who identified a 1 to 4 ft (30 to 122 cm) thick interval of clayey, slightly glauconitic, fossiliferous olive-gray, coarse sand containing fine pebbles of phosphate. This thin interval of late Oligocene age occurs near the top of the Piney Point Formation and appears to correlate with the Old Church Formation in Virginia. This formation appears to thicken downdip between Piney Point and Point Lookout (Hansen, 1996). The absence of middle Oligocene deposits in most of the CCNPP site region indicates possible emergence or non-deposition during this time interval. Erosion or nondeposition during this relatively long interval of time produced an unconformity on the top of the Piney Point Formation that is mapped as a southeast dipping surface in the CCNPP site vicinity (Figure 2.5-14).

Renewed downwarping within the Salisbury Embayment resulted in marine transgression across older Cretaceous and Eocene deposits in Southern Maryland. The resulting

Miocene-age Chesapeake Group consists of three marine formations; from oldest to youngest these are the Calvert, Choptank and St. Marys Formations (Figure 2.5-224). The basal member of the group, the Calvert Formation, is exposed in Anne Arundel, Calvert, Prince Georges, St. Mary's and Charles Counties. Although these formations were originally defined using biostratigraphic data, they are difficult to differentiate in well logs (Hansen, 1996) (Glaser, 2003a). The basal sandy beds are generally 10 to 20 ft (3 to 6 m) thick and consist of yellowish green to greenish light gray, slightly glauconitic fine to medium, quartz sand. The basal beds unconformably overlie older Oligocene and Eocene units and represent a major early Miocene marine transgression (Hansen, 1996). The overlying Choptank and St. Marys formations are described in greater detail in Section 2.5.1.2.3.

The Upper Miocene Eastover Formation and the Lower to Upper Pliocene Yorktown Formation occur in St. Mary's County and to the south in Virginia (McCartan, 1989b) (Ward, 2004). These units appear to have not been deposited to the north of St. Mary's County and that portion of the Salisbury Embayment may have been emergent (Ward, 2004).

Surficial deposits in the Coastal Plain consist, in general, of two informal stratigraphic units: the Pliocene-age Upland deposits and the Pleistocene to Holocene Lowland deposits (Figure 2.5-224). McCartan (McCartan, 1989b) recognized that an Upper Pliocene sand with gravel cobbles and boulders that blankets topographically high areas in the southeast third of St. Mary's County. The Upland Deposits are areally more extensive in St. Mary's County than in Calvert County (Glaser, 1971). The map pattern has a dendritic pattern and since it caps the higher interfluvial divides, this unit is interpreted as a highly dissected sediment sheet whose base slopes toward the southwest (Glaser, 1971) (Hansen, 1996). This erosion might have occurred due to differential uplift during the Pliocene or down cutting in response to lower base levels when sea level was lower during period of Pleistocene glaciation.

2.5.1.1.3.5.3 Plio-Pleistocene and Quaternary Stratigraphic Units

As stated previously, surficial deposits in the Coastal Plain consist, in general, of two informal stratigraphic units: the Pliocene-age Upland deposits and the Pleistocene to Holocene Lowland deposits. McCartan (1989b) differentiates three Upper Pleistocene estuarine deposits, Quaternary stream terraces, Holocene alluvial deposits and colluvium in St. Mary's County. The Lowland deposits in southern Maryland were laid down in fluvial to estuarine environments (Hansen, 1996) and are generally found along the Patuxent and Potomac River valleys and Chesapeake Bay. These deposits occur in only a few places along the eastern shore of Chesapeake Bay. The Lowland deposits extend beneath Chesapeake Bay and the Potomac River filling deep, ancestral river channels with 200 ft (61 m) or more of fluvial or estuarine sediments (Hansen, 1996). These deep channels and erosion on the continental slope probably occurred during periods of glacial advances and lower sea levels. Deposition most likely occurred as the glaciers retreated and melt waters filled the broader ancestral Susquehanna and Potomac Rivers.

2.5.1.1.4 Regional Tectonic Setting

In 1986, the Electric Power Research Institute (EPRI) developed a seismic source model for the Central and Eastern United States (CEUS), which included the CCNPP site region (EPRI, 1986). The CEUS is a stable continental region (SCR) characterized by low rates of crustal deformation and no active plate boundary conditions. The EPRI source model included the independent interpretations of six Earth Science Teams and reflected the general state of knowledge of the geoscience community as of 1986. The seismic source models developed by each of the six teams were based on the tectonic setting and the occurrence, rates, and distribution of

historical seismicity. The original seismic sources identified by EPRI (1986) are thoroughly described in the EPRI study reports (EPRI, 1986) and are summarized in Section 2.5.2.2.

Since 1986, additional geological, seismological, and geophysical studies have been completed in the CEUS and in the CCNPP site region. The purpose of this section is to summarize the current state of knowledge on the tectonic setting and tectonic structures in the site region and to highlight new information acquired since 1986 that is relevant to the assessment of seismic sources.

A global review of earthquakes in SCRs by Johnston et al. (Johnston, 1994) shows that areas of Mesozoic and Cenozoic extended crust are positively correlated with large SCR earthquakes. Nearly 70% of SCR earthquakes with M 6 occurred in areas of Mesozoic and Cenozoic extended crust (Johnston, 1994). Additional evidence shows an association between Late Proterozoic rifts and modern seismicity in eastern North America (Johnston, 1994) (Wheeler, 1995) (Ebel, 2002). Paleozoic and older crust extended during the Mesozoic underlies the entire 200 mi (322 km) CCNPP site region (Figure 2.5-15). The EPRI SOG ESTs were aware of the major conclusions of the Johnston et al. (1994) study - that there is a correlation between Mesozoic and Cenozoic extended crust and large SCR earthquakes. Thus, the findings of Johnston et al. (1994) are not considered new information that would prompt an update of the EPRI-SOG source characterization of the CCNPP COLA.

In a more recent study, Schulte and Mooney (Schulte, 2005) reassessed the correlation between earthquakes and extended and non-extended SCRs. Schulte and Mooney (Schulte, 2005) compiled an updated catalog of SCR earthquakes containing 1,221 earthquakes with magnitudes greater than or equal to Mw 4.5, approximately 58% more earthquakes than in the catalog used by Johnston et al. (Johnston, 1994). Schulte and Mooney (Schulte, 2005) then classified the earthquakes as having occurred in one of five different domains: interior rifts, rifted margins, non-rifted crust, possible interior rifts, and possible rifted margins. Based on their analysis of this classification, Schulte and Mooney (Schulte, 2005) made numerous observations and conclusions that largely support the conclusions of Johnston (Johnston, 1994). In particular, Schulte and Mooney (Schulte, 2005) concluded that:

- Extended SCR crust only has slightly more earthquakes with Mw > 4.5 than non-extended SCR crust; and
- The largest SCR earthquakes (Mw > 7.0) occur predominantly within the extended crust.

The reanalysis of earthquakes with respect to SCRs and extended crust by Schulte and Mooney (Schulte, 2005) supports the conclusions of Johnston (1994) and thus does not provide new information that would motivate an update or revision of the EPRI-SOG source model for this COLA.

As discussed in this section and determined from a comprehensive literature review, discussion with local and regional experts, field and aerial reconnaissance, and review of aerial photography and LiDAR data (See Subsection 2.5.1.1.4.4 for further details), no potential capable faults or tectonic -related features were identified within the site region. These findings are consistent with Crone (2000) and Wheeler (2005) that performed primarily a literature review of existing information for previously identified faults in the Central and Eastern United States.

Although recent characterization of several tectonic features has modified our understanding of the tectonic evolution and processes of the mid Atlantic margin, no structures or features have been identified in the site region since 1986 that show clear evidence of seismogenic potential greater than what was recognized and incorporated in the EPRI study (EPRI, 1986) seismic source model.

The following sections describe the tectonic setting of the site region by discussing the: (1) plate tectonic evolution of eastern North America at the latitude of the site, (2) origin and orientation of tectonic stress, (3) gravity and magnetic data and anomalies, (4) principal tectonic features, and (5) seismic sources defined by regional seismicity. Historical seismicity occurring in the site region is described in Section 2.5.2.1. The geologic history of the site region was discussed in Section 2.5.1.1.2.

2.5.1.1.4.1 Plate Tectonic Evolution of the Atlantic Margin

The Late Precambrian to Recent plate tectonic evolution of the site region is summarized in Section 2.5.1.1.2 and in Figure 2.5-8. Most of the present-day understanding of the plate tectonic evolution comes from research performed prior to the 1986 EPRI report (EPRI, 1986). Fundamental understanding about the timing and architecture of major orogenic events was clear by the early 1980's, after a decade or more of widespread application of plate tectonic theory to the evolution of the Appalachian orogenic belt (e.g., (Rodgers, 1970) (Williams, 1983)). Major advances in understanding of the plate tectonic history of the Atlantic continental margin since the EPRI study report (EPRI, 1986) include the organization of lithostratigraphic units and how they relate to the timing and kinematics of Paleozoic events (e.g., Hatcher, 1989) (Hibbard, 2006) (Hibbard, 2007) and the refinement of the crustal architecture of the orogen and passive margin (e.g., (Hatcher, 1989) (Glover, 1995b) (Klitgord, 1995)).

The following subsections divide the regional plate tectonic history into: (1) Late Proterozoic and Paleozoic tectonics and assembly of North American continental crust, (2) Mesozoic rifting and passive margin formation, and (3) Cenozoic vertical tectonics associated with exhumation, deposition, and flexure.

2.5.1.1.4.1.1 Late Proterozoic and Paleozoic Plate Tectonic History

Although details about the kinematics, provenance, and histories of lithostratigraphic units within the Appalachian orogenic belt continue to be debated and reclassified (e.g., (Hatcher, 1989) (Horton, 1991) (Glover, 1995b) (Hibbard, 2006)), it is well accepted that plate boundary deformation has occurred repeatedly in the site region since middle Proterozoic time. Two complete Wilson cycles, the paired large-scale events of suturing of continents to form supercontinents and rifting to breakup the supercontinents and form ocean basins, occurred twice during this time period (see Fig. 2.5-8). Numerous studies have been published reviewing in detail the individual tectonic events that comprised these two Wilson cycles (e.g., Faill, 1997a; Faill, 1997b, 1998; Hatcher et al., 2007; Thomas, 2006; Whitmeyer and Karlstrom, 2007). The largest-scale events that comprised these Wilson cycles are:

- The Grenville orogeny: The Grenville orogeny marked the beginning of the first Wilson cycle with the suturing of numerous tectonic blocks to Laurentia forming the supercontinent Rodinia. The orogeny occurred over a prolonged period of time extending from approximately 1.3 to 1.0 Ga.

- Rodinia breakup and opening of Iapetus Ocean: This stage of rifting marks the completion of the first Wilson cycle. Extension began as early as approximately 760 to

650 Ma with major rifting occurring around 620 to 550 Ma. The final stages of minor rifting are thought to have been completed by approximately 530 Ma.

- The Appalachian orogeny: The Appalachian orogeny is a broad term used to describe the successive collisional episodes that mark the beginning of the second Wilson cycle and resulted in the formation of Pangea. Three main compressive, orogenic episodes led to the formation of Pangea: Taconic (Ordovician-Silurian), Acadian (Devonian-Mississippian), and Alleghanian (Mississippian-Permian). However, some researchers also explicitly identify the Avalonian (Late Proterozoic-Cambrian), Potomac (pre-Early Ordovician) and Penobscot (Cambrian-Ordovician) orogenies and periods of subduction as key compressional events in the formation of Pangea.

- Pangea breakup and opening of the Atlantic Ocean: The breakup of Pangea during Jurassic time marks the end of the second Wilson cycle.

Evidence for most of these compressive tectonic events are preserved in the geologic record based on foreland strata, deformation structures, and metamorphism (Figure 2.5-8). Synrift basins, normal faults, and postrift strata associated with the opening of the Iapetus and Atlantic Ocean basins record the break-up of the supercontinents. The principal structures that formed during the major events are relevant to the current seismic hazards in that: (1) they penetrate the seismogenic crust, (2) they subdivide different crustal elements that may have contrasting seismogenic potential, and (3) their associated lithostratigraphic units make up the North American continental crust that underlies most of the site region. Many of the principal structures are inherited faults that have been reactivated repeatedly through time. Some are spatially associated with current zones of concentrated seismic activity and historical large earthquakes. For example, the 1811 - 1812 New Madrid earthquake sequence ruptured a failed Late Proterozoic rift that also may have been active in the Mesozoic (Ervin, 1975).

During the interval between opening of the Iapetus Ocean and opening of the Atlantic Ocean, the eastern margin of the ancestral North America continent was alternately (1) an active rift margin accommodating lithospheric extension with crustal rift basins and synrift strata and volcanism; (2) a passive continental margin accumulating terrestrial and shallow marine facies strata; and (3) an active collisional margin with accretion of microcontinents, island arcs, and eventually the African continent. Major Paleozoic mountain building episodes associated with the collision and accretion events included the Taconic, Acadian, and Allegheny Orogenies. More localized collisional events in the site region include the Avalon, Virgilina and Potomac (Penobscot) orogenies (Hatcher, 1987) (Hatcher, 1989) (Glover, 1995b) (Hibbard, 1995) (Drake, 1999) (Figure 2.5-8). The geologic histories of these orogenies are described in Section 2.5.1.1.2.

Tectonic structures developed during the interval between the Late Proterozoic and Triassic Periods are variable in sense of slip and geometry. Late Proterozoic and early Cambrian rifting associated with the breakup of Rodinia and development of the Iapetus Ocean formed east-dipping normal faults through Laurentian (proto-North American) crust (Figure 2.5-16 and Figure 2.5-17). Late Proterozoic extended crust of the Iapetan margin probably underlies the Appalachian fold belt southeastward to beneath much of the Piedmont Province (Wheeler, 1996). Paleozoic compressional events associated with the Taconic, Acadian, and Allegheny orogenies formed predominantly west-vergent structures that include (1) Valley and Ridge Province shallow folding and thrusting within predominantly passive margin strata, (2) Blue Ridge Province nappes of Laurentian crust overlain by Iapetan continental margin deposits, (3) Piedmont Province thrust-bounded exotic and suspect terranes including island arc and accretionary complexes interpreted to originate in the Iapetan Ocean, and (4)

Piedmont Province and sub-Coastal Plain Province east-dipping thrust, oblique, and reverse fault zones that collectively are interpreted to penetrate much of the crust and represent major sutures that juxtapose crustal elements (Hatcher, 1987) (Horton, 1991) (Glover, 1995b) (Hibbard, 2006) (Figure 2.5-16 and Figure 2.5-17). Many investigators recognize significant transpressional components to major faults bounding lithostratigraphic units (Hatcher, 1987) (Glover, 1995b) (Hibbard, 2006) (Figure 2.5-8 and Figure 2.5-16).

2.5.1.1.4.1.2 Mesozoic and Cenozoic Passive Margin Evolution

At the time of the EPRI (1986) study much was published about the structure and crustal elements of the Mesozoic to Cenozoic Atlantic passive margin (e.g., (Klitgord, 1979)). However, it was not until the Geological Society of America's Decade of North American Geology (DNAG) volume on the U.S. Atlantic continental margin (Sheridan, 1988), seminal papers within it (e.g., (Klitgord, 1988)), and later summary publications (e.g., (Klitgord, 1995) (Withjack, 1998) (Schlische, 2003) (Withjack, 2005)) that the current understanding of the margin structure and tectonic history was formulated comprehensively.

The current Atlantic passive continental margin has evolved since rifting initiated in the Early Triassic. The progression from active continental rifting to sea-floor spreading and a passive continental margin included: (1) initial rifting and hot-spot plume development, (2) thinning of warm, buoyant crust with northwest-southeast extension, normal faulting and deposition of synrift sedimentary and volcanic rocks, and (3) cooling and subsidence of thinned crust and deposition of postrift sediments on the coastal plain and continental shelf, slope, and rise (Klitgord, 1988) (Klitgord, 1995). The transition between the second (rifting) and third (drifting) phases during the Late Triassic and Early Jurassic marked the initiation of a passive margin setting in the site region, in which active spreading migrated east away from the margin (Withjack, 1998) (Withjack 2005). As the thinned crust of the continental margin cooled and migrated away from the warm, buoyant crust at the mid-Atlantic spreading center, horizontal northwest-southeast tension changed to horizontal compression as gravitational potential energy from the spreading ridge exerted a lateral "ridge push" force on the oceanic crust. Northwest-southeast-directed postrift shortening, manifested in Mesozoic basin inversion structures, provides the clearest indication of this change in stress regime (Withjack, 1998) (Schlische, 2003). The present-day direction of maximum horizontal compression-east-northeast to west-southwest-is rotated from this hypothesized initial postrift direction.

The crustal structure of the passive continental margin includes areas of continental crust, (Iapetan-extended crust (Wheeler, 1996)), rifted continental crust, rift-stage (transitional) crust, marginal oceanic crust, and oceanic crust (Klitgord, 1995) (Figure 2.5-18 and Figure 2.5-19). Rifted continental crust is crust that has been extended, faulted, and thinned slightly. In the site region, rifted-continental crust extends from the western border faults of the exposed synrift Danville, Scottsville, Culpeper, Gettysburg, and Newark basins to the basement hinge zone, approximately coincident with the seaward edge of the continental shelf (Klitgord, 1995) (Figure 2.5-12 and Figure 2.5-19). Rifted crust also includes exposed and buried Upper Triassic to Lower Jurassic basins within the eastern Piedmont and Coastal Plain Provinces, including the Richmond, Taylorsville, and Norfolk basins (LeTourneau, 2003) (Schlische, 2003) (Figure 2.5-10). Several additional basins with poorly defined extent also underlie the Coastal Plain and Continental Shelf and are shown directly east and northeast of the site (Figure 2.5-10). Buried synrift basins are delineated based on sparse drillhole data, magnetic and gravity anomalies, and seismic reflection data (e.g., (Benson, 1992)). Figure 2.5-19 shows east-dipping basin-bounding faults that penetrate the seismogenic crust and have listric geometries at depth. Many of the synrift normal faults within the site region are interpreted as

Paleozoic thrust faults reactivated during Mesozoic rifting. The Mesozoic basins are discussed further in Section 2.5.1.1.4.4.3 as well as the hypothesized Queen Anne basin shown as lying beneath the site (Figure 2.5-10) as one alternate interpretation of basement lithology.

Rift-stage (transitional) crust is extended continental crust intruded by mafic magmatic material during rifting. In the site region, this crustal type coincides with the basement hinge zone and postrift Baltimore Canyon Trough (Klitgord, 1995) (Figure 2.5-12). The basement hinge zone is defined where pre-Late Jurassic basement abruptly deepens seaward from about 1 to 2.5 mi (1.6 to 4 km) to more than 5 mi (8 km) . Overlying this lower crustal unit seaward of the basement hinge zone is the Jurassic volcanic wedge, representing a period of excess volcanism and is greater than 65 mi (105 km) wide and 1 to 5 mi (1.5 to 8 km) thick. The wedge is identified on seismic reflection lines as a prominent sequence of seaward-dipping reflectors. The East Coast magnetic anomaly (ECMA) coincides with the seaward edge of the wedge (Figure 2.5-18) (Section 2.5.1.1.4.3.2).

The last transitional crustal unit between continental and oceanic crust is marginal oceanic crust (Klitgord, 1995) (Figure 2.5-18). Marginal oceanic crust is located east of the ECMA where the Jurassic volcanic wedge merges with the landward edge of oceanic crust. Here, the transition from rifting to sea-floor spreading created a thicker than normal oceanic crust with possible magmatic underplating.

A postrift unconformity separates synrift from postrift deposits and represents the change in tectonic regime in the Middle Jurassic from continental rifting to the establishment of the passive margin ("drifting"). Sedimentary rocks below the unconformity are cut by numerous faults. In contrast, the rocks and strata above the unconformity accumulated within the environment of a broadly subsiding passive margin and are sparsely faulted. Sediments shed from the faulted blocks of the rifting phase and from the core of the Allegheny orogen accumulated on the coastal plain, continental shelf, slope, and rise above the postrift unconformity and contributed to subsidence of the cooling postrift crust by tectonic loading.

Postrift deformation is recorded in synrift basins and within postrift strata as normal faults seaward of the basement hinge zone and as contractional features landward of the basement hinge zone. Extensive normal faulting penetrates the postrift strata (and upper strata of the volcanic wedge) of the marginal basin overlying the volcanic wedge (Figure 2.5-18 and Figure 2.5-19). This set of faults is thought to have been caused by sediment loading on the outer edge of the margin due to differential compaction of the slope-rise deposits relative to adjacent carbonate platform deposits (Poag, 1991) (Klitgord, 1995). These faults are interpreted as margin-parallel structures that bound large mega-slump blocks and are not considered active tectonic features (Poag, 1991).

The evidence for postrift shortening and positive basin inversion (defined as extension within basins followed by contraction) is well documented in several Atlantic margin basins, including the Newark, Taylorsville, and Richmond basins in the site region (LeTourneau, 2003) (Schlische, 2003) (Withjack, 2005) (Figure 2.5-10). Contractional postrift deformation is interpreted to record the change in stress regime from horizontal maximum extension during rifting to horizontal maximum compression during passive margin drifting. The hypothesis that the change in stress regime following rifting was recorded in reverse and strike slip faulting and folding was known prior to the 1986 EPRI study (e.g., (Sanders, 1963) (Swanson, 1982) (Wentworth, 1983)), but significant advances in the documentation and characterization of the rift to drift transition and postrift deformation has occurred since the mid-1980s (Withjack, 1998) (Schlische, 2003). Based on structural analysis and age control of widespread

approximately 200 Ma basaltic dikes and faulting, much of the site region was under a state of northwest-southeast maximum compression by Late Triassic and Early Jurassic time (Withjack, 1998) (Schlische, 2003a) (Withjack, 2005). This deformation regime may have persisted locally into the Cenozoic based on the recognized early Cenozoic contractional growth faulting associated with the northeast-striking Brandywine fault system (Jacobeen, 1972) (Wilson, 1990), Port Royal fault zone (Mixon, 1984) (Mixon, 2000) and Skinkers Neck anticline (Mixon, 1984) (Mixon, 2000) (Section 2.5.1.1.4.4.4). The present-day stress field of east-northeast to west-southwest maximum horizontal compression (Zoback, 1989a) is rotated from the hypothesized Jurassic and Cretaceous northwest-southeast orientation. The east-northeast to west-southwest maximum horizontal stress direction is consistent with resolved dextral transpressive slip locally documented on the northeast-striking Stafford fault system (Mixon, 2000), a recognized Tertiary tectonic feature (Section 2.5.1.1.4.4.4.1).

2.5.1.1.4.1.3 Cenozoic Passive Margin Flexural Tectonics

Tectonic processes along the Atlantic passive continental margin in the Cenozoic Era include vertical tectonics associated with lithospheric flexure. Vertical tectonics are dominated by: (1) cooling of the extended continental, transitional, and oceanic crust as the spreading center migrates eastward, and (2) the transfer of mass from the Appalachian core to the Coastal Plain and Continental Shelf, Slope, and Rise via erosion. Erosion and exhumation of the Allegheny crustal root of the Piedmont, Blue Ridge, Valley and Ridge, and Appalachian Plateau Provinces has been balanced by deposition on and loading of the Coastal Plain and offshore provinces by fluvial, fluvial-deltaic, and marine sediment transport. Margin-parallel variations in the amount of uplift and subsidence have created arches (e.g. South New Jersey and Norfolk Arches) and basins or embayments (e.g. Salisbury Embayment) along the Coastal Plain and Continental Shelf (Figure 2.5-12).

Flexural zones show both passive-margin-normal and passive-margin-parallel trends. Flexure normal to the passive margin is clearly recorded in the basement hinge zone (Figure 2.5-19). The vertical relief across the offshore basement hinge zone accounts for a change in postrift sediment thickness from 1 to 2.5 mi (1.6 to 4 km) to over 5 mi (8 km) and indicates lateral changes in tectonic loading (Klitgord, 1995). It has been proposed that the downwarping of the margin in the vicinity of the main depocenter of the Baltimore Canyon Trough led to the flexural uplift of the Coastal Plain units to the west (Watts, 1982). However, more recent studies show that sea-level variations since the Cretaceous are compatible with the present elevations of exposed Coastal Plain strata and thus do not support flexural uplift of the Coastal Plain (e.g., (Pazzaglia, 1993)).

A simple elastic model of Cenozoic flexural deformation across the Atlantic passive margin has been used to approximate the response of rifted continental crust to surface erosion of the Piedmont and deposition on the Coastal Plain and Continental Shelf (Pazzaglia, 1994) (Figure 2.5-12 and Figure 2.5-19). The boundary between areas of net Cenozoic erosion and deposition, the Fall Line, marks the flexural hinge between uplift and downwarping. Geologic correlation and longitudinal profiles of Miocene to Quaternary river terraces on the Piedmont with deltaic and marine equivalent strata on the Coastal Plain provide data for model validation (Pazzaglia, 1993). A one-dimensional elastic plate model replicates the form of the profiles and maintenance of the Fall Line with flexure driven by exhumation of the Piedmont and adjacent Appalachian provinces coupled with sediment loading in the Salisbury Embayment and Baltimore Canyon Trough (Pazzaglia, 1994). Model results suggest a long-term denudation rate of approximately 33 ft (10 m) per million years and about 115 to 426 ft (35 to 130 m) of upwarping of the Piedmont in the last 15 million years.

The flexural hinge zones (Fall Line and basement hinge zone) do not appear to be seismogenic. The spatial association between the Fall Line and observed Cenozoic faults such as the Stafford and Brandywine fault systems is commonly attributed to the fact that those faults are recognizable where Cenozoic cover is thin and there is greater exposure of bedrock compared to areas farther east toward the coast (e.g., (Wentworth, 1983)). It is suggested (Pazzaglia, 1994) that low rates of contractional deformation on or near the hinge zone documented on Cenozoic faults may be a second-order response to vertical flexure and horizontal compressive stresses. Neither the Fall Line nor basement hinge zone was considered a potential tectonic feature by EPRI (1986). They were considered zones where ground amplification could be affected. It is also suggested (Weems, 1998) that multiple fall lines (i.e., alignments of anomalously steep river gradients) located near or within the Fall Line may be of neo-tectonic origin. Subsequent studies performed during the North Anna ESP study demonstrates that the fall lines (Weems, 1998) are erosional features and not capable tectonic sources (NRC, 2005) (Section 2.5.1.1.4.4.5.1) Post-EPRI seismicity also shows no spatial patterns suggestive of seismicity aligned with either the basement hinge zone or Fall Line. Crone and Wheeler (Crone, 2000) and Wheeler (Wheeler, 2005) (Wheeler, 2006) also do not list these as potentially Quaternary active features. Accordingly, it is concluded that these features are not capable tectonic sources. Post-EPRI seismicity also shows no spatial patterns suggestive of seismicity aligned with either the basement hinge zone or Fall Line (Section 2.5.2).

Along-strike variations in the amount of epeirogenic movement along the Atlantic continental margin has resulted in a series of arches and embayments identified based on variations in thickness of Coastal Plain strata from Late Cretaceous through Pleistocene time. The Salisbury Embayment is a prominent, broad depocenter in the site region, and coincides with Chesapeake Bay and Delaware Bay (Figure 2.5-12). In general, it appears that downwarping associated with the Salisbury Embayment (Figure 2.5-12) began early in the Cretaceous and continued intermittently throughout the Cretaceous and Tertiary periods. Deposition apparently kept pace, resulting in a fluvial-deltaic environment. Biostratigraphic data from test wells on the west side of Chesapeake Bay indicate that Upper Cretaceous sediments reach maximum thickness in Anne Arundel County and show progressive thinning to the south. This appears to reflect deposition within the downwarping, northwest-trending Salisbury Embayment during the Cretaceous (Hansen, 1978). At the margins of the Salisbury Embayment are the South New Jersey Arch to the northeast and the Norfolk Arch to the south. Both arches are broad anticlinal warps reflected in the top of basement and overlying sediments. Thinning and overlapping within the Upper Cretaceous interval suggests that the northern flank of the Norfolk Arch was tectonically active during late Cretaceous time (Hansen, 1978) (Figure 2.5-12). The processes that form and maintain the arches and embayments are poorly understood, and there has been little advancement in the thinking about these features since publication of the EPRI study report (EPRI, 1986). Poag (2004), however, uses new basement data obtained from seismic reflection profiles and exploratory boreholes in the region of the main Chesapeake Bay impact crater to show that the Norfolk Arch is not as well expressed as originally interpreted by earlier authors (Brown, 1972) using limited data. Previous elevation differences cited as evidence for the basement arch appear to be due to subsidence differential between the impact crater and the adjacent deposits (Poag, 2004) (Section 2.5.1.1.4.4.4). Regardless, no published hypothesis was found suggesting causality between epeirogenic processes maintaining these specific arches and the embayment and potentially seismogenic structures, and there is no spatial association of seismicity with the basement arches. Thus, it is concluded that these features are not capable tectonic sources.

2.5.1.1.4.2 Tectonic Stress in the Mid-Continent Region

Expert teams that participated in the 1986 EPRI evaluation of intra-plate stress generally concluded that tectonic stress in the CEUS region is characterized by northeast-southwest-directed horizontal compression. In general, the expert teams concluded that the most likely source of tectonic stress in the mid-continent region was ridge-push force associated with the Mid-Atlantic ridge, transmitted to the interior of the North American plate by the elastic strength of the lithosphere. Other potential forces acting on the North American plate were judged to be less significant in contributing to the magnitude and orientation of the maximum compressive principal stress. Some of the expert teams noted local deviations from this regional trend. They assessed the quality of stress indicator data and discussed various hypotheses to account for their interpreted variations in the regional stress trajectories.

Since 1986, an international effort to collate and evaluate stress indicator data has resulted in publication of a new world stress map (Zoback, 1989a) (Zoback, 1989b). Data for this map are ranked in terms of quality, and plate-scale trends in the orientations of principal stresses are assessed qualitatively based on analysis of high-quality data (Zoback, 1992). Subsequent statistical analyses of stress indicators confirmed that the trajectory of the maximum compressive principal stress is uniform across broad continental regions at a high level of statistical confidence. In particular, the northeast-southwest orientation of principal stress in the CEUS inferred by the EPRI experts is statistically robust, and is consistent with the theoretical trend of compressive forces acting on the North American plate from the mid-Atlantic ridge (Coblentz and Richardson, 1995). However, local variations in the regional stress field similar to those recognized by the EPRI teams are also present in the more recent datasets (e.g., Kim, 2005; Reinecker, 2008).

In addition to better documenting the orientation of stress, research conducted since 1986 has addressed quantitatively the relative contributions of various forces that may be acting on the North American plate to the total stress within the plate. Richardson and Reding (Richardson, 1991) performed numerical modeling of stress in the continental U.S. interior, and considered the contribution to total tectonic stress to be from three classes of forces:

- Horizontal stresses that arise from gravitational body forces acting on lateral variations in lithospheric density. These forces commonly are called buoyancy forces. Richardson and Reding emphasize that what is commonly called ridge-push force is an example of this class of force. Rather than a line-force that acts outwardly from the axis of a spreading ridge, ridge-push arises from the pressure exerted by positively buoyant, young oceanic lithosphere near the ridge against older, cooler, denser, less buoyant lithosphere in the deeper ocean basins (Turcotte, 2002). The force is an integrated effect over oceanic lithosphere ranging in age from about 0 to 100 million years (Dahlen, 1981). The ridge-push force is transmitted as stress to the interior of continents by the elastic strength of the lithosphere.

- Shear and compressive stresses transmitted across major plate boundaries (strike-slip faults and subduction zones).

- Shear tractions acting on the base of the lithosphere from relative flow of the underlying asthenospheric mantle.

Richardson and Reding (Richardson, 1991) concluded that the observed northeast-southwest trend of principal stress in the CEUS dominantly reflects ridge-push body forces. They estimated the magnitude of these forces to be about 2 to 3 X 10^{12} N/m (i.e., the total vertically

integrated force acting on a column of lithosphere 1 m wide), which corresponds to average equivalent stresses of about 40 to 60 MPa distributed across a 30 mi (50 km) thick elastic plate. The fit of the model stress trajectories to data was improved by the addition of compressive stress (about 5 to 10 MPa) acting on the San Andreas Fault and Caribbean plate boundary structures. The fit of the modeled stresses to the data further suggested that shear stresses acting on these plate boundary structures is in the range of 5 to 10 MPa.

Richardson and Reding (Richardson, 1991) noted that the general northeast-southwest orientation of principal stress in the CEUS also could be reproduced in numerical models that assume a shear stress, or traction, acting on the base of the North American plate. Richardson and Reding (Richardson, 1991) and Zoback and Zoback (Zoback, 1989) do not favor this as a significant contributor to total stress in the mid-continent region. A basal traction predicts or requires that the horizontal compressive stress in the lithosphere increases by an order of magnitude moving east to west, from the eastern seaboard to the Great Plains. Zoback and Zoback (Zoback, 1989) noted that the state of stress in the southern Great Plains is characterized by north-northeast to south-southwest extension, which is contrary to this prediction. They further observed that the level of background seismic activity is generally higher in the eastern United States than in the Great Plains, which is not consistent with the prediction of the basal traction model that compressive stresses (and presumably rates of seismic activity) should be higher in the middle parts of the continent than along the eastern margin.

To summarize, analyses of regional tectonic stress in the CEUS since EPRI (1986) have not significantly altered the characterization of the northeast-southwest orientation of the maximum compressive principal stress. The orientation of a planar tectonic structure relative to the principal stress direction determines the magnitude of shear stress resolved onto the structure. Given that the current interpretation of the orientation of principal stress is similar to that adopted in EPRI (1986), a new evaluation of the seismic potential of tectonic features based on a favorable or unfavorable orientation to the stress field would yield similar results. Thus, there is no significant change in the understanding of the static stress in the CEUS since the publication of the EPRI source models in 1986, and there are no significant implications for existing characterizations of potential activity of tectonic structures.

2.5.1.1.4.3 Gravity and Magnetic Data and Features of the Site Region and Site Vicinity

Gravity and magnetic anomaly datasets of the site region have been published following the 1986 EPRI study. Significant datasets include regional maps of the gravity and magnetic fields in North America by the Geological Society of America (GSA), as part of the Society's DNAG project (Tanner, 1987) (Hinze, 1987). The DNAG datasets are widely available in digital form via the internet (Hittelman, 1994). A magnetic anomaly map of North America was published in 2002 that featured improved reprocessing of existing data and compilation of a new and more complete database (Bankey, 2002) (Figure 2.5-20).

These maps present the potential field data at 1:5,000,000-scale, and thus are useful for identifying and assessing gravity and magnetic anomalies with wavelengths on the order of tens of kilometers or greater (Bankey, 2000) (Hittelman, 1994). Regional gravity anomaly maps are based on Bouguer gravity anomalies onshore and free-air gravity anomalies offshore. The primary sources of magnetic data reviewed for this CCNPP Unit 3 study are from aeromagnetic surveys onshore and offshore (Bankey, 2002), and the DNAG datasets available digitally from the internet (Hittelman, 1994).

Most of the contributed gravity and magnetic data that went into the regional compilations were collected prior to the 1986 EPRI study; thus, most of the basic data were available for interpretation at local and regional scales. Large-scale compilations (1:2,500,000-scale) of the free-air anomalies offshore and Bouguer anomalies onshore were published in 1982 by the Society of Exploration Geophysicists (Lyons, 1982) (Sheridan, 1988). The DNAG magnetic anomaly maps were based on a prior analog map of magnetic anomalies of the U.S. published in the early 1980's (Zietz, 1982) (Behrendt, 1983) (Sheridan, 1988).

In addition, the DNAG Continent-Ocean transect program published a synthesis of gravity and magnetic data with seismic and geologic data (Klitgord, 1995). Transect E-3, which crosses the site region, is presented in Figure 2.5-16 and Figure 2.5-17. Much of the seismic and geophysical data through the Piedmont region was reanalyzed from a geophysical survey conducted along Interstate I-64 in Virginia that was published prior to release of the 1986 EPRI study (e.g., (Harris, 1982)).

In summary, the gravity and magnetic data published since 1986 do not reveal any new anomalies related to geologic structures that were not identified prior to the 1986 EPRI study. Rather, post-EPRI publications have refined the characteristics and tectonic interpretation of the anomalies. Discussion of the gravity and magnetic anomalies is presented in the following sections.

2.5.1.1.4.3.1 Gravity Data and Features

Gravity data compiled at 1:5,000,000-scale for the DNAG project provide documentation of previous observations that the gravity field in the site region is characterized by a long-wavelength, east-to-west gradient in the Bouguer gravity anomaly over the continental margin (Harris, 1982) (Hittelman, 1994) (Figure 2.5-21). The free-air gravity anomaly shows broad gravity lows over offshore oceanic crust near the continental margin and over the broad marginal embayments. Offshore marginal platforms are marked by shorter-wavelength, higher-amplitude gravity highs and lows. The present shelf edge is marked by a prominent free-air gravity anomaly that also corresponds to the continent-ocean boundary (Sheridan, 1988) (Klitgord, 1995).

Bouguer gravity values increase eastward from about -80 milligals (mgal) in the Valley and Ridge Province of western Virginia to about +10 mgal in the Coastal Plain Province, corresponding to an approximately 90 mgal regional anomaly across the Appalachian Orogen (Figure 2.5-17 and Figure 2.5-21). This regional gradient is called the "Piedmont gravity gradient" (Harris, 1982), and is interpreted to reflect the eastward thinning of the North American continental crust and the associated positive relief on the Moho discontinuity with proximity to the Atlantic margin.

The Piedmont gravity gradient is punctuated by several smaller positive anomalies with wavelengths ranging from about 15 to 50 mi (25 to 80 km) , and amplitudes of about 10 to 20 mgal. Most of these anomalies are associated with accreted Taconic terranes such as the Carolina/Chopawamsic terrane (Figure 2.5-17). Collectively, they form a gravity high superimposed on the regional Piedmont gradient that can be traced northeast-southwest on the 1:5,000,000-scale DNAG map relatively continuously along the trend of the Appalachian orogenic belt through North Carolina, Virginia, and Maryland (Figure 2.5-21). The continuity of this positive anomaly diminishes to the southwest in South Carolina, and the trend of the anomaly is deflected eastward in Maryland, Pennsylvania, and Delaware.

The short-wavelength anomalies and possible associations with upper crustal structure are illustrated by combining gravity profiles with seismic reflection data and geologic data (Harris, 1982) (Glover, 1995b). In some cases, short-wavelength positive anomalies are associated with antiformal culminations in Appalachian thrust sheets. For example, there is a positive anomaly associated with an anticline at the western edge of the Blue Ridge nappe along the Interstate I-64 transect (Harris, 1982) (Figure 2.5-17). The anomaly is presumably due to the presence of denser rocks transported from depth and thickened by antiformal folding in the hanging wall of the thrust.

The Salisbury geophysical anomaly (SGA) is a paired Bouguer gravity anomaly and magnetic high that is located along the west side of the Salisbury Embayment (Klitgord, 1995) (Figure 2.5-17, Figure 2.5-18, Figure 2.5-20, and Figure 2.5-21). The SGA is located about 10 mi (16 km) west of the CCNPP site (Figure 2.5-22). The anomaly is expressed most clearly as a magnetic lineation that separates a zone of short-wavelength, high-amplitude magnetic lineations to the west from a zone of low-amplitude, long-wavelength anomalies to the east. The gravity data show the SGA to form the western margin of a broad gravity low that extends seaward to the basement hinge zone. The anomaly takes the form of a north-northeast-trending gravity high having about 30 mgal relief (Johnson, 1973). The anomaly has also been named the Sussex-Curioman Bay trend (Levan, 1963) or the Sussex-Leonardtown anomaly (Daniels, 1985), and is believed to reflect an east-dipping mafic rock body associated with a suture zone buried beneath coastal plain sediments (Figure 2.5-17). The SGA is interpreted (Klitgord, 1995) to mark the likely location of the Taconic suture that separates the Goochland terrane on the west from a zone of island arc and oceanic metavolcanics formed in the Iapetus Ocean on the east. The SGA is shown (Horton, 1991) to be associated with the buried Sussex terrane is a probable mafic mélange that was interpreted by Lefort and Max (Lefort, 1989) to mark the Alleghenian "Chesapeake Bay suture" (Figure 2.5-16).

The offshore portions of the site region contain a prominent, long-wavelength free-air gravity anomaly associated with the transition from continental to oceanic crust (Sheridan, 1988) (Klitgord, 1995) (Figure 2.5-19). This anomaly is large (75 to 150 mgal peak to trough) and is 45 to 80 mi (72 to 129 km) wide. Variations in the amplitude and shape of the anomaly along the Atlantic margin are due to seafloor relief, horizontal density variations in the crust, and relief on the crust-mantle boundary (Sheridan, 1988) (Klitgord, 1995).

In summary, gravity data published since the mid-1980s confirm and provide additional documentation of previous observations of a gradual "piedmont gravity gradient" across the Blue Ridge and Piedmont Provinces of Virginia and a prominent gravity anomaly at the seaward margin of the continental shelf. Shorter-wavelength anomalies such as the SGA also are recognized in the data. All anomalies were known at the time of the 1986 EPRI study. The "piedmont gravity gradient" is interpreted to reflect eastward thinning of the North American crust and lithosphere. The free-air anomaly at the outer shelf edge is interpreted as reflecting the transition between continental and oceanic crust. Second-order features in the regional field, such as the Salisbury geophysical anomaly and the short discontinuous northeast-trending anomaly east of the site, primarily reflect density variations in the upper crust associated with the boundaries and geometries of Appalachian thrust sheets and accreted terranes.

2.5.1.1.4.3.2 Magnetic Data and Features

Magnetic data compiled for the 2002 Magnetic Anomaly Map of North America reveal numerous northeast-southwest-trending magnetic anomalies, generally parallel to the structural features of the Appalachian orogenic belt (Bankey, 2002) (Figure 2.5-20). Unlike the

gravity field, the magnetic field is not characterized by a regional, long-wavelength gradient that spans the east-west extent of the site region. A magnetic profile along Interstate-64 published to accompany a seismic reflection profile (Harris, 1982) shows anomalies with wavelengths of about 6 to 30 mi (10 to 48 km). It has been concluded (Harris, 1982) that anomalies in the magnetic field primarily are associated with upper-crustal variations in magnetic susceptibility and, unlike the gravity data, do not provide information on crustal-scale features in the lithosphere.

Prominent north- to northeast-trending magnetic anomalies in the CCNPP site region include the interior New York-Alabama, Ocoee, and Clingman lineaments, the Coastal Plain Salisbury geophysical anomaly and near shore Brunswick magnetic anomaly, and the offshore East Coast magnetic anomaly (King, 1978) (Klitgord, 1988) (Klitgord, 1995) (Bankey, 2002) (Figure 2.5-20). The offshore Blake Spur magnetic anomaly is outside the site region.

King and Zietz (1978) identified a 1,000 mi (1,600 km) long lineament in aeromagnetic maps of the eastern U.S. that they referred to as the "New York-Alabama lineament" (NYAL) (Figure 2.5-20). The NYAL primarily is defined by a series of northeast-southwest-trending linear magnetic anomalies in the Valley and Ridge province of the Appalachian fold belt that systematically intersect and truncate other magnetic anomalies. The NYAL is located about 160 mi (257 km) northwest of the CCNPP site.

The Clingman lineament is an approximately 750 mi (1,200 km) long, northeast-trending aeromagnetic lineament that passes through parts of the Blue Ridge and eastern Valley and Ridge provinces from Alabama to Pennsylvania (Nelson, 1981). The Ocoee lineament splays southwest from the Clingman lineament at about latitude 36°N (Johnston, 1985a). The Clingman-Ocoee lineaments are sub-parallel to and located about 30 to 60 mi (48 to 97 km) east of the NYAL. These lineaments are located about 60 mi northwest of the CCNPP site.

King and Zietz (King, 1978) interpreted the NYAL to be a major strike-slip fault in the Precambrian basement beneath the thin-skinned fold-and-thrust structures of the Valley and Ridge province, and suggested that it may separate rocks on the northwest that acted as a mechanical buttress from the intensely deformed Appalachian fold belt to the southeast. Shumaker (Shumaker, 2000) interpreted the NYAL to be a right-lateral strike-slip fault that formed during an initial phase of Late Proterozoic continental rifting that eventually led to the opening of the Iapetus Ocean.

The Clingman lineament also is interpreted to arise from a source or sources in the Precambrian basement beneath the accreted and transported Appalachian terranes (Nelson, 1981). Johnston (Johnston, 1985a) observed that the "preponderance of southern Appalachian seismicity" occurs within the "Ocoee block", a Precambrian basement block bounded by the NYAL and Clingman-Ocoee lineaments (the Ocoee block was previously defined by (Johnston, 1985b)). Based on the orientations of nodal planes from focal mechanisms of small earthquakes, it was noted (Johnston, 1985) that most events within the Ocoee block occurred by strike-slip displacement on north-south and east-west striking faults, Johnston (Johnston, 1985a) did not favor the interpretation of seismicity occurring on a single, through-going northeast-southwest-trending structure parallel to the Ocoee block boundaries.

The Ocoee block lies within a zone defined by Wheeler (Wheeler, 1995) (Wheeler, 1996) as extended continental crust of the Late Proterozoic to Cambrian Iapetan terrane. Synthesizing geologic and geophysical data, Wheeler (Wheeler, 1995) mapped the northwest extent of the

Iapetan normal faults in the subsurface below the Appalachian detachment, and proposed that earthquakes within the region defined by Johnston and Reinbold (Johnston, 1985b) as the Ocoee block may be the result of reactivation of Iapetan normal faults as reverse or strike-slip faults in the modern tectonic setting.

The East Coast magnetic anomaly (ECMA) is a prominent, linear, segmented magnetic high that extends the length of the Atlantic continental margin from the Carolinas to New England (Figure 2.5-20). The anomaly is about 65 mi (105 mi) wide and has an amplitude of about 500 nT. This anomaly approximately coincides with the seaward edge of the continental shelf, and has been considered to mark the transition from continental to oceanic crust. Klitgord et al. (1995) note that the anomaly is situated above the seaward edge of the thick Jurassic volcanic wedge and lower crustal zone of magmatic under plating along the boundary between rift-stage and marginal oceanic crust (Figure 2.5-18 and Figure 2.5-19). The ECMA is not directly associated with a capable tectonic feature, and thus is not considered as a seismic source.

The Brunswick magnetic anomaly (BMA) is located along the basement hinge zone offshore of the Carolinas, at the southern portion of the site region about 200 mi (322 km) from the CCNPP site (Figure 2.5-20). The lineament is narrower and has less amplitude than the ECMA (Klitgord, 1995). The BMA may continue northward along the hinge zone of the Baltimore Canyon Trough, but the magnetic field there is much lower in amplitude and the lineament is diffuse. The BMA is not directly related to a fault or other tectonic structure, and thus is not a potential seismic source.

The Blake Spur magnetic anomaly (BSMA) is located east of the site region above oceanic crust, about 290 mi (465 km) from the CCNPP site (Figure 2.5-20). The BSMA is a low-amplitude magnetic anomaly that lies subparallel to the East Coast magnetic anomaly (Klitgord et al., 1995). The BSMA probably formed during the Middle Jurassic as the midocean ridge spreading center shifted to the east. The BSMA coincides with a fault-bounded, west-side-down scarp in oceanic basement. Since its formation, the BSMA has been a passive feature in the Atlantic crust, and thus is not a potential seismic source.

The Salisbury geophysical anomaly (SGA), as mentioned above, is a paired Bouguer gravity and magnetic anomaly along the west side of the Salisbury embayment that is located about 10 mi (16 km) of the CCNPP site (Figure 2.5-22). The anomaly is expressed in the magnetic data as a lineament separating short-wavelength, high-amplitude magnetic lineations to the west from a zone of low-amplitude, long-wavelength anomalies to the east. The contrast in magnetic signature is related to the juxtaposition of terranes of contrasting affinity beneath coastal plain sediments, and in particular the mafic to ultramafic rocks and mélange termed the Sussex terrane by Horton et al. (1991) and believed to represent alternatively a Taconic (Glover, 1995b) or Alleghenian (Lefort, 1989) suture (Figure 2.5-16). Lower intensities to the west are associated with the Goochland terrane, which represents continental basement (Figure 2.5-17).

Discrete magnetic lows associated with the Richmond and Culpeper basins are discernible on the 2002 North America magnetic anomaly map (Bankey, 2002) (Figure 2.5-22). Basaltic and diabase dikes and sills are a component of the synrift fill of the exposed basins in the Piedmont and of the Taylorsville basin (Schlische, 2003) (Klitgord, 1995). The distinctive, elongate magnetic anomalies associated with these igneous bodies within the synrift basins of the Piedmont are also used beneath the Coastal Plain to delineate the Taylorsville, Queen Anne, and other synrift basins (e.g., (Benson, 1992)). The elongate magnetic anomalies are less

prevalent in the magnetic field east of the Salisbury geophysical anomaly. Either the eastern rift basins do not contain as much volcanic material as the western set of rift basins or the depth to this volcanic material is considerably greater (Klitgord, 1995). Small, circular magnetic highs across the coastal plain have been interpreted as intrusive bodies (Horton, 1991) (Klitgord, 1995).

Approximately 5 to 7 mi (8 to 11 km) east of the CCNPP site is an unnamed short, discontinuous weak to moderate northeast-trending magnetic anomaly that aligns subparallel to the SGA (Figure 2.5-22). Similar features to the south have been interpreted as granitic intrusive anomalies, whereas Benson (1992) interprets the feature as being bound by a Mesozoic basin (Figure 2.5-10). A deep borehole (SM-DF-84, Figure 2.5-11) drilled near the southern margin of this feature encountered Jurassic (?) volcanic rocks (dated at 169 ± 8 million years old) related to Mesozoic rifting, or perhaps basic metavolcanic rocks accreted to North America as part of the Brunswick Terrane (Hansen, 1986).

A magnetic profile along an approximately west-northwest to east-southeast transect through central Pennsylvania (Glover, 1995b) (Figure 2.5-17) indicates that paired high and low magnetic anomalies are associated with the margins of crustal units. Many of these anomalies have very high amplitudes and short wavelengths. For example, there is a 400-600 nT anomaly associated with the western margin of the Blue Ridge thrust nappe. Similarly, along a continuing transect line through Virginia, Glover and Klitgord (Glover, 1995a) show a 1500-2000 nT anomaly associated with the western edge of the Potomac mélange. This transect crosses the Salisbury geophysical anomaly where it is expressed as an 600 nT anomaly (Figure 2.5-17). In summary, magnetic data published since the mid-1980's confirm and provide additional documentation of previous observations (i.e., pre-EPRI) across this region of eastern North America, and do not reveal any new anomalies related to geologic structures previously unknown to EPRI (EPRI, 1986).

2.5.1.1.4.4 Principal Tectonic Structures

Research since the EPRI study (EPRI, 1986) has advanced the understanding of the character and timing of the crustal architecture and tectonic history of the Atlantic continental margin. The research has explained the significance of many geophysical anomalies and has clarified the timing and kinematics of tectonic processes from the Late Precambrian through the Cenozoic. Since the EPRI study (EPRI, 1986) was completed, new Cenozoic tectonic features have been proposed and described in the site region, and previously described features have since been characterized in more detail. New features identified since the EPRI study (EPRI, 1986) in the CCNPP site region area include gentle folds and a hypothesized minor fault on the western shore of Chesapeake Bay directly south of the CCNPP site (Kidwell, 1997). Also, new geologic data collected since 1986 has clarified the geometry and location of the Port Royal fault zone and Skinkers Neck anticline, and tectonic features representing the southern continuation of the Brandywine fault system, all of which are discussed further in the following sections. Tectonic features suggested by poorly constrained data include an unnamed fault underlying the upper Chesapeake Bay inferred by Pazzaglia (Pazzaglia, 1993), a series of warps beneath the lower Patuxent River and Chesapeake Bay near the CCNPP site hypothesized by McCartan (McCartan, 1995), and a hypothesized Stafford fault system by Marple and Talwani (Marple, 2004b) that is significantly longer and more active than previously recognized (Mixon, 2000). An additional geologic feature discovered since EPRI (1986) in the site region is the Eocene Chesapeake Bay impact crater (Figure 2.5-5 and Figure 2.5-6) (King, 1974) (Schruben, 1994). Based on the absence of published literature documenting Quaternary tectonic deformation and spatially associated with seismicity, we conclude that this feature is not a capable tectonic source (Section 2.5.1.1.4.4.4).

In the sections below, specific tectonic features and their evidence of Cenozoic activity published since the EPRI (1986) study are discussed. We find that no new information has been published since 1986 on any tectonic feature within the CCNPP site region that would cause a significant change in the EPRI seismic source model. These findings are based in part on a review of existing published literature by Crone and Wheeler (Crone, 2000) and Wheeler (Wheeler, 2005) (Wheeler, 2006), and studies performed for this COL. The investigation of potential Quaternary faults or features within the site vicinity included a multi-step process, including: (1) compilation and review of existing published and unpublished literature; (2) phone and in-person interviews of regional and local experts; (3) field and aerial reconnaissance, and (4) review of aerial photography (5-mile-radius), digital elevation maps, and LiDAR coverage. Each step included the following:

1. The references of Crone (2000), Wheeler (2005), and Wheeler (2006), were used as screening tools to initially characterize and identify possible late Cenozoic structures within a 200-mile-radius of the site. The references listed in Crone (2000), Wheeler (2005), and Wheeler (2006) were obtained and reviewed for structures located within a 200-mile-radius, as well as a few located directly outside of the 200-mile-radius. An internal internet- and library-based reference search for authors and topics related to potential Cenozoic seismogenic structures along the East Coast of the United States was performed to capture studies that post-date Crone (2000) and Wheeler (2005) (2006), as well as references the authors missed during their own compilation (e.g., Hansen and Edwards, 1986; Kidwell, 1997; McCartan et al., 1995; Pazzaglia, 1993).

2. To complement the comprehensive literature search, UniStar geologists contacted regional and local experts with field experience in Virginia, Maryland, Pennsylvania, Washington, D.C. and Calvert County, Maryland. At the U.S. Geological Survey in Reston, Virginia, both in-person and over-the-phone interviews were performed with experts regarding previously known and unknown potential seismic sources in the region. Experts contacted to discuss their knowledge on the structural and geologic setting of Chesapeake Bay and the eastern seaboard of the United States included: Richard Harrison, David Russ, David Powars, Wayne Newell, Lucy McCartan, Wylie Poag, Milan Pavich, and Steve Schindler of the U.S. Geological Survey. In addition, UniStar geologists visited the Maryland Geological Survey (MGS) and discussed similar topics with John Wilson who provided references related to studies performed by former MGS geologist Harry Hansen. In-house experts, Scott Lindvall and Ross Hartleb, who worked on numerous similar nuclear-related sites in the southeast, were contacted to provide a summary of potential regional seismic sources (i.e., Charleston, etc.). In addition, UniStar geologists contacted Dr. Susan Kidwell to discuss a detailed biostratigraphy and basin analysis of the Miocene Coastal Plain section exposed along Calvert Cliffs, and her basis for inferring a hypothetical fault at Moran Landing. Dr. Steve Obermier (retired from the U.S. Geological Survey) and Dr, Martitia Tuttle (an expert in paleoliquefaction investigations in the Central-Eastern United States) were contacted to discuss their knowledge of liquefaction-related features, if any, along the East Coast near the CCNPP site. UniStar also spoke with Martin Chapman of Virginia Tech, and Duane Braun of Bloomsberg University, Pennsylvania.

3. To independently evaluate the information collected through the literature searches and interviews, UniStar conducted field reconnaissance of: (a) previously mapped geologic features and potential seismic sources within a 200-mi-radius of the site (e.g., Crone, 2000; Wheeler, 2005; Wheeler 2006), (b) site vicinity geomorphology and Quaternary geology with respect to neotectonic deformation, and (c) local cliff exposures for evidence of faulting and/or folding. Reconnaissance of key potential

structures was conducted during and after consultation with local experts and literature review. Field reconnaissance was performed on the Stafford, Brandywine, Port Royal, Skinkers Neck, Mountain Run, Hazel Run, Fall Hill, Dumfries, Fall Line, Upper Marlboro, and Hillville fault zones. Field reviews of faults were followed by aerial reconnaissance. Dr. David Powars of the U.S. Geological Survey provided UniStar geologists with a tour of the Rock Creek fault zone and recent exposures of ancient gravels at the National Cathedral. The location of field stops and the aerial reconnaissance flight path are shown on Figure 2.5-229. UniStar geologists performed reconnaissance of several hypothesized faults/folds (Hansen, 1978; Kidwell, 1997; McCartan et al., 1995, and Pazzaglia, 1993) that were not evaluated by Crone (2000) or Wheeler (2005) or Wheeler (2006). UniStar geologists attended a three-day field trip affiliated with the Geological Society of America (Philadelphia, 2006) and lead by Dr. Frank Pazzaglia entitled: Rivers, glaciers, landscape evolution, and active tectonics of the central Appalachians, Pennsylvania and Maryland (Pazzaglia et al., 2006) . The field trip was attended by a diverse group of geologists and geomorphologists. The trip afforded UniStar geologists the opportunity to engage with other regional experts on questions pertaining to the Quaternary and structural geology and tectonic framework of the Chesapeake Bay region (a portion of the field trip route is depicted in Figure 2.5-229).

4. Previously mapped structures and tectonic-related geomorphology were evaluated utilizing aerial photography within a 5-mi-radius of the site and LiDAR data that encompassed St Mary's, Charles, and Calvert Counties, Maryland (a map depicting some of the LiDAR reviewed is provided in Figure 2.5-26). Multiple flights of fluvial terraces mapped previously by McCartan (1989a and 1989b) were evaluated where the Hillville and inferred Kidwell faults would project across fluvial surfaces of the Patuxent and Potomac Rivers. Lastly, aerial reconnaissance of many of the structures listed above was performed to assess their geomorphic expression and lateral continuity, if any (Figure 2.5-229).

For discussion purposes, principal tectonic structures within the 200 mi (322 km) CCNPP site region were divided into five categories based on their age of formation or most recent reactivation. These categories include Late Proterozoic, Paleozoic, Mesozoic, Tertiary, and Quaternary. Late Proterozoic, Paleozoic, and Mesozoic structures are related to major plate tectonic events and generally are mapped regionally on the basis of geological and/or geophysical data. Late Proterozoic structures include normal faults active during post-Grenville orogeny rifting and formation of the Iapetan passive margin. Paleozoic structures include thrust and reverse faults active during Taconic, Acadian, Alleghanian, and other contractional orogenic events. Mesozoic structures include normal faults active during break-up of Pangaea and formation of the Atlantic passive margin.

Tertiary and Quaternary structures within the CCNPP site region are related to the tectonic environment of the Atlantic passive margin. This passive margin environment is characterized by southwest- to northeast-oriented, horizontal principal compressive stress, and vertical crustal motions. The vertical crustal motions associated with loading of the coastal plain and offshore sedimentary basins and erosion and exhumation of the Piedmont and westward provinces of the Appalachians. Commonly, these structures are localized, and represent reactivated portions of older bedrock structures. Zones of seismicity not clearly associated with a tectonic feature are discussed separately in Section 2.5.1.1.4.5.

2.5.1.1.4.4.1 Late Proterozoic Tectonic Structures

Extensional structures related to Late Proterozoic-Early Cambrian rifting of the former supercontinent Rhodinia and formation of the Iapetan Ocean basin are located along a northeast-trending belt between Alabama and Labrador, Canada, and along east-west-trending branches cratonward (Wheeler, 1995) (Johnston, 1994) (Figure 2.5-23). Major structures along this northeast-trending belt include the Reelfoot rift, the causative tectonic feature of the 1811-1812 New Madrid earthquake sequence. Within the 200 mi (322 km) site region, a discrete Late Proterozoic feature includes the New York-Alabama lineament (King, 1978) (Shumaker, 2000). The Rome Trough (Ervin and McGinnis, 1975) is located directly outside the 200-mile (322 km) site region. Within the eastern Piedmont physiographic province, extended crust of the Iapetan passive margin extends eastward beneath the Appalachian thrust front approximately to the eastern edge of Paleozoic crust extended during the Mesozoic (Johnston, 1994) (Wheeler, 1996) (Figure 2.5-15). This marks the western boundary of major Paleozoic sutures that juxtapose Laurentian crust against exotic crust amalgamated during the Paleozoic orogenies (Wheeler, 1996) (Figure 2.5-16 and Figure 2.5-17). At its closest approach, the area of largely intact and slightly extended Iapetan crust is located about 70 mi (113 km) northwest of the CCNPP site (Figure 2.5-23).

The earthquake potential of Iapetan normal faults was recognized by the EPRI team members due to the association between the Reelfoot rift and the 1811 to 1812 New Madrid earthquake sequence (EPRI, 1986). Seismic zones in eastern North America spatially associated with Iapetan normal faults include the Giles County seismic zone of western Virginia, and the Charlevoix, Quebec seismic zone, both of which are located outside the CCNPP site region (Wheeler, 1995) (Figure 2.5-23). Because the Iapetan structures are buried beneath Paleozoic thrust sheets and/or strata, their dimensions are poorly known except in isolated, well studied cases.

Although published literature since the EPRI study (EPRI, 1986) has made major advances in showing the association between local seismic sources and Late Proterozoic structures (Wheeler, 1992) (Wheeler, 1995) and has highlighted the extent of extended Iapetan passive margin crust (Wheeler, 1995) (Wheeler, 1996), no new information has been published since 1986 on any Late Proterozoic feature within the CCNPP site region that would cause a significant change in the EPRI study (EPRI, 1986) seismic source model.

2.5.1.1.4.4.2 Paleozoic Tectonic Structures

The central and western portions of the CCNPP site region encompass portions of the Piedmont, Blue Ridge, Valley and Ridge, and Appalachian Plateau physiographic provinces (Figure 2.5-1). Structures within these provinces are associated with thrust sheets, shear zones, and sutures that formed during convergent and transpressional Appalachian orogenic events of the Paleozoic Era. Tectonic structures of this affinity exist beneath the sedimentary cover of the Coastal Plain and Continental Shelf Provinces. Paleozoic structures shown on Figure 2.5-23 include: 1) sutures juxtaposing allochthonous (tectonically transported) rocks against proto-North American crust, 2) regionally extensive Appalachian thrust faults and oblique-slip shear zones, and 3) a multitude of smaller structures that accommodated Paleozoic deformation within individual blocks or terranes (Figure 2.5-16, Figure 2.5-17, and Figure 2.5-18). The majority of these structures dip eastward and sole into either a low angle thrust or the low angle, basal Appalachian decollement (Figure 2.5-17). Below the decollement are rocks that form the North American basement complex (Grenville or Laurentian crust).

Researchers have observed that much of the sparse seismicity in eastern North America occurs within the North American basement below the basal decollement. Therefore, seismicity

within the Appalachians may be unrelated to the abundant, shallow thrust sheets mapped at the surface (Wheeler, 1995). For example, seismicity in the Giles County seismic zone, located in the Valley and Ridge Province, is occurring at depths ranging from 3 to 16 mi (5 to 25 km) (Chapman, 1994), which is generally below the Appalachian thrust sheets and basal decollement (Bollinger, 1988).

2.5.1.1.4.4.2.1 Appalachian Structures

Paleozoic faults within 200 mi (322 km) of the CCNPP site and catalog seismicity are shown on Figure 2.5-23 and Figure 2.5-24 (see section 2.5.2 for a complete discussion on seismicity). Paleozoic faults with tectonostratigraphic units are shown on Figure 2.5-16, Figure 2.5-17 and Figure 2.5-18. Faults mapped within the Appalachian provinces (Piedmont, Blue Ridge, Valley and Ridge) are discussed in this section along with postulated Paleozoic faults in the Coastal Plain that are buried by Cenozoic strata. No new information has been published since 1986 on any Paleozoic fault in the site region that would cause a significant change in the EPRI study (EPRI, 1986) seismic source model. Paleozoic faults are discussed below from west to east across the CCNPP site region.

Major Paleozoic tectonic structures of the Appalachian Mountains within 200 mi (322 km) of the site include the Little North Mountain-Yellow Breeches fault zone, the Hylas shear zone, the Mountain Run-Pleasant Grove fault system, the Brookneal shear zone, and the Central Piedmont shear zone (including the Spotsylvania fault) (Figure 2.5-23). These structures bound lithotectonic units as defined in recent literature (Horton, 1991) (Glover, 1995b) (Hibbard, 2006) (Hibbard, 2007).

The northeast-striking Little North Mountain fault zone is located within the eastern Valley and Ridge Physiographic Province of western Virginia, eastern Maryland, and southern Pennsylvania (Figure 2.5-16 and Figure 2.5-23). The fault zone forms the tip of an upper level thrust sheet that attenuated Paleozoic shelf deposits of the Laurentian continental margin during the Alleghenian Orogeny (Hibbard, 2006). The east-dipping Little North Mountain thrust sheet soles into a decollement shown as a couple miles deep (Figure 2.5-17). This decollement represents an upper-level detachment above a deeper decollement about 5 mi (8 km) deep (Glover, 1995b) (Figure 2.5-17). The Little North Mountain fault and Yellow Breeches fault to the northeast mark the approximate location of the westernmost thrusts that daylight within the Valley and Ridge Province (Figure 2.5-23). Farther west, thrust ramps branching from the deeper decollement rarely break the surface and overlying fault-related folds control the morphology of the Valley and Ridge Province.

The Little North Mountain-Yellow Breeches fault zone is not considered a capable tectonic source. The decollement associated with the Little North Mountain thrust is within a couple miles of the surface, suggesting the fault probably does not penetrate to seismogenic depths. No seismicity is attributed to the Little North Mountain-Yellow Breeches fault zone and published literature does not indicate that it offsets late Cenozoic deposits or exhibits geomorphic expression indicative of Quaternary deformation. Therefore, this Paleozoic fault is not considered to be a capable tectonic source.

The Hylas shear zone, active between 330 and 220 million years ago during the Alleghenian orogeny, comprises a 1.5 mi (2.4 km) wide zone of ductile shear fabric and mylonites located 71 mi (115 km) southwest of the site (Bobyarchick, 1979, Gates, 1989). The Hylas shear zone also locally borders the Mesozoic Richmond and Taylorsville basins and appears to have been reactivated during Mesozoic extension to accommodate growth of the basin (Figure 2.5-10) (LaTourneau, 2003; Hibard, 2006). Discussions of the post-Paleozoic reactivation of the Hylas

shear zone are presented in Section 2.4.1.1.4.4.3, Mesozoic Tectonic Structures, and in Section 2.4.1.1.4.4.4, Tertiary Tectonic Structures. Based on review of published literature and historical seismicity, there is no reported geomorphic expression, historical seismicity, or Quaternary deformation along the Hylas shear zone, and thus this feature is not considered to be a capable tectonic source.

The Mountain Run-Pleasant Grove fault system is located within the Piedmont Physiographic Province in Virginia and Maryland and may extend to near Newark, New Jersey (Hibbard, 2006) (Figure 2.5-17 and Figure 2.5-23). This fault system extends across the entire site region and juxtaposes multiple-tectonized, allochthonous rocks and terranes to the east against the passive margin rocks of North American affinity to the west. Included in this fault system are portions of the Bowens Creek fault, the Mountain Run fault zone, the Pleasant Grove fault, and the Huntingdon Valley fault (Horton, 1991; Mixon, 2000; Hibbard, 2006). Fault zones along this fault system exhibit mylonitic textures, indicative of the ductile conditions in which it formed during the Paleozoic Era. Locally the allochthonous rocks are the Potomac composite terrane (Horton, 1991), which consists of a stack of thrust sheets containing tectonic mélange deposits that include ophiolites, volcanic arc rocks, and turbidites. This east-dipping thrust probably shallows to a decollement a couple miles below ground surface, and is shown to be truncated by the Brookneal shear zone (Figure 2.5-17) (Glover, 1995b). In the site region, the southeastern boundary of the Mesozoic Culpeper basin locally is bounded by the Mountain Run fault zone (Mixon, 2000), suggesting that portions of the Paleozoic thrust fault system may have been reactivated since the Paleozoic (Figure 2.5-10). Discussions of the Culpeper basin and local reactivation of portions of the Mountain Run-Pleasant Grove fault system are in Section 2.5.1.1.4.4.3.

Within the Mountain Run-Pleasant Grove fault system, only local portions of the Mountain Run fault zone have been identified with possible late Cenozoic tectonic activity (Cron, 2000; Wheeler, 2006). These portions of the Mountain Run fault zone are discussed in Section 2.5.1.1.4.4.5.2. For other faults within the Mountain Run-Pleasant Grove fault system, published literature does not indicate that it offsets late Cenozoic deposits or exhibits geomorphic expression indicative of Quaternary deformation, and no seismicity has been attributed to it. Therefore, these faults are not considered to be capable tectonic sources.

The Brookneal shear zone is located within the Piedmont in Virginia and probably extends beneath the Coastal Plain across Virginia and Maryland to within about 50 mi (80 km) of the site (Figure 2.5-16 and Figure 2.5-23). The dextral-reverse shear zone is the northern continuation of the Brevard zone, a major terrane boundary extending from Alabama to North Carolina (Hibbard, 2002). The Brookneal shear zone juxtaposes magmatic and volcaniclastic rocks of the Chopawamsic volcanic arc to the east against the Potomac mélange to the west. This east-dipping thrust possibly truncates the Mountain Run fault at about 2.5 mi (4 km) depth, then flattens to a decollement at about 4 to 5 mi (6 to 8 km) depth that dips gently eastward beneath the surface trace of the Spotsylvania fault (Figure 2.5-17) (Glover, 1995b). Southwest of the site region, the Mesozoic Danville basin locally overlies the Brookneal shear zone. The depositional contact defining the southeastern margin of the Danville basin crosses the Brookneal shear zone and is unfaulted, suggesting that the Paleozoic fault was not reactivated as a normal fault during Triassic rifting. The Brookneal shear zone is not considered a capable tectonic source. No seismicity is attributed to it and published literature does not indicate that it offsets late Cenozoic deposits or exhibits geomorphic expression indicative of Quaternary deformation. Therefore, this Paleozoic fault is not considered to be capable tectonic source.

The northeast-striking Spotsylvania fault has been mapped in the Virginia piedmont as far north as Fredericksburg and beneath the Coastal Plain in eastern Virginia and Maryland (Hibbard, 2006) (Horton, 1991) (Glover, 1995b) (Figure 2.5-16, Figure 2.5-17 and Figure 2.5-23). At its closest approach, the fault is about 40 mi (64 km) northwest of the site (Figure 2.5-16). The fault juxtaposes terranes of different affinity, placing Proterozoic continental rocks of the Goochland terrane to the east against Early Paleozoic (Ordovician) volcanic arc rocks of the Chopawamsic terrane to the west (Glover, 1995b; Hibbard, 2006) (Figure 2.5-9). The Spotsylvania fault is a Late Paleozoic dextral-reverse fault active during the Alleghenian orogeny (Pratt, 1988; Bailey, 2004). The fault is the norther continuation of the Central Piedmont shear zone, a zone of ductile and brittle shear that accommodated thrust and right-lateral movement of various exotic volcanic arc terranes to the east against rocks of the Piedmont domain (including the Chopawamsic terrane) to the west (Hibbard, 1998; Hibbard, 2000; Bailey, 2004; Hibbard, 2006). The Hycoshear zone, the part of the Central Piedmont shear zone located direly southeast of the Spotsylvania fault (Hibbard, 1998; Bailey, 2004), is partially located within the 200-mile site region (Figure 2.5-9 and Figure 2.5-23). The east-dipping Spotsylvania fault and Hyco shear zone likely penetrate the crust at gentle to intermediate angles (Hibbard, 1998; Pratt, 1988; Glover, 1995b), and the Spotsylvania fault may truncate the basal Appalachian decollement and higher decollement of the Brookneal shear zone (Figure 2.5-17) (Glover, 1995b).

The Spotsylvania fault and the Hyco shear zone are not considered capable tectonic sources. Specific studies of the Spotsylvania fault by Dames and Moore (DM, 1977b) demonstrate that it exhibits negligible vertical deformation of a pre- to early-Cretaceous erosion surface and is not related to Tertiary faulting along the younger Stafford fault zone (Section 2.5.1.1.4.4.4). The fault was determined by the NRC (AEC) to be not capable within the definition of 10 CFR 100, Appendix A (CFR, 2006). No subsequent evidence has been published since the Dames and Moore (DM, 1977b) study to indicate potential Quaternary activity on the Spotsylvania fault. Additionally, no geomorphic, geologic, or seismic evidence has been identified that indicates that the Hyco shear zone (the portion of the Central Piedmont shear zone within the 200-mile site region) has been active in Quaternary time. The Hyco shear zone is not considered a capable tectonic source.

2.5.1.1.4.4.2.2 Coastal Plain Structures

Major Paleozoic tectonic structures beneath the Coastal Plain in the 25 mi (40 km) CCNPP site vicinity include faults bounding the Sussex terrane west of the site and unnamed faults mapped seaward of the CCNPP site by Glover and Klitgord (Glover, 1995a) (Figure 2.5-16, Figure 2.5-17 and Figure 2.5-23). These fault zones, cited here as the western and eastern zones, are interpreted to dip steeply east, penetrate the crust, and juxtapose lithostratigraphic terranes.

The western fault zone coincides with the margins of the Sussex Terrane of Horton (Horton, 1991) (Figure 2.5-16 and Figure 2.5-17). The narrow Sussex Terrane and potential bounding faults are delimited in part by the Salisbury geophysical anomaly, a positive gravity and magnetic high described in Section 2.5.1.1.4.3. The eastern fault zone is shown to extend from coastal North Carolina to southern Delaware, trending north along the eastern part of southern Chesapeake Bay before branching into two splays that trend northeast across the Delmarva Peninsula (Figure 2.5-16 and Figure 2.5-23). The regional crustal cross section shows the fault zone as dipping east at moderate to steep angles (Figure 2.5-17).

No seismicity is attributed to the buried Paleozoic faults and published literature does not indicate that these faults offset late Cenozoic deposits or exhibit geomorphic expression

indicative of Quaternary deformation. Therefore, the Paleozoic structures (faults bounding the Sussex terrane west of the site and unnamed faults mapped seaward of the CCNPP site by Glover and Klitgord (Glover, 1995a) in the site vicinity are not considered to be capable tectonic sources.

Other Paleozoic faults mapped by Hibbard (Hibbard, 2006) within the 200 mi (322 km) site region are smaller features that typically are associated with larger Paleozoic structures and accommodate internal deformation within the intervening structural blocks (Figure 2.5-23). No seismicity is attributed to these faults and published literature does not indicate that any of these faults offset late Cenozoic deposits or exhibit geomorphic expression indicative of Quaternary deformation. Therefore, these Paleozoic structures in the site region are not considered to be capable tectonic sources.

2.5.1.1.4.4.3 Mesozoic Tectonic Structures

Mesozoic basins have long been considered potential sources for earthquakes along the eastern seaboard and were considered by most of the EPRI teams in their definition of seismic sources (EPRI, 1986). A series of elongate rift basins of early Mesozoic age are exposed in a belt extending from Nova Scotia to South Carolina and define an area of crust extended during the Mesozoic (Figure 2.5-10)(Benson, 1992). These Mesozoic rift basins, also commonly referred to as Triassic basins, exhibit a high degree of parallelism with the surrounding structural grain of the Appalachian orogenic belt. The parallelism generally reflects reactivation of pre-existing Paleozoic structures (Ratcliffe, 1986a; Schlische, 2003; LeTourneau, 2003; Schlische, 2003a). The rift basins formed during extension and thinning of the crust as Africa and North America rifted apart to form the modern Atlantic Ocean (Section 2.5.1.1.4.1.2) (Withjack, 2005).

Generally, the rift basins are asymmetric half-grabens with the primary rift-bounding faults on the western margin of the basin (Figure 2.5-10, Figure 2.5-18 and Figure 2.5-19) (Benson, 1992; Schlische, 1990; Withjack, 1998; Schlische, 2003). The rift-bounding normal faults are interpreted by some authors to be listric at depth and merge into Paleozoic low -angle detachments (Crespi, 1988) (Harris, 1982) (Manspeizer, 1988). Other authors interpret rift-bounding faults to penetrate deep into the crust following deep crustal fault zones (Wentworth, 1983) (Pratt, 1988) (Klitgord, 1995) (Figure 2.5-19).

Within the 200 mi (322 km) CCNPP site region, rift basins with rift-bounding faults on the western margin include the exposed Danville, Richmond, Culpeper, Gettysburg, and Newark basins, and the buried Taylorsville, Norfolk, hypothesized Queen Anne, and other smaller basins (Figure 2.5-10). As discussed below, most of the above-mentioned basins are bound by reactivated Paleozoic thrust or reverse faults (e.g. the Richmond basin and the Paleozoic Hylas shear zone) (Figure 2.5-10 and Figure 2.5-23). Field data also indicate that the Ramapo Fault was reactivated with both strike-slip and dip-slip displacement during Paleozoic orogenies and Mesozoic extension (Ratcliff, 1971). The principal basins within the site region are discussed below in further detail.

The Culpepper, Gettysburg, and Newark basins (i.e. the composite Birdsboro basin of Faill [2003]) form an east- to northeast-trending band of mostly exposed Mesozoic basins located 60 to 125 miles west, northwest, and north of the CCNPP Unit 3 site (Figure 2.5-10). These basins are asymmetric half-grabens bounded on the west or northwest by a series of interconnected east- to southeast-dipping fault zones (Lindholm, 1978) (Hibbard, 2006). The fault bounding the western margin of the Culpeper basin was observed to follow a well-developed foliation in metamorphic rocks by Lindholm (1978), indicating to him that the Mesozoic faulting was controlled by Paleozoic structure. However, a named Paleozoic fault

zone associated with the western margin of the Culpeper basin is not clearly identified in the published literature. The southeast margin of the Culpeper basin is locally in fault contact with the Paleozoic Mountain Run fault zone (Mixon, 2000) (Hibbard, 2006) (Figure 2.5-10). This southeast-dipping fault contact probably represents post-Triassic, east-side up movement, although the total post-Triassic throw on the fault is limited and does not seem to strongly influence the basin architecture (Mixon, 2000). The Mountain Run fault zone is discussed further in FSAR sections 2.5.1.1.4.4.2.1 and 2.5.1.1.4.4.5.2.

The Gettysburg and Newark basins are bounded on their northwestern margins by southeast-dipping faults with a recognized Paleozoic history. The Gettysburg basin is bounded by the Shippenburg and Carbaugh-Marsh Creek faults (Root, 1989). The Newark basin is at least partially bounded by the Ramapo Fault zone (Ratcliffe, 1985; 1986a) (Schlische, 1992). Detailed studies of these basin-bounding faults confirm they formed as a result of reactivation of Paleozoic faults or metamorphic structures (Ratcliffe, 1985) (Root, 1989) (Schlische, 1993) (Swanson, 1986). None of these basinbounding faults have demonstrable associated Quaternary seismic activity or conclusive evidence for recent fault activity (Section 2.5.1.1.4.4.5). The northeast-striking, narrow Danville basin (also grouped with the larger Dan River-Danville basin) is located about 170 miles southwest of the CCNPP Unit 3 site (Figure 2.5-10). The primary basin-bounding fault is located on the northwest margin of the basin and dips southeast (Benson, 1992) (Hibbard, 2006), creating a highly asymmetric cross-section (Schlische, 2003). Swanson (1986) summarizes evidence suggesting the main basin-bounding fault reactivated ductile Paleozoic faults, specifically the Stony Ridge fault zone, a probable northern extension of the Paleozoic Chatham fault. The Danville basin and the basin-bounding Chatham fault separates the Smith River Terrane on the northwest against the Milton terrane on the southeast within the central portion of the basin, but farther northeast the fault and basin are located within the Potomac terrane as mapped by Horton (1991).

The northeast-striking Richmond Taylorsville basins are located about 80 miles and 30 miles west and southwest of the CCNPP Unit 3 site, respectively within central Virginia and Maryland (Figure 2.5-10). The Richmond basin is subaerially exposed and its extent is well defined by mapping. In contrast, the Taylorsville basin is mainly buried beneath the coastal plain and its extent is constrained by limited geologic mapping, multiple seismic lines, boreholes, and interpretation of gravity and aeromagnetic data (Milici, 1995) (LeTourneau, 2003). The extent of the buried portions of the Taylorsville basin is well-defined in Virginia, but poorly constrained within Maryland based on limited subsurface data (Jacobeen, 1972) and a lack of seismic lines.

Where exposed, both the Taylorsville and Richmond basins are bounded on the west by the northeast-striking, southeast-dipping Paleozoic Hylas shear zone (Section 2.5.1.1.4.4.2.1) (Figure 2.5-10 andFigure 2.5-23). Bobyarchick and Glover (Bobyarchick,1979) argue that the Hylas shear zone was reactivated as an extensional fault to accommodate the growth of the Richmond and Taylorsville basins during Mesozoic rifting based on a 220 million year old phase of brittle extensional deformation mapped throughout the fault zone. Evidence for later Mesozoic and early Tertiary inversion of the Taylorsville basin is based on interpretation of seismic reflection profiles (LeTourneau, 2003) and the coincidence of the eastern margin of the Taylorsville basin with contractional structures that disrupt the Cretaceous and early Tertiary coastal plain sediments (i.e. Skinker's Neck anticline, Port Royal fault zone, and Brandywine fault zone) (Section 2.5.1.1.4.4.4) (Figure 2.5-25).

The extension of the basin bounding fault of the Taylorsville basin (Hylas shear zone) beneath the CCNPP site can be hypothesized based on a range of possible down-dip geometries. The northwestern boundary of the Taylorsville basin is approximately 27 to 30 miles (44 to 48 km) northwest of the CCNPP site (Figure 2.5-10) (Schlische, 1990)(Benson, 1992). Available crustal-scale cross sections provide a range of dip angles from 20 degrees (Withjack 1998) (Schlische, 2003a) to 25 degrees (Glover, 1995) (Klitgord, 1995) (Figure 2.5-17 and Figure 2.5-19) to 30 degrees (Pratt, 1988). Based on this range in dip angle the Hylas shear zone would be 10-11 mi (16-18 km), 12-14 mi (20-22 km), and 15-17 mi (25-28 km) beneath the CCNPP site within crystalline bedrock. The thickness of the seismogenic upper crust (i.e. depth to the Moho) is variable in these cross sections and is typically depicted as either 9 mi (15 km) thick (Schlische, 1990)(Schlische, 2003a) or 18-25 mi (30-40 km thick). The 9 mi (15 km) thick model suggests that the Hylas shear zone should sole into the Moho before the fault extends beneath the CCNPP site.

The geometry and continuity of the buried Queen Anne basin and other smaller rift basins beneath the Coastal Plain and Continental Shelf are not clear, but the recognition and interpretation of these basins have expanded since the EPRI (1986) study (Figure 2.5-10).

Data constraining the location of the buried Queen Anne basin with respect to the CCNPP Unit 3 Site are sparse and thus the geometry and continuity of the basin are unclear. Seismic reflection studies (Hansen, 1988)(Benson, 1992), borehole data (Hansen, 1978) (Figure 2.5-11), and gravity and magnetic signatures (Benson, 1992)(Hansen, 1988)(Figure 2.5-23) were used to characterize the limits of the Queen Anne basin. These data permit multiple interpretations of the location of a basin at or near the CCNPP Site (Klitgord, 1988) (Schlische, 1990) (Horton, 1991) (Bensen, 1992) (Klitgord 1995) (Withjack 1998) (LeTourneau, 2003) (Figure 2.5-10, Figure 2.5-12, Figure 2.5-16, and Figure 2.5-22).

The delineation of the Queen Anne basin by Benson (1992) (shown on Figure 2.5-10) is derived from a seismic reflection profile (Hansen, 1988) approximately 40 mi northeast of the site, "extensive proprietary seismic reflection profiling" data south of CCNPP, a borehole located about 13 miles southwest of the site, and aeromagnetic and gravity data. The Queen Anne basin first named and imaged by Hansen (1988) in the TXC-10C Vibroseis profile located 40 mi northeast of the CCNPP site. This seismic line crosses the eastern boundary of the basin imaging west-dipping Triassic basin deposits above high-angle west-side-down faults offsetting crystalline basement (Hansen, 1988), but does not cross the western boundary of the basin. The Coastal Plain section is not deformed by the underlying faults. As discussed below, Benson (1992) extends the Queen Anne basin to the south based on the presence of proprietary seismic lines. Although Benson (1992) did not review the data, he inferred, based on the local concentration of these proprietary seismic lines, that they were acquired to better image a known Tertiary basin. A borehole located about 13 miles southwest of the CCNPP Unit 3 site encountered a diabase dike at depth (Benson, 1992). Although suggestive, Benson (1992) acknowledges that the diabase dike may or may not be associated with a Mesozoic basin. Benson (1992) summarizes: "The areas of inferred buried rift basins/synrift rocks shown in this map might best be considered as areas where efforts should be concentrated to verify their presence or absence." To convey this uncertainty, Benson (1992) shows the southern extension of the Queen Anne basin with a dashed and queried boundary, whereas to the north-northeast of the site the basin boundary is depicted as a solid line where geophysical data are available (and verifiable). Subsequent authors have relied upon and modified Benson (1992), yet no new published information is available near the CCNPP site to better constrain the presence or absence of a Triassic basin beneath the site. The Hillville fault (Hansen,1986) may represent a fault along the western margin of the Queen Anne basin or the eastern

margin of the Taylorsville basin reactivated during Cretaceous and early Tertiary time. The geometry of this fault discussed in Section 2.5.1.1.4.4.5—is poorly constrained in the vibroseis line by Hansen (1978), which illustrates offset crystalline basement. There are limited data to constrain its length and no data to constrain its down-dip geometry (Hansen, 1986). In addition, there is no evidence for Quaternary activity of the Hillville fault or any other structure associated with the hypothesized Queen Anne basin.

In summary, there are no specific Mesozoic basin-bounding faults within the site region that have demonstrable associated seismic activity or evidence of recent fault activity (Figure 2.5-10). The major postulated basins closest to the site (Taylorsville and Queen Anne) were considered during the 1980s to exist and several were incorporated into seismic sources by the different EPRI teams. Seismicity potentially associated with reactivation of faults bordering or beneath the Mesozoic basins is captured in the existing EPRI seismic source model. No new data have been developed to demonstrate that any of the Mesozoic basins are currently active, and Crone and Wheeler (Crone, 2000), and Wheeler (Wheeler, 2006) do not recognize any basin-margin faults that have been reactivated during the Quaternary in the site region. No Mesozoic basin in the site region is associated with a known capable tectonic source, and no new information has been developed since 1986 that would require a significant revision to the EPRI seismic source model.

2.5.1.1.4.4.4 Tertiary Tectonic Structures

Several faults were active during the Tertiary Period within the 200 mi (322 km) CCNPP site region (Figure 2.5-25). These faults have been recognized in the western part of the Coastal Plain Province where Tertiary strata crop out in river valleys and where the faults have bee investigated using seismic and borehole data. These faults include the relatively well characterized Stafford fault system in Virginia, the Brandywine fault system in Maryland, and the National Zoo/Rock Creek faults in Washington, D.C. Additional faults and fault-related folds defined by seismic and borehole data include the Port Royal fault zone and Skinkers Neck anticline in Virginia, and the Hillville fault in Maryland. Tertiary structures that have been proposed but are poorly constrained by data include east-facing monoclines along the western shore of Chesapeake Bay (McCartan, 1995) and a northeast-striking fault in the upper Chesapeake Bay (Pazzaglia, 1993). In addition, Kidwell (Kidwell, 1997) uses detailed stratigraphic analysis of the Calvert Cliffs area to postulate the existence of several broad folds developed in Miocene strata as well as a poorly constrained postulated fault. All of these structures are located within about 50 mi (80 km) of the site, and the proposed east-facing monoclines of McCartan (McCartan, 1995) are within a few miles of the CCNPP site. Within 25 mi (40 km) of the site, the only fault with documented Tertiary displacement is the Hillville fault (Hansen, 1978) (Hansen, 1986) (Figure 2.5-25).

Several faults associated with the Eocene Chesapeake Bay impact crater have been identified near the mouth of the Chesapeake Bay about 60 mi (97 km) south of the site (Powars, 1999) (Figure 2.5-5). The impact crater formed on a paleo-continental shelf when the Eocene sea in this location was approximately 1,000 ft (305 m) deep. The Chesapeake Bay impact crater was discovered in 1993, and thus post-dates the EPRI study (EPRI, 1986). The 35-million year old Chesapeake Bay impact crater is a 56 mi (90 km) wide, complex peak-ring structure. Fault styles observed within the impact include a series of inner and outer ring, post-impact, compaction related growth faults, sin-impact faults that offset Proterozoic and Paleozoic crystalline basement rocks, and syn-impact faults related to secondary craters (Powars, 1999; Poag, 2004; Poag, 2005). These faults and others within the outer and inner ring include normal-faulted slump blocks and compaction faults that extend up-section into upper

Miocene and possibly younger deposits. Published literature does not indicate that any faults related to the impact crater are seismogenic or offset Quaternary deposits.

Multiple, fault-bounded secondary craters of Eocene age also have been interpreted from multichannel seismic profiles previously collected by Texaco along the Potomac River and Chesapeake Bay 20 and 40 mi (32 and 64 km) north and northwest of the main Chesapeake Bay impact crater (Poag, 2004). The secondary impact craters have diameters ranging from 0.25 to 2.9 mi (0.4 to 4.7 km). Faults associated with the secondary craters occasionally penetrate Proterozoic and Paleozoic crystalline basement rocks (Poag, 2004). Primarily middle Miocene to Quaternary sediments thicken and sag into the primary and secondary craters. Faults associated with the impact crater are not considered capable tectonic sources and are not discussed further in this section.

Faults and folds mapped within the 200 mi (322 km) CCNPP site region that displace Tertiary Coastal Plain deposits are described below. These structures include the Stafford fault system, Brandywine fault system, National Zoo/Rock Creek faults, Port Royal fault zone, Skinkers Neck anticline, and the Hillville fault. Additional hypothesized Tertiary structures for which compelling geologic or geophysical evidence is lacking are then described. These structures include hypothesized east-facing monoclines along the western shore of Chesapeake Bay near the CCNPP site described by McCartan (McCartan, 1995), a hypothesized fault in the upper Chesapeake Bay mapped by Pazzaglia (Pazzaglia, 1993), and structures interpreted in Calvert Cliffs by Kidwell (Kidwell, 1997).

2.5.1.1.4.4.4.1 Stafford Fault of Mixon,et al.

The Stafford fault (#10 on Figure 2.5-31) approaches within 47 mi (76 km) southwest of the site (Figure 2.5-25). The 42 mi (68 km) long fault system strikes approximately N35°E (Newell, 1976). The fault system consists of several northeast-striking, northwest-dipping, high-angle reverse to reverse oblique faults including, from north to south, the Dumfries, Fall Hill, Brooke, Tank Creek, Hazel Run, and an unnamed fault (Mixon et al., 2000). Two additional northeast-striking, southeast-side-down faults, the Ladysmith and the Acadia faults, are included here as part of the Stafford fault system. These individual faults are 10 to 25 mi (16 to 40 km) long and are separated by 1.2 to 3 mi (2 to 5 km) wide en echelon, left step-overs. The left-stepping pattern and horizontal slickensides found on the Dumfries fault suggest a component of dextral shear on the fault system (Mixon, 2000).

Locally, the Stafford fault system coincides with the Fall Line and a northeast-trending portion of the Potomac River (Figure 2.5-25). Mixon and Newell (Mixon, 1977) suggest that the Fall Line and river deflection may be tectonically controlled. Drilling, trenching, and mapping in the Fredericksburg region showed that most fault movement on any of the four primary faults comprising the Stafford fault system was pre-middle Miocene in age. Mixon, 1978; 1982). Mesozoic and Tertiary movement is documented by displacement of Ordovician bedrock over lower Cretaceous strata along the Dumfries fault and abrupt thinning of the Paleocene Aquia Formation across multiple strands of the fault system (Mixon, 1977). Minor late Tertiary activity of the fault system is documented by an 11-14-inch (28-36 cm) displacement by the Fall Hill fault of a Pliocene terrace deposit along the Rappahannock River (Mixon, 1978) (Mixon, 1982) (Mixon, 2000) and an 18 in (46 cm) displacement near the Hazel Run fault of upland gravels of Miocene or Pliocene age (Mixon, 1978). Both offsets suggest southeast-side-down displacement (Mixon, 1978).

Subsequent studies of the Stafford fault system better document the timing of displacement, mostly by refining the age of units. For example, the Rappahannock River terrace deposit was

originally cited as Late Pliocene or early Pleistocene. However, later work has revealed that the deposit is Pliocene in age (Mixon et al., 2000). Similarly, the Miocene or Pliocene upland gravels offset 18" are now interpreted as the Pliocene sand and gravel unit, Tps (Mixon et al., 2000).

Recent geologic and geomorphic analysis of the Stafford fault system for the application of North Anna Early Site Permit (ESP) to the NRC provides additional constraints on the age of deformation (Dominion, 2004a). Geomorphic analyses (structure contour maps and topographic profiles) of upland surfaces capped by Neogene marine deposits and topographic profiles of Pliocene and Quaternary fluvial terraces of the Rappahannock River near Fredericksburg, Virginia, indicate that these surfaces are not visibly deformed across the Stafford fault system (Dominion, 2004a). In addition, field and aerial reconnaissance of these features during the North Anna ESP, and as part of this CCNPP Unit 3 study, indicate that there are no distinct scarps or anomalous breaks in topography on the terrace surfaces associated with the mapped fault traces. The NRC (2005) agreed with the findings of the subsequent study for the North Anna ESP, and stated: "Based on the evidence cited by the applicant, in particular the applicant's examination of the topography profiles that cross the fault system, the staff concludes that the applicant accurately characterized the Stafford fault system as being inactive during the Quaternary Period." Collectively, this information indicates that the Stafford fault system is not a capable tectonic source as defined in Appendix A of Regulatory Guide 1.165 (NRC, 1997).

Marple (Marple, 2004a) recently proposed a significantly longer Stafford fault system that extends from Fredericksburg, Virginia to New York City as part of a northeastern extension of the postulated East Coast fault system (ECFS), (Figure 2.5-31) (Section 2.5.1.1.4.4.5.14). The proposed northern extension of the Stafford fault system is based on: (1) aligned apparent right-lateral deflections of the Potomac (22 mi (35 km) deflection), Susquehanna (31 mi (50 km) deflection) and Delaware Rivers (65 mi (105 km) deflection) (collectively these are named the "river bend trend"), (2) upstream incision along the Fall Line directly west of the deflections, and (3) limited geophysical and geomorphic data. Marple and Talwani (Marple, 2004b) proposed that the expanded Stafford fault system of Marple (Marple, 2004a) was a northeast extension of the ECFS of Marple and Talwani (Marple, 2000). Marple and Talwani (Marple, 2004b) further speculate that the ECFS and the Stafford fault system were once a laterally continuous and through-going fault, but subsequently were decoupled to the northwest and southeast, respectively, during events associated with the Appalachian orogeny.

Data supporting the extended Stafford fault system of Marple (Marple, 2004a) is limited. Marple and Talwani (Marple, 2004b) suggest that poorly located historical earthquakes that occurred in the early 1870's and 1970's lie close to the southwestern bend in the Delaware River and concluded an association between historical seismicity and the postulated northern extension of the Stafford fault system. Review of seismicity data available both before and after the EPRI study (EPRI, 1986) indicates a poor correlation in detail between earthquake epicenters and the expanded Stafford fault system (Figure 2.5-25). Geophysical, borehole and trench data collected by McLaughlin (McLaughlin, 2002), near the Delaware River across the trace of the postulated expanded Stafford fault system of Marple (Marple, 2004a), provide direct evidence for the absence of Quaternary deformation. Collectively, there is little geologic and seismologic evidence to support this extension of the fault system beyond that mapped by Mixon (Mixon, 2000).

In summary, all significant information on timing of displacement for the Stafford fault system was available prior to 1986 and incorporated into the EPRI (1986) seismic source models. New significant information published since 1986 regarding the activity of the Stafford fault system includes the geomorphic and geologic analysis performed for the North Anna ESP that concluded the fault system was not active (Dominion, 2004a). Field and aerial reconnaissance performed for the North Anna ESP and this CCNPP COL application also did not reveal any geologic or geomorphic features indicative of potential Quaternary activity along the fault system. Therefore, on the basis of a review of existing geologic literature, the Stafford fault system is not considered a capable tectonic source, and there is no new information that would require a significant revision to the EPRI (1986) seismic source model.

2.5.1.1.4.4.4.2 Brandywine Fault System

The Brandywine fault system is located approximately 30 mi (48 km) west of the site and north of the Potomac River (Figure 2.5-25). The 12 to 30 mi (19 to 48 km) long Brandywine fault system consists of a series of en echelon northeast-trending, southeast-dipping reverse faults with east-side-up vertical displacement. Jacobeen (Jacobeen, 1972) and Dames and Moore (DM, 1973) first described the fault system from Vibroseis™ profiles and a compilation of borehole data as part of a study for a proposed nuclear power plant at Douglas Point along the Potomac River. The fault system is composed of the Cheltenham and Danville faults, which are 4 mi and 8 mi (6 to 13 km) long, respectively. These two faults are separated by a 0.6 to 1 mi (1 to 1.6 km) wide left step-over (Jacobeen, 1972). Later work by Wilson and Fleck (Wilson, 1990) interpret one continuous 20 to 30 mi (32 to 48 km) long fault that transitions into a west-dipping flexure to the south near the Potomac River. The mapped trace of the Brandywine fault system is generally coincident with (within 1.0 to 2.5 miles (2 to 4 km)) and parallel to the aeromagnetic and gravity anomalies used to define the western boundary of the Taylorsville basin but they do not precisely coincide (Mixon, 1977) (Hansen, 1986) (Wilson, 1990) (Benson, 1992). This observation lead Mixon and Newell (Mixon, 1977) to speculate the origin of the Brandywine fault system may be related to the reversal of a pre-existing zone of crustal weakness (i.e., Taylorsville Basin border fault).

The Brandywine fault system was active in the Early Mesozoic and reactivated during late Eocene and possibly middle Miocene time (Jacobeen, 1972) (Wilson, 1990). Basement rocks have a maximum vertical displacement of approximately 250 ft (76 m) across the fault (Jacobeen, 1972). Also, the Cretaceous Potomac Formation is 150 ft (46 m) thinner on the east (up-thrown) side of the fault indicating syndepositional activity of the fault. The faulting is interpreted to extend upward into the Eocene Nanjemoy Formation (70 ft (21 m) offset) (Wilson, 1990), and die out as a subtle flexure developed within the Miocene Calvert Formation (8 ft (2.4 km) flexure) (Jacobeen, 1972).

Wilson and Fleck (Wilson, 1990) speculate that the fault system continues northeast toward the previously mapped Upper Marlboro faults, near Marlboro, Maryland (Figure 2.5-25). Dryden (Dryden, 1932) reported several feet of reverse faulting in Pliocene Upland deposits in a railroad cut near Upper Marlboro, Maryland (Prowell, 1983). However, these faults are not observed beyond this exposure. Wheeler (Wheeler, 2006) suggests that the Upper Marlboro faults have a surficial origin (i.e., landsliding) based on the presence of very low dips and geometric relations inconsistent with tectonic faulting. Field reconnaissance conducted as part of this CCNPP Unit 3 study used outcrop location descriptions from Prowell (Prowell, 1983) but failed to identify any relevant exposures associated with the faults of Dryden (Dryden, 1932). Wheeler's (Wheeler, 2006) assessment of the Upper Marlboro fault appears to be consistent with the outcrop described by Dryden (Dryden, 1932) as not being associated with the Brandywine fault system.

Geologic information indicates that the Brandywine fault system was last active during the Miocene. All geologic information on the timing of displacement on the Brandywine fault system was available and incorporated into the EPRI seismic source models in 1986. The post-EPRI study by Wilson and Fleck (Wilson, 1990) extended the fault north and south as an anticline, but offers no new information about the timing of the deformation. There is no pre-EPRI or post-EPRI seismicity associated with this fault system. This fault system is identified only in the subsurface and geologic mapping along the surface projection of the fault zone does not show a fault (DM, 1973) (McCartan, 1989a) (McCartan, 1989b). Field and aerial reconnaissance performed as part of this CCNPP Unit 3 study, coupled with interpretation of Light Detection and Ranging (LiDAR) data (see Section 2.5.3.1 for additional information regarding the general methodology), revealed no anomalous geomorphic features indicative of potential Quaternary activity. The Brandywine fault system, therefore, is not a capable tectonic source and there is no new information developed since 1986 that would require a significant revision to the EPRI seismic source model.

2.5.1.1.4.4.4.3 Port Royal Fault Zone and Skinkers Neck Anticline

The Port Royal fault zone and Skinkers Neck anticline are located about 32 mi (51 km) west of the CCNPP site, south of the Potomac River (Figure 2.5-25). First described by Mixon and Powars (Mixon, 1984), these structures have been identified within the subsurface by: (1) contouring the top of the Paleocene Potomac Formation, (2) developing isopach maps of the Lower Eocene Nanjemoy Formation, and (3) interpreting seismic lines collected in northern Virginia (Milici, 1991) (Mixon, 1992) (Mixon, 2000). The fault and anticline are not exposed in surface outcrop. The Port Royal fault zone is located about 4 to 6 mi (6 to 10 km) east and strikes subparallel to the Skinkers Neck anticline and the Brandywine fault system. In our discussion, we consider the Skinkers Neck anticline to consist of a combined anticline and fault zone, following previous authors.

Mixon and Newell (Mixon, 1977) first hypothesized that a buried fault zone existed beneath Coastal Plain sediments and connected the Taylorsville basin in the north to the Richmond basin in the south along a fault zone coincident with the Brandywine fault zone of Jacobeen (Jacobeen, 1972). The inferred fault of Mixon and Newell (Mixon, 1977) coincides with a gravity gradient used to target exploration studies that led to the discovery of the Port Royal fault and Skinkers Neck anticline in 1984 (Mixon, 1984) (Mixon, 1992).

The Port Royal fault zone consists of a 32 mi (51 km) long, north to northeast-striking fault zone that delineates a shallow graben structure that trends parallel to a listric normal fault bounding the Taylorsville basin (Mixon, 2000) (Milici, 1991). In map view, the fault zone makes a short left-step to the Brandywine fault system (Figure 2.5-25). Along the northern part of the fault zone, near the town of Port Royal, Virginia, the fault is expressed in the subsurface as a 3 mi (5 km) wide zone of warping with a west-side-up sense of displacement. Water well and seismic reflection data show an apparent west-side-up vertical component for the southwestern part of the structure also (Mixon, 1992) (Mixon, 2000) (Milici, 1991).

The Skinkers Neck anticline is located directly west of the Port Royal fault zone and southwest of the mapped terminus of the Brandywine fault system (Figure 2.5-25). The north- to northeast-striking structure is 30-mi (48 km) long and 3 to 5 mi (5 to 8 km) wide, and is defined as an asymmetric, low-amplitude, north-plunging anticline with a west-bounding fault (Mixon, 2000). Locally, Mixon (Mixon, 2000) map the feature as two separate, closely-spaced anticlines. Along the west side of the structure, a fault zone strikes north-to-northeast and is interpreted as a fault-bounded, down-dropped block. The Skinkers Neck anticline is not mapped north of the Potomac River by Mixon (Mixon, 1992) (Mixon, 2000). However, McCartan (McCartan,

1989a) shows two folds north of the Potomac River, west of the Brandywine fault system, and along trend with the Skinkers Neck anticline as mapped by Mixon (Mixon, 2000).

The Port Royal fault zone and Skinkers Neck anticline likely are associated with Paleozoic structures that were reactivated in the Early Mesozoic, Paleocene, and possibly middle Miocene (Mixon, 1992) (Mixon, 2000) (McCartan, 1989c). Similar to the Brandywine fault system, these structures closely coincide with the Mesozoic Taylorsville basin (Mixon, 1992) (Milici, 1991). This apparent coincidence with a Mesozoic basin suggests that the Port Royal fault zone and the Skinkers Neck anticline represent possible pre-existing zones of crustal weakness. Post-Mesozoic deformation includes as much as 30 to 33 ft (9 to 10 km) of Paleocene offset, and less than 25 ft (7.6 m) of displacement across the basal Eocene Nanjemoy Formation. Deformation on the order of 5 to 10 ft (1.5 to 3 m) is interpreted to extend upward into the Middle Miocene Calvert and Choptank Formations (Mixon, 1992). The overlying Late Miocene Eastover Formation is undeformed across both the Port Royal fault zone and Skinkers Neck anticline, constraining the timing of most recent activity (Mixon, 1992) (Mixon, 2000).

Although the Port Royal fault zone and Skinkers Neck anticline where characterized after the EPRI study (EPRI, 1986), geological information available to the EPRI teams regarding the pre-Quaternary activity of the structures was available (Mixon, 1984). Both of these structures are mapped in the subsurface as offsetting Tertiary or older geologic units (Mixon, 2000). Field and aerial (inspection by plane) reconnaissance, coupled with interpretation of aerial photography (review and inspection of features preserved in aerial photos) and LiDAR data (see Section 2.5.3.1 for additional information regarding the general methodology), conducted during this CCNPP Unit 3 study shows that there are no geomorphic features indicative of potential Quaternary activity along the surface-projection of the fault zone (i.e., along the northern banks of the Potomac River and directly northeast of the fault zone). Also, there is no pre-EPRI or post-EPRI (EPRI, 1986) seismicity spatially associated with the Port Royal fault zone or the Skinkers Neck anticline. In summary, the Port Royal fault zone and Skinkers Neck anticline are not considered capable tectonic sources, there is no new information developed since 1986 that would require revision to the EPRI seismic source model regarding these features.

2.5.1.1.4.4.4.4 National Zoo Faults

The National Zoo faults in Washington D.C. approach to within 47 mi (76 km) of the site (Figure 2.5-25). The National Zoo faults are primarily low-angle to high-angle, northwest-striking, southwest-dipping thrust faults that occur within a 1.0 to 1.5 mi (1.6 to 2.4 km) long, north to northeast-trending fault zone (Prowell, 1983) (McCartan, 1990) (Fleming, 1994) (Froelich, 1975). The mapped surface traces of these faults range from 500 to 2000 ft (152 to 610 km) with up to 20 ft (6 m) of post-Cretaceous reverse displacement visible in outcrops at the National Zoo (Fleming, 1994). The faults were first identified by Darton (Darton, 1950) in exposures along Rock Creek in historic excavations between the National Zoo and Massachusetts Avenue in Washington D.C.

The National Zoo faults were active during the Early Mesozoic with probable reactivation during the Pliocene (Darton, 1950) (McCartan, 1990) (Fleming, 1994). This fault zone is coincident with the mapped trace of the Early Paleozoic Rock Creek shear zone, which led several researches to infer that the National Zoo faults are related to reversal of a pre-existing zone of crustal weakness (McCartan, 1990) (Fleming, 1994). Combined with the Rock Creek fault zone, the National Zoo faults could be up to 16 mi (26 km) long. Differential offset across basement and Potomac Group contacts also suggests Paleozoic fault reactivation (Fleming,

1994). The Cretaceous Potomac formation offsets are primarily less than 50 ft (15 m) and isopach maps show a thickening of Coastal Plain sediments east of these faults (Fleming, 1994) (Darton, 1950). The youngest two faults juxtapose basement rocks over Pliocene Upland gravels (Fleming, 1994) (McCartan, 1990). One exposure of these two faults is still preserved along Adams Mill road as a special monument (Prowell, 1983). Based on our field reconnaissance with USGS researchers, future additional investigations are planned by the USGS to further investigate the age of the gravels and lateral continuity of the National Zoo faults.

All information on timing of displacement of the National Zoo faults was available and incorporated into the EPRI seismic source models in 1986. Although later detailed mapping of these thrust faults with the Rock Creek shear zone was published after completion of the EPRI study (EPRI, 1986), Darton (Darton, 1950) and Prowell (Prowell, 1983) identified these faults as active during Cenozoic time. In addition, there is no pre-EPRI or post-EPRI seismicity spatially associated with this fault zone. Therefore, the conclusion is that the National Zoo faults are not a capable tectonic source. There also is no new published geologic information developed since 1986 that would require a significant revision to the EPRI seismic source model.

2.5.1.1.4.4.4.5 Hillville Fault Zone

The Hillville fault zone of Hansen (1978) approaches to within 5 mi (8 km) of the site in the subsurface (Figure 2.5-25, Figure 2.5-26, and Figure 2.5-27). The 26 mi (42 km) long, northeast-striking fault zone is composed of steep southeast-dipping reverse faults that align with the east side of the north-to northeast-trending Sussex-Currioman Bay aeromagnetic anomaly (i.e. SGA,Figure 2.5-11 and Figure 2.5-22) (Hansen, 1986). Based on seismic reflection data, collected about 9 mi (15 km) west-southwest of the site, the fault zone consists of a narrow zone of discontinuities that vertically separate basement by as much as 250 ft (76 m) (Hansen, 1978). (Figure 2.5-26 and Figure 2.5-233). With the exception of the single seismic reflection profile St. M-1 of Hansen (1978) there are no other data to indicate the down-dip geometry of the fault. The strike of the fault is inferred entirely from the inferred coincidence of the fault with the Sussex Currioman Bay aeromagnetic anomaly (Figure 2.5-11)(Hansen, 1986).

The Hillville fault zone delineates a possible Paleozoic suture zone reactivated in the Mesozoic and Early Tertiary. The fault zone is interpreted as a lithotectonic terrane boundary that separates basement rocks associated with Triassic rift basins on the west from low-grade metamorphic basement on the east (i.e., Sussex Terrane/Taconic suture of Glover and Klitgord, (Glover, 1995a) (Figure 2.5-17) (Hansen, 1986). The apparent juxtaposition of the Hillville fault zone with the Sussex-Currioman Bay aeromagnetic anomaly suggests that the south flank of the Salisbury Embayment may be a zone of crustal instability that was reactivated during the Mesozoic and Tertiary. Cretaceous activity is inferred by Hansen (Hansen, 1978) who extends the fault up into the Cretaceous Potomac Group. The resolution of the geophysical data does not allow an interpretation for the upward projection of the fault into younger overlying Coastal Plain deposits (Hansen, 1978). Hansen (Hansen, 1978), however, used stratigraphic correlations (i.e. "pinchouts") of Coastal Plain deposits from borehole data to speculate that the Hillville fault may have been active during the Early Paleocene.

There is no geologic data to suggest that the Hillville fault is a capable tectonic source. Field and aerial reconnaissance, coupled with interpretation of aerial photography and LiDAR data (see Section 2.5.1.1.4.4 for additional information regarding the general methodology), conducted during this COL study shows that there are no geomorphic features indicative of potential Quaternary activity along the surface-projection of the Hillville fault zone. A review

of geologic cross sections (McCartan, 1989a) (McCartan, 1989b) (Glaser, 2003b) (Glaser, 2003c) show south-dipping Lower to Middle Miocene Calvert Formation and no faulting along projection with the Hillville fault zone. A structure contour map of the top of the Eocene Piney Point-Nanjemoy Aquifer appears undeformed in the vicinity of the Hillville fault, indicating the likely absence of faulting of this regionally recognized stratigraphic marker (Figure 2.5-14). A geologic cross section prepared by Achmad and Hansen (Achmad, 1997) that intersects the Hillville fault, also shows no demonstrable offset across the contact between the Piney Point and Nanjemoy Formations (Figure 2.5-13). Furthermore Quaternary terraces mapped by McCartan (McCartan, 1989b) and Glaser (Glaser, 2003b) (Glaser, 2003c) bordering the Patuxent and Potomac Rivers were evaluated for features suggestive of tectonic deformation by interpreting LiDAR data and through field and aerial reconnaissance (Figure 2.5-26 and Figure 2.5-27 and Figure 2.5-229). No northeast-trending linear features coincident with the zone of faulting were observed where the surface projection of the fault intersects these Quaternary surfaces. Aerial reconnaissance of this fault zone also demonstrated the absence of linear features coincident or aligned with the fault zone (Figure 2.5-229). The interpretation of the detailed stratigraphic profiles collected along Calvert Cliffs and the western side of Chesapeake Bay provide geologic evidence for no expression of the fault where the projected fault would intersect the Miocene-aged deposits (Kidwell, 1997; see Section 2.5.3 for further explanation). Lastly, abundant shallow seismic reflection data acquired and interpreted by Colman (1990) in Chesapeake Bay intersect the northeast projection of the Hillville fault (Figure 2.5-29). Colman (1990) makes no mention of encountering the Hillville fault in their interpretations of the seismic data. Therefore, we conclude that the Hillville fault zone is not a capable tectonic source, and there is no new information developed since 1986 that would require a significant revision to the EPRI model.

2.5.1.1.4.4.4.6 Unnamed Fault beneath Northern Chesapeake Bay, Cecil County, Maryland

Pazzaglia (1993a) proposed a fault in northern Chesapeake Bay that comes to within 70 mi (113 km) north of the site (Figure 2.5-25, and Figure 2.5-230). On the basis of geologic data and assuming that the bay is structurally controlled, Pazzaglia (1993a) infers a 14 mi (23 km) long, northeast-striking fault with a southeast-side up sense of displacement. Pazzaglia (1993a) interprets this fault as beneath the Northeast River and northern Chesapeake Bay based on a vertical elevation difference of the early Pleistocene Turkey Point beds across the bay in Cecil County, Maryland (Figure 2.5-230). Specifically:

> "The Turkey Point beds at Turkey Point, Grove Point, and Betterton lie 6 - 8 m higher than at the mouth of the Susquehanna River…These elevation disparities suggests ~8 m of post-early Pleistocene offset along a northeast-southwest - trending fault beneath the upper Chesapeake Bay."(Pazzaglia, 1993a; p. 1632).

Central to the Pazzaglia (1993a) interpretation of a fault is the argument that the Turkey Point beds exposed in a three meter deep trench on Coudon Farm terrace west of Chesapeake Bay correlate with, and are equivalent to, the Turkey Point beds exposed in a sea cliff at Turkey Point, located 10 km to the southeast on the opposite side of the bay (Figure 2.5-230). This fault interpretation assumes that the depositional base of the Turkey Point beds should lie at a very similar elevation over considerable lateral distances. Pazzaglia clarified several key aspects of the fault interpretation during expert interviews. First, he stated that only the Turkey Point and Coudon Farm sites were used to estimate the six to eight meters of vertical separation. Second, he indicated that there may be original depositional relief on the base of the Turkey Point beds, which could account for the elevation disparity between Coudon Farms and Turkey Point.

Despite the information discussed above, the hypothesized fault from Pazzaglia (1993a) is unconfirmed based on evidence that supports the absence of faulting and the lack of direct supporting geologic evidence. First, the hypothetical fault inferred by Pazzaglia (1993a) is coincident with a fault inferred previously by Higgins (1974) that was re-evaluated by Edwards (1979). Motivated by speculations from Higgins (1974) - that the northern Chesapeake Bay magnetic anomaly was created by faulting of Coastal Plain stratigraphy, Edwards (1979) drilled three borings on either side of the magnetic anomaly and compiled existing boring and geophysical data to construct the top-of-basement structure contour map shown in Figure 2.5-230. Based on their findings, Edwards (1979) make several key statements on the absence of a fault, including: "A regional map of the basement surface… does not reveal any structural anomalies… that could not be explained by relict topographic relief on the pre-Coastal Plain surface" (p. 20) and "within the scale of resolution (50 feet) of the data obtained in this project, offset at the base of the Coastal Plain cannot be demonstrated. Thus any fault associated with the shear zone can be dated no younger than Early Cretaceous" (p. 21). Similarly, geologic cross-sections from Benson (2006), developed from the borings of Edwards (1979), provide a line of evidence that is inconsistent with faulting beneath the northern part of Chesapeake Bay. Second, geologic mapping by Higgins (1986) along the northeast on-land projection of the inferred fault of Pazzaglia (1993a) does not show any northeast-striking fault(s) near Indian Falls and Northeast (Figure 2.5-232). Likewise, Higgins (1990) report unfaulted Cretaceous deposits along a northeast projection of the inferred fault and state: "No irregularities such as local steepening, flattening, or reversal of the dip of the Coastal Plain strata have been found in Cecil County which would indicate that there has been significant post-depositional tectonic movements." (p. 123).

There is no direct geologic evidence to suggest that this unnamed fault zone from Pazzaglia (1993a) is a capable tectonic source. There is no pre-EPRI or post-EPRI seismicity spatially associated with this fault zone. Field and aerial reconnaissance conducted to support CCNPP Unit 3 (Figure 2.5-229) and inspection of detailed 'bare earth' LiDAR data (Figure 2.5-232) shows that there are no geomorphic features indicative of potential Quaternary activity along the surface-projection of the unnamed fault. Based on the sum of published literature (Higgins, 1986)(Higgins, 1990), structure contour maps (Edwards, 1979), field and aerial reconnaissance, and reasonable alternate explanations presented by F. Pazzaglia himself, it is concluded that this hypothetical fault is not a capable tectonic source.

2.5.1.1.4.4.4.7 Unnamed Monocline beneath Chesapeake Bay

McCartan (McCartan, 1995) show east-facing monoclinal structures bounding the western margin of Chesapeake Bay 1.8 and 10 mi (2.9 and 16 km) east and southeast, respectively, of the site (Figure 2.5-25). Also, McCartan (McCartan, 1995) interprets an east-facing monocline about 10 mi (16 km) west of the site. The three monoclinal structures are depicted on two cross sections as warping Lower Paleocene to Upper Miocene strata with approximately 60 to 300 ft (18 to 91 m) of relief. The monoclines exhibit a west-side up sense of structural relief that projects upward into the Miocene Choptank Formation (McCartan, 1995). The overlying Late Miocene St. Marys Formation is not shown as warped. Boreholes shown with the cross sections accompanying the McCartan (MaCartan, 1995) map provide the only direct control on cross section construction. The boreholes are widely spaced and do not appear to provide a constraint on the existence and location of the warps. No borehole data is available directly west of the cliffs and within the bay to substantiate the presence of the warp. No surface trace or surface projection of the warps is indicated on the accompanying geologic map. Based on text accompanying the map and cross sections, we infer that the cross sections imply two approximately north- to northeast-striking, west-side up structures, of presumed tectonic origin.

McCartan (McCartan, 1995) interpret the existence of the monocline based on three observations in the local landscape. Firstly, the north to northeast-trending western shore of Chesapeake Bay within Calvert County is somewhat linear and is suggestive of structural control (McCartan, 1995). Secondly, land elevation differences west and east of Chesapeake Bay are on the order of 90 ft (27 m), with the west side being significantly higher in elevation, more fluvially dissected, and composed of older material compared to the east side of Chesapeake Bay. On the west side of the bay, the landscape has surface elevations of 100 to 130 ft (30 to 40 m) msl and drainages are incised into the Pliocene Upland Deposits and Miocene-aged deposits of the St. Mary's, Choptank, and Calvert Formations. Along the eastern shoreline of the Delmarva Peninsula, surface elevations are less than 20 to 30 ft (6 to 9 m) msl and the surface exhibits minor incision and a more flat-lying topographic surface. These eastern shore deposits are mapped as Quaternary estuarine and deltaic deposits. Thirdly, variations in unit thickness within Tertiary deposits between Calvert Cliffs and Delmarva Peninsula are used to infer the presence of a warp. Based on these physiographic, geomorphic and geologic observations, McCartan (McCartan, 1995) infer the presence of a fold along the western shore of Chesapeake Bay (Figure 2.5-25).

Based on the paucity of geologic data constraining the cross sections of McCartan (McCartan, 1995), the existence of the monocline is speculative. The borehole data that constrain the location of the monocline are approximately 18 to 21 mi (29 to 34 km) apart and permit, but do not require the existence of a monocline. McCartan (McCartan, 1995) do not present additional data that are inconsistent with the interpretation of flat-lying, gently east-dipping Miocene strata shown in prior published cross sections north and south of this portion of Chesapeake Bay (Cleaves et al., 1968; Milici, et al., 1995) and within Charles and St. Mary's Counties, Maryland (McCartan, 1989a) (McCartan, 1989b) (DM, 1973). No geophysical data are presented as supporting evidence for this feature. In contrast, shallow, high-resolution geophysical data collected along the length of Chesapeake Bay to evaluate the ancient courses of the submerged and buried Susquehanna River provide limited evidence strongly indicating that Tertiary strata are flat lying and undeformed along the western shore of Chesapeake Bay (Colman, 1990) (Figure 2.5-29).

Alternatively, the change in physiographic elevation and geomorphic surfaces between the western and eastern shores of Chesapeake Bay can be explained by erosional processes directly related to the former course of the Susquehanna River, coupled with eustatic sea level fluctuations during the Quaternary (Colman, 1990) (Owens, 1979). Colman and Halka (Colman, 1989) also provide a submarine geologic map of Chesapeake Bay at and near the site which depicts Tertiary and Pleistocene deposits interpreted from high-resolution geophysical profiles. No folding or warping or faulting is depicted on the Colman and Halka (Colman, 1989) map which encompasses the warp of McCartan (McCartan, 1995). Colman (Colman, 1990) utilize the same geophysical data to track the former courses of the Susquehanna River between northern Chesapeake Bay and the southern Delmarva Peninsula. Paleo-river profiles developed from the geophysical surveys that imaged the depth and width of the paleochannels show that the Eastville (150 ka) and Exmore (200 to 400 ka) paleochannels show no distinct elevation changes within the region of the Hillville fault and McCartan (McCartan, 1995) features.

There is no geologic data to suggest that the postulated monocline along the western margin of Chesapeake Bay of McCartan (McCartan, 1995), if present, is a capable tectonic source. Field and aerial reconnaissance, coupled with interpretation of aerial photography and LiDAR data (see Section 2.5.3.1 for additional information regarding the general methodology), conducted during this COL study, shows that there are no geomorphic features indicative of

folding directly along the western shores of Chesapeake Bay. There is no pre-EPRI or post-EPRI seismicity spatially associated with this structure. These data indicate that the McCartan (McCartan, 1995) warps, if present, most likely do not deform Pliocene to Quaternary deposits, and thus are not capable tectonic sources that would require a revision to the EPRI (1986) seismic source model.

2.5.1.1.4.4.4.8 Unnamed Folds and Postulated Fault within Calvert Cliffs, Western Chesapeake Bay, Calvert County, Maryland

The Calvert Cliffs along the west side of Chesapeake Bay provide a 25 mile (40 km) long nearly continuous exposure of Miocene, Pliocene and Quaternary deposits (Figure 2.5-26). Kidwell (1988 and 1997) prepared over 300 comprehensive lithostratigraphic columns along a 25 mi (40 km) long stretch of Calvert Cliffs (Figure 2.5-30). Because of the orientation of the western shore of Chesapeake Bay, the cliffs intersect any previously potential structures (i.e., Hillville fault) trending northeast or subparallel to the overall structural trend of the Appalachians. The cliff exposures provide a 230 ft (70 m) thick section of Cenozoic deposits that span at least 10 million years of geologic time.

On the basis of the stratigraphic profiles, Kidwell (Kidwell, 1997) develops a chronostratigraphic sequence of the exposed Coastal Plain deposits and provides information on regional dip and lateral continuity. The Miocene Choptank Formation is subdivided into two units and is unconformably overlain by the St .Marys Formation. The St. Marys Formation is subdivided into three subunits each of which is bound by a disconformity. The youngest subunit is unconformably overlain by the Pliocene Brandywine Formation (i.e., Pliocene Upland gravels). The exposed Coastal Plain deposits strike northeast and dip south-southeast between 1 and 2 degrees. The southerly dip of the strata is disrupted occasionally by several low amplitude broad undulations in the Choptank Formation, and decrease in amplitude upward into the St Marys Formation (Figure 2.5-30). Kidwell (Kidwell, 1997) interprets the undulations as monoclines and asymmetrical anticlines. The undulations typically represent erosional contacts that have wavelengths on the order of 2.5 to 5 mi (4 to 8 km) and amplitudes of 10 to 11 ft (about 3 m). Any inferred folding of the overlying Pliocene and Quaternary fluvial strata is very poorly constrained or obscured because of highly undulatory unconformities within these younger sand and gravel deposits. For instance, the inferred folding of the overlying Pliocene and Quaternary channelized sedimentary deposits consist of intertidal sand and mud-flats, tidal channels and tidally-influenced rivers exhibit as much as 40 ft (12 m) of erosional elevation change (Figure 2.5-30).

About 1.2 mi (1.9 km) south of the site, Kidwell (Kidwell, 1997) interprets an apparent 6 to 10 ft (2 to 3 m) elevation change in Miocene strata by extrapolating unit contacts across the approximatley 0.6 mile wide (1 km) gap at Moran Landing (Figure 2.5-25 and Figure 2.5-30). Kidwell (Kidwell, 1997) also interprets a 3 to 12 ft (1 to 3.6 m) elevation change in younger (Quaternary(?)) fluvial material across the same gap. Because of the lack of cliff exposures at Moran Landing (only the valley margins), no direct observations of these elevation changes can be made. Kidwell (Kidwell,1997) explains the differences in elevation of the Miocene-Quaternary stratigraphy by hypothesizing the existence of a fault at Moran Landing that strikes northeast and accomodates a north-side down sense of separation. However, the postulated fault of Kidwell (Kidwell, 1997) is not shown on any of Kidwell's (Kidwell, 1997) cross- sections, or any published geologic map (e.g., Glaser, 2003b and 2003c). In addition, Hansen (Hansen, 1978) does not describe faulting in seismic reflection lin St. M-2 that intersects the inferred southwest projection of the hypothesized Kidwell (Kidwell, 1997) fault (Figure 2.5-27).

The observations of offset younger gravels do not provide any evidence for the existence of a fault because the surface on which the gravels are deposited is an erosional unconformity with extensive variable relief (Kidwell, 1997). Observations made during field reconnaissance, as part of the FSAR preparation, confirmed that this contact was an erosional unconformity with significant topography north and south of Moran Landing consistent with stratigraphic representations in Kidwell (1997) profiles. The observations of several feet of elevation change in the Miocene units over several thousands of feet of horizontal distance is at best weak evidence for faulting within the Miocene deposits. For example, subtle elevation variations in Miocene strata characterized along a near-continuous exposure south of Moran Landing contain similar vertical and lateral dimensions as to the inferred elevation change across Moran Landing; however, the features are interpreted as subtle warps and not faults by Kidwell (1997). On the basis of association with similar features to the south and the lack of a continuous exposure, there is little to no evidence to support a fault across Moran Landing. The lack of evidence for Quaternary faulting within the observations made by Kidwell (Kidwell, 1997). and the results of the studies undertaken as part of the CCNPP Unit 3 COLA effort (field and aerial reconnaissance, air photo and LiDAR analysis) (see FSAR Section 2.5.3.1), collectively support the conclusion that the hypothesized fault of Kidwell (Kidwell, 1997) is not a capable fault.

2.5.1.1.4.4.5 Quaternary Tectonic Features

In an effort to provide a comprehensive database of Quaternary tectonic features, Crone and Wheeler (Crone, 2000), Wheeler (Wheeler, 2005), and Wheeler (Wheeler, 2006) compiled geological information on Quaternary faults, liquefaction features, and possible tectonic features in the CEUS. Crone and Wheeler (Crone, 2000) and Wheeler (Wheeler, 2005) evaluated and classified these features into one of four categories (Classes A, B, C, and D; see Table 2.5-1 for definitions (Crone, 2000) (Wheeler, 2005)) based on strength of evidence for Quaternary activity.

Within a 200 mi (322 km) radius of the CCNPP site, Crone and Wheeler (Crone, 2000), Wheeler (Wheeler, 2005) and Wheeler (Wheeler, 2006) identified 17 potential Quaternary features (Figure 2.5-31). Work performed as part of the CCNPP Unit 3 investigation, including literature review, interviews with experts, and geologic reconnaissance, did not identify any additional potential Quaternary tectonic features within the CCNPP site region, other than those previously mentioned (McCartan, 1995) (Kidwell, 1997). Within approximately 200 mi (322 km) of the site, Crone and Wheeler (Crone, 2000) found only one feature described in the literature that exhibited potential evidence for Quaternary activity (Figure 2.5-31). This feature (shown as number 12) is the paleo-liquefaction features within the Central Virginia seismic zone.

The following sections provide descriptions of 15 of the 17 potential Quaternary features identified by Crone and Wheeler (Crone, 2000), Wheeler (Wheeler, 2005) (Wheeler, 2006), and of the postulated East Coast fault system of Marple and Talwani (Marple, 2004). Note that the Central Virgina and Lancaster seismic zones are discussed in Section 2.5.1.1.4.5 and Section 2.5.2. Out of the 17 features evaluated for this CCNPP Unit 3 study, nearly all are classified as Class C features, with the exception of the Central Virginia seismic zone (Class A).

The features are labeled with the reference numbers utilized in Figure 2.5-31:

1. Fall lines of Weems (1998) (Class C)
2. Ramapo fault system (Class C)
3. Kingston fault (Class C)

4. New York Bight fault (offshore) (Class C)
5. Cacoosing Valley earthquake (Class C)
6. Lancaster seismic zone (Class C)
7. New Castle County faults (Class C)
8. Upper Marlboro faults (Class C)
9. Everona fault and Mountain Run fault zone (Class C)
10. Stafford fault of Mixon et al. (Class C)
11. Lebanon Church fault (Class C)
12. Central Virginia seismic zone (Class A)
13. Hopewell fault (Class C)
14. Old Hickory faults (Class C)
15. Stanleytown-Villa Heights faults (Class C)
16. (The Stafford fault system of Marple is included in (17), i.e. the East Coast fault system)
17. East Coast fault system (Class C)

2.5.1.1.4.4.5.1 Fall Lines of Weems (1998)

In 1998, Weems defined seven fall lines across the Piedmont and Blue Ridge Provinces of North Carolina and Virginia (Figure 2.5-31). The eastern fall line is located approximately 47 mi (76 km) west of the CCNPP site. The fall lines, not to be confused with the Fall Line separating the Piedmont and Coastal Plain provinces, are based on the alignment of short stream segments with anomalously steep gradients. Weems (1998) explores possible ages and origins (rock hardness, climatic, and tectonic) of the fall lines and "based on limited available evidence favors a neo-tectonic origin" for these geomorphic features during the Quaternary. Weems (1998) interprets longitudinal profiles for major drainages flowing primarily southeast and northwest across the Piedmont and Blue Ridge Provinces to assess the presence and origin of the "fall zones".

A critical evaluation of Weems' (1998) study, as part of the North Anna ESP, demonstrates that there are inconsistencies and ambiguities in Weems' (1998) correlations and alignment of steep reaches of streams used to define continuous fall lines (Dominion, 2004b). The North Anna ESP study concludes that that the individual fall zones of Weems (1998) may not be as laterally continuous as previously interpreted. For instance, stratigraphic, structural and geomorphic relations across and adjacent to the Weems (1998) fall zones can be readily explained by differential erosion due to variable bedrock hardness rather than Quaternary tectonism (Dominion, 2004b). Furthermore, there is no geomorphic expression of recent tectonism, such as the presence of escarpments, along the trend of the fall lines between drainages where one would expect to find better preservation of tectonic geomorphic features. Similarly, Wheeler (2005) notes that the Weems (1998) fall zones are not reproducible and are subjective, thus tectonic faulting is not yet demonstrated as an origin, and the fall lines are designated as a Class C feature. In the Safety Evaluation Report for the North Anna

ESP site study, the NRC staff agrees with the assessment that the fall lines of Weems (1998) are nontectonic features (NRC, 2005). In summary, based on review of published literature, field reconnaissance, and geologic and geomorphic analysis performed previously for the North Anna ESP application, the fall lines of Weems (1998) are erosional features related to contrasting erosional resistances of adjacent rock types, and are not tectonic in origin, and thus are not capable tectonic sources.

2.5.1.1.4.4.5.2 Everona Fault and Mountain Run Fault Zone

The Mountain Run fault zone is located approximately 71 mi (114 km) southwest of the site (Figure 2.5-9). The 75 mi (121 m) long, northeast-striking fault zone is mapped from the southeastern margin of the Triassic Culpeper Basin near the Rappahannock River southwestward to near Charlottesville, in the western Piedmont of Virginia (Pavlides, 1986) (Horton, 1991). The fault zone consists of a broad zone of sheared rocks, mylonites, breccias, phyllonites, and phyllites up to 2.5 to 3 mi (4 to 5 km) wide (Pavlides, 1989) (Crone, 2000) (Mixon, 2000). Within this broad fault zone are three features that have been identified by Crone and Wheeler (Crone, 2000) as having possible Quaternary tectonic activity. From northeast to southwest, these are: (1) the northwest-facing, 1-mi- (1.6-km-) long Kelly's Ford scarp, (2) the northwest-facing, 7-mi- (11-km-) long Mountain Run scarp, and (3) the northwest-dipping fault exposed near the town of Everona, Virginia, named informally the Everona fault (Pavlides, 1983) (Pavlides, 1986) (Pavlides, 1994) (Crone, 2000) (Mixon, 2000) (Figure 2.5-31).

The Mountain Run fault zone is interpreted to have formed initially as a thrust fault upon which back-arc basin rocks (mélange deposits) of the Mine Run Complex were accreted onto ancestral North America at the end of the Ordovician (Pavlides, 1989). This major structure separates the Blue Ridge and Piedmont terranes (Pavlides, 1983) (Figure 2.5-9, Figure 2.5-16, and (Figure 2.5-17). Subsequent reactivation of the fault during the Paleozoic and/or Mesozoic produced strike-slip and dip-slip movements. Horizontal slickenside lineations within phyllite found in borehole samples beneath the alluvium-filled valley of Mountain Run suggest strike-slip movement, whereas small scale folds in the uplands near the scarp suggest an oblique dextral sense of slip (Pavlides, 2000). The timing of the reverse and strike-slip histories of the fault zone, and associated mylonitization and brecciation, is constrained to be pre-Early Jurassic, based on the presence of undeformed Early Jurassic diabase dikes that cut rocks of the Mountain Run fault zone (Pavlides, 2000). The northern portion of the Mountain Run fault zone bounds the southeastern margin of the Culpeper basin (Mixon, 2000) (Figure 2.5-9 and Figure 2.5-10), indicating that the fault locally has been active since the Triassic (Crone, 2000) (Section 2.5.1.1.4.4.3).

Two features within the northeast-striking Mountain Run fault zone are moderately to well-expressed geomorphically (Pavlides, 2000). Two northwest-facing scarps occur along the fault zone, including: (1) the 1 mi (1.6 km) long Kelly's Ford scarp located directly northeast of the Rappahannock River and; (2) the 7 mi (11 km) long Mountain Run scarp located along the southeast margin of the linear Mountain Run drainage. The presence of these two locally conspicuous bedrock scarps in the Piedmont, an area characterized by deep weathering and subdued topography, has led some experts to suggest that the scarps formed due to a Late Cenozoic phase of movement within the mountain run fault zone (Pavlides, 2000) (Pavlides, 1983).

Field and aerial reconnaissance, and geomorphic analysis of deposits and features associated with the fault zone, recently performed for the North Anna ESP provide new information on the Mountain Run and Kelly's Ford scarps in particular, and the Mountain Run fault zone in

general (Dominion, 2004a). In response to NRC comments for the North Anna ESP, geologic cross sections and topographic profiles were prepared along the Mountain Run fault zone across and between the Mountain Run and Kelly's Ford scarps to further evaluate the inferred tectonic geomorphology coincident with the fault zone first proposed by Pavlides (1986). The results of the additional analysis were presented in the response to an NRC Request for Additional Information (RAI) (Dominion, 2004a) and demonstrated that the Mountain Run and Kelly's Ford scarps are probably a result of a differential erosion and not late Cenozoic tectonic activity. Three main findings from the Dominion (2004a) study are summarized below:

- There is no consistent expression of a scarp along the Mountain Run fault zone in the vicinity of the Rappahannock River. The northwest-facing Kelly's Ford scarp is similar to a northwest-facing scarp along the southeastern valley margin of Mountain Run; both scarps were formed by streams that preferentially undercut the southeastern valley walls, creating asymmetric valley profiles.

- There is no northwest-facing scarp associated with the 10 mile (16 km) long portion of the Mountain Run fault zone between the Rappahannock and Rapidan Rivers (i.e., between the Kelly's Ford and Mountain Run scarps). Undeformed late Neogene colluvial deposits bury the Mountain Run fault zone in this region, demonstrating the absence of Quaternary fault activity.

- The northwest-facing Mountain Run scarp southwest of the Rappahannock River alternates with a southeast-facing scarp on the opposite side of Mountain Run valley; both sets of scarps have formed by the stream impinging on the edge of the valley.

Near Everona, Virginia, a small reverse fault, found in an excavation, vertically displaces a "probable Late Tertiary" or "Pleistocene" gravel layer by 5 ft (1.5 m) (Pavlides, 1983) (Manspeizer, 1989) (Crone, 2000). The fault strikes northeast and dips between about 55 to 20 degrees northwest, shallowing up-dip (Manspeizer, 1989) (Crone, 2000). This isolated fault exposure, called the Everona fault by Crone and Wheeler (Crone, 2000), is located about 0.4 mi (0.6 km) northwest of the Mountain Run scarp and is within but near the northwest margin of the Mountain Run fault zone (Pavlides, 1983) (Mixon, 2000). There is no geomorphic expression associated with the exposure (Crone, 2000). The CCNPP Unit 3 investigation did not reveal additional investigations of the Everona fault since the initial exposure was documented in 1983 (Pavlides, 1983). Crone and Wheeler (Crone, 2000) assessed that the faulting at Everona is likely to be of Quaternary age, but because the likelihood has not been tested by detailed paleoseismological or other investigations, this feature was assigned to Class C.

All of the basic information on the style and timing of displacement of the Everona fault was available to the EPRI SOG team in 1986. Significant new information developed since 1986 includes the work performed for the North Ana ESP that shows the Mountain Run fault zone in the vicinity of the Kelly's Ford and Mountain Run scarps has not been active during the Quaternary. In addition, the NRC staff agrees that the scarps along the Mountain Run Fault zone were not produced by Cenozoic fault activity (NRC, 2005). Similarly, Crone and Wheeler (Crone, 2000) do not show the Mountain Run fault zone as a known Quaternary structure in their compilation of active tectonic features in the CEUS, having assigned it to Class C. Based on the lack of new information on the Everona fault and the findings of the previous studies performed for the North Anna ESP (Dominion, 2004a), it is concluded that the Everona-Mountain Run fault zone is not a capable tectonic source. No new information has been developed since 1986 that would require a significant revision to the EPRI seismic source model.

2.5.1.1.4.4.5.3 Stafford Fault of Mixon, et al.

The Stafford fault (#10 on Figure 2.5-31) approaches within 47 mi southwest of the site (Figure 2.5-25). The Stafford fault (Mixon, 2000) is discussed in more detail in Section 2.5.1.1.4.4.1 (Stafford Fault System). The northern extension of the Stafford fault system as proposed by Marple (#16 on Figure 2.5-31) is discussed in Section 2.5.1.1.4.4.1 and Section 2.5.1.1.4.5.14. The 42 mile (68 km) long fault system strikes approximately N35°E and was identified and described first by Newell (Newell, 1976). The fault system consists of a series of five northeast-striking, northwest-dipping, high-angle reverse faults including, from north to south, the Dumfries, Fall Hill, Hazel Run, and Brooke faults, and an unnamed fault. The Brooke fault also includes the Tank Creek fault located northeast of the Brooke fault (Mixon, 2000).

No new significant information has been developed since 1986 regarding the activity of the Stafford fault system with the exception of the response to an NRC RAI for the North Anna ESP (Dominion, 2004a). Field reconnaissance performed for the CCNPP Unit 3 study also did not reveal any geologic or geomorphic features indicative of potential Quaternary activity along the fault system. In addition, near the site and along the portion of the Stafford fault mapped by Mixon et al. (2000) no seismicity is attributed to the Stafford fault. Similarly, Wheeler (Wheeler, 2005) does not show the Stafford fault system as a Quaternary structure in his compilation of active tectonic features in the CEUS. The NRC (NRC, 2005) agreed with the findings of the subsequent study for the North Anna ESP, and stated: "Based on the evidence cited by the applicant, in particular the applicant's examination of the topography profiles that cross the fault system, the staff concludes that the applicant accurately characterized the Stafford fault system as being inactive during the Quaternary Period." Based on a review of existing information for the Stafford fault system, including the response to the NRC RAI for the North Anna ESP, the Stafford fault system is not a capable tectonic source and there is no new information developed since 1986 that would require a significant revision to the EPRI seismic source model.

2.5.1.1.4.4.5.4 Ramapo Fault System

The Ramapo fault is located in northern New Jersey and southern New York State, approximately 200 mi (320 km) north-northeast of the CCNPP site (Figure 2.5-31, Figure 2.5-227 and Figure 2.5-234). The Ramapo fault is one segment of a system of northeast-striking, southeast-dipping, normal faults that bound the northwest side of the Mesozoic Newark basin (Figure 2.5-10, and Figure 2.5-227), (Drake, 1996) (Ratcliffe, 1971) (Schlische, 1992). Bedrock mapping by Drake et al. (Drake et al., 1996) shows primarily northwest-dipping Lower Jurassic and Upper Triassic Newark Supergroup rocks in the hanging wall and tightly folded and faulted Paleozoic basement rocks in the footwall of the fault. The Ramapo fault proper extends for 50 mi (80 km) from Peapack, NJ to the Hudson River (Ratcliffe, 1971). To the south the Ramapo fault splays into several fault strands and merges with the Flemington Fault zone. On the north side of the Hudson River the fault splays into several northeast- to east-trending faults in Rockland and Westchester Counties, New York.

The Ramapo fault first received significant attention as a potentially capable fault during the licensing process for the Indian Point Nuclear Power Plant in the late 1970s (Aggarwal, 1978). Due to the close proximity of a proposed strand of this fault to the Indian Point plant (several miles at most) and the questions raised regarding the capability of the fault during the licensing process, a considerable amount of research has been conducted to address the potential capability of the fault. The vast majority of the research was conducted prior to the development of the EPRI source characterizations (EPRI, 1986) that are used as the base source model for the CCNPP Unit 3 COLA (see discussion in Section 2.5.2). Therefore, much of this information was known to the EPRI teams and considered by them in the development of the

existing source characterizations for the Ramapo fault (Subsection 2.5.2.2.1). Of the information on the Ramapo fault that has been published since the EPRI study (Kafka, 1996) (Kafka, 1989) (Newman, 1987) (Ratcliffe, 1990) (Sykes, 2008) none has presented any new information or data that requires updating of the EPRI model. The primary basis for this conclusion is the observation that none of the more recent publications provide conclusive evidence that the Ramapo and related faults are capable structures.

Interest in the Ramapo fault as a potential seismogenic fault was initially driven by the work of seismologists at what is now referred to as the Lamont Doherty Earth Observatory in New Jersey. Largely based on earthquake locations generated from local network data, these researchers noticed a spatial association between earthquakes and the Ramapo fault (Aggarwal, 1978) (Kafka, 1985) (Page, 1968). The study of Page et al. (Page, 1968) used the locations of four earthquakes that they located near the Ramapo fault as the basis for concluding that the earthquakes were occurring on the Ramapo fault, and, therefore, the Ramapo was experiencing small slip events. In a later study, Aggarwal and Sykes (Aggarwal, 1978) located 33 earthquakes with magnitudes less than or equal to mb 3.3 that occurred between 1962 and 1977 within the New York - New Jersey region surrounding the Ramapo fault. Based on the locations of these earthquakes, Aggarwal and Sykes (Aggarwal, 1978) also noted a spatial association between the locations of the earthquakes and the Ramapo and related faults. Aggarwal and Sykes (Aggarwal, 1978) described this association as "leav[ing] little doubt that earthquakes in this area occur along preexisting faults" (page 426) (Aggarwal, 1978). In particular, Aggarwal and Sykes (Aggarwal, 1978) focused on the Ramapo fault: (1) noting that over half of the 32 events plot along the Ramapo fault, and (2) concluding that that Ramapo fault is an active fault with the capability of generating large earthquakes. Aggarwal and Sykes (Aggarwal, 1978) based this conclusion on: (1) the spatial association of seismicity; (2) focal mechanisms for earthquakes near the Ramapo fault that show high-angle thrust faulting along roughly northeast trending faults, implying a northwest maximum compressive stress direction; and (3) earthquake hypocenters from within 10 km of the Ramapo fault surface trace that align with a dip of approximately 60°.

Despite the strong insistence from earlier authors that there was little doubt the Ramapo fault is active, numerous studies (Kafka, 1985) (Quittmeyer, 1985) (Seborowski, 1982) (Thurber, 1985) post-dating those of Aggarwal and Sykes (Aggarwal, 1978) and Page et al. (Page, 1968) presented revised analyses of the seismicity that contradict the earlier work and clearly demonstrate that there is considerable uncertainty as to whether or not slip on the Ramapo and related faults is causing the recorded seismicity. Seborowski et al. (Seborowski, 1982) analyzed a sequence of aftershocks in 1980 near the northern end of the Ramapo fault close to Annsville, NY (Figure 2.5-227). Seborowski et al. (Seborowski, 1982) demonstrated that the alignment of these earthquakes and their composite focal mechanism suggest thrusting on a north-northwest trending fault plane. This observation led Seborowski et al. (Seborowski, 1982) to conclude that their observations are not consistent with the conclusion of Aggarwal and Sykes (Aggarwal, 1978) that the Ramapo fault is active because their slip direction and corresponding maximum compressive stress direction is perpendicular to that hypothesized by Aggarwal and Sykes (Aggarwal, 1978).

Quittmeyer et al. (Quittmeyer, 1985) analyzed another earthquake sequence that occurred in 1983 approximately 7 miles from the sequence analyzed by Seborowski et al. (Seborowski, 1982) and also reanalyzed one of the earthquakes used by Aggarwal and Sykes (Aggarwal, 1978) explicitly to address the discrepancy between the expected slip directions, and thus maximum compressive stress directions, of the Aggarwal and Sykes (Aggarwal, 1978) and Seborowski et al. (Seborowski, 1982) studies. Quittmeyer et al. (Quittmeyer, 1985)

demonstrated two main points: (1) a composite fault plane solution for the 1983 earthquake sequence indicates thrust faulting along faults striking northwest with a maximum compressive stress direction oriented to the northeast; and (2) the earthquake analyzed by Aggarwal and Sykes (Aggarwal, 1978) has a non-unique fault plane solution that could be consistent with either the results of Aggarwal and Sykes (Aggarwal, 1978) or consistent with the fault plane solution for the 1983 earthquake sequence. Based on these observations, Quittmeyer et al. (Quittmeyer, 1985) hypothesized the maximum compressive stress direction is directed roughly northeast and implied that the Ramapo fault is not likely a source of earthquakes within the region.

Kafka et al. (Kafka, 1985) presented a revised and extended seismicity catalog for the New York - New Jersey area surrounding the Ramapo fault region extending from 1974 to 1983. Kafka et al. (Kafka, 1985) described this compilation as an improvement over previous catalogs because the increased robustness of the network during that timeframe provides more accurate earthquake locations and uniform magnitude estimates. During this time period, Kafka et al. (Kafka, 1985) recorded a total of 61 earthquakes, all with magnitudes less than or equal to mbLg 3.0. Assuming that their earthquake catalog is complete down to magnitudes of mbLg > 2.0, Kafka et al. (Kafka, 1985) reported that 7 out of 15 earthquakes occur within 10 mi (6 km) of the Ramapo fault. Kafka et al. (Kafka, 1985) describe the remaining earthquakes as occurring around the outside of the Newark basin. Importantly, Kafka et al. (Kafka, 1985) concluded that while "much emphasis was placed on the significance of the Ramapo fault and its relationship to seismicity" (page 1279), the other seismicity occurring throughout the region suggests that "the geologic structures associated with most (if not all) earthquakes in this region are still unknown" (page 1285). In a later publication in which Kafka and Miller (Kafka, 1996) analyze updated seismicity with respect to geologic structures, Kafka and Miller (Kafka, 1996) further discredit the association between seismicity and the Ramapo fault by saying, "…the currently available evidence is sufficient to rule out … a concentration of earthquake activity along the Ramapo fault" (page 83).

Thurber and Caruso (Thurber, 1985) derived new, one- and three-dimensional crustal velocity models of the upper crust in the region of the northern Ramapo fault to provide better earthquake locations in that area. These new velocity models are considered improvements over those used in previous studies (e.g., Aggarwal, 1978). The new models resulted in some changes in depths for the 15 earthquakes examined by Thurber and Caruso (Thurber, 1985). Based on their work, Thurber and Caruso (Thurber, 1985) concluded that: (1) there are significant lateral velocity variations within the region surrounding the Ramapo fault that can impact earthquake locations made using simple velocity models; and (2) "the Ramapo fault proper is not such a salient seismic feature in New York State, unlike the findings of Aggarwal and Sykes" (page 151). As with the Quittmeyer et al. (Quittmeyer, 1985), Seborowski et al. (Seborowski, 1982), and Kafka et al. (Kafka, 1985) studies, these conclusions of Thurber and Caruso (1985) indicate that there is considerable uncertainty surrounding the potential activity of the Ramapo fault.

Primarily triggered by the seismological suggestions that the Ramapo fault is active, geological investigations also were conducted to look for evidence of Quaternary slip on the Ramapo fault. The primary researcher involved in these efforts was Nicholas Ratcliffe of the U.S. Geological Survey. Ratcliffe and his colleagues' work consisted of detailed geologic mapping, seismic reflection profiling, petrographic analysis, borings and core analysis along much of the Ramapo fault and its corollary northern and southern extension (Ratcliffe, 1980) (Ratcliffe, 1983) (Ratcliffe, 1985a) (Ratcliffe 1985b) (Ratcliffe 1986a) (Ratcliffe 1986b) (Ratcliffe 1988) (Ratcliffe 1992). Much of Ratcliffe's work was explicitly focused on investigating the

potential relationship between the Ramapo fault and the seismicity that had been noted in the surrounding region (Aggarwal, 1978). The primary conclusions of the cumulative work of Ratcliffe and his colleagues' with respect to the potential for Quaternary slip on the Ramapo fault are:

- The most recent episodes of slip along the Ramapo fault, as determined from rock core samples taken across the fault, were in a normal sense with some along-strike slip motion (i.e., oblique normal faulting). Ratcliffe and others concluded that the evidence for extension across the fault as the most recent slip and the lack of compression (i.e., thrust faulting), as would be required in the modern day stress field (Zoback, 1980) (Zoback, 1989), is evidence that the Ramapo fault has not been reactivated since the latest episode of extension in the Mesozoic.

- The Ramapo fault generally has a dip that is less than that inferred from the earthquake epicenters of Aggarwal and Sykes (Aggarwal, 1978), with the exception of the northernmost end of the fault where the dip measured from borings is approximately 70°. The implication of this observation is that earthquakes near the Ramapo fault hypothesized as being due to slip on the Ramapo fault are more likely occurring within the Proterozoic footwall rocks of the Ramapo fault.

Ratcliffe and his colleagues' results provide additional evidence of the uncertainty with respect to the potential activity of the Ramapo fault because they found positive evidence for a lack of slip along the fault since the Mesozoic.

Most, if not all, of this geologic and seismologic information was known at the time of the EPRI-SOG study (EPRI, 1986-1989) when the seismic source characterizations that are used as the base model for CCNPP Unit 3 were developed (Section 2.5.2). As such, the EPRI characterizations take into account uncertainty in the potential for the Ramapo fault to be a capable fault. For example, some of the EPRI Earth Science Teams explicitly characterized the Ramapo fault, and the probability of activity for the Ramapo fault given by those teams is less than 1.0 (Subsection 2.5.2.2.1).

Since the research pre-dating the ERPI-SOG study, there has been some additional research on the Ramapo fault. However, none of this additional research has provided any certainty with respect to the potential for activity of the Ramapo fault. For example, a fieldtrip guidebook of Kafka et al. (Kafka, 1989) for the New York region briefly discusses geomorphic evidence of the Ramapo fault including valley tilting, concentrations of terraces on only one valley side, and tributary offsets as evidence of Quaternary activity along the Ramapo fault. The use of these observations of Kafka et al. (Kafka, 1989) as evidence supporting Quaternary activity of the Ramapo fault should be treated cautiously based on the following:

- Kafka et al. (Kafka, 1989) present no data or evidence supporting these observations;

- Some of the noted geomorphic features may be older than Quaternary in age; and

- The observations themselves are not necessarily positive evidence of seismogenic, Quaternary faulting.

Newman et al. (Newman, 1987) (Newman, 1983) also presents observations that they interpret as evidence of Quaternary activity along the Ramapo fault. In their studies, Newman et al. (Newman, 1987) (Newman, 1983) constructed marine transgression curves based on radiocarbon dating of peat deposits for a series of tidal marsh sites along the Hudson River where it crosses the Ramapo fault. A total of eleven sites were investigated by Newman et al.

(Newman, 1987), six of which were within the Ramapo fault zone as it crosses Hudson River. Of the six sites within the Ramapo fault zone, Newman et al. (Newman, 1987) report that three of the sites show a discontinuity in transgression curves that they conclude reflects Holocene normal faulting within the Ramapo fault zone. These observations and conclusions of Newman et al. (Newman, 1987) (Newman, 1983) are questionable with respect to the argument for Quaternary faulting along the Ramapo fault because:

- There is considerable uncertainty in the radiocarbon and elevation data used to develop the transgression curves that was not clearly taken into account in testing the faulting or no faulting hypotheses;
- The sense of motion indicated by the transgression curves (normal faulting) is contrary to the current state of stress (reverse faulting is expected);
- Trenching studies across the Ramapo fault have not revealed any evidence of Quaternary faulting (Ratcliffe, 1990; Stone, 1984); and
- If the inferred offsets within the transgression curves are from fault movement, there is no evidence that the movement could have been accumulated through a seismic slip).

Finally, in an abstract for a regional Geological Society of America meeting, Nelson (Nelson, 1980) reported the results of pollen analysis taken from a core adjacent to the Ramapo fault near Ladentown, NY (Figure 2.5-227). In the brief abstract Nelson (Nelson, 1980) reports that the pollen history can be interpreted as either a "continuous, complete Holocene pollen profile suggesting an absence of postglacial seismicity along the fault" or as a pollen profile with a reversal, potentially suggesting a disruption of the infilling process caused by faulting. In summarizing his work, Nelson (Nelson, 1980) concludes that, "the pollen evidence is equivocal but certainly not strongly suggestive of seismicity."

More recently, another reanalysis of the seismicity within the region surrounding the Ramapo fault has been conducted by Sykes et al. (Sykes, 2008), who compiled a seismicity catalog extending from 1677 through 2006 for the greater New York City - Philadelphia area. This catalog contains 383 earthquakes occurring within parts of New York, Connecticut, Pennsylvania, and New Jersey (Figure 2.5-227). Of these 383 earthquakes, those occurring since 1974 are thought to have the best constraints on location due to the establishment of a more robust seismograph network at that time. Sykes et al. (Sykes, 2008) claim that one of the striking characteristics of their seismicity catalog is the concentration of seismicity within what they refer to as the Ramapo Seismic Zone (RSZ), a zone of seismicity approximately 7.5 mi (12 km) wide extending from the Ramapo fault to the west and from northern New Jersey north to approximately the Hudson River (Figure 2.5-227). The RSZ defined by Sykes et al. (Sykes, 2008) is approximately 200 mi (320 km) from the CCNPP site. All of the instrumentally located earthquakes within the RSZ have magnitudes less than mb 3.0 (Sykes, 2008). The only earthquake with mb > 3.0 is the historical mb 4.3 earthquake of 30 October 1783. However, uncertainty in the location of this earthquake is thought to be as much as 100 km (62 mi) (Sykes, 2008) raising significant suspicion as to whether the event occurred within the RSZ given the small extent of the RSZ relative to the location uncertainty.

From analyzing cross sections of the earthquakes, Sykes et al. (Sykes, 2008) concluded that the earthquakes within the RSZ occur within the highly deformed middle Proterozoic to early Paleozoic rocks to the west of the Mesozoic Newark basin and not the Ramapo fault proper. Figure 2.5-228 shows the Sykes et al. (Sykes, 2008) seismicity from the box in Figure 2.5-227 plotted along a cross section perpendicular to the Ramapo fault with the range of expected dips for the Ramapo fault (approximately 45° near the south end and 70° near the north end)

(Ratcliffe, 1980) (Ratcliffe, 1985a) (Sykes, 2008) specifically noted that, with the exception of three earthquakes with magnitudes less than or equal to mb 1.0 that are poorly located, earthquake hypocenters are almost vertically aligned beneath the surface trace of the Ramapo fault and not aligned with the Ramapo fault at depth (Figure 2.5-228). Instead of associating the earthquakes with the Ramapo fault, Sykes et al. (Sykes, 2008) attributed the observed seismicity within the RSZ to minor slip events on numerous small faults within the RSZ. However, neither Sykes et al. (Sykes, 2008), nor any other researchers (Kafka, 1985) (Wheeler, 2001) (Wheeler, 2005) (Wheeler, 2006) (Wheeler, 2008), have identified distinct faults on which they believe the earthquakes may be occurring thus preventing the characterization of any potentially active faults. Also, Sykes et al. (Sykes, 2008) only vaguely described the geometry of the RSZ and did not provide robust constraints on the geometry of the zone, the orientation of the potentially active faults they interpret to exist within the zone, or the maximum expected magnitude of earthquakes within the zone. As such, the Sykes et al. (Sykes, 2008) study presents no new information that suggests changes to the EPRI model are required to adequately represent the potential capability of the Ramapo fault or the Ramapo seismic zone.

A good summary of the current state of knowledge concerning the capability of the Ramapo fault is provided by Wheeler (Wheeler, 2006). While the Wheeler (Wheeler, 2006) paper did not consider the results of the Sykes et al. (Sykes, 2008) study, Wheeler's (Wheeler, 2006) comments accurately describe the current state of knowledge concerning the capability of the Ramapo fault of RSZ. Wheeler (Wheeler, 2006) states that: "No available arguments or evidence can preclude the possibility of occasional small earthquakes on the Ramapo fault or other strands of the fault system, or of rarer large earthquakes whose geologic record has not been recognized. Nonetheless, there is no clear evidence of Quaternary tectonic faulting on the fault system aside from the small earthquakes scattered within and outside the Ramapo fault system" (page 178). The implication for the CCNPP Unit 3 site is that there is no new information to suggest that the EPRI (EPRI, 1986) characterizations for the Ramapo fault do not adequately capture the current technical opinion with respect to the seismic hazard posed by the Ramapo fault or RSZ.

2.5.1.1.4.4.5.5 Kingston Fault

The Kingston fault is located in central New Jersey, approximately 175 mi (282 km) northeast of the CCNPP site (Figure 2.5-31) and (Figure 2.5-234). The Kingston fault is a 7 mi (11 km) long north to northeast-striking fault that offsets Mesozoic basement and is overlain by Coastal Plain sediments (Owens, 1998) (Figure 2.5-235) Stanford (Stanford, 1995) use borehole and geophysical data to interpret a thickening of as much as 80 ft (24 m) of Pliocene Pensauken Formation across the surface projection of the Kingston fault (Figure 2.5-236). Stanford (Stanford, 1995) interprets the thickening of the Pensauken Formation as a result of faulting rather than fluvial processes. Geologic cross sections prepared by Stanford (Stanford, 2002) do not show that the bedrock-Pensauken contact is vertically offset across the Kingston fault (Figure 2.5-236). Therefore, it seems reasonable to conclude that faulting of the Pensauken Formation is not required and that apparent thickening of the Pliocene gravels may represent a channel-fill from an ancient pre-Pliocene channel (Figure 2.5-236). Wheeler (Wheeler, 2006) reports that the available geologic evidence does not exclusively support a fault versus a fluvial origin for the apparent thickening of the Pensauken Formation. Wheeler (Wheeler, 2005) assigns the Kingston fault as a Class C feature based on a lack of evidence for Quaternary deformation. Given the absence of evidence for Quaternary faulting and the presence of undeformed Pleistocene glaciofluvial gravels overlying the fault trace, we conclude that the fault is not a capable tectonic feature.

2.5.1.1.4.4.5.6 New York Bight Fault

On the basis of seismic surveys, the New York Bight fault is characterized as an approximately 31 mile (50 km) long, north-northeast-striking fault, located offshore of Long Island, New York (Hutchinson, 1985) (Schwab, 1997a) (Schwab, 1997b) (Figure 2.5-31 and Figure 2.5-234). The fault is located about 208 mi (335 km) northeast of the CCNPP site. Seismic reflection profiles indicate that the fault originated during the Cretaceous and continued intermittently with activity until at least the Eocene. The sense of displacement is northwest-side down and displaces bedrock as much as 357 ft (109 m), and Upper Cretaceous deposits about 236 ft (72 m) (Hutchinson, 1985). High-resolution seismic reflection profiles that intersect the surface projection of the fault indicate that middle and late Quaternary sediments are undeformed within a resolution of 3 ft (1 m) (Hutchinson, 1985) (Schwab, 1997a) (Schwab, 1997b).

The Mesozoic New York Bight basin is located immediately east of the New York Bight fault (Hutchinson et al., 1986) (Figure 2.5-10). On the basis of seismic reflection data, Hutchinson (1986) interpret the basin to be structurally controlled by block faulting in the crystalline basement accompanied by syn-rift Mesozoic sedimentation. There is no evidence reported by Hutchinson (1986) that the basin bounding faults extend into the overlying Cretaceous sediments. Although not explicitly stated in the published literature (Hutchinson,1985) (Schwab, 1997a) (1997b), the association of the New York Bight fault along the western edge of the New York Bight basin suggests late Cretaceous through Eocene reactivation of the early Mesozoic basin bounding fault.

Only a few, poorly located earthquakes are spatially assoiciated within the vicinity of the New York Bight fault (Wheeler, 2006) (Figure 2.5-31 and Figure 2.5-234). Wheeler (Wheeler, 2006) defines the fault as a feature having insufficient evidence to demonstrate that faulting is Quaternary and assigns the New York Bight fault as a Class C feature. Based on the seismic reflection surveys of Schwab (Schwab, 1997a) (Schwab, 1997b) and Hutchinson (1985) and the absence of Quaternary deformation, we conclude that the New York Bight fault is not a capable tectonic source.

2.5.1.1.4.4.5.7 Cacoosing Valley Earthquake Sequence

The 1993 to 1997 Cacoosing Valley earthquake sequence occurred along the eastern margin of the Lancaster seismic zone with the main shock occurring on January 16, 1994, near Reading, Pennsylvania, about 135 mi (217 km) north of the CCNPP site (Seeber, 1998) (Figure 2.5-31). This earthquake sequence also is discussed as part of the Lancaster seismic zone discussion (Section 2.5.1.1.4.5.2). The maximum magnitude earthquake associated with this sequence is an event of mbLg 4.6 (Seeber, 1998). Focal mechanisms associated with the main shock and aftershocks define a shallow subsurface rupture plane confined to the upper 1.5 mi (2.4 km) of the crust. It appears that the earthquakes occurred on a pre-existing structure striking N45°W in contrast to the typical north-trending alignment of microseismicity that delineates the Lancaster seismic zone. Seeber (Seeber, 1998) use the seismicity data, as well as the shallow depth of focal mechanisms, to demonstrate that the Cacoosing Valley earthquakes likely were caused by anthropogenic changes to a large rock quarry. Wheeler (Wheeler, 2006) defines the fault as a feature having insufficient evidence to demonstrate that faulting is Quaternary and assigns the Cacoosing Valley earthquake sequence as a Class C feature. Based on the findings of Seeber (Seeber, 1998), we interpret this earthquake sequence to be unrelated to a capable tectonic source.

2.5.1.1.4.4.5.8 New Castle County Faults

The New Castle faults are interpreted as 3 to 4 mi (4.8 to 6.4 km) long buried north and northeast-striking basement faults (Spoljaric, 1972) (Spolijaric, 1973). The faults are interpreted

from structural contours of the top of Precambrian to Paleozoic crystalline basement derived from geophysical and borehole data, and define a 1 mi (1.6 km) wide, N25°E-trending graben in basement rock (Spoljaric, 1973). The faults are located in northern Delaware, near New Castle, about 97 mi (156 km) northeast of the CCNPP site (Figure 2.5-31). The graben is bounded by faults that displace the basement surface on the order of 32 to 98 ft (10 to 30 m) (Spoljaric, 1972). Spoljaric (1973) suggests that the overlying Cretaceous deposits are tilted in a direction consistent with fault deformation; however, no direct evidence is reported to indicate that the faults extend into the Cretaceous sediments. Sbar (Sbar, 1975) evaluates a 1973 M3.8 earthquake and its associated aftershocks, and note that the microseismicity defines a causal fault striking northeast and parallel to the northeast-striking graben of Spoljaric (Spoljaric, 1973). Subsequently, subsurface exploration by the Delaware Geological Survey (McLaughlin, 2002), that included acquisition of high resolution seismic reflection profiles, borehole transects, and paleoseismic trenching, provides evidence for the absence of Quaternary faulting on the New Castle faults. Wheeler (Wheeler, 2005) characterizes the New Castle County faults as a Class C feature. Based on McLaughlin (McLaughlin, 2002) there is strong evidence to suggest that the New Castle County faults as mapped by Spolijaric (Spolijaric, 1972) are not a capable tectonic source.

2.5.1.1.4.4.5.9 Upper Marlboro Faults

The Upper Marlboro faults are located in Prince George's County, Maryland, approximately 36 mi (58 km) northwest of the CCNPP site (Figure 2.5-31). These faults were first shown by Dryden (Dryden, 1932) as a series of faults offsetting Coastal Plain sediments. The faults were apparently exposed in a road cut on Crain Highway at 3.3 mi (5.3 km) south of the railroad crossing in Upper Marlboro, Maryland (Prowell, 1983). Two faults displace Miocene and Eocene sediments and a third fault is shown offsetting a Pleistocene unit. These faults are not observed beyond this exposure. No geomorphic expression has been reported or was noticed during field reconnaissance for the CCNPP Unit 3 study. Based on a critical review of available literature, Wheeler (Wheeler, 2006) re-interprets the Upper Marlboro faults as likely related to surficial landsliding because of the very low dips and concavity of the fault planes. The Marlboro faults are classified by Crone and Wheeler (Crone, 2000) and Wheeler (Wheeler, 2006), as a Class C feature based on a lack of evidence for Quaternary faulting. Given the absence of seismicity along the fault, lack of published literature documenting Quaternary faulting, coupled with the interpretation of Crone and Wheeler (Crone, 2000) and Wheeler (Wheeler, 2006), we conclude that the Upper Marlboro faults are not a capable tectonic source.

2.5.1.1.4.4.5.10 Lebanon Church Fault

The Lebanon Church fault is a poorly-known northeast-striking reverse fault located in the Appalachian Mountains of Virginia, near Waynesboro, about 119 mi (192 km) southwest of the CCNPP site (Prowell, 1983) (Figure 2.5-31). The fault is exposed in a single road cut along U.S. Route 250 as a small reverse fault that offsets Miocene-Pliocene terrace gravels up to as about 5 ft (1.5 m) (Prowell, 1983). The terrace gravels overlie Precambrian metamorphic rocks of the Blue Ridge Province. An early author (Nelson, 1962) considered the gravels to be Pleistocene, whereas Prowell (1983) interprets the gravel to be Miocene to Pliocene. Wheeler (Wheeler, 2006) classifies the Lebanon Church fault as a Class C feature having insufficient evidence to demonstrate that faulting is Quaternary. As part of this CCNPP Unit 3 study, inquiries with representatives with the Virginia Geological Survey and United States Geological Survey indicate that there is no new additional geologic information on this fault. Based on literature review, discussion with representatives with Virginia Geological Survey, as well as the absence of seismicity spatially associated with the feature, we conclude that the Lebanon Church fault is not a capable tectonic source.

2.5.1.1.4.4.5.11 Hopewell Fault

The Hopewell fault is located in central Virginia, approximately 89 mi (143 km) southwest of the CCNPP site (Figure 2.5-31). The Hopewell fault is a 30 mi (48 km) long, north-striking, steeply east-dipping reverse fault (Mixon, 1989) (Dischinger, 1987). The fault was originally named the Dutch Gap fault by Dischinger (Dischinger, 1987), and was renamed the Hopewell fault by Mixon (Mixon, 1989). The fault displaces a Paleocene-Cretaceous contact and is inferred to offset the Pliocene Yorktown Formation (Dischinger, 1987). Mixon (Mixon, 1989) extend the mapping of Dischinger (Dischinger, 1987), but include conflicting data regarding fault activity. For instance, a cross section presented by Mixon (Mixon, 1989) shows the Hopewell fault displacing undivided upper Tertiary and Quaternary units, whereas the geologic map used to produce the section depicts the fault buried beneath these units. A written communication from Newell (Wheeler, 2006) explains that the Hopewell fault was not observed offsetting Quaternary deposits and the representation of the fault in the Mixon (Mixon, 1989) cross section is an error. Thus, the Hopewell fault zone is assigned as a Class C feature because no evidence is available to demonstrate Quaternary surface deformation. Based on the written communication of Newell (Wheeler, 2006), an absence of published literature documenting Quaternary faulting, and an absence of seismicity spatially associated with the feature, we conclude that the Hopewell fault is not a capable tectonic source.

2.5.1.1.4.4.5.12 Old Hickory Faults

The Old Hickory faults are located near the Fall Line in southeastern Virginia, approximately 115 mi (185 km) south-southwest of the CCNPP site (Figure 2.5-31). Based on mining exposures of the Old Hickory Heavy Mineral deposit, the Old Hickory faults consist of a series of five northwest-striking reverse faults that offset Paleozoic basement and Pliocene Coastal Plain sediments. The northwest-striking reverse faults juxtapose Paleozoic Eastern Slate Belt diorite over the Pliocene Yorktown Formation (Berquist, 1999). Strike lengths range between 330 to 490 ft (100 to 150 m) and are spaced about 164 ft (50 m) apart. Berquist and Bailey (Berquist, 1999) report up to 20 ft (6 m) of oblique dip-slip movement on individual faults, and suggest that the faults may be reactivated Mesozoic structures. There is no stratigraphic or geomorphic evidence of Quaternary or Holocene activity of the Old Hickory faults (Berquist, 1999). Crone and Wheeler (Crone, 2000) and Wheeler (Wheeler, 2006) conclude that "no Quaternary fault is documented" and assign a Class C designation to the Old Hickory faults. Based on the absence of published literature documenting the presence of Quaternary deformation, and the absence of seismicity spatially associated with this feature, we conclude that the Old Hickory faults are not a capable tectonic source.

2.5.1.1.4.4.5.13 Stanleytown-Villa Heights Faults

The postulated Stanleytown-Villa Heights faults are located in the Piedmont of southern Virginia, approximately 223 mi (359 km) southwest of the CCNPP site (Figure 2.5-31). The approximately 660 ft long (201 m long) faults juxtapose Quaternary alluvium against rocks of Cambrian age, and reflect an east-side-down sense of displacement (Crone, 2000). No other faults are mapped nearby (Crone, 2000). Geologic and geomorphic evidence suggests the "faults" are likely the result of landsliding. Crone and Wheeler (Crone, 2000) classify the Stanleytown-Villa Heights faults as a Class C feature based on lack of evidence for Quaternary faulting. Based on the absence of published literature documenting the presence of Quaternary faulting, and the absence of seismicity spatially associated with this feature, we conclude that the Stanleytown-Villa Heights faults are not a capable tectonic source.

2.5.1.1.4.4.5.14 East Coast Fault System

The postulated East Coast fault system (ECFS) of Marple and Talwani (2000) trends N34°E and is located approximately 70 mi (113 km) southwest of the site (Figure 2.5-31). The 370 mi

(595 km) long fault system consists of three approximately 125 mi (201 km) long segments extending from the Charleston area in South Carolina northeastward to near the James River in Virginia (Figure 2.5-31). The three segments were initially referred to as the southern, central, and northern zones of river anomalies (ZRA-S, ZRA-C, ZRA-N) and are herein referred to as the southern, central and northern segments of the ECFS. The southern segment is located in South Carolina; the central segment is located primarily in North Carolina. The northern segment, buried beneath Coastal Plain deposits, extends from northeastern North Carolina to southeastern Virginia, about 70 mi (113 km) southwest of the CCNPP site. Marple and Talwani (Marple, 2000) map the northern terminus of the ECFS between the Blackwater River and James River, southeast of Richmond. Identification of the ECFS is based on the alignment of geomorphic features along Coastal Plain rivers, areas suggestive of uplift, and regions of local faulting. The right-stepping character of the three segments, coupled with the northeast orientation of the fault system relative to the present day stress field, suggests a right-lateral strike-slip motion for the postulated ECFS (Marple and Talwani, 2000).

The southern segment of the fault system, first identified by Marple and Talwani (1993) as an approximately 125 mi (201 km) long and 6 to 9 mi (10 to 14.5 km) wide zone of river anomalies, has been attributed to the presence of a buried fault zone. The southern end of this segment is associated with the Woodstock fault, a structure defined by fault-plane solutions of microearthquakes and thought to be the causative source of the 1886 Charleston earthquake (Marple, 2000). The southern segment is geomorphically the most well-defined segment of the fault system and is associated with micro-seismicity at its southern end. This segment was included as an alternative geometry to the areal source for the 1886 Charleston earthquake in the 2002 USGS hazard model (Section 2.5.2) for the National Seismic Hazard Mapping Project (Frankel, 2002).

Crone and Wheeler (Crone, 2000) do not include the central and northern segments of the ECFS in their compilation of potentially active Quaternary faults. The segments also were not presented in workshops or included in models for the Trial Implementation Project (TIP), a study that characterized seismic sources and ground motion attenuation models at two nuclear power plant sites in the southeastern United States (Savy, 2002). As a member of both the USGS and TIP workshops, Talwani did not propose the northern and central segments of the fault system for consideration as a potential source of seismic activity. There is no pre-EPRI or post-EPRI seismicity spatially associated with the northern and central segments of the fault system.

Recent geologic and geomorphic analysis of stream profiles across sections of the ECFS, and critical evaluation of Marple and Talwani (Marple, 2000) for the North Anna ESP, provides compelling evidence that the northern segment of the ECFS, which lies nearest to the CCNPP site, has a very low probability of existence (Dominion, 2004b). Wheeler (Wheeler, 2005) states that although the evidence for a southern section of the ECFS is good, there is less evidence supporting Quaternary tectonism along the more northerly sections of the ECFS, and designates the northern portion of the fault system as a Class C feature.

In the Safety Evaluation Report for the North Anna ESP site, the NRC staff agreed with the assessment of the northern segment of the East Coast Fault System (ECFS-N) presented by the North Anna applicant (NRC, 2005). Based on their independent review, the NRC staff concluded that:

- "Geologic, seismologic, and geomorphic evidence presented by Marple and Talwani is questionable."

- "The majority of the geologic data cited by Marple and Talwani in support of their postulated ECFS apply only to the central and southern segments."
- There are "no Cenozoic faults or structure contour maps indicating uplift along the ECFS-N."
- "The existence and recent activity of the northern segment of the ECFS is low."

Despite the statements above, the NRC concluded that the ECFS-N could still be a contributor to the seismic hazard at the North Anna site and should be included in the ground motion modeling to determine the Safe Shutdown Earthquake. The NRC agreed with the 10% probability of existence and activity proposed in the North Anna ESP application. The results of the revised ground motion calculations indicate that the ECFS-N does not contribute to the seismic hazard at the North Anna ESP site. The CCNPP site is approximately 70 mi (113 km) northeast of the ECFS-N, or 7 mi (11 km) further away than the North Anna site is from the ECFS-N. Based on the above discussion and the large distance between the site and the ECFS-N, this fault is not considered a contributing seismic source and need not be included in the seismic hazard calculations for the CCNPP site.

Marple and Talwani (Marple, 2004) suggest a northeast extension of the ECFS of Marple and Talwani (Marple, 2000), based on existing limited geologic, geophysical and geomorphic data. Marple and Talwani (Marple, 2004) postulate that the northern ECFS may step left (northwest) to the Stafford fault system near northern Virginia and southern Maryland (Figure 2.5-31) and thus extending the ECFS along the Stafford fault up to New York. As stated in Section 2.5.1.1.4.4.4.1, the NRC (NRC, 2005) agreed with an analysis of the Stafford fault performed as part of the North Anna ESP application and states: "Based on the evidence cited by the applicant, in particular the applicant's examination of the topography profiles that cross the fault system, the staff concludes that the applicant accurately characterized the Stafford fault system as being inactive during the Quaternary Period."

In summary, the ECFS in its entirety represents a new postulated tectonic feature that was not known to the EPRI Earth Science Teams in 1986. The 1986 EPRI models include areal sources to model the Charleston seismic source; therefore, the southern segment of the East Coast fault system is in essence covered by the different Charleston sources zone geometries. A review of the seismic sources that contribute 99% of the seismic hazard to the CCNPP shows that the Charleston source is not a contributor. The central and northern segments of the ECFS represent a new tectonic feature in the Coastal Plain that postdates the EPRI studies. The closest approach of the northern segment to the site is approximately 77 mi (124 km) as described above. Although the postulated ECFS represents a potentially new tectonic feature in the Coastal Plain of Virginia and North Carolina (Marple, 2000), current interpretations of the ECFS based on existing data indicate that the fault zone probably does not exist (especially the northern segment) and, if it does exists, has a very low probability of activity and does not contribute to hazard at the site.

2.5.1.1.4.5 Seismic Sources Defined by Regional Seismicity

Within 200 mi (322 km) of the CCNP site, two potential seismic sources are defined by a concentration of small to moderate earthquakes. These two seismic sources include the Central Virginia seismic zone in Virginia and the Lancaster seismic zone in southeast Pennsylvania, both of which are discussed below (Figure 2.5-31).

2.5.1.1.4.5.1 Central Virginia Seismic Zone

The Central Virginia seismic zone is an area of persistent, low level seismicity in the Piedmont Province (Figure 2.5-24 and Figure 2.5-31). The zone extends about 75 mi (121 km) in a north-south direction and about 90 mi (145 km) in an east-west direction from Richmond to Lynchburg and is coincident with the James River (Bollinger, 1985). The CCNPP site is located 47 to 62 mi (76 to 100 km) northeast of the northern boundary of the Central Virginia seismic zone. The largest historical earthquake to occur in the Central Virginia seismic zone was the body-wave magnitude (mb) 5.0 Goochland County event on December 23, 1875 (Bollinger, 1985). The maximum intensity estimated for this event was Modified Mercalli Intensity (MMI) VII in the epicentral region. More recently, an mb 4.5 earthquake (two closely-spaced events that when combined = Mw 4.1) occurred on December 9, 2003 within the Central Virginia seismic zone (Kim and Chapman, 2005). The December 9, 2003 earthquake occurred close to the Spotsylvania fault, but due to the uncertainty in the location of the epicenter (3.7 to 5 mi (6 to 8 km)), no attempt could be made to locate the epicenter with a specific fault or geologic lineament in the CVSZ (Kim, 2005).

Seismicity in the Central Virginia seismic zone ranges in depth from about 2 to 8 mi (3 to 13 km) (Wheeler, 1992). It is suggested (Coruh, 1988) that seismicity in the central and western parts of the zone may be associated with west-dipping reflectors that form the roof of a detached antiform, while seismicity in the eastern part of the zone near Richmond may be related to a near-vertical diabase dike swarm of Mesozoic age. However, given the depth distribution of 2 to 8 mi (3 to 13 km) (Wheeler, 1992) and broad spatial distribution, it is difficult to uniquely attribute the seismicity to any known geologic structure and it appears that the seismicity is generally above the Appalachian detachment.

No capable tectonic sources have been identified within the Central Virginia seismic zone, but two paleo-liquefaction sites have been identified within the seismic zone (Crone, 2000) (Obermier, 1998). The presence of these paleo-liquefaction features on the James and Rivanna Rivers shows that the Central Virginia seismic zone reflects both an area of paleo-seismicity as well as observed historical seismicity. Based on the absence of widespread paleo-liquefaction, however, it was concluded (Obermier, 1998) that an earthquake of magnitude 7 or larger has not occurred within the seismic zone in the last 2,000 to 3,000 years, or in the eastern portion of the seismic zone for the last 5,000 years. It was also conclude that the geologic record of one or more magnitude 6 or 7 earthquakes might be concealed between streams, but that such events could not have been abundant in the seismic zone. In addition, these isolated locations of paleo-liquefaction may have been produced by local shallow moderate magnitude earthquakes of M 5 to 6.

The paleo-liquefaction sites reflect pre-historical occurrences of seismicity within the Central Virginia seismic zone, and do not indicate the presence of a capable tectonic source. Recently, Wheeler (Wheeler, 2006) hypothesizes that there may be two causative faults for the small dikes of Obermier and McNulty (Obermier, 1998), and that earthquakes larger than those represented by historic seismicity are possible; whereas Marple and Talwani (Marple, 2004) interpret seismicity data to infer the presence of a hypothesized northwest-trending basement fault (Shenandoah fault) that coincides with the Norfolk fracture zone (Marple, 2004). However, no definitive causative fault or faults have been identified within the Central Virginia seismic zone (Wheeler, 2006).

The 1986 EPRI source model includes various source geometries and parameters to capture the seismicity of the Central Virginia seismic zone. Subsequent hazard studies have used maximum magnitude (M_{max}) values that are within the range of maximum magnitudes used

by the six EPRI models. Collectively, upper-bound maximum values of M_{max} used by the EPRI teams range from mb 6.6 to 7.2 (Section 2.5.2.2). More recently, Bollinger (Bollonger, 1992) has estimated a M_{max} of mb 6.4 for the Central Virginia seismic source. Also, Chapman and Krimgold (Chapman, 1994) have used a M_{max} of Mw 7.53 (mb 7.25) for the Central Virginia seismic source zone based on the estimated magnitude of the 1886 Charleston earthquake. More recent estimates of the 1886 earthquake magnitude are lower (Bakun and Hopper, 2004; Johnston, 1996) indicating that the M_{max} of Chapman and Krimgold (Chapman, 1994) should also be lowered. These more recent estimates of M_{max} values for the Central Virginia seismic zone are within the range of the M_{max} values used in the 1986 EPRI studies (Section 2.5.2.2.1.7). Also, the distribution and rate of seismicity in the Central Virginia seismic source have not changed since the 1986 EPRI study (Section 2.5.2.2.8). Thus, there is no new information or data that motivates modifying the source geometry, rate of seismicity, or M_{max} values for the Central Virginia seismic zone in the EPRI-SOG model. The same conclusion was reached in the North Anna ESP application, and in 2005 the NRC agreed with this conclusion (NRC, 2005).

2.5.1.1.4.5.2 Lancaster Seismic Zone

The Lancaster seismic zone, as defined by Armbruster and Seeber (Armbruster, 1987), of southeast Pennsylvania has been a persistent source of seismicity for at least two centuries. The seismic zone is about 80 mi (129 km) long and 80 mi (129 km) wide and spans a belt of allochthonous Appalachian crystalline rocks between the Great Valley and Martic Line about 111 mi (179 km) northwest of the CCNPP site (Figure 2.5-31). The Lancaster seismic zone crosses exposed Piedmont rocks that include thrust faults and folds associated with Paleozoic collisional orogenies. It also crosses the Newark-Gettysburg Triassic rift basin which consists of extensional faults associated with Mesozoic rifting. Most well-located epicenters in the Lancaster seismic zone lie directly outside the Gettysburg-Newark basin (Scharnberger, 2006). The epicenters of 11 events with magnitudes 3.04 to 4.61 rmb from 1889 to 1994 from the western part of Lancaster seismic zone define a north-south trend that intersects the juncture between the Gettysburg and Newark sub-basins. This juncture is a hinge around which the two sub-basins subsided, resulting in east-west oriented tensile stress. Numerous north-south trending fractures and diabase dikes are consistent with this hypothesis. It is likely that seismicity in at least the western part of the Lancaster seismic zone is due to present-day northeast-southwest compressional stress which is activating the Mesozoic fractures, with dikes perhaps serving as stress concentrators (Armbruster, 1987).

It also is probable that some recent earthquakes in the Lancaster seismic zone have been triggered by surface mining. For instance, the 16 January 1994 Cacoosing earthquake (mb 4.6) is the largest instrumented earthquake occurring in the Lancaster seismic zone (Section 2.5.1.1.4.4.5.7). This event was part of a shallow (depths generally less than 1.5 mi (2.4 km)) earthquake sequence linked to quarry activity (Seeber, 1998). The earthquake sequence that culminated in the January 16 event initiated after a quarry was shut down and the quarry began to fill with water. Seeber (Seeber, 1998) interprets the reverse-left lateral oblique earthquake sequence to be due to a decrease in normal stress caused by quarrying followed by an increase in pore fluid pressure (and decrease in effective normal stress) when the pumps were turned off and the water level increased.

Prior to the Cacoosing earthquake sequence, the 23 April 1984 Martic earthquake (mb 4.1) was the largest instrumented earthquake in the seismic zone and resembles pre-instrumental historical events dating back to the middle 18th century (Armbruster, 1987). The 1984 earthquake sequence appears centered at about 2.8 mi (4.5 km) in depth and may have ruptured a steeply east-dipping, north-to northeast-striking fault aligned subparallel to Jurassic dikes with a reverse-right lateral oblique movement, consistent with east-northeast

horizontal maximum compression. These dikes are associated with many brittle faults and large planes of weakness suggesting that they too have an effect on the amount of seismicity in the Lancaster seismic zone (Armbruster, 1987). Most of the seismicity in the Lancaster seismic zone is occurring on secondary faults at high angles to the main structures of the Appalachians (Armbruster, 1987) (Seeber, 1998). The EPRI study (EPRI, 1986) source models do not identify the Lancaster seismic zone as a separate seismic source. However, the 5.3 to 7.2 Mb maximum magnitude distributions of EPRI source zones are significantly greater than any reported earthquake in this Lancaster seismic zone. Thus, the EPRI study (EPRI, 1986) models adequately characterized this region and no significant update is required.

2.5.1.2 Site Geology

Sections 2.5.1.2.1 through 2.5.1.2.6 are added as a supplement to the U.S. EPR FSAR.

2.5.1.2.1 Site Area Physiography and Geomorphology

The CCNPP site area is located within the Western Shore Uplands of the Atlantic Coastal Plain Physiographic Province and is bordered by the Chesapeake Bay to the east and the Patuxent River to the west (Figure 2.5-4 and Figure 2.5-7).

The site vicinity geologic map (Figure 2.5-27 and Figure 2.5-28), compiled from the work of several investigators, indicates that the counties due east from the CCNPP site across Chesapeake Bay are underlain by Pleistocene to Recent sands. Most of the site vicinity is underlain by Tertiary Coastal Plain deposits. Quaternary to Recent alluvium beach deposits and terrace deposits are mapped along streams and estuaries. Quaternary terrace and Lowland deposits are shown in greater detail on the scale of the site area geologic map (Figure 2.5-32). Geologic cross sections in the site area indicate that the Tertiary Upland deposits are underlain by gently dipping Tertiary Coastal Plain deposits described in Section 2.5.1.2.2 (Figure 2.5-33).

The topography within 5 mi (8 km) of the site consists of gently rolling hills with elevations ranging from about sea level to nearly 130 ft (40 m) msl (Figure 2.5-4). The site is well-drained by short, ephemeral streams that form a principally dendritic drainage pattern with many streams oriented in a northwest-southeast direction (Figure 2.5-5). As shown on the site area and site topographic and geological maps, the ground surface above approximately 100 ft (30 m) msl is capped by the Upper Miocene-Pliocene Upland deposits (Figure 2.5-4, Figure 2.5-5, Figure 2.5-32, and Figure 2.5-33). These deposits occupy dissected upland areas of the Cove Point quadrangle in which the CCNPP site is located (Figure 2.5-32 and Figure 2.5-33) (Glaser, 2003a). The longest stream near the site is Johns Creek, which is approximately 3.5 mi (5.6 km) long before it drains into St. Leonard Creek (Figure 2.5-4 and Figure 2.5-34). The ephemeral stream channels near the CCNPP site are either tributary to Johns Creek or flow directly to the Chesapeake Bay. These stream channels maintain their dendritic pattern as they cut down into the underlying Choptank and St. Marys Formations (Figure 2.5-27, Figure 2.5-32 and Figure 2.5-33).

The Chesapeake Bay shoreline forms the eastern boundary of the CCNPP site and generally consists of steep cliffs with narrow beach at their base. The cliffs reach elevations of about 100 ft (30 m) msl along the eastern portion of the site's shoreline. Narrow beaches whose width depends upon tidal fluctuations generally occur at the base of the cliffs. Field observations indicate that these steep slopes fail along nearly vertical irregular surfaces. The slope failure appears to be caused by shoreline erosion along the base of the cliffs. Shoreline processes and slope failure along Chesapeake Bay are discussed in Section 2.4.9. Approximately 2500 ft (762 m) of the shoreline from the existing CCNPP Units 1 and 2 intake

structure southward to the existing barge jetty is stabilized against shoreline erosion (Figure 2.5-50). The CCNPP Unit 3 will be constructed at a final grade elevation of approximately 85 ft (26 km) msl and will be set back approximately 1,000 ft (305 m) from the Chesapeake Bay shoreline.

As described in Section 2.5.1.1.1, the Chesapeake Bay was formed toward the end of the Wisconsinan glacial stage, which marked the end of the Pleistocene epoch. As the glaciers retreated, the huge volumes of melting ice fed the ancestral Susquehanna and Potomac Rivers, which eroded older Coastal Plain deposits forming a broad river valley. The rising sea level covered the Continental Shelf and reached the mouth of the Bay about 10,000 years ago. Sea level continued to rise, eventually submerging the area now known as the Susquehanna River Valley prior to sea level dropping to the current elevation. The Bay assumed its present dimensions about 3000 years ago (Section 2.4.9).

2.5.1.2.2 Site Area Geologic History

The site area geologic history prior to the early Cretaceous is inferred from scattered borehole data, geophysical surveys and a synthesis of published information. These data indicate that the rock beneath the Coastal Plain sediments in the site area may be either extended or rifted exotic crystalline magmatic arc material (Glover, 1995b) or, alternatively, Triassic rift basin sediments (Benson, 1992). Although the base of the Coastal Plain section has not been penetrated directly beneath the site with drill holes, regional geologic cross sections developed from geophysical, gravity and aeromagnetic, as well as limited deep borehole stratigraphic data beyond the site area, suggest that the base of the Coastal Plain section is most likely at a depth of about 2,600 ft (792 m) beneath the site (Section 2.5.1.2.3 and Section 2.5.1.2.4).

Tectonic models discussed in Section 2.5.1.1.4.3.1 hypothesize that the crystalline basement was first accreted to the pre-Taconic North American margin during the Paleozoic along a suture that lies about 10 mi (16 km) west of the site (Klitgord, 1995) (Figure 2.5-17 and Figure 2.5-23). These models also suggest this basement is rifted crust that was thinned after accretion during the Mesozoic rifting of Pangea (Section 2.5.1.1.4.1.2). Therefore, the crystalline basement beneath the Coastal Plain sediments in the site area might consist of an accreted nappe-like block of Carolina-Chopawamsic magmatic arc terrane with windows of Laurentian Grenville basement cut by later phase normal faults (Figure 2.5-16 and Figure 2.5-17) (Klitgord, 1995).

As discussed in Section 2.5.1.1.2, Section 2.5.1.1.4.4.3, and Section 2.5.1.2.4, Mesozoic rift basins are exposed in the Piedmont Physiographic Province and are buried beneath Coastal Plain sediments (Figure 2.5-10). Whether or not the CCNPP Site is underlain by a Mesozoic basin (e.g., the Queen Anne Basin) preserved beneath the thick Coastal Plain section is unclear. The available data in the site area include only regional gravity and aeromagnetic data that allow multiple (often contradictory) interpretations of the location of a basin at or near the CCNPP Site beneath the Coastal Plain sediments. For example, Horton (1991) (Figure 2.5-9 and Figure 2.5-16) and Benson (1992) (Figure 2.5-10) show the CCNPP site underlain by the Mesozoic Queen Anne basin, whereas Schlische (1990) (Figure 2.5-22) and Withjack (1998) (Figure 2.5-10) do not show a Mesozoic basin beneath the site. There are no deep boreholes or seismic lines that allow for a definitive interpretation of the presence, geometry, or thickness of a Mesozoic rift basin beneath the CCNPP site. See Section 2.5.1.1.4.4.3 for further discussion regarding the Queen Anne basin.

During the early Cretaceous, sands, clays, sandy clays, and arkosic sands of the Arundel/ Patuxent Formations (undivided) were deposited on the crystalline basement in a continental and fluviatile environment. Individual beds of sand or silt grade rapidly into sediments with different compositions or gradations, both vertically and horizontally, which suggests they were deposited in alluvial fan or deltaic environments. Clay layers containing carbonized logs, stumps and other plant remains indicate the existence of quiet-water, swamp environments between irregularly distributed stream channels. Thicker clays near the top of this unit in St. Mary's County are interpreted to indicate longer periods of interfluvial quiet water deposition (Hansen, 1984).

The overlying beds of the Patapsco Formation are similar to the deposits in the Arundel/ Patuxent (undivided) formations and consist chiefly of materials derived from the eroded crystalline rocks of the exposed Piedmont to the west and reworked Lower Cretaceous sediments. These sediments were deposited in deltaic and estuarine environments with relatively low relief. The Upper Cretaceous Raritan Formation appears to be missing from the site area due either to non-deposition or erosion on the northern flank of the structurally positive Norfolk Arch.

The Magothy Formation represents deposits from streams flowing from the Piedmont and depositing sediments in the coastal margins of the Upper Cretaceous sea. Subsequent uplift and tilting of the Coastal Plain sediments mark the end of continental deposition and the beginning of a marine transgression of the region. This contact is a regional unconformity marked in places by a basal layer of phosphatic clasts in the overlying Brightseat Formation.

During the Early Paleocene Epoch, the Brightseat Formation marks a marine advance in the Salisbury embayment (Ward, 2004). Uplift or sea level retreat is indicated by the burrowed contact (unconformity) of the Brightseat Formation with the overlying Aquia Formation. The marine Aquia Formation which is noted for its high glauconite content and shell beds was deposited in a shoaling marine environment indicated by a generally coarsening upward lithology (Hansen, 1996). A mix of light-colored quartz grains and greenish to blackish glauconite grains and iron staining indicated the change to a sandbank facies in the upper Aquia formation (Hansen, 1996). A marine transgression during the Late Paleocene/Early Eocene into the central portion of the Salisbury Embayment deposited the Marlboro Clay (Ward, 2004). During the Early Eocene, a moderately extensive marine transgression deposited the Potopaco Member of the Nanjemoy Formation. A subsequent transgression deposited the Woodstock Member of the Nanjemoy Formation (Ward, 2004). The most extensive marine transgression during the middle Eocene resulted in the deposition of the Piney Point Formation (Ward, 2004). The site area may have been emergent during the Oligocene as the Late Oligocene Old Church Formation indicates sea level rise and submergence to the north and south of the site area (Ward, 2004). A brief regression was followed by nearly continuous sedimentation in the Salisbury Embayment punctuated by short breaks, resulting in a series of thin, unconformity-bounded beds (Ward, 2004). A series of marine transgressions into the Salisbury Embayment during the Miocene produced the Calvert, Choptank and St. Marys Formations. Pliocene and Quaternary geologic history is discussed in Section 2.5.1.2.1.

2.5.1.2.3 Site Area Stratigraphy

The CCNPP site area is located on Coastal Plain sediments ranging in age from Lower Cretaceous to Recent, which, in turn, were deposited on the pre-Cretaceous basement. As discussed above in Section 2.5.1.2.2, there is uncertainty regarding whether Mesozoic rift basin deposits underlie the Coastal Plain sediments or whether the Coastal Plain sediments are deposited directly over extended crystalline basement. Figure 2.5-36 is a site-specific

stratigraphic column based on correlations by Hansen (Hansen, 1996), Achmad and Hansen (Achmad, 1997) and Ward and Powars (Ward, 2004).

Site specific information on the stratigraphy underlying the CCNPP site is constrained by the total depths of the various borings advanced by site investigators over the years. Figure 2.5-35 shows the locations of the various borings at the site and identifies those completed as either water supply wells or observation wells based on the 2007 drilling program and the plot plan at that time. Many of these borings were drilled to 200 ft (61 m) in total depth; two were advanced to a total depth of 400 ft (122 m). Figure 2.5-103 includes the additional boring locations based on the 2008 drilling program. Only a few scattered borings have been advanced below the Aquia Formation (Figure 2.5-13)(Hansen, 1986). The deepest boring known to have been advanced at the site is CA-Ed 22 which was drilled to a total depth of 789 ft (240 m) and completed as a water supply well in 1968 (Hansen, 1996). This boring penetrates the full Tertiary stratigraphic section and intersects the contact between the Tertiary and the Cretaceous section at the base of the Aquia Formation.

The closest boring which advances to pre-Cretaceous bedrock is approximately 13 mi (21 km) south of the site at Lexington Park in St. Mary's County, (Figure 2.5-11) (Hansen, 1986). This boring cored a Jurassic diabase dike that may have intruded either Triassic rift-basin deposits or extended crystalline basement (Section 2.5.1.1.3). The few other borings that have reached basement rock near the site are widely scattered (Figure 2.5-11) but the majority indicates that the crystalline basement beneath the site area is likely to be similar to the schists and gneisses found in the Piedmont Physiographic Province approximately 50 mi (80 km) to the west (Figure 2.5-1). Alternatively, this crystalline basement might have been accreted to the exposed Piedmont as a result of continental collision during a Paleozoic orogeny (Section 2.5.1.1.1.4 and Section 2.5.1.2.2).

Coastal Plain sediments were deposited in a broad basement depression known as the Salisbury Embayment extending from eastern Virginia to southern New Jersey (Figure 2.5-12) (Ward, 2004). These sediments were deposited during periods of marine transgression/ regression and exhibit lateral and vertical variation in both lithology and texture.

2.5.1.2.3.1 Lower Cretaceous Potomac Group and pre-Potomac sediments

As discussed in Section 2.5.1.1.3, Hansen and Wilson (Hansen, 1984) assign the lowermost 30 ft (9 m) of the Lexington Park well (SM-Df 84), 13 mi (21 km) south of the CCNPP site (Figure 2.5-11) (Hansen, 1986), to the Waste Gate formation. These sediments are described as gray silts and clays, interbedded with fine to medium silty fine to medium sands. Although these sediments might correlate with the Waste Gate Formation identified in a well in Crisfield, Maryland (Do-CE 88), east of the Chesapeake Bay (Figure 2.5-11), there is no direct evidence indicating whether this unit occurs beneath the CCNPP site.

The Potomac Group is comprised of a sequence of interbedded sands and silty to fine sandy clays. Because this formation was not encountered by any borings drilled at the CCNPP site, the description of these units is based on published data (Hansen, 1984) (Achmad, 1997). Regionally, the Potomac Group consists of, from oldest to youngest, the Patuxent Formation, the Arundel Formation and the Patapsco Formation. These units are considered continental in origin and are in unconformable contact with each other.

The Lower Cretaceous Patuxent Formation consists of a sequence of variegated sands and clays which form a major aquifer in the Baltimore area, approximately 50 mi (80 km) up-dip from the site, but which have not been tested in the vicinity of the site. The nearest well

intercepting the Patuxent is approximately 13 mi (21 km) south of the site and here the formation contains much less sand than is found in the upper part of the Potomac Group. The Patuxent is approximately 600 to 700 ft (182 m to 213 m) thick and is overlain by the Arundel/ Patapsco formations (undivided)

In the Baltimore area, the Arundel Formation consists of clays which are brick red near the Fall Line. Further down-dip toward the southeast, the color changes to gray and this unit is difficult to separate in the subsurface from those clays present in the underlying Patuxent and overlying Patapsco formations. Consequently, the Arundel and the Patuxent are often undivided (Hansen, 1984) in the literature and referred as the Arundel/Patuxent formations (undivided). Hansen and Wilson (Hansen, 1984) describe the upper portion of the Arundel/ Patuxent formations (undivided) as variegated silty clay with thin very fine sand and silt interbeds that may be as thick as 150 to 200 ft (46 to 61 m) beneath the CCNPP site (Figure 2.5-13). The Arundel Formation is not recognized in southern Maryland (Hansen, 1996).

2.5.1.2.3.2 Upper Cretaceous Formations

The Patapsco formation is the uppermost unit in the Potomac Group and consists of gray, brown and red variegated silts and clays interbedded with lenticular, cross-bedded clayey sands and minor gravels. This formation is a major aquifer near the Fall Line in the Baltimore area, but the Patapsco is untested near the CCNPP site. The thickness of the Patapsco Formation based on regional correlations is 1,000 to 1,100 ft thick beneath the CCNPP site.

The Mattaponi (?) formation described as overlying the Potomac group in Hansen and Wilson (Hansen, 1984) is no longer recognized by the Maryland Geological Survey. The section formerly assigned to the Mattaponi (?) has been included within the Patapsco Formation.

The Magothy Formation unconformably overlies the Patapsco Formation beneath the site. The Magothy is comprised chiefly of pebbly, medium coarse sand, although there are clayey portions in the upper part (Achmad, 1997). This formation is much thinner at the site than further north in Calvert County and pinches out within a few mi to the south (Achmad, 1997). The Monmouth and Matawan formations have not been differentiated from the Magothy Formation in the site area.

2.5.1.2.3.3 Tertiary Formations

The earliest Tertiary sediments beneath the site are assigned to the Lower Paleocene Brightseat Formation, a thin dark gray sandy clay identified in the deepest boring (CA-Ed 22) at the site as the Lower Confining Unit (Figure 2.5-13). The Brightseat Formation is identified in the gamma log as a higher than normal gamma response below the Aquia sand. According to Ward and Powars (Ward, 2004) the Brightseat Formation marks a marine advance in the Salisbury Embayment and occurs principally in the northeastern portion of the Embayment. This stratigraphic unit was reached by the water supply well CA-Ed 22 in 1968 (Figure 2.5-13). Achmad and Hansen (Achmad, 1997) describe the Brightseat Formation as approximately 10 ft (3 m) thick consisting mainly of very fine sand and clay with a bioturbated fabric. The absence of a bioturbated contact with the underlying beds suggests an unconformable contact.

The Aquia Formation unconformably overlies the Brightseat Formation and consists of clayey, silty, very shelly glauconitic sand (Ward, 2004). Microfossil study has placed the Aquia in the upper Paleocene. In the type section, the Aquia Formation is divided into two members, the Piscataway Creek and the Paspotansa, but at the CCNPP site, these members are not differentiated. Achmad and Hansen (Achmed, 1997) describe the Aquia Formation as

approximately 150 ft (46 m) thick. The sand becomes fine-grained in the lower 50 ft (15 m) of the formation.

The Marlboro clay is a silvery-gray to pale-red plastic clay interbedded with yellowish-gray to reddish silt occurring at the base of the Nanjemoy Formation (Ward, 2004). Achmad and Hansen (1997) describe approximately 10 ft (3 m) of clay with thin, indistinct laminae of differing colored silt. Its contact with the underlying Aquia Formation is somewhat gradational while the contact between the Marlboro and the overlying Nanjemoy appears to be sharp indicating that the Nanjemoy unconformably overlies the Marlboro. Microfossil studies indicate the presence of a mixture of very late Paleocene and very early Eocene flora. Based on geophysical logs from CA-Ed 22, the Marlboro clay appears to be approximately 15 ft (4.6 m) thick beneath the CCNPP site (Figure 2.5-13).

At the CCNPP site, the Nanjemoy Formation is divided into the Potapaco and Woodstock members between the overlying Piney Point Formation and the underlying Marlboro clay. The Nanjemoy Formation is described as olive black, very fine grained, well-sorted silty glauconitic sands (Ward, 2004). Based on electric log data, the thickness of the Nanjemoy Formation beneath the CCNPP site is approximately 180 ft (55 m). About 80 ft (24 m) of this unit was penetrated by CCNPP Unit 3 borings, B-301 and B-401 (Figure 2.5-37 and Figure 2.5-38), drilled during the subsurface investigation.

The Piney Point Formation is a thin glauconitic sand and clay unit unconformably overlying the Nanjemoy formation. According to Achmad and Hansen (Achmad, 1997), the Piney Point is approximately 20 ft (6 m) thick at the CCNPP site and extends from about the middle of Calvert County, north of the CCNPP site, toward the south to beyond the Potomac River; increasing in thickness to approximately 130 ft (40 m) at Point Lookout at the confluence of the Potomac River and Chesapeake Bay. Formerly considered late Eocene in age, the Piney Point is assigned to the middle Eocene (Achmad, 1997) (Ward, 2004). The unit has a distinctive natural gamma signature associated with the presence of glauconite and is a useful marker bed.

This distinctive natural gamma signature is present in boring B-301 at a depth of 302 ft (92 m) (205 ft (62 m) msl). This interval is described as dark greenish gray, dense clayey sand grading to very dense silty sands in their bottom 25 ft (8 m). Boring B-401 encountered the Piney Point Formation at a depth of 278 ft (85 m) (-181 ft (-55 m) msl).

According to Hansen (Hansen, 1996), the top of the Piney Point Formation occurs at an approximate elevation of -200 ft (-61 m) msl in the CCNPP site area (Figure 2.5-14). The absence of late Eocene and early Miocene sediments indicate the absence of deposition or erosion for millions of years. A structure contour map of the top of the Piney Point Formation shows an erosion surface that dips gently toward the southeast (Figure 2.5-14).

The Chesapeake Group at the CCNPP site is divided into three marine formations which are, from oldest to youngest, the Calvert Formation, the Choptank Formation and the St. Marys Formation. These units are difficult to distinguish in the subsurface due to similar sediment types and are undivided at the CCNPP site (Glaser, 2003c). Achmad and Hansen (Achmad, 1997) indicate that the Chesapeake Group is approximately 245 ft (75 m) thick beneath the CCNPP site, based on boring CA-Ed 22 data. Kidwell (Kidwell, 1997) states that the stratigraphic relations within this group are highly complex. Based on cross sections presented in Kidwell (Kidwell, 1997), the contact between the St. Marys Formation and the underlying Choptank is estimated to be approximately 22 ft (7 m) deep in boring B-301 and at 10 ft (3 m)

deep in B-401. The thickness of the Chesapeake Group (undifferentiated) is 280 ft in boring B-301 and 268 ft in B-401. The difference in these thicknesses and that in CA-Ed 22 is attributed to the geophysical log of the latter boring not continuing to the top of the boring and/or difference in the chosen top of the St. Marys Formation.

Although the formational contacts within the Chesapeake Group are difficult to impossible to identify, there are several strata which are encountered in most of the CCNPP Unit 3 investigation borings. The most persistent of these is the calcite-cemented sand shown in Figure 2.5-42 and probably is one of the units Kidwell (Kidwell, 1997) interprets as the Choptank Formation.

About 20 ft below the base of this cemented sand unit as a second, but much thinner cemented sand which is identified primarily by "N" values (the sum of the blow counts for the intervals 6 to 12 in (15 to 30 cm) and 12 to 18 in (30 to 46 cm) sample intervals in a standard SPT) higher than those immediately above and below.

The base of the Chesapeake Group (Piney Point Formation) is clearly identified in the geophysical log (Figure 2.5-37 and Figure 2.5-38) by the characteristic gamma curve response. Based on the boring log, this gamma curve response appears to be related to calcite-cemented sand.

The surficial deposits consist of two informal stratigraphic units: the Pliocene-age Upland deposits and Pleistocene to Holocene Lowland deposits. The Upland deposits consist of two units deposited in a fluviatile environment. The Upland deposits are areally more extensive in St. Mary's County than in Calvert County (Glaser, 1971). The outcrop distribution has a dendritic pattern and since it caps the higher interfluvial divides, this unit is interpreted as a highly dissected sediment sheet whose base slopes toward the southwest (Glaser, 1971) (Hansen, 1996). This erosion might have occurred due to differential uplift during the Pliocene or down cutting in response to lower base levels when sea level was lower during periods of Pleistocene glaciation.

2.5.1.2.3.4 Quarternary Formations

The Lowland deposits are considered to consist of three lithologic units. The basal unit is estimated to be 10 to 20 ft (3 to 6 m) thick and is often described as cobbly sand and gravel. This unit may represent high energy stream deposits in an alluvial environment near the base of eroding highlands to the west. The basal unit is overlain by as much as 90 ft (27 m) of bluish gray to dark brown clay that may be silty or sandy (Glaser, 1971) The uppermost of the three units consists of 10 to 30 ft (3 to 9 m) of pale gray, fairly well sorted, medium to coarse sand (Glaser, 1971). The Lowland deposits were laid down in fluvial to estuarine environments (Hansen, 1996) and are generally found along the Patuxent and Potomac River valleys and the Chesapeake Bay. These deposits occur in only a few places along the east shore of Chesapeake Bay.

Sands overlying the Chesapeake Group at the CCNPP site are mapped by Glaser (2003c) as Upland Deposits. Within the CCNPP Unit 3 power block these sands range in thickness from a feather edge in borings on the southern edge, to more than 50 ft in B-405.

Boring B-301 intersected 22 ft (7 m) of silty sand above the contact with the Chesapeake Group, while B-401 has 10 ft (3 m) of silty sand (Figure 2.5-37 and Figure 2.5-38). The sand in both borings grades into a coarser sand unit just above the contact. These sands are attributed to the Upland deposits previously mapped (Glaser, 2003c).

Terrace deposits in the CCNPP site area (Figure 2.5-32 and Figure 2.5-34) consist of interbedded light gray to gray silty sands and clay with occasional reddish brown pockets and are approximately 50 ft (15 m) thick. These units are Pliocene to Holocene in age.

Holocene deposits, mapped as Qal on the site Geologic Map, includes heterogeneous sediments underlying floodplains and beach sands composed of loose sand.

2.5.1.2.4 Site Area Structural Geology

The local structural geology of the CCNPP site area described in this section is based primarily on a summary of published geologic mapping (Cleaves, 1968) (Glaser, 1994) (McCartan, 1995) (Achmad, 1997) (Glaser, 2003b) (Glaser, 2003c), aeromagnetic and gravity surveys (Hansen, 1978) (Hittelman, 1994) (Milici, 1995) (Bankey, 2002), detailed lithostratigraphic profiles along Calvert Cliffs (Kidwell, 1988) (Kidwell, 1997), results of earlier investigations performed at the CCNPP site (BGE, 1968) (CEG, 2005), as well as CCNPP site reconnaissance and subsurface exploration performed for the CCNPP Unit 3 site investigation.

Sparse geophysical and borehole data indicate that the basement consists of exotic crystalline magmatic arc material (Hansen, 1986) (Glover, 1995b) or Triassic rift basin sedimentary rocks (Benson, 1992). Although the basement beneath the site area has not been penetrated with drill holes, regional geologic cross sections developed from geophysical, gravity and aeromagnetic, as well as limited deep borehole data from outside of the CCNPP site area, suggest that the based of the Coastal Plain section is present at a depth of approximately 2,500 ft (762 m) msl (Section 2.5.1.2.2).

Tectonic models hypothesize that the crystalline basement underlying the site was accreted to a pre-Taconic North American margin in the Paleozoic along a suture that lies about 10 mi (16 km) west of the site (Klitgord, 1995) (Figure 2.5-17 and Figure 2.5-23). The plate-scale suture is defined by a distinct north-northeast-trending magnetic anomaly that dips easterly between 35 and 45 degrees and lies about 7.5 to 9 mi (12 to 14.5 km) beneath the CCNPP site (Glover, 1995b) (Figure 2.5-17). Directly west of the suture lies the north to northeast-trending Taylorsville Basin (LeTourneau, 2003) and to the east, the postulated Queen Anne Mesozoic rift basin (Figure 2.5-9) (Benson, 1992). These rift basins are delineated from geophysical data subject to alternate interpretations and a limited number of deep boreholes that penetrate the Coastal Plain section located outside the Site Area, and generally are considered approximately located where buried beneath the Coastal Plain (Jacobeen, 1972) (Hansen, 1986) (Benson, 1992) (LeTourneau, 2003). Because the available geologic information used to constrain the basin locations is sparse, some authors, but not all, depict the CCNPP site area to be underlain by a Mesozoic basin (Klitgord, 1988) (Schlische, 1990) (Horton, 1991) (Benson, 1992) (Klitgord, 1995) (Withjack, 1998) (LeTourneau, 2003) (Figure 2.5-10, Figure 2.5-12, Figure 2.5-16, and Figure 2.5-22). However, based on a review of existing published geologic literature, there is no known basin-related fault or geologic evidence of basin-related faulting in the basement directly beneath the CCNPP site area.

Recent 1:24,000-scale mapping (Glaser, 2003b) (Glaser, 2003c) for Calvert County and St. Mary's County shows the stratigraphy at the CCNPP site area consisting of nearly flat-lying Cenozoic Coastal Plain sediments that have accumulated within the west-central part of the Salisbury Embayment (Figure 2.5-32 and Figure 2.5-33). The Salisbury Embayment is defined as a regional depocenter that has undergone slow crustal and regional downwarping as a result of sediment overburden during the Early Cretaceous and much of the Tertiary. The Coastal Plain deposits within this region of the Salisbury Embayment generally strike northeast-southwest and have a gentle dip to the southeast at angles close to or less than one

to two degrees (Figure 2.5-32 and Figure 2.5-33). The gentle southerly dip of the sediments result in a surface outcrop pattern in which the strata become successively younger in a southeast direction across the embayment. The gentle-dipping to flat-lying Miocene Coastal Plain deposits are exposed in the steep cliffs along the western shoreline of Chesapeake Bay and provide excellent exposures to assess the presence or absence of tectonic-related structures.

Local geologic cross sections of the site area depict unfaulted, southeast-dipping Eocene-Miocene Coastal Plain sediments in an unconformable contact with overlying Pliocene Upland deposits (Glaser, 1994) (Achmad, 1997) (Glaser, 2003b) (Glaser, 2003c) (Figure 2.5-13, Figure 2.5-32, and Figure 2.5-33). No faults or folds are depicted on these geologic cross sections. A review of an Early Site Review report (BGE, 1977), i.e. Perryman site, and a review of the Preliminary Safety Analysis Report for the Douglas Point site (Potomac Electric Power Company, 1973), located along the eastern shore of the Potomac River about 45 mi (72 km) west-southwest of the CCNPP site, also reported no faults or folds within a 5 mi (8 km) radius of the CCNPP site. The Updated Final Safety Analysis Report for the Hope Creek site, located in New Jersey along the northern shore of Delaware Bay, also was reviewed for tectonic features previously identified within 5 mi (8 km) of the CCNPP site, yet none were identified (PSEG, 2002). Review of a seismic source characterization study (URS, 2000) for a liquidefied natural gas plant at Cove Point, about 3 mi (5 km) southeast of the site, also identified no faults or folds projecting toward or underlying the CCNPP site area.

On the basis of literature review, and aerial and field reconnaissance, the only potential structural features at and within the CCNPP site area consist of a hypothetical buried northeast-trending fault (Hansen, 1986), two inferred east-facing monoclines developed within Mesozoic and Tertiary deposits along the western shore of Chesapeake Bay (McCartan, 1995), and multiple subtle folds or inflections in Miocene strata and a postulated fault directly south of the site (Kidwell, 1997) (Figure 2.5-25). The Hillville fault of Hansen and Edwards (Hansen, 1986) and inferred fold of McCartan (McCartan, 1995) and Kidwell (Kidwell, 1997) are described in Sections 2.5.1.1.4.4.4 and Section 2.5.3. As previously discussed in Section 2.5.1.1.4.4.4, none of these features are considered capable tectonic sources, as defined in RG 1.165, Appendix A. Each of these features is discussed briefly below. Only the Hillville fault has been mapped within or directly at the 5 mi (8 km) radius of the CCNPP site area (Figure 2.5-27, Figure 2.5-28, and Figure 2.5-32).

Hillville fault of Hansen and Edwards (Hansen, 1986): The 26 mile long Hillville fault approaches to within 5 mi (8 km) of the CCNPP site (Figure 2.5-32). The fault consists of a northeast-striking zone of steep southeast-dipping reverse faults that coincide with the Sussex-Currioman Bay aeromagnetic anomaly. The style and location of faulting are based on seismic reflection data collected about 9 mi (14 km) west-southwest of the site. A seismic line imaged a narrow zone of discontinuities that vertically separate basement by as much as 250 ft (76 m) (Hansen, 1978). Hansen and Edwards (Hansen, 1986) interpret this offset as part of a larger lithotectonic terrane boundary that separates basement rocks associated with Triassic rift basins on the west and low-grade metamorphic basement on the east. The Hillville fault may represent a Paleozoic suture zone that was reactivated in the Mesozoic and Early Tertiary. Based on stratigraphic correlation between boreholes within Tertiary Coastal Plain deposits, Hansen and Edwards (Hansen, 1986) speculate that the Hillville fault was last active in the Early Paleocene. There is no pre-EPRI and post-EPRI (1986) seismicity spatially associated with this feature (Figure 2.5-25) nor is there any geomorphic evidence of Quaternary deformation. The Hillville fault is not considered a capable tectonic source.

In addition, two speculative and poorly constrained east-facing monoclines along the western margin of Chesapeake Bay are mapped within the 5 mi (8 km) radius of the CCNPP site area. East-facing monoclines (McCartan, 1995): The unnamed monoclines are not depicted on any geologic maps of the area, including those by the authors, but they are shown on geologic cross sections that trend northwest-southeast across the existing site and south of the CCNPP site near the Patuxent River (McCartan, 1995) (Figure 2.5-25). East-facing monoclines are inferred beneath Chesapeake Bay at about 2 and 10 mi (3.2 to 16 km) east and southeast, respectively, from the CCNPP site. Along a northerly trench, the two monoclines delineate a continuous north-trending, east-facing monocline. As mapped in cross section and inferred in plan view, the monoclines trend approximately north along the western shore of Chesapeake Bay. The monoclines exhibit a west-side up sense of structural relief that projects into the Miocene Choptank Formation (McCartan, 1995). The overlying Late Miocene St. Marys Formation is not shown as warped. Although no published geologic data are available to substantiate the existence of the monoclines, McCartan (McCartan, 1995) believes the distinct elevation change across Chesapeake Bay and the apparent linear nature of Calvert Cliffs are tectonically controlled. CCNPP site and aerial reconnaissance, coupled with literature review, for the CCNPP Unit 3 study strongly support a non-tectonic origin for the physiographic differences across the Chesapeake Bay (Section 2.5.1.1.4.4.4). There is no pre-EPRI or post-EPRI (1986) seismicity spatially associated with this feature, nor is there geologic data to suggest that the monocline proposed by McCartan (McCartan, 1995) is a capable tectonic source.

Multiple subtle folds or inflections developed in Miocene Coastal Plain strata including a postulated fault are mapped in the cliff exposures along the west side of Chesapeake Bay. Kidwell's (Kidwell, 1997) postulated folds and fault: Kidwell (Kidwell, 1988) (Kidwell, 1997) prepared over 300 lithostratigraphic columns along a 25 mi (40 km) long stretch of Calvert Cliffs that intersect much of the CCNPP site (Figure 2.5-30). When these stratigraphic columns are compiled into a cross section, they collectively provide a 25 mi (40 km) long nearly continuous exposure of Miocene, Pliocene and Quaternary deposits. Kidwell's (Kidwell, 1997) stratigraphic analysis indicates that the Miocene Coastal Plain deposits strike northeast and dip very shallow between 1 and 2 degrees to the south-southeast, which is consistent with the findings of others (McCartan, 1995) (Glaser 2003b) (Glaser, 2003c). The regional southeast-dipping strata are disrupted occasionally by several low amplitude broad undulations developed within Miocene Coastal Plain deposits (Figure 2.5-30). The stratigraphic undulations are interpreted as monoclines and asymmetrical anticlines by Kidwell (Kidwell, 1997). In general, the undulatory stratigraphic contacts coincide with basal unconformities having wavelengths of 2.5 to 5 mi (4 to 8 km) and amplitudes of 10 to 11 ft (approximately 3 meters). Based on prominent stratigraphic truncations, the inferred warping decreases upsection into the overlying upper Miocene St. Marys Formation. Any inferred folding of the overlying Pliocene and Quaternary fluvial deposits is poorly constrained and can be readily explained by highly variable undulating unconformities.

About 1.2 mi (1.9 km) south of the site, Kidwell (Kidwell, 1997) interprets an apparent 6 to 10 ft (2 to 3 m) elevation change in Miocene strata by extrapolating unit contacts across the approximately 0.6 mile wide (1 km) gap at Moran Landing (Figure 2.5-25 and Figure 2.5-30). Kidwell (Kidwell, 1997) also interprets a 3 to 12 (0.9 to 3.7 m) ft elevation change in younger (Quaternary (?)) fluvial material across this same gap. Because of the lack of cliff exposures at Moran Landing (only the valley margins), no direct observations of these elevation changes can be made. Kidwell (Kidwell, 1997) explains the differences in elevation of the Miocene-Quaternary stratigraphy by hypothesizing the existence of a fault at Moran Landing that strikes northeast and accommodates a north-side down sense of separation. However, the postulated fault of Kidwell (Kidwell, 1997) is not shown on any of Kidwell's (Kidwell, 1997)

cross-sections, or any published geologic map (e.g., Glaser, 2003b and 2003c). In addition, Hansen (1978) does not describe faulting in seismic reflection line St. M-2 that intersects the inferred southwest projection of the hypothesized Kidwell (1997) fault (Figure 2.5-27).

The observations of offset younger gravels do not provide any evidence for the existence of a fault because the surface on which the gravels are deposited is an erosional unconformity with extensive variable relief (Kidwell, 1997). Observations made during field reconnaissance, as part of the FSAR preparation, confirmed that this contact was an erosional unconformity with significant topography north and south of Moran Landing consistent with stratigraphic representations in Kidwell (1997) profiles. The observations of several feet of elevation change in the Miocene units over several thousands of feet of horizontal distance is at best weak evidence for faulting within the Miocene deposits. For example, subtle elevation variations in Miocene strata characterized along a near-continuous exposure south of Moran Landing contain similar vertical and lateral dimensions as to the inferred elevation change across Moran Landing; however, the features are interpreted as subtle warps and not faults by Kidwell (1997). On the basis of association with similar features to the south and the lack of a continuous exposure, there is little to no evidence to support a fault across Moran Landing. The lack of evidence for Quaternary faulting within the observations made by Kidwell (Kidwell, 1997), and the results of the studies undertaken as part of the CCNPP Unit 3 COLA effort (field and aerial reconnaissance, air photo and LiDAR analysis) (see FSAR Section 2.5.3.1), collectively support the conclusion that the hypothesized fault of Kidwell (Kidwell, 1997) is not a capable fault.

There is no pre-EPRI or post-EPRI study (EPRI, 1986) seismicity spatially associated with the Kidwell (Kidwell, 1997) features, the hypothetical features are not aligned or associated with gravity and magnetic anomalies, nor is there data to indicate that the features proposed by Kidwell (Kidwell, 1997) are capable tectonic sources.

The most detailed subsurface exploration of the site was performed by Dames & Moore as part of the original PSAR (BGE, 1968) for the existing CCNPP foundation and supporting structures. The PSAR study included drilling as many as 85 geotechnical boreholes, collecting downhole geophysical data, and acquiring seismic refraction data across the site. Dames and Moore (BGE, 1968) developed geologic cross sections extending from Highway 2/4 northwest of the site to Camp Conoy on the southeast which provide valuable subsurface information on the lateral continuity of Miocene Coastal Plain sediments and Pliocene Upland deposits (Figure 2.5-32 and Figure 2.5-34). Cross sections C-C′ and D-D′ pre-date site development and intersect the existing and proposed CCNPP site for structures trending north-northeast, parallel to the regional structural grain. These sections depict a nearly flat-lying, undeformed geologic contact between the Middle Miocene Piney Point Formation and the overlying Middle Miocene Calvert Formation at about –200 ft (-61 m) msl (Figure 2.5-41 and Figure 2.5-42).

Geologic sections developed from geotechnical borehole data collected as part of the CCNPP Unit 3 study also provide additional detailed sedimentological and structural relations for the upper approximately 400 ft (122 m) of strata directly beneath the footprint of the site. Similar to the previous cross sections prepared for the site, new geologic borehole data support the interpretation of flat-lying and unfaulted Miocene and Pliocene stratigraphy at the CCNPP site (Figure 2.5-39 and Figure 2.5-43). A cross section prepared oblique to previously mapped northeast-trending structures (i.e., Hillville fault), inferred folds (McCartan, 1995) (Kidwell, 1997), and the fault of Kidwell (Kidwell, 1997) shows nearly flat-lying Miocene and Pliocene stratigraphy directly below the CCNPP site. Multiple key stratigraphic markers provide

evidence for the absence of Miocene-Pliocene faulting and folding beneath the site. Minor perturbations are present across the Miocene-Pliocene stratigraphic boundary, as well as other Miocene-related boundaries, however these minor elevation changes are most likely related to the irregular nature of the fluvial unconformities and are not tectonic-related.

Numerous investigations of the Calvert Cliffs coastline over many decades by government researchers, stratigraphers, and by consultants for Baltimore Gas and Electric, as well as investigations for the CCNPP Unit 3, have reported no visible signs of tectonic deformation within the exposed Miocene deposits near the site, with the only exception being that of Kidwell (Kidwell, 1997) (Figure 2.5-44). Collectively, the majority of published and unpublished geologic cross sections compiled for much of the site area and site, coupled with regional sections (Achmad, 1997) (Glaser, 2003b) (Glaser, 2003c) and site and aerial reconnaissance, indicate the absence of Pliocene and younger faulting and folding. A review and interpretation of aerial photography, digital elevation models, and LiDAR data of the CCNPP site area, coupled with aerial reconnaissance, identified few discontinuous north to northeast-striking lineaments. None of these lineaments were interpreted as fault-related, nor coincident with the Hillville fault or the other previously inferred Miocene-Pliocene structures mapped by McCartan (McCartan, 1995) and Kidwell (Kidwell, 1997) (Section 2.5.3). A review of regional geologic sections and interpretation of LiDAR data suggest that the features postulated by Kidwell (Kidwell, 1997), if present, are not moderate or prominent structures, and do not deform Pliocene and Quaternary strata. In summary, on the basis of regional and site geologic and geomorphic data, there are no known faults within the site area, with the exception of the poorly constrained Hillville fault that lies along the northwestern perimeter of the 5 mi (8 km) radius of the site (Hansen, 1986).

2.5.1.2.5 Site Area Geologic Hazard Evaluation

No geologic hazards have been identified within the CCNPP site area. No geologic units at the site are subject to dissolution. No deformation zones were encountered in the exploration or excavation for CCNPP Units 1 and 2 and none have been encountered in the site investigation for CCNPP Unit 3. Because the CCNPP Unit 3 plant site is located at an elevation of approximately 85 ft (26 m) msl and approximately 1,000 ft (305 m) from the Chesapeake Bay shoreline, it is unlikely that shoreline erosion or flooding will impact the CCNPP site.

2.5.1.2.6 Site Engineering Geology Evaluation

2.5.1.2.6.1 Engineering Soil Properties and Behavior of Foundation Materials

Engineering soil properties, including index properties, static and dynamic strength, and compressibility are discussed in Section 2.5.4. Variability and distribution of properties for the foundation bearing soils will be evaluated and mapped as the excavation is completed.

Settlement monitoring will based on analyses performed for the final design.

2.5.1.2.6.2 Zones of Alteration, Weathering, and Structural Weakness

No unusual weathering profiles have been encountered during the site investigation. No dissolution is expected to affect foundations. Any noted desiccation, weathering zones, joints or fractures will be mapped during excavation and evaluated.

2.5.1.2.6.3 Deformational Zones

No deformation zones were encountered in the exploration or excavation for CCNPP Units 1 and 2 and none have been encountered in the site investigation for CCNPP Unit 3. Excavation mapping is required during construction and any noted deformational zones will be evaluated

and assessed as to their rupture and ground motion generating potential while the excavations' walls and bases are exposed. Additionally, the NRC will be notified when excavations are open for inspection. No capable tectonic sources as defined by Regulatory Guide 1.165 (NRC, 1997) exist in the CCNPP site region.

2.5.1.2.6.4 Prior Earthquake Effects

Outcrops are rare within the CCNPP site area. Studies of the CCNPP Unit 1 and 2 excavation, available outcrops, and small streams, and extensive exposures along the western shore of Chesapeake Bay have not indicated any evidence for earthquake activity that affected the Miocene deposits. The findings of a field and aerial reconnaissance (Figure 2.5-229), coupled with literature and aerial photography review, as well as discussions with experts in the assessment of paleoliquefaction in the central and eastern United States, indicate the absence of evidence for paleoliquefaction in Maryland. For example, one study entitled "Paleoliquefaction Features along the Atlantic Seaboard" by Amick (1990) searched for paleoliquefaction features in the state of Maryland. This NRC funded study performed a regional paleoliquefaction survey between Cape May, New Jersey and the Georgia/Florida state line, which included portions of the Delmarva Peninsula and Chesapeake Bay. Amick (1990) reported no liquefaction in the Delmarva Peninsula portion of the investigation (Amick, 1990) where Quaternary-aged deposits are ubiquitous. These findings are consistent with Crone (2000) and Wheeler (2005)(2006), which make no reference to paleoliquefaction features in the State of Maryland.

2.5.1.2.6.5 Effects of Human Activities

No mining operations, excessive extraction or injection of ground water or impoundment of water has occurred within the site area that can affect geologic conditions.

2.5.1.2.6.6 Site Ground Water Conditions

A detailed discussion of ground water conditions is provided in Section 2.4.12.

2.5.1.3 References

This section is added as a supplement to the U.S. EPR FSAR.

Achmad, 1997. Hydrogeology, model simulation, and water-supply potential of the Aquia and Piney Point-Nanjemoy Aquifers in Calvert and St. Mary's Counties, Maryland, Department of Natural Resources, Maryland Geological Survey Report of Investigations No. 64, 197 p., G. Achmad and H. Hansen, 1997.

Aggarwal, 1978. Earthquakes, Faults, and Nuclear Power Plants in Southern New York and Northern New Jersey, Science, Volume 200, p 425-429, Y. Aggarwal, and L. Sykes, 1978.

Amick, 1990. Paleoliquefaction features along the Atlantic Seaboard, NUREG/CR-5613, D. Amick, R. Gelinas, G. Maurath, R. Cannon, D. Moore, E. Billington, and H. Kemppmen, October, 1990.

Armbruster, 1987. The 23 April 1984 Martic Earthquake and The Lancaster Seismic Zone In Eastern Pennsylvania, Bulletin of the Seismological Society of America, Volume 77, Number 2, p 877-890, J. Armbruster, and L. Seeber, 1987.

Bailey, 1999. The Geology of Virginia: Generalized Geologic Terrane Map of the Virginia Peidmont and Blue Ridge, Physiographic Map of Virginia, College of William and Mary,

Department of Geology, C. Bailey, 1999, Website: www.wm.edu/geology/virginia/phys_regions.html, Date accessed: June 25, 2007.

Bailey, 2004. Strain and vorticity analysis of transpressional high-strain zones from the Virginia Piedmont, USA, in Alsop, G.I., and Holdsworth, R.E., eds., Flow processes in faults and shear zones: Geological Society [London] Special Publication 224, p. 249-264, C. Bailey, B. Frances, and E. Fahrney, 2004.

Barineau, 2008. The Taconic Orogeny: Collisional vs. Accretionary orogenesis in the southern Appalachians. Geological Society of America Abstracts with Programs, Vol. 40, No. 4, p. 68, C. I. Barineau, 2008.

Bartholomew, 2004. Northern ancestry for the Goochland terrane as a displaced fragment of Laurentia, Geology, Volume 32; Number 8, 669-672, M. J. Bartholomew and R. P. Tollo, 2004.

BGE, 1968. Preliminary Safety Analysis Report Calvert Cliffs Nuclear Power Plant Units 1 and 2, Volume 1, Docket 50-317 and 50-318, Baltimore Gas and Electric, 1968.

BGE, 1977. Limited Early Site Review Perryman Site Suitability-Site Safety Report, Volume III, Baltimore Gas and Electric, July 1977.

Bankey, 2002. Magnetic Anomaly Map of North America, U.S. Geological Survey, 1 sheet, scale 1:10,000,000, V. Bankey, A. Cuevas, D. Daniels, C. Finn, I. Hernandez, P. Hill, R. Kucks, W. Miles, M. Pilkington, C. Roberts, W. Roest, V. Rystrom, S. Shearer, S. Snyder, R. Sweeney, and J. Velez, 2002.

Behrendt, 1983. Structural elements of the U.S. Atlantic margin delineated by the second vertical derivative of the aeromagnetic data, U.S. Geological Survey Geophysical Investigation Map GP-956, scale 1:2,500,000, J. Behrendt and M. Grim, 1983.

Benson, 1992. Map of Exposed and Buried Early Mesozoic Rift Basins/Synrift Rocks of the U.S. Middle Atlantic Continental Margin, Delaware Geological Survey Miscellaneous Map Series No. 5, R. Benson, 1992.

Benson, 2006. Internal stratigraphic correlation of the subsurface Potomac Formation, New Castle County, Delaware, and adjacent areas in Maryland and New Jersey, Delaware Geological Survey Report of Investigations No. 71, R.N. Benson, 2006.

Berquist, 1999. Late Cenozoic Reverse Faulting in the Fall Zone, Southeastern Virginia, The Journal of Geology, Volume 107, p 727-732, C. Berquist, Jr and C. Bailey, 1999.

Bobyarchick, 1979. Deformation and Metamorphism in the Hylas Zone and Adjacent Parts of the Eastern Piedmont in Virginia, Geological Society of America Bulletin, Volume 90, p 739–752, A. Bobyarchick and L. Glover, 1979.

Bollinger, 1985. Seismicity, Seismic Reflection Studies, Gravity and Geology of the Central Virginia Seismic Zone: Part I. Seismicity, Geological Society of America Bulletin, Volume 96, 49–57, G. Bollinger and M. Sibol, January 1985.

Bollinger, 1988. The Giles County, Virginia, Seismic Zone – Seismological Results and Geological Interpretations, U.S. Geological Survey Professional Paper 1355, G. Bollinger and R. Wheeler, 1988.

Bollinger, 1992. Specification of Source Zones, Recurrence Rates, Focal Depths, and Maximum Magnitudes for Earthquakes Affecting the Savannah River Site in South Carolina, U.S. Geological Survey Bulletin 2017, G. Bollinger, 1992.

Brezinski, 2004. Stratigraphy of the Frederick Valley and its Relationship to Karst Development, Maryland Geological Survey, Report of Investigations Number 75, D. Brezinski, 2004.

Bridge, 1994. Marine transgressions and regressions recorded in Middle Devonian shore-zone deposits of the Catskill clastic wedge, Geological Society of America Bulletin, Volume 106, Number 11, pgs 1440-1458, J.S. Bridge and B.J. Willis, 1994.

Brown, 1972. Structural and stratigraphic framework and spatial distribution of permeability of the Atlantic Coastal Plain, North Carolina to New York, U.S. Geological Survey Professional Paper 796, p 79, P. Brown, J. Miller, and F. Swain, 1972.

Burton, 1985. Attitude, movement history, and structure of cataclastic rocks of the Flemington fault—Results of core drilling near Oldwick, New Jersey, U.S. Geological Survey Miscellaneous Field Studies, Map MF-1781, 1 sheet, W. Burton and N. Ratcliffe, 1985.

Carr, 2000. Geologic transect across the Grenville orogen of Ontario and New York. Canadian Journal of Earth Science 37(2-3): 193–216, S. D. Carr, R. M. Easton, R. A. Jamieson and N. G. Culshaw, 2000.

Carter, 1976. Soil Survey of Louisa County, Virginia, U.S. Department of Agriculture, Soil Conservation Service, J. Carter, March 1976.

Cecil, 2004. Geology of the National Capital Region: Field trip guidebook, Stop 11; Upper Devonian and Lower Mississippian strata on Interstate 68 at Sideling Hill, Md., in Southworth, S., and Burton, W., eds., The Paleozoic record of changes in global climate and sea level; central Appalachian basin: U.S. Geological Survey Circular 1264, p 112- 116, C. B. Cecil, D. K. Brezinski, V. Skema and R. Stamm, 2004.

Cederstrom, 1957. Structural Geology of Southeastern Virginia, American Association of Petroleum Geologists Bulletin, Volume 29, D. Cederstrom, 1957.

CFR, 2007. Geologic and Seismic Siting Criteria, Title 10, Code of Federal Regulations, Part 100.23, 2007.

Chapman, 1994. Seismic Hazard Assessment for Virginia, Virginia Tech Seismological Observatory, Department of Geological Sciences, M. Chapman and F. Krimgold, February 1994.

Clark, 1992. Central Appalachian Periglacial Geomorphology, A Field Excursion Guidebook under the auspices of the 27th International Geographical Congress, Commission on Frost Action Environments, Agronomy Series Number 120, G. Clark, R. Behling, D. Braun, E. Ciolkosz, J. Kite, and B. Marsh, August 1992.

Cleaves, 1968. Geologic Map of Maryland, Maryland Geologic Survey, 1 sheet, scale 1:250,000, E. Cleaves, J. Edwards, Jr, and J. Glaser, 1968.

Cleaves, 2000. Regoliths of the Middle-Atlantic Piedmont and Evolution of a Polymorphic Landscape, Southeastern Geology, Volume 39, Numbers 3 and 4, p 199-122, E. Cleaves, October 2000.

Coblentz, 1995. Statistical Trends in the Intraplate Stress Field, Journal of Geophysical Research, Volume 100, p. 20, 245–20, 255, D. Coblentz, and R. Richardson, 1995.

Colman, 1989. Quaternary Geology of the Southern Maryland Part of the Chesapeake Bay, U.S Geological Survey, MF-1948-C, Scale 1:125,000, 3 plates, S. Colman, and J. Halka, 1989.

Colman, 1990. Ancient channels of the Susquehanna River beneath Chesapeake Bay and the Delmarva Peninsula, Geological Society of America Bulletin, Volume 102, p 1268-1279, S. Colman, J. Halka, C. Hobbs, R. Mixon, and D. Foster, 1990.

Colton, 1970. The Appalachian Basin – Its Depositional Sequences and Their Geologic Relationships, Chapter 2 in Studies of Appalachian Geology: Central and Southern by G. Fisher, F. Pettijohn, J. Reed, Jr, and K. Weaver, Interscience Publishers, G. Colton, 1970.

Conley, 1973. Geology of the Snow Creek, Martinsville East, Price, and Spray Quadrangles: Virginia Division of Mineral Resources Report of Investigations 33, p 71, J. F. Conley and W. S. Henika, 1973.

Conners, 1986. Quaternary Geomorphic Processes in Virginia, in The Quaternary of Virginia – A Symposium Volume, edited by J. McDonald and S. Bird, Virginia Division of Mineral Resources, Publication 75, J. Conners, 1986.

CEG, 2005. Calvert Cliffs Independent Spent Fuel Storage Installation, Updated Environmental Report, Volume 3, Revision 7, Constellation Energy Group, 2005.

Coruh, 1988. Seismogenic Structures in the Central Virginia Seismic Zone, Geology, Volume 16, p 748-751, C.Coruh, G. Bollinger, and J. Costain, August 1988.

Crespi, 1988. Using balanced cross sections to understand early Mesozoic extensional faulting, in A.J., Froelich and G.R. Robinson Jr. eds, Studies of the Early Mesozoic Basins of the Eastern United States, U.S. Geological Survey Bulletin no 1776, P. 220-229, J. Crespi, 1988.

Crone, 2000. Data for Quaternary Faults, Liquefaction Features, and Possible Tectonic Features in the Central and Eastern United States, east of the Rocky Mountain front, U.S. Geological Survey Open-File Report 00-260, A. Crone and R. Wheeler, 2000.

Dahlen, 1981. Isostacy and Ambient State of Stress in the Oceanic Lithosphere, Journal of Geophysical Research, Volume 86, p 7801–7807, F. Dahlen, 1981.

DM, 1973. Supplemental Geologic Data, North Anna Power Station, Louisa County, Virginia, Virginia Electric and Power Company Report, , Dames and Moore, August 17, 1973.

DM, 1977a. A Seismic Monitoring Program at the North Anna Site in Central Virginia, January 24, 1974 through August 1, 1977, for Virginia Electric and Power Company, Dames and Moore, September 13, 1977.

DM, 1977b. Lateral Continuity of a Pre- or Early Cretaceous Erosion Surface Across Neuschel's Lineament Northern Virginia, for Virginia Electric and Power Company, Dames and Moore, April 1977.

Daniels, 1985. Geologic Interpretation of Basement Rocks of the Atlantic Coastal Plain, United States Department of Interior Geological Survey Open-File Report 85-655, D. Daniels and G. Leo, 1985.

Darton, 1950. Configuration of the Bedrock Surface of the District of Columbia and Vicinity, Maryland Geological Survey, 4 sheets, scale 1:31,680, N. Darton, 1950.

de Boer, 2003. Evidence for Predominant lateral Magma flow Along Major Feeder-Dike Segments of the Eastern North America Swarm Based Magmatic Fabric, in The Great Rift Valleys of Pangea in Eastern North America, in P.M. Letourneau, and P.E. Olsen. (eds), J.Z. de Boer, R.E. Ernst, A.G. Lindsey, p 189-206.

Dischinger, 1987. Late Mesozoic and Cenozoic Stratigraphic and Structural Framework near Hopewell, Virginia, U.S. Geological Survey Bulletin 1567, p 48, J. Dischinger, 1987.

Dominion, 2004a. Response to 6/1/04 RAI 2.5.1-5, 2.5.1-6, 2.5.3-2, and 2.5.1-5, Letter No. 5, U.S. Nuclear Regulatory Committee, Serial No. 04-347, and Docket No. 52-008, Dominion, 2004.

Dominion, 2004b. Response to 4/15/04 RAI 2.5.1-1 to 2.5.1-4, 2.5.2-2 to 2.5.2-4, and 2.5.3-1, Letter No. 3, U.S. Nuclear Regulatory Committee, Serial No. 04-270, and Docket No. 52-008, Dominion, 2004.

Drake, 1989. The Taconic Orogen, in Hatcher, R.D. William T., and Viele, G.W., eds., The Appalachian –Ouachita Orogen in the United States, DNAG, Volume F-2, p 101-177, A. Drake Jr, A. Sinha, J. Laird, and R. Guy, 1989.

Drake, 1999. Geologic map of the Seneca quadrangle, Montgomery County, Maryland, and Fairfax and Loudon Counties, Virginia, U.S. Geological Survey, Geologic Quadrangle Map GQ-1802, A. Drake Jr, S. Southworth, and K. Lee, 1999.

Drake, 1996. Bedrock Geological Map of Northern New Jersey, U.S. Geological Survey, 2 sheets, scale 1:100,000, A. Drake Jr, R. Volkert, D. Monteverde, G. Herman, H. Houghton, R. Parker, and R. Dalton, 1996.

Dryden, 1932. Faults and joints in the Costal Plain of Maryland, Journal of the Washington Academy of Sciences, Volume 22, p 469-472, A. Dryden Jr, 1932.

Ebel, 2002. Earthquakes in the Eastern Great Lakes Basin from a regional perspective, Tectonophysics, p 17-30, J. Ebel and M. Tuttle, 2002.

Edwards, 1979. New Data Bearing on the Structural Significance of the Upper Chesapeake Bay Magnetic Anomaly; Maryland Geological Survey Report of Investigation No. 30, 44 p. J. Edwards and H. Hansen ,1979.

Edwards, 1981. A Brief Description of the Geology of Maryland, Maryland Geological Survey, Pamphlet Series, J. Edwards Jr, 1981, Website: www.mgs.md.gov/esic/brochures/mdgeology.html, Date accessed: June 25, 2007.

EPRI, 1986. Seismic Hazard Methodology for the Central and Eastern United States, EPRI Report NP-4726, Electric Power Research Institute, July 1986.

Ervin, 1975. Reelfoot Ridft: reactivated precursor to the Mississippi Embayment, Geological Society of America Bulletin, Volume 86, Number 9, p 1287-1295, C. Ervin and L. McGinnis, 1975.

Faill, 1997a. A Geologic History of the North-Central Appalachians, Part 1, Orogenesis from the Mesoproterozoic through the Taconic Orogeny, Journal of Science, Volume 297, p 551–619, R. Faill, 1997.

Faill, 1997b. A Geologic History of the North-Central Appalachians, Part 2, The Appalachian basin from the Silurian through the Carboniferous, Journal of Science, Volume 297, p 729-761, R. Faill, 1997.

Faill, 1998. A Geologic History of the North-Central Appalachians, Part 3, The Allegheny Orogeny, American Journal of Science, Volume 298, p 131–179, R. Faill, February 1998.

Fenneman, 1946. Physical Divisions of the United States, U.S. Geological Survey, 1:7,000,000-scale map, N. Fenneman and D. Johnson, 1946.

Fichter, 2000. The Geological Evolution of Virginia and the Mid-Atlantic Region: Chronology of Events in the Geologic History of Virginia, Stages A through M, James Madison University, L. Fichter and S. Baedke, September 2000, Website: geollab.jmu.edu/vageol/vahist.html, Date accessed: June 25, 2007.

Fisher, 1964. Triassic Rocks of Montgomery County in Geology of Howard and Montgomery Counties, Maryland Geological Survey, p 10-17, G. Fisher, 1964.

Fleming, 1994. Geologic Map of the Washington West Quadrangle, District of Columbia, Montgomery and Prince Georges Counties, Maryland, and Arlington and Fairfax Counties, Virginia, U.S. Geological Survey, 1 sheet, scale 1:24,000, A. Fleming, A. Drake Jr, and L. McCartan, 1994.

Frankel, 2002. Documentation for the 2002 Update of the National Seismic Hazard Maps: U.S. Geological Survey Open-File Report 02-420, A. Frankel, M. Petersen, C. Mueller, K. Haller, R. Wheeler, E. Leyendecker, R. Wesson, S. Harmsen, C. Cramer, D. Perkins, and K. Rukstales, 2002.

Froelich, 1975. Preliminary Geologic Map, District of Columbia, U.S. Geological Survey, 1 sheet, scale 1: 24,000, A. Froelich and J. Hack, 1975.

Frye, 1986. Roadside Geology of Virginia, Mountain Press Publishing Company, K. Frye, 1986.

Gates, 1989. Alleghanian tectono-thermal evolution of the dextral transcurrent Hylas zone, Virginia Piedmont, U.S.A.: Journal of Structural Geology, v. 11, p. 407-419, A. Gates and L. Glover, 1989.

Gates, 2004. Vestiges of an Iapetan rift basin in the New Jersey Highlands: implications for the Neoproterozoic Laurentian margin Journal of Geodynamics, Volume 37, Issues 3-5, p 381-409, A. E. Gates and R. A. Volkert, 2004.

Glaser, 1971. Geology and mineral resources of Southern Maryland: Maryland Geological Survey Report of Investigations No 15, 85 p., J. Glaser, 1971.

Glaser, 1994. Geologic Map of Calvert County, Department of Natural Resources Maryland Geological Survey, scale 1:62,500, J. Glaser, 1994.

Glaser, 2003a. Geologic Map of Prince George's County, Maryland, Maryland Geological Survey, 1 sheet, scale 1:62,500, J. Glaser, 2003.

Glaser, 2003b. Geologic Map of the Broomers Island Quadrangle, Calvert and St. Mary's Counties, Maryland, Maryland Geological Survey, 1 sheet, scale 1: 24,000, J. Glaser, 2003.

Glaser, 2003c. Geologic Map of the Cove Point Quadrangle, Calvert County, Maryland, Maryland Geological Survey, 1:24,000 scale, J. Glaser, 2003c.

Glover, 1995a. E-3 Southwestern Pennsylvania to Baltimore Canyon Trough, Geological Society of America Centennial Continent/Ocean Transect #19, L. Glover III, and K. Klitgord, 1995.

Glover, 1995b. Chapter 1, Tectonics of the central Appalachian orogen in the vicinity of corridor E-3, with implications for tectonics of the southern Appalachians, in L. Glover III and K. Klitgord, Chief Compilers, E-3 Southwestern Pennsylvania to Baltimore Canyon Trough, Geological Society of America Continent/Ocean Transect #19, Explanatory Pamphlet, p 2–49, L. Glover III, J. Costain, and C. Coruh, 1995.

Glover, 1997. Paleozoic collisions, Mesozoic rifting and structure of the Middle Atlantic states continental margin: An "EDGE" Project report, in Glover, L., and Gates, A. E., eds., Central and Southern Appalachian Sutures: Results of the EDGE Project and Related Studies: Boulder, Colorado, Geological Society of America Special Paper 314, L. Glover, R. E. Sheridan, W. S. Holbrook, J. Ewing, M. Talwani, R. B. Hawman, and P. Wang, 1997.

Hack, 1989. Geomorphology of the Appalachian Highlands, R. Hatcher Jr, W. Thomas, and G. Viele, eds., The Geology of North America, Volume F-2, The Appalachian-Ouachita Orogen in the United States, Geological Society of America, J. Hack, 1989.

Hackley, 2007 Northward extension of Carolina slate belt stratigraphy and structure, south-central Virginia: Results from geologic mapping, American Journal of Science, Volume 325, Number 4, p 749-771, P. C. Hackley, J. D Peper, W. C. Burton and J. W. Horton (Jr), 2007.

Hansen, 1978. Upper Cretaceous (Senonian) and Paleocene (Danian) Pinchouts on the South Flank of the Salisbury Embayment, Maryland and their relationship to antecedent basement structures, Department of Natural Resources Maryland Geological Survey Report of Investigations No. 29, p 36, H. Hansen, 1978.

Hansen, 1984. Summary of Hydrogeologic Data from a Deep (2678 ft.) Well at Lexington Park, St. Mary's County, Maryland, Maryland Geological Survey Open File Report No. 84-02-1, H. Hansen and J. Wilson, 1984.

Hansen, 1986. The Lithology and Distribution of Pre-Cretaceous basement rocks beneath the Maryland Coastal Plain, Department of Natural Resources Maryland Geological Survey Report of Investigations No. 44, p 27, H. Hansen and J. Edwards Jr, 1986.

Hansen, 1988. Buried rift basin underlying coastal plain sediments, central Delmarva Peninsula, Maryland, Geology, Volume 49, p 779-782, H. Hansen, September 1988.

Hansen, 1996. Hydrostratigraphic Framework of the Piney Point-Nanjemoy Aquifer and Aquia Aquifer in Calvert and St. Mary's Counties, Maryland, Maryland Geological Survey, Open-File Report No 96-02-8, p 45, H. Hansen, 1996.

Harris, 1982. Interpretive seismic profile along Interstate I-64 from the Valley and Ridge to the Coastal Plain in central Virginia, United States Geological Survey Oil and Gas Investigations Chart OC-123, L. Harris, W. deWitt Jr, and K. Bayer, 1982.

Hatcher, 1983. Basement massifs in the Appalachians: their role in deformation during the Appalachian Orogenies, Geological Journal, Volume 18, p 255-265, R. D. Hatcher (Jr), 1983.

Hatcher, 1987. Tectonics of the southern and central Appalachian internides, Annual Reviews of Earth and Planetary Science, Volume 15, p 337–362, R. Hatcher Jr, 1987.

Hatcher, 1989. Alleghenian Orogen, in Hatcher, R.D., William, A., Viele, G., eds., The Appalachian-Ouachita Orogen in the United States, Geological Society of America DNAG, Volume F-2, p 233-318, R. Hatcher, W. Thomas, P. Geiser, A. Snoke, S. Mosher, and D. Wiltschko, 1989.

Hatcher, 2004. Paleozoic structure of internal basement massifs, southern Appalachian Blue Ridge, incorporating new geochronologic, Nd and Dr isotopic, and geochemical data, in Tollo, R. P., Corriveau, L., McLelland, J., and Bartholomew, M.J., eds. Proterozoic tectonic evolution of the Grenville orogen in North America: Boulder, Colorado, Geological Society of America Memoir 197, p 525-547, R. Hatcher (Jr), B. R. Bream, C. F. Miller, J. O. Eckert (Jr), P. D. Fullagar, and C. W. Carrigan, 2004.

Hatcher, 2007. Basement Massifs in the Appalachians: Their role in deformation during the Appalachian Orogenies. Geological Journal, Volume 18, p. 255-265, R. D. Hatcher (Jr), 2007.

Henika, 2006. Geology of the Southside Piedmont, in Virginia Museum of National History Guidebook #6, Henika, W.S., Hibbard, J., and Beard, J. eds, W. S. Henika, J. P. Hibbard, J. Beard, P. Bradley, B. Cattanach, M. Ozdogau, E. Robbins, and P. Thayer, 2006.

Hibbard, 1995. Orogenesis exotic to the Iapetan cycle in the Southern Appalachians, J. Hibbard, C. van Staal, and P. Cawood, eds., Current Perspectives in the Appalachian-Caledonian Orogen, Special Paper - Geological Association of Canada, Volume 41, p 191-206, J. Hibbard and S. Samson, 1995.

Hibbard, 1998. The Hyco shear zone in North Carolina and southern Virginia: implications for the Piedmont zone-Carolina zone boundary in the southern Appalachians: American Journal of Science, v. 298, p. 85-107, J. Hibbard, G. Shell, P. Bradley, S. Samson, and G. Worthman, 1998.

Hibbard, 2000. Docking Carolina: Mid-Paleozoic accretion in the southern Appalachians: Geology, v. 28, p. 127-130, J. Hibbard, 2000.

Hibbard, 2002. The Carolina Zone: overview of Neoproterozoic to early Paleozoic per-Gondwanan terranes along the eastern flank of the southern Appalachians, Earth Science Reviews, Volume 57, p 299-399, J. Hibbard, E. Stoddard, D. Secor, and A. Dennis, 2002.

Hibbard, 2003. Smith River allochthon: A southern Appalachian peri-Gondwanan terrane emplaced directly on Laurentia? Geology, Volume 31, p. 215-218 J. P. Hibbard, R. J. Tracy and W. S. Henika, 2003.

Hibbard, 2007. A Comparative Analysis of Pre-Silurian Crustal Building Blocks of the Northern and the Southern Appalachian Orogen, American Journal of Science, Volume 307, p 23, J. Hibbard, C. van Staal, and D. Rankin, 2007.

Hibbard, 2006. Lithotectonic map of the Appalachian orogen, Canada – United States of America, Geological Survey of Canada Map 02096A, 2 sheets, Scale1:1,500,000, J. Hibbard, C. van Staal, D. Rankin, and H. Williams, 2006.

Higgins, 1974. Interpretation of aeromagnetic anomalies bearing on the origin of Upper Chesapeake Bay and river course changes in the central Atlantic seaboard region: Speculations; Geology, v. 2 no. 1, p. 73-76, M.W. Higgins, I. Zietz, and G.W. Fisher, 1974.

Higgins, 1986. Geologic Map of Cecil County, State of Maryland, U.S. Geological Survey, 1 sheet, Scale 1:62500, M. Higgins and L. Conant, 1986.

Higgins, 1990. The geology of Cecil County, Maryland; Maryland Geological Survey, Bulletin 37, p. 183, M.W. Higgins, and L.B. Conant, 1990.

Hinze, 1987. Magnetic Anomaly map of North America, Decade of North American Geology (DNAG), Geological Society of America, Scale 1:5,000,000, 5 plates, W. Hinze and P. Hood, 1987.

Hittelman, 1994. Geophysics of North America, National Oceanic and Atmospheric Administration, A. Hittelman, J. Kinsfather, and H. Meyers, 1994.

Horton, 1989. Tectonostratigraphic terranes and their Paleozoic boundaries in the central and southern Appalachians. Geological Society of America, Special paper 230, p 213-245, J. Horton, A. Drake, and D. Rankin, 1989.

Horton, 1991. Preliminary Tectonostratigraphic Terrane Map of the Central and Southern Appalachians, U.S. Geological Survey Miscellaneous Investigations Series Map I-2163, J. Horton, A. Drake, D. Rankin, and R. Dallmeyer, 1991.

Howell, 1995. Principles of terrane analysis: new applications for global tectonic, Chapman and Hall, Topics in the Earth Sciences 8, 2nd edition, p 245, D. G. Howell, 1995.

Huber, 2000. Warm Climates in Earth History, Cambridge University Press, p. 480, B.T. Huber, K.G. MacLeod, S.L. Wing, 2000.

Hunt, 1967. Physiography of the United States, W.H. Freeman and Company, p 480, C. Hunt, 1967.

Hunt, 1972. Geology of Soils; Their Evolution, Classification, and Uses, W.H. Freeman and Company, p 344, C. Hunt, 1972.

Hutchinson, 1985. New York Bight Fault, Geologic Society of America Bulletin, Volume 96, p. 975-989. D.R. Hutchinson and J.A. Grow, 1985.

Jacobeen, 1972. Seismic Evidence for High Angle Reverse Faulting in the Coastal Plain of Prince Georges and Charles County, Maryland, Maryland Geological Survey, Information Circular No. 13, F. Jacobeen Jr, 1972.

Johnson, 1973. Bouguer gravity of northeastern Virginia and the Eastern Shore Peninsula, Virginia Division of Mineral Resources Report of Investigations 32, p 48, S. Johnson, 1973.

Johnston, 1985a. Seismotectonics of the Southern Appalachians, Bulletin of the Seismological Society of America, Volume 75, Number 1, p 291-312, A. Johnston, D. Reinbold, and S. Brewer, 1985.

Johnston, 1985b. A basement block model for Southern Appalachian seismicity, Geological Society of America - Abstracts with Programs, Volume 17, Number 2, p 97, A. Johnston, and D. Reinbold, 1985.

Johnston, 1994. The Earthquakes of Stable Continental Regions: Volume 1 - Assessment of Large Earthquake Potential, EPRI, TR-102261-V1, A. Johnston, K. Coppersmith, L. Kanter, and C. Cornell, 1994.

Kafka, 1985. Earthquake Activity in the Greater New York City Area: Magnitudes, Seismicity, and Geologic Structures, Bulletin of the Seismological Society of America, Volume 75, Number 5, p 1285-1300, A. Kafka, E. Schlesinger-Miller, and N. Barstow, 1985.

Kafka, 1989. Earthquake activity in the greater New York City area—A faultfinder's guide, in Weiss, D., ed. Field trip guidebook: New York State Geological Association, 61st Annual Meeting, Middletown, New York, October 13-15, 1989, Guidebook, p 177-203, A. Kafka, M. Winslow, and N. Barstow, 1989.

Kafka, 1996. Seismicity in the area surrounding two Mesozoic rift basins in the northeastern United States, Seismological Research Letters, Volume 67, p 69-86, A.L. Kafka and P.E. Miller, 1996.

Karabinos, 2008. External Basement Massifs in the Northern Appalachians: the Link Between Rodinia and angea. Geological Society of America Abstracts with Programs, Vol. 40, No. 6, p. 289, P. Karabinos, 2008.

Keppie, 1989. Tectonic map of Pre-Mesozoic terranes in circum-Atlantic Phanerozoic orogens, Nova Scotia Department of Mines and Energy, Halifax, N.S., scale 1:5,000,000, J. D. Keppie and D. Dallmeyer, 1989.

Kidwell, 1988. Reciprocal sedimentation and noncorrelative hiatuses in marine-paralic siliciclastics: Miocene outcrop evidence, Geology, Volume 16, p 609-612, S. Kidwell, 1988.

Kidwell, 1997. Anatomy of Extremely Thin Marine Sequences Landward of a Passive-Margin Hinge Zone: Neogene Calvert Cliffs Succession, Maryland, Journal of Sedimentary Research, Volume 67, Number 2, p 322-340, S. Kidwell, 1997.

Kim, 2005. The 9 December 2003 Central Virginia Earthquake Sequence: A Compound Earthquake in the Central Virginia Seismic Zone: Bulletin of the Seismological Society of America, Volume 95, Number 6, p 2428-2445, W. Kim and M. Chapman, 2005.

King, 1978. The new York-Alabama lineament: geophysical evidence for a major crustal break in the basement beneath the Appalachian basin, Geology, Volume 6, p 312-318, E. King and I. Zietz, 1978.

Klitgord, 1979. Basin structure of the U.S. Atlantic margin, J. Watkins, L. Montadert, and P. Dickerson, eds, Geological and geophysical investigations of continental margins: American Association of Petroleum Geologists Memoir 29, p 85-112, K. Klitgord and J. Behrendt, 1979.

Klitgord, 1988. U.S. Atlantic continental margin; Structural and tectonic framework, R. Sheridan and J. Grow, eds., The Atlantic Continental Margin, U.S., Geological Society of America, The Geology of North America, Volume I-2, p 19-55, K. Klitgord, D. Hutchinson, and H. Schouten, 1988.

Klitgord, 1995. Mid-Atlantic Continental Margin: The Mesozoic-Cenozoic Continent-Ocean Boundary, in L. Glover III, and K. Klitgord, Chief Compilers, E-3 Southwestern Pennsylvania to Baltimore Canyon Trough, Geological Society of America Continent/Ocean Transect #19, Explanatory Pamphlet, K. Klitgord, C. Poag, L. Glover, R. Sheridan, D. Hutchinson, R. Mixon, and R. Benson, 1995.

Lane, 1983. Physiographic Provinces of Virginia, Virginia Geographer, Volume XV, Fall-Winter, C. Lane, 1983.

Lash, 1989. Documentation and significance of progressive microfabric changes in Middle Ordovician trench mudstones, Geological Society of America Bulletin, Volume 101, p. 1268-1279, G. G. Lash, 1989.

Lefort, 1989. Is there an Archean crust beneath Chesapeake Bay (abs): Abstracts, 28th International Geological Congress, p 2-227, J. Lefort and M. Max, July 1989.

LeTourneau, 2003. Tectonic and climatic controls on the stratigraphic architecture of the Late Triassic Taylorsville Basin, Virginia and Maryland, P. Olsen, eds., The great rift valleys of Pangea in eastern North America, Sedimentology, Stratigraphy and Paleontology, Volume 2, p 12-58, P. LeTourneau, 2003.

LeVan, 1963. A magnetic survey of the Coastal Plain in Virginia, Virginia Division of Mineral Resources Report of Investigations 4, p 17, D. LeVan and R. Pharr, 1963.

Lyons, 1982. Gravity anomaly map of the United States, Society of Exploration Geophysicists, scale 1:2,500,000, sheets, P. Lyons, N. O'Hara, 1982.

Lindholm, 1978. Triassic-Jurassic in eastern North America – A model based on pre-Triassic structures: Geology, V. 6, p. 365-368. R.C. Lindholm, 1977.

Maguire, 2003. Continuation of Appalachian Piedmont under New Jersey Coastal Plain, in D. W. Valentino and A.E. Gates, eds, The Mid-Atlantic Piedmont: Tectonic Missing Link of the Appalachians: Boulder, Colorado, Geological Society of America Special Paper 330, T. J. Maguire, R. E. Sheridan, R. A. Volkert, M. D. Feigenson, M. D., and L. C. Patino, 2003,

Manspeizer, 1988. Late Triassic-early Jurassic synrift basins of the U.S. Atlantic margin, in R.E. Sheridan and J.A. Grow (eds.), The Atlantic Continental Margin, vol. 1-2 of The Geology of North America, Geological Society of America, Boulder CO., p. 197-216, W. Manspeizer, and H. Cousminer, 1988.

Manspeizer, 1989. Post-Paleozoic Activity, Geology of North America, Volume F-2, The Appalachian-Ouachita Orogen in the United States, Geological Society of America, W.

Manspeizer, J. DeBoer, J. Costain, A. Froelich, C. Coruh, P. Olsen, G. McHone, J. Puffer, and D. Prowell, 1989.

Markewich, 1990. Contrasting Soils and Landscapes of the Piedmont and Coastal Plain, Eastern United States, Geomorphology, Volume 3, p 417–447, H. Markewich, M. Pavich, and G. Buell, 1990.

Marple, 1993. Evidence for Possible Tectonic Upwarping Along the South Carolina Coastal Plain from an Examination of River Morphology and Elevation Data, Geology, Volume 21, p 651–654, R. Marple and P. Talwani, 1993.

Marple, 2000. Evidence for a Buried Fault System in the Coastal Plain of the Carolinas and Virginia - Implications for Neotectonics in the Southeastern United Sates, Geological Society of America Bulletin, Volume 112, Number 2, p 200–220, R. Marple and P. Talwani, February 2000.

Marple, 2004a. Relationship of the Stafford fault zone to the right-stepping bends of the Potomac, Susquehanna, and Delaware Rivers and related upstream incision along the U.S. Mid-Atlantic fall line; in Southeastern Geology, Volume 42, Number 3, p 123-144, R. Marple, 2004.

Marple, 2004b. Proposed Shenandoah Fault and East Coast-Stafford Fault System and Their Implications for Eastern U.S. Tectonics, Southeastern Geology, Volume 43, Number 2, p 57-80, R. Marple and P. Talwani, 2004.

MGS, 2007. Physiographic Provinces and their Subdivisions in Maryland, Maryland Geological Survey, 2007, Website: http://www.mgs.md.gov, Date accessed: June 25, 2007.

McCartan, 1989a. Geologic Map of Charles County, Maryland, Maryland Geological Survey, 1 sheet, Scale 1:62,500, L. McCartan, 1989.

McCartan, 1989b. Geologic Map of St. Mary's County, Maryland: Maryland Geological Survey map, Scale 1:62,500, L. McCartan, 1989.

McCartan, 1989c. Atlantic Coastal Plain Sedimentation and Basement Tectonics Southeast of Washington, D.C., Field Trip Guide Book T214, 28th International Geological Congress, July 13, L. McCartan, 1989.

McCartan, 1990. Geologic Map of the Coastal Plain and Upland Deposits, Washington, D.C., Maryland, and Virginia, U.S. Geological Survey, 1 sheet, Scale 1:24,000, L. McCartan, 1990.

McCartan, 1995. Geologic Map and Cross Sections of the Leonardtown 30 X 60 minute quadrangle, Maryland and Virginia. U.S. Geological Survey Open-file report OFR 95-665, p 38, 1 plate, L. McCartan, W. Newell, J. Owens and G. Bradford, 1995.

McLaughlin, 2002. Results of Trenching Investigations along the New Castle Railroad Survey-1 Seismic Line, New Castle, Delaware, Delaware Geological Survey, Open File Report 43, p 17, P. McLaughlin, S. Baxter, K. Ramsey, T. McKenna, S. Strohmeier, 2002.

Merchat, 2007. The Cat Square terrane: Possible Siluro=Devonian remnant ocean basin in the Inner Piedmont, southern Appalachians, USA, in Hatcher, R,D, et al (eds), 40D Framework of Continental Crust, Geological Society of America Memoir 200, p. 553-565, 2007.

Milici, 1991. Preliminary geologic section across the buried part of the Taylorsville basin, Essex and Caroline Counties, Virginia: Virginia Division of Mineral resources Open File Report 91-1, p 31, R. Milici, K. Bayer, P. Pappano, J. Costain, C. Coruh, J. Cahit, 1991.

Milici, 1995. Structural Section Across the Atlantic Coastal Plain, Virginia and Southeasternmost Maryland, Virginia Division of Mineral Resources, Publication 140, 2 plates, R. Milici, J. Costain, C. Coruh, and P. Pappano, 1995.

Mixon, 1977. Stafford Fault System: Structures Documenting Cretaceous and Tertiary Deformation Along the Fall Line in Northeastern Virginia, Geology, Volume 5, p 437–440, R. Mixon and W. Newell, 1977.

Mixon, 1978. The Faulted Coastal Plain Margin at Fredericksburg, Virginia, Tenth Annual Virginia Geology Field Conference, R. Mixon and W. Newell, October 1978.

Mixon, 1982. Mesozoic and Cenozoic Compressional Faulting Along the Atlantic Coastal Plain Margin, Virginia, in Lyttle ed., Central Appalachian Geology NE-SE Geological Society of America Field Trip Guidebook, p. 29-54, R. B. Mixon, and W. L. Newell, 1982.

Mixon, 1984. Folds and faults in the Inner Coastal Plain of Virginia and Maryland – Their effects on distribution and thickness of Tertiary rock units and local geomorphic history, in Frederiksen, N.O., and Krafft, K., eds., Cretaceous and Tertiary stratigraphy, paleontology, and structure, southwestern Maryland and northeastern Virginia: Field trip volume and guidebook (for field trip held October 17, 1984), Reston, Va. American Association of Stratigraphic Palynologists, p 112-122, R. Mixon and D. Powars, 1984.

Mixon, 1989. Geologic Map and Generalized Cross Sections of the Coastal Plain and Adjacent Parts of the Piedmont, Virginia, U.S. Geological Survey, Miscellaneous Investigations Series Map I-2033, 2 sheets, Scale 1:250,000, R. Mixon, C. Berquist, W. Newell, G. Johnson, D. Powers, J. Schindler, and E. Rader, 1989.

Mixon, 1992. Nature and Timing of Deformation of Upper Mesozoic and Cenozoic Deposits in the Inner Atlantic Coastal Plain, Virginia and Maryland, U.S. Geological Survey Circular C1059, p 65-73, R. Mixon, D. Powars, and D. Daniels, 1992.

Mixon, 2000. Geologic Map of the Fredericksburg 30' x 60' Quadrangle, Virginia and Maryland, U.S. Geological Survey, Geologic Investigations Series Map I-2607, R. Mixon, L. Pavlides, D. Powars, A. Froelich, R. Weems, J. Schindler, W. Newell, L. Edwards, and L. Ward, 2000.

Mulvey, 2004. 40Ar/39Ar Constraints on the Age of Fabric Development in the Westminster Terrane, North-Central Maryland, Northeastern Section (39th Annual) and Southeastern Section (53rd Annual) Joint Meeting, B. K. Mulvey, M. J. Kunk, S. Southworth, and R. P. Wintsch, 2004.

Murphy, 2004. Neoproterozoic—Early Paleozoic evolution of peri-Gondwanan terranes: implications for Laurentia-Gondwana connections. International Journal of Earth Sciences, Volume. 93, Number 5, p. 659-682, J. B. Murphy, S. A. Pisarevsky, R. D. Nance and J. D. Keppie, 2004.

Nelson, 1962. Geology and Mineral resources of Albermarle County, Virginia Division of Mineral Resources Bulletin 77, 92 p., 1 folded map, Scale 1:62,500, W. Nelson, 1962.

Nelson, 1980. Determination of Holocene fault movement along the Ramapo fault in southeastern New York using pollen stratigraphy, Geological Society of America Abstracts with Programs, Volume 12, Number 2, p 75, S. Nelson, 1980.

Nelson, 1981. The Clingman Lineament; Aeromagnetic Evidence for a Major Discontinuity in the North American Basement, Geological Society of America, Southeastern Section, Abstracts with Programs, Volume 13, Number 1, p 31, A. Nelson and I. Zietz, January 1981.

Newell, 1976. Detailed Investigation of a Coastal Plain-Piedmont Fault Contact in Northeastern Virginia, U.S. Geological Survey Open-File Report 76-329, W. Newell, D. Prowell, and R. Mixon, 1976.

Newman, 1983. Holocene neotectonics of the lower Hudson Valley: Geological Society of America Abstracts with Programs, Volume 15, Number 3, p 148, W. Newman, L. Cinquemani, J. Sperling, L. Marcus, and R. Pardi, 1983.

NRC, 1978. Standard Format and Content of Safety Analysis Reports for Nuclear Power Plants, LWR Edition, Regulatory Guide 1.70, Revision 3, U.S. Nuclear Regulatory Commission, November 1978.

NRC, 1997. Identification and Characterization of Seismic Sources and Determination of Safe Shutdown Earthquake Ground Motion, U.S. Nuclear Regulatory Commission, Regulatory Guide 1.165, March 1997.

NRC, 2005. Safety Evaluation Report for an Early Site Permit (ESP) at the North Anna ESP Site – NUREG-1835, Nuclear Regulatory Commission, September 2005.

NRC, 2007. Basis Geologic and Seismic Information, Regulatory Guide 1.206, Section 2.5.1, U.S. Nuclear Regulatory Commission, June, 2007.

Obermier, 1998. Paleoliquefaction Evidence for Seismic Quiescence in Central Virginia During the Late and Middle Holocene Time (abs), Eos Transactions of the American Geophysical Union, Volume 79, Number 17, p S342, S. Obermier and W. McNulty, 1998.

Otton, 1955. Ground-Water Resources of the Southern Maryland Coastal Plain, Maryland Department of Geology, Mines and Water Resources, Bulletin 15, p 347, E. Otton, 1955.

Owens, 1979. Upper Cenozoic Sediments of the Lower Delaware Valley and the Northern Delmarva Peninsula, New Jersey, Pennsylvania, Delaware, and Maryland, Geological Survey Professional Paper 1067-D, U.S. Geological Survey, J. Owens and J. Minard, 1979.

Owens, 1998. Bedrock geologic map of central and southern New Jersey, U.S. Geological Survey M.I. Series Map I-2540-B, 4 sheets, Scale 1:100,000, J. Owens, P. Sugarman, N. Sohl, R. Parker, H. Houghton, R. Volkert, Jr., and R. Orndoff, 1998.

Page, 1968. Seismicity in the vicinity of the Ramapo fault, New Jersey-New York, Bulletin of Seismological Society of America, Volume. 58, p 681-687, R.A. Page, P.H. Molnar, and J. Oliver, 1968.

Pavlides, 1980. Revised Nomenclature and Stratigraphic Relationships of the Fredericksburg Complex and Quantico Formation of the Virginia Piedmont, U.S. Geological Survey Professional Paper 1146, L. Pavlides, 1980.

Pavlides, 1983. Late Cenozoic faulting along the Mountain Run Fault Zone, central Virginia Piedmont, GSA Abstracts with Programs, Volume 15, Number 2, L. Pavlides, 1983.

Pavlides, 1986. Mountain Run Fault Zone of Virginia, U.S. Geological Survey Open-File Report 87-93, 93–94, L. Pavlides, 1986.

Pavlides, 1989. Early Paleozoic Composite Mélange Terrane, Central Appalachian Piedmont, Virginia and Maryland: Its Origin and Tectonic History, Geological Society of America Special Paper 228, p 135–193, L. Pavlides, 1989.

Pavlides, 1994. Early Paleozoic Alkalic and Calc-Alkalic Plutonism and Associated Contact Metamorphism, Central Virginia Piedmont, U.S. Geological Survey Professional Paper 1529, L. Pavlides, J. Arth, J. Sutter, T. Stern, and H. Cortesini Jr, 1994.

Pavlides, 2000. Geology of the Piedmont and Blue Ridge Provinces, Chapter II of the pamphlet to accompany the U.S. Geological Survey, Geologic Investigations Series Map I-2607, L. Pavlides, 2000.

Pazzaglia, 1993. Stratigraphy, petrography, and correlation of late Cenozoic middle Atlantic Coastal Plain deposits: Implications for late-stage passive-margin geologic evolution, Geological Society of America Bulletin, Volume 105, p 1617-1634, F. Pazzaglia, 1993.

Pazzaglia, 1993. Fluvial terraces of the lower Susquehanna River, Geomorphology, Volume 8, p 83-113, F. Pazzaglia and T. Gardner, 1993.

Pazzaglia, 1994. Late Cenozoic flexural deformation of the middle U.S. Atlantic passive margin, Journal of Geophysical Research, Volume 99, Number B6, p 12, 143-12, 157, F. Pazzaglia and T. Gardner, 1994.

Pazzaglia, 2006. Rivers, glaciers, landscape evolution, and active tectonics of the central Appalachians, Pennsylvania and Maryland, in Pazzaglia, F.J., ed, Excursions in Geology and History: Field Trips in the Middle Atlantic States: Geological Society of America Field Guide 8. P. 169-197, F.J. Pazzaglia, D.D. Braun, M. Pavich, P. Bierman, N. Potter, D. Merritts, R. Walter, D. Germanoski, 2006.

Pesonen, 2003. Palaeomagnetic configuration of continents during the Proterozoic, Tectonophysics Volume 375, Issues 1-4, Pages 289-324, L. J. Pesonen, S. A. Elming, S. Mertanen, S. Pisarevsky, M. S. D'Agrella-Filho, J. G. Meert, P. W. Schmidt, N. Abrahamsen, and g. Bylundi, 2003.

Poag, 1991. Rise and demise of the Bahama-Grand Banks gigaplatform, northern margin of the Jurassic proto-Atlantic seaway, Marine Geology, Volume 102, p 63-130, C. Poag, 1991.

Poag, 2004. The Chesapeake Bay Crater; geology geophysics of a late Eocene submarine impact structure, Springer-Verland: Berlin, p 522, W. Poag, C. Koeberl, and W. Reimold, 2004.

Poag, 2005. Stratigraphy and Paleoenvironments of Early Postimpact Deposits at the USGS NASA Langley Corehole, Chesapeake Bay Impact Crater, Chapter F of Studies of the

Chesapeake Bay Impact Structure - The USGS-NASA Langley Corehole, Hampton, Virginia, and Related Coreholes and Geophysical Surveys, U.S. Professional Paper 1688, pages F1 to F51, Poag, W. and Norris, R.D., 2005.

PEPC, 1973. Preliminary safety analysis report, Douglas Point Nuclear Generating Station, Units 1 and 2, Volume 2, Dames and Moore for the Potomac Electric Power Company, Docket Number 50448-2 and 50449-2, 1973.

Powars, 1999. The effects of the Chesapeake Bay Impact Crater on the Geological Framework and Correlation of Hydrogeologic Units of the Lower York-James Peninsula, Virginia, U.S. Geological Survey Professional Paper 1612, p 82, 9 plates, D. Powars and T. Bruce, 1999.

Pratt, 1988. A geophysical study of the Earth's crust in Central Virginia: Implications for Appalachian Crustal structure: Journal of Geophysical Research, V. 93 p. 6649-6667, T. Pratt, C. Coruh, J. Costain, and L. Glover III, 1988.

Prowell, 1983. Index of Faults of Cretaceous and Cenozoic Age in the Eastern United States, U.S. Geological Survey Miscellaneous Field Studies Map MF-1269, D. Prowell, 1983.

PSEG, 2002. Section 2.5, Geology, Seismology, and Geotechnical Engineering, Updated Final Safety Analysis Report, Revision 12, Hope Creek Generating Station, submitted to the NRC (LR-N02-0179), 2002.

Quittmeyer, 1985. Possible implications of recent microearthquakes in sourthern New York state: Earthquake Notes, Volume 56, p 35-42, R.C. Quittmeyer, C.T. Statton, K.A. Mrotek and M. Houlday, 1985.

Rader, 1993. Geologic map of the Virginia – expanded explanation: Virginia Division of Mineral Resources, E. Rader and N. Evans, eds., 1993.

Rankin, 1989. Pre-orogenic terranes, in Hatcher (Jr), R.D., et al., eds., The Appalachian-Ouachita orogen in the United States: Boulder, Colorado, Geological Society of America, The Geology of North America, Volume F-2, p 7-100, D.W. Rankin, A. A. Drake (Jr), L. Glover, R. Goldsmith, L. M. Hall, D. P Murray, N. M. Ratcliffe, J. F. Read, D. T. Secor (Jr), and R. S. Stanley, 1989.

Ratcliffe, 1971. The Ramapo fault system in New York and Adjacent Northern New Jersey—A case of tectonic heredity, Geological Society of America Bulletin, Volume 82, p 125-142, N. Ratcliffe, 1971.

Ratcliffe, 1980. Brittle faults (Ramapo fault) and phyllonitic ductile shear zones in the basement rocks of the Ramapo seismic zones New York and New Jersey, and their relationship to current seismicity, in Manspeizer, W., ed., Field studies of New Jersey geology and guide to field trips Newark, New Jersey, Rutgers University, Geology Department, U.S., New York State Geological Association, 52nd annual meeting, October 10, 1980, Guidebook, p 278-312, N. Ratcliffe, 1980.

Ratcliffe, 1982. Results of core drilling of the Ramapo fault at Sky Meadow Road, Rockland County, New York, and assessment of evidence for reactivation to produce current seismicity, U.S. Geological Survey Miscellaneous Investigations, Map I-1401, 1 sheet, N. Ratcliffe, 1982.

Ratcliffe, 1983. Fault reactivation models for the origin of eastern United States seismicity, Does the solution to Charleston reside at Charleston, in Hays, W.W., and Gori, P.L., eds., Proceedings of Conference XX: A workshop on the 1886 Charleston, South Carolina, earthquake and its implications for today, US Geological Survey Open-File Report 83-843, N.M. Ratcliffe, 1983.

Ratcliffe, 1985a. Fault reactivation models for origin of the Newark basin and studies related to eastern U.S. seismicity, in Robinson, G.R., and Froelich, A.J., eds., Proceedings of the Second U.S. Geological Survey Workshop on the Early Mesozoic Basins of the Eastern United States, US Geological Survey Circular 946, p 36-45, N.M. Ratcliffe, and W. Burton, 1985.

Ratcliffe, 1985b. Northeast Seismicity and Tectonics, in Jacobson, M.L., and R., R.T., eds., National Earthquake Hazards Reduction Program summaries of technical reports, Volume XX, US Geological Survey Open File Report 85-464, p 54-58, N.M. Ratcliffe, and J. Costain, 1985.

Ratcliffe, 1986. Seismic Reflection Geometry of the Newark Basin Margin in Eastern Pennsylvania, NUREG/CR-4676, N. Ratcliffe, W. Burton, R. D' Angelo, and J. Costain, 1986.

Ratcliff, 1986a. Low-angle extensional faulting, reactivated mylonites and seismic reflection geometry of the Newark basin margin in eastern Pennsylvania, Geology, v. 14. p 766-770, N.W. Ratcliff, W.C. Burton, and R.M. D'Angelo, and J.K. Costain, 1986.

Ratcliffe, 1986b. Low-angle extensional faulting, reactivated mylonites, and seismic reflection geometry of the Newark basin margin in eastern Pennsylvania, Geology, Volume 14 , p 766-770, N.M. Ratcliffe, W. Burton, R.M. D'Angelo, and J.K.Costain, 1986.

Ratcliffe, 1988. Structural analysis of the Furlong fault and the relation of mineralization to faulting and diabase intrusion, Newark basin, Pennsylvania, in Froelich, A.J., and Robinson, G.R., eds., Studies of the early Mesozoic Basins of the Eastern United States, US Geological Survey Bulletin 1776, p 176-193, N.M. Ratcliffe and W.C. Burton, 1988.

Ratcliffe, 1990. Orientation, movement history, and cataclastic rocks of Ramapo fault based on core drilling and trenching along the western margin of the Newark basin near Bernardsville, New Jersey, U.S., Geological Survey Miscellaneous Investigations, Map I-1982, 1 sheet, N. Ratcliffe, W. Burton, and M. Pavich, 1990.

Ratcliffe, 1992. Bedrock geology and seismotectonics of the Oscawana Lake quadrangle, New York, p 38, N.M. Ratcliffe, 1992.

Reinecker, 2008. The release 2008 of the World Stress Map (www.world-stress-map.org), Heidelberg Academy of Sciences and Humanities, J. Reinecker, O. Heidbach, M. Tingay, B. Sperner, and B. Müller.

Richardson, 1991. North American Plate Dynamics, Journal of Geophysical Research, Volume 96, R. Richardson and L. Reding, 1991.

Rodgers, 1970. The tectonics of the Appalachians, Wiley-Interscience: New York, NY, p 271, J. Rodgers, 1970.

Root, 1989. Basement control of structure in the Gettysburg rift basin, Pennsylvania and Maryland: Tectonophysics, v. 166, p. 281-292. S.I. Root, 1989.

Sanders, 1963. Late Triassic tectonic history of northeaster United States, American Journal of Science 261, p 501-524, J. Sanders, 1963.

Savy, 2002. Guidance for Performing Probabilistic Seismic Hazard Analysis for a Nuclear Plant Site: Example Application to the Southeastern United States, Nuclear Regulatory Commission, NUREG-CR/6607, J. Savy, W. Foxall, N. Abrahamson, and D. Bernreuter, 2002.

Sbar, 1975. The Delaware-New Jersey earthquake of February 28, 1973, Bulletin of the Seismological Society of America, Volume 65, p 85-92, M. Sbar, R. Jordan, C. Stephens, T. Pickett, K. Woodruff, and C. Sammis, 1975.

Scharnberger, 2006. The Lancaster Seismic Zone of southeast Pennsylvania in relation to the Gettysburg-Newark basin, Geological Society of America Abstracts with Programs, Volume 38, Number 2, p 83, C. Scharnberger, 2006.

Schlische, 1990. Quantitative filling model for continental extensional basins with applications to early Mesozoic rifts of eastern North America, Journal of Geology, 98, p. 135-155, R. Schlische., and P. Olsen., 1990.

Schlische, 1992. Structural and Stratigraphic Development of the Newark Extension Basin, Eastern North America: Evidence for the Growth of the Basin and its Bounding Structures, Geological Society of America Bulletin, Volume 104, p 1246-1263, R. Schlische, October 1992.

Schlische, 1993. Anatomy and evolution of the Triassic-Jurassic Continental Rift System, Eastern North America, Tectonics, v. 12, p. 1026-1042, R.W. Schlische, 1993.

Schlische, 2003. Progress in Understanding the Structural Geology, Basin Evolution, and Tectonic History of the Eastern North America Rift System, P. LeTourneau and P. Olsen, eds., The Great Rift Valleys of Pangea in Eastern North America, Volume 1, R. Schlische, 2003.

Schlische, 2003a. Relative timing of CAMP, rifting, continental breakup, and inversion: tectonic significance, by The Central Atlantic Magmatic Province: in Hames, W.E., McHone, G.C., Renne, P.R., and Ruppel, C., eds., American Geophysical Union Monograph 136, p. 33-59, R.W. Schlische, M.O. Withjack, and P.E. Olsen, 2003.

Schlische, 2005. The early Mesozoic Birdsboro central Atlantic Margin basin in the Mid-Atlantic region, eastern United States: Discussion, Geological Society of America Bulletin, V. 117, p. 823-828, R.W. Schlische, and M.O. Withjack, 2005.

Schmidt, 1993. Maryland's Geology, Tidewater Publishers, Centreville, Maryland, p 164, M. Schmidt Jr, 1993.

Schruben, 1994. Geology of the conterminous United States at 1:250,000, 000 scale; a digital representation of the 1974 P. B. King and H. M. Beikman map, U.S. Geological Survey Digital Data Series DDS-0011, P. Schruben, R. Arndt, W. Bawiec, and R. Ambroziak, 1994.

Schulte, 2005. An updated global earthquake catalogue for stable continental regions: reassessing the correlation with ancient rifts: Geophys. J. Int., v. 161, p. 707-72. S.M. Schulte, and W.D. Mooney, 2005.

Schwab, 1997a. Initial results of high-resolution sea-floor mapping offshore of the New York–New Jersey metropolitan area using sidescan sonar, Northeastern Geology and Environmental

Sciences Volume 9, Number 4, p 243–262, W. Schwab, M. Allison, W. Corso, L. Lotto, B. Butman, M. Bucholtz ten Brink, J. Denny, W. Danforth, and D. Foster, 1997.

Schwab, 1997b. Mapping the sea floor offshore of the New York–New Jersey metropolitan area using sidescan sonar—preliminary report, U.S. Geological Survey Open-File Report 97-61, 3 sheets, W. Schwab, W. Corso, M. Allison, B. Butman, J. Denny, L. Lotto, W. Danforth, D. Foster, T. O'Brien, D. Nichols, B. Irwin, and K. Parolski, 1997.

Scott, 2006. Correlating Late Pleistocene Deposits on the Coastal Plain of Virginia with the Glacial-Eustatic sea-level curve (MS Thesis), Old Dominion University, p 112, T. Scott, May 2006.

Seborowski, 1982. Tectonic implications of recent earthquakes near Annsville, New York, Bulletin of Seismological Society of America, Volume 72, p 1601-1609, D.K. Seborowski, G. Williams, J.A. Kelleher, and C.A. Statton, 1982.

Seeber, 1998. The 1994 Cacoosing Valley earthquakes near Reading, Pennsylvania: A shallow rupture triggered by quarry unloading, Journal of Geophysical Research, Volume 103, Number B10, p 24, 505-24, 521, L. Seeber, J. Armbruster, W. Kim, N. Barstow, and C. Scharnberger, 1998.

Sevon, 2000. Regolith in the Piedmont Upland section, Piedmont Province, York, Lancaster, and Chester Counties, Southeastern Pennsylvania, Southeastern Geology, Volume 39, Number 3 and 4, p 223–241, W. Sevon, October 2000.

Sheridan, 1988. The Atlantic Continental Margin, U.S.Geological Society of America, The Geology of North America, Volume 1-2, p 610, R. Sheridan and J. Grow, 1988.

Sheridan, 1988. Geophysical Data, R. Sheridan and J. Grow, eds., The Atlantic Continental Margin, U.S. Geological Society of America, The Geology of North America, Volume 1, p 177-196, R. Sheridan, J. Grow, and K. Klitgord, 1988.

Sheridan, 1993. Deep seismic reflection data of EDGE U.S. mid-Atlantic continentalmargin experiment: Implications for Appalachian sutures and Mesozoic rifting and magmatic underplating, Geology; Volume 21; Number 6; p 563-567, R. E. Sheridan, D. L. Musser, L. Glover, M. Talwani, J. I. Ewing, W. S. Holbrook, G. M. Purdy, R. Hawman and S. Smithson, 1993.

Sheridan, 1998. Grenville age of basement rocks in Cape May NJ well: new evidence for Laurentian crust in U.S, Atlantic Coastal Plain basement Chesapeake terrane. Journal of Geodynamics, Volume 27, pages 623-633, Sheridan, R.E., Maguire, T.J., Feigenson, M.D., Patino, W. C., Volkert, R.A., 1998.

Shumaker, 2000. The New York-Alabama Lineament; An Early Iapetian Wrench Fault?, American Association of Petroleum Geologists Bulletin, Volume 84, Number 9, p 1393, R. Shumaker, September 2000.

Southworth, 2004. Guidebook to Field Trips in the National Capital Region, Central Appalachians: U.S. Geological Survey Circular 1264, p 298, S. Southworth, W. C. Burton and K. Schindler eds., 2004.

Southworth, 2006. Central Appalachian Piedmont and Blue Ridge tectonic transect, Potomac River corridor, in Pazzaglia, F.J., ed., Excursions in Geology and History: Field Trips in the Middle Atlantic States: Geological Society of America Field Guide 8, p 135- 167, S. Southworth, A. A.

Drake (Jr), D. K. Brezinski, R. P. Wintsch, M. J. Kunk, J. N. Aleinikoff, C. W. Naeser and N. D. Naeser, 2006.

Spears, 2002. Geology of the central Virginia Piedmont between the Arvonia syncline and the Spotsylvania high-strain zone, Thirty-Second Annual Virginia Geological Field Conference Guidebook Charlottesville, Virginia, October 11-13, Virginia Division of Mineral Resources. p.36, D. Spears and C. Bailey, 2002.

Spoljaric, 1972. Geology of the Fall Zone in Delaware, Delaware Geological Survey, p 30, N. Spoljaric, March 1972.

Spoljaric, 1973. Normal Faults in Basement Rocks of the Northern Coastal Plain, Delaware, Geological Society of America Bulletin, Volume 84, p 2781-2783, N. Spoljaric, 1973.

Stanford, 1995. Possible Pliocene-Pleistocene Movement on a Reactivated Mesozoic Fault In Central New Jersey, Geological Society of America Abstracts with Programs, Volume 27, Number 1, p 83, S. Stanford, D. Jagel, and D. Hall, 1995.

Stanford, 2002. Surficial Geology of the Monmouth Junction Quadrangle, Somerset, Middlesex, and Mercer Counties, New Jersey, Department of Environment Protection New Jersey Geological Survey Open-File Map OFM 47, 1 plate, Scale 1: 24,000, S. Stanford, 2002.

Stewart, 2002. Late Mississippian paleoseismites from southeastern West Virginia and southwestern Virginia, in Ettensohn, F. F. Rast, N., and Brett, C.E., eds, Ancient seismites: Boulder, Colorado, Geological Society of America Special Paper 359, p 127- 144, K. G. Stewart, J. M. Dennison and M. J. Bartholomew, 2002.

Stone, 1984. Faults in Pleistocene sediments at trace of Ramapo fault in Geological Survey research, fiscal year 1981, U.S. Geological Survey, Professional Paper 1375, p. 49, B. Stone and N. Ratcliffe, 1984.

Swanson, 1982. Preliminary model for early transform history in central Atlantic rifting, Geology, 10:317-320, M. Swanson, 1982.

Swanson, 1986. Preexisting fault control for Mesozoic basin formation in eastern North America, Geology, v. 14 p. 419-422, M.T. Swanson, 1986.

Sykes, 2008. Observations and Tectonic Setting of Historic and Instrumentally Located Earthquakes in the Greater New York City-Philadelphia Area, Bulletin of the Seismological Society of America, Volume 98, p 1696-1719, L.R. Sykes, J.G. Armbruster, W.Y. Kim, and L. Seeber, 2008.

Tanner, 1987. Gravity Anomaly map of North America, Decade of North American Geology (DNAG), Geological Society of America, Scale 1:5,000,000, 5 plates, J. Tanner, 1987.

Thelin, 1991. Landforms of the Conterminous United States–A Digital Shaded-Relief Portrayal, U.S. Geological Survey, pamphlet to accompany Geological Investigation Series Map I-2206, G. Thelin and R. Pike, April 17 1991.

Thomas, 1989. Tectonic map of the Ouachita orogen: In Hatcher, R.D., Jr., Thomas, W.A., and Viele, G.W., eds., The Appalachian-Ouachita orogen in the United States: Geological Society of

America, The Geology of North America, v. F-2, plate 9, W. A. Thomas, G. W. Viele, J. K. Arbenz, R. L. Nicholas, R. E. Denison, W. R. Muehlberger, and P. R. Tauvers, 1989.

Thomas, 2006. Tectonic inheritance at a continental margin: GSA Today, v. 16, no. 2, p. 4–11, W. A. Thomas, 2006.

Thurber, 1985. Crustal structure along the Ramapo fault zone, New York State, Earthquake Notes, Volume 56, p 145-152, C. Thurber and T. Caruso, 1985.

Turcotte, 2002. Geodynamics, Cambridge University Press, p 456, D. Turcotte and G. Schubert, 2002.

USGS, 2008. Catskills Geology, retrieved on 7/27/2009, http://catskillmountainkeeper.org/node/653, United States Geological Survey, 2008.

URS, 2000. Seismic Characterization study for the expansion of the Williams Gas Pipeline – Transco LNG facility, Cove Point, Maryland, URS Corporation, October 2000.

van Staal, 1998. The Cambrian-Silurian tectonic evolution of the northern Appalachians and British Caledonides: history of a complex, west and southwest Pacific-type segmentof Iapetus, Geological Society, London, Special Publications; v. 143; p. 197-242, C. R. van Staal, J. F. Dewey, C. Mac Niocaill and W.S. McKerrow, 1998.

Vigil, 2000. A Tapestry of Time and Terrain, U.S. Geological Survey, pamphlet to accompany U.S. Geological Survey, Geological Investigation Series Map I-2720, J. Vigil, R. Pike, and D. Howell, February 24, 2000.

Walker, 1971. Nondeltaic depositional environments in the Catskill Clastic Wedge (Upper Devonian) of Central Pennsylvania., Geological Society of America Bulletin, Volume 82, Number 5, pgs 1305-1326, R.G. Walker., 1971.

Ward, 2004. Tertiary Lithology and Paleontology, in Southworth, S. and Burton, W., eds., Geology of the National Capital Region- Field Trip Guidebook: U.S. Geological Survey Circular 1264, p 263-279, L. Ward and D. Powars, 2004.

Watts, 1982. Tectonic Subsidence, Flexure, and Global Changes of Sea Level, Nature, Volume 297, p 469-474, A. Watts, 1982.

Weems, 1998. Newly Recognized En Echelon Fall Lines in the Piedmont and Blue Ridge Provinces of North Carolina and Virginia, With a Discussion of Their Possible Ages and Origins, U.S. Geological Survey Open-File Report 98-374, R. Weems,1998.

Wentworth, 1983, Regenerate Faults of Small Cenozoic Offset - Probable Earthquake Sources in the Southeastern United States, U.S. Geological Survey, Professional Paper 1313-S, C. Wentworth and M. Mergner-Keefer, 1983.

Wheeler, 1992. Geologic Implications of Earthquake Source Parameters in Central and Eastern North America, Seismological Research Letters, Volume 63, Number 4, p 491–505, R. Wheeler and A. Johnston, 1992.

Wheeler, 1995. Earthquakes and the Cratonward Limit of Iapetan Faulting in Eastern North America, Geology, Volume 23, 105–108, R. Wheeler, 1995.

Wheeler, 1996. Earthquakes and the Southeastern Boundary of the Intact Iapetan margin in Eastern North America, Seismological Research letters, Volume 67, Number 5, p 77-83, R. Wheeler, 1996.

Wheeler, 2001. Known and suggested Quaternary faulting in the midcontinent United States, Engineering Geology, Volume 62, p 51-78, R.L. Wheeler, and A.J. Crone, 2001.

Wheeler, 2005. Known or Suggested Quaternary Tectonic Faulting, Central and Eastern United States – New and Updated Assessments for 2005, U.S. Geological Survey, Open File Report 2005-1336, p 37, R. Wheeler, 2005.

Wheeler, 2006. Quaternary tectonic faulting in the Eastern United States, Engineering Geology, Volume 82, p 165-186, R. Wheeler, 2006.

Wheeler, 2008. Paleoseismic Targets, Seismic Hazard, and Urban Areas in the Central and Eastern United States, Bulletin of Seismological Society of America, Volume 98, p 1572-1580, R.L. Wheeler, 2008.

Williams, 1983. Appalachian suspect terranes, R. Hatcher Jr, H. Williams and I. Zietz, eds., Contributions to the Tectonics and Geophysics of Mountain Chains, Geological Society of America Memoir 159, p 33-53, H. Williams and R. Hatcher, 1983.

Wilson, 1990. Geology and Hydrologic Assessment of Coastal Plain Aquifiers in the Waldorf Area, Charles County, Maryland, Maryland Geological Survey, Report of Investigations No. 53,138 p., 8 plates, J. Wilson and W. Fleck, 1990.

Withjack, 1998. Diachronous rifting drifting, and inversion on the passive margin of eastern North America: An analog for other passive margins, American Association of Petroleum Geologist Bulletin, Volume 82, p 817-835, M. Withjack, R. Schlische, and P. Olsen, 1998.

Withjack, 2005. A review of tectonic events on the passive margin of eastern North America: in Post, P., ed., Petroleum Systems of Divergent Continental Margin Basins:25th Bob S. Perkins Research Conference, Gulf Coast Section of SEPM, p. 203-235..M.O. Withjack, and R. W. Schlische, 2005.

Zietz, 1982. Composite magnetic anomaly map of the United States, Part A: Conterminous United States, U.S. Geological Survey Map GP-54923, Scale 1:2,500,000, I. Zietz, 1982.

Zoback, 1980. State of Stress in the Conterminous United States, Journal of Geophysical Research, Volume 85, p 6113-6156, M.L. Zoback, and M. Zoback, 1980.

Zoback, 1989a. Tectonic Stress Field of the Coterminous United States, in L. C. Pakiser and M. D. Mooney, eds., Geophysical Framework of the Continental United States, Geological Society of America Memoir 172, p 523–539, M. Zoback and M. Zoback, 1989.

Zoback, 1989b. Global patterns of tectonic stress, Nature, Volume 341, p 291-296, M. Zoback, M. Zoback, J. Adams, M. Assumpcao, S. Bell, E. Bergman, P. Blumling, N. Brereton, D. Denham, J. Ding, K. Fuchs, N. Gay, S. Gregersen, H. Gupta, A. Gvishiani, K. Jacob, R. Klein, P. Knoll, M. Magee, J. Mercier, B. Muller, C. Paquin, K. Rajendran, O. Stephansson, G. Suarez, M. Suter, A. Udias, Z. Xu, and M. Zhizhin,. 1989.

Zoback, 1992. Stress Field Constraints on Intraplate Seismicity in Eastern North America, Journal of Geophysical Research, Volume 97, p 11,761–11,782, M. Zoback, 1992.

2.5.2 Vibratory Ground Motion

The U.S. EPR FSAR includes the following COL Item for Section 2.5.2:

> A COL applicant that references the U.S. EPR design certification will review and investigate site-specific details of the seismic, geophysical, geological, and geotechnical information to determine the safe shutdown earthquake (SSE) ground motion for the site and compare site-specific ground motion to the Certified Seismic Design Response Spectra (CSDRS) for the U.S. EPR.

This COL Item is addressed as follows:

{This section provides a detailed description of the vibratory ground motion assessment that was carried out for the CCNPP Unit 3 site, resulting in the development of the CCNPP Unit 3 ground motion response spectra. The starting point for this site assessment is the EPRI-SOG probabilistic seismic hazard analysis (PSHA) methodology outlined in EPRI NP-4726-A 1988 (EPRI, 1988) and tectonic interpretations in EPRI NP-4726 1986 (EPRI, 1986).

Nuclear Regulatory Commission (NRC) Regulatory Guide 1.165, "Identification And Characterization of Seismic Sources and Determination of Safe Shutdown Earthquake Ground Motion," March, 1997, (NRC, 1997a) states in Section B, Discussion:

> "The CEUS is considered to be that part of the United States east of the Rocky Mountain front, or east of Longitude 105 West (Refs. 4, 5). To determine the SSE in the CEUS, an accepted PSHA methodology with a range of credible alternative input interpretations should be used. For sites in the CEUS, the seismic hazard methods, the data developed, and seismic sources identified by Lawrence Livermore National Laboratory (LLNL) (Refs. 4-6) and the Electric Power Research Institute (EPRI) (Ref. 7) have been reviewed and accepted by the staff."

Reference 7 is Electric Power Research Institute, "Probabilistic Seismic Hazard Evaluations at Nuclear Power Plant Sites in the Central and Eastern United States," NP-4726, All Volumes, 1989-1991. The title and number of the referenced document are not in agreement. The title of EPRI-4726 is "Seismic Hazard Methodology for the Central and Eastern United States." No document could be found that had the title provided by the NRC.

In lieu of the reference 7, i.e., EPRI document, NP-4726, All Volumes, 1989-1991, Section 2.5.2 will implement EPRI NP-4726, "Seismic Hazard Methodology for the Central and Eastern United States," 1986 and EPRI-4726-A, "Seismic Hazard Methodology for the Central and Eastern United States,"1988. EPRI NP-4726-1986 and EPRI-4726-A, 1988 have been determined to be acceptable as described below.

Additionally, the PSHA methodology used for the CCNPP 3 site is described in EPRI NP-6395-D-1989 (EPRI, 1989a). EPRI NP-6395-D (EPRI, 1989a) has been determined to be an acceptable PSHA methodology by the NRC is also described below.

The NRC has accepted the use of the following, which were included in the North Anna Early Site Permit Application by Dominion Nuclear North Anna, LLC, which was approved in

NUREG-1835, Safety Evaluation Report for an Early Site Permit (ESP) at the North Anna Site, 2005. (NRC, 2005).

- EPRI 4726, 1986, "Seismic Hazard Methodology for the Central and Easter United States" was included in the Early Site Permit Application as reference 120. It is also specifically included as a reference in Section C of NUREG-1835.
- EPRI-NP-6395-D, 1989, "Probabilistic seismic hazard evaluation at nuclear plant sites in the central and eastern United States, Resolution of the Charleston Earthquake Issue."
    a. Early Site Permit Application as reference 115.
    b. Generic Letter 88-20, "Individual Plant Examinations of External Events (IPEEE) for Severe Accident Vulnerabilities" (NRC, 1991).

The NRC has accepted the use of the EPRI NP-4726-A, 1988 in the letter dated Oct 31, 2005, T. Mundy, Exelon to NRC, Subject: Response Supplemental Draft Safety Evaluation Report (DSER) Item, page 16 of 112 and page 54 of 112, (Adams Accession No. ML053120131) (Exelon, 2005).

The EPRI-SOG tectonic interpretations in EPRI NP-4726 1986 (EPRI, 1986). were updated with more recent geological, seismological, and geophysical data under the guidance of NRC Regulatory Guide 1.165, (NRC, 1997a). Sections 2.5.2.1 through 2.5.2.3 document this review and update, as needed, of the EPRI-SOG seismicity, seismic source, and ground motion models.

Section 2.5.2.4 develops PSHA parameters at the site assuming the very hard rock foundation conditions implied by currently accepted ground motion attenuation models.

Section 2.5.2.5 summarizes information about the seismic wave transmission characteristics of the CCNPP Unit 3 site with reference to more detailed discussion of all engineering aspects of the subsurface in Section 2.5.4.

Section 2.5.2.6 describes the development of the horizontal ground motion response spectra (GMRS) for the CCNPP Unit 3 site. The selected ground motion is based on the risk-consistent/ performance-based approach of Regulatory Guide 1.208, A Performance-Based Approach to Define the Site-Specific Earthquake Ground Motion (NRC, 2007a), with reference to NUREG/ CR-6728 (NRC, 2001), NUREG/CR-6769 (NRC, 2002b), and ASCE/SEI 43-05 (ASCE 2005). Horizontal ground motion amplification factors are developed using site-specific data and estimates of near-surface soil and rock properties. These amplification factors are then used to scale the hard rock spectra to develop Uniform Hazard Spectra accounting for site-specific conditions using Approach 2A of NUREG/CR-6728 (NRC, 2001) and NUREG/CR-6769 (NRC, 2002). Horizontal spectra are developed from these soil Uniform Hazard Spectra using the performance-based approach of ASCE/SEI 43-05 (ASCE 2005), as implemented in Regulatory Guide 1.208 (NRC, 2007a). The GMRS is defined at the free ground surface of a hypothetical outcrop at the base of the nuclear island foundation. See Sections 2.5.4 and 2.5.2.5 for further discussion of the subsurface conditions.

Section 2.5.2.6 also describes vertical spectra, which are developed by scaling the horizontal spectra by a frequency-dependent vertical-to-horizontal (V:H) factor.

The spectra that are described in this section are considered performance goal-based (risk-informed) site specific safe shutdown earthquake response spectra. The GMRS, and its specific location at a free ground surface, reflect the seismic hazard in terms of a PSHA and

geologic characteristics of the site and represent the site-specific ground motion response spectrum (GMRS) of Regulatory Guide 1.208 (NRC, 2007a). These spectra are expected to be modified as appropriate to develop ground motion for design considerations.

The GMRS developed in this section is smaller than the minimum Safe Shutdown Earthquake Ground Motion for design identified in paragraph (d)(1) of 10 CFR 100.23 (CFR, 2007). Therefore a Safe Shutdown Earthquake (SSE) for design is developed in Section 3.7.1.

2.5.2.1 Seismicity

The seismic hazard analysis conducted by EPRI as delineated in NP-6395-D 1989 (EPRI, 1989a) relied, in part, on an analysis of historical seismicity in the central and eastern United States (CEUS) to estimate seismicity parameters (rates of activity and Richter b-values) for individual seismic sources. The historical earthquake catalog used in the EPRI analysis was complete through 1984. The earthquake data for the site region that has occurred since 1984 was reviewed and used to update the EPRI catalog (EPRI, 1988).

Geologic evidence for prehistoric seismicity in the site region is discussed in Section 2.5.2.2.1.7.

Sections 2.5.2.1.1 and 2.5.2.1.2 are added as a supplement to the U.S. EPR FSAR.

2.5.2.1.1 Regional Seismicity Catalog Used for 1989 Seismic Hazard Analysis Study

Many seismic networks record earthquakes in the CEUS. A large effort was made during the EPRI seismic hazard analysis study to combine available data on historical earthquakes and to develop a homogeneous earthquake catalog that contained all recorded earthquakes for the region. "Homogeneous" means that estimates of body-wave magnitude, m_b, for all earthquakes are consistent, that duplicate earthquakes have been eliminated, that non-earthquakes (e.g., mine blasts and sonic booms) have been eliminated, and that significant events in the historical record have not been missed. Thus, the EPRI catalog (EPRI, 1988) forms a strong basis on which to estimate seismicity parameters.

2.5.2.1.2 Updated Seismicity Data

Regulatory Guide 1.165 (NRC, 1997a) specifies that earthquakes of a Modified Mercalli Intensity (MMI) greater than or equal to IV or of a magnitude greater than or equal to 3.0 should be listed for seismic sources, "any part of which is within a radius of 200 mi (320 km) of the site (the site region)." While updating the EPRI catalog (EPRI, 1988) for this evaluation of vibratory ground motion a latitude-longitude window of 35° to 43° N, 71° to 83° W was used. This window incorporates the 200 mi (320 km) radius "site region" and seismic sources contributing significantly to CCNPP Unit 3 site earthquake hazard. Figure 2.5-1 shows the CCNPP Unit 3 site and its associated site region. Figure 2.5-45 through Figure 2.5-50 show this site region and the defined latitude-longitude window.

The updated catalog was compiled from the following sub-catalogs:

- EPRI Catalog (EPRI, 1988). The various data fields of the EPRI catalog are described in EPRI NP-4726-A 1988 (EPRI, 1988).
- Southeastern US Seismic Network (SEUSSN) Catalog. The SEUSSN catalog is available from the Virginia Tech Seismological Observatory web site (SEUSSN, 2006). On the date of September 8, 2006, the SEUSSN catalog had 1223 records dating from March 1568 to December 2004 within the site region latitude-longitude window. Of these, 230 records occurred in 1985 or later.

- Advanced National Seismic System (ANSS) Catalog. The ANSS catalog (ANSS 2006) was searched on September 8, 2006, for all records within the site region latitude-longitude window, resulting in 570 records from 1964 to July 11, 2006. Of these, 402 records occurred in 1985 or later.

- Canada On-line Bulletin (Canada). The Canadian catalog is available from the Natural Resources Canada online earthquake database site (Canada, 2006). On the date of the catalog update, September 13, 2006, the Canadian catalog had 189 records dating from April 25, 1969 to July 11, 2006 within the site region latitude-longitude window. Of these, 160 records occurred in 1985 or later.

- Ohio Seismic Network Catalog (Ohio). The Ohio catalog is available from the Ohio Department of Natural Resources website (Ohio, 2006). On the date of the catalog update, September 8, 2006, the Ohio catalog had 92 records dating from December 3, 1951 to July 1, 2006 within the site region latitude-longitude window. Of these, 83 records occurred in 1985 or later.

An examination of the eastern US seismic networks indicated that no single network has complete coverage over the full project region. The large, reputable networks that have partial coverage of the project region include: Lamont-Doherty Seismic Network, Weston Observatory, ANSS (ANSS, 2006), SEUSSN (SEUSSN, 2006), Canada On-line Bulletin (Canada, 2006) and Ohio Seismic Network (Ohio, 2006). A search of the available information from each network was made to determine what data were available and what combination of catalogs would provide the best coverage of the project region.

The SEUSSN, and ANSS catalogs (SEUSSN, 2006) (ANSS, 2006) were determined to be the best seismicity catalogs to be used for a temporal update (1985 to present) of the EPRI catalog (EPRI, 1988) in the CCNPP Unit 3 site region. As a national catalog, the ANSS catalog (ANSS, 2006) compiles data from several regional networks, including SEUSSN. Where these catalogs spatially overlap, the more primary SEUSSN catalog (SEUSSN, 2006) was preferred, though there are some events uniquely listed in the ANSS catalog and these are retained in the updated catalog presented here as Table 2.5-2. The SEUSSN (SEUSSN, 2006) catalog has consistent coverage over the southern and central portions of the project region. The ANSS (ANSS, 2006) catalog was used for coverage in the remaining northern portion of the project region. There appears, however, diminished coverage of the ANSS (ANSS, 2006) catalog in the very northwest portion of the project region near and along the border of Canada. Given the apparent diminished coverage, additional regional catalogs with northern coverage are evaluated.

It was found that the Weston Observatory and Lamont-Doherty Seismic Networks contribute their information to ANSS, so that further independent information from these seismic networks in the Northeast was not sought.

The Canada (Canada, 2006) and Ohio (Ohio, 2006) catalogs both have coverage in the northern and northwestern portion of the project region and were included as supplemental material to the SEUSSN and ANSS catalogs (SEUSSN, 2006) (ANSS 2006). The ranking order used in creating a composite catalog was: EPRI, SEUSSN, ANSS, Canada and Ohio (EPRI, 1988) (SEUSSSN, 2006) (ANSS, 2006)(Canada, 2006)(Ohio, 2006).

The magnitudes given in these catalogs were converted to best or expected estimate of m_b magnitude ($E(m_b)$, also called Emb), using the conversion factors given as Eq. 4-1 and Table 4-1 in EPRI NP-4726-A 1988 (EPRI, 1988):

$$Emb = 0.253 + 0.907 \cdot Md \quad \text{Eq. 2.5.2-1}$$

$$Emb = 0.655 + 0.812 \cdot ML \quad \text{Eq. 2.5.2-2}$$

where Md is duration or coda magnitude and ML is "local" magnitude.

The EPRI-SOG methodology modifies the Emb values to develop unbiased estimates of seismicity recurrence parameters. The modified Emb magnitudes are designated m_b^* (or Rmb). Eq. 4-2 of NP-4726-A 1988 (EPRI, 1988) indicates that the equation from which m_b^*, or Rmb, is estimated from the best estimate of magnitude $E(m_b)$, or Emb, and the variance of m_b, σ^2_{mb}, or Smb^2 is:

$$m_b^* = E(m_b) + (1/2) \cdot \ln(10) \cdot b \cdot \sigma^2_{mb} \quad \text{Eq. 2.5.2-3}$$

where b = 1.0

Values for σ_{mb} or Smb were estimated for each event of the composite catalog and an m_b^* (Rmb) was calculated using Eq. 2.5.2-3 and added to the updated catalog, as listed in Table 2.5-2.

The result of the above process was a catalog of 113 earthquakes listed in Table 2.5-2 as the update of the EPRI NP-4726-A (EPRI, 1988) seismicity catalog recommended for the site region.

Regulatory Guide 1.206 (NRC, 2007c) provides for a discussion of each earthquake, provide information, whenever available, on the epicenter coordinates, depth of focus, date, origin time, highest intensity, magnitude, seismic moment, source mechanism, source dimensions, distance from the site, and any strong-motion recordings. Additionally it request an identification of the sources of the information. It also requests that that application identifies all magnitude designations such as mb, ML, Ms, or Mw.

The data/information was not available in all cases; however, in those cases where the requested information was available, it has been included in the discussion and in appropriate tables. Specifically, date, origin time, location, depth (when available), epicentral distance, and intensity (when available) are included in the discussion and applicable tables and/or figures. All available magnitudes were considered in development of Emb, in analogy with the EPRI-SOG catalog NP-4726-A (EPRI, 1988) being updated. Other information, such as seismic moment, source mechanism, source dimensions, and any strong motion readings, was not found. For the purpose of recurrence analysis, all earthquakes in Table 2.5-2 are considered independent events.

The 113 events in the 35° to 43° N, 71° to 83° W latitude-longitude window, incorporating the 200 mi (320 km) radius site region, from 1985 to July 11, 2006 with Emb magnitude 2.8 or greater have been incorporated into a number of figures, including figures presenting tectonic features, as discussed in Section 2.5.1, and presenting seismic sources in Section 2.5.2.2 (e.g., Figure 2.5-45 through Figure 2.5-50).

The EPRI PSHA study (EPRI, 1989a) expressed maximum magnitude (M_{max}) values in terms of body-wave magnitude (m_b), whereas most modern seismic hazard analyses describe M_{max} in terms of moment magnitude (**M**). To provide a consistent comparison between magnitude scales, this study relates body-wave magnitude to moment magnitude using the arithmetic average of three equations, or their inversions, presented by Atkinson (Atkinson, 1995) and by Frankel (USGS, 1996), and in EPRI TR-102293 (EPRI,1993). The conversion relations are very

consistent for magnitudes 4.5 and greater and begin to show divergence at lower magnitudes. (Table 2.5-3 lists m_b and **M** equivalences developed from these relations over the range of interest for this study.) Throughout the discussion below in Sections 2.5.2.2 and 2.5.2.3, the largest assigned values of M_{max} distributions assigned by the Earth Science Teams described in EPRI NP-4726 1986 (EPRI, 1986) to seismic sources are presented for both magnitude scales (m_b and **M**) to give perspective on the maximum earthquakes that were considered possible in each seismic source. For example, EPRI m_b values of M_{max} are followed by the equivalent **M** value. A table of conversion values from m_b to **M** and **M** to m_b is provided in Table 2.5-3.

2.5.2.2 Geologic and Tectonic Characteristics of Site and Region

As described in Section 2.5.1, a comprehensive review of available geological, seismological, and geophysical data has been performed for the CCNPP Unit 3 site region and adjoining areas. As discussed in Section 2.5.1.2.6, excavation mapping is required during construction and any noted deformational zones will be evaluated and NRC notified when excavations are open for inspection. The following sections summarize the seismic source interpretations (EPRI,1986) from the 1989 EPRI PSHA study (EPRI, 1989a), relevant post-EPRI seismic source characterization studies, and updated interpretations of new and existing sources provided by the more recent data. Based on evaluation of this information, no new information was found that would suggest potentially significant modifications to the EPRI seismic source model (EPRI, 1989a), with the following two exceptions:

- The East Coast fault system (ECFS) represents a new postulated seismic source along the Atlantic Seaboard, as described previously in Section 2.5.1.1.4.4. The hypothesized ECFS is separated into a southern, central, and northern segment. The southern segment of the ECFS has been proposed by Marple (Marple, 2000) as being the source for the 1886 Charleston earthquake.

- The average recurrence interval for large magnitude earthquakes in the Charleston seismic source zone, located 465 mi (748 km) from the CCNPP Unit 3 site, is currently believed to be 550 years based on paleoliquefaction data, rather than several thousand years based on seismicity used in the EPRI seismic source mode (EPRI, 1989a). The Charleston source geometry also has been modified to include the possibility that the 1886 Charleston earthquake occurred on the southern segment of the ECFS.

Although the Charleston source lies outside the site region (200-mi radius), a preliminary sensitivity analysis performed for the CCNPP Unit 3 site shows that this source is a significant contributor of low frequency (1 Hz) ground motion, and thus the Charleston source has been included in the PSHA study for the site. Since publication of the EPRI seismic source model (EPRI, 1989a), significant new information has been developed for assessing the earthquake source that produced the 1886 Charleston earthquake. Paleoliquefaction features and other new information published since the 1986 EPRI project (EPRI,1986) have significant implications regarding the geometry, M_{max}, and recurrence of M_{max} in the Charleston seismic source. A summary of the Updated Charleston Seismic Source (UCSS) model prepared by Bechtel (Bechtel, 2006) and incorporated into the PSHA study for the CCNPP Unit 3 site is presented below in Section 2.5.2.2.2.7. As for the high frequency seismic ground motion hazard at the site, it is captured by the existing EPRI NP-6395-D (EPRI, 1989a) study, and therefore, no modifications are recommended. The following sections present a summary of the EPRI NP-4726 (EPRI, 1986) seismic sources (Section 2.5.2.2.1) and post-EPRI seismic source characterization studies (Section 2.5.2.2.2).

Sections 2.5.2.2.1 and 2.5.2.2.2 are added as a supplement to the U.S. EPR FSAR.

2.5.2.2.1 Summary of EPRI Seismic Sources

Summarized in this section are the seismic sources and parameters used in the 1989 EPRI project EPRI NP-6452-D (EPRI, 1989b). The following description of seismic sources is limited to those sources within 200 mi (320 km) of the CCNPP Unit 3 site (the "site region") followed by those at distances greater than 200 mi (320 km) (i.e., Charleston) (Section 2.5.2.2.2) that appear to impact the hazard at the CCNPP Unit 3 site.

In the 1986 EPRI project (EPRI, 1986), six independent Earth Science Teams (ESTs) evaluated geological, geophysical, and seismological data to develop seismic sources in the CEUS. These sources were used to model the occurrence of future earthquakes and evaluate earthquake hazards at nuclear power plant sites across the CEUS. The six ESTs involved in the EPRI project were Bechtel Group, Dames & Moore, Law Engineering, Rondout Associates, Weston Geophysical Corporation, and Woodward-Clyde Consultants. Each team produced a report which was included in EPRI NP-4726, 1986 (EPRI, 1986) that provides detailed descriptions of how they identified and defined seismic sources. The results were implemented into a probabilistic seismic hazard analysis (PSHA) reported in EPRI NP-6395-D (EPRI, 1989a). EPRI NP-6452-D (EPRI,1989b) summarized the parameters used in the final PSHA calculations and this reference is the primary source for the seismicity parameters used in this current CCNPP Unit 3 COL application. For the computation of hazard in the 1989 study (EPRI, 1989a) a few of the seismic source parameters were modified or simplified from the original parameters determined by the six ESTs as discussed in EPRI NP-6452-D (EPRI, 1989b).

The seismic source models developed for each of the six EST teams are shown on Figure 2.5-45 through Figure 2.5-50. The sources that contributed 99 percent of the CCNPP Unit 3 site hazard are shown and labeled on the figures. For the 1989 EPRI seismic hazard calculations, a screening criterion was implemented to identify those sources whose combined hazard exceeded 99 percent of the total hazard from all sources for two ground motions measurements (EPRI, 1989). These sources are identified in the descriptions below as "primary" seismic sources. Other sources, which together contributed less than one percent of the total hazard from all sources for the two ground motion measures, are identified in the descriptions below as "additional" seismic sources. Earthquakes with $m_b > 3.0$ are also shown in Figure 2.5-45 through Figure 2.5-50 to show the spatial relationships between seismicity and seismic sources. Earthquake epicenters include events from both the EPRI earthquake catalog (EPRI, 1988) and for the period between 1985 and June 2006, as described in Section 2.5.2.1.2.

Earthquake epicenters from the EPRI earthquake catalog include events from the period between 1627 and 1984, updated with seismicity in the CEUS from the period between 1985 and 2006, as described in Section 2.5.2.1.2 (Table 2.5-2). The maximum magnitude, the closest distance to the CCNPP Unit 3 site, and the probability of activity of each EST's seismic sources are summarized in Table 2.5-4 through Table 2.5-9. These tables present the parameters assigned to each source and specify whether or not the source contributed to 99 percent of the site hazard in the original EPRI seismic hazard analyses. The tables also indicate whether new information has been identified that would lead to a significant revision of the source's geometry, maximum earthquake magnitude, or recurrence parameters. The seismicity recurrence parameters (a- and b-values) used in the EPRI seismic hazard study were computed for each one-degree latitude and longitude cell that intersects any portion of a seismic source.

Each EST used separate nomenclature to describe the seismic sources in the CEUS and the CCNPP Unit 3 site region. A number of different names may have been used by the EPRI teams

to describe the same or similar tectonic features or sources, or one team may describe seismic sources that another team does not. For example, the Woodward-Clyde team identified their source that covers the seismicity of central Virginia as the "State Farm Complex," whereas most of the other teams named their source as the Central Virginia Seismic Zone (CVSZ). Each team's source names, data, and rationale are included in their team-specific documentation (EPRI, 1986). Brief descriptions of the seismic sources that contribute 99 percent of the site seismic hazard are described in the following sections.

As indicated in this section, the EPRI PSHA study (EPRI, 1989a) expressed maximum magnitude (M_{max}) values in terms of body-wave magnitude (m_b), whereas most modern seismic hazard analyses describe M_{max} in terms of moment magnitude (**M**). To provide a consistent comparison between magnitude scales, this study relates body-wave magnitude to moment magnitude using the arithmetic average of three equations, or their inversions, presented by Atkinson (Atkinson, 1995) and by Frankel (USGS, 1996) and in EPRI TR-102293 (EPRI, 1993). The conversion relations are very consistent for magnitudes 4.5 and greater and begin to show divergence at lower magnitudes. Throughout this section, the largest assigned values of M_{max} distributions assigned by the ESTs to seismic sources are presented for both magnitude scales (m_b and **M**) to give perspective on the maximum earthquakes that were considered possible in each seismic source. For example, EPRI m_b values of M_{max} are followed by the equivalent **M** value.

The most significant EPRI sources for each of the six ESTs, with respect to the CCNPP Unit 3 site, are described below. For each team, the listed sources contributed to 99 percent of the total seismic hazard for that team at the CCNPP Unit 3 site. The assessment of these and other EPRI sources within the site region has found that the EPRI source parameters (maximum magnitude, geometry, recurrence rate) are sufficient to capture the current understanding of the seismic hazard in the site region.

Except for the two specific cases described earlier, no new seismological, geological, or geophysical information in the literature published since the 1986 EPRI source model (EPRI, 1986) suggests that these sources should be modified for the CCNPP Unit 3 site. The two cases where new information suggests modification of the EPRI source characterizations is the addition of the postulated northern segment of the ECFS (ECFS-N) and the new recurrence rates and geometry parameters for the existing Charleston source. The ECFS-N segment, as discussed in Section 2.5.1.1.4.4, is a hypothesized fault with a very low probability of exisistence and activity. A sensitivity analysis performed for the Dominion North Anna site (Dominion, 2005) demonstrates that the postulated ECFS-N has a negligible affect on ground motions at the North Anna site. Because the CCNPP Unit 3 site is approximately 70 mi (113 km) northeast of the ECFS-N, or 7 mi (11 km) further away than the North Anna site is from the ECFS-N, and based on the sensitivity analysis performed for the Dominion North Anna site, this postulated fault is not considered a contributing seismic source and does not need to be included in the seismic hazard calculations for the CCNPP Unit 3 site. Furthermore, several features used to define the postulated ECFS-N segment have been shown to be non-tectonic features or inactive (see Section 2.5.1.1.4.4).

Each EST's characterization of the Charleston seismic source was replaced by four alternative source geometries. For each geometry, large earthquake occurrences (**M** 6.7 to 7.5) were modeled with a range of mean recurrence rates, and smaller earthquakes (m_b from 5.0 to 6.7) were modeled with an exponential magnitude distribution, with rates and b-values determined from historical seismicity. Also, all surrounding sources for each team were redrawn so that the new Charleston source geometries were accurately represented as

a "hole" in the surrounding source, and seismic activity rates and b-values were recalculated for the modified surrounding sources, based on historical seismicity. Further details and the results of sensitivity analyses performed on the modified seismic sources are presented in Section 2.5.2.4.

2.5.2.2.1.1 Sources Used for EPRI PSHA – Bechtel Group

Bechtel Group identified and characterized three seismic sources that contribute to 99 percent of the hazard at the CCNPP Unit 3 site. All three of these sources are within the site region and include the:

- Southern Appalachians Region (BZ5)
- Central Virginia (E)
- Atlantic Coastal Region (BZ4)

Also identified within the site region are five other seismic sources that do not contribute to 99 percent of the hazard at the site. These sources include the:

- Stafford Fault (17)
- Eastern Mesozoic Basins (13)
- Bristol Trends (24)
- Lebanon Trend (23)
- New York-Alabama Lineament (25)

Seismic sources identified by the Bechtel Group team within the site region are listed in Table 2.5-4. A map showing the locations and geometries of the Bechtel Group seismic sources contributing 99% of the seismic hazard is provided in Figure 2.5-45. The seismic source identified by the Bechtel Group that contributes most to the site hazard at 1 Hz and 10^{-4} mean annual frequency of exceedance is the Atlantic Coastal Region (source BZ4). The following is a brief discussion of each of the seismic sources that contribute to 99 percent of the site hazard.

Southern Appalachians Region (BZ5)

The CCNPP Unit 3 site is located within the Southern Appalachians Region background source (BZ5). It is a large background source that extends from New York to Alabama and encompasses a majority of the site region. The largest M_{max} assigned by the Bechtel Group to this zone is m_b 6.6 (**M** 6.5).

Central Virginia (E)

The CCNPP Unit 3 site is located approximately 49 mi (79 km) (northwest of the Central Virginia Seismic Zone (E). The source is defined exclusively on the basis of seismicity in the central Virginia region. No tectonic features were identified within the source. The largest maximum earthquake magnitude (M_{max}) that the Bechtel Group assigned to this zone is body-wave magnitude (m_b) 6.6 (**M** 6.5).

Atlantic Coastal Region (BZ4)

The Atlantic Coastal Region background source (BZ4) is located about 65 mi (105 km) southeast and east of the CCNPP Unit 3 site. This source is a large background zone that extends from offshore New England to Alabama and encompasses the easternmost portion of the site region. The largest M_{max} assigned by the Bechtel Group to this zone is m_b 7.4 (**M** 7.9), reflecting its assumption that there is a small probability that a Charleston-type earthquake could occur within this region.

2.5.2.2.1.2 Sources Used for EPRI PHSA – Dames & Moore

Dames & Moore identified and characterized seven seismic sources that contribute to 99 percent of the hazard at the CCNPP Unit 3 site. These sources include:

- Connecticut Basin (47)
- Southern Appalachian Mobile Belt (53)
- Southern Cratonic Margin "Default Zone 10" (41)
- Newark-Gettysburg Basin (42)
- Central Virginia Seismic Zone (40)
- Appalachian Fold Belt (4)
- Kink in Fold Belt "1" (4A)

All of these source zones are within the site region except the Kink in Fold Belt (4A), which is 416 mi (669 km) away from the CCNPP Unit 3 site. Twelve (12) other seismic sources were identified within the site region that did not contribute to 99 percent of the hazard. These less significant sources include the:

- Stafford Fault Zone (44)
- Combination Zone 4-4A-4B-4C-4D (C01)
- Kink in Fold Belt (4C)
- Hopewell Fault Zone (45)
- Buried Triassic Basins (48)
- Dan River Basin (46)
- East Marginal Basin (8)
- Combination Zone 8-9 (C02)
- Kink in Fold Belt (Giles Co. Area) (4B)
- Kink in Fold Belt (4D)
- Jonesboro Basin (49)

- Ramapo Fault (43)

Seismic sources identified by Dames & Moore within the site region are listed in Table 2.5-5. A map showing the locations and geometries of the Dames & Moore seismic sources contributing 99% of the seismic hazard is provided in Figure 2.5-46. The seismic source identified by the Dames & Moore that contributes most to the site hazard at 1 Hz and 10^{-4} mean annual frequency of exceedance is the Central Virginina Seismic Zone (source 40). The following is a brief discussion of each of the seismic sources that contribute to 99 percent of the hazard at the CCNPP Unit 3 site.

Connecticut Basin (47)

The CCNPP Unit 3 site is located within the Connecticut Basin (47) source. Similar to the Newark-Gettysburg Basin (42), this source is defined based on the presence of a Triassic basin and the assumption that the bounding Mesozoic rift structures could be reactivated. The largest earthquake M_{max} assigned by the Dames & Moore team to this zone is m_b 7.2 (**M** 7.5).

Southern Appalachian Mobile Belt (53)

The CCNPP Unit 3 site is located within the Southern Appalachian Mobile Belt default zone (53). This default source comprises crustal rocks that have undergone several periods of divergence and convergence. The source is bounded on the east by the East Coast magnetic anomaly and on the west by the westernmost boundary of the Appalachian gravity gradient. The largest M_{max} assigned by the Dames & Moore team to this zone is m_b 7.2 (**M** 7.5).

Southern Cratonic Margin "Default Zone 10" (41)

The CCNPP Unit 3 site is located 40 mi (64 km) east of the Southern Cratonic Margin default zone (41). This large default background zone is located between the Appalachian Fold Belt (4) and the Southern Appalachian Mobile Belt (53) and includes the region of continental margin deformed during Mesozoic rifting. Located within this default zone are many Triassic basins and border faults. The largest M_{max} assigned by the Dames & Moore team to this zone is m_b 7.2 (**M** 7.5).

Newark-Gettysburg Basin (42)

The Newark-Gettysburg Basin source (42) is about 57 mi (92 km) northwest of the CCNPP Unit 3 site. This source incorporates the Newark, Gettysburg, and Culpeper Triassic basins that formed during Mesozoic rifting. The largest M_{max} assigned by the Dames & Moore team to this zone is m_b 7.2 (**M** 7.5).

Central Virginia Seismic Zone (40)

The Central Virginia Seismic Zone (40) is about 68 mi (109 km) southwest of the CCNPP Unit 3 site. This source is defined based on the pattern of clustered seismicity in the central Virginia area. No known tectonic features were associated with this seismic activity. The largest M_{max} assigned by the Dames & Moore team to this zone is m_b 7.2 (**M** 7.5).

Appalachian Fold Belts (4)

The Appalachian Fold Belts source (4) is about 86 mi (138 km) west of the CCNPP Unit 3 site. This source extends from New York to Alabama and consists of the Appalachian folded

mountain belt of Paleozoic age. The largest M_{max} assigned by the Dames & Moore team to this zone is m_b 7.2 (**M** 7.5).

Kink in Fold Belt "1" (4a)

The Kink in Fold Belt source (4a) is about 416 mi (669 km) west of the CCNPP Unit 3 site and is a contributing source outside the site region. Kinks in Paleozoic fold belts were defined based on bends of the fold belts and areas of greater seismicity. The largest M_{max} assigned by the Dames & Moore team to this zone is m_b 7.2 (**M** 7.5).

2.5.2.2.1.3 Sources Used for EPRI PSHA – Law Engineering

Law Engineering identified and characterized 12 seismic sources that contribute to 99 percent of the hazard at the CCNPP Unit 3 site. These sources include:

- Combination Zone 22-35 (C11)
- Reactivated Eastern Seaboard Normal (22)
- Combination Zone 8-35 (C10)
- Mesozoic Basins (8-bridged) (C09)
- Eastern Piedmont (107)
- Eastern Basement (17)
- Six individual mafic plutons (M16, M17, M18, M19, M20, M21)

Law Engineering also characterized 15 other seismic sources within the site region that do not contribute to 99 percent of the hazard. These less significant sources include the:

- Combination Zone 22 -24-35 (C13)
- Mesozoic Basins-16 (8-16)
- Eastern Basement Background (217)
- Mafic Pluton (M25)
- Mafic Pluton (M22)
- Mafic Pluton (M26)
- Mafic Pluton (M23)
- Mafic Pluton (M24)
- Mesozoic Basins – 12 (8-12)
- Western New England (101)
- Mafic Pluton (M29)
- Mafic Pluton (M27)

- Mafic Pluton (M30)
- Ohio-Pennsylvania Block (112)
- Mafic Pluton (M28)

Note that half of these sources are mafic pluton seismic sources. Seismic sources identified by Law Engineering within the site region are listed in Table 2.5-6. A map showing the locations and geometries of the Law Engineering seismic sources contributing 99% of the seismic hazard is provided in Figure 2.5-47. The seismic source identified by the Law Engineering that contributes most to the site hazard at 1 Hz and 10^{-4} mean annual frequency of exceedance is the Eastern Basement (source 17). The following is a brief discussion of each of the seismic sources that contribute to 99 percent of the site hazard.

Combination Source 22-35 (C11)

The CCNPP Unit 3 site is located within the C11 combination source. The C11 combination zone has the same geometry as the Reactivated Eastern Seaboard Normal (22) source zone, excluding the Charleston seismic source zone (35). The largest M_{max} assigned by the Law Engineering team to this combination zone is m_b 6.8 (**M** 6.8).

Reactivated Eastern Seaboard Normal (22)

The CCNPP Unit 3 site is located within the Reactivated Eastern Seaboard Normal (22) source. This source is characterized as a region along the eastern seaboard in which Mesozoic normal faults are reactivated as high-angle reverse faults. Law Engineering assigned a single M_{max} of m_b 6.8 (**M** 6.8) to this zone.

Combination Sources 8-35 (C10)

The CCNPP Unit 3 site is located approximately 5 mi (8 km) southeast of the C10 combination zone. The C10 combination source zone has the same geometry as the Mesozoic Basins combination zone (C09), excluding the Charleston region (35). The largest M_{max} assigned by the Law Engineering team to both combination sources is m_b 6.8 (**M** 6.8).

Mesozoic Basins (8-bridged) (C09)

The Mesozoic basins (C09) source includes eight bridged basins, the closest of which is about 5 mi northwest from the CCNPP Unit 3 site. This source was defined based on northeast-trending, sediment-filled troughs in basement rock bounded by normal faults. The largest M_{max} assigned by the Law Engineering team to this zone was m_b 6.8 (**M** 6.8).

Eastern Piedmont (107)

The Eastern Piedmont (107) is about 5 mi (8 km) west of the CCNPP Unit 3 site. This source is characterized as a seismotectonic region having a positive Bouguer gravity anomaly field and a pattern of short wavelength magnetic anomalies. Law Engineering interprets this source to represent a crustal block underlain by mafic or transitional crust east of the relict North American continental margin. The largest M_{max} assigned by the Law Engineering team to this zone is m_b 5.7 (**M** 5.3).

Eastern Basement (17)

The CCNPP Unit 3 site is located 44 mi (71 km) southeast of the Eastern Basement source (17). This source is defined as an area containing pre-Cambrian and Cambrian normal faults, which developed during the opening of the Iapetus Ocean, in the basement rocks beneath the Appalachian decollement. The Giles County and eastern Tennessee zones of seismicity are included in this source and are located approximately 230 mi and 415 mi, respectively, from the CCNPP Unit 3 site. The largest M_{max} assigned by the Law Engineering team to this zone is m_b 6.8 (**M** 6.8).

Six Individual Mafic Plutons (M16, M17, M18, M19, M20, and M21)

The six significant mafic pluton sources (M16, M17, M18, M19, M20, and M21) are located between 52 mi (and 116 mi from the CCNPP Unit 3 site. Mafic pluton M21 is located 52 mi west of the site. Law Engineering considers pre- and post-metamorphic mafic plutons in the Appalachians to be stress concentrators and, therefore, earthquake sources. Law Engineering does not define a seismic source in central Virginia, but the plutons, of small areal extent, capture a majority of the seismicity of central Virginia, due to the method in which 70 percent of the seismicity from the surrounding one degree square area 69 mi by 69 mi (111 km x 111 km) is assigned to each pluton. A single M_{max} of m_b 6.8 (**M** 6.8) is assigned by the Law Engineering team to all mafic pluton sources.

2.5.2.2.1.4 Sources Used for EPRI PSHA – Rondout Associates

Rondout identified and characterized four seismic sources that contribute to 99 percent of the hazard at the CCNPP Unit 3 site. All four sources are within the site region and include:

- Background 49 (C01)
- Shenandoah (30)
- Central Virginia (29)
- Quakers (31)

Rondout also identified seven other seismic sources within the site region that did not contribute to 99 percent of the hazard at the site. These sources include:

- Combination Zone 49 + 32 (C09)
- Appalachian Basement 3 and 4 (49-03 and 49-04)
- Norfolk Fracture Zone (32)
- Combination Zone 50 (02) + 12 (C07)
- Grenville Province 2 (50-02)
- Giles County (28)

Seismic sources identified by Rondout within the site region are listed in Table 2.5-7. A map showing the locations and geometries of the Rondout seismic sources contributing 99% of the seismic hazard is provided in Figure 2.5-48. The seismic source identified by the Rondout that contributes most to the site hazard at 1 Hz and 10^{-4} mean annual frequency of exceedance is the Central Virginia source (source 107). The following is a discussion of each of the seismic sources that contribute to 99 percent of the hazard at the CCNPP Unit 3 site.

Background 49 (C01)

The CCNPP Unit 3 site is located within the Background 49 source. This background source contains Paleozoic or younger crust that is east of the Precambrian cratonic margin. Rondout assigned a M_{max} of m_b 5.8 (**M** 5.4) to this source.

Shenandoah (30)

The CCNPP Unit 3 site is located 13 mi (21 km) east of the Shenandoah source. This Shenandoah source is defined based on geophysical and geologic features. The source includes the intersection of the Pittsburg-Washington lineament and the strong gravity gradient associated with the edge of the ancient Paleozoic craton. It also includes both the post-Cretaceous Brandywine and Stafford fault zones. Rondout assigned a M_{max} of m_b 6.5 (**M** 6.3) to this source.

Central Virginia (29)

The CCNPP Unit 3 site is located 55 mi (89 km) northeast of the Central Virginia source. This source is defined based on seismicity and the possible intersection of the extension of the Norfolk fault zone and a northeast-trending linear zone defined by aeromagnetic, gravity, and volcanic-plutonic rocks. The largest M_{max} assigned by Rondout to this source is m_b 7.0 (**M** 7.2).

Quakers (31)

The CCNPP Unit 3 site is located 70 mi (113 km) south of the Quakers source. This source contains the old buried Paleozoic cratonic edge, which was mapped using gravity data. This region was reactived multiple times during the opening and closing of the Iapetus Ocean and during Mesozoic rifting. Rondout assigned a M_{max} of m_b 6.8 (**M** 6.8) to this source.

2.5.2.2.1.5 Sources Used for EPRI PSHA – Weston Geophysical

Weston Geophysical identified and characterized 11 seismic sources that contributed to 99 percent of the hazard at the CCNPP Unit 3 site. All 11 of these sources are within the site region and include:

- Combination Zone 104 – 22–26 (C23)
- Combination Zone 104 – 25 (C21)
- Combination Zone 104 – 22–25 (C24)
- Combination Zone 104 – 28BCDE – 22 – 25 (C27)
- Combination Zone 104 – 28BCDE – 22 – 26 (C28)
- Combination Zone 104 – 28BE – 26 (C34)
- Combination Zone 104 – 28BE – 25 (C35)
- Zone of Mesozoic Basins (28E)
- Central Virginia Seismic Zone (22)
- Combination Zone 103 – 23 – 24 (C19)

- Combination Zone 21 –19 (C07)

Weston Geophysical also identified 17 seismic sources within the site region that do not contribute to 99 percent of the hazard at the site. These less significant sources include the:

- Combination Zone 104-26 (C22)
- Combination Zone 104-28BCDE (C25)
- Combination Zone 104-28BCDE-22 (C26)
- Southern Coastal Plain (104)
- Combination Zone 28A thru E (C01)
- Zone of Mesozoic Basin (28B)
- Southern Appalachians (103)
- Combination Zone 103-23 (C17)
- Combination Zone 103-24 (C18)
- New York Nexus (21)
- Combination Zone 21-19-10A (C08)
- Mesozoic Basin (or intersection of Sources 28 and 21) (28A)
- Zone of Mesozoic Basin (28D)
- Combination Zone 21-19-10A -28A (C09)
- Combination Zone 21-19-28A (C10)
- Zone of Mesozoic Basin (28C)
- Appalachian Plateau (102)

The majority of these sources are combination zones. Seismic sources identified by Weston Geophysical within the site region are listed in Table 2.5-8. A map showing the locations and geometries of the Weston Geophysical seismic sources contributing 99% of the seismic hazard is provided in Figure 2.5-49. The seismic source identified by the Weston Geophysical that contributes most to the site hazard at 1 Hz and 10^{-4} mean annual frequency of exceedance is the Central Virginia Seismic Zone (source 22). The following is a discussion of each of the seismic sources that contribute to 99 percent of the hazard at the site.

Seven Combination Zones 104-25 (C21); 104-22-26 (C23); 104-22-25 (C24); 104-28BCDE-22-25 (C27); 104-28BCDE-22-26 (C28); 104-28BE-26 (C34); 104-28BE-25 (C35))

Weston Geophysical specified a seven combination seismic source zones that encompass the CCNPP Unit 3 and contribute to the 99 percent seismic hazard. These seven combination zones all represent the combination of different seismic sources within a large South Coastal Plain Background zone (104). Although not shown on Figure 2.5-49, the South Coastal Plain

Background zone (104) has the same perimeter as the seven combination zones described here. The largest M_{max} assigned by the Weston team to each of these seven combination sources is m_b 6.6 (**M** 6.5).

Zone of Mesozoic Basins (28E)

The CCNPP Unit 3 site is located 4 mi (6 km) east of the Zone of Mesozoic Basins source (28E). This source surrounds three northeast-trending elongated zones of Mesozoic basins that extend from South Carolina to southern New Jersey. The largest M_{max} value assigned by Weston to this zone is m_b 6.6 (**M** 6.5).

Central Virginia Seismic Zone (22)

The CCNPP Unit 3 site is located 45 mi (72 km) northeast of the CVSZ (22) source. This source is defined based on a northwest trending alignment of seismicity that extends from Richmond to Waynesboro, Virginia. The largest Mmax value assigned by Weston Geophysical to this zone is mb 6.6 (**M** 6.5).

Two Combination Zones 21-19 (C07) and 103-23-24 (C19)

Two additional combination sources, 21 – 19 (C07) and 103 – 23 – 24 (C19), are located 113 mi (182 km) and 73 (117 km) mi from the CCNPP Unit 3 site, respectively. Combination zone 21-19 is the New York Nexus source zone minus the Moodus (19) source zone. Combination zone 103-23-24 is the Southern Appalachinas (103) source zone minus the Giles County (23) and New York Alabama-Clingman (24) source zones. The largest M_{max} assigned by the Weston team to each of these two combination sources is m_b 6.6 (**M** 6.5).

2.5.2.2.1.6 Sources Used for EPRI PSHA - Woodward-Clyde Consultants

Woodward-Clyde Consultants identified and characterized seven seismic sources that contributed to 99 percent of the hazard at the CCNPP Unit 3 site. All seven of these sources are within the site region and include:

- Calvert Cliffs Background (B20)
- Tyrone-Mt. Union Lineament (61)
- New Jersey Isostatic Gravity Saddle (21)
- Pittsburg-Washington Lineament (63)
- Central Virginia Gravity Saddle (26)
- State Farm Complex (27)
- Newark Basin Perimeter (23)

Woodward-Clyde Consultants also identified eight seismic sources within the site region that do not contribute to 99 percent of the hazard at the site. These sources include:

- New Jersey Isostatic Gravity Saddle No. 2 (Combo c2) (21A)
- Richmond Basin (28)
- Continental Shelf Int. (02)

- Southeast NY/NJ/PA NOTA Zone (53)
- Continental Shelf (01)
- Newark Basin (22)
- Ramapo Fault (24)
- Hudson Valley (25)

Seismic sources identified by Woodward-Clyde within the site region are listed in Table 2.5-9. A map showing the locations and geometries of the Woodward-Clyde seismic sources contributing 99% of the seismic hazard is provided in Figure 2.5-50. The seismic source identified by Woodward-Clyde that contributes most to the site hazard at 1 Hz and 10^{-4} mean annual frequency of exceedance is the Calvert Cliffs Background source (B20). Following is a brief discussion of each of the seismic sources that contributed to 99 percent of the site hazard.

Calvert Cliffs Background (B20)

The CCNPP Unit 3 site is located within the Woodward-Clyde Consultants Calvert Cliffs Background source, a large, rectangular background source that is centered on the site. T his source is not based on any geological, geophysical, or seismological features. The largest M_{max} assigned by Woodward-Clyde Consultants to this zone is m_b 6.6 (**M** 6.5).

Tyrone-Mt. Union Lineament (61)

The CCNPP Unit 3 site is located within the Tyrone-Mt. Union Lineament source. This source is based on a northwest-trending lineament, inferred to be a deep crustal fracture, mapped using geologic and geophysical data. The 435 mi (700 km) long and 62 mi (100 km) wide source surrounds the lineament. The largest M_{max} assigned to this source is m_b 7.1 (**M 7.3**).

New Jersey Isostatic Gravity Saddle (21)

The New Jersey Isostatic Gravity Saddle is located 48 mi (77 lm) northeast of the CCNPP Unit 3 site. This source is based on a gravity saddle mapped using isostatic gravity from coastal New Jersey to south of New York City and surrounds a region of concentrated historical earthquakes. The largest M_{max} assigned to this source is m_b 6.9 (**M** 7.0).

Pittsburg-Washington Lineament (63)

The Pittsburg-Washington Lineament source is located 52 mi (84 km) northeast of the CCNPP Unit 3 site. This northwest-trending lineament is based on offset features in gravity and magnetic data. The 435 mi (700 km) long and 62 mi (100 km) wide source surrounds the lineament. The largest M_{max} assigned to this source is m_b 7.1 (**M 7.3**).

Central Virginia Gravity Saddle (26)

The Central Virginia Gravity Saddle source is about 67 mi (108 km) southwest of the CCNPP Unit 3 site. This source was defined based on a saddle in the northeast-trending gravity high associated with the Appalachians. Central Virginia seismicity is located along the south and southwest margin of the gravity saddle. This source is an alternative interpretation of the

seismicity in the central Virginia area. The largest M_{max} assigned by Woodward-Clyde Consultants to this zone is m_b 7.0 (**M** 7.2).

State Farm Complex (27)

The State Farm Complex source is about 69 mi (111 km) southwest of the CCNPP Unit 3 site. This source was defined based on pre-Cambrian gneissic terrain located in central Virginia and bounded on the east by the Richmond Basin and on the west by Goochland fault. There is a strong concentration of seismicity on either side of the feature, which is centered in the CVSZ. The largest M_{max} assigned by Woodward-Clyde Consultants to this source is m_b 6.9 (**M** 7.0).

Newark Basin Perimeter (23)

The Newark Basin Perimeter source is located 103 mi (165 km) northeast of the CCNPP Unit 3 site. This source is based on a northeast-trending Triassic basin, named the Newark basin, that extends from New Jersey to New York. The largest M_{max} assigned to this source was m_b 6.8 (**M 6.8**).

2.5.2.2.1.7 Characterization of the Central Virginia Seismic Zone

In the 1989 EPRI seismic hazard study (EPRI, 1989a), the CVSZ represented an important contributor to seismic hazard for the CCNPP Unit 3 site, particularly for low structural frequencies (see Section 2.5.2.6.1 below). The EPRI study (EPRI, 1989a) is designed to incorporate multiple expert opinions into one PSHA to capture the epistemic uncertainty related to lack of knowledge regarding seismic sources in the CEUS. Each EST characterized the CVSZ differently, as shown on Figure 2.5-51 and listed in Table 2.5-10. In spite of these different interpretations, the central portion of each source represents the densest cluster of earthquake activity in the region. The largest M_{max} for these different characterizations of the CVSZ range from m_b 6.6 to m_b 7.2 (**M** 6.5 to 7.5), as listed in Table 2.5-10.

With the exception of Law Engineering, all of the ESTs identified a source representing the CVSZ. Law Engineering instead identified multiple mafic plutons in the region. The seismicity parameters for these mafic plutons were calculated from a large region surrounding each pluton, which effectively captures the majority of seismicity in central Virginia. Thus, the mafic plutons indirectly represent a local seismic source for Law Engineering as provided in EPRI Report NP-4726, 1986, Volume 7) (EPRI, 1986).

Seismicity in the CVSZ ranges in depth from about 2 mi (3 km) to 8 mi (13 km) (Wheeler, 1992). Coruh (Coruh, 1988) suggest that seismicity in the central and western parts of the zone may be associated with west-dipping reflectors that form the roof of a detached antiform, while seismicity in the eastern part of the zone near Richmond may be related to a near-vertical diabase dike swarm of Mesozoic age. However, given the depth distribution of 2 mi (3 km) to 8 mi (13 km) (Wheeler, 1992) and broad spatial distribution, it is difficult to uniquely attribute the seismicity to any known geologic structure and it appears that the seismicity extends both above and below the Appalachian detachment.

Since the EPRI study (EPRI, 1989a), two liquefaction features have been found within the CVSZ (Obermeier, 1998). As described in Section 2.5.1.1.4.5, these new observations are consistent with the M_{max} values and recurrence parameters assigned by the EPRI teams. The lack of widespread liquefaction features in the 186 mi (300 km) of stream exposures searched within the CVSZ, despite the presence of mid- to late-Holocene potentially liquefiable deposits, has led some researchers (Obermeier, 1998) to conclude that it is unlikely that an earthquake of

magnitude 7 or larger has occurred within the seismic zone in the last 2,000 to 3,000 years, or in the eastern portion of the seismic zone for the last 5,000 years.

Within the CCNPP Unit 3 site region, the paleo-liquefaction features found within the Central Virginia seismic zone are only two recorded occurrences of Quaternary earthquake-induced geologic failure. Within the CCNPP Unit 3 site region, the literature review conducted for the development of this section, which included compilations of potential Quaternary features by Crone and Wheeler (Crone, 2000), Wheeler (Wheeler, 2005), and Wheeler (Wheeler, 2006), found no other documented evidence of Quaternary earthquake-induced geologic failure, such as earthquake-induced liquefaction, landsliding, land spreading, or lurching. Outside of the CCNPP Unit 3 site region, widespread liquefaction is recorded near Charleston, South Carolina. These data are incorporated in the Updated Charleston Seismic Source Model presented in Section 2.5.2.2.2.7.

The 1986 EPRI source model (EPRI, 1986) includes various source geometries and parameters to capture the seismicity of the Central Virginia seismic zone (Figure 2.5-51). Subsequent hazard studies have used maximum magnitude (M_{max}) values that are within the range of maximum magnitudes used by the six EPRI models. Collectively, upper-bound M_{max} values used by the EPRI teams range from m_b 6.6 to 7.2 (**M** 6.5 to 7.5) (Table 2.5-10). More recently, Bollinger (USGS, 1992) has estimated a M_{max} of **M** 6.2 (m_b 6.4) for the Central Virginia seismic source, and Chapman, and Krimgold (Chapman, 1994) have used a M_{max} of **M** 7.53 (m_b 7.22) for the Central Virginia seismic source based on the estimated magnitude of the 1886 Charleston earthquake from Johnston (1992) (as cited in Chapman and Krimgold (Chapman, 1994)). However, more recent estimates of the 1886 earthquake magnitude made by Johnston (1996) and Bakun and Hopper (2004) are lower, **M** 7.3 (m_b 7.1) and **M** 6.9 (m_b 6.9), respectively.

Based on Chapman and Krimgold's (1994) reliance on the magnitude of the 1886 Charleston earthquake as the basis for their Central Virginia seismic zone Mmax value, it is reasonable and appropriate to assume that the Mmax for the Central Virginia seismic zone described in Chapman and Krimgold (1994) should be lowered to account for the updated magnitude (i.e., Johnston, 1996; Bakun and Hopper, 2004) estimate of the 1886 earthquake. It is concluded that the more recent estimates of Mmax for the Central Virginia seismic zone are within the range of Mmax values used in the 1986 EPRI studies (EPRI, 1986) because (1) the original Mmax of the Chapman and Krimgold (1994) Central Virginia seismic zone is only 0.02 Mw magnitude units above the EPRI-SOG range, and (2) the revised Mmax values for the Chapman and Krimgold (1994) Central Virginia seismic zone that are derived from newer estimates of the magnitude of the 1886 earthquake lie within the range of EPRI-SOG Mmax values for the Central Virginia seismic zone. Also, the distribution and rate of seismicity in the Central Virginia seismic source has not changed since the 1986 EPRI study (EPRI, 1986). Thus, there is no new information or data that motivates modifying the source geometry, rate of seismicity, or Mmax values for the Central Virginia seismic zone in the EPRI-SOG model. The same conclusion was reached in the North Anna ESP application, and the NRC agreed with these findings as part of a review of Dominion Nuclear North Anna LLC's ESP application and assessment of the Central Virginia seismic zone as documented in NUREG-1835, Safety Evaluation Report for an Early Site Permit (ESP) at the North Anna ESP Site, (NRC, 2005). This supports the conclusion that no new information has been developed since 1986 that would require a significant revision to the EPRI seismic source model (EPRI, 1986).

2.5.2.2.2 Post-EPRI Seismic Source Characterization Studies

Since the EPRI seismic hazard project (EPRI, 1989), seven studies have been performed to characterize seismic sources relevant to the CCNPP Unit 3 site probabilistic seismic hazard

analysis. Four of these studies characterize seismic sources within the CCNPP Unit 3 site region and include the following:

- Sources and parameters for the Savannah River nuclear site in South Carolina (USGS, 1992).
- Seismic hazard of Virginia (Chapman, 1994).
- United States Geological Survey's National Seismic Hazard Mapping Project (USGS, 1996) (USGS, 2002).
- North Anna ESP Application (Dominion, 2005).

These four studies are described below in Sections 2.5.2.2.2.1 through 2.5.2.2.2.4.

Three additional studies centered outside the CCNPP Unit 3 site area have been performed to characterize seismic sources in the southeastern United States. These studies include the following:

- South Carolina Department of Transportation's seismic hazard mapping project (Chapman, 2002).
- The Nuclear Regulatory Commission's Trial Implementation Project (TIP) study (NRC, 2002a).
- The Southern Nuclear Company's ESP application for Vogtle Units 2 and 3 that included the Updated Charleston Seismic Source model (Bechtel, 2006).

These studies are described below in Sections 2.5.2.2.2.5 through 2.5.2.2.2.7.

Based on review of these recent studies that lie outside of the site region, it was determined that an update of the Charleston seismic source for the EPRI (EPRI, 1986) (EPRI, 1989a) seismic hazard project was required to assess the seismic hazard at the CCNPP Unit 3 site (Figure 2.5-52). For example, a preliminary sensitivity analysis of the Charleston source zone that included the postulated East Coast Fault system (Section 2.5.1.1.4.4) indicates that, at low frequencies (1 Hz), the Charleston source is a significant contributor to the seismic hazard at the CCNPP Unit 3 site. Thus, new PSHA models that have been developed to address the Charleston source are summarized in the following sections. In particular, the PSHA for the CCNPP Unit 3 site incorporates the Updated Charleston Seismic Source (UCSS) model developed by Bechtel (Bechtel, 2006) for the Vogtle nuclear power plant in Georgia. The UCSS (Bechtel, 2006) is presented in Section 2.5.2.2.2.7.

In addition, located in the CCNPP Unit 3 site region is the Lancaster seismic zone of Pennsylvania, 120 mi (193 km) North of the CCNPP Unit 3 site (Figure 2.5-52). The significance of the Lancaster seismic zone with respect to the CCNPP Unit 3 site seismic hazard is discussed in Section 2.5.2.2.2.8. In addition, several small earthquake clusters that post-date EPRI (EPRI, 1989a) include the Howard County earthquake sequence of Maryland (Reger, 1994). The Howard County earthquake swarm is discussed in Section 2.5.2.2.2.9.

2.5.2.2.2.1 Seismic Sources and Parameters for the Savannah River Nuclear Site

USGS (USGS, 1992) specified sources, recurrence rates, focal depths, and maximum magnitudes for earthquake sources in the southeastern United States to be used in probabilistic seismic hazard analyses at the Savannah River nuclear site in South Carolina (

Table 2.5-11). Bollinger's approach to seismic zonation in the Eastern United States was based primarily on the historical record of earthquake activity. Maximum magnitudes were derived from a combination of three different estimates based on the 1000 year earthquake, the maximum historical earthquake plus one magnitude unit, and the calculated values from various published relationships between magnitude and fault rupture area. Bollinger identified two seismic sources within the CCNPP Unit 3 site region (200 mi radius). These sources are the CVSZ (RZ6) and a complementary background zone (CZ1) (Table 2.5-11). The CVSZ was defined by Bollinger as a rectangular zone centered on the majority of the seismicity in the central Virginia area. The maximum magnitude earthquake value estimated for this source was m_b 6.4 (**M** 6.2) (USGS, 1992). For the complimentary background zone a M_{max} value of m_b 5.75 (**M** 5.36) was used. The M_{max} values for the Central Virginia and complementary background sources in the USGS (USGS, 1992) study are lower than the largest M_{max} values assigned by most of the EPRI teams (Table 2.5-10).

2.5.2.2.2.2 Seismic Hazard of Virginia

In 1994, a seismic hazard assessment of Virginia was performed to examine the seismic hazard within Virginia on a county-by-county basis (Chapman, 1994). Seismic sources and earthquake frequency-magnitude recurrence relationships were defined using the results of network monitoring by the Seismological Observatory at Virginia Polytechnic Institute and State University and published geologic and geophysical investigations. The study defined a total of 10 seismic sources (Table 2.5-12). Within the CCNPP Unit 3 site region, Chapman (Chapman, 1994) defined six contiguous, non-overlapping sources that were based primarily on patterns of seismicity. The most prominent area of historical seismicity within the site region is defined as the Central Virginia Seismic Zone. An M_{max} value of **M** 7.53 (m_b 7.22) was assigned to all sources in their model, with the exception of New Madrid. Chapman (Chapman, 1994) assumed that a Charleston-size event was capable of occurring in any of the sources within the CCNPP Unit 3 site region.

Subsequent to the Chapman and Krimgold study, Johnston (Johnston, 1996) reduced his magnitude estimate of the Charleston earthquake to **M** 7.3 from the prior estimate of **M** 7.53 as cited in Chapman (Chapman, 1994). Using the magnitude conversion described in Section 2.5.2.2.1, **M** = 7.3 converts to m_b = 7.1, which is within the range of largest M_{max} values (m_b 6.6 to 7.2) assigned by the EPRI teams to the Central Virginia seismic zone. These later studies, therefore, are consistent with the interpretations of the EPRI EST teams.

2.5.2.2.2.3 United States Geological Survey (USGS) Model

In 2002, the USGS produced updated seismic hazard maps for the conterminous United States based on new seismological, geophysical, and geological information (USGS, 2002). The 2002 maps reflect changes to the source model used to construct the previous version of the national seismic hazard maps (USGS, 1996). The most significant modifications to the CEUS portion of the source model include changes in the recurrence, M_{max}, and geometry of the Charleston and New Madrid sources. Unlike the EPRI models that incorporate many local sources, the USGS source model in the CCNPP Unit 3 site region (200 mi (320 km) radius) includes only three sources that are important to the site hazard: the Extended Margin background, Stable Craton background, and the New Madrid (Table 2.5-13). Except for the Charleston and New Madrid zones, where earthquake recurrence is modeled by paleoliquefaction data, the hazard for the large background or "maximum magnitude" zones is largely based on historical seismicity and the variation of that seismicity.

As part of the 2002 update of the National Seismic Hazard Maps, the USGS developed a model of the Charleston source that incorporates available data regarding recurrence, M_{max}, and

geometry of the source zone. The USGS model uses two equally weighted source geometries: a) an areal source enveloping most of the tectonic features and liquefaction data in the greater Charleston area, and b) a north-northeast-trending elongated areal source enveloping the southern half of the southern segment of the proposed East Coast fault system (ECFS) (Table 2.5-13 and Figure 2.5-53). The USGS (USGS, 2002) report does not specify why the entire southern segment of the ECFS is not contained in the source geometry. For M_{max}, the study defines a distribution of magnitudes and weights for Charleston of **M** 6.8 (0.20), 7.1 (0.20), 7.3 (0.45), 7.5 (.15). For recurrence, USGS (USGS, 2002) adopt a mean paleoliquefaction-based recurrence interval of 550 years and represent the uncertainty with a continuous lognormal distribution.

2.5.2.2.2.4 North Anna ESP Application

A seismic source characterization study was performed as part of an Early Site Permit application for the North Anna nuclear power plant, located in central Virginia, by Dominion Nuclear North Anna LLC (Dominion, 2005). Aspects of the study have been summarized previously in Sections 2.5.1.1.4.4 and 2.5.1.1.4.4. In particular, Dominion Nuclear North Anna LLC (Dominion, 2004a) (Dominion, 2004b) performed additional studies and/or addressed Requests for Additional Information (RAI) associated with several potential seismic sources, including the fall lines of Weems (USGS, 1998), Everona-Mountain Run Fault Zone, Stafford Fault System, postulated East Coast Fault System (ECFS) (Marple, 2000), and CVSZ. All of these features have been discussed previously in Section 2.5.1. With the exception of the southern segment of the postulated East Coast fault system, the presence of these features does not warrant modification to the EPRI (EPRI, 1989a) PSHA study (see Section 2.5.1.1.4.4). The ECFS-south is included in the updated Charleston Source Study Bechtel (Bechtel, 2006) presented below in Section 2.5.2.2.2.7.

2.5.2.2.2.5 South Carolina Department of Transportation Model

Chapman (Chapman, 2002) created probabilistic seismic hazard maps for the South Carolina Department of Transportation (SCDOT). In the SCDOT model, treatment of the 1886 Charleston, South Carolina, earthquake and similar events dominates estimates of hazard statewide (Chapman, 2002). The SCDOT model (Chapman, 2002) employs a combination of line and area sources to characterize Charleston-type earthquakes in three separate geometries and uses a slightly different M_{max} range (**M** 7.1 to 7.5) than the USGS 2002 model (USGS, 2002) model (Table 2.5-14 and Figure 2.5-54). Three equally-weighted seismic sources defined for this study include:

- a larger Coastal South Carolina zone called the Charleston area source that includes most of the paleoliquefaction sites.
- a line source capturing the intersection of the Woodstock and Ashley River faults, that is modeled as three parallel line sources.
- a southern ECFS line source called the ZRA fault source.

The respective magnitude distributions and weights used for all sources for M_{max} are **M** 7.1 (0.20), 7.3 0(0.60), 7.5 (0.20). The mean recurrence interval used in the SCDOT study is 550 years, based on the paleoliquefaction record.

2.5.2.2.2.6 The Trial Implementation Project Study

The Lawrence Livermore National Laboratory Trial Implementation Project (TIP) (NRC, 2002a) study focuses on seismic zonation and earthquake recurrence models for two nuclear plant

sites in the southeastern U.S. i.e., the Vogtle site in Georgia and the Watts Bar site in Tennessee. The TIP study (NRC, 2002a) uses an expert elicitation process to characterize the Charleston seismic source, considering published data through 1996. The TIP study (NRC, 2002a) identifies multiple alternative zones for the Charleston source and for the South Carolina–Georgia seismic zone, as well as alternative background seismicity zones for the Charleston region. However, the TIP study (NRC, 2002a) focuses primarily on implementing the Senior Seismic Hazard Advisory Committee (SSHAC) PSHA methodology (NRC, 1997b) and was designed to be as much of a test of the methodology as a real estimate of seismic hazard. As a result, its findings are not included explicitly in this report for the CCNPP Unit 3 site.

2.5.2.2.2.7 Updated Charleston Seismic Source (UCSS) Model

It has been nearly 20 years since the six EPRI ESTs evaluated hypotheses for earthquake causes and tectonic features and assessed seismic sources in the CEUS (EPRI, 1986). The EPRI Charleston source zones developed by each EST are shown in Figure 2.5-55 and summarized in Table 2.5-15. Several studies that post-date the 1986 EPRI EST assessments have demonstrated that the source parameters for geometry, M_{max}, and recurrence of M_{max} in the Charleston seismic source require an update to capture a more current understanding for both the 1886 Charleston earthquake and the seismic source that produced this earthquake. In addition, recent PSHA studies of the South Carolina region (NRC, 2002a) (Chapman, 2002), southeastern United States (USGS, 2002), and for the Vogtle site (Bechtel, 2006) have developed models of the Charleston seismic source that differ significantly from the earlier EPRI characterizations. The Updated Charleston Seismic Source model of Bechtel (Bechtel, 2006) was included in the PSHA study for the CCNPP Unit 3 site.

The UCSS model prepared by Bechtel (Bechtel, 2006) is summarized below. Methods used to update the Charleston seismic source follow guidelines provided in Regulatory Guide 1.165 (NRC, 1997a). Bechtel (Bechtel, 2006) performed a SSHAC Level 2 study to incorporate current literature and data and the understanding of experts into an update of the Charleston seismic source model. This level of effort is outlined in the NUREG/CR-6372 (NRC,1997b) report, which provides guidance on incorporating uncertainty and the use of experts in PSHA studies.

The UCSS model also incorporates new information to re-characterize geometry, M_{max}, and recurrence for the Charleston seismic source. These components are summarized in the following sections. Paleoliquefaction data imply that the Charleston earthquake process is defined by repeated, relatively frequent, large earthquakes located in the vicinity of Charleston, indicating that the Charleston source behaves differently from the rest of the eastern seaboard.

UCSS Geometry

The UCSS model includes four mutually exclusive source zone geometries (A, B, B′, and C; Figure 2.5-56). The latitude and longitude coordinates that define these four source zones are presented in Table 2.5-16. Details regarding each source geometry are given below. The four geometries of the UCSS are defined based on the following: current understanding of geologic and tectonic features in the 1886 Charleston earthquake epicentral region; the 1886 Charleston earthquake shaking intensity; distribution of seismicity; and geographic distribution, age, and density of liquefaction features associated with both the 1886 and prehistoric earthquakes. These features, shown in Figure 2.5-57 and Figure 2.5-58, strongly suggest that the majority of evidence for the Charleston source is concentrated in the Charleston area and is not widely distributed throughout South Carolina. Table 2.5-17 provides a subset of the Charleston tectonic features differentiated by pre- and post-EPRI

(EPRI, 1986) information. In addition, pre- and post-1986 instrumental seismicity, m_b 3, are shown on Figure 2.5-57 and Figure 2.5-58. Seismicity continues to be concentrated in the Charleston region in the Middleton Place–Summerville seismic zone (MPSSZ), which has been used to define the intersection of the Woodstock and Ashley River faults (SSA, 1981) (SSA, 1993). In addition, two earthquakes in 2002 (m_b 3.5 and 4.4) are located offshore of South Carolina along the Helena Banks fault zone in an area previously devoid of seismicity of m_b > 3. A compilation of the EPRI ESTs Charleston source zones is provided in Figure 2.5-55 as a comparison to the UCSS geometries shown in Figure 2.5-56.

Geometry A – Charleston

Geometry A is an approximately 62 mi x 31 mi (100 km x 50 km), northeast-oriented area centered on the 1886 Charleston meizoseismal area (Figure 2.5-56). Geometry A is intended to represent a localized source area that generally confines the Charleston source to the 1886 meizoseismal area (i.e., a stationary source in time and space). Geometry A completely incorporates the 1886 earthquake MMI X isoseismal (Bollinger, 1977), the majority of identified Charleston-area tectonic features and inferred fault intersections, and the majority of reported 1886 liquefaction features. Geometry A excludes the northern extension of the southern segment of the East Coast fault system because this system extends well north of the meizoseismal zone and is included in its own source geometry (Geometry C). Geometry A also excludes outlying liquefaction features, because liquefaction occurs as a result of strong ground shaking that may extend well beyond the areal extend of the tectonic source. Geometry A also envelopes instrumentally located earthquakes spatially associated with the MPSSZ (SSA, 1981) (USGS, 1983b) (SSA, 1993).

The preponderance of evidence strongly supports the conclusion that the seismic source for the 1886 Charleston earthquake is located in a relatively restricted area defined by Geometry A. Geometry A envelopes (a) the meizoseismal area of the 1886 earthquake, (b) the area containing the majority of local tectonic features (although many have large uncertainties associated with their existence and activity, as described earlier), (c) the area of ongoing concentrated seismicity, and (d) the area of greatest density of 1886 liquefaction and prehistoric liquefaction. These observations show that future earthquakes with magnitudes comparable to the Charleston earthquake of 1886 will most likely occur within the area defined by Geometry A. A weight of 0.70 is assigned to Geometry A (Figure 2.5-59). To confine the rupture dimension to within the source area and to maintain a preferred northeast fault orientation, Geometry A is represented in the model by a series of closely spaced, northeast-trending faults parallel to the long axis of the zone.

Geometries B, B′, and C

While the preponderance of evidence supports the assessment that the 1886 Charleston meizoseismal area and Geometry A define the area where future events will most likely be centered, it is possible that the tectonic feature responsible for the 1886 earthquake either extends beyond or lies outside Geometry A. Therefore, the remaining three geometries (B, B′, and C) are assessed to capture the uncertainty that future events may not be restricted to Geometry A. The distribution of liquefaction features along the entire coast of South Carolina and observations from the paleoliquefaction record that a few events were localized (moderate earthquakes to the northeast and southwest of Charleston), suggest that the Charleston source could extend well beyond Charleston proper. Geometries B and B′ are assessed to represent a larger source zone, while Geometry C represents the southern segment of the hypothesized East Coast fault system as a possible source zone. The combined

geometries of B and B′ are assigned a weight of 0.20, and Geometry C is assigned a weight of 0.10. Geometry B′ a subset of B, formally defines the onshore coastal area as a source (similar to the SCDOT coastal source zone) that would restrict earthquakes to the onshore region. Geometry B, which includes the onshore and offshore regions, and Geometry B′ are mutually exclusive and given equal weight in the UCSS model. Therefore, the resulting weights are 0.10 for Geometries B and B′.

Geometry B – Coastal and Offshore Zone

Geometry B is a coast-parallel, approximately 162 mi x 62 mi (260 km x 100 km) source area that a) incorporates all of Geometry A, b) is elongated to the northeast and southwest to capture other, more distant liquefaction features in coastal South Carolina (Amick, 1990a) (Amick, 1990b) (NRC, 1990) (Talwani, 2001), and c) extends to the southeast to include the offshore Helena Banks fault zone (Behrendt, 1987; Figure 2.5-56 and Figure 2.5-58). The elongation and orientation of Geometry B is roughly parallel to the regional structural grain as well as roughly parallel to the elongation of 1886 isoseismals. The northeastern and southwestern extents of Geometry B are controlled by the mapped extent of paleoliquefaction features (Amick, 1990a) (Amick, 1990b) (NRC, 1990) (Talwani, 2001).

The location and timing of paleoliquefaction features in the Georgetown and Bluffton areas to the northeast and southwest of Charleston have suggested to some researchers that the earthquake source may not be restricted to the Charleston area (Obermeier, 1989) (NRC, 1990) (Talwani, 2001). A primary reason for defining Geometry B is to account for the possibility that there may be an elongated source or multiple sources along the South Carolina coast. Paleoliquefaction features in the Georgetown and Bluffton areas may be explained by an earthquake source both northeast and southwest of Charleston, as well as possibly offshore.

Geometry B extends southeast to include an offshore area and the Helena Banks fault zone. The Helena Banks fault zone is clearly shown by multiple seismic reflection profiles and has demonstrable late Miocene offset (Behrendt, 1987). Offshore earthquakes in 2002 (m_b 3.5 and 4.4) suggest a possible spatial association of seismicity with the mapped trace of the Helena Banks fault system (Figure 2.5-56 and Figure 2.5-58). Whereas these two events in the vicinity of the Helena Banks fault system do not provide a positive correlation with seismicity or demonstrate recent fault activity, these small earthquakes are considered new data since the EPRI studies. The EPRI earthquake catalog (EPRI, 1988) was devoid of any events ($m_b > 3.0$) offshore from Charleston. The recent offshore seismicity also post-dates the development of the USGS and SCDOT source models that exclude any offshore Charleston source geometries.

A low weight of 0.10 is assigned to Geometry B (Figure 2.5-59), because the preponderance of evidence indicates that the seismic source that produced the 1886 earthquake lies onshore in the Charleston meizoseismal area and not in the offshore region. To confine the rupture dimension to within the source area and to maintain a preferred northeast fault orientation, Geometry B is represented in the model by a series of closely spaced, northeast-trending faults parallel to the long axis of the zone.

Geometry B′ – Coastal Zone

Geometry B′ is a coast-parallel, approximately 162 mi x 31 mi (260 km x 50 km source area that incorporates all of Geometry A, as well as the majority of reported paleoliquefaction features (Amick, 1990a) (Amick, 1990b) (NRC, 1990) (Talwani, 2001). Unlike Geometry B, however,

Geometry B′ (Figure 2.5-55) does not include the offshore Helena Banks Fault Zone (Figure 2.5-58).

The Helena Banks fault system is excluded from Geometry B′ to recognize that the preponderance of the data and evaluations support the assessment that the fault system is not active. It is also excluded because most evidence strongly suggests that the 1886 Charleston earthquake occurred onshore in the 1886 meizoseismal area and not on an offshore fault. Whereas there is little uncertainty regarding the existence of the Helena Banks fault, there is a lack of evidence that this feature is still active. Isoseismal maps documenting shaking intensity in 1886 indicate an onshore meizoseismal area (the closed bull's eye centered onshore north of downtown Charleston, Figure 2.5-58). An onshore source for the 1886 earthquake as well as the prehistoric events is supported by the instrumentally recorded seismicity in the MPSSZ and the corresponding high density cluster of 1886 and prehistoric liquefaction features.

Similar to Geometry B above, a weight of 0.10 is assigned to Geometry B′ and reflects the assessment that Geometry B′ has a much lower probability of being the source zone for Charleston-type earthquakes than Geometry A (Figure 2.5-59). To confine the rupture dimension to within the source area and to maintain a preferred northeast fault orientation, Geometry B′ is represented in the model by a series of closely spaced, northeast-trending faults parallel to the long axis of the zone.

Geometry C – East Coast Fault System – South (ECFS-s)

Geometry C is an approximately 123 mi x 19 mi (200 km x 30 km), north-northeast-oriented source area enveloping the southern segment of the proposed East Coast fault system (ECFS-s) shown inFigure 3 of Marple (Marple, 2000) (Figure 2.5-56 and Figure 2.5-60). The USGS hazard model (USGS, 2002) (Figure 2.5-53) incorporates the postulated ECFS-S as a distinct source geometry (also known as the zone of river anomalies (ZRA) depicted in Figure 2.5-60); however, as described earlier, the USGS model truncates the northeastern extent of the proposed fault segment. The South Carolina Department of Transportation hazard model (Chapman, 2002) also incorporates the ECFS-S as a distinct source geometry; however, this model extends the southern segment of the proposed East Coast fault system farther to the south than originally postulated by Marple (Marple, 2000) to include, in part, the distribution of liquefaction in southeastern South Carolina (Figure 2.5-56).

In this CCNPP Unit 3 site evaluation, the area of Geometry C is restricted to envelope the original depiction of the proposed ECFS-S by Marple (Marple, 2000). Truncation of the zone to the northeast as shown by the 2002 USGS model is not supported by available data, and the presence of liquefaction in southeastern South Carolina is best captured in Geometries B and B′, rather than extending the ECFS-S farther to the south than defined by the data of Marple (Marple, 2000).

A low weight of 0.10 is assigned to Geometry C to reflect the assessment that Geometries B, B′, and C all have equal, but relatively low, likelihood of producing Charleston-type earthquakes (Figure 2.5-59). As with the other UCSS geometries, Geometry C is represented as a series of parallel, vertical faults oriented northeast-southwest and parallel to the long axis of the narrow rectangular zone. The faults and extent of earthquake ruptures are confined within the rectangle depicting Geometry C.

UCSS Model Parameters

Based on studies by Bollinger (Bollinger, 1985) (Bollinger,1991) (USGS, 1992), a 20-km-thick seismogenic crust is assumed for the UCSS. To model the occurrence of earthquakes in the characteristic part of the Charleston distribution (**M** > 6.7), the model uses a series of closely-spaced, vertical faults parallel to the long axis of each of the four source zones (A, B, B′, and C). Faults and earthquake ruptures are limited to within each respective source zone and are not allowed to extend beyond the zone boundaries, and ruptures are constrained to occur within the depth range of 0 mi to 12.5 mi (0 km to 20 km). Modeled fault rupture areas are assumed to have a width-to-length aspect ratio of 0.5, conditional on the assumed maximum fault width of 0 mi to 12.5 mi (0 km to 20 km). To obtain M_{max} earthquake rupture lengths from magnitude, the empirical relationship reported in Wells (SSA, 1994) between surface rupture length and **M** for earthquakes of all slip types is used. To maintain as much similarity as possible with the original EPRI model, the UCSS model treats earthquakes in the exponential part of the distribution (**M** < 6.7) as point sources uniformly distributed within the source area (full smoothing), with a constant depth fixed at 10 km.

UCSS Maximum Magnitude

The six EPRI ESTs developed a distribution of weighted M_{max} values and weights to characterize the largest earthquakes that could occur on Charleston seismic sources (Table 2.5-15). On the low end, the Law Engineering team assessed a single M_{max} of m_b 6.8 to seismic sources it considered capable of producing earthquakes comparable in magnitude to the 1886 Charleston earthquake. On the high end, four teams defined M_{max} upper bounds ranging between m_b 7.2 and m_b 7.5. For the CCNPP Unit 3 PSHA, the m_b magnitude values have been converted to moment magnitude (**M**), as described previously. The m_b value and converted moment magnitude value for each team are shown below. The range in **M** for the six ESTs is 6.5 to 8.0.

Team	Charleston Mmax range
Bechtel Group	m_b 6.8 to 7.4 (M 6.8 to 7.9)
Dames & Moore	m_b 6.6 to 7.2 (M 6.5 to 7.5)
Law Engineering	m_b 6.8 (M 6.8)
Rondout	m_b 6.6 to 7.0 (M 6.5 to 7.2)
Weston Geophysical	m_b 6.6 to 7.2 (M 6.5 to 7.5)
Woodward-Clyde Consultants	m_b 6.7 to 7.5 (M 6.7 to 8.0)

The **M** equivalents of EPRI m_b estimates for Charleston M_{max} earthquakes show that the upper bound values are similar to, and in two cases exceed, the largest modern estimate of **M** 7.3 ± 0.26 (Johnston, 1996) for the 1886 earthquake. The upper bound values for five of the six ESTs also exceed the preferred estimate of **M** 6.9 by Bakun (Bakun, 2004) for the Charleston event. The EPRI M_{max} estimates are more heavily weighted toward the lower magnitudes, with the upper bound magnitudes given relatively low weights by several ESTs (Table 2.5-3 through Table 2.5-8). Therefore, updating the M_{max} range and weights to reflect the current range of technical interpretations is warranted for the UCSS.

Based on assessment of the currently available data and interpretations regarding the range of modern M_{max} estimates (Table 2.5-18), the UCSS model modifies the USGS magnitude distribution (USGS, 2002) to include a total of five discrete magnitude values, each separated by 0.2 **M** units (Figure 2.5-59). The UCSS M_{max} distribution includes a discrete value of **M** 6.9 to represent the Bakun best estimate of the 1886 Charleston earthquake magnitude, as well as a lower value of **M** 6.7 to capture a low probability that the 1886 earthquake was smaller than

the Bakun mean estimate of **M** 6.9. Bakun did not explicitly report a 1-sigma range in magnitude estimate of the 1886 earthquake, but do provide a 2-sigma range of **M** 6.4 to **M** 7.2 (Bakun, 2004).

The UCSS magnitudes and weights are as follows:

M	Weight	
6.7	0.10	
6.9	0.25	(Bakun ,2004) mean
7.1	0.30	
7.3	0.25	(Johnston, 1996) mean
7.5	0.10	

This results in a weighted M_{max} mean magnitude of **M** 7.1 for the UCSS, which is slightly lower than the mean magnitude of **M** 7.2 in the USGS model (USGS, 2002).

UCSS Recurrence Model

In the 1989 EPRI study (EPRI, 1989a), the six EPRI ESTs used an exponential magnitude distribution to represent earthquake sizes for their Charleston sources. Parameters of the exponential magnitude distribution were estimated from historical seismicity in the respective source areas. This resulted in recurrence intervals for M_{max} earthquakes (at the upper end of the exponential distribution) of several thousand years.

The current model for earthquake recurrence is a composite model consisting of two distributions. The first is an exponential magnitude distribution used to estimate recurrence between the lower-bound magnitude used for hazard calculations and m_b 6.7. The parameters of this distribution are estimated from the earthquake catalog, as they were for the 1989 EPRI study (EPRI, 1989a). This is the standard procedure for smaller magnitudes and is the model used, for example, by the USGS 2002 national hazard maps (USGS, 2002). In the second distribution, M_{max} earthquakes (**M** > 6.7) are treated according to a characteristic model, with discrete magnitudes and mean recurrence intervals estimated through analysis of geologic data, including paleoliquefaction studies. In this document, M_{max} is used to describe the range of largest earthquakes in both the characteristic portion of the UCSS recurrence model and the EPRI exponential recurrence model.

This composite model achieves consistency between the occurrence of earthquakes with **M** < 6.7 and the earthquake catalog and between the occurrence of large earthquakes (**M** > 6.7) with paleoliquefaction evidence. It is a type of "characteristic earthquake" model, in which the recurrence rate of large events is higher than what would be estimated from an exponential distribution inferred from the historical seismic record.

M_{max} Recurrrence Intervals

This section describes how the UCSS model determines mean recurrence intervals for M_{max} earthquakes. The UCSS model incorporates geologic data to characterize the recurrence intervals for M_{max} earthquakes. As described earlier, identifying and dating paleoliquefaction features provides a basis for estimating the recurrence of large Charleston area earthquakes. Most of the available geologic data pertaining to the recurrence of large earthquakes in the Charleston area were published after 1990 and, therefore, were not available to the six EPRI ESTs. In the absence of geologic data, the six EPRI EST estimates of recurrence for large,

Charleston-type earthquakes were based on a truncated exponential model using historical seismicity (EPRI, 1986) (EPRI, 1989a). The truncated exponential model also provided the relative frequency of all earthquakes greater than m_b 5.0 up to M_{max} in the EPRI PSHA (EPRI, 1989a). The recurrence interval of M_{max} earthquakes in the EPRI models was on the order of several thousand years, which is significantly greater than more recently published estimates of about 500 to 600 years, based on paleoliquefaction data (Talwani, 2001).

Paleoliquefaction Data

Strong ground shaking during the 1886 Charleston earthquake produced extensive liquefaction, and liquefaction features from the 1886 event are preserved in geologic deposits at numerous locations in the region. Documentation of older liquefaction-related features in geologic deposits provides evidence for prior strong ground motions during prehistoric large earthquakes. Estimates of the recurrence of large earthquakes in the UCSS are based on dating paleoliquefaction features. Many potential sources of ambiguity and/or error are associated with dating and interpreting paleoliquefaction features. This assessment does not reevaluate field interpretations and data; rather, it reevaluates criteria used to define individual paleoearthquakes in the published literature. In particular, the UCSS reevaluates the paleoearthquake record interpreted by Talwani and Shaeffer (Talwani, 2001) based on that study's compilation of sites with paleoliquefaction features.

Talwani and Schaeffer compiled radiocarbon ages from paleoliquefaction features along the coast of South Carolina. These data include ages that provide contemporary, minimum, and maximum limiting ages for liquefaction events. Radiocarbon ages were corrected for past variability in atmospheric ^{14}C using well established calibration curves and converted to "calibrated" (approximately calendric) ages. From the compilation of calibrated radiocarbon ages from various geographic locations, they correlated individual earthquake episodes. They identified an individual earthquake episode based on samples with a "contemporary" age constraint that had overlapping calibrated radiocarbon ages at approximately 1-sigma confidence interval. The estimated age of each earthquake was "calculated from the weighted averages of overlapping contemporary ages" They defined as many as eight events from the paleoliquefaction record (named 1886, A, B, C, D, E, F, and G, in order of increasing age), and offered two scenarios to explain the distribution and timing of paleoliquefaction features (Table 2.5-19). (Talwani, 2001)

The two scenario paleoearthquake records proposed by Talwani and Schaeffer (Talwani, 2001), Scenario 1 and Scenario 2, have different interpretations for the size and location of prehistoric events (Table 2.5-19). In Scenario 1, the four prehistoric events that produced widespread liquefaction features similar to the large 1886 Charleston earthquake (A, B, E, and G) are interpreted to be large, Charleston-type events. Three events, C, D, and F, are defined by paleoliquefaction features that are more limited in geographic extent than other events and are interpreted to be smaller, moderate-magnitude events (approximately M 6). Events C and F are defined by features found north of Charleston in the Georgetown region, and Event D is defined by sites south of Charleston in the Bluffton area. In Scenario 2, all events are interpreted as large, Charleston-type events. Furthermore, Events C and D are combined into a large Event C′. Talwani and Schaeffer (Talwani, 2001) justify the grouping of the two events based on the observation that the calibrated radiocarbon ages that constrain the timing of Events C and D are indistinguishable at the 95 percent (2-sigma) confidence interval.

The length and completeness of the paleoearthquake record based on paleoliquefaction features is a source of epistemic uncertainty in the UCSS. The paleoliquefaction record along

the South Carolina coast extends from 1886 to the mid-Holocene. The consensus of the scientists who have evaluated these data is that the paleoliquefaction record of earthquakes is complete only for the most recent ~2000 years and that it is possible that liquefaction events are missing from the older portions of the record. The suggested incompleteness of the paleoseismic record is based on the argument that past fluctuations in sea level have produced time intervals of low water table conditions (and thus low liquefaction susceptibility), during which large earthquake events may not have been recorded in the paleoliquefaction record. While this assertion may be true, it cannot be ruled out that the paleoliquefaction record is complete back to the mid-Holocene. (Talwani, 2001)

2-Sigma Analysis of Event Ages

Analysis of the coastal South Carolina paleoliquefaction record is based on the Talwani and Schaeffer data compilation. As described above, Talwani and Schaeffer use calibrated radiocarbon ages with 1-sigma error bands to define the timing of past liquefaction episodes in coastal South Carolina. The standard in paleoseimology, however, is to use calibrated ages with 2-sigma (95.4 percent confidence interval) error bands (e.g., (Sieh, 1989) (Grant, 1994)). Likewise, in paleoliquefaction studies, to more accurately reflect the uncertainties in radiocarbon dating, the use of calibrated radiocarbon dates with 2-sigma error bands (as opposed to narrower 1-sigma error bands) is advisable (Tuttle, 2001). The Talwani and Schaeffer use of 1-sigma error bands may lead to over-interpretation of the paleoliquefaction record such that more episodes are interpreted than actually occurred. In recognition of this possibility, the conventional radiocarbon ages presented in Talwani and Schaeffer have been recalibrated and reported with 2-sigma error bands. The recalibration of individual radiocarbon samples and estimation of age ranges for paleoliquefaction events show broader age ranges with 2-sigma error bands which are used to obtain broader age ranges for paleoliquefaction events in the Charleston area. (Talwani, 2001)

Event ages based on overlapping 2-sigma ages of paleoliquefaction features are presented in Table 2.5-19. Paleoearthquakes have been distinguished based on grouping paleoliquefaction features that have contemporary radiocarbon samples with overlapping calibrated ages. Event ages have then been defined by selecting the age range common to each of the samples. For example, an event defined by overlapping 2-sigma sample ages of 100–200 cal. yr. BP (before present) and 50–150 cal. yr. BP would have an event age of 100–150 cal. yr. BP. The UCSS study considers the "trimmed" ages to represent the approximately 95 percent confidence interval, with a "best estimate" event age as the midpoint of the approximately 95 percent age range.

The 2-sigma analysis identified six distinct paleoearthquakes in the data presented by Talwani and Schaeffer. As noted by that study, Events C and D are indistinguishable at the 95 percent confidence interval, and in the UCSS, those samples define Event C' (Table 2.5-19). Additionally, the UCSS 2-sigma analysis suggests that Talwani and Schaeffer Events F and G may have been a single, large event, defined in the UCSS as F'. One important difference between the UCSS result and that of Talwani and Schaeffer is that the three Events C, D, and F in their Scenario 1, which are inferred to be smaller, moderate-magnitude events, are grouped into more regionally extensive Events C' and F' (Table 2.5-19). Therefore, in the UCSS, all earthquakes in the 2-sigma analysis have been interpreted to represent large, Charleston-type events. Analysis suggests that there have been four large earthquakes in the most-recent, ~2000-year, portion of the record (1886 and Events A, B, and C'). In the entire ~5000-year paleoliquefaction record, there is evidence for six large, Charleston-type earthquakes (1886, A, B, C', E, and F') (Table 2.5-19). (Talwani, 2001).

Recurrence intervals developed from the earthquakes recorded by paleoliquefaction features assume that these features were produced by large M_{max} events and that both the ~2000-year and ~5000-year records are complete. However, the UCSS mentions at least two concerns regarding the use of the paleoliquefaction record to characterize the recurrence of past M_{max} events. First, it is possible that the paleoliquefaction features associated with one or more of these pre-1886 events were produced by multiple moderate-sized events closely spaced in time. If this were the case, then the calculated recurrence interval would yield artificially short recurrence for M_{max}, because it was calculated using repeat times of both large (M_{max}) events and smaller earthquakes. Limitations of radiocarbon dating and limitations in the stratigraphic record often preclude identifying individual events in the paleoseismologic record that are closely spaced in time (i.e., separated by only a few years to a few decades). Several seismic sources have demonstrated tightly clustered earthquake activity in space and time that are indistinguishable in the radiocarbon and paleoseismic record:

- New Madrid (December 1811, January 1812, February 1812)
- North Anatolian Fault (August 1999 and November 1999)
- San Andreas Fault (1812 and 1857)

Therefore, the UCSS acknowledges the distinct possibility that M_{max} occurs less frequently than what is calculated from the paleoliquefaction record.

A second concern is that the recurrence behavior of the M_{max} event may be highly variable through time. For example, the UCSS considers it unlikely that **M** 6.7 to **M** 7.5 events have occurred on a Charleston source at an average repeat time of about 500 to 600 years (Talwani, 2001) throughout the Holocene Epoch. Such a moment release rate would likely produce tectonic landforms with clear geomorphic expression, such as are present in regions of the world with comparably high rates of moderate to large earthquakes (for example, faults in the Eastern California shear zone with sub-millimeter per year slip rates and recurrence intervals on the order of about 5000 years have clear geomorphic expression (SSA, 2000). Perhaps it is more likely that the Charleston source has a recurrence behavior that is highly variable through time, such that a sequence of events spaced about 500 years apart is followed by quiescent intervals of thousands of years or longer. This sort of variability in inter-event time may be represented by the entire mid-Holocene record, in which both short inter-event times (e.g., about 400 years between Events A and B) are included in a record with long inter-event times (e.g., about 1900 years between Events C' and E).

Recurrence Rates

The UCSS model calculates two average recurrence intervals covering two different time intervals, which are used as two recurrence branches on the logic tree (Figure 2.5-59). The first average recurrence interval is based on the four events that occurred within the past ~2000 years. This time period is considered to represent a complete portion of the paleoseismic record based on published literature e.g., (Talwani, 2001)) and feedback from those researchers questioned (Talwani , 2001). These events include 1886, A, B, and C' (Table 2.5-19). The average recurrence interval calculated for the most recent portion of the paleoliquefaction record (four events over the past ~2000 years) is given 0.80 weight on the logic tree (Figure 2.5-59).

The second average recurrence interval is based on events that occurred within the past ~5000 years. This time period represents the entire paleoseismic record based on

paleoliquefaction data (Talwani, 2001). These events include 1886, A, B, C', E, and F', as listed in Table 2.5-19. As mentioned previously, published papers and researchers questioned suggest that the older part of the record (older than ~2000 years ago) may be incomplete. Whereas this assertion may be true, it is also possible that the older record, which exhibits longer inter-event times, is complete. The average recurrence interval calculated for the ~5000-year record (six events) is given 0.20 weight on the logic tree (Figure 2.5-59). The 0.80 and 0.20 weighting of the ~2000-year and ~5000-year paleoliquefaction records, respectively, reflect incomplete knowledge of both the current short-term recurrence behavior and the long-term recurrence behavior of the Charleston source.

The mean recurrence intervals for the most-recent ~2000-year and past ~5000-year records represent the average time interval between earthquakes attributed to the Charleston seismic source. The mean recurrence intervals and their parametric uncertainties were calculated according to the methods outlined by Savage (SSA, 1991) and Cramer (Cramer, 2001). The methods provide a description of mean recurrence interval, with a best estimate mean Tave and an uncertainty described as a lognormal distribution with median T0.5 and parametric lognormal shape factor σ 0.5.

The lognormal distribution is one of several distributions, including the Weibull, Double Exponential, and Gaussian, among others, used to characterize earthquake recurrence (Ellsworth, 1999). Ellsworth (Ellsworth,1999) and Matthews (SSA, 2002) propose a Brownian-passage time model to represent earthquake recurrence, arguing that it more closely simulates the physical process of strain build-up and release. This Brownian-passage time model is currently used to calculate earthquake probabilities in the greater San Francisco Bay region (USGS, 2003). Analyses show that the lognormal distribution is very similar to the Brownian-passage time model of earthquake recurrence for cases where the time elapsed since the most recent earthquake is less than the mean recurrence interval (Cornell, 1988) (Ellsworth, 1999). This is the case for Charleston, where 120 years have elapsed since the 1886 earthquake and the mean recurrence interval determined over the past ~2000 years is about 548 years. The UCSS study has calculated average recurrence interval using a lognormal distribution because its statistics are well known (NIST, 2006) and it has been used in numerous studies (e.g., those performed by Savage (SSA, 1991), Working Group on California Earthquake Probabilities (WGCEP, 1995), and Cramer (Cramer 2001).

The average interval between earthquakes is expressed as two continuous lognormal distributions. The average recurrence interval for the ~2000-year record, based on the three most recent inter-event times (1886-A, A-B, and B-C′), has a best estimate mean value of 548 years and an uncertainty distribution described by a median value of 531 years and a lognormal shape factor of 0.25. The average recurrence interval for the ~5000-year record, based on five inter-event times (1886-A, A-B, B-C′, C′-E, and E-F′), has a best estimate mean value of 958 years and an uncertainty distribution described by a median value of 841 years and a lognormal shape factor of 0.51. At one standard deviation, the average recurrence interval for the ~2000-year record is between 409 and 690 years; for the ~5000-year record, it is between 452 and 1,564 years. Combining these mean values of 548 and 958 years with their respective logic tree weights of 0.8 and 0.2 results in a weighted mean of 630 years for Charleston M_{max} recurrence.

The mean recurrence interval values used in the UCSS model are similar to those determined by earlier studies. Talwani and Schaeffer consider two possible scenarios to explain the distribution in time and space of paleoliquefaction features. In Scenario 1, large earthquakes have occurred with an average recurrence of 454 ± 21 years over about the past ~2000 years;

in Scenario 2, large earthquakes have occurred with an average recurrence of 523 ±100 years over the past ~2,000 years. Talwani and Schaeffer state that, "In anticipation of additional data we suggest a recurrence rate between 500 and 600 years for **M** 7+ earthquakes at Charleston." For the ~2000-year record, the 1-standard-deviation range of 409 to 690 years completely encompasses the range of average recurrence interval reported by Talwani and Schaeffer. The best-estimate mean recurrence interval value of 548 years is comparable to the midpoint of the Talwani and Schaeffer best-estimate range of 500 to 600 years. The best estimate mean recurrence interval value from the ~5000-year paleoseismic record of 958 years is outside the age ranges reported by Talwani and Schaeffer, although they did not determine an average recurrence interval based on the longer record (Talwani, 2001).

In the updated seismic hazard maps for the conterminous United States, Frankel (USGS, 2002) used a mean recurrence value of 550 years for characteristic earthquakes in the Charleston region. This value is based on the above-quoted 500–600 year estimate from Talwani and Schaeffer (Talwani, 2001). Frankel (USGS, 2002) did not incorporate uncertainty in mean recurrence interval in their calculations.

For computation of seismic hazard, discrete values of activity rate (inverse of recurrence interval) are required as input to the PSHA code (SSA, 1968). To evaluate PSHA based on mean hazard, the mean recurrence interval and its uncertainty distribution should be converted to mean activity rate with associated uncertainty. The final discretized activity rates used to model the UCSS in the PSHA reflect a mean recurrence of 548 years and 958 years for the ~2000-year and ~5000-year branches of the logic tree, respectively. Lognormal uncertainty distributions in activity rate are obtained by the following steps: (1) invert the mean recurrence intervals to get mean activity rates; (2) calculate median activity rates using the mean rates and lognormal shape factors of 0.25 and 0.51 established for the ~2000-year and ~5000-year records, respectively; and (3) determine the lognormal distributions based on the calculated median rate and shape factors. The lognormal distributions of activity rate can then be discredited to obtain individual activity rates with corresponding weights.

Characterization of Lancaster Seismic Zone

The Lancaster Seismic Zone (LSZ) of southeastern Pennsylvania is identified as a post-EPRI seismic zone located about 111 mi (179 km) northwest of the CCNPP Unit 3 site (Figure 2.5-52). This region of seismicity in the Appalachian mountains of Pennsylvania is described in Section 2.5.1.1.4.5 and includes roughly two centuries of seismicity. Despite its moderate rate of activity, the largest known earthquake was magnitude mbLg 4.1 (SSA, 1987). One larger event has been attributed to anthropogenic causes (i.e. Cacoosing Valley Earthquake mbLg 4.6; (Seeber, 1998). No evidence of larger prehistoric earthquakes, such as paleoliquefaction features, has been discovered (Wheeler, 2006). While the lack of large earthquakes in the relatively short historical record cannot preclude the future occurrence of large events, there is a much higher degree of uncertainty associated with the assignment of M_{max} for the LSZ than other CEUS seismic source zones, such as New Madrid and Charleston, where large historical earthquakes are known to have occurred.

Although the Lancaster seismic zone is not explicitly included in the original EPRI source model (EPRI, 1986), various EPRI source geometries and parameters provide conservative M_{max} distributions for the LSZ. A wide range of M_{max} values and associated probabilities were assigned to these EPRI sources to reflect the uncertainty of multiple experts from each EST. The body-wave magnitude (m_b) M_{max} values assigned by the ESTs for source geometries that envelop the LSZ range from m_b 5.3 to 7.2 (**M** 4.88 to 7.5). The Dames & Moore sources that

envelop the LSZ include an upper-bound M_{max} value of m_b 7.2 (**M** 7.5). Sources from the Woodward-Clyde and Rondout teams that envelop the LSZ were also assigned large upper-bound M_{max} values of m_b 6.8 to 7.1 (**M** 6.8 to 7.33). Thus, the maximum magnitude distributions of EPRI source zones are significantly greater than the largest reported earthquake in the LSZ.

Despite the identification of the LSZ by Armbruster and Seeber (SSA, 1987), subsequent post-EPRI seismic source characterizations studies (Chapman, 1994) (USGS, 1992) (USGS, 2002) do not identify the zone as a seismic source zone. The M_{max} distribution assigned to the seismic source zones that cover, but do not define, the LSZ are m_b 7.2 (**M** 7.5) (Chapman, 1994), m_b 5.78 (**M** 5.4) (Bollinger, 1992), and m_b 7.2 (**M** 7.5) (USGS, 1996) (USGS, 2002). Like the EPRI models, these magnitude distributions are larger than any instrumented or pre-instrumental historical events dating back to the 18th century (SSA, 1987). However, all of the post-EPRI (EPRI, 1986) background sources zones that encompass the LSZ effectively capture the EPRI background zones for the LSZ. Based on the available seismological and geologic evidence and available published literature for the LSZ, the existing EPRI seismic source model does not require a significant change. Therefore, it is concluded that no new information has been developed since 1986 that would require a significant revision to the EPRI seismic source model.

Earthquake Swarm of Howard County, Maryland

Howard County of Maryland, located about 12 mi (19 km) southwest of Baltimore, experienced 21 confirmed and probable shallow (approximately 1650 ft t(503 m) to 1980 ft (604 m) deep) earthquakes between March and November 1993 (Reger, 1994). The largest events recorded are mbLg 2.5 and mbLg 2.7 and occurred early in the sequence. Some minor cosmetic damage was reported near the epicenters (e.g., plaster cracked; light objects fell from shelves; bicycles fell over); however, there were no reports of structural damage. Analyses of seismicity data define a short (1000 ft (305 m) long) northwest-striking reverse fault with a minor component of left-lateral slip. Researchers speculate that the earthquakes may be associated with a diabase dike either aligned with the inferred reverse fault or offset by the inferred reverse fault; however, the cause of the earthquake swarm remains unknown. Field examination by the Maryland Geological Survey did not find any evidence for surface fault rupture in the region of the inferred surface projection of the fault (Reger, 1994). This earthquake swarm occurred in a region that historically has been aseismic and post-dates the EPRI source model (EPRI, 1986). Based on the small size of the maximum earthquakes and shallow depth, as well as the absence of a well-defined geologic structure aligned with the microseismicity, the Howard County earthquake swarm is not interpreted as a capable tectonic source. In summary, the EPRI model (EPRI, 1986) does not need to be revised to accommodate this minor earthquake swarm.

2.5.2.3 Correlation of Earthquake Activity with Seismic Sources

The updated EPRI seismicity catalog was reviewed in order to evaluate the spatial pattern of seismicity relative to the EPRI seismic source model (EPRI, 1986) and potential correlation of seismicity to possible geologic or tectonic structures. The EPRI seismicity catalog covers earthquakes in the CEUS for the time period from 1627 to 1984, as described in Section 2.5.2.1. This catalog has been updated for this CCNPP Unit 3 site investigation for the time period from 1985 to 2006, as described in Section 2.5.2.1. Figure 2.5-45 through Figure 2.5-50 show the distribution of earthquake epicenters from both the EPRI (pre-1985) and updated (post-1984) earthquake catalogs in comparison to the seismic sources identified by each of the EPRI ESTs.

Comparison of the updated earthquake catalog to the EPRI earthquake catalog (EPRI, 1988) yields the following conclusions:

- The updated catalog does not show any earthquakes within the site region that can be associated with a known geologic or tectonic structure. As described in Section 2.5.1, the majority of seismicity in the CCNPP Unit 3 site region appears to be occurring at depth within the basement beneath the Appalachian decollement.
- The updated catalog does not show a unique cluster of seismicity that would suggest a new seismic source outside of the EPRI seismic source model (EPRI, 1986).
- The updated catalog does not show a pattern of seismicity that would require significant revision to the EPRI seismic source geometry.
- The updated catalog does not show or suggest any increase in M_{max} for any of the EPRI seismic sources (EPRI, 1986).
- The updated catalog does not show any increase in seismicity parameters (rate of activity, b value) for any of the EPRI seismic sources (EPRI, 1986) (see Section 2.5.2.6.5).

2.5.2.4 Probabilistic Seismic Hazard Analysis and Controlling Earthquake

Sections 2.5.2.4.1 through 2.5.2.4.6 are added as a supplement to the U.S. EPR FSAR.

2.5.2.4.1 1989 EPRI Probabilistic Seismic Hazard Analysis

Following the recommendation of Regulator Guide 1.165 (NRC, 1997)), the 1989 EPRI study, EPRI NP-6395-D (EPRI, 1989a) forms a basis with which to start seismic hazard calculations. The first step was to replicate the results published from the 1989 EPRI study (EPRI, 1989a), to verify that seismic sources were modeled correctly and that the current seismic hazard software could accurately reproduce the 1989 results. The PSHA software used determines the annual frequency of exceedance as a function of minimum ground motion in an integration of hazard contribution of seismic sources - characterized by various parameters, including spatial extent and location, magnitude frequency recurrence, and tectonic environment - propagating the ground motion from the sources to the site through an appropriate attenuation relation. This software and the manner in which it is used allows for the incorporation of numerous elements of modeling and parametric variability, including alternative models and parametric distributions, as well as consideration of statistical uncertainties. This replication was made using the ground motion equations from the 1989 EPRI study, and it was made for rock hazard conditions in order to remove any effect that soil amplification might have on the comparison.

Table 2.5-20 compares the mean seismic hazard calculated for several amplitudes for peak ground acceleration (PGA) and for spectral velocity (SV) at 10 and 1 Hz. Spectral velocity was the response spectrum measure used in the 1989 EPRI study. For amplitudes corresponding to annual exceedance frequencies in the range 10^{-4} to 10^{-6}, the 2006 calculations replicate the 1989 EPRI results (EPRI, 1989a) to an accuracy that is in the range of 3 percent to 12 percent, with the 2006 calculations indicating slightly higher hazard. This is acceptable agreement, given that independent software was used to perform these calculations. Comparisons were also made for the median hazard and the 85 percent hazard, and these comparisons showed somewhat larger differences, with the 2006 results generally (but not always) showing higher hazards than the EPRI results (EPRI, 1989a). These comparisons are of less importance and concern because the mean hazard will be used to derive recommended seismic design levels.

2.5.2.4.2 Effects of New Regional Earthquake Catalog

One of the important sensitivity studies examined the effect of earthquakes that have occurred since the 1989 EPRI study (EPRI, 1989a) was performed in order to determine if activity rates have changed. Seismicity rates in the EPRI study were based on an earthquake catalog that extended through 1984. This sensitivity study examined additional earthquakes that occurred during the period of 1985 to 2005 and calculated rates of activity in regions surrounding the CCNPP Unit 3 site.

Figure 2.5-61 shows historical seismicity in the region of the site, with three areas that were used to examine the effect of additional seismicity: a 124 mi (200 km) × 124 mi (200 km) square region centered on the site, a 249 mi (400 km) × 249 mi (400 km) square region centered on the site, and a Rondout source 29. The latter source was selected as a representative source for the Central Virginia seismic zone.

To examine the effect of additional seismicity, the EPRI software discussed in EPRI NP-6452-D 1989 (EPRI, 1989b) was run, first with the original earthquake catalog (through 1984) (EPRI, 1986), and then with the extended catalog (through 2005). This software calculates seismicity parameters (a- and b-values) from which annual rates of earthquake occurrence can be derived. For these calculations, the seismicity was assumed to be spatially homogeneous within each source.

Figure 2.5-62, Figure 2.5-63, and Figure 2.5-64 compare annual rates of earthquake occurrence verses magnitude for the three sources examined in this sensitivity study (the 124 mi (200 km) × 124 mi (200 km) square region centered on the site, the 249 mi (400 km) × 249 mi (400 km) square region centered on the site, and the Rondout source 29). All three plots are in terms of m_b magnitude, which is the scale used in the original EPRI calculations. All three plots show that the additional seismicity from 1985-2005 indicates lower seismicity rates for the square sources surrounding the site and virtually the same seisicity rate in the Central Virginia Seismic Zone that was calculated using the original EPRI earthquake catalog (EPRI, 1986).

These comparisons indicate that the original seismicity rates that were calculated for seismic sources are adequate. These seismicity rates were developed during the 1989 EPRI study (EPRI, 1989a) for seismic sources developed by the six Earth Science Teams and do not need to be updated.

2.5.2.4.3 New Maximum Magnitude Information

As discussed above in Section 2.5.2.2, no new scientific information has been published that would lead to a change in the EPRI seismic source characterization or parameters, including the assessment of maximum magnitude. The only exception is the Charleston source, which is addressed in the next subsection. Therefore, the maximum magnitude distributions assigned by the EPRI EST teams to their sources have not been modified for the assessment of seismic hazard.

2.5.2.4.4 New Seismic Source Characterizations

As described above in Section 2.5.2.2.2.7, a new Charleston source model (the UCSS) has been developed to reflect updated estimates of the possible geometries of seismic sources in the Charleston region, the possible characteristics magnitudes that might occur, and the possible mean recurrence rates associated with those characteristic magnitudes. There are four geometries:

- Geometry A, weight 0.7

- Geometry B, weight 0.1
- Geometry B', weight 0.1
- Geometry C, weight 0.1

The distribution of characteristic magnitudes for these sources is described in Section 2.5.2.2.7.2. A discrete distribution with 5 values and weights is used. The distribution of mean recurrence intervals is described in Section 2.5.2.2.7.3, and it is developed using two data periods for paleoliquefaction events. Each data period has its own mean and uncertainty estimate for mean recurrence interval, and a discrete distribution with 5 values and weights is used to model each distribution, thus resulting in a total of 10 mean recurrence values (with weights) describing uncertainty in mean recurrence interval.

The above four geometries were represented with parallel faults oriented Northeast-Southwest and spaced at 6 mi (10 km) apart, and the activity rate of each geometry was distributed among the parallel faults. A general rupture length equation was used (Wells and Coppersmith 1994) to model a finite rupture length for each earthquake. The large distance between the CCNPP Unit 3 site and the Charleston seismic sources means that the exact details of the fault models and rupture lengths are not critical to the calculation of hazard from the Charleston source.

None of the six EPRI Earth Science Teams had a Charleston source that contributed to the 99 percent hazard in the original EPRI 1989 (EPRI, 1989a) calculations, in part because the implicit recurrence interval for large Charleston earthquakes was much longer than is now modeled (i.e., the activity rate was estimated to be lower). To include possible re-occurrences of large earthquakes in the Charleston region, the UCSS was added to each EST's list of sources.

2.5.2.4.5 New Ground Motion Models

Since publication of the 1989 EPRI study (EPRI, 1989a), much work has been done to evaluate strong earthquake ground motion in the central and eastern United States. This work was summarized EPRI TR-1009684 (EPRI, 2004) in the form of updated ground motion equations that estimate median spectral acceleration and uncertainty as a function of earthquake magnitude and distance. Epistemic uncertainty is modeled using multiple ground motion equations and multiple estimates of aleatory uncertainty (sigma), all with associated weights. Different sets of equations are recommended for sources that represent rifted verses non-rifted parts of the earth's crust. Equations are available for spectral frequencies of 100 Hz (equivalent to PGA), 25 Hz, 10 Hz, 5 Hz, 2.5 Hz, 1 Hz, and 0.5 Hz, and these equations apply to hard rock conditions.

EPRI published an update, EPRI TR-1014381 (EPRI, 2006a) in 2006 to the estimates of aleatory uncertainty. This update reflected the observation that the aleatory uncertainties in the original EPRI attenuation study (EPRI, 2004) were probably too large, resulting in over-estimates of seismic hazard. The 2006 EPRI study (EPRI, 2006a) recommends a revised set of aleatory uncertainties (sigmas) with weights, that can be used to replace the original aleatory uncertainties published in the 2004 EPRI study (EPRI, 2004).

The ground motion model used in the seismic hazard calculations consisted of the median equations from the EPRI 2004 study (EPRI 2004), with the updates for the aleatory uncertainties (EPRI, 2006a). EPRI TR-1014381 (EPRI, 2006a) was used in lieu of the Regulatory Guide 1.208 cited document, i.e. EPRI Report 1013105 (EPRI, 2006b). EPRI Report 1013105 (EPRI, 2006b) was an Update Report while EPRI TR-1014381 (EPRI, 2006a) is the final report. For

the purposes of revised estimates of aleatory uncertainty in the central and eastern U.S., there is no technical difference between the documents. The "Recommended CEUS Sigma" values and "Conclusions" of both reports are identical.

Additionally, Equation 7 of Regulatory Guide 1.208 (NRC, 2007a), Appendix D, Page D-5, was not used as written, in the determination mean distance of the controlling earthquake.

The deviation is described as follows:

Equation 7 is addressed in Appendix D, Step 3, Determining Controlling Earthquakes, as:

"The mean distance of the controlling earthquake is based on magnitude-distance bins greater than distances of 100 km (63 mi) as discussed in Step 5 and determined according to the following:

$$\mathrm{Ln}\{D_C(1-2.5\mathrm{Hz})\} = \sum_{d>100} \mathrm{Ln}(d) \sum_{m} P>100(m,d)_2 \qquad \text{Equation 7}$$

where d is the centroid distance value for each distance bin."

The definition for the term "P" is provided in Appendix D, Step 1, Determining Controlling Earthquakes."

P is defined as: This distribution, P > 100 (m,d), is defined by the following:

$$P>100(m,d)_1 = [P(m,d)_1] \div \left[\sum_{m} \sum_{d>100} [P(m,d)_1]\right] \qquad \text{Equation 3}$$

As written Equation 7 is in error. The specific error is that the term P > 100 $(m,d)_2$ in Equation 7 should be P> 100 $(m,d)_1$ as defined in Step 1, i.e., difference in subscript 2 in Step 3 versus subscript 1 in Step 1.

By the definition in Step 1, P > 100 $(m,d)_1$ refers to the probability of the fractional contribution of each magnitude and distance bin (beyond 100 km) to the total hazard for the average of 1 and 2.5 Hz, whereas P > 100 $(m,d)_2$ refers to of the fractional contribution of each magnitude and distance bin to the total hazard for the average of 5 and 10 Hz. Step 3 explicitly refers to mean magnitude and distance of the controlling earthquakes associated with the ground motions determined in Regulatory Guide 1.208, Appendix D, Step 2 for the average of 1 and 2.5 Hz.

The corrected equation provides for evaluating the mean distance of the controlling earthquake for distances of 100 km or greater for the average of 1 and 2.5 Hz (NRC, 2007a).

2.5.2.4.6 Updated EPRI Probabilistic Seismic Hazard Analysis Deaggregation, and 1 Hz, 2.5 Hz, and 10 Hz Spectral Accelerations Incorporating Significant Increases Based on the Above Sensitivity Studies

With the above assumptions on seismic sources (the original EPRI EST teams sources, plus the Charleston sources) and the substitution of the updated ground motion model and aleatory uncertainty model, the seismic hazard was recalculated for the CCNPP Unit 3. This calculation

was first made for hard rock conditions, and these results were then modified (as described below) to account for local site conditions.

The calculation of seismic hazard consists of calculating annual frequencies of exceeding different amplitudes of ground motion, for all combinations of seismic sources, seismicity parameters, maximum magnitudes, ground motion equations, and ground motion aleatory uncertainties. This calculation is made separately for each of the six EPRI EST teams and results in a family of seismic hazard curves. The alternative assumptions on seismic sources, seismicity parameters, maximum magnitudes, ground motion equations, and ground motion aleatory uncertainties are weighted, resulting in a combined weight associated with each hazard curve. From the family of hazard curves and their weights, the mean hazard (and the distribution of hazard) can be calculated.

Figure 2.5-95 through Figure 2.5-101 are plots of the resulting updated probabilistic seismic hazard hard rock curves for the seven spectral ordinates (100 Hz (equivalent to PGA), 25 Hz, 10 Hz, 5 Hz, 2.5 Hz, 1 Hz, and 0.5 Hz). The mean and fractile (15%, 50% (median), and 85%) hazard curves are indicated.

Figure 2.5-65 shows mean and median uniform hazard spectra for 10^{-4} and 10^{-5} annual frequencies of exceedance from these calculations at the seven structural frequencies at which ground motion equations are available. Numerical values of these spectra are documented in Table 2.5-24.

The seismic hazard was deaggregated for implementation of Regulatory Guide 1.208 (NRC, 2007a). That is, the contributions by earthquake magnitude and distance to hazard at the 10^{-4}, 10^{-5}, and 10^{-6} ground motions were determined for 1 Hz, 2.5 Hz, 5 Hz, and 10 Hz. The deaggregations for 1 Hz and 2.5 Hz were combined to produce a single mean low-frequency (LF) deaggregation, and the deaggregations for 5 Hz and 10 Hz were combined to produce a single mean high-frequency (HF) deaggregation. These deaggregations were done for ground motions corresponding to mean 10^{-4}, 10^{-5}, and 10^{-6} annual frequencies of exceedance. The resulting deaggregations by magnitude and distance are shown in Figure 2.5-66 through Figure 2.5-69, Figure 2.5-89, and Figure 2.5-90 for 10^{-4} (Figure 2.5-66 and Figure 2.5-67) 10^{-5} (Figure 2.5-68 and Figure 2.5-69) and 10^{-6} (Figure 2.5-89 and Figure 2.5-90). These figures also show the contribution by ground motion epsilon, which is the number of standard deviations that the 10^{-4}, 10^{-5}, or 10^{-6} (log) ground motion is above or below the median (log) ground motion. (This deaggregation is done in logarithmic space because ground motions are assumed to follow a lognormal distribution.) In Figure 2.5-66 through Figure 2.5-69, Figure 2.5-89, and Figure 2.5-90 earthquake magnitudes have been converted to the moment magnitude scale.

Figure 2.5-66 through Figure 2.5-69, Figure 2.5-89, and Figure 2.5-90 show that small, local earthquakes dominate the HF motion, but that a significant contribution to hazard (from 15 percent to 30 percent) occurs for LF motions from large, distant earthquakes in the Charleston SC region. Representative earthquake magnitudes and distances were developed for the 10^{-4} and 10^{-5} ground motions as these are used to develop the recommended ground motion response spectrum (GMRS).

A deviation was taken to the formulas presented in Regulatory Guide 1.208 (NRC, 2007a). Appendix D, Development of Seismic Hazard Information Base and Determination of Controlling Earthquakes for determination of the controlling earthquake for high frequencies (5-10 Hz). The procedure in Regulatory Guide 1.208 (NRC, 2007a), Appendix D specifies

averaging the high frequency contributions to hazard across the entire magnitude-distance bins matrix to determine the overall mean magnitude and mean distance of the controlling earthquake.

Use of this process leads to a less accurate description of the magnitudes and distances contributing most significantly to the high frequency hazard than the alternative adopted.

The alternative was to select the mean magnitude and mean distance contributing to the high frequency ground motion from the R < 100 km results only. Use of all distances in the calculation of mean magnitude and distance controlling earthquake values of **M** = 5.5 and R = 97 for the 10^{-4} event. It is clear from the total deaggregation results (see Figure 2.5-67 of the FSAR) that this is not the distance of the earthquake controlling high frequency motions. Use of the alternative method leads to the same mean magnitude but to the closer distance, **R**, of 35 km, in better agreement with the deaggregation results (again, as shown in the figure). The same method was followed for the 10^{-5} annual frequency of exceedance results.

This alternative process is acceptable as use of the procedure in Regulatory Guide 1.208 (NRC, 2007a), Appendix D would have resulted in a lesser representative controlling magnitude.

The deaggregation of seismic hazard at annual frequencies of exceedance of 10^{-4} and 10^{-5} was divided into two groups: those contributions for R < 62 mi) 100 km, and those contributions for R > 62 mi (100 km). Table 2.5-21 shows the mean magnitudes and distances for each group, as well as the mean magnitude and distance overall.

With these deggregations, the representative LF earthquake was selected using the R > 62 mi (100 km) mean magnitude and mean distance (the dark-shaded cells in Table 2.5-21). In order to accurately represent the magnitudes and distances contributing to the HF ground motion, the mean magnitude and mean distance was selected from the R <62 mi (100 km) results (the light-shaded cells in Table 2.5-21). The alternative, selecting the overall mean magnitude and mean distance to represent the HF earthquake, would have meant using **M** = 5.5 and R = 97 for the 10^{-4} HF event. From Figure 2.5-67 this has a lower contribution to hazard than the **M** = 5.5, R = 22mi (35 km) result from the R < 62 mi (100 km) results. This method of selecting mean magnitude and mean distance was followed for the 10^{-5} annual frequency of exceedance results as well.

As an example of how individual seismic sources contribute to mean seismic hazard, Figure 2.5-91 and Figure 2.5-92 show the mean seismic hazard by source for the Rondout team. This team is selected as an example because they have the simplest interpretation of seismic sources among all EPRI EST teams. For the Rondout team, the following sources were modeled:

- Source RND-29: central Virginia seismic zone
- Source RND-30: source in northern Virginia and central Maryland
- Source RND-31: source in eastern Pennsylvania, New Jersey, and southern New England
- Source RND-C01: background source for the eastern seaboard
- Sources Charleston: the UCSS source described above

These plots confirm the sensitivities described in the deaggregation plots. That is, local sources, particularly the central Virginia seismic zone, tend to dominate the hazard, particularly for high frequency ground motions (10 Hz). However, for low frequency ground motion (1 Hz) the Charleston source has an important contribution to hazard.

Figure 2.5-93 and Figure 2.5-94show the median seismic hazard by source for the Rondout team, for 10 Hz and 1 Hz, respectively. Qualitatively these plots show the same effects as the plots for mean seismic hazard (Figure 2.5-91 and Figure 2.5-92).

Figure 2.5-65 shows mean and median uniform hazard response spectra (UHRS) for the CCNPP Unit 3 site for rock conditions, accounting for all seismic sources in the analysis. Important factors affecting the analysis are the Charleston seismic source (as shown in Figure 2.5-66 through Figure 2.5-69, Figure 2.5-89, and Figure 2.5-90), the updated ground motions equations from EPRI TR-1009684 (EPRI, 2004) and the revised estimates of aleatory uncertainty provided by EPRI EPRI TR-1014381 (EPRI, 2006a).

2.5.2.5 Seismic Wave Transmission Characteristics of the Site

The uniform hazard spectra described in the preceding section are defined on hard rock (shear-wave velocity of 9200 ft/sec (2804 m/sec)), which is located more than 2500 ft (762 m) below the current ground surface at the CCNPP Unit 3 site. The seismic wave transmission effects of this thick soil column on hard rock ground motions are described in this section.

Section 2.5.2.5.1 is added as a supplement to the U.S. EPR FSAR.

2.5.2.5.1 Development of Site Amplification Functions

2.5.2.5.1.1 Methodology

The calculation of site amplification factors is performed in the following 4 steps:

1. Develop a base-case soil and rock column in which mean low-strain shear wave velocities and material damping values, and strain-dependencies of these properties, are estimated for relevant layers from the hard rock horizon to the surface. At the CCNPP Unit 3 site, hard rock (V_S = 9200 ft/sec (~2.8 km/sec) is at a depth of approximately 2600 ft (792 m).

2. Develop a probabilistic model that describes the uncertainties in the above properties, locations of layer boundaries, and correlation between these properties, and generate a set of 60 artificial "randomized" profiles.

3. Use the seismic hazard results at 10^{-4}, 10^{-5} and 10^{-6} annual frequencies of exceedance to generate smooth spectra, representing LF and HF earthquakes at the three annual frequencies, for input into dynamic response analysis.

4. Use an equivalent-linear site-response formulation together with Random Vibration Theory (RVT) to calculate the dynamic response of the site for each of the 60 artificial profiles, and calculate the mean and standard deviation of site response. This step is repeated for each of the six input motions (10^{-4}, 10^{-5}, and 10^{-6} annual frequencies, HF and LF smooth spectra).

   RVT methods characterize the input rock motion using its powerspectrumand duration instead of using time domain earthquake input motions. This spectrum is propagated through the soil to the surface using frequency domain transfer functions and computing peak ground accelerations, spectral accelerations,or

peak strains using extreme value statistics. The RVT analysis that was conducted accounted for the strain dependent soil properties in the same manner as time-history based methods.

These steps are described in the following subsections.

2.5.2.5.1.2 Base Case Soil/Rock CCNPP Unit 3 and Uncertainties

Development of a base case soil/rock column is described in detail in Section 2.5.4. Summaries of the low strain shear wave velocity, material damping, and strain-dependent properties of the base case materials are provided below in this section. These parameters are used in the site response analyses.

The geology at the CCNPP Unit 3 site consists of marine and fluvial deposits overlying bedrock. The approximately upper 400 ft (122 m) of the site soils was investigatedand characterized using test borings, cone penetration testing, test pits, geophysical methods, and RCTS tests. Information on subsurface conditions below this depth was assembled from available geologic information from various resources.

Natural Soils in the upper 400 ft (122 m) of the site can generally be divided into the following geotechnical strata:

- Stratum I: Terrace Sand
- Stratum IIa: Chesapeake Clay/Silt
- Stratum IIb: Chesapeake Cemented Sand
- Stratum IIc: Chesapeake Clay/Silt
- Stratum III: Nanjemoy Sand

Two borings, B-301 and B-401 provide the deepest site-specific soils information collected during the geotechnical investigation for the CCNPP Unit 3 site, and they were also used to obtain the deepest suspension P-S velocity logging profile at the site. The P-S measurements provide shear and compressional wave velocities and Poisson's ratios in soils at 1.6 ft (0.5 m) intervals to a depth of about 400 ft (122 m).

Various available geologic records were reviewed and communications were made with staff at the Maryland Geological Survey, the United States Geological Survey, the Triassic-Jurassic Study Group, Lamont-Doherty Earth Observatory, and Columbia University to develop estimates of subsurface soil properties below 400 ft (122 m) depth. Further details, including associated references, are presented in Subsection 2.5.1. Soils below 400 ft (122 m) consist of Coastal Plain sediments of Eocene, Paleocene, and Cretaceous eras, extending to an estimated depth of about 2555 ft (779 m) below the ground surface. These soils contain sequences of sand, silt, and clay. Given their geologic age, they are expected to be competent soils, consolidated to at least the weight of the overlying soils.

Several available geologic records were reviewed to estimate bedrock characteristics below the site. Various bedrock types occur in the CCNPP Unit 3 site region, including Triassic red beds, Jurassic diabase, granite, schist, and gneiss. However, only granitoid rocks (metamorphic gneiss, schist, or igneous granitic rocks) similar to those exposed in the Piedmont, could be

discerned as the potential regional rock underlying the CCNPP Unit 3 site. This rock type was assumed as the predominant rock type at the CCNPP Unit 3 site.

Two sonic profiles were found for wells in the area that penetrated the bedrock, one at Chester, Maryland (about 40 mi (64 km) north of the site) and another at Lexington Park, Maryland (about 10 mi (16 km) south of the site). These two profiles were digitized and converted to shear wave velocity, based on a range of assumed Poisson's ratios for soil and rock.

Unit weights for the soils beneath the site are in the range of about 115 to 120 pcf (pounds per cubic foot) (1842 kg/m^{3}to 1922 kg/m^3). The bedrock unit weight was assigned a value of 162 pcf (2595 kg/m^3).

Initially, generic EPRI curves from EPRI TR-102293 (EPRI, 1993) were adopted to describe the strain dependencies of shear modulus and damping for all subsurface soils. The EPRI "sand" curves cover a depth range up to 1,000 ft (305 m). Since soils at the CCNPP Unit 3 site extend beyond 1,000 feet (305 m), similar curves were extrapolated from the EPRI curves, extending beyond 1000 ft (305 m), to obtain data for deeper soils. EPRI curves for the upper 400 ft (122 m) of the site soils were based on available results from the site investigation as described in Section 2.5.4.2.5.9. Below 400 ft (122 m), a site-specific geologic profile was used as a basis for the soil profiles, including engineering judgment to arrive at the selected EPRI curves. The damping curves for soils were truncated at 15 percent for the initial site response analysis.

Bedrock was assumed to behave elastically with a damping ratio of 1 percent.

Subsequent dynamic laboratory RCTS test results were used to obtain site-specific data on shear modulus and damping characteristics of in situ soils in the upper 400 ft (122 m) and of the backfill material as detailed in Section 2.5.4. The site-specific RCTS-based shear modulus degradation and damping ratio curves were used for all final site amplification factor analysis. A subsurface soil profile extending only to the base of the nuclear island foundation, and including no backfill, was used for the calculation of the GMRS. For the development of FIRS in Section 3.7.1, the soil profile appropriate for any given structure was developed from the material properties described and discussed in Section 2.5.4.

2.5.2.5.1.3 Site Properties Representing Uncertainties and Correlations

To account for variations in shear-wave velocity across the site, 60 artificial profiles were generated using the stochastic model developed by Toro (Toro, 1996), with some modifications to account for conditions at the CCNPP Unit 3 site. These artificial profiles represent the soil column from the top of bedrock (with a bedrock shear-wave velocity of 9,200 ft/s (~2.8 km/sec) to the ground surface (or to the base of the nuclear island, for the soil column used in the calculation of the GMRS). This model uses as inputs the following quantities:

- The median shear-wave velocity profile, which is equal to the base-case soil and rock profiles described above.
- The standard deviation of ln(Vs) (the natural logarithm of the shear-wave velocity) as a function of depth, which is developed using available site and regional data (refer to Section 2.5.4).
- The correlation coefficient between ln(Vs) in adjacent layers, which is taken from generic studies.

- The probabilistic characterization of layer thickness as a function of depth, which is also taken from generic studies, and then modified to allow for sharp changes in the base-case velocity profile.

- The depth to bedrock, which is randomized to account for epistemic uncertainty in the bedrock-depth data described in Section 2.5.4.

- The median or best-estimate shear stiffness (G/G_{MAX}) and damping curves, which are based on site-specifc RCTS test in the upper 400 ft (122 m) of the profile (refer to Section 2.5.4).

- The uncertainty in the shear stiffness (G/G_{MAX}) and damping curves.

Figure 2.5-72 shows the median V_S value as a function of depth, and it also shows actual values obtained from boreholes B-301 and B-401 from the P-S velocity logging measurement, both as recorded and smoothed over a window of 9.8 ft (3 m). The bottom Figure in Figure 2.5-72 shows the logarithmic standard deviations calculated from the smoothed data, which were used to generate multiple profiles. Below 400 ft (122 m), data are available from two profiles from Chester and Lexington Park. The shear-wave velocities from these two profiles, and the logarithmic standard deviation computed from them, are shown in Figure 2.5-73.

Values for the standard deviation of $\ln(V_s)$ as a function of depth were developed using V_s data from site boreholes B-301 and B-401 (for the top 400 ft (122 m) of the profile), and from boreholes at Chester and Lexington Park (for greater depths). Refer to Section 2.5.4 for more details on these data.

This study uses the inter-layer correlation model from Toro for U.S. Geological Survey category "C" as documented in Toro. (Toro, 1996)

The probabilistic characterization of layer thickness consists of a function that describes the rate of layer boundaries as a function of depth. This study utilized a generic form of this function, taken from Toro (Toro, 1996), and then modified to allow for sharp changes in the adopted base-case velocity profile.

Section 2.5.4 indicates that the shear-wave velocity of 9,200 ft/s (~2.8 km/sec) (for bedrock) is estimated at a depth of approximately 2531 ft (771 m). This value is taken as the base case or median depth. This information on bedrock depth is based on boreholes located tens of miles away from the site where are discussed in Section 2.5.4. The uncertainty associated with depth to bedrock is characterized by a uniform distribution over the interval of 2531 ft (771 m), plus or minus 50 ft (15 m) (the latter number is one half the contouring interval used to estimate the depth to bedrock). Because bedrock occurs at a large depth, the specific details of modeling uncertainty in this depth are not critical to the calculation of site response.

Figure 2.5-74 illustrates the V_S profiles generated for profiles 1 through 10, using the median, logarithmic standard deviation, and correlation model described. These profiles include uncertainty in depth to bedrock. In total, 60 profiles were generated. Figure 2.5-75 compares the median of these 60 V_S profiles to the median V_S profile described in the previous section, indicating excellent agreement. ThisFigure also shows the ±1 standard deviation values of the 60 profiles, reflecting the standard deviations indicated in Figure 2.5-72 and Figure 2.5-73.

Median values of shear stiffness (G/G_{MAX}) and damping for each geologic unit are described in Section 2.5.4. Uncertainties in the properties for each curve-type are characterized using the values obtained by Costantino (Costantino, 1996). In addition, the correlation coefficient between the ln (G/G_{MAX}) and ln (damping) residuals is given a value of -0.75. Figure 2.5-76 and Figure 2.5-77 illustrate the shear stiffness and damping curves generated for one of the geologic units, the Chesapeake silt/clay that is present at the depth range from approximately 100 ft (30 m) to 280 ft (85 m).

This set of 60 profiles, consisting of V_S versus depth, depth to bedrock, stiffness, and damping, are used to calculate and quantify site response and its uncertainty, as described in the following sections.

2.5.2.5.1.4 Development of Low-Frequency and High-Frequency Smooth Spectra

In order to derive smooth spectra corresponding to the 10^{-4} and 10^{-5} amplitudes, the mean magnitudes and distances summarized in Table 2.5-21 were used in the following way. The magnitudes and distances were applied to spectral shape equations from NUREG/CR-6728 (NRC, 2001) to determine realistic spectral shapes for the four representative earthquakes (10^{-4} and 10^{-5}, HF and LF events) – see Figure 2.5-70 and Figure 2.5-71. The HF shapes were scaled to the Uniform Hazard Spectra mean values for 10^{-4} or 10^{-5}, as appropriate, from Table 2.5-24 for 5 Hz, 10 Hz, 25 Hz, and 100 Hz. The shapes were used to interpolate between these 4 structural frequencies. Below 5 Hz, the HF spectral shape was extrapolated from 5 Hz, without regard to Uniform Hazard Spectra amplitudes at lower frequencies. The LF shapes were scaled to the Uniform Hazard Spectra values for 10^{-4} or 10^{-5}, as appropriate, from Table 2.5-24 for 0.5 Hz, 1 Hz, and 2.5 Hz. Below 0.5 Hz the spectral shape was extrapolated from 0.5 Hz. Above 2.5 Hz the spectral shape was extrapolated from 2.5 Hz, without regard to Uniform Hazard Spectra amplitudes at higher frequencies.

Creation of smoothed 10^{-4} and 10^{-5} spectra in this way ensures that the HF spectra match the 10^{-4} and 10^{-5} Uniform Hazard Spectra values at high frequencies (5 Hz and above), and ensures that the LF spectra match the 10^{-4} and 10^{-5} Uniform Hazard Spectra values at low frequencies (2.5 Hz and below). In between calculated values, the spectra have smooth and realistic shapes that reflect the magnitudes and distances dominating the seismic hazard, as reflected in Table 2.5-21.

2.5.2.5.1.5 Site Response Analysis

The site response analysis performed for the CCNPP Unit 3 site used Random Vibration Theory (RVT). The application of RVT to site response has been described by Schneider (Schneider, 1991), Stepp (Stepp, 1991), Silva (Silva, 1997), and Rathje (Rathje, 2006), and a theoretical description of the method will not be presented here. Given a site-specific soil column and the above studies, the fundamental assumptions are as follows:

- The site response can be modeled using horizontal soil layers and a one-dimensional analysis.
- Vertically-propagating shear waves are the dominant contributor to site response.
- An equivalent-linear formulation of soil nonlinearity is appropriate for the characterization of site response.

These are the same assumptions that are implemented in the SHAKE program (Idriss, 1992) and that constitute standard practice for site-response calculations. In this respect, RVT and SHAKE are similar. Both use an iterative, frequency-domain equivalent-linear calculation to

determine site response, and the frequency-domain representation of wave propagation in the the layered medium is identical for both approaches. The difference is that RVT works with ground-motion power spectrum (and its relation to the response spectrum and other peak-response quantities), thus representing an ensemble of ground motions, while SHAKE works with individual time histories and their Fourier transforms, thus representing one specific ground motion. Starting from the same inputs (e.g. the site properties described in Section 2.5.2.5.1.3 and the same rock response spectrum), both procedures will lead to similar estimates of site response (see, for example, Rathje (Rathje, 2006)).

The RVT site-response analysis requires the estimation of an additional parameter, strong motion duration, which does not have a strong influence on the calculated site response. Strong motion durations of the rock motions are calculated from the mean magnitudes and distances of the controlling earthquakes as taken from the deaggregation results (see Table 2.5-21). Estimates of strong motion duration depend on crustal shear-wave velocity and seismic stress drop, Δσ, as follows:

$$T = \frac{1}{f_c} + 0.05R \qquad \text{Eq. 2.5.2-1}$$

where R is the distance of controlling earthquake and earthquake corner frequency f_c is defined as:

$$f_c = 4.9 \times 10^6 \beta \left(\frac{\Delta\sigma}{M_0}\right)^{1/3}$$

$$M_0 = 10^{(1.5\mathbf{M} + 16.05)}$$

where M_0 is the seismic moment and **M** is the moment magnitude of the controlling earthquake (Rathje, 2006). A value of 3.5 km/s was used for β and 120 bars for Δσ, reflecting eastern US conditions.

One parameter that is used by both the RVT method and SHAKE is the effective strain ratio. This parameter is estimated using the expression (**M**-1)/10 (Idriss, 1992), where **M** is the magnitude of the controlling earthquake taken from the deaggregation analysis. A value of 0.5, rather than 0.45, was used for the 10^{-4}, 10^{-5}, and 10^{-6} HF runs to remain within the 0.5 - 0.7 range found empirically by Kramer (Kramer, 1996). Values of 0.58, 0.59, and 0.61 derived from Idriss (Idriss, 1992) formula, were used for the 10^{-4}, 10^{-5}, and 10^{-6} LF runs. As is the case for strong motion duration, computed site response is not very sensitive to estimates of effective strain ratio.

The RVT method starts with the response spectrum of rock motion (for example, the 10^{-4} HF spectrum). It then generates a Fourier spectrum corresponding to that input response spectrum, using an estimate of strong motion duration (calculated as described above) as an additional input. This step is denoted as the Inverse RVT (or IRVT) step. An iterative procedure (similar to that in SHAKE) is then applied to calculate peak and effective shear strains in each layer using RVT, update the stiffness and damping in each layer using the calculated effective strains and the G/G_{max} and damping curves for the layer, and repeat the process until it

converges. The final (or strain-compatible) stiffness and damping are then used to calculate the strain-compatible site transfer function. This transfer function is then multipled by the Fourier spectrum of the input rock motion to obtain the Fourier spectrum of the motion at the top of the profile or at the desired elevation (for either outcrop or in-column conditions), from which response spectra are calculated using RVT.

This process is repeated multiple times, once for each artificial profile . For sixty site profiles, sixty response spectra are calculated, from which statistics of site response are obtained.

The above calculations are repeated multiple times, once for each input rock spectrum. Thus the site response is calculated separately for the 10^{-4} HF, 10^{-4} LF, 10^{-5} HF, 10^{-5} LF, 10^{-6} HF, and 10^{-6} LF spectra.

In comparison to the SHAKE approach, the RVT approach avoids the requirement of performing spectral matching on the input time histories to match an input rock spectrum, and avoids analyzing each individual time history with a site-response program.

The site amplification factor is defined as the surface response spectral amplitude at each frequency, computed using the set of profiles that do not contain the 41 feet of fill above the nuclear island, divided by the input rock spectral amplitude. Figure 2.5-78 shows the logarithmic mean and standard deviation of site amplification factor from the 60 profiles for the 10^{-4} HF input motion. As would be expected by the large depth of sediments at the site, amplifications are largest at low frequencies, and de-amplification occurs at high frequencies because of soil damping. The maximum strains in the soil column are low for this motion, and this is shown in Figure 2.5-79, which plots the maximum strains calculated for the 60 profiles versus depth. Maximum strains are generally less than 0.01 percent, with some profiles having strains in shallow layers up to 0.03 percent.

Figure 2.5-80 and Figure 2.5-81 show similar plots of amplification factors and maximum strains for the 10^{-4} LF motion. The results are similar to those for the HF motion, with the soil column generally exhibiting maximum strains less than 0.01 percent.

Figure 2.5-82 through Figure 2.5-85 show comparable plots of amplification factors and maximum strains for the 10^{-5} input motion, both HF and LF. For this higher motion, larger maximum strains are observed, but they are still generally less than 0.03 percent. A few profiles exhibit maximum strains of about 0.1 percent at shallow depths. These strains are within the range for which the equivalent linear site response formulation has been validated.

Table 2.5-23 documents the mean amplification factors for 10^{-4}, 10^{-5}, and 10^{-6} rock input motions, and for HF and LF spectra.}

2.5.2.6 Ground Motion Response Spectra

The U.S. EPR FSAR includes the following COL Item in Section 2.5.2.6:

> A COL applicant that references the U.S. EPR design certification will compare the final site-specific soil characteristics with the U.S. EPR design generic soil parameters and verify that the site-specific seismic characteristics are enveloped by the CSDRS (anchored at 0.3 g PGA) and the 10 generic soil profiles discussed in Section 2.5.2 and Section 3.7.1 and summarized in Table 3.7.1-6.

This COL Item is addressed as follows:

{This section and Section 3.7.1 describes the reconciliation of the site-specific soil characteristics and site-specific seismic characteristics for CCNPP Unit 3 and demonstrates that these parameters are enveloped by the Certified Seismic Design Response Spectra (CSDRS), anchored at 0.3 g PGA, and the 10 generic soil profiles used in the design of the U.S. EPR.

Table 5.0-1 of the U.S. EPR FSAR identifies shear wave velocity as a required parameter to be enveloped, defined as "Minimum shear wave velocity of 1000 feet per second (Low strain best estimate average value at bottom of basemat)."

Figure 2.5-102 compares the 10 generic soil profile cases used for the U.S. EPR and the average shear wave velocity profile that was adopted for the CCNPP site (shown in Figure 2.5-74 and Figure 2.5-75.

The CCNPP Unit 3 Average Profile shown in the Figure 2.5-102 is for soils below El. +44 ft (bottom of the basemat is zero in the figure). Soils such as Stratum I Terrace Sand will not be used for support of foundations of Category I structures. Therefore, shear wave velocity measurements in the CCNPP site soils above El. +44 ft. regardless of value, are excluded from this evaluation as they lie above the basemat. Results from the above Figure indicate that:

1. The CCNPP Unit 3 Average Profile is bounded by the 10 generic profiles used for the U.S. EPR.
2. The CCNPP Unit 3 Average Profile offers a shear wave velocity at the bottom of the basemat (approx. El. +44 ft (or depth = 0 in Figure 2.5-102)) of 1,450 ft/sec.
3. The minimum shear wave velocity from the CCNPP Unit 3 Average Profile is 1,130 ft/sec.
4. The characteristic shear wave velocity of the soil column (weighted with respect to the 344 ft soil column) is 1,510 ft/sec.

On the basis of the above, the idealized CCNPP Unit 3 site shear wave velocity profile is bounded by the 10 generic soil profiles used for the U.S. EPR and meets the minimum 1,000 ft/sec criterion identified in the U.S. EPR FSAR.

GMRS was conducted in accordance with the performance-based approach described in Regulatory Position 5 of Regulatory Guide 1.208 (NRC, 2007a).

The GMRS was developed starting from the 10^{-4} and 10^{-5} rock Uniform Hazard Spectra. At high frequencies, the appropriate (10^{-4} or 10^{-5}) HF mean amplification factor was applied to the 10^{-4} and 10^{-5} rock spectrum, to calculate site spectral amplitudes for 10^{-4} and 10^{-5} annual frequencies of exceedance. At low frequencies, a similar technique was used with the LF mean amplification factors. At intermediate frequencies the larger of the HF and LF site spectral amplitudes was used.

Figure 2.5-86 illustrates the resulting site spectra. At high frequencies the HF spectral amplitudes are always greater, and at low frequencies the LF spectral amplitudes are always greater. The two sets of spectral amplitudes cross at 2-3 Hz.

This procedure corresponds to Approach 2A in NUREG/CR-6728 (NRC, 2001) and NUREG/CR-6769 (NRC, 2002b), wherein the rock Uniform Hazard Spectra (for example, at 10^{-4}) is multiplied by a mean amplification factor at each frequency to estimate the 10^{-4} site Uniform Hazard Spectra. Note that the amplification factors plotted in Figure 2.5-78, Figure 2.5-80,

Figure 2.5-82, and Figure 2.5-84 are mean logarithmic amplification factors, which correspond approximately to the median. The amplification factors used to prepare Figure 2.5-86 are arithmetic mean amplification factors, which are slightly higher than the median.

The low-frequency character of the spectra in Figure 2.5-86 reflects the low-frequency amplification of the site, as shown in the amplification factors of Figure 2.5-78, Figure 2.5-80, Figure 2.5-82, and Figure 2.5-84. That is, there is a fundamental site resonance at about 0.22 Hz, with a dip in site response at about 0.4 Hz, and this dip occurs for all 60 of the site profiles that were used to characterize the site profile. As a result, there is a dip in the site spectra for 10^{-4} and 10^{-5} at 0.4 Hz that reflects the site characteristics.

The ASCE (ASCE, 2005) performance-based approach was used to derive a GMRS from the 10^{-4} and 10^{-5} site spectra. The spectrum is derived at each structural frequency as follows:

$$A_R = SA(10^{-5})/SA(10^{-4})$$

$$DF = 0.6\ A_R^{0.8}$$

$$GMRS = max(SA(10^{-4}) \times max(1.0, DF), 0.45 \times SA(10^{-5}))$$

The last term in the above equation was not published in this form in ASCE (ASCE, 2005) but is a supplemental modified form, as presented in NRC Regulatory Guide 1.208 (NRC, 2007a). The resulting horizontal spectrum is plotted in Figure 2.5-87. This spectrum has been smoothed slightly, particularly around 1.5 Hz, to remove slight bumps and dips in the spectrum resulting from the site amplification calculations that are not statistically significant. The average change in spectral amplitudes for the 5 frequencies that were smoothed was an increase of 1%, which is not significant.

A vertical spectrum was calculated by deriving vertical-to-horizontal (V:H) ratios and applying them to the horizontal spectrum. As background and for comparison purposes, V:H ratios were obtained by the following methods:

1. Rock V:H ratios for the central and eastern United States (CEUS) were calculated from NUREG-6728 (NRC, 2001), using the recommended ratios for PGA < 0.2g, which applies at this site (see Figure 2.5-88).

2. Soil V:H ratios for the western United States (WUS) were calculated from two publications (Abrahamson, 1997) (Campbell, 1997) that have equations estimating both horizontal and vertical motions on soil. Horizontal and vertical motions were predicted from these two references for M = 5.5 and R = 9 mi (15 km). M = 5.5 was selected because earthquakes around this magnitude dominate the high frequency motions, and R = 9 mi (15 km) was selected because this distance resulted in a horitontal PGA of approximately 0.1 g at the site, which is close to the PGA associated with the horizontal SSE. For each reference, the V:H ratio was formed, and the average ratio (average from the two references) was then calculated.

3. The WUS V/H ratios for soil were modified in an approximate way for CEUS conditions by shifting the frequency axis of the V:H ratios so that they more closely resemble what might be expected at a soil site. This shifted the WUS peak V/H ratio from about 15 Hz to about 45 Hz.

Figure 2.5-88 shows these three V:H ratios plotted vs. structural frequency. As a conservative choice, the envelope V/H ratio shown as a thick dashed line was selected because this envelops all three approaches. The recommended V:H ratio is 1.0 for frequencies greater than 25 Hz, 0.75 for frequencies less than 5 Hz, and is interpolated (log-linear) between 5 and 25 Hz. Figure 2.5-87 plots the resulting vertical spectrum, calculated in this manner from the horizontal spectrum. Table 2.5-22 lists the horizontal and vertical GMRS amplitudes.

2.5.2.7 Conclusions

This section is added as a supplement to the U.S. EPR FSAR.

Calvert Cliffs 3 Nuclear Project, LLC and UniStar Nuclear Operating Services, LLC used the seismic source and ground motion models published by the Electric Power Research Institute (EPRI) for the central and eastern United States (CEUS), Seismic Hazard Methodology for the Central and Eastern United States, (EPRI, 1986). As such, FSAR Section 2.5.2 focuses on those data developed since publication of this 1986 EPRI report. Regulatory Guide 1.165, Identification and Characterization of Seismic Sources and Determination of Safe Shutdown Earthquake Ground Motion, (NRC, 1997), indicates that applicants may use the seismic source interpretations developed by Lawrence Livermore National Laboratory (LLNL) in the "Eastern Seismic Hazard Characterization Update," published in 1993, or the EPRI document as inputs for a site-specific analysis.

Calvert Cliffs 3 Nuclear Project, LLC and UniStar Nuclear Operating Services, LLC also used the guidance of Regulatory Guide 1.208, A Performance–Based Approach to Define the Site-Specific Earthquake Ground Motion, (NRC, 2007a) to develop the Ground Motion Response Spectrum (GMRS).

Calvert Cliffs 3 Nuclear Project, LLC and UniStar Nuclear Operating Services, LLC has provided a characterization of the seismic sources surrounding the site, as required by 10 CFR 100.23. Calvert Cliffs 3 Nuclear Project, LLC and UniStar Nuclear Operating Services, LLC has adequately addressed the uncertainties inherent in the characterization of these seismic sources through a PSHA, and that this PSHA followed the guidance provided in Regulatory Guide 1.208 (NRC, 2007a).

The GMRS developed by UniStar Nuclear Operating Services, LLC uses the performance-based approach described in Regulatory Guide 1.208 (NRC, 2007a), adequately representing the regional and local seismic hazards and accurately includes the effects of the local CCNPP Unit 3 subsurface properties.

The performance-based approach outlined in Regulatory Guide 1.208 (NRC, 2007a) is an advancement over the solely hazard-based reference probability approach recommended in Regulatory Guide 1.165 (NRC, 1997) and it was used where appropriate in the determination of the GMRS. The performance-based approach uses not only the seismic hazard characterization of the site from the PSHA but also basic seismic fragility SSC modeling in order to obtain an SSE that directly targets a structural performance frequency value. Calvert Cliffs 3 Nuclear Project, LLC and UniStar Nuclear Operating Services, LLC conclude that the application for the CCNPP Unit 3 site is acceptable from a geologic and seismologic standpoint and meets the requirements of 10 CFR 100.23(d) (CFR, 2007). However, because the site specific SSE is smaller than the minimum Safe Shutdown Earthquake Ground Motion for design identified in paragraph (d)(1), a design SSE is developed in Section 3.7.1.

Deviations from the NRC guidance in Regulatory Guide 1.165 (NRC, 1997), Regulatory Guide 1.208 (NRC, 2007a), or review criteria in Standard Review Plan 2.5.2 (NRC, 2007b) have been identified and acceptable alternatives, including technical justification, have been provided.

2.5.2.8 References

This section is added as a supplement to the U.S. EPR FSAR.

Abrahamson, 1997. Empirical Response Spectral Attenuation Relations for Shallow Crustal Earthquakes. N. A. Abrahamson and W. J. Silva, Seismological Research Letter, Volume 68, Number 1, pp. 94-127, 1997.

Amick 1990a. Paleoliquefaction Investigations Along the Atlantic Seaboard With Emphasis on the Prehistoric Earthquake Chronology of Coastal South Carolina, D. Amick, unpublished Ph.D. dissertation, University of South Carolina, selected pages, 1990.

Amick, 1990b. Characteristics of Seismically Induced Liquefaction Sites and Features Located In the Vicinity of the 1886 Charleston, South Carolina Earthquake, D. Amick, G. Maurath, and R. Gelinas, Seismological Research Letter, Volume 61, Number 2, pp. 117-130, 1990.

ANSS, 2006. Advanced National Seismic System catalog, catalog-search2_pl_ search_090806.htm, obtained from the ANSS website on September 8, 2006. Website: http:// www.ncedc.org/anss/catalog-search.html, Date accessed: September 8, 2006.

ASCE, 2005. American Society of Civil Engineers, "Seismic Design Criteria for Structures, Systems, and Components in Nuclear Facilities," American Society for Civil Engineers/ Structural Engineering Institute, Report ASCE/SEI 43-05, 2005.

Atkinson, 1987. Stochastic prediction of ground motion and spectral response parameters at hard-rock sites in eastern North America, G. M. Atkinson and D. M. Boore, Seismological Society of America, Bulletin, Volume 77, Number 2, pp. 440-467, 1987.

Atkinson, 1995. Ground-Motion Relations for Eastern North America, G. M. Atkinson and D. M. Boore, Seismological Society of America, Bulletin, Volume 85, Number 1, pp 17-30, 1995.

Bakun, 2004. Magnitudes and Locations of the 1811-1812 New Madrid, Missouri, and the 1886 Charleston, South Carolina, Earthquakes, W. H. Bakun and M. G. Hopper, Seismological Society of America, Bulletin, Volume 94, Number 1, pp. 64-75, 2004

Bechtel, 2006. Update of Charleston Seismic Source and Integration with EPRI Source Models, Bechtel engineering study report 25144-006-V14-CY06-00006, revision 001002, September 8, 2006. S. C Lindvall and R. D. Hartleb. Release was provided by letter AR-07-0883, dated April 19, 2007 from Charles Pierce, Southern Company to Rod Krich, Constellation.

Behrendt, 1981. Cenozoic Faulting in the Vicinity of the Charleston, South Carolina, 1886 Earthquake: Geology, J. C. Behrendt, R. M. Hamilton, H. D. Ackermann, and V. J. Henry, Volume 9, Number 3, pp. 117-122, 1981.

Behrendt, 1983. Marine Multichannel Seismic-reflection Evidence for Cenozoic Faulting and Deep Crustal Structure Near Charleston, South Carolina, C. Behrendt, R. M. Hamilton, H. D. Ackermann, V. J. Henry, and K. C. Bayer, U. S. Geological Survey Professional Paper 1313-J, pp. J1-J29, 1983.

Behrendt, 1987. The Helena Banks Strike-slip (?) Fault Zone in the Charleston, South Carolina, Earthquake Area: Results From a Marine, High-resolution, Multichannel, Seismic-reflection Survey, J. C. Behrendt and A. Yuan, Geological Society of America, Bulletin, Volume 98, pp. 591-601, 1987.

Bollinger, 1977. Reinterpretation of the Intensity Data for the 1886 Charleston, South Carolina, Earthquake in Studies Related to the Charleston, South Carolina, Earthquake of 1886-A Preliminary Report, D. W. Rankin, edition, G. A. Bollinger, U. S. Geological Survey Professional Paper 1028, pp. 17-32, 1977.

Bollinger, 1985. An Analysis of Earthquake Focal Depths in the Southeastern U. S., G. A. Bollinger, M. C. Chapman, M. S. Sibol, and J. K. Costain, American Geophysical Union, Geophysical Research Letter, Volume 12, Number 11, pp. 785-788, 1985.

Bollinger, 1989. Magnitude recurrence relations for the Southeastern United States and its subdivisions, G. A. Bollinger, F. C. Davison Jr., M. S. Sibol, and J. B. Birch, Journal of Geophysical Research, Volume 94, Number B3, pp. 2857-2873, 1989.

Bollinger, 1991. Seismicity of the Southeastern United States; 1698-1986 in Neotectonics of North America, Decade Map Volume to Accompany the Neotectonic Maps, D. B. Slemmons, E. R. Engdahl, M. D. Zoback, and D. D. Blackwell G. A. Bollinger, A. C. Johnston, P. Talwani, L. T. Long, K. M. Shedlock, M. S. Sibol, and M. C. Chapman, pp. 291-308, 1991.

Campbell, 1997. Empirical near-source attenuation relationships for horizontal and vertical components of peak ground acceleration, peak ground velocity, and pseudo-absolute acceleration response spectra, K. W. Campbell, Seismological Society Of America, Seismological Research Letter, Volume 68, Number 1, pp. 154-179, 1997.

Canada, 2006. Canadian catalog is searchable through the on-line bulletin from the Natural Resources Canada, Earthquake Search, Website: http://earthquakescanada.nrcan.gc.ca/stnsdata/nedb/bull_e.php, Date accessed: September 13, 2006.

CFR, 2007. Geologic and Seismic Siting Factors, Title 10, Code of Federal Regulations, Part 100.23(d), 2007.

Chapman, 1994. Seismic Hazard Assessment for Virginia, M. C. Chapman and F. Krimgold, Virginia Tech Seismological Observatory, Department of Geological Sciences, February 1994.

Chapman, 2002. Seismic Hazard Mapping for Bridge and Highway Design in South Carolina, M. C. Chapman and P. Talwani, South Carolina Department of Transportation Report, 2002.

Cook, 1979. Thin-skinned Tectonics in the Crystalline Southern Appalachians: COCORP Seismic Reflection Profiling of the Blue Ridge and Piedmont, F. A. Cook, A. Albaugh, D. S., Brown, L. D., Kaufman, S., Oliver, J. E., Hatcher, R. D. Jr., Geology, Volume 7, pp. 563-567, 1979.

Cook, 1981. COCORP Seismic Profiling of the Appalachian Orogen Beneath the Coastal Plain of Georgia, F. A. Cook, L. D. Brown, S. Kaufman, J. E. Oliver, and T. A. Petersen, Geological Society of America Bulletin, Volume 92, Number 10, pp. 738-748, 1981.

Cornell, 1988. Temporal and Magnitude Dependence in Earthquake Recurrence Models, C. A. Cornell and S. R. Winterstein, Seismological Society of America, Bulletin, Volume 79, pp. 1522-1537, 1988.

Coruh, 1988. Seismogenic structures in the central Virginia seismic zone, C. Coruh, G. A. Bollinger, and J. K Costain, Geology, Volume 16, pp. 748-751, 1988.

Costantino, 1996. Recommendations for Uncertainty Estimates in Shear Modulus Reduction and Hysteretic Damping Relationships, C. J. Costantino, (1996). Published as an appendix in "Description and validation of the stochastic ground motion model," W.J. Silva, N. Abrahamson, G. Toro and C. Costantino. (1997). Report Submitted to Brookhaven National Laboratory, Associated Universities, Inc. Upton, New York 11973, Contract No. 770573.

Cramer, 2001. A Seismic Hazard Uncertainty Analysis for the New Madrid Seismic Zone, C. H. Cramer, Engineering Geology, Volume 62, pp. 251-266, 2001.

Crone, 2000. Data for Quaternary Faults, Liquefaction Features, and Possible Tectonic Features in the Central and Eastern United States, east of the Rocky Mountain front, U.S. Geological Survey Open-File Report 00-260, A. J. Crone and R. L. Wheeler, 2000.

Deere, 1966. Engineering Classification and Index Properties of Intact Rock, University of Illinois, Prepared for Air Force Weapons Laboratory, Technical Report No AFWL-TR-65-116, D. Deere and R. Miller, December, 1966.

Dominion, 2004a. Dominion Nuclear North Anna LLC, Docket No. 52-008, Response to 6/1/04 RAI 2.5.1-5, 2.5.1-6, 2.5.3-2, and 2.5.1-5, Letter No. 5, U.S. Nuclear Regulatory Commission, Serial No. 04-347, 2004.

Dominion, 2004b. Dominion Nuclear North Anna LLC, Docket No. 52-008, Response to 4/15/04 RAI 2.5.1-1 to 2.5.1-4, 2.5.2-2 to 2.5.2-4, and 2.5.3-1, Letter No. 3, U.S. Nuclear Regulatory Committee, Serial No. 04-270, 2004.

Dominion, 2005. Dominion North Anna LLC, Docket No. 52-008, North Anna Early Site Permit Application, Revision 5, Adams Accession No. ML052150253, July 2005.

Ellsworth, 1999. A Physically-Based Earthquake Recurrence Model for Estimation of Long-Term Earthquake Probabilities, W. L. Ellsworth, M. V. Matthews, R. M. Nadeau, S. P. Nishenko, P. A. Reasenberg, and R. W. Simpson, U.S. Geological Survey Open-File Report 99-522, 1999.

EPRI, 1986. Seismic Hazard Methodology for the Central and Eastern United States, Tectonic Interpretations, Electric Power Research Institute, Report NP-4726, Volumes 5–10, July 1986.

EPRI, 1988. Seismic Hazard Methodology for the Central and Eastern United States, Electric Power Research Institute, Report NP-4726-A, Revision 1, Volume 1, Part 2, 1988.

EPRI, 1989a. Probabilistic Seismic Hazard Evaluations at Nuclear Power Plant Sites in the Central and Eastern United States: Resolution of the Charleston Earthquake Issue, Electric Power Research Institute, Report NP-6395-D, 1989.

EPRI, 1989b. EQHAZARD Primer, Electric Power Research Institute, Report NP-6452-D, June 1989.

EPRI, 1992. The stable continental region earthquake database: in Methods for assessing maximum earthquakes in the central and eastern U.S., Electric Power Research Institute, Report RP-2556-12, 1992.

EPRI, 1993. Guidelines for Determining Design Basis Ground Motions, Volume 5: Quantification of Seismic Source Effects, Electric Power Research Institute, Report TR-102293, November 1993.

EPRI, 1994. The earthquakes of stable continental regions, Volume I: Assessment of Large Earthquake Potential, Electric Power Research Institute, Final Report TR-102261-V1, 1994.

EPRI, 2004. CEUS Ground Motion Project Final Report, Electric Power Research Institute, TR-1009684 2004, December 2004.

EPRI, 2006a. Program on Technology Innovation: Truncation of the Lognormal Distribution and Value of the Standard Deviation for Ground Motion Models in the Central and Eastern United States, Electric Power Research Institute, Report TR-1014381, August 2006.

EPRI, 2006b. Program on Technology Innovation: Truncation of the Lognormal Distribution and Value of the Standard Deviation for Ground Motion Models in the Central and Eastern United States, Electric Power Research Institute, Technical Update 1013105, February 2006.

Exelon, 2005. Letter dated October 31, 2005, T. Mundy, Exelon to NRC, Subject: Response Supplemental Draft Safety Evaluation Report (DSER) Item, page 16 of 112 and page 54 of 112, (Adams Accession Number ML053120131), 2005.

Fletcher, 1978. Seismic Trends and Travel-time Residuals in Eastern North America and Their Tectonic Implications, J. B. Flectcher, M. L. Sbar, and L. R. Sykes, Geological Society of America Bulletin, Volume 89, pp. 1656-1676, 1978.

Grant, 1994. Paleoseismic Evidence of Clustered Earthquakes on the San Andreas Fault in the Carrizo Plain, California, L. B. Grant, and K. Sieh, Journal of Geophysical Research, Volume 99, Number B4, pp. 6819-6841, 1994.

Idriss, 1992. SHAKE91: A computer program for conducting equivalent linear seismic response analyses of horizontally layered soil deposits, I. M. Idriss, and J. I Sun, Department of Civil and Environmental Engineering, Center for Geotechnical Modeling, University of California, Davis, Calif., 1992.

Johnston, 1985. Recurrence rates and probability estimates for the New Madrid seismic zone, A. C. Johnston and S. J. Nava, Journal of Geophysical Research, Volume 90, pp. 6737–6753, 1985.

Johnston, 1996. Seismic Moment Assessment of Earthquake in Stable Continental Regions – III. New Madrid 1811-1812, Charleston 1886 and Lisbon 1755, A. C. Johnston, Geophysical Journal International, Volume 126, pp. 314-344, 1996.

Kramer, 1996. Geotechnical Earthquake Engineering, S. L. Kramer, Prentice-Hall, 1996.

Marple, 1990. Field Investigations of the Woodstock Lineament, R. T. Marple and P. Talwani, Seismological Society of America, Seismological Research Letter, Volume 61, Number 3-4, p. 156, 1990.

Marple, 1993. Evidence For Possible Tectonic Upwarping Along The South Carolina Coastal Plain From An Examination Of River Morphology And Elevation Data, R. T. Marple and P. Talwani, Geology, Volume 21, pp. 651-654, 1993.

Marple, 2000. Evidence for a Buried Fault System in the Coastal Plain of the Carolinas and Virginia - Implications for Neotectonics in the Southeastern United Sates, R. T. Marple and P. Talwani, Geological Society of America Bulletin, Volume 112, Number 2., pp. 200-220, 2000.

Marple, 2004. P., Proposed Shenandoah Fault and East Coast-Stafford Fault System and Their Implications for Eastern U. S. Tectonics, R. T. Marple and P. Talwani, Southeastern Geology, Volume 43, Number 2, pp. 57-80, 2004.

Martin, 1994. G. W., Seismic Parameters from Liquefaction Evidence, J. R. Martin and G. W. Clough, Journal of Geotechnical Engineering, Volume 120, Number 8, pp. 1345-1361, 1994.

NIST, 2006. NIST/SEMATECH, e-Handbook of Statistical Methods, http://www.itl.nist.gov/div898/handbook/, accessed 11 January 2006, Chapter 1 downloaded in PDF form from http://www.itl.nist.gov/div898/handbook/toolaids/pff/1-eda.pdf.

NRC, 1986. Identification of a Northwest Trending Seismogenic Graben Near Charleston, South Carolina, NUREG/CR-4075, U.S. Nuclear Regulatory Commission 1986.

NRC, 1990. Paleoliquefaction Features Along the Atlantic Seaboard, NUREG/CR-5613, U. S. Nuclear Regulatory Commission, 1990

NRC, 1991. Generic Letter 88-20, Individual Plant Examinations of External Events (IPEEE) for Severe Accident Vulnerabilities, U. S. Nuclear Regulatory Commission, 1991.

NRC, 1997a. Identification and Characterization of Seismic Sources and Determination of Safe Shutdown Earthquake Ground Motion**,** Regulatory Guide 1.165, U. S. Nuclear Regulatory Commission, March 1997.

NRC, 1997b. Recommendations for Probabilistic Seismic Hazard Analysis: Guidance on Uncertainty and Use of Experts, Prepared by Senior Seismic Hazard Analysis Committee (SSHAC), NUREG/CR-6372, U. S. Nuclear Regulatory Commission, 1997.

NRC, 2001. Technical Basis for Revision of Regulatory Guidance on Design Ground Motions, Hazard- and Risk-Consistent Ground Motion Spectra Guidelines, NUREG/CR-6728, U. S. Nuclear Regulatory Commission, 2001.

NRC, 2002a. Guidance for Performing Probabilistic Seismic Hazard Analysis for a Nuclear Plant Site: Example Application to the Southeastern United States, NUREG/CR-6607, U. S. Nuclear Regulatory Commission, 2002.

NRC, 2002b. Technical Basis for Revision of Regulatory Guidance on Design Ground Motions: Development of Hazard- & Risk-Consistent Seismic Spectra for Two Sites, NUREG/CR-6769, U.S. Nuclear Regulatory Commission**,** 2002.

NRC, 2005. Safety Evaluation Report for an Early Site Permit (ESP) at the North Anna ESP Site, NUREG-1835, U. S. Nuclear Regulatory Commission, September 2005.

NRC, 2007a. A Performance-Based Approach to Define the Site-Specific Earthquake Ground Motion, U. S. Nuclear Regulatory Commission, Regulatory Guide 1.208, March 2007.

NRC, 2007b. Vibratory Ground Motion, Standard Review Plan, NUREG-0800, Section 2.5.2, Revision 4, U.S. Nuclear Regulatory Commission, March 2007.

NRC, 2007c. Combined License Applications For Nuclear Power Plants (LWR Edition), Regulatory Guide 1.206, U.S. Nuclear Regulatory Commission, March 2007.

Obermeier, 1989. Liquefaction evidence for Repeated Holocene Earthquakes in the Coastal Region of South Carolina, S. F. Obermeier, R. E. Weems, R. B. Jacobson, and G. S. Gohn, Annals of the New York Academy of Sciences, Volume 558, pp. 183-195, 1989.

Obermeier, 1998. Paleoliquefaction Evidence for Seismic Quiescence in Central Virginia During the Late and Middle Holocene Time (abs), S. F. Obermier and W. E. McNulty. Eos Transactions, American Geophysical Union, Volume 79, No. 17, p S342, 1998.

Ohio, 2006. Ohio Seismic Network catalog, "http://www.dnr.state.oh.us/OhioSeis, KEY TO COLUMN DATA.htm, Oh_eq_1950 to 1999.htm, and Oh_eq_2000_to_present.htm," Ohio Department of Natural Resources, September 8, 2006. Website: http://www.dnr.state.oh.us/OhioSeis.

Ramsey, 1995. Radiocarbon calibration and analysis of stratigraphy: the OxCal program, C. Bronk Ramsey, C., Radiocarbon, Volume 37, Number 2, pp. 425-430, 1995.

Ramsey, 2001. Development of the radiocarbon program OxCal: Radiocarbon, C. Bronk Ramsey, Volume 43, Number 2A, pp. 355-363, 2001.

Rathie, 2006. Site-Specific Validation of Random Vibration Theory Based Seismic Site Response Analysis, Journal of Geotechnical and Geoenvironmental Engineering, American Society of Civil Engineers, Volume 132, No. 7, G. M. Rathie, C. Ozbey, July, 2006.

Reger, 1994. Summary of the Howard County, Maryland, Earthquakes of 1993, Southeastern U.S. Seismic Network Bulletin No. 28, Appendix A., Website: http://www.geol.vt.edu/outreach/vtso/anonftp/catalog/bul28.list1, J. P. Reger, 1994.

Schneider, 1991. Estimation of Ground Motion at Close Distances Using the Band-Limited White Noise Model, Proceedings 4th International Conference on Seismic Zonation, Bol. 4, Earthquake Engineering Research Institute, J. F. Schneider, W. J. Silva, S. J. Chiou, and J. C. Stepp, Stanford, CA, pp 187-194, 1991.

Seeber, 1981. The 1886 Charleston, South Carolina earthquake and the Appalachian detachment, L. Seeber and J. G. Armbruster, Journal of Geophysical Research, Volume 86, Number B9, pp. 7874-7894, 1981.

Seeber, 1998. The 1994 Cacoosing Valley earthquakes near Reading, Pennsylvania: A shallow rupture triggered by quarry unloading, L. Seeber, J. G. Armbruster, W. Y. Kim, N. Barstow, C. Scharnberger, Journal of Geophysical Research, Volume 103, Number B10, pp. 24,505-24,521, 1998.

SEUSSN, 2006. South Eastern United States Seismic Network catalog, "susn2004cat.txt," Virginia Tech Seismic Observatory, September 8, 2006. Website: http://www.geol.vt.edu/outreach/vtso/.

Sieh, 1989. Precise Chronology of Earthquakes Produced by the San Andreas fault in Southern California, K. Sieh, M. Stuiver, and D. A. Brillinger, Journal of Geophysical Research, Volume 94, Number B1, pp. 603-623, 1989.

Silva, 1997. Description and validation of the stochastic ground motion model, Final report, Brookhaven National Laboratory, Contract No. 770573, W. J. Silva, N. Abrahamson, G. Toro, C. Costantino, Associated Universities, Inc., Upton, N.Y., 1997.

Smith, 1985. Preliminary interpretation of a detailed gravity survey in the Bowman and Charleston, S.C. Seismogenic zones: Abstracts with Programs, W. A. Smith and P. Talwani, Geological Society of America southeastern section, Volume 17, Number 2, p. 137, 1985.

SSA, 1968. Engineering Seismic Risk Analysis, Seismological Society of America, Bulletin, Volume 58, Number 5, pp. 1583-1606, C. A. Cornell, 1968.

SSA, 1981. Results of recent South Carolina seismological studies, Seismological Society of America, Bulletin, Volume 71, Number 6, pp. 1883-1902, A. C. Tarr, P. Talwani, S. Rhea, D. Carver, and D. Amick, 1981.

SSA, 1987. The 23 April 1984 Martic Earthquake and The Lancaster Seismic Zone In Eastern Pennsylvania, Bulletin of the Seismological Society of America, Vol. 77, No. 2, pp. 877-890, J. Armbruster and L. Seeber, 1987.

SSA, 1991. Criticism of Some Forecasts of the National Earthquake Evaluation Council, Seismological Society of America, Bulletin, Volume 81, Number 3, pp. 862-881, J. C. Savage, 1991.

SSA, 1993. Fault Plane Solutions and Relocations of Recent Earthquakes in Middleton Place-Summerville Seismic Zone near Charleston, South Carolina, Seismological Society of America, Bulletin, Volume 83, Number 5, pp. 1442-1466, S. Madabhushi and P. Talwani, 1993.

SSA, 1994. New Empirical Relationships Among Magnitude, Rupture Length, Rupture Width, Rupture Area, and Surface Displacement, Seismological Society of America, Bulletin, Volume 84, Number 4, pp. 974-1002, D. L. Wells and K. J Coppersmith, August 1994.

SSA, 1995. Seismic Hazards in Southern California: Probable earthquakes, 1994 to 2024, Bulletin of the Seismological Society of America, Volume 85, pp. 379-439, Working Group on California Earthquake Probabilities, 1995.

SSA, 2000. Paleoseismology of the Johnson Valley, Kickapoo, and Homestead Valley faults: clustering of earthquakes in the Eastern California shear zone, Seismological Society of America, Bulletin, Volume 90, Number 5, pp. 1200-1236, T. K. Rockwell, S. Lindvall, M. Herzberg, D. Murbach, T. Dawson, and G. Berger 2000.

SSA, 2002. A Brownian model for recurrent earthquakes, Seismological Society of America, Bulletin, Volume 92, pp. 2233-2250, M. V. Matthews, W. L. Ellsworth, and P. A. Reasenberg, 2002.

Stepp, 1991. Site response evaluations based upon generic soil profiles using random vibration methodology. Proceedings 4th International Conference on Seismic Zonation, Vol. 4, Earthquake Engineering Research Institute, J.C. Stepp, W. J. Silva, H.B. Seed, I. M. Idriss, R. McGuire, J. Schneider, Stanford, Calif., pp. 739-746, 1991.

Sykes, 1978. Intraplate Seismicity, Reactivation of Preexisting Zones of Weakness, Alkaline Magmatism, and Other Tectonism Postdating Continental Fragmentation, L. R. Sykes, Reviews of Geophysics, Volume 16, pp. 621-688, 1978.

Talwani, 1982. An internally consistent pattern of seismicity near Charleston, South Carolina, P. Talwani, Geology, Volume 10, pp. 655–658, 1982.

Talwani, 1999. Fault Geometry and Earthquakes in Continental Interiors, P. Talwani, Tectonophysics, Volume 305, pp. 371-379, 1999.

Talwani, 2000. Macroscopic Effects of the 1886 Charleston Earthquake, A Compendium of Field Trips of South Carolina Geology, P. Talwani, South Carolina Geological Survey, pp. 1-6, 2000.

Talwani, 2001. Recurrence Rates of Large Earthquakes in the South Carolina Coastal Plain Based on Paleoliquefaction Data, P. Talwani and W. T. Schaeffer, Journal of Geophysical Research, Volume 106, Number B4, pp. 6621-6642, 2001.

Talwani, 2004. Macroseismic effects of the 1886 Charleston earthquake, P. Talwani and M. Katunam, Carolina Geological Society field trip guidebook, p. 18, 2004.

Toro, 1996. Probabilistic Models of Site Velocity Profiles for Generic and Site-Specific Ground Motion Amplification Studies, G. R. Toro, Published as an appendix in W. J. Silva, N. Abrahamson, G. Toro and C. Costantino, (1997), Description and validation of the stochastic ground motion model, Report Submitted to Brookhaven National Laboratory, Associated Universities, Inc. Upton, New York 11973, Contract No. 770573, 1996.

Tuttle, 2001. The Use of Liquefaction Features in Paleoseismology: Lessons Learned in the New Madrid Seismic Zone, central United States, M. P. Tuttle, Journal of Seismology, Volume 5, pp. 361-380, 2001.

USGS, 1983a. Land multichannel seismic-reflection evidence for tectonic features near Charleston, South Carolina, Studies Related to the Charleston, South Carolina, Earthquake of 1886- Tectonics and Seismicity, U.S. Geologic Survey, Professional Paper 1313-I, pp. I1-I18, R. M. Hamilton, J.C. Behrendt, and H. D. Ackermann, 1983.

USGS, 1983b. Seismicity Near Charleston, South Carolina, March 1973 to December 1979 in Studies Related to the Charleston, South Carolina Earthquake of 1886: Tectonics and Seismicity, G. S. Gohn (ed.), U. S. Geological Survey, Professional Paper 1313, pp. R1-R17, A. C. Tarr and S. Rhea, 1983.

USGS, 1983c. Regenerate Faults of the Southeastern United States, in Studies Related to the Charleston, South Carolina, Earthquake of 1886: Tectonics and seismicity, Gohn, G. S. (ed.), C. M. Wentworth and M. Mergener-Keefer, US Geological Survey Professional Paper 1313, pp. S1-S20, 1983.

USGS, 1992. Specification of Source Zones, Recurrence Rates, Focal Depths, and Maximum Magnitudes for Earthquakes Affecting the Savannah River Site in South Carolina, U.S. Geological Survey, Bulletin 2017, G. A. Bollinger, 1992.

USGS, 1996. National seismic-hazard maps: documentation, U. S Geological Survey, Open-File Report 96-532, A. Frankel, T. Barnhard, D. Perkins, E. V. Leyendecker, N. Dickman, S. Hanson, and M. Hopper, 1996.

USGS, 1997. Geology of the Pringletown, Ridgeville, Summerville, and Summerville Northwest 7.5-minute quadrangles, Berkeley, Charleston, and Dorchester counties, South Carolina:

Miscellaneous Investigations Series, U. S. Geological Survey, R. E. Weems, E. M. Lemon, Jr. and M. S. Nelson, 1997.

USGS, 1998. Newly Recognized En Echelon Fall Lines in the Piedmont and Blue Ridge Provinces of North Carolina and Virginia, With a Discussion of Their Possible Ages and Origins, U.S. Geological Survey, Open-File Report 98-374, R. E. Weems, 1998.

USGS, 2002. Documentation for the 2002 Update of the National Seismic Hazard Maps, U.S. Geological Survey Open-File Report 02-420, A. D. Frankel, M. D. Petersen, C. S. Mueller, K. M Haller, R. L. Wheeler, E. V. Leyendecker, R. L. Wesson, S. C. Harmsen, C. H. Cramer, D. M. Perkins, and K. S. Rukstales, 2002.

USGS, 2003. Earthquake Probabilities in the San Francisco Bay region: 2002-2031, U. S. Geological Survey Open-File Report 03-2134, Working Group on California Earthquake Probabilities, 2003.

Weems, 2002. Structural and tectonic setting of the Charleston, South Carolina, region; evidence from the Tertiary stratigraphic record, R. E. Weems and W. C. Lewis, Geological Society of America, Bulletin, Volume 114, Number 1, pp. 24-42, 2002.

WGCEP, 1995. Working Group on California Earthquake Probabilities, Seismic Hazards in Southern California: Probable earthquakes, 1994 to 2024, Bulletin of the Seismological Society of America, Volume 85, pp. 379-439, 1995.

Wheeler, 1992. Geologic Implications of Earthquake Source Parameters in Central and Eastern North America, Seismological Research Letters, R. L. Wheeler, and A. C. Johnston Volume 63, No. 4, pp. 491–505, 1992.

Wheeler, 2005. Known or Suggested Quaternary Tectonic Faulting, Central and Eastern United States – New and Updated Assessments for 2005, U.S. Geological Survey, Open File Report 2005-1336, R. L. Wheeler, 2005.

Wheeler, 2006. Quaternary tectonic faulting in the Eastern United States, Engineering Geology, Volume 82, pp. 165-186, R. L. Wheeler, 2006.

2.5.3 Surface Faulting

The U.S. EPR FSAR includes the following COL Item in Section 2.5.3:

> A COL applicant that references the U.S. EPR design certification will investigate site-specific surface and subsurface geologic, seismic, geophysical, and geotechnical aspects within 25 miles around the site and evaluate any impact to the design. The COL applicant will demonstrate that no capable faults exist at the site in accordance with the requirements of 10 CFR 100.23 and 10 CFR 50, Appendix S. If non-capable surface faulting is present under foundations for safety-related structures, the COL applicant will demonstrate that the faults have no significant impact on the structural integrity of safety-related structures, systems or components.

This COL Item is addressed as follows:

{There is no potential for tectonic fault rupture and there are no capable tectonic sources within a 25 mi (40 km) radius of the CCNPP site. A capable tectonic source is a tectonic structure that can generate both vibratory ground motion and tectonic surface deformation, such as faulting or folding at or near the earth's surface in the present seismotectonic regime (NRC, 1997). The following sections provide the data, observations, and references to support this conclusion. Information contained in these sections was developed in accordance with RG 1.165 (NRC, 1997), and is intended to satisfy 10 CFR 100.23, "Geologic and Seismic Siting Criteria" (CFR, 2007a) and 10 CFR 50, Appendix S, "Earthquake Engineering Criteria for Nuclear Power Plants" (CFR 2007b).

Sections 2.5.3.1 through 2.5.3.9 are added as a supplement to the U.S. EPR FSAR.

2.5.3.1 Geological, Seismological, and Geophysical Investigations

The following investigations were performed to assess the potential for surface fault rupture at and within a 25 mi (40 km) radius of the CCNPP Unit 3 site (for a more complete description of the methodology, see Section 2.5.1.1.4.4):

- Compile and review existing geologic and seismologic data.
- Interpret aerial photography.
- Interpret satellite and LiDAR imagery.
- Field and aerial (inspection by plane) reconnaissance.
- Review of pre-EPRI and post-EPRI (1989) seismicity (e.g. earthquake catalog used in EPRI (1989) ended in 1983. Pre-EPRI catalog is 1500's through 1983; post-EPRI is 1983 through 2006).
- Discuss site area geology with researchers at the U.S. Geological Survey (USGS), Maryland Geological Survey (MGS), and academic institutions.

The geologic and geotechnical information available for the existing CCNPP Units 1 and 2 site, as well as the proposed CCNPP Unit 3 site, is contained in three principal sources:

1. Work performed for the existing CCNPP Units 1 and 2 and complementary structures (BGE, 1968) (Constellation, 2005); and geotechnical foundation studies for adjacent parking lots (BPC, 1981).
2. Published and unpublished geologic mapping performed primarily by the USGS and MGS.
3. Seismicity data compiled and analyzed in published journal articles and, more recently, as part of Section 2.5.2.

Existing information was supplemented by aerial and field reconnaissance within a 25 mi (40 km) radius of the site, and interpretation of aerial photography along all known faults within the 5 mi (8 km) radius of the site. In addition, Light Detection and Ranging (LiDAR) data acquired from surrounding counties (Charles County, St Mary's County and Calvert County), that covered all known faults within much of the approximately 25 mi (40 km) radius and the entire 5 mi (8 km) radius, was reviewed and interpreted with respect to published Quaternary geologic maps as shown in Figure 2.5-26. Satellite imagery (raster imagery) of the CCNPP site region also was acquired for review and interpretation. These field and office-based studies

were performed to verify, where possible, the existence of mapped bedrock faults in the CCNPP site area and to assess the presence or absence of geomorphic features suggestive of potential Quaternary fault activity along the mapped faults, or previously undetected faults. Features reviewed during the field reconnaissance and office-based analysis of aerial photography, satellite imagery, and LiDar data, were based on a compilation of existing regional geologic information, as well as discussions with experts at the USGS and MGS who have worked in the vicinity of the CCNPP site.

Field reconnaissance of the site and within a 25 mi (40 km) radius of the site was conducted by geologists in teams of two or more. Two field reconnaissance visits in late summer and autumn, 2006 focused on exposed portions of the Calvert Cliffs, other cliff exposures along the west shore of Chesapeake Bay, and roads traversing the site and a 5 mi (8 km) radius of the site. Key observations and discussion items were documented in field notebooks and photographs. A general summary of the key observations includes: 1) the nearly flat-lying Miocene Coastal Plain stratigraphy in the cliffs was generally well exposed and field descriptions matched published literature, 2) no faults were exposed in the Miocene Coastal Plain deposits along the cliffs, and 3) no liquifaction features were identified.

Aerial reconnaissance within a 25 mi (40 km) radius of the site was conducted by two geologists in a top-wing Cessna aircraft on January 3, 2007. The aerial reconnaissance investigated the geomorphology of the Chesapeake Bay area and targeted numerous previously mapped geologic features and potential seismic sources within a 200 mi (322 km) radius of the site (e.g., Mountain Run fault zone, Stafford fault system, Brandywine fault zone, Port Royal fault zone, and Skinkers Neck anticline). The flight crossed over the CCNPP site briefly but did not circle or approach the site closely in order to comply with restrictions imposed by the Federal Aviation Administration. Key observations and discussion items were documented in field notebooks and photographs. In general, the aerial reconnaissance coupled with interpretation of LiDAR data revealed no anomalous geomorphic features suggestive of Quanternary activity (e.g. tonal lineaments, fault scarps or deflected terrace back edges) along the surface-projection of the fault zones.

The investigations of regional and site physiographic provinces and geomorphic process, geologic history, and stratigraphy were conducted by Bechtel Power Corporation. The investigations of regional and site tectonics and structural geology were conducted by William Lettis and Associates.

2.5.3.1.1 Previous Site Investigations

Previous site investigations performed for the existing units are summarized in the CCNPP Units 1 and 2 Preliminary Safety Analysis Report (PSAR) (BGE, 1968) and Independent Spent Fuel Storage Installation (ISFSI) Safety Analysis Report (SAR) (CGG, 2005). As cited in the CCNPP Units 1 and 2 PSAR and ISFSI SAR, these previous investigations provide the following results documenting the absence of Quaternary faults at and within the area of the CCNPP Unit 3 site:

- Interpretation of air photos and topographic maps. This interpretation revealed no evidence of surface rupture, surface warping, or offset of geomorphic features indicative of active faulting.

- Interviews with personnel from government agencies and private organizations. These interviews concluded that no known faults are present beneath the existing CCNPP Units 1 and 2 or CCNPP Unit 3 site areas.

- Seismicity Analysis -This analysis showed that: no microseismic activity has occurred in the site area; the site is located in a region that has experienced only infrequent minor earthquake activity; the closest epicentral location is greater than 25 mi (40 km) away. No earthquake within 50 mi (80 km) of the CCNPP site has been large enough to cause significant damage since the region has been populated over the past approximately 300 years. Section 2.5.2 provides a full discussion on the seismicity analysis for the CCNPP site.

- Approximately 85 exploratory boreholes were drilled at the CCNPP Units 1 and 2 site area. Borehole data have provided evidence for the lateral continuity of strata across the existing CCNPP Units 1 and 2 site area and the inspection of soil samples has revealed no adverse effects indicative of geologically recent or active faulting.

- Field reconnaissance of limited surface outcrops at the site and along the western shore of Chesapeake Bay, coupled with geophysical surveys, provided evidence for no faulting at the CCNPP site.

At the time of the original studies for the PSAR (BGE, 1968), there were no published maps showing bedrock faults within a 5 mi (8 km) radius of the CCNPP site. The closest significant bedrock faults mapped prior to 1968 were faults located about 50 mi (80 km) west of the CCNPP site in the Piedmont Province (BGE, 1968). The Geologic Map of Maryland (MGS, 1968) shows no faults within a 25 mi (40 km) radius of the CCNPP site.

2.5.3.1.2 Regional and Local Geological Studies

Since the late 1960's, extensive mapping of the CCNPP site region within the Coastal Plain Province by the MGS (MGS, 1971) (MGS, 1994) (MGS, 2003a) (MGS, 2003b) (MGS, 2003c) (MGS, 1986) and by the USGS (USGS, 1989c) (USGS, 1989d) (USGS, 1979a) (USGS, 1986), (USGS, 1979b) (USGS, 1995) (USGS, 2000b) has been performed to improve the industry's knowledge of the Coastal Plain stratigraphy and geologic structure within the region. Coastal Plain mapping includes geologic cross sections across the CCNPP site area (USGS, 2003b) (USGS, 2003c) and a developed geologic cross Section based on mapping and borehole data (Achmad, 1997). In addition, closely-spaced shallow-penetration seismic-reflection profiles in the Chesapeake Bay provide limited below-water information on the Tertiary-Quaternary history of Chesapeake Bay (USGS, 1989a) (USGS, 1989b) (GSA, 1990), as well as limited information on the absence of Middle Miocene faulting. This compilation of previous mapping and exploration studies, coupled with site-specific reconnaissance for CCNPP Unit 3, provides the principal basis for the few, if any, bedrock faults recognized within the site area.

In addition, the USGS recently completed a compilation of all Quaternary faults, liquefaction features, and possible tectonic features in the eastern U.S. (USGS, 2000a) (USGS, 2005) (Wheeler, 2006). These compilations do not show any Quaternary faults or features within a 25 mi (40 km) or 5 mi (8 km) radius of the site as shown in Figure 2.5-31. The nearest potential Quaternary features (USGS, 2000a) (USGS, 2005) (Wheeler, 2006) are the Stafford fault 47 mi (76 km) west-southwest, and the Upper Marlboro faults 36 mi (58 km) to the northeast, respectively, of the CCNPP site as shown in Figure 2.5-31. Two documented paleo-liquefaction sites (Obermier, 1998) on the James and Rivanna Rivers within the Central Virginia seismic zone are both located over 25 mi (40 km) from the CCNPP site as shown in Figure 2.5-31.

Local geologic cross-sections oriented northwest-southeast within the site area (5 mi (8 km) radius) depict unfaulted southeast-dipping Eocene-Miocene Coastal Plain sediments that are unconformably overlain by Pliocene Upland deposits (MGS, 1994) (Achmad, 1997) (MGS, 2003b) (MGS, 2003c) as shown in Figure 2.5-13, Figure 2.5-32, and Figure 2.5-33. No faults or

folds are depicted on these geologic cross-sections. A review of a PSAR for a proposed nuclear power plant along the eastern shore of the Potomac River (e.g., Douglas Point), located 45 mi (72 km) west-southwest of the CCNPP site, also reported no faults or folds within a 5 mi (8 km) radius of the CCNPP site (PEPCO, 1973). Lastly, review of a seismic source characterization study (URS, 2000) for a liquefied natural gas plant at Cove Point, about 3 mi (4.8 km) southeast of the CCNPP site, also mentions no faults or folds present in the Cove Point area that could project toward the CCNPP site.

The most detailed subsurface exploration of the CCNPP site was performed by Dames and Moore as part of the original PSAR (BGE, 1968) for the CCNPP Units 1 and 2 foundation and supporting structures. This PSAR study included drilling 85 geotechnical boreholes, collecting down-hole geophysical data, and acquiring seismic refraction data across the site. As summarized in the PSAR (BGE, 1968), geologic cross sections were developed extending from Highway 2/4 northwest of the CCNPP site to Camp Conoy on the southeast, which provide valuable subsurface information on the lateral continuity of Miocene Coastal Plain sediments and Pliocene Upland deposits as shown in Figure 2.5-32, Figure 2.5-41, and Figure 2.5-42. Cross-sections C-C′ to D-D′ pre-date site development in the Conoy Landing area, and shadow the existing CCNPP Units 1 and 2 site and the proposed CCNPP Unit 3 site for structures trending north-northeast, parallel to the regional structural grain. These sections depict a nearly flat-lying, undeformed geologic contact between the Eocene Piney Point Formation and the overlying Middle Miocene Calvert Formation at about -200 ft (-61 m) msl as shown in Figure 2.5-41 and Figure 2.5-42.

Geologic cross-sections developed from geotechnical data collected from approximately 85 boreholes as part of the CCNPP Unit 3 study also provide additional detailed information for the upper approximately 400 ft (123 km) of strata on the presence or absence of structures directly beneath the footprint of the site. Similar to the previous cross sections prepared for the site, the new geologic borehole data support an interpretation of gently-dipping to flat-lying and unfaulted Miocene and Pliocene stratigraphy at the CCNPP site as shown in Figure 2.5-34, Figure 2.5-39 and Figure 2.5-43. Cross Section E-E′ prepared oblique to previously mapped northeast-trending structures (i.e., Hillville fault; inferred folds (USGS, 1995) (Kidwell, 1997) and postulated fault (Kidwell, 1997)) shows nearly flat-lying Miocene and Pliocene stratigraphy directly underling the CCNPP site as shown in Figure 2.5-39. Multiple key stratigraphic markers within the Chesapeake Group provide evidence for the absence of Miocene-Pliocene faulting and folding beneath the CCNPP site. Minor perturbations are present across the Miocene-Pliocene stratigraphic boundary, as well as other subunits within the Miocene Chesapeake Group. Although the stratigraphic contacts between the Calvert and Choptank Formations, as well as the Choptank and St. Marys Formation, cannot be readily delineated, there are several key lithologic contacts (i.e., cemented sand separated by uncemented sand layers) that exhibit flat-lying bedding and lateral continuity. The near-horizontal subunits provide evidence for the absence of surface-fault rupture beneath the CCNPP site as shown in Figure 2.5-39. A prominent geologic contact between the Piney Point and Calvert Formations, and Nanjemoy and Piney Point Formations, identified in exploratory boreholes B-303 and B-403 also provides evidence for a very low-gradient, nearly flat-lying Miocene deposit directly beneath the site as shown in Figure 2.5-39.

Geotechnical data collected directly to the south of the CCNPP site were compiled along sections E-E′ and E′-E″ and shown in Figure 2.5-39 and Figure 2.5-43. Although these geotechnical boreholes are limited in depth (from -325 ft to 37.5 ft (-99 to 11.4 m) msl), they provide additional evidence of the lateral continuity between the Pliocene Upland gravel deposits and Miocene St. Marys Formation, as well as a cemented sand unit in the upper part

of the St. Marys Formation. The nearly flat-lying and undisrupted nature of these shallow Miocene-Pliocene deposits are consistent with sections E-E′ and E′-E′′, and observations of the exposed Miocene and Pliocene strata along the western shore of Chesapeake Bay near the existing the CCNPP site as shown in Figure 2.5-44.

2.5.3.2 Geological Evidence, or Absence of Evidence, for Surface Deformation

As shown on Figure 2.5-32, only one inferred bedrock fault (i.e., Hillville fault) has been mapped at or near the 5 mi (8 km) radius of the CCNPP site (Hansen, 1978). In addition to the Hillville fault (Hansen, 1978), several other structures have been proposed within the 5 mi (8 km) radius of the site that have either shown in geologic cross-sections or published papers: (a) that two hypothesized east-facing monoclines are postulated beneath Chesapeake Bay (USGS, 1995) and (b) multiple stratigraphic undulations (inferred folds and warps) and a fault are postulated along the western margin of Chesapeake Bay (Kidwell, 1997). The Hillville fault (MGS, 1978) and inferred folds (USGS, 1995) (Kidwell, 1997) are described in Section 2.5.1 and below. None of these features are considered capable tectonic sources, as defined in Appendix A of Regulatory Guide 1.165 (NRC, 1997). Only the Hillville fault has been mapped within or near the 5 mi (8 km) radius of the CCNPP site, whereas the other features (USGS, 1995) (Kidwell, 1997) are only shown on cross sections as shown in Figure 2.5-25.

No deformation or geomorphic evidence indicative of potential Quaternary activity has been reported in the literature for the Hillville fault; whereas the features (USGS, 1995) (Kidwell, 1997) have been loosely inferred to have been active during the Quaternary. No evidence of Quaternary deformation along these inferred structures was identified during aerial and field reconnaissance, as well as during air photo and LiDAR interpretation undertaken for the CCNPP Unit 3 study. The Hillville fault is interpreted as a lithotectonic terrane boundary that coincides with the Sussex-Currioman Bay aeromagnetic anomaly (MGS, 1986), whereas the other postulated features have not been attributed to a known tectonic structure.

2.5.3.2.1 Hillville Fault Zone

The 26 mi (42 km) long Hillville fault (MGS, 1978) approaches to within 5 mi (8 km) of the CCNPP site as shown in Figure 2.5-11, Figure 2.5-26, and Figure 2.5-32. The fault consists of a northeast-striking zone of steep southeast-dipping reverse faults that coincide with the Sussex-Currioman Bay aeromagnetic anomaly (Hansen, 1986). The style and location of faulting are based on seismic reflection data collected about 9 mi (14.5 km) west-southwest of the CCNPP site. Seismic line St M-1 (location shown on Figure 2.5-26) imaged a narrow zone of discontinuities that vertically separate basement by as much as 250 ft (76 m) (MGS, 1978) as shown in Figure 2.5-32. It has been interpreted (MGS, 1986) that this offset is part of a larger lithotectonic terrane boundary that separates basement rocks associated with Triassic rift basins on the west from low-grade metamorphic basement on the east. The Hillville fault may represent a Paleozoic suture zone that was reactivated in the Mesozoic and Early Tertiary similar to the Brandywine fault system located to the west of the CCNPP site. Based on stratigraphic correlation (e.g., "pinchouts") between boreholes within Tertiary Coastal Plain deposits, it is speculated (MGS, 1986) that the Hillville fault was last active in the Early Paleocene. However, MGS (1986) concludes that the Upper Paleocene Aquia Formation and Miocene Calvert Formation provide evidence for the absence of deformation upsection. For example, a structure contour map of the top of the Eocene Piney Point-Nanjemoy Aquifer appears undeformed in the vicinity of the Hillville fault that likely reflects the absence of considerable faulting of this regionally extensive stratigraphic marker (Figure 2.5-14). Lastly, a geologic cross section prepared by Achmad and Hansen (Achmad, 1997) that intersects the Hillville fault shows no demonstrable offset across the contact between the Piney Point and Nanjemoy Formations (Figure 2.5-13).

Field and aerial (inspection by plane) reconnaissance, coupled with interpretation of aerial photography (review and inspection of features preserved in aerial photos) and LiDAR data shows that there are no geomorphic features indicative of potential Quaternary activity along the surface-projection of the Hillville fault zone. Multiple Quaternary fluvial terraces of the Patuxent and Potomac Rivers previously mapped (USGS, 1989c) (USGS, 1989d) (MGS, 1994) (MGS, 2003b) (MGS, 2003c) were evaluated for features suggestive of tectonic deformation using the LiDAR data as shown in Figure 2.5-26. Furthermore, where the Hillville fault would intersect the steep cliffs of Chesapeake Bay, there is direct observation of no faulting in the exposed Miocene strata. This is consistent with cross sections (Kidwell, 1997) (Achmad, 1997) (MGS, 2003b) (MGS, 2003c) that trend oblique to and across the northeast strike of the Hillville fault and do not show a fault as shown in Figure 2.5-13, Figure 2.5-30, and Figure 2.5-33. There is no pre-Electric Power Research Institute (EPRI) or post-EPRI (EPRI, 1986) study of seismicity spatially associated with this feature, or any geomorphic evidence of Quaternary deformation as shown in Figure 2.5-25. Abundant shallow seismic reflection data acquired and interpreted by Colman (1990) in Chesapeake Bay intersect the northeast projection of the Hillville fault (Figure 2.5-29). Colman (1990) makes no mention of encountering the Hillville fault in their interpretations of the seismic data. Thus, based on the absence of geomorphic expression, seismicity, and offset of Miocene to Quaternary surficial deposits, it is concluded that the Hillville fault is not a surface-fault rupture hazard at the CCNPP site.

2.5.3.2.2 East Facing Monoclines

Two speculative and poorly constrained east-facing monoclines along the western margin of Chesapeake Bay are depicted in geologic cross sections (USGS, 1995) within the 5 mi (8 km) radius of the CCNPP site. East-facing monoclines are inferred beneath Chesapeake Bay at about 2 and 10 mi (3.2 and 16 km) east and southeast, respectively, of the CCNPP site as shown in Figure 2.5-25. The east-facing monoclines (USGS, 1995) are not depicted on any geologic maps of the area but they are shown on geologic cross-sections (USGS, 1995) that trend northwest-southeast across the CCNPP site and south of the site near the Patuxent River. A partial representation of cross sections A-A' and E-E' is provided in Figure 2.5-40 (USGS, 1995). As mapped in cross Section and inferred in plan view, the monoclines align with the western shore of Chesapeake Bay and by association define a north-trending structure beneath the Chesapeake Bay. The monoclines exhibit a west-side up sense of motion that projects into the Miocene Choptank Formation (USGS, 1995). The monoclines are shown deforming the Lower Paleocene to Upper Miocene strata with approximately 60 to 300 ft (18 to 91 m) of structural relief. The overlying Late Miocene St. Marys Formation is not shown as warped. Boreholes used to construct the Section are widely spaced and do not provide good constraint on the existence and location of the postulated monoclines (cross sections A-A' and E-E') (USGS, 1995). Although no published geologic data are available to substantiate the existence of the monoclines, it is inferred (USGS, 1995) that the distinct elevation change (about 100 ft (30 m)) between Calvert Cliffs and the Delmarva Peninsula to the east, and the apparent linear nature of the Calvert Cliffs, to be tectonically controlled.

Existing published geologic, aeromagnetic, and gravity data provide evidence for the absence of a prominent north-trending monocline directly underlying Chesapeake Bay. Regional aeromagnetic and gravity maps show that the overall trend of potential structures buried beneath the Coastal Plain and Chesapeake Bay near the site trend northeast or subparallel to mapped faults and folds in the Piedmont Province to the west of the CCNPP site as shown in Figure 2.5-20, Figure 2.5-21, and Figure 2.5-22. A structural contour map of the top of the Middle Eocene Piney Point and Nanjemoy contact shows a northeast-striking undeformed contact across the Chesapeake Bay, consistent with regional bedding, yet inconsistent with a postulated more north-trending structure approximately parallel to the western margin of the

Chesapeake Bay as shown in Figure 2.5-14. Lastly, an east-west oriented cross-Section located about 30 mi (48 km) north of the CCNPP site also depicts nearly flat-lying Cretaceous and Paleocene stratigraphy across the Chesapeake Bay, and does not depict a fold or fault (MGS, 1978).

The change in physiographic elevation and geomorphic surfaces between the western and eastern shores of Chesapeake Bay can be explained by erosional processes directly related to the former course of the Susquehanna River, coupled with eustatic sea level fluctuations during the Quaternary (USGS, 1989a) (USGS, 1989b) (GSA, 1990) (USGS, 1979a) (USGS, 1979b). It is interpreted (GSA, 1990) by high resolution, shallow geophysical data to delineate several former river course(s) and provide geometrical constraints on the width and depth of the paleo-Susquehanna River between northern Chesapeake Bay and the southern Delmarva Peninsula as shown in Figure 2.5-29. Paleo-river profiles of the Eastville (150 ka) and Exmore (200 to 400 ka) Susquehanna paleochannels show no distinct elevation changes within the CCNPP site area and along projection features (USGS, 1995), as well as the Hillville fault (MGS, 1978). A submarine geologic map of Tertiary and Pleistocene deposits below the Chesapeake Bay at and near the CCNPP site developed from the shallow, high-resolution seismic reflection profiles has been developed (USGS, 1989a) (USGS, 1989b). No folds, warps or faults are depicted on these maps (USGS, 1989a) (USGS, 1989b) which encompass the hypothesized (USGS, 1995) east-facing monocline. Lastly, structure contour maps of the top of Tertiary deposits, developed from shallow seismic reflection data, show no geomorphic features that could be interpreted as fault or fold related (USGS, 1989b).

In summary, site and aerial reconnaissance, coupled with literature review, do not provide evidence for the existence of the hypothesized east-facing monocline (USGS, 1995). There also is no pre-EPRI or post-EPRI (EPRI, 1986) study of seismicity spatially associated with these features. If the feature does exist, the Miocene St. Marys Formation is not depicted (USGS, 1995) to be deformed. Therefore, the inferred monoclines (USGS, 1995) are older than Late Miocene in age and do not represent a surface-fault rupture or deformation hazard at the CCNPP site.

2.5.3.2.3 Stratigraphic Undulations and Hypothesized Fault

Multiple subtle folds or inflections and a postulated fault have been mapped (Kidwell, 1997) in cliff exposures of the Miocene Choptank and St. Marys Formations along the west side of Chesapeake Bay. Based on structural relations, such as an apparent decrease in warping up-section through the exposed Miocene section, it is suggested (Kidwell, 1997) that the postulated deformation may reflect growth faulting, or the presence of other tensional structures at depth. Over 300 lithostratigraphic columns along an approximately 25 mi (40 km) long stretch of Calvert Cliffs between Chesapeake Beach and Little Cove Point were prepared (Kidwell, 1988) (Kidwell, 1997) as shown in Figure 2.5-30. When these stratigraphic columns are compiled into a cross section, they provide an approximately 25 mi (40 km) long nearly continuous log of Miocene, Pliocene and Quaternary deposits exposed in the cliffs directly east of the CCNPP site as shown in Figure 2.5-30. A stratigraphic analysis (Kidwell, 1997) indicates that the Miocene Coastal Plain deposits strike northeast and dip 1 to 2 degrees to the south consistent with the findings of others (USGS, 1995) (MGS, 2003b) (MGS, 2003c). However, the very low regional southerly dip is disrupted occasionally by several subtle low amplitude and broad undulations developed within the Miocene Coastal Plain deposits. The stratigraphic undulations (represented at 150 times vertical exaggeration in Figure 2.5-30) are interpreted (Kidwell, 1997) as monoclines and asymmetrical anticlines. The undulatory stratigraphic contacts of the Miocene deposits often coincide with basal unconformities having wavelengths typically on the order of 2.5 to 5 mi (4 to 8 km) and amplitudes of 10 to

11 ft (3 to 3.4 m). South of the CCNPP site, near Little Cove Point, the stratigraphic undulations within the Miocene St. Marys Formation decrease in wavelength (approaching one mile) and amplitude (approximately 9 ft (2.7 m) or less). Based on stratigraphic truncations, the inferred warping also appears to decrease up-Section into the overlying upper Miocene St. Marys Formation near the CCNPP site. Any inferred folding of the overlying Pliocene and Quaternary fluvial strata is very poorly constrained or obscured, because of highly undulatory unconformities within these sand and gravel deposits.

About 1.2 mi (1.9 km) south of the CCNPP site, Kidwell (Kidwell, 1997) interprets an apparent 6 to 10 ft (1.8 to 3 m) elevation change in Miocene strata by extrapolating unit contacts across the approximately 0.6 mile wide (1 km) gap at Moran Landing (Figure 2.5-25 and Figure 2.5-30). Kidwell (Kidwell, 1997) also interprets a 3 to 12 (0.9 to 3.7 m) ft elevation change in younger (Quaternary (?)) fluvial material across this same gap. Because of the lack of cliff exposures at Moran Landing (only the valley margins), no direct observations of these elevation changes can be made. Kidwell (1997) explains the differences in elevation of the Miocene-Quaternary stratigraphy by hypothesizing the existence of a fault at Moran Landing that strikes northeast and accommodates a north-side down sense of separation. However, the postulated fault of Kidwell (Kidwell, 1997) is not shown on any of Kidwell's (Kidwell, 1997) cross-sections, or any published geologic map (e.g., Glaser, 2003b and 2003c). In addition, Hansen (1978) does not describe faulting in seismic reflection line St. M-2 that intersects the inferred southwest projection of the hypothesized Kidwell (1997) fault (Figure 2.5-27).

The observations of offset younger gravels do not provide any evidence for the existence of a fault because the surface on which the gravels are deposited is an erosional unconformity with extensive variable relief (Kidwell, 1997). Observations made during field reconnaissance, as part of the FSAR preparation, confirmed that this contact was an erosional unconformity with significant topography north and south of Moran Landing consistent with stratigraphic representations in Kidwell (1997) profiles. The observations of several feet of elevation change in the Miocene units over several thousands of feet of horizontal distance is at best weak evidence for faulting within the Miocene deposits. For example, subtle elevation variations in Miocene strata characterized along a near-continuous exposure south of Moran Landing contain similar vertical and lateral dimensions as to the inferred elevation change across Moran Landing; however, the features are interpreted as subtle warps and not faults by Kidwell (1997). On the basis of association with similar features to the south and the lack of a continuous exposure, there is little to no evidence to support a fault across Moran Landing.

Field and aerial (inspection by plane) reconnaissance, coupled with interpretation of aerial photography (review and inspection of features preserved in aerial photos) and LiDAR data, conducted for this investigation shows that there are no geomorphic features indicative of potential Quaternary activity along trend with the postulated folds and fault interpreted by Kidwell (Kidwell, 1997). LiDAR data was reviewed for the presence of northeast-striking lineaments in the region of Moran Landing and to the southeast between the Patuxent and Potomac Rivers as shown in Figure 2.5-26. No features suggestive of tectonic deformation were interpreted in the Pliocene (Upland deposits) or Quaternary fluvial surfaces (USGS, 1989c) (USGS, 1989d) (MGS, 2003b) (MGS, 2003c), some of which approach approximately 450 ka in age. There is no pre-EPRI or post-EPRI (EPRI, 1986) study seismicity spatially associated with the Kidwell (Kidwell, 1997) features, nor is there geomorphic evidence to strongly suggest that these features, including the postulated fault, pose a surface-fault rupture hazard at the CCNPP site. The hypothesized fault also is not aligned with any magnetic or gravity anomaly previously interpreted by others, suggesting that the apparent elevation change across Moran Landing is surficial in origin.

In summary, with the exception of Kidwell (Kidwell, 1997), numerous investigations of the Chesapeake Bay coastline by government researchers, stratigraphers, and consultants for Baltimore Gas and Electric have reported no visibly distinct signs of tectonic deformation within the exposed Miocene deposits near the CCNPP site as shown in Figure 2.5-44. Collectively, the majority of published and unpublished geologic information for the CCNPP site area, coupled with regional geologic sections (Achmad, 1997) (MGS, 2003b) (MGS, 2003c) and site and aerial reconnaissance, indicate the absence of Late Miocene and younger faulting and folding. A review of regional geologic sections and interpretation of LiDAR data suggest that the features, if present, are not prominent structures and do not appear to be developed within the Pliocene to Quaternary landscape. In summary, on the basis of regional and site data, there are no known faults within the site area, with the exception of the poorly constrained Hillville fault that lies along the western perimeter of the 5 mi (8 km) radius of the site. The Hillville fault has been documented as being last active in the Paleocene epoch (MGS, 1986).

2.5.3.3 Correlation of Earthquakes with Capable Tectonic Sources

No reported historical earthquake epicenters have been associated with bedrock faults within the 25 mi (40 km) radius of the CCNPP site vicinity as shown in Figure 2.5-25.

2.5.3.4 Ages of Most Recent Deformations

As presented in Section 2.5.3.2, the Hillville fault and postulated folds and faults within 5 mi (8 km) of the CCNPP site do not exhibit evidence of Quaternary activity. It is interpreted (MGS, 1978) that the Hillville fault formed during the Paleozoic Era as part of the regional Taconic orogeny, and locally may have been reactivated during the Paleozoic with the youngest deformation being Paleocene. Based on a review of available published geologic literature, field and aerial (inspection by plane) reconnaissance, and interpretation of aerial photography (review and inspection of features preserved in aerial photos) and LiDAR data, the postulated structures (USGS, 1995) (Kidwell, 1997), if they exist, are constrained to the Miocene and do not appear to affect Pliocene and Quaternary deposits.

2.5.3.5 Relationship of Tectonic Structures in the Site Area to Regional Tectonic Structures

Of the three features evaluated within the 5 mi (8 km) radius of the CCNPP site, only the Hillville fault has been linked with a regional tectonic structure. The Hillville fault zone delineates a possible Paleozoic suture zone reactive in the Mesozoic and Early Tertiary. Tectonic models hypothesize that the crystalline basement underlying the CCNPP site was accreted to a pre-Taconic North American margin in the Paleozoic along a suture that lies about 10 mi (16 km) west of the CCNPP site as shown in Figure 2.5-17 and Figure 2.5-23. The lithosphere plate-scale suture is defined by a distinct north-northeast-trending magnetic anomaly that dips easterly between 35 and 45 degrees and lies about 8 to 9 mi (12.9 to 14.5 km) beneath the CCNPP site (GSA, 1995) as shown in Figure 2.5-17. Directly west of the suture lies the north-to northeast-trending Taylorsville basin and to the east, the postulated Queen Anne Mesozoic rift basin as shown in Figure 2.5-10. The fault zone is interpreted as a lithotectonic terrane boundary that separates basement rocks associated with Triassic rift basins on the west from low-grade metamorphic basement on the east (i.e., Sussex Terrane/ Taconic suture (GSA, 1995); see Figure 2.5-17) (MGS, 1986). The apparent juxtaposition of the Hillville fault zone with the Sussex-Currioman Bay aeromagnetic anomaly suggests that the south flank of the Salisbury Embayment may be a zone of crustal instability that was reactivated during the Mesozoic and Tertiary. Cretaceous activity is inferred (MGS, 1978) and the fault extended up into the Cretaceous Potomac Group. The resolution of the geophysical data does not permit an interpretation for the upward projection of the fault into the younger

overlying Coastal Plain deposits. Stratigraphic correlations of Coastal Plain deposits from borehole data were used (MGS, 1978) to speculate that the Hillville fault may have been active during the Early Paleocene.

2.5.3.6 Characterization of Capable Tectonic Sources

Based on previous discussions in Section 2.5.3.4, there are no capable tectonic sources within 5 mi (8 km) of the CCNPP site.

2.5.3.7 Designation of Zones of Quaternary Deformation Requiring Detailed Fault Investigation

There are no zones of Quaternary deformation requiring detailed investigation within the CCNPP site area. A review and interpretation of aerial photography, digital elevation models, and LiDAR data of the site area, coupled with aerial reconnaissance, identified a few discontinuous north to northeast-striking lineaments. None of these lineaments are interpreted as fault-related, or coincident with the Hillville fault or the other previously inferred Miocene-Pliocene structures. Aerial and field reconnaissance of the western shoreline of Chesapeake Bay suggests that some of the lineaments along the western shoreline may be related to a weak to poorly developed, near-vertical, north to northeast-trending fracture or joint set. These fractures provide discontinuities by which large blocks of the St. Marys and Choptank Formations spall and form colluvial rubble at the base of the steep cliffs; however, these weak fractures do not represent a surface-fault rupture hazard at the site.

2.5.3.8 Potential for Tectonic or Non-Tectonic Deformation at the Site

The potential for tectonic deformation at the site is negligible. This is based on:

1. The nearly flat-lying Miocene stratigraphy beneath the site interpreted from both existing and new borehole data,

2. The absence of faulting in Miocene deposits exposed along the cliffs at the eastern boundary of the CCNPP site as shown in Figure 2.5-43,

3. The interpretation of aerial photography and LiDAR data.

Collectively, these data support the interpretation for the absence of any Quaternary surface faults or capable tectonic sources within the site area. In addition, there is no evidence of non-tectonic deformation at the site, such as glacially induced faulting, collapse structures, growth faults, salt migration, or volcanic intrusion.

2.5.3.9 References

Achmad, 1997. Hydrogeology, model simulation, and water-supply potential of the Aquia and Piney Point-Nanjemoy Aquifers in Calvert and St. Marys Counties, Maryland, G. Achmad and H. Hansen, 1997.

BPC, 1981. Subsurface Investigation and Foundation Report, North Parking Area, Calvert Cliffs Nuclear Power Plant, Lusby, Maryland, Bechtel Power Corporation, June 1981.

BGE, 1968. Preliminary Safety Analysis Report Calvert Cliffs Nuclear Power Plant Units 1 and 2, Volume 1, Docket 50-317 and 50-318, Baltimore Gas and Electric Company, 1968.

CFR, 2007a. Geologic and Seismic Siting Criteria, Title 10, Code of Federal Regulations, Part 100.23, 2007.

CFR, 2007b. Earthquake Engineering Criteria for Nuclear Power Plants, Title 10, Code of Federal Regulations, Part 50, Appendix S, 2007.

CEG, 2005. Calvert Cliffs Independent Spent Fuel Storage Installation, Updated Environmental Report, Volume 3, Revision 7, Constellation Energy, 2005.

EPRI, 1986. Seismic Hazard Methodology for the Central and Eastern United States: EPRI NP-4726, Electric Power Research Institute, 1986.

GSA, 1990. Ancient channels of the Susquehanna River beneath Chesapeake Bay and the Delmarva Peninsula, Geological Society of America Bulletin, Volume 102, p 1268-1279, S. Colman, J. Halka, C. Hobbs III, R. Mixon, D. Foster, 1990.

GSA, 1995. E-3 Southwestern Pennsylvania to Baltimore Canyon Trough, Geological Society of America Centennial Continent/Ocean Transect #19, L. Glover III and K. Klitgord, 1995.

Kidwell, 1988. Reciprocal Sedimentation and Noncorrelative Hiatuses in Marine-Paralic Siliciclastics: Miocene Outcrop Evidence, Geology, Volume 16, p 609-612, S. Kidwell, 1988.

Kidwell, 1997. Anatomy of Extremely Thin Marine Sequences Landward of a Passive-Margin Hinge Zone: Neogene Calvert Cliffs Succession, Journal of Sedimentary Research, Volume 67, Number 2, p 322-340, S. Kidwell,1997.

MGS, 1968. Geologic Map of Maryland, Scale 1:250,000, Department of Natural Resources, Maryland Geological Survey, E. Cleaves, J. Edwards Jr., and J. Glaser, 1968.

MGS, 1971. Geology and mineral resources of Southern Maryland, Report of Investigations Number 15, p 85, Maryland Geological Survey, J. Glaser, 1971.

MGS, 1978. Upper Cretaceous (Senonian) and Paleocene (Danian) Pinchouts on the South Flank of the Salisbury Embayment, Maryland and their relationship to antecedent basement structures, Report of Investigations Number 29, p 36, Department of Natural Resources, Maryland Geological Survey, H. Hansen, 1978.

MGS, 1986. The Lithology and Distribution of Pre-Cretaceous basement rocks beneath the Maryland Coastal Plain, Report of Investigations Number 44, p 27, Department of Natural Resources, Maryland Geological Survey, H. Hansen and J. Edwards Jr., 1986.

MGS, 1994. Geologic Map of Calvert County, Department of Natural Resources, Maryland Geological Survey, Scale 1:62,500, J. Glaser, 1994.

MGS, 2003a. Geologic Map of Prince George's County, Maryland, Maryland Geological Survey, Scale 1:62,500, J. Glaser, 2003a.

MGS, 2003b. Geologic Map of the Broomers Island Quadrangle, Calvert and St. Marys Counties, Maryland, Maryland Geological Survey, Scale 1: 24,000, J. Glaser, 2003.

MGS, 2003c. Geologic Map of the Cove Point Quadrangle, Calvert County, Maryland, Maryland Geological Survey, Scale 1:24,000, J. Glaser, 2003c.

NRC, 1997. Identification and Characterization of Seismic Sources and Determination of Safe Shutdown Earthquake Ground Motion, Regulatory Guide 1.165, U.S. Nuclear Regulatory Commission, March 1997.

Obermier, 1998. Paleoliquifaction Evidence for Seismic Quiescence in Central Virginia During the Late and Middle Holocene Time (abs), Eos Transactions of the American Geophysical Union, Volume 79, Number 17, p S342, S. Obermier and W. McNulty, 1998.

PEPCO, 1973. Preliminary Safety Analysis Report, Douglas Point Nuclear Generating Station, Units 1 and 2, Volume 2, Docket Number 50448-2 and 50449-2, Potomac Electric Power Company, 1973.

URS, 2000. Seismic Characterization Study for the Expansion of the Williams Gas Pipeline-Tranco LNG Facility, Cove Point, Maryland, URS Corporation, October 2000.

USGS, 1979a. Upper Cenozoic Deposits of the Central Delmarva Peninsula, Maryland and Delaware, U.S. Geological Survey, Professional Paper 1067-A, J. Owens and C. Denny, 1979.

USGS, 1979b. Upper Cenozoic Sediments of the Lower Delaware Valley and the Northern Delmarva Peninsula, New Jersey, Pennsylvania, Delaware, and Maryland, U.S. Geological Survey, Professional Paper 1067-D, J. Owens and J. Minard, 1979.

USGS, 1986. Geologic Map of Dorchester County, Maryland, U.S. Geological Survey, Scale 1:62,500, J. Owens and C. Denny, 1986.

USGS, 1989a. Quaternary Geology of the Southern Maryland Part of the Chesapeake Bay, U.S. Geological Survey, Miscellaneous Field Studies Map MF-1948-C, Scale 1:125,000, S. Colman and J. Halka, 1989.

USGS, 1989b. Quaternary Geology of the Northern Maryland part of the Chesapeake Bay, U.S. Geological Survey, Miscellaneous Field Studies Map MF-1948-B, Scale 1:125,000, S. Colman and J. Halka, 1989.

USGS, 1989c. Geologic Map of Charles County, Maryland, U.S. Geological Survey, Scale 1:62,500, L. McCartan, 1989.

USGS, 1989d. Geologic Map of St. Marys County, Maryland, U.S. Geological Survey, Scale 1:62,500, L. McCartan, 1989.

USGS, 1995. Geologic Map and Cross Sections of the Leonardtown 30 X 60 minute quadrangle, Maryland and Virginia, U.S. Geological Survey, L.McCartan, W. Newell, J. Owens, and G. Bradford, 1995.

USGS, 2000a. Data for Quaternary Faults, Liquefaction Features, and Possible Tectonic Features in the Central and Eastern United States, East of the Rocky Mountain Front, Open-File Report 00-260, U.S. Geological Survey, A. Crone and R. Wheeler, 2000.

USGS, 2000b. Geologic Map of the Fredericksburg 30' x 60' Quadrangle, Virginia and Maryland, Geologic Investigations Series Map I-2607, U.S. Geological Survey, R. Mixon, L. Pavlides, D. Powars, A. Froelich, R. Weems, J. Schindler, W. Newell, L. Edwards, L. Ward, 2000.

USGS, 2005. Known or Suggested Quaternary Tectonic Faulting, Central and Eastern United States – New and Updated Assessments for 2005, Open File Report 2005-1336, U.S. Geological Survey, R. Wheeler, 2005.

Wheeler, 2006. Quaternary tectonic faulting in the Eastern United States, Engineering Geology, Volume 82, p 165-186, R. Wheeler, 2006.}

2.5.4 Stability of Subsurface Materials and Foundations

The U.S. EPR FSAR includes the following COL Item for Section 2.5.4:

> A COL applicant that references the U.S. EPR design certification will present site-specific information about the properties and stability of soils and rocks that may affect the nuclear power plant facilities, under both static and dynamic conditions including the vibratory ground motions associated with the CSDRS and the site-specific SSE.

This COL Item is addressed as follows:

{This section addresses site-specific subsurface materials and foundation conditions. It was prepared based on the guidance in relevant sections of NRC Regulatory Guide 1.206, Combined License Applications for Nuclear Power Plants (LWR Edition) (USNRC, 2007a).

The CCNPP Units 1 and 2 Updated Final Safety Analysis Report (UFSAR) (BGE, 1982) contains a summary of the geotechnical information collected previously for the construction of CCNPP Units 1 and 2. The planned CCNPP Unit 3 is approximately 2,000 ft south of the existing units. CCNPP Units 1 and 2 UFSAR (BGE, 1982) contains mostly general information that is quantitatively limited in its extent and depth of exploration relative to the investigation performed for the CCNPP Unit 3. Therefore, comparison to CCNPP Units 1 and 2 is limited, but provided when relevant information is available. The information presented in this section is based on results of a site specific subsurface investigation program implemented at the CCNPP Unit 3 site, and evaluation of the collected data, unless indicated otherwise.

Geotechnical and geophysical site investigations have been completed in three stages as follows:

- **Phase I** – Performed in 2006, this is the initial investigation effort and is reported in the Geotechnical Subsurface Investigation Data Reports (Schnabel, 2007a) (Schnabel, 2007b). The investigation includes the boring program for the CCNPP Unit 3 and laboratory testing, including the Resonant Column Torsional Shear (RCTS) tests of the in-situ soils.
- **Phase II** – Performed in 2008, the second phase investigation incorporates the following items:
  - Drilling and sampling of 48 additional Standard Penetration Test (SPT) borings.
  - Installation and Development of 7 additional observation wells.
  - 11 Cone Penetration Tests (CPT) with shear wave velocity measurements.
  - Borehole geophysical including P-S suspension tests in the Intake Area.
  - Two pressuremeter tests.

Information from the Phase II investigation is presented in several geotechnical and laboratory testing data reports (Schnabel, 2009) (MACTEC, 2009a). The investigation incorporates information from additional borings and additional laboratory testing.

- **Phase III** – Performed in 2009, incorporating the following items:
  - Intake samples laboratory testing, including both static and dynamic RCTS tests.
  - Structural fill static testing, including chemical tests, triaxial tests, grain size tests, and Modified Proctor tests.
  - Structural fill dynamic testing (RCTS).

    Information from the Phase III investigation is presented in several geotechnical and laboratory testing data reports (MACTEC, 2009b) (MACTEC, 2009c) (MACTEC, 2009d).

The referenced geotechnical reports for the three phases of the investigation are provided in COLA Part 11J: Geotechnical Data Report and COLA Part 11K: Mactec Report.

The CCNNP3 Unit 3 site covers an area of approximately 460 acres. Figure 2.5-103 provides the site utilization plan. The following areas are identified:

1. Powerblock Area – Safety-related facilities in this area include the Reactor Building (RB), Fuel Building (FB) and Safeguard Buildings (Nuclear Island, NI), Essential Service Water Buildings (ESWB), and Emergency Power Generation Buildings (EPGB); other important facilities are the Nuclear Auxiliary Building (NAB), the Radioactive Waste Processing Building (RWPB), the Access Building (AB), and the Turbine Building (TB). The Powerblock Area is enlarged in Figure 2.5-104.
2. Intake Area – Safety-related facilities in this area include the Ultimate Heat Sink Makeup Water Intake Structure (UHS-MWIS) and the Forebay. Other facilities are the Circulating Water Makeup Intake Structure and the Fish Return. The Intake Area is enlarged in Figure 2.5-105.
3. Utility Corridor Area.
4. Construction Laydown Area (CLA).
5. Unit 3 Switchyard.
6. Unit 3 Cooling Basin and Cooling Tower.

The Powerblock, Construction Laydown Area, switchyard and cooling tower and basin are collectively referred to as the CCNPP Unit 3 Area.

The natural topography at the CCNPP site varies throughout the site with differences in elevation up to 100 ft. In the area where CCNPP Unit 3 is planned, ground surface elevations at the time of the exploration ranged from approximately El. 47 ft to El. 121 ft, with an average of 86 ft. The planned elevation (rough grade) in the Powerblock Area ranges from about El. 75 ft to El. 85 ft, with the centerline of Unit 3 at El. 84.7 ft, or approximately El. 85 ft.

In the Intake Area, ground surface elevations at the time of the exploration ranged from approximately El. 7 ft to 12 ft with an average of approximately 9.5 ft. The planned rough grade in the Intake Area is El. 10 ft.

The focus of Section 2.5.4 is the Powerblock Area and the Intake Area. These zones house the safety-related, Seismic-Category I facilities, with the Utility Corridor Area in between. Numerous natural and man-made slopes are identified across the plan. The safety of slopes is addressed in Section 2.5.5.

The subsurface conditions were established from the information contained in the Geotechnical Subsurface Investigation Data Reports from all Phases of the investigation (MACTEC, 2009a) (MACTEC, 2009b) (MACTEC, 2009c) (MACTEC, 2009d) (Schnabel, 2007a) (Schnabel, 2007b) (Schnabel, 2009). The maximum depth explored was about 400 ft beneath the ground surface at boring locations B-301 and B-401. The maximum depth explored by CPT soundings below the ground surface was 138.0 ft at C-302 and 152.4 ft at C-725 (CPT soundings encountered repeated refusal and, therefore, could not be consistently extended to greater depths). Field tests (borings, CPTs, etc.) identified as 300-series, e.g., B-301 or C-301, are located in the Powerblock Area. Tests identified as 400-series, e.g., B-401 or C-401, are located in an area adjacent to the CCNPP Powerblock Area, hereafter referred to as Construction Laydown Area (CLA). Field tests identified as 700 series, e.g., B-701 or C-701, are located outside of these two areas, and include the proposed cooling tower, switchyard, Utility Corridor, Intake Slope, and intake/discharge piping locations. Locations of various test areas are identified in Figure 2.5-103, Figure 2.5-104, and Figure 2.5-105. The major strata identified from the boring logs are described in detail in the next subsections.

References to elevation values in this subsection are based on the National Geodetic Vertical Datum of 1929 (NGVD29), unless stated otherwise.

2.5.4.1 Geologic Features

The CCNPP Unit 3 is located in the Atlantic Coastal Plain physiographic province. The soils in the site vicinity were formed by ancient rivers carrying large quantities of solids from the northern and western regions into the Atlantic Ocean. These deposits were placed under both freshwater (fluvial) and saltwater (marine) environments, and are about 2,500 ft thick at the site (BGE, 1982). The upper soils are Quaternary, Holocene- and/or Pleistocene-Age deposits formed as beaches or terraces. The lower soils are Miocene-, Eocene-, Paleocene-, and Cretaceous-Age deposits. The Miocene and Eocene soils belong to the Chesapeake and Nanjemoy groups. The Holocene, Pleistocene, Miocene, and Eocene soils were the subject of a detailed subsurface exploration for the COL investigation.

Detail narrative of the geologic features is provided in Section 2.5.1. Section 2.5.1.1 addresses the regional geologic settings, including regional physiography and geomorphology, regional geologic history, regional stratigraphy, regional tectonic and non-tectonic conditions, and geologic hazards, as well as maps, cross-sections, and references. Section 2.5.1.2 addresses the geologic conditions specific to the site, including site structural geology, site physiography and geomorphology, site geologic history, site stratigraphy and lithology, site structural geology, seismic conditions, and site geologic hazard evaluation, accompanied by figures, maps, and references.}

2.5.4.2 Properties of Subsurface Materials

The U.S. EPR FSAR includes the following COL Item in Section 2.5.4.2:

A COL applicant that references the U.S. EPR design certification will reconcile the site-specific soil properties with those used for design of U.S. EPR Seismic Category I structures and foundations described in Section 3.8.

This COL Item is addressed as follows:

{A comprehensive field investigation and associated laboratory testing has been performed for the CCNPP Unit 3 site. This subsection presents the properties of underlying materials encountered. It is divided into five subsections, as follows.

- Section 2.5.4.2.1 provides an introduction to the soil profile and subsurface conditions,
- Section 2.5.4.2.2 provides a description of the field investigation program, including borings, sampling, and in-situ tests,
- Section 2.5.4.2.3 provides a narrative on the origin of the engineered fill soils samples,
- Section 2.5.4.2.4 provides a description of the laboratory testing program,
- Section 2.5.4.2.5 provides the CCNPP Unit 3 soil properties for analysis and design of foundations.

The description of the field investigation and laboratory testing data incorporate information from all three phases of the investigation (Phase I, II, and III).

2.5.4.2.1 Description of Subsurface Materials

The site geology is comprised of deep Coastal Plain sediments underlain by bedrock, which is about 2,500 ft below the ground surface for CCNPP Units 1 and 2 UFSAR (BGE, 1982). The site soils consist of marine and fluvial deposits. The upper 400 ft of the site soils were the subject of the CCNPP Unit 3 subsurface investigation. In general, the soils at the site can be divided into the following stratigraphic units:

- ***Stratum I: Terrace Sand*** – light brown to brown sand with varying amounts of silt, clay, and/or gravel, sometimes with silt or clay interbedded layers.
- ***Stratum IIa: Chesapeake Clay/Silt*** – light to dark gray clay and/or silt, predominantly clay, with varying amounts of sand.
- ***Stratum IIb: Chesapeake Cemented Sand*** – interbedded layers of light to dark gray silty/clayey sands, sandy silts, and low to high plasticity clays, with varying amounts of shell fragments and with varying degrees of cementation. For the purposes of settlement analysis, Stratum IIb was further divided into three sub-layers. The investigation encountered variation of SPT values both in depth and horizontal distribution. The position of the sub layers beneath the Powerblock Area footprint is variable and this condition needs to be accounted for in a detailed three dimensional settlement analysis. Section 2.5.4.10 provides the details of the settlement model.
- ***Stratum IIc: Chesapeake Clay/Silt*** – gray to greenish gray clay/silt soils, they contain interbedded layers of sandy silt, silty sand, and cemented sands with varying amount of shell fragments.

- ***Stratum III: Nanjemoy Sand*** – primarily dark greenish-gray glauconitic sand with interbedded layers of silt, clay, and cemented sands with varying amounts of shell fragments and varying degrees of cementation.

Figure 2.5-106 provides an idealized soil column for the CCNPP Unit 3 site. The actual depth of layer interfaces varies throughout the site. This condition is revealed by the following subsurface profiles identified on Figure 2.5-103, Figure 2.5-104, and Figure 2.5-105:

Figure 2.5-107	Subsurface profile A-A' at the Powerblock looking east through the NI (local plant coordinates).
Figure 2.5-108	Subsurface profile B-B' at the Powerblock looking east through the EPGBs and NI.
Figure 2.5-109	Subsurface profile C-C' at the Powerblock looking south through the NI and TB.
Figure 2.5-110	Subsurface profile D-D' at the Powerblock looking south through 1EPBG, 3ESWB, and the RWPB.
Figure 2.5-111	Subsurface profile E-E' at the Powerblock looking east through the RWPB, NAB, NI (Safeguard North), 2ESWB and 1ESWB.
Figure 2.5-112	Subsurface profile F-F' at the Intake Area, looking east through the UHS-MWIS.

The recommendations for soil properties (Section 2.5.4.2.5) to be used for analysis and design of foundation are provided in tabular form for each layer identified. Table 2.5-25 presents the depths and thicknesses of the layers encountered at the site. The data is provided for the entire site and independently for the Powerblock Area and the Intake Area. Information on deeper soils (below 400 ft) was obtained from literature research and it is discussed in Section 2.5.4.2.5. Identification of Strata I through III was based on their physical and engineering characteristics. The characterization of the soils was based on a suite of tests performed on these soils, consisting of standard penetration tests (SPT) in soil borings including hammer energy measurements, cone penetration test (CPT) soundings, test pits, geophysical suspension P-S velocity logging, field electrical resistivity testing, and observation wells, as well as extensive laboratory testing.

2.5.4.2.1.1 Stratum I – Terrace Sand

The Terrace Sand stratum consists primarily of light-brown to brown sand with varying amounts of silt, clay, and/or gravel, sometimes with silt or clay interbeds. This stratum was fully penetrated by boreholes installed within CCNPP Unit 3 Powerblock Area and the adjoining CLA area (the 300 and 400 series borings) and by a majority of boreholes drilled outside of these two areas including the Intake Slope and the Utility Corridor (the 700 series borings). This stratum was not encountered in low lying areas.

The thickness of Stratum I soils was estimated from the boring logs and CPT logs. In CCNPP Unit 3 area, its thickness with respect to the existing ground surface is shown in Table 2.5-25. The average bottom for Stratum I soils is about El. 62 ft in CCNPP Unit 3 area. Stratum I Terrace Sand does not exist in the Intake Area.

At isolated locations, sandy soils with an appearance similar to Stratum I soils were encountered. Materials that were probably man-made, (hereafter referred to as "fill"), and disturbed soils were encountered, beginning at the existing ground surface at isolated locations at the CCNPP Unit 3 site. These materials were predominantly sand with varying

amounts of silt and clay. In the Intake Area (B-701, B-702, B-771 through B-776, B-780 through B-782, and B-821), the depth of these materials varied from approximately 6 to 11 ft below existing grade. They were present at the ground surface and were encountered in 25 borings (B-303, B-309, B-318, B-336, B-340, B-341, B-352, B-356, B-357, B-406, B-409, B-412, B-415, B-419, B-420, B-432, B-437, B-438/A, B-439, B-440, B-701, B-710, B-713, B-768, and B-791). Mainly, they were found in areas which had previously been developed at the site, such as Camp Conoy, roadways, and ball field areas. Their thickness ranged from approximately 0.5 ft to 17 ft, with an average thickness of about 6 ft.

Stratum I soils are characterized, on average, as non-plastic with an average fines content (materials passing No. 200 Sieve) of 20 percent. Grain size analyses indicated that these soils are primarily fine or fine-medium sands. The Unified Soil Classification System (USCS) designations were poorly-graded sand/silty sand, silty sand, well-graded sand, clayey sand, clay of high plasticity, silt, clay, and silt with high plasticity, with the predominant classifications of SP-SM and SM. The often plastic and fine-grained soil classifications are from the interbeds within this stratum.

2.5.4.2.1.2 Stratum IIa – Chesapeake Clay/Silt

The Chesapeake Clay/Silt was encountered at all locations except the Intake Area. When present, it was encountered beneath the Terrace Sand, except in low lying areas where Stratum I soils had been eroded. Stratum IIa typically consists of light to dark gray clay and/or silt, although it is predominately clay, with varying amounts of sand.

The thickness of Stratum IIa soils was estimated from the boring logs and CPT logs. The thickness of this stratum is presented in Table 2.5-25. Only data from borings that fully penetrated the layer were considered for determination of termination elevations.

The stratum IIa soils were characterized, on average, as medium-high plasticity clays. Their predominant USCS designation was clay of high plasticity and silt of high plasticity (CH and MH); sometimes with silty sand, silty sand to clayey sand, and organic clay. The organic designation was based on laboratory (liquid limit) tests. With less than 1 percent organic matter on average, and observations during sampling, these soils are not considered organic.

2.5.4.2.1.3 Stratum IIb – Chesapeake Cemented Sand

The Chesapeake Cemented Sand stratum was encountered beneath Stratum IIa in all the boreholes except at the Intake Area where it was encountered beneath fill. This stratum includes interbedded layers of light to dark gray silty/clayey sands, sandy silts, and low to high plasticity clays, with varying amounts of shell fragments and with varying degrees of cementation. The predominant soils, however, are sandy. The thickness and termination elevations of this layer are presented in Table 2.5-25. Only data from borings that fully penetrated the layer were considered for determination of termination elevations.

Layer IIb is further subdivided into three sub-layers, as shown by Figure 2.5-106. The layers are denominated Layer 1, Layer 2, and Layer 3. In general, Layer 1 is characterized by standard penetration test (SPT) N-values greater than 20, Layer 2 is characterized by SPT N-values less than 20, and Layer 3 is characterized by SPT N-values greater than 20. Additional information on SPT data is provided in Section 2.5.4.2.2.

Grain size analyses indicated that Stratum IIb soils are primarily medium-fine sands. The USCS designations were silty sand, poorly-graded sand to silty sand, clayey sand, silt, silt of high

plasticity, clay of high plasticity, clay, and organic clay. The predominant classifications, however, were silty sand, clayey sand, and poorly-graded sand to silty sand (SM, SC, and SP-SM). Three Phase I investigation samples were classified as organic clay or organic silt, although evidence of high organic content was not present during the field exploration. Organic content testing on three samples indicated an average organic content of 1.4 percent. Eleven Phase II samples from Intake Area borings were tested for organic content. The average organic content in the Intake Area was 1.5 percent. Despite the presence of organic matter in these samples, Stratum IIb soils are not considered organic soils since organic materials are virtually absent in these soils. The plastic and fine-grained soil classifications are generally from the clayey/silty interbeds within this stratum. For engineering analysis purposes, and given the predominance of granular proportions, Stratum IIb soils were characterized, on average, as sands with low plasticity, and with fines content of 25 percent.

2.5.4.2.1.4 Stratum IIc – Chesapeake Clay/Silt

Underlying the Stratum IIb sands, another Chesapeake Clay/Silt stratum was encountered, although distinctly different from the soils in Stratum IIa. This stratum was encountered in areas and in borings that were sufficiently deep to encounter these soils. Although primarily gray to greenish gray clay/silt soils, they contain interbedded layers of sandy silt, silty sand, and cemented sands with varying amounts of shell fragments. The greenish tone is the result of glauconite in these soils. Glauconite is a silicate mineral of greenish color with relatively high iron content (about 20 percent). Galuconite oxidizes on contact with air, producing a dark color tone. It is normally found as sand-size, dark green nodules. It can precipitate directly from marine waters or develop as a result of decaying of organic matter in animal shells or bottom-dwellers.

The thickness of Stratum IIc soils was estimated from the boring logs. Only two borings, B-301 and B-401, were sufficiently deep to completely penetrate this stratum. Based on borings B-301 and B-401, the thickness of this stratum is estimated as 190 ft. The stratum thickness and termination elevations of this Stratum are provided in Table 2.5-25.

For engineering analysis purposes, CCNPP Unit 3 Stratum IIc soils were characterized, on average, as high plasticity clay and silt, with an average PI = 50. Their predominant USCS designation was clay of high plasticity and silt of high plasticity (CH and MH), however, sometimes with silty sand, clay, and organic clay classifications indicated. Based on observations during sampling, the organic soil designation based on laboratory (Liquid Limit) testing is not representative of these soils, and therefore, they are not considered organic soils. The organic designation may be impacted by the glauconite content in the soils. Organic content testing was performed on 53 Stratum IIc soil samples (all areas). Results indicated organic contents ranging from 1.0 to 9.3 percent with an average of 3.3 percent. The measured values are indicative of the presence of slight organics in these soils.

2.5.4.2.1.5 Stratum III – Nanjemoy Sand

Underlying the Chesapeake Clay/Silt stratum are the Nanjemoy soils (Stratum III). Stratum III was encountered in deep borings B-301 and B-401. This stratum consists primarily of dark, greenish-gray glauconitic sand, however, it contains interbedded layers of silt, clay, and cemented sands with varying amounts of shell fragments and varying degrees of cementation. The glauconite in these soils could vary from less than 10 percent to as much as 50 percent.

The thickness of Stratum III soils cannot be estimated from the information obtained from the CCNPP Unit 3 subsurface investigation (boring logs B-301 and B-401), as these borings did not

penetrate these soils in their entirety, although they penetrated them by about 100 ft. It is estimated that the Nanjemoy soils are about 200 ft thick at the site (Hansen, 1996), consisting of primarily sandy soils in the upper 100 ft and clayey soils in the lower 100 ft. On this basis, the termination (bottom) of the upper sandy portion can be estimated at about El. -315 ft and the termination of the lower clayey portion can be estimated at about El. -415 ft. Information from borings B-301 and B-401 sufficiently characterizes the upper half of this geologic unit, as these borings were terminated at El. -308 ft and El. -329 ft, respectively.

For engineering analysis purposes, Stratum III soils were characterized, on average, as sand of high plasticity. Their predominant USCS designations were clayey sand and silty sand (SC and SM), although clay of high plasticity and silt of high plasticity were also indicated.

2.5.4.2.1.6 Subsurface Materials below 400 Feet

The field exploration for the CCNPP Unit 3 extended to a maximum depth of about 400 ft below ground. Coastal Plain sediments, however, are known to extend below this depth, to a depth of approximately 2,500 ft, or to top of bedrock (BGE, 1982). The subsurface conditions below 400 ft were addressed through reference to existing literature and work that had been done by others, primarily for the purpose of seismic site characterization. The subsurface conditions below 400 ft are addressed in Sections 2.5.2.5 and 2.5.4.2.5.

2.5.4.2.2 Field Investigation Program

The planning of the field investigation referred to the guidance provided in NRC Regulatory Guide 1.132, "Site Investigations for Foundations of Nuclear Power Plants" (USNRC, 2003a). References to the industry standards used for field tests completed for the CCNPP Unit 3 subsurface investigation are shown in Table 2.5-26. The details and results of the field investigation are included as COLA Part 11J. The work was performed under the Bechtel QA program with work procedures developed specifically for the CCNPP Unit 3 subsurface investigation, including a subsurface investigation plan developed by Bechtel. A complementary Phase II investigation was performed in 2008 as part of the detailed design of the project, with reference to guidance in Regulatory Guide 1.132 (USNRC, 2003a) to verify subsurface uniformity at locations where coverage was not available in the initial phase of the investigation due to shifting locations of some structures. Results of the additional (Phase II) investigation are presented herein, and in the data report (Schnabel, 2009) (MACTEC, 2009a). Locations of the field tests are shown in Figure 2.5-103, Figure 2.5-104, and Figure 2.5-105.

2.5.4.2.2.1 Previous Subsurface Investigations

Based on limited information available from the CCNPP Units 1 and 2 UFSAR (BGE, 1982), the original subsurface investigations for the CCNPP Units 1 and 2 performed in 1967 consisted of a total of 10 exploratory borings, ranging in depth from 146 to 332 ft, with soil samples obtained at various intervals for soil identification and testing. Seven piezometers were also installed for groundwater observation and monitoring. The 1967 investigation included other field investigations (two seismic survey lines using Microtremor) and laboratory testing (moisture content, density, particle size, permeability, cation exchange, and x-ray diffraction). Supplemental investigations in support of detailed design were performed in July 1967 (5 borings), August 1967 (23 borings), December 1968 (18 borings), and 1969 (5 borings). Additional investigations were performed in 1980/1981 (borings, CPT soundings, and observation wells) in order to site a "generic Category I structure," and in 1992 additional investigations (borings, dilatometer soundings, crosshole seismic survey, field resistivity) were performed for an additional Diesel Generator Building (Bechtel, 1992). Various laboratory testing was also performed on selected portions of the recovered soils.

Geological descriptions in CCNPP Units 1 and 2 UFSAR (BGE, 1982) indicate the surficial deposits to be Pleistocene Age soils extending from the ground surface to about El. 70 ft. These soils were estimated to extend to an average El. 60 ft based on the CCNPP subsurface investigation. CCNPP Units 1 and 2 UFSAR (BGE, 1982) indicates that Chesapeake Group soils were encountered in the 1967 investigation between El. 70 ft and El. -200 ft. These soils were estimated to extend to approximately El. -200 ft based on the CCNPP Unit 3 investigation. CCNPP Units 1 and 2 UFSAR (BGE, 1982) indicates that Eocene deposits lie below El. -200 ft and consist of glauconitic sands. Comparable observations were made on these, and the overlying deposits, from the CCNPP Unit 3 subsurface investigation borings. The CCNPP Units 1 and 2 UFSAR (BGE, 1982) remarked that "good correlation of subsurface stratigraphy was obtained between the borings." This remark is corroborated by the results obtained from the CCNPP subsurface investigation.

The CCNPP Unit 3 subsurface investigation involved a significantly larger quantity of testing than performed for the original CCNPP Units 1 and 2. Given the reasonably parallel geologic conditions between CCNPP Units 1 and 2 and the CCNPP Unit 3 site, and the greater intensity in exploration and testing at the CCNPP Unit 3 site which should result in enhanced characterization of the subsurface conditions, findings from previous investigations are not discussed further, unless a differing condition is reported from the previous investigations.

2.5.4.2.2.2 CCNPP Unit 3 Field Investigation

The subsurface investigation program was performed in accordance with the guidance outlined in Regulatory Guide 1.132 (USNRC, 2003a). Deviations are identified at point of use, alternatives and/or basis for deviation are provided. The fieldwork was performed under the contractors QA program and work procedures developed specifically for the CCNPP Unit 3 subsurface investigation.

Regulatory Guide 1.132 (USNRC, 2003a) provides guidance on spacing and depth of borings, sampling procedures, in-situ testing, geophysical investigations, etc. This guidance was used in preparing a technical specification, addressing the basis for the CCNPP Unit 3 subsurface investigation. The quantity of borings and CPTs for Seismic Category I structures was based on a minimum of one boring per structure and the one boring per 10,000-square ft criterion. The maximum depths of the borings for Seismic Category I structures were based on a foundation to overburden stress ratio criterion of 10 percent. The sampling intervals typically exceeded the guidance document by decreasing the sample spacing in the upper 15 ft and maintaining 5-ft sampling intervals at depths greater than 50 ft, except for the 400-ft borings. Continuous sampling was also performed, and is later described.

Regulatory Guide 1.132 (USNRC, 2003a) provides guidance in selecting the boring depth (dmax) based on a foundation to overburden stress ratio of 10 percent. Regulatory Guide 1.132 (USNRC, 2003a), also indicates that at least one-fourth of the principal borings should penetrate to a depth equal to dmax. Given the previously available knowledge of subsurface conditions as documented in the CCNPP Units 1 and 2 UFSAR (BGE, 1982) indicating stable, geologically old deposits at the site which would not adversely impact foundation stability, it was determined that one boring should be extended to about 400 ft, 4 borings extended to about 200 ft, and 4 borings extended to about 150 ft for the Common Basemat. (The consistency across the site of the Miocene-age Chesapeake Group clays and silts that exist below about 100 ft depth and the underlying Nanjemoy Formation sands that start at around 300 ft depth is aptly demonstrated by the similarity of the shear wave velocity profiles obtained in boreholes almost 1,000 ft apart. Also included were 3 CPT soundings. Borings associated with the Common Basemat extended at least 33 ft below the foundation level. An

additional (Phase II) field investigation was completed in 2008 (Schnabel, 2009) (MACTEC, 2009a) in conformance with guidance in Regulatory Guide 1.132.

The current quantity and locations of tests for the combined initial and Phase II investigations, are shown in Figure 2.5-103, Figure 2.5-104, and Figure 2.5-105. These provide the necessary coverage at the footprint structures, although several of the test locations required relocation during the field investigation to reduce cutting trees, and for accessibility for drilling equipment.

A team consisting of a geologist, a geotechnical engineer, and a member of UniStar project management performed a site reconnaissance prior to start of the field investigation. The focus of this task was to observe the site and access conditions, locations of borings and wells, and identify potential test relocation areas. Information on site geology and geotechnical conditions, used as a basis for developing the soils investigation plan for the CCNPP subsurface investigation was obtained from the information contained in the CCNPP Units 1 and 2 UFSAR (BGE, 1982).

Regulatory Guide 1.132, (USNRC, 2003a) provides that boreholes with depths greater than about 100 ft should be surveyed for deviation. In lieu of surveying for deviation in boreholes greater than 100 ft, deviation surveys were used in the 10 suspension P-S velocity logging boreholes to depths ranging from about 200 to 400 ft. The results indicated minimum, maximum, and average deviation of 0.6, 1.6, and 1.0 percent, respectively. The information collected the necessary data for proper characterization of the CCNPP Unit 3 subsurface materials.

Regulatory Guide 1.132, (USNRC, 2003a) provides guidance for color photographs of all cores to be taken soon after removal from the borehole to document the condition of the soils at the time of drilling. For soil samples, undisturbed samples are sealed in steel tubes, and cannot be photographed. SPT samples are disturbed, and by definition they do not resemble the condition of the material in-situ. Sample photography is a practice typically limited to rock core samples, not soils, therefore, it was not used for the initial investigation. However, it was used during the Phase II investigation. X-ray imaging was performed on tube samples selected for RCTS testing.

The Phase I CCNPP Unit 3 subsurface field exploration was performed from April through August 2006; the Phase II exploration was performed from May through December 2008. This work consisted of an extensive investigation to define the subsurface conditions at the project area. The scope of work and investigation methods was determined to be as follows:

- Surveying to establish the horizontal and vertical locations of exploration points.
- Evaluating the potential presence of underground utilities at exploration points.
- Drilling 200 test borings with SPT sampling and collecting in excess of 275 intact samples (using Shelby push tubes, Osterberg sampler, and Pitcher sampler) to a maximum depth of 403 ft, including 6 borings with continuous SPT samples (B-305, B-409, B-774, B-324, B-417, and B-775), with the first three borings being 150 ft deep each and the last three borings being 100 ft deep each. Note that "continuous sampling" was defined as one SPT sample for every 2.5-ft interval with a one ft distance between each SPT sample. In addition to the 6 continuous borings noted above, 13 borings were continuously sampled between El. 50 ft and El. -20 ft (B-342, B-343, B-344, B-345, B-347, B-348, B-352 through B-357, and B-357A).

- Installing and developing 47 groundwater observation wells to a maximum depth of 122 ft, including Slug testing in each well.
- Excavating 20 test pits to a maximum depth of 10 ft and collecting bulk soil samples.
- Performing 74 CPT soundings, including off-set soundings that required pre-drilling to overcome CPT refusal, to a maximum depth of 152 ft, as well as seismic CPT and 37 pore pressure dissipation measurements.
- Conducting 13 P-S Suspension Logging tests to measure dynamic properties.
- Conducting 2-dimensional field electrical resistivity testing along four arrays.
- Performing borehole geophysical logging, consisting of suspension P-S velocity logging, natural gamma, long- and short-term resistivity, spontaneous potential, 3-arm caliper, and directional survey in 13 boreholes.
- Two pressuremeter tests, one in the CCNPP Unit 3 Powerblock Area and another in the Intake Area.
- Two Dilatometer tests, one in the CCNPP Unit 3 Powerblock Area and another in the Intake Area.
- Conducting SPT hammer-rod combination energy measurements on drilling rigs.

Table 2.5-26 provides a summary of the number of field tests performed. The location of each exploration point was investigated for the presence of underground utilities prior to commencing exploration at that location. Locations of several exploration points had to be adjusted due to proximity to utilities, inaccessibility due to terrain conditions, or proximity to wetlands. Access had to be created to most exploration locations, via clearing roads and creating temporary roads, due to heavy brush and forestation. These areas were restored subsequent to completion of the field investigation.

An on-site storage facility for soil samples was established before the exploration program commenced. Each sample was logged into an inventory system. Samples removed from the facility were noted in the inventory logbook. A chain-of-custody form was also completed for all samples removed from the facility. Material storage handling was in accordance with ASTM D4220 (ASTM, 2000a).

Complete results of the investigation are in COLA Part 11J. Geophysical test results are discussed and summarized in Section 2.5.4.4. Further details pertaining to field activities related to borings, CPTs, Slug tests, geophysical surveys, and other activities are summarized below.

Borings, Standard Penetration Test and Sampling

Soils were sampled using the SPT sampler in accordance with ASTM D1586 (ASTM, 1999). The soils were sampled at continuous intervals (one sample every 2.5-ft) to 15 ft depth. Subsequent SPT sampling was performed at regular 5 ft intervals. At boring B-401, with a total depth of 401.5 ft, SPT sampling was performed at about 10 ft intervals below a depth of 300 ft. The recovered soil samples were visually described and classified by the engineer or geologist in accordance with ASTM D2488 (ASTM, 2006). A representative portion of the soil sample was

placed in a glass jar with a moisture-preserving lid. The sample jars were labeled, placed in boxes, and transported to the on-site storage facility.

Table 2.5-27 provides a summary of all test borings performed. The boring locations are shown in Figure 2.5-103, Figure 2.5-104, and Figure 2.5-105. The boring logs are included in COLA Part 11J. At boring completion, the boreholes were tremie-grouted using cement-bentonite grout.

Soil samples were collected from the borings via SPT and tube samples. Samples were collected more frequently in the upper portion of the borings than in the lower portion, e.g., typically 6 samples were obtained in the upper 15 ft. Thereafter, SPT samples were typically obtained at 5 ft intervals. SPT N-values were measured during the sampling and recorded on the boring logs. SPT N-values in Stratum I soils registered 0 blows/ft (SPT weight of hammer (WOH) or weight of rod (WOR)). The WOH and WOR values were very infrequent in Stratum I soils. A total of 5 WOH and WOR conditions were encountered in borings at CCNPP Unit 3 location, and a total of 5 were observed in all other borings. At the CCNPP Unit 3 location, three of these conditions were in boring B-309 in materials designated as "fill," which will be removed during construction. The fourth episode was in boring B-314 at the ground surface which will also be removed during construction. The fifth value was in boring B-322 at about El. 70 ft, at the location of the Essential Service Water System (ESWS) Cooling Tower. The cause of this low SPT value is likely due to sampling disturbance. A review of the boring logs and stratigraphic profiles for the same soils at other locations does not indicate this to be the predominant situation. Rather, the low SPT value is an isolated, infrequent situation, most likely caused by factors other than the natural condition of Stratum I soils. Nonetheless, these soils will be removed during excavation for the ESWS Cooling Tower to at least El. 60 ft. In conclusion, at the CCNPP Unit 3 location, the 5 WOH and WOR results are inconsequential to the stability of Stratum I soils.

The data clearly indicates the need to further subdivide Layer IIb into three sub-stratums. Figure 2.5-113 provides a graphic representation of the SPT distribution in the CCNPP Unit 3 Powerblock Area. Figure 2.5-114 provides equivalent information for the Intake Area. SPT data is summarized in Table 2.5-28. For the Powerblock Area, 177 out of 359 N-values are greater than 63 blows/ft, which is approximately 49 percent of the N-values reported. Out of these 177 values, 153 N-values are 100 blows/ft, which is difficult to clearly portray in scatter plots. The plot does not show clearly these 153 points at a N-value of 100 because the deeper layer overrides those points. Values for analysis and design are provided in Section 2.5.4.2.

Intact samples were obtained in accordance with ASTM D1587 (ASTM, 2000c) using the push Shelby tubes, Osterberg sampler, and rotary Pitcher sampler. Upon sample retrieval, the disturbed portions at both ends of the tube were removed, both ends were trimmed square to establish an effective seal, and pocket penetrometer (PP) tests were performed on the trimmed lower end of the samples. Both ends of the sample were then sealed with hot wax, covered with plastic caps, and sealed once again using electrician tape and wax. The tubes were labeled and transported to the on-site storage area. Table 2.5-29 provides a summary of undisturbed sampling performed during the subsurface investigation. A total of 375 sample retrievals were attempted. Intact samples are also identified on the boring logs included in COLA Part 11J.

Energy Measurements

Several drill rigs were used for the Phase I and II COL subsurface exploration. SPT hammer energies were measured for each of the drilling rigs used. Energy measurements were made in 10 borings (B-348, B-354, B-356, B-357, B-401, B-403, B-404, B-409, B-744, and B-791). Because

the SPT N-value used in correlations with engineering properties is the value corresponding to 60 percent hammer efficiency, the measured SPT N-values were adjusted in accordance with ASTM D6066 (ASTM, 2004b). A summary of the measured ETR values for each drill rig is shown in Table 2.5-30. The measured SPT N-values from each boring were adjusted using the appropriate ETR value also shown in Table 2.5-30 for the drill rig used.

The energy measurements were made on the hammer-rod system on drilling rigs used in the subsurface investigation. A Pile Driving Analyzer (PDA) was used to acquire and process the data. Energy measurements were made at sampling intervals of 15 ft, with the total number of measurements made per boring ranging from 6 (at boring B-744) to 26 (at boring B-401), depending on boring depth. Energy transfer to the gage locations was estimated using the Case Method, in accordance with ASTM D4633 (ASTM, 2005a). The resultant energy transfer efficiency measurements ranged from 78 to 90 percent, with an average energy transfer efficiency of 84 percent. Detailed results are presented in COLA Part 11J.

Cone Penetration Testing

CPT soundings were performed using an electronic seismic piezocone compression model, with a 15 cm^2 tip area and a 225 cm^2 friction sleeve area. CPT soundings were performed in accordance with ASTM D5778 (ASTM, 2000b), except that tolerances for wear of the cone tip were in accordance with report SGF 1:93E, Recommended Standard for Cone Penetration Tests, (SGS, 1993) which are comparable to ASTM. For the 10-cm^2 base cone, the ASTM D5778 (ASTM, 2005b) specified dimensions for "base diameter," "cone height," and "extension" are a minimum of 34.7 mm, 24 mm, and 2 mm, respectively, compared to the report SGF 1:93E (SGS, 1993) which recommended tolerances of a minimum of 34.8 mm, 24 mm, and 2 mm, for the same cone. The 2-mm SGF Report (SGS, 1993) value accounts for a constant 5-mm porous filter. Pore pressures were measured in the soundings. The equipment was mounted on a track-operated rig dedicated only to the CPT work. Cone tip resistance, sleeve friction, and dynamic pore pressure were recorded every 5 cm (approximately every 2 in) as the cone was advanced into the ground. Seismic shear wave velocity tests were also performed using a geophone mounted in the cone, a digital oscilloscope, and a beam, which was struck on the ground surface with a sledge hammer. Pore pressure dissipation data were also obtained, with the data recorded at 5-sec intervals.

A total of 74 CPT soundings were performed, including additional off-set soundings due to persistent refusal in dense/hard or cemented soils. At selected sounding locations, the soils causing refusal were pre-augered so that deeper CPT penetration could be obtained at the sounding location. Pre-augering was performed at several locations, and often several times at the same sounding. The sounding depths ranged from about 12 ft to 152 ft. Seismic CPT was performed at eight sounding locations. Pore pressure dissipation tests were performed, with 37 results at various depths. Table 2.5-31 provides a summary of CPT locations. The locations are shown in Figure 2.5-103, Figure 2.5-104, and Figure 2.5-105. The CPT logs, shear wave velocity, and pore pressure dissipation results are contained in COLA Part 11J.

The cone tip resistance, qc, in the Stratum I soils ranged from about 2 to 570 tons per square ft (tsf), with an average of about 120 tsf. The results indicate the qc values in Stratum I soils to be typically limited to about 200 tsf, with values peaking much higher between elevation 80 ft to elevation 90 ft. The CPT results also indicate the presence of clay zones within this stratum, at about elevation 115 ft, elevation 100 ft, and elevation 90 ft. Estimated relative density from CPT data ranges from about 30 to near 95 percent, with an average of about 75 percent. Stratum I Terrace Sand was not encountered in CPTs in the Intake Area. In the Utility Corridor it was present at higher elevations.

For Stratum IIa soils, the cone tip resistance values ranged from about 10 to 200 tsf, with an average value of about 50 tsf. Stratum IIa Chesapeake Clay/Silt was not encountered in the Intake Area. The results also indicate a mild increase in tip resistance with depth.

CPT soundings were attempted in Stratum IIb soils. However, the soils could only be partly penetrated. All CPT soundings experienced refusal when encountering the highly cemented portions of these soils. The CPT soundings could only be advanced after predrilling through the highly cemented zones, and sometimes the predrilling had to be repeated due to the intermittent presence of hard zones at the same sounding. Values of qc from the soundings ranged from about 40 to over 600 tsf. The average qc value ranges from 200 to 300 tsf. The results are consistent with the SPT N-values where the highest N-values were measured in zones that CPT soundings encountered refusal or could not penetrate these soils, approximately between elevation 20 and elevation 40 ft. Stratum IIb Cemented Sand was encountered in the Intake Area with similar but somewhat lower average tip resistance. Average qc value for the Intake Area is approximately 210 tsf. Low SPT N-values and qc values are very infrequent in this stratum, given the influence of cementation. The low values are very likely the result of sampling disturbance, or in one case (at C-406, elevation ~30 ft, qc~10 tsf) the low tip resistance is due to the relatively low overburden pressure at that location. They could also be influenced by groundwater, given that the "confined" groundwater level is roughly near the top of this stratum (refer to Section 2.5.4.6 for groundwater information). The cementation in Stratum IIb soils varies, including zones that are highly cemented and others with little or no cementation. The degree of cementation was subjectively evaluated during the field exploration by observing the degree of shell fragmentation present and testing the soils with diluted hydrochloric acid, as noted on the boring logs. The cementation is affected by the presence of shells in these soils. The influence of iron oxide may also be a factor, although no specific test was performed on the samples for verification of iron contents. These soils, however, have been studied in the past by others, as follows.

Based on a study of soils near Calvert Cliffs (Rosen, et al., 1986), dolomite or calcite, which is present in the local soils, is identified as the cementing agent. The absence of dolomite or calcite in certain parts may be due to low pH groundwater. Abundant iron cement is also reported in some areas near Calvert Cliffs, with significant accumulation of shells that had dissolved. The degree of cementation is affected by the level of dolomitization in the sandy soils, a process that began in the Chesapeake Groups soils once they were covered by the clayey soils above.

The abundant shells in some zones within this stratum render these zones very porous. In a few borings, loss of drilling fluid was noted, (e.g., in borings B-302, B-309, B-354, B-357, B-357A, B-406, B-414, B-426, B-703, B-710, B-786A and B-790). These zones were encountered either near the upper or the lower part of the stratum. Fluid loss was estimated to be in the range of 300 to 600 gallons at B-354, B-357 and B-357A, and at each of the 400-series borings. The loss was judged to be due to the nested accumulation of coarse materials, particularly shell fragments at these locations. The fluid loss in boring B-309, and in the upper portion of boring B-710, was in suspected fill materials.

Refusal was also encountered for Stratum IIc soils. Profiles of qc versus elevation are shown in Figure 2.5-115 and Figure 2.5-116 for the Powerblock and Intake Areas respectively. The results suggest relative uniformity in qc values with depth and lateral extent, as well as evidence of cemented (or hardened zones) near elevation -40 ft which was similarly reflected in the SPT N-value profiles in Figure 2.5-113. The qc values for CCNPP Powerblock Area range

from about 50 to 100 tsf, with an average of about 75 tsf. Stratum IIc Clay/Silt was encountered in the Intake Area with a slightly lower average tip resistance of 70 tsf.

Observation Wells and Slug Testing

A total of 47 observation wells were installed to a maximum depth of 122 ft during the CCNPP Unit 3 subsurface investigation under the full-time supervision of geotechnical engineers or geologists. Wells were installed either in SPT boreholes or at an off-set location, in accordance with ASTM D5092 (ASTM, 2004a). Wells installed in SPT boreholes were grouted to the bottom of the well, and the portion above was reamed to a diameter of at least 6 in using rotary methods and biodegradable drilling fluid. Off-set wells were installed using either 6¼-in ID hollow-stem augers or 6-in diameter holes using the rotary method and biodegradable drilling fluid. Each well was developed by pumping and/or flushing with clean water. Table 2.5-33 provides a summary of the observation well locations and details. The locations are shown in Figure 2.5-103, Figure 2.5-104, and Figure 2.5-105. Complete observation well details are provided in Section 2.4.12.

Slug testing, for the purposes of measuring the in-situ hydraulic conductivity of the soils, was performed in all 47 wells. The tests were conducted using the falling head method, in accordance with Section 8 of ASTM D4044 (ASTM, 2002b). Slug testing included establishing the static water level, lowering a solid cylinder (slug) into the well to cause an increase in water level in the well, and monitoring the time rate for the well water to return to the pre-test static level. Electronic transducers and data loggers were used to measure the water levels and times during the test. Table 2.5-33 also provides the hydraulic conductivity values. Details on testing are provided in Section 2.4.12. COLA Part 11J contains the details of well installation records, boring logs for observation wells, and the hydraulic conductivity test results.

Test Pits

A total of 20 test pits were excavated to a maximum depth of 10 ft each using a mechanical excavator. Bulk samples were collected at selected soil horizons in some of the test pits for laboratory testing. Table 2.5-34 provides a summary of the test pit locations. The locations are shown in Figure 2.5-103, Figure 2.5-104, and Figure 2.5-105. COLA Part 11J contains the test pit records.

Field Electrical Resistivity Testing

A total of four field electrical resistivity (ER) tests were performed to obtain apparent resistivity values for the site soils. Table 2.5-35 provides a summary of the ER test locations. ER testing was conducted using an Advanced Geosciences, Inc., Sting resistivity meter, a Wenner four-electrode array, and "a" spacings of 1.5 ft, 3 ft, 5 ft, 7.5 ft, 10 ft, 15 ft, 20 ft, 30 ft, 40 ft, 50 ft, 100 ft, 200 ft, and 300 ft in accordance with ASTM G57 (ASTM, 2001a) and IEEE 81 (IEEE, 1983), except as noted below. The arrays were centered on each of the staked locations R-1 and R-2, R-3, and R-4, and are shown in Figure 2.5-103 and Figure 2.5-104. The electrodes were located using a 300-ft measuring tape along the appropriate bearings using a Brunton compass.

ASTM G57 (ASTM, 2001a) states that electrodes not be driven more than 5 percent of the electrode separation, which is about 0.9 in for the smallest "a" spacing of 1.5 ft used. Electrodes, however, were driven about 2.25 in (or about 12 percent) at locations where leaves and vegetation were present on the ground, to ensure adequate contact with the soils. ASTM G57 (ASTM, 2001a) states that a decade box be used to check the accuracy of the resistance meter. This verification, however, was conducted using a resistor supplied by the equipment manufacturer in compliance with the manufacturer's recommendations. ASTM G57 (ASTM, 2001a) states that measurement alignments be chosen along uniform topography. Given the

topography at the site, however, the array alignments along R-1 and R-2 contained topographic variation. Finally, IEEE 81 (IEEE, 1983) states that electrodes not be driven into the ground more than 10 percent of the "a" spacing. As discussed above, at some locations electrodes were driven about 2.25 in (or about 12 percent) into the ground. Despite the noted deviations, the collected resistivity values are considered valid and suitable for use.

The results of field resistivity surveys are presented in COLA Part 11J, and summarized in Table 2.5-36.

Suspension P-S Velocity Logging Survey

Borehole geophysical logging was performed in a total of 13 boreholes. The geophysical survey consisted of natural gamma, long- and short-normal resistivity, spontaneous potential, three-arm caliper, direction survey, and suspension P-S velocity logging. Geotechnical engineers or geologists provided full-time field inspection of borehole geophysical logging activities. Detailed results are provided in COLA Part 11J.

Suspension P-S velocity logging was performed in borings B-301, B-304, B-307, B-318, B-323, B-401, B-404, B-407, B-418, B-423, B-773, B-786, and B-821. The measurement at B-786 was performed directly underneath the UHS-MWIS in the Intake Area during the Phase II investigation. The boreholes were uncased and filled with drilling fluid. Boreholes B-301 and B-401 were approximately 400 ft deep each, while the remaining boreholes were approximately 200 ft deep each. The OYO/Robertson Model 3403 unit and the OYO Model 170 suspension logging recorder and probe were used to obtain the measurements. Details of the equipment are described in Ohya (Ohya, 1986). The velocity measurement techniques used for the project are described in Electric Power Research Institute (EPRI) Report TR-102293, Guidelines for Determining Design Basis Ground Motions, (EPRI, 1993). The results are provided as tables and graphs in COLA Part 11J. Figure 2.5-117 and Figure 2.5-118 present the results of the P-S logging surveys. Figure 2.5-119 provides the test result of the PS log performed in the Intake Area. Overall, the result is consistent with the measurements in the Powerblock Area. Section 2.5.4.2.5.8 and 2.5.4.4 provide the analysis of the P-S data along with the development of the best estimate soil profiles for the Unit 3 Area and the Intake Area.

The suspension P-S velocity logging used a 23-ft probe containing a source near the bottom, and two geophone receivers spaced 3.3 ft (1 m) apart, suspended by a cable. The probe is lowered into the borehole to a specified depth where the source generates a pressure wave in the borehole fluid (drilling mud). The pressure wave is converted to seismic waves (P-wave and S-wave) at the borehole wall. At each receiver location, the P- and S-waves are converted to pressure waves in the fluid and received by the geophones mounted in the probe, which in turn send the data to a recorder on the surface. At each measurement depth, two opposite horizontal records and one vertical record are obtained. This procedure is typically repeated every 1.65 ft (0.5 m) or 3.3 ft (1 m) as the probe is moved from the bottom of the borehole toward the ground. The elapsed time between arrivals of the waves at the geophone receivers is used to determine the average velocity of a 3.3-ft high column of soil around the borehole. For quality assurance, analysis is also performed on source-to-receiver data.

Ignoring the measurements above El. 85 ft (approximate finished grade), V_p measurements in Stratum I Terrace Sand ranged from about 850 ft/sec to 5,560 ft/sec, with an increasing trend with depth. Vp measurements in Stratum IIa Chesapeake Clay/Silt ranged from about 3,000 ft/sec to 5,750 ft/sec. V_p measurements in Stratum IIb Chesapeake Cemented Sand ranged from about 2,000 ft/sec to 8,130 ft/sec, with initially increasing trend with depth, however, with fairly uniform values after a few feet of penetration, except at intermittent cemented zones

with peak V_p values. V_p measurements in Stratum IIc Chesapeake Clay/Silt ranged from about 4,800 ft/sec to 5,600 ft/sec, with relatively uniform values throughout the entire thickness, except for occasional minor peaks at intermittent depths. V_p measurements in Stratum III Nanjemoy Sand ranged from about 5,420 ft/sec to 7,330 ft/sec, with relatively uniform values, except for occasional minor peaks at intermittent depths. Results are relatively consistent with those reported from CCNPP Units 1 and 2 (Table 2.5-37 and Figure 2.5-120) for similar soils. V_p values below about El. 80 ft are typically at or above 5,000 ft/sec; these measurements reflect the saturated condition of the soils below the referenced elevation.

V_s measurements in Stratum IIa Chesapeake Clay/Silt ranged from about 590 ft/sec to 1,430 ft/sec, with typically increasing trend with depth. V_s measurements in Stratum IIb Chesapeake Cemented Sand ranged from about 560 ft/sec to 3,970 ft/sec, with significant variation with depth owing to significant changes in density and cementation. V_s measurements in Stratum IIc Chesapeake Clay/Silt ranged from about 1,030 ft/sec to 1,700 ft/sec, with relatively uniform trend in values throughout the entire thickness, except for occasional minor peaks at intermittent depths. V_s measurements in Stratum III Nanjemoy Sand ranged from about 1,690 ft/sec to 3,060 ft/sec, with initially increasing trend in depth, however, relatively uniform at greater depth, except for occasional minor peaks at intermittent depths.

The P-S logging results are discussed in detail in Section 2.5.4.4.

Pressuremeter

Pressuremeter testing was performed in pre-drilled boreholes using a cylindrical probe that expanded radially. The deformation of the borehole wall was measured relative to the stress induced by the pressuremeter on the soil. Geotechnical engineers or geologists were on site to inspect the work. One pressuremeter test was performed in the Unit 3 Powerblock Area to a depth of about 360 ft at borehole PM-301. Another pressuremeter test was performed in the Intake Area to a depth of about 150 ft in borehole PM-701. The data are presented in COLA Part 11J. Sixty-seven (67) tests were completed in PM-301 and 29 in PM-701. Almost all of the tests produced useful data, although not all tests could be completely analyzed for all possible parameters. In instances where not all parameters could be determined, this was due to borehole disturbance or uneven expansion of the instrument resulting in less than complete information on the soil.

The pressuremeter used was a digital electronic instrument of the Cambridge design and is a much more sensitive instrument than the Menard type specified by ASTM. The pressuremeter data was analyzed to determine the pressuremeter modulus and limit pressure as determined by ASTM D4719 (ASTM, 2007). Additional analyses were performed to determine the unload/reload modulus which usually included one to three cycles per tests at various strain levels. Strength parameters were determined using modeling techniques. Pressuremeter data has been used as means, among other methodologies, to estimate the elastic modulus for settlement. It is also used to establish the ratio of the Unload/Reload Modulus to the Elastic Modulus.

Table 2.5-38 and Table 2.5-39 provide the data recordings of the pressuremeter tests at PM-301 and PM-701. Figure 2.5-121 shows a graphic representation of the data for the Powerblock and Intake Area in the form of elastic modulus. An average for the site is plotted as references. This information is used as one of the criteria to provide a recommendation for elastic modulus.

Dilatometer

An in-situ penetration and expansion test with a steel dilatometer blade with a sharp cutting edge was incrementally forced into the soil in a generally vertical orientation. At a specified depth a flat circular, metallic membrane is expanded into the surrounding soil. Inspected by a geotechnical engineer or geologist, the soil deformation is measured relative to the stress induced on the soil by the expanding membrane. One dilatometer test was performed in the Powerblock Area to a depth of about 350 ft in boring B-301. Another dilatometer test was performed in the Intake Area to a depth of about 150 ft at boring B-701. Due to the large amount of data, the results of the tests are included only in COLA Part 11J.

2.5.4.2.3 Backfill Investigation

During the Phase III investigation, a backfill characterization study was conducted. Structural fill has been identified and the material sampled was sent to the laboratory to establish their static, chemical, and dynamic properties. The results are evaluated to verify that the candidate backfill materials meet the design requirements for structural fill. The structural fill for CCNPP Unit 3 is sound, durable, well graded sand or sand and gravel, with a maximum 25 percent fines content, and free of organic matter, trash, and other deleterious materials. Backfill and related topics are further addressed in Section 2.5.4.5. It is estimated that about 2 million cubic yards of structural backfill are required.

The field sampling campaign was performed as follows:

- Batch 1: sampling of six buckets from Vulcan Quarry in Havre de Grace, Maryland was performed in September of 2008. Sample testing directive to laboratory was performed on unblended samples.
- Batch 2: sampling of six buckets from Vulcan Quarry. Sample testing directive to laboratory was performed on blended samples. Sample testing directive to laboratory was performed on composite samples.
- Batch 3: eight buckets of CR6, eight buckets of GAB, and six buckets of coarse aggregate- 57 sampled from the Vulcan Quarry on December, 2008. Sample testing directive to laboratory was performed on composite samples.
- Batch 4: seventeen buckets of CR6, GAB, and coarse aggregate-57 sampled from the Vulcan Quarry on March, 2009. Sample testing directive to laboratory was performed on composite samples. Batch 4 was used for Resonant Column Torsional Shear Testing.

2.5.4.2.4 Laboratory Testing Program

The laboratory investigations of soils and rock were performed in accordance with the guidance outlined in Regulatory Guide 1.138, Laboratory Investigations of Soils for Engineering Analysis and Design of Nuclear Power Plants (USNRC, 2003b). Deviations are identified and alternatives and/or basis for deviation are provided.

The detailed results of all laboratory tests performed as part of the subsurface investigation is provided in the following reports:

- Geotechnical Subsurface Investigation Data Report (Schnabel, 2007a), with Phase I laboratory testing program.

- Geotechnical Subsurface Investigation Data Report (Schnabel, 2007b).
- Reconciliation of EPRI and RCTS Results Calvert Cliffs Nuclear Power Plant Unit 3 (Bechtel, 2007), with the RCTS data and analysis for the Powerblock Area.
- Revised Laboratory Testing Results, Rev.2 (MACTEC, 2009a).
- Structural Fill Static Laboratory Testing Results, Rev. 1 (MACTEC, 2009b).
- Structural Fill Dynamic Laboratory Testing Results, Rev.1 (MACTEC, 2009c).
- Intake Samples Laboratory Testing Results, Rev. 1 (MACTEC, 2009d).

The referenced reports are included in COLA Part 11J and COLA Part 11K.

The laboratory work was performed under the Bechtel QA program with work procedures developed specifically for the CCNPP Unit 3 subsurface investigation. Soil samples were shipped under chain-of-custody protection from the on-site storage to the testing laboratories. ASTM D4220 (ASTM, 2000a) provides guidance on standard practices for preserving and transporting soil samples. This guidance was referenced in preparing technical specifications for the CCNPP Unit 3 subsurface investigation, addressing sample preservation and transportation, as well as other subsurface investigation and geotechnical requirements.

Laboratory testing consisted of testing soils and groundwater samples obtained from the investigation program. Testing of groundwater samples is addressed in Section 2.4.13. Laboratory testing of soil samples consisted of index and engineering property tests on selected SPT, undisturbed, and bulk samples. The SPT and undisturbed samples were recovered from the borings and the bulk samples were obtained from the test pits.

Testing of index properties included the following items:

- Soil classification,
- Water content,
- Grain size (sieve and hydrometer),
- Atterberg limits,
- Organic content,
- Specific gravity,
- Unit weight.

Chemical tests included:

- pH,
- Chloride content,
- Sulfate content.

Performance and strength tests under static conditions included:

- Consolidation,
- Unconfined compression (UC),
- Unconsolidated-undrained triaxial compression with pore pressure measurement (UU),
- Consolidated-undrained triaxial compression with pore pressure measurement (CU-Bar),
- Direct shear (DS),
- Modified Proctor compaction (Moisture–Density),
- California Bearing Ratio (CBR).

Performance and strength tests under dynamic conditions included:

- Resonant Column Torsional Shear (RCTS) tests.

Unit weight is also obtained from direct volume/mass measurements from miscellaneous tests. The number of tests performed is provided in Table 2.5-40.

Regulatory Guide 1.138 (USNRC, 2003b) provides guidance for laboratory testing procedures for certain specific tests, including related references. Laboratory testing of samples for the CCNPP Unit 3 subsurface investigation used commonly accepted, and updated practices such as more recent ASTM and EPA standards which are equivalent to the testing procedures referenced in the Regulatory Guide. Laboratory testing of samples for the CCNPP Unit 3 subsurface investigation did not rely upon non-U.S. or out-of-date versions of practices or standards.

The soil and rock laboratory tests listed in Regulatory Guide 1.138 (USNRC, 2003b) are common tests performed in most well-equipped soil and rock testing laboratories, and they are covered by ASTM standards. Additional test that are not covered in regulatory guidance were also performed for the CCNPP Unit 3 subsurface investigation (e.g., CBR tests to assess suitability of subgrade or fill materials for pavement, and RCTS tests, which were used in lieu of the resonant column test alone to obtain shear modulus and damping ratio values for a wide range of strains). Results of Cation Exchange Capacity tests are addressed with the groundwater chemistry data in Section 2.4.13.

The following subsections present a summary of the most relevant laboratory testing data. A recommendation of soil properties for use of foundation analysis and design is provided in Section 2.5.4.2.5. The complete set of laboratory test results is included in COLA Part 11J and COLA Part 11K. References are made to property data tables. Each table presents a line item for each of the soil layers and one line item for backfill.

2.5.4.2.4.1 Index Testing

Laboratory index tests and testing for determination of engineering properties were performed on selected samples. Laboratory test quantities are summarized in Table 2.5-40. Sample selection for testing was primarily based on the observed soil uniformity from the field classification, or conversely, the variation in material description based on logging in the field, in order to obtain a quantitative measure of the uniformity, or the variation, respectively.

Values of index testing are provided in Table 2.5-41 and Table 2.5-42. Figure 2.5-122 and Figure 2.5-123 provide a plot of Moisture Content and Atterberg limits as a function of elevation for the Powerblock and Intake Area respectively. Figure 2.5-124 and Figure 2.5-125 provide the plasticity chart for the Powerblock Area and Intake Area respectively.

2.5.4.2.4.2 Chemical Testing

Chemical testing consisted of pH, chloride, and sulfate tests, performed on selected soil samples collected during the COL exploration. The pH tests were performed on samples in both calcium chloride and deionized water. Seventy-seven sets of chemical tests were performed on soil samples collected from depths ranging from the ground surface to 104 ft below the ground surface. The test results are provided in the data report and summarized in Table 2.5-43.

2.5.4.2.4.3 Performance and Strength Tests under Static Conditions

Summary data of performance and strength properties are presented in the following tables:

- Table 2.5-44 and Table 2.5-45 provide the summary of the consolidation test results for the Powerblock Area and Intake Area respectively.
- Table 2.5-46 and Table 2.5-47 provide the summary of shear strength test results for the Powerblock Area and Intake Area respectively; the tests include unconsolidated-undrained triaxial, consolidated-drained triaxial, unconfined compression and direct shear.
- Table 2.5-48 provides the results of Modified Proctor tests for the samples tested for backfill. These samples have been selected based on performance under compaction tests and RCTS tests (Section 2.5.4.2.4.4).

2.5.4.2.4.4 Resonant Column Torsional Shear Tests (RCTS)

Testing was performed on resonant column and torsional shear (RCTS) equipment to measure the material properties (shear modulus and material damping in shear) of soil specimens. The RCTS equipment used is of the fixed-free type, with the bottom of the specimen fixed and shear stress applied to the top. Both the resonant column (RC) and torsional shear (TS) tests were performed in a sequential series on the same specimen over a shearing strain range from about 10^{-4} percent to about 1 percent, depending upon specimen stiffness. RCTS testing was performed on each soil specimen at selected confining pressures of 0.25, 0.5, 1, 2, and 4 times the estimated effective stress. Testing at each successive stage (i.e., confining pressure condition) occurred after the specimens were allowed to consolidate at each pressure step. At each level of shear strain amplitude, the shear modulus and material damping ratio were determined.

EPRI curves were fitted to the data to provide the recommendation (EPRI, 1990). For the Powerblock Area, the EPRI curve fitting is provided in the report "Reconciliation of EPRI and RCTS Results, Calvert Cliffs Nuclear Power Plant Unit 3" (Bechtel, 2007), and is included as COLA Part 11J. Section 2.5.4.2.5 provides a detailed discussion about the criteria for selection of strain dependant property curves based on generic curves and site specific laboratory information.

RCTS testing was performed for the samples in the Powerblock Area, the Intake Area, and Backfill. Table 2.5-49 provides a list of the RCTS samples tested and their index properties. The

following samples were used for RCTS testing. The associated figure shows the results for that specific sample.

- Powerblock Area
  - B-437-6 (13.5′), Figure 2.5-126
  - B-301-10 (33.5′), Figure 2.5-127
  - B-305-17 (39.5′), Figure 2.5-128
  - B-404-14 (52.0′), Figure 2.5-129
  - B-401-31 (138.5′), Figure 2.5-130
  - B-401-67 (348.5′), Figure 2.5-131
  - B-401-48 (228.5′), Figure 2.5-132
  - B-301-78 (385.2′), Figure 2.5-133
  - B-306-17 (68.0′), Figure 2.5-134
  - B-409-15 (35.0′), Figure 2.5-135
  - B-404-22 (83.5′), Figure 2.5-136
  - B-401-42 (198.5′), Figure 2.5-137
  - B-409-39 (95.0′), Figure 2.5-138
- Intake Area
  - B-773-2 (15.9′), Figure 2.5-139
  - B-773-3 (27.0′), Figure 2.5-140
  - B-773-4 (37.0′), Figure 2.5-141
  - B-773-5 (47.0′), Figure 2.5-142
  - B-773-6 (57.0′), Figure 2.5-143
  - B-773-7 (66.1′), Figure 2.5-144
  - B-773-9 (87.0′), Figure 2.5-145
  - B-773-11 (107.0′), Figure 2.5-146
  - B-773-13 (127.0′), Figure 2.5-147
  - B-773-15 (147.0′), Figure 2.5-148
- Backfill
  - CR6 Composite (Bulk), Figure 2.5-149
  - GAB Composite (Bulk), Figure 2.5-150
  - CR6 Vulcan Average (Bulk), Figure 2.5-151

The backfill low strain RCTS test shear wave velocity measurements are used to aid in the development of the best estimate velocity profiles. These measurements are provided in Table 2.5-50. The confining pressures in the test ranged from 0.5 ksf to 17.3 ksf. Since the backfill will be placed near the surface in the uppermost 43.5 feet, and an increase in confining

pressures is expected from building facilities, the relevant results correspond to the confining pressures reported in Table 2.5-50.

2.5.4.2.5 Soil Properties for Foundation Analysis and Design

Sections 2.5.4.2.2, 2.5.4.2.3, and 2.5.4.2.4 provide a comprehensive summary of the results from field and laboratory testing. This section uses the data retrieved and develops soil properties to be used for foundation analysis and design. The selection of properties takes into account the wealth of information generated from the field and laboratory, and is developed based on simplified soil profiles that are derived with the use of common geotechnical engineering principles and engineering judgment.

Figure 2.5-106 shows the general soil profile for the CCNPP Unit 3 Site. The profile is applicable throughout the site, though at the Intake Area, due to the difference in elevation and proximity to the shoreline, the Stratum I Terrace Sand and Stratum IIa Chesapeake Clay/Silt are not present. Instead, a man made fill sits on top of Layer IIb Chesapeake Cemented Sand. Figure 2.5-112 shows the conditions at the Intake Area.

The soil properties provided in this section are applicable to the soil layers portrayed by Figure 2.5-106. The settlement analysis for the CCNPP3 Unit 3 Site accounts for a three-dimensional representation of the subsurface conditions. Details of the settlement analysis are provided in Section 2.5.4.10.

2.5.4.2.5.1 General Classification and Index Properties

Stratum I soils are characterized, on average, as non-plastic with an average fines content (materials passing No. 200 Sieve) of 20 percent. Grain size analyses indicated that these soils are primarily fine or fine-medium sands. The Unified Soil Classification System (USCS) designations were poorly-graded sand/silty sand, silty sand, well-graded sand, clayey sand, clay of high plasticity, silt, clay, and silt with high plasticity, with the predominant classifications of SP-SM and SM. The often plastic and fine-grained soil classifications are from the interbeds within this stratum.

Stratum IIa soils are characterized as medium-high plasticity clays. Their predominant USCS designation was clay of high plasticity and silt of high plasticity (CH and MH); sometimes with silty sand, silty sand to clayey sand, and organic clay. The organic designation was based on laboratory (liquid limit) tests. With less than 1 percent organic matter on average, and observations during sampling, these soils are not considered organic.

Stratum IIb soils are primarily medium-fine sands. The USCS designations were silty sand, poorly-graded sand to silty sand, clayey sand, silt, silt of high plasticity, clay of high plasticity, clay, and organic clay. The predominant classifications, however, were silty sand, clayey sand, and poorly-graded sand to silty sand (SM, SC, and SP-SM).

Stratum IIc soils are characterized as high plasticity clay and silt, with an average PI = 50. Their predominant USCS designation was clay of high plasticity and silt of high plasticity (CH and MH), however, sometimes silty sand, clay, and organic clay classifications were indicated. Based on observations during sampling, the organic soil designation based on laboratory (Liquid Limit) testing is not representative of these soils, and therefore, they are not considered organic soils.

Stratum III soils are characterized as sand of high plasticity. Their predominant USCS designations were clayey sand and silty sand (SC and SM), although clay of high plasticity and silt of high plasticity were also indicated.

Table 2.5-51 provides the USCS classification of soils and index properties for each stratum. Unit weights were determined based on numerous unit weight tests performed on specimens during different types of tests such as unit weight, triaxial, RCTS. The USCS classification is based on the predominant classification of tested samples.

2.5.4.2.5.2 Chemical Properties

Table 2.5-43 provides the data obtained for the CCNPP Unit 3 site. Guidelines for interpretation of chemical test results are provided in Table 2.5-52, based on the following consensus standards, API Recommended Practice 651 (API, 2007), Reinforced Soil Structures (FHWA, 1990), Standard Specification for Portland Cement (ASTM 2005b), Manual of Concrete Practice (ACI, 1994), and Standard Specification for Blended Hydraulic Cement (ASTM, C595). From the average values of available results shown in Table 2.5-43, the field resistivity surveys in Table 2.5-12, and guidelines in Table 2.5-52, the following conclusions were developed:

Attack on Steel (Corrosiveness): The resistivity test results indicate that all soils are "little corrosive," except for Stratum IIc Chesapeake Clay/Silt that may be "little to mildly corrosive." Based on the chloride contents typically being below 10 ppm, all soils are essentially non-corrosive. The pH results, however, indicate that all soils are "corrosive to very corrosive," except for Stratum IIc Chesapeake Clay/Silt that may be "mildly corrosive." Few chemical test results are available from Stratum IIc; however, that should be of no special importance because no Seismic Category I structure (or piping) is anticipated within these soils. The pH data dominate the corrosive characterization of the soils. Nevertheless, all natural soils at the site will be considered corrosive to metals, requiring protection if placed within these soils. Protection of steel against corrosion may include cathodic protection, or other measures. Additional pH testing on groundwater samples obtained from the observation wells (refer to Section 2.4.13) indicate pH values of average 5.5, 6.8, and 7.1 for wells screened in Stratum I, Stratum IIa, and Stratum IIb soils, respectively. Except for values obtained in groundwater associated with Stratum I soils indicating "corrosive" conditions, remaining pH data from other strata only indicate "mildly corrosive" conditions.

Attack on Concrete (Aggressiveness): The sulfate test results in all tested soils indicate a "severe" potential for attack on concrete, except for Stratum IIc Chesapeake Clay/Silt that may cause a "moderate" attack. As noted above, few chemical test results are available for Stratum IIc; however, based on the available information, Seismic Category I structures (or piping) may encounter Stratum IIc soils in the Intake Area. Nevertheless, all natural soils at the site will be considered aggressive to concrete, requiring protection if placed within these soils.

2.5.4.2.5.3 Performance Properties Under Static Conditions

The required performance properties under static conditions are the following:

- C_r - Recompression index,
- C_c - Compression index,
- e_o - Initial void ratio,
- p'_c - Preconsolidation pressure,
- OCR - Overconsolidation ratio,

- c_v - Coefficient of consolidation.
- k - Permeability (hydraulic conductivity),

The selected values for the consolidation properties are based on average parameters obtained from laboratory testing. Permeability is obtained from well field tests and development and calibration of hydrogeologic models. Details of the tests and models are provided in Sections 2.4.12 and 2.4.13. Hydraulic conductivity for backfill is based on laboratory results of tests performed on bulk samples. Table 2.5-53 provides the soil performance properties for each stratum.

2.5.4.2.5.4 Strength Properties Under Static Conditions

The required strength properties under static conditions are the following:

- N - Standard Penetration Test (SPT) Resistance (N);
- c′ - Cohesion under drained conditions;
- Φ′ - Friction angle under drained conditions;
- c - Cohesion under undrained conditions;
- Φ - Friction angle under undrained conditions;
- s_u - Undrained shear strength.

Table 2.5-28 provides the SPT test data. The average SPT N corrected values are used.

The shear strength parameters are based on laboratory testing data. Table 2.5-54 provides the strength properties for each stratum.

2.5.4.2.5.5 Elastic Properties Under Static Loading

The required elastic properties of soil under static loading are the following:

- E - Elastic modulus (large strain).
- $E_{u/r}$ - Unload/Reload Elastic modulus.
- $E_{u/r}$/E- - Ratio of to unload/reload Elastic modulus to Elastic modulus.
- G - Shear modulus (large strain).
- *v* - Poisson's ratio.

The elastic moduli significantly impact settlement estimates and therefore numerous methods have been applied to estimate these parameters. The Shear modulus (G) and elastic modulus (E) are estimated for each soil strata using the following three criteria:

1. Geophysical test results: Shear wave velocities (V_s), P-wave velocities (V_p), and Poisson's ratios from borehole surveys are used to estimate the shear modulus (G) and Elastic modulus (E) at depth intervals between 1.6 ft and 1.7 ft below the ground surface. The geophysical survey data are grouped based on the soil strata. Average G and E values and their corresponding standard deviations of each soil layer are estimated. The G and E values estimated based on the geophysical tests correspond to very low strain values; therefore, they are reduced to account for the material's strain softening due to higher strains. The moduli are determined from elasticity theory equations:

$G = \rho V_s^2$

$E = 2G(1+\nu)$

The value of the static Poisson Ratio is adopted from typical values reported in the literature (Salgado, 2008).

2. Pressuremeter testing data obtained from two borehole locations are used to calculate the shear modulus (G) and elastic modulus (E) for each soil layer. Results from Pressuremeter testing correspond to high strain values, therefore, it is expected that the elastic modulus values fall in the lower bound range.

3. Elastic modulus is calculated using different correlations as a function of corrected SPT N-values and undrained shear strength (s_u):

$E = 18N_{60}$	Coarse grained Materials (Davie, et al.,1988)
$E = \beta_0\sqrt{OCR} + \beta_1 N_{60}$	Coarse grained materials (Coduto, 2001)
$E = 450s_u$	Fine grained materials (Davie, et al., 1988)
$E = 2G(1 + \nu)$, $G = s_u$	Fine grained materials (Senapathy, et al., 2001)

Table 2.5-55 provides the estimates of elastic modulus using the previously listed criteria.

The unload/reload modulus ($E_{u/r}$) is required for the estimation of heave and of settlement between excavation and reload. The pressuremeter test data were used to estimate the ratio of unload/reload modulus. The data provided by Table 2.5-38 and Table 2.5-39 indicate that the unload/reload values are consistently above 3.0, with average values above 4.0 and in many instances higher than 6.0. Due to the uncertainty involved in settlement computations and the uncertainty in relating pressuremeter data to actual field conditions it is prudent to adopt a conservative approach. Therefore, the maximum value for the $E_{u/r}/E$ ratio adopted is 3.0 except when the minimum recorded value for a given layer is higher than 3.0. In those instances the minimum value of $E_{u/r}/E$ is adopted. Table 2.5-56 shows the minimum, average, and maximum values of the $E_{u/r}/E$ ratio reported from pressuremeter testing. Table 2.5-57 provides the static elastic properties for each stratum.

By establishing a limit of 3.0, the previous criterion is conservative for the estimation of total settlements. By using a larger value than 3.0 whenever $(E_{u/r}/E)_{min}$ is larger, the previous criterion is conservative for the estimation of tilt. This approach accounts for the asymmetric topographic conditions and the effect that they have on the unloading throughout the footprint of the foundation. Additional explanation is provided in the settlement analysis in Section 2.5.4.10.

2.5.4.2.5.6 Earth Pressure Coefficients

Active, passive, and at-rest static earth pressure coefficients, K_a, K_p, and K_0, respectively, were estimated assuming frictionless vertical walls and horizontal backfill using Rankine's Theory and based on the following relationships (Lambe, et al., 1969):

Active Earth Pressure Coefficient: $K_a = \tan^2\left(45 - \frac{\Phi'}{2}\right)$

Passive Earth Pressure Coefficient: $K_p = \tan^2\left(45 + \frac{\Phi'}{2}\right)$

At Rest Earth Pressure Coefficient: $K_0 = 1 - \sin(\Phi')$

The values for earth pressure coefficients for each stratum are provided in Table 2.5-58.

2.5.4.2.5.7 Sliding Coefficient

The sliding coefficient is tangent δ, where δ is the friction angle between the soil and the material it is bearing against, in this case concrete. Based on "Foundations & Earth Structures" (NFEC, 1986), the sliding coefficient, tangent δ, for each stratum is provided in Table 2.5-58.

2.5.4.2.5.8 Low Strain Dynamic Properties

The low strain dynamic properties are the basis to develop the Best Estimate soil profile for the purposes of site amplification analysis. The following properties are discussed:

- γ - Moist unit weight;
- G_o - Low strain shear modulus;
- V_S - Shear wave velocity;
- V_p - Compression wave velocity;
- *v* - Poisson's Ratio;

The moist unit weight is obtained directly from the index properties. Based on all 10 suspension P-S velocity measurements, an average V_s profile was estimated for the upper 400 ft. Poisson's ratio values were determined based on the V_p and V_s measurements. The measurement of dynamic properties reflects the conditions for the approximately upper 400 ft of the site, or to about El. -317 ft. Information on deeper soils, as well as bedrock, was obtained from the available literature.

Shear wave velocity measurements were made using a seismic cone at ten soundings (C-301, C-304, C-307, C-308, C-401, C-404, C-407, C-408, C-724, and C-725). The measurements were made at 3.3 ft (1 m) intervals. At several locations, the soils required pre-drilling to advance the cone, particularly in the cemented zones. Although the deepest CPT sounding was about 142 ft, the combined measurements provided information for the upper approximately 200 ft of the site soils, extending to about elevation -80 ft. Further penetration was not possible due to continued cone refusal. The CPT results are found to be relatively consistent with the suspension P-S velocity logging results. The variations in different soils that were observed in the suspension P-S velocity logging data are readily duplicated by the CPT results, including the peaks associated with cemented or hard zones. Further details on testing and the results are provided, in tables and graphs, in COLA Part 11J and COLA Part 11K.

Given the similarity between the suspension P-S velocity logging and the seismic CPT results, and that the CPT results only extend to limited depth, the suspension P-S velocity logging results were used as the basis for determination of shear wave velocity profile for the site. It is also well established that the P-S logging technique is specifically designed to measure wave velocities and is a superior measurement technique when compared to the CPT.

The best estimate of the shear and compression shear wave velocity profiles are presented by the following four figures:

1. Figure 2.5-166, showing the best estimate velocity profiles in the Powerblock Area;

2. Figure 2.5-167, showing the best estimate velocity profiles in the Powerblock Area, after placement of fill;

3. Figure 2.5-168, showing the best estimate velocity profiles in the Intake Area;

4. Figure 2.5-169, showing the best estimate velocity profiles in the Intake Area, after placement of fill;

In these four figures, 0 depth corresponds to site grade, El 83 ft.

The following apply to the best estimate profiles and the previous figures:

- The figures indicate the position of the groundwater. For the Powerblock Area, the groundwater level at the site has an approximate depth of 16 ft. Once construction is finalized, due to new drainage patterns the expected depth of the groundwater is 30 ft. A detailed discussion related to groundwater is provided in Section 2.4.12.

- The shear wave velocity of the fill has been estimated by adjusting the low strain dynamic properties measured by the RCTS tests to the field conditions. Table 2.5-50 provides the RCTS test results for the range of confining pressures that will prevail after backfill placement. Based on the results, a three-step velocity profile is proposed, as shown by the four previously listed figures. The shear wave velocity for the backfill below the EPGB is 900 fps. This value is below the 1,000 fps specified in the U.S. EPR FSAR. This constitutes a departure. The lower shear wave velocity will be used in the soil-structure interaction analysis in section 3.7.

- For the Intake Area, the best estimate is based in the P-S logging measurement of boring B-773. The shear wave velocity in Stratum II-C, Chesapeake Clay/Silt is consistent with the measurements at the Powerblock Area, though slightly lower with a value of 1150 fps, as opposed to 1250 fps. The measurement at B-773 reached a depth of approximately 150 ft. The values for deeper strata are taken from the best estimate profile in the Powerblock Area.

- The development of the deep soil column, location of bedrock, and location of the 9,200 fps horizon was based on the study of geologic conditions and deep well exploration records in the site vicinity. A detailed discussion with the basis for parameter selection is provided in the following paragraphs.

To develop the deep soil velocity profile, various geologic records were reviewed and communication made with staff at the Maryland Geological Survey, the United States Geological Survey, and the Triassic-Jurassic Study Group of Lamont-Doherty Earth Observatory, Columbia University. The results of this work, and associated references, are addressed in Section 2.5.1. In summary, a soil column profile was prepared, extending from the ground surface to the top of rock. Soils below 400 ft consist of Coastal Plain sediments of Eocene, Paleocene, and Cretaceous eras, extending to an estimated depth of about 2,500 ft below the ground surface. These soils contain sequences of sand, silt, and clay. Given their

geologic age, they are expected to be competent soils, consolidated to at least the weight of the overlying soils.

Several available geologic records were also reviewed in order to obtain information on both the depth to bedrock and the bedrock type, as addressed in Section 2.5.1. Accordingly, the estimated depth to bedrock in the proximity of the site is about 2,555 ft, which is consistent with the depth of 2,500 ft reported in the CCNPP Units 1 and 2 UFSAR (BGE, 1982). Top of rock elevation at the CCNPP site is estimated, and adopted, at approximately El. -2,446 ft which corresponds to a depth of about 2,531 ft. Regional geologic data were also researched for information on bedrock type. This revealed various rock types in the region, including Triassic red beds and Jurassic diabase, granite, schist, and gneiss. However, only granitoid rocks (metamorphic gneiss, schist, or igneous granitic rocks), similar to those exposed in the Piedmont, could be discerned as the potential regional rock underlying the CCNPP Unit 3 site. For the purpose of rock response to dynamic loading, granitoid was considered as the predominant rock type at the CCNPP Unit 3 site.

With the geology established below a depth of 400 ft, velocity profiles also needed to be established. The velocity data were found through a research of available geologic information for the area. From the Maryland Geological Survey data, two sonic profiles were discovered for wells in the area that penetrated the bedrock, one at Chester, MD (about 38 miles north the site, (USGS, 1983) and another at Lexington Park, MD (about 13 miles south of the site, (USGS, 1984); their locations relative to the site are shown in Figure 2.5-152. These two sonic profiles were digitized and converted to shear wave velocity, based on a range of Poisson's ratios for the soil and the rock. The two Vs profiles for Chester and Lexington Park are plotted versus elevation, with the superimposed measured velocity profile from the upper 400 ft at the CCNPP site, as shown in Figure 2.5-153 and Figure 2.5-154.

The bottom of the measured V_s profile in the upper 400 ft fits well with the Chester data for which a soil's Poisson's ratio = 0.4 was used, whereas, in the case of Lexington Park data, the bottom of the measured data in the upper 400 ft fits well with the profile for which the soil's Poisson's ratio = 0.45 was used. Geologically, the soils at the two sites are quite comparable. (Refer to Section 2.5.1 for more details on site geology). The reason for the different "fits" is not clear. However, based on actual Poisson's ratio measurement at another deep Coastal Plain site (SNOC, 2006), where suspension P-S velocity logging measurements extended to a depth of over 1,000 ft, a Poisson's ratio of 0.4 was adopted to represent the soil conditions at the CCNPP site, given the geologic similarity of the soils at both sites.

If a Poisson's ratio of 0.4 is used to convert the Chester sonic log to a shear wave velocity log, this shear wave velocity log fits well with the bottom of the site Vs profile measured with suspension logging at comparable elevations. A similarly good fit is obtained for the Lexington Park data when a Poisson's ratio of 0.45 is used.

Although geologically the soils at the Chester and Lexington Park sites are quite comparable, there are reasons why the soils at the elevation of the bottom of the site profile could have slightly different Poisson's ratio values, e.g., the Lexington Park soils may be more cohesive than the Chester soils. Nevertheless, a single Poisson's ratio value was needed for below the bottom of the measured profile for the CCNPP site. Based on actual Poisson's ratio measurements at another deep Coastal Plain site (SNOC, 2006), where suspension P-S velocity logging measurements extended to a depth of over 1,000 ft, a Poisson's ratio of 0.4 was adopted to represent the soil conditions at the CCNPP site, given the geologic similarity of the soils at CCNPP site and the other Coastal Plain site.

Both profiles (particularly the Chester profile) include significant "peaks," giving a visual impression that the difference in the two profiles may be large. To further look at the variation in these two profiles based on the adopted Poisson's ratio of 0.4, both profiles were averaged over 100-ft intervals along the entire depth to "smooth" the peaks. The original profiles for the two sites (based on a Poisson's ratio of 0.4) and the 100-ft interval average for the two measurements are shown in Figure 2.5-155. A comparison of the two 100-ft interval averages show that once the effect of the "peaks" are removed, the two profiles are relatively similar for the same Poisson's ratio of 0.4. Finally, an average of the 100-ft interval data for both sites was taken. This latter profile was compared with an available measured profile in deep Coastal Plain soils (SNOC, 2006); its similarity to the measured profile is indicative of its appropriateness for the geologic setting, as shown in Figure 2.5-156.

Similar to the soil profiles addressed above, two velocity profiles were also available for bedrock, based on the sonic data from Chester (USGS, 1983) and Lexington Park (USGS, 1984) sites. Rock was encountered at different depths at these two sites; however, the elevation difference in top of rock is only 11 ft between the two sites. The bottom portions of Figure 2.5-153 and Figure 2.5-154 (near the soil-rock interface) are enlarged for clarity and are shown in Figure 2.5-157 and Figure 2.5-158 for the Poisson's ratios shown.

A comparison of the shear wave velocity profiles in bedrock for the two sites reveals different velocity responses, regardless of the Poisson's ratio values considered. The Chester profile is somewhat transitional and does not approach 9,200 ft/sec at termination of measurements. The Lexington Park profile is rather abrupt, and is in excess of 9,200 ft/sec. The difference in these two responses is found in the geologic description of the bedrock at the two sites. At Chester, the bedrock is described as more the typical, regional metamorphic rock (granitic, schist, or gneiss). At Lexington Park, the bedrock is described as an intrusive diabase. Based on further evaluation of regional bedrocks, as addressed in Section 2.5.1, the following description was established for the CCNPP Unit 3 site: bedrock is probably granitoid rock, less likely to be sandstone or shale, even less likely to be diabase. Accordingly, the Lexington Park profile (that is for diabase rock) was excluded from further consideration.

Closer examination of the Chester bedrock velocity results reveal that the velocities are rather "insensitive" to the assumption of Poisson's ratio, as is evident in Figure 2.5-157. For all practical purposes, the assumption of Poisson's ratio of 0.2, 0.25, or 0.3 for the bedrock renders identical velocity profiles. The responses also follow a particular velocity gradient. For a Poisson's ratio of 0.3 for the rock, one could assume a bedrock velocity starting at some value at the soil-rock interface, transitioning to the 9,200 ft/sec at some depth. This approach was followed, as shown in Figure 2.5-159, showing the shear wave velocity profile versus elevation in bedrock. From this figure, starting at Vs of 5,000 ft/sec at the soil-rock interface, the 9,200 ft/sec velocity is reached within about 20 ft depth into rock. Many variations were tried (varying the starting velocity at soil-rock interface, varying the slope of transitioning velocity profile, transition in "slope" or in "step," different Poisson's ratios, etc.); the end result appeared relatively unchanged, i.e., the 9,200 ft/sec velocity is achieved within a short distance of penetrating the rock. On this basis, the "stepped" velocity gradient shown in Figure 2.5-159 was adopted to define the velocity profile for the rock. The recommended velocity profile for bedrock begins with Vs = 5,000 ft/sec at the soil-rock interface, as indicated from the sonic data, transitioning to 9,200 ft/sec in the steps shown in Figure 2.5-159. The top of rock elevation was adjusted to conform to the estimated rock elevation for the CCNPP Unit 3 site, or El. -2,446 ft. (Refer to Section 2.5.1).

Accordingly, based on measured data in the upper 400 ft and data obtained from available literature in areas surrounding the CCNPP site, the shear wave velocity profile in soils at the CCNPP Unit 3 site is shown in Figure 2.5-166 and Figure 2.5-167. For the Intake Area the profiles are provided in Figure 2.5-168 and Figure 2.5-169. The profiles in the figures are considered as the design shear wave velocity profiles. Tabular data related to velocity profiles is provided in Table 2.5-59 and Table 2.5-60 for the Powerblock and Intake Area respectively.

2.5.4.2.5.9 Strain Dependant Properties

The strain dependant properties for the CCNPP3 project are developed by fitting generic curves to the site specific data reported by RCTS tests. EPRI curves from EPRI TR-102293 were used as generic curves (EPRI, 1993). EPRI "sand" curves were used for predominately granular soils and "clay" curves were used for predominately clay soils based on estimated PI values. The EPRI "sand" curves cover a depth range up to 1,000 ft. Since soils at the CCNPP site extend beyond 1,000 ft, similar curves were extrapolated from the EPRI curves, extending beyond the 1,000-ft depth, to characterize the deeper soils. For instance, the "1,000-2,000 ft" curve was extrapolated by "off-setting" this curve by the amount shown between the "250-500 ft" and "500-1,000 ft" curves in EPRI TR-102293 (EPRI, 1993). To assess the adequacy of EPRI curves for the deeper soils, these were compared with the set of curves derived from the RCTS results for the upper soils, as shown in Figure 2.5-237. The comparison indicates that:

- Marlboro Clay and Patuxent/Arundel Clay Curves: the EPRI curves are identical and fall nearly half-way between the RCTS-based curves for the Stratum I Sand (Curve 3) and Strata II and III soils (Curve 2) in their G/Gmax relationship and closer to Curve 3 in their damping relationship. Based on the available RCTS results, it is inconceivable for these soils at such great depths (and expected high strength) to behave as "softly" as Stratum I Sand (Curve 3) which is at relatively shallow depths and primarily non-plastic. Therefore, as a minimum, the Marlboro and Patuxent/Arundel clays are expected to behave closer to that represented by Curve 2. On this basis. Curve 2 is a reasonable representation for these soils and is used for the dynamic characterization of Marlboro Clay and Patuxent/Arundel Clay.

- Aguia/Brightseat Sand and Patapsco Sand: the EPRI curves are nearly identical and follow Curve 2 closely in their G/Gmax and damping relationship. Based on the RCTS results, and given their depths, these soils are expected to behave somewhere in the region represented by Curves 1 and 2, and possibly closer to Curve 1. Given that a number of the RCTS tests on sandy soils banded closely and were represented by Curve 2, the deeper sandy soils of the Aguia/Brightseat and Patapsco are expected to produce relationships that are mimicked by Curve 2, as a minimum. On this basis., Curve 2 is a reasonable representation for these soils and is used for the dynamic characterization of Aguia/Brightseat Sand and Patapsco Sand.

The calculated maximum strains based on the initially adopted EPRI curves for soils below 1000 feet are in the 10^{-3}% to 10^{-2}% range for the 1E-4 and 1E-5 rock input motions, respectively, as shown in Figure 2.5-238. At such strain levels, the difference between the EPRI-based and RCTS-based curves are minor to insignificant as evident in Figure 2.5-237. Therefore the potential impact of variation of the extrapolated curves on the site response analysis is negligible and is conservatively covered by the randomization of the soil column and strain dependant properties as described in Section 2.5.2.

EPRI curve selection for the upper 400 ft of the site soils was based on available soil characterization data from the site investigation.

A detailed description of the RCTS curve fitting process is provided in the report "Reconciliation of EPRI and RCTS Results, Calvert Cliffs Nuclear Power Plant Unit 3" (Bechtel, 2007), and is included as COLA Part 11J.

The strain dependent properties are first developed for the Powerblock Area. After fitting EPRI curves to the RCTS data in the Powerblock, the resulting curves were used as a starting point to fit the data of the Intake Area and develop properties for that zone. The damping ratio curves are truncated at 15 percent, consistent with the maximum damping values that will be used for the site response analysis. The backfill RCTS results were used to develop strain dependent properties following the same fitting approach and using EPRI curves for granular soils. The following tables and figures provide the strain dependant properties for the CCNPP project:

- Table 2.5-61 and Figure 2.5-170 provide the properties for the Powerblock Area.
- Table 2.5-62 and Figure 2.5-171 provide the properties for the Intake Area.
- Table 2.5-63 and Figure 2.5-172 provide the properties for Backfill.

Bedrock Properties

The two velocity profiles for the Chester and Lexington Park sites (Figure 2.5-157 and Figure 2.5-158), indicate the presence of "hard" rock (identified with V_s = 9,200 ft/sec). Hard rocks typically exhibit an elastic response to loading, with little, if any, change is stiffness properties. For the range of shear strains anticipated in the analysis (10^{-4} to 1 percent range), essentially no shear modulus reduction is expected; therefore, for rocks at the site, the estimated shear moduli should remain unaffected, given the relatively high velocity observed from the area rocks.

Hard rocks are considered to have damping, but it is not strain dependent. A damping ratio of 1 percent has been used for bedrock at other sites, e.g., for the Vogtle Early Site Permit application (SNOC, 2006) in order to obtain compatibility with soils above bedrock. Experience on similar work has indicated that using damping ratios of 0.5 percent, 1 percent, 2 percent, and 5 percent produces essentially identical results (Dominion, 2006). Therefore, for CCNPP Unit 3, a damping ratio of 1 percent was adopted for the bedrock. Bedrock shear modulus was considered to remain constant, i.e., no degradation, in the shear strain range of 10^{-4} percent to 1 percent.

The rock unit weight was estimated from the available literature (Deere, et al., 1996), as 162 pcf.

2.5.4.3 Foundation Interfaces

Subsurface profiles (at the corresponding locations shown in Figure 2.5-103, Figure 2.5-104, and Figure 2.5-105) depicting the inferred subsurface Stratigraphy with the location of the plant's facilities are presented in the following figures:

- Subsurface and excavation profile Powerblock Area A-A': Figure 2.5-160.
- Subsurface and excavation profile Powerblock Area B-B': Figure 2.5-161.
- Subsurface and excavation profile Powerblock Area C-C': Figure 2.5-162.

- Subsurface and excavation profile Powerblock Area D-D': Figure 2.5-163.
- Subsurface and excavation profile Powerblock Area E-E': Figure 2.5-164.
- Subsurface and excavation profile Powerblock Area F-F': Figure 2.5-165.

Excavation and dewatering issues are addressed in Section 2.5.4.5. Settlement and bearing capacity are discussed in Section 2.5.4.10. Slope stability analysis is discussed in Section 2.5.5.

2.5.4.4 Geophysical Surveys

Section 2.5.4.2.2 provides a description of the geophysical surveys performed. Section 2.5.4.2.5.8 provides a detailed description of the interpretation and recommendation of properties for dynamic soil profiles. The main goal of the surveys was to gather the information to provide a recommendation for velocity profiles underneath foundation footprints.

The best estimate of the shear and compression shear wave velocity profiles are presented by the following four figures:

1. Figure 2.5-166, showing the best estimate velocity profiles in the Powerblock Area.
2. Figure 2.5-167, showing the best estimate velocity profiles in the Powerblock Area, after placement of fill.
3. Figure 2.5-168, showing the best estimate velocity profiles in the Intake Area.
4. Figure 2.5-169, showing the best estimate velocity profiles in the Intake Area, after placement of fill.

2.5.4.5 Excavation and Backfill

Sections 2.5.4.5.1 through 2.5.4.5.4 are added as a supplement to the U.S. EPR FSAR.

2.5.4.5.1 Source and Quantity of Backfill and Borrow

A significant amount of earthwork is anticipated in order to establish the final site grade and to provide for the final embedment of the structures. It is estimated that approximately 3.5 million cubic yards (cyd) of materials will be moved during earthworks to establish the site grade.

The materials excavated as part of the site grading are primarily the surficial soils belonging to the Stratum I Terrace Sand. To evaluate these soils for construction purposes, 20 test pits were excavated at the site. The maximum depth of the test pits was limited to 10 ft. Results of laboratory testing on the bulk samples collected from the test pits for moisture-density and other indices are included in COLA Part 11J and Part 11K. The results clearly indicate that there are both plastic and non-plastic soils included in Stratum I soils, including material designated as fill. These fill soils are predominantly non-plastic. A similar observation was made from the borings that extended deeper than the test pits. Their composition consists of a wide variety of soils, including poorly-graded sand to silty sand, well graded sand to silty sand, clayey sand, silty sand, clay, clay of high plasticity, and silt of high plasticity, based on the USCS. The highly plastic or clay portion of these soils will not be suitable for use as structural fill, given the high

percentage of fines (average 59 percent) and the average natural moisture content nearly twice the optimum value of 10 percent. The remaining sand or sandy portion will be suitable; however, these materials are typically fine (sometimes medium to fine) sand in gradation, and likely moisture-sensitive that may require moisture-conditioning. Additionally, the suitable portions of the excavated soils are used for site grading purposes, with very little, if any, remaining to be used as structural fill.

It is estimated that about 2 million cyd of structural backfill are needed. Therefore, structural fill will be obtained from off-site borrow sources. An off-site borrow source of structural fill for CCNPP Unit 3 has been identified, Vulcan Quarry in Havre de Grace, Maryland. Details of the engineering and chemical properties of the backfill are provided in Section 2.5.4.2.4.

2.5.4.5.2 Extent of Excavations, Fills, and Slopes

In the area of CCNPP Unit 3, the current ground elevations range from approximately El. 50 ft to El. 120 ft, with an approximate average El. 88 ft. The finished grade in CCNPP Unit 3 Powerblock Area ranges from about El. 75 ft to El. 85 ft; with the centerline of Unit 3 at approximately El. 85 ft. Earthwork operations are performed to achieve the planned site grades, as shown on the grading plan in Figure 2.5-173. All safety-related structures are contained within the outline of CCNPP Unit 3, except for the water intake structures that are located near the existing intake basin, also shown in Figure 2.5-173. Seismic Category I structures with their corresponding foundation are:

- Nuclear Island Common Basemat (El. 41.5).
- Emergency Power Generating Building (El. 76).
- Essential Service Water Buildings (El. 61.0).
- Ultimate Heat Sink Makeup Water Intake Structure (El. -26.5).

Excavation profiles (at the corresponding locations shown in Figure 2.5-103, Figure 2.5-104, and Figure 2.5-105) are shown in:

- Subsurface and excavation profile Powerblock Area A-A': Figure 2.5-160.
- Subsurface and excavation profile Powerblock Area B-B': Figure 2.5-161.
- Subsurface and excavation profile Powerblock Area C-C': Figure 2.5-162.
- Subsurface and excavation profile Powerblock Area D-D': Figure 2.5-163.
- Subsurface and excavation profile Powerblock Area E-E': Figure 2.5-164.
- Subsurface and excavation profile Intake Area F-F': Figure 2.5-165.

These figures illustrate that excavations for foundations of Seismic Category I structures will result in removing Stratum I Terrace Sand and Stratum IIa Chesapeake Clay/Silt in their entirety, and will extend to the top of Stratum IIb Chesapeake Cemented Sand, except in the Intake Area. In the Intake Area, the foundations are supported on Stratum IIc soils, given the interface proximity of Strata IIb and IIc.

The depth of excavations to reach Stratum IIb is approximately 40 ft to 45 ft below the final site grade in the Powerblock Area. Since foundations derive support from these soils,

variations in the top of this stratum were evaluated, reflected as elevation contours for the top of Stratum IIb in CCNPP Unit 3 and in CLA areas, as shown in Figure 2.5-174. The variation in top elevation of these soils is very little, approximately 5 ft or less (about 1 percent) across each major foundation area. The extent of excavations to final subgrade, however, is determined during construction based on observation of the actual soil conditions encountered and verification of their suitability for foundation support. Once subgrade suitability in Stratum IIb soils is confirmed, the excavations are backfilled with compacted structural fill or, if necessary, lean concrete is placed in lieu of structural fill.

The properties of lean concrete are controlled through controlling its compressive strength. A minimum 28-day compressive strength of 2,500 psi is used. Properties of lean concrete are controlled during construction. Detailed project specifications include requirements for mix design, placement, sampling and testing, frequency of testing, applicable standards, and acceptance criteria. Lean concrete may be used in lieu of structural fill in the following cases: below the foundations as leveling mats, to counteract seepage forces at the bottom of the excavation and to help preserve soil subgrade integrity, and in restricted spaces to expedite construction.

Subsequent to foundation construction, the structural fill is extended to the final site grade, or near the final site grade, depending on the details of the final civil design for the project. Compaction and quality control/quality assurance programs for backfilling are addressed in Section 2.5.4.5.3.

Once the design foundation elevation is reached, two methods of verifying the competent foundation soils may be used. The first method is to proof roll the entire excavated area with a compaction vehicle or approved equivalent until the grade offers a relatively unyielding surface (i.e., less than one inch). Any areas that exhibit excessive (i.e., greater than one inch) rutting, pumping or yielding will be identified by the Geotechnical Engineer and the construction contractor will undercut these areas until the intended competent Stratum is encountered as verified by additional proof rolling. The second method is to perform in-situ compaction testing by means of ASTM D7380-08 "Standard Test Method for Soil Compaction Determination (Dynamic Cone Penetration)" (ASTM 2008b) and/or ASTM D1556 "Test Method for Density and Unit Weight of Soil in-Place by Sand-Cone Method" (ASTM 2007b). Structural backfill placement will not begin until the unsuitable material of the final excavation grade has been verified and approval received from the Geotechnical Engineer.

Permanent excavation and fill slopes, created due to site grading, are addressed in Section 2.5.5. Temporary excavation slopes, such as those for foundation excavation, are graded on an inclination not steeper than 2:1 horizontal:vertical (H:V) or even extended to inclination 3:1 H:V, if found necessary, and having a factor of safety for stability of at least 1.30 for static conditions.

Excavation for the Ultimate Heat Sink Makeup Water Intake Structure is different than that for other CCNPP Unit 3 structures, as shown in Figure 2.5-165. Given the proximity of this excavation to the Chesapeake Bay, this excavation is made by installing a sheetpile cofferdam that not only provides excavation support but also aids with the dewatering needs. This is addressed further in Section 2.5.4.5.4.

Excavation for Seismic Category I electrical duct banks and pipes in the Powerblock Area involve the removal of Stratum I Terrace Sand in its entirety to the top of Stratum IIa

Chesapeake Clay/Silt. Such excavation is required since the Stratum I layer has potential for liquefaction, as indicated in Section 2.5.4.8.

2.5.4.5.3 Compaction Specifications

Testing of structural backfill is described in Section 2.5.4.2.4. For foundation support and backfill against walls, structural fill should be granular in nature, with well-graded sand, gravel or crushed gravel, and typically should not contain more than 10 percent by weight of material passing No. 200 sieve and no less than 95 percent by weight passing the 3/4-inch sieve. The maximum allowable aggregate size shall be 1 inch. Gradation shall be determined in accordance with ASTM D422 and D1140. Structural fill should consist of durable materials free from organic matters or any other deleterious or perishable substances, and of such a nature that it can be compacted readily to a firm and non-yielding state.

Structural fill will be compacted at a moisture content of ±3 percent of the optimum, and compaction will be done to 95 percent of Modified Proctor optimum dry density. The maximum dry density and optimum moisture content is determined in accordance with ASTM D1557, "Standard Test Methods for Laboratory Compaction Characteristics of Soil Using Modified Effort (56,000 ft-lbf/ft^3(2700 kN-m/m^3))," (ASTM, 2009).

Fill materials need to be placed in horizontal layers usually not greater than 8 inches in loose thickness. Each layer is required to be spread evenly and mixed thoroughly to obtain uniformity of material and moisture in each layer. When the moisture content of the fill material is below that specified, water needs to be added until the moisture content is as specified. When the moisture content of the fill material is too high, the fill material needs to be aerated through blading, mixing, or other satisfactory methods until the moisture content is as specified. After each fill layer has been placed, mixed and spread evenly, it needs to be thoroughly compacted to the specified degree of compaction. Compaction needs to be accomplished by acceptable types of compacting equipment. The equipment is required to be of such design and nature that it is able to compact the fill to the specified degree of compaction. Compaction should be continuous over the entire area and the equipment should make sufficient passes to obtain the desired uniform compaction.

Continuous geotechnical engineering observation and inspection of fill placement and compaction operations is required to certify and ensure that the fill is properly placed and compacted in accordance with the project plans and specifications. Field density tests in accordance with ASTM D1556 "Standard Test Method for Density and Unit Weight of Soil in Place by Sand-Cone Method, American Society for Testing and Materials" (ASTM, 2007b) are required to be performed for each layer of fill. Moisture content may be determined in the laboratory in accordance with ASTM D2216, "Standard Test Methods for Laboratory Determination of Water (Moisture) Content of Soil and Rock by Mass" (ASTM, 2005c) or in the field using nuclear methods in accordance with ASTM D6938 "Standard Test Method for In-Place Density and Water Content of Soil and Soil-Aggregate by Nuclear Methods (Shallow Depth)," (ASTM, 2008b). If the surface is disturbed, the density tests are to be made in the compacted materials below the disturbed zone. When these tests indicate that the degree of compaction of any layer of fill or portion thereof does not meet the specified minimum requirement, the particular layer or portions requires reworking until the specified relative compaction is obtained.

At least one in-place moisture content and field density test are required on every 10,000 square feet of each lift of fill, and further placement is not allowed until the required relative compaction has been achieved. The number of tests is increased if a visual inspection

determines that the moisture content is not uniform or if the compacting effort is variable and not considered sufficient to meet the project specification. For critical areas, at least one in-place moisture content and field density test are required at least every 200 cubic yards of compacted fill.

Testing and analysis will be performed to confirm the structural fill shear wave velocity at the bottom of the basemats for Seismic Category I and Seismic Category II-SSE structures meets or exceeds the requirements in Table 2.4-1. The testing will consist of shear wave velocity (V_S) measurements using Spectral Analysis of Surface Waves (SASW). The testing frequency will be selected to produce a V_S profile with depth, at three locations per SASW line. The initial SASW testing will be performed at the foundation elevation along a line (either east-west or north-south) beneath the center line of each structure. A second line, parallel to the first line (and at the same elevation) will be carried out adjacent to each structure in areas free from foundations or other structures. The third and final SASW line will be performed at the final rough or finished grade elevations directly above the second line tested in the area free from foundations. The first and second lines of testing allow direct comparison of the fill quality and variability at the level of the foundation. The second and final testing allows assessment of the increase in V_S with increasing confining pressure due to the backfill loading at the same vertical location. Given the consistency between the first and second SASW lines, conclusions can be drawn regarding the relationship between V_S and confining pressure beneath the structure. The recorded V_S measurements will also be compared with V_S measurements from RCTS testing at comparable confining pressures, allowing correlation of design (laboratory-based) and actual (field-based) measurements.

In addition to SASW testing, a second geophysical method (e.g., down-hole testing) will be utilized to measure VS at one location at final rough or finished grade for each structure for redundancy and confirmation purposes. The NRC will be informed of critical dates for testing of structural fill so they may observe the testing process.

The backfill supplier will submit samples of backfill prior to placement to perform tests such as Modified Proctor, grain size and chemical properties. The number of samples should adequately cover each of the backfill supply batches. Samples should be collected in accordance with ASTM D75. Each sample should be representative of the material from a single source. Testing will be performed by an independent qualified laboratory.

Careful inspection and testing during fill placement will be enforced and fill placement progress interrupted if required. The number of tests will be sufficient to adequately represent the backfill for each lift. The number of samples and quality control testing will be indicated by the testing specification.

2.5.4.5.4 Dewatering and Excavation Methods

Groundwater control is required during construction. Groundwater conditions and dewatering are addressed in Sections 2.4.12.5 and 2.5.4.6.

Given the soil conditions, excavations are performed using conventional earth-moving equipment, likely using self-propelled scrapers with push dozers, excavators and dump trucks. Most excavations should not present any major difficulties. Blasting is not anticipated. The more difficult excavations would have been in Stratum IIb Cemented Sand, due to the cemented nature and proximity to groundwater, but the cemented portions are not planned to be excavated, except where minor excavations are needed due to localized conditions or due to deeper foundation elevations such as at the Ultimate Heat Sink Makeup Water Intake

Structure area. Excavations in localized, intermittent cemented soils may require greater excavating effort, such as utilizing hoe-rams or other ripping tools; however, these zones are very limited in thickness, with probably only occasional need for expending additional efforts. Excavations for the CCNPP Unit 3 powerblock foundations are planned as open cut. Upon reaching the final excavation levels, all excavations are cleaned of any loose materials, by either removal or compaction in place. All final subgrades are inspected and approved prior to being covered by backfill or concrete. The inspection and approval procedures are addressed in the foundation and earthworks specifications developed during the detailed design stage of the project. These specifications include measures, such as proof-rolling, excavation and replacement of unsuitable soils, and protection of surfaces from deterioration.

As discussed in Section 2.5.4.5.2, excavation for the Ultimate Heat Sink Makeup Water Intake Structure requires the installation of a sheetpile cofferdam. The sheetpile structure extends from the ground surface to a depth of about 50 ft. The full scope of the sheetpile cofferdam is developed during the detailed design stage of the project. Excavation of soils in this area should not present any major difficulties given their compactness.

Foundation rebound (or heave) is monitored in excavations for selected Seismic Category I structures. Rebound estimates are addressed in Section 2.5.4.10. Monitoring program specifications are developed during the detailed design stage of the project. The specification document addresses issues, such as the installation of a sufficient quantity of instruments in the excavation zone, monitoring and recording frequency, and evaluation of the magnitude of rebound and settlement during excavation, dewatering, and foundation construction.

2.5.4.6 Groundwater Conditions

Sections 2.5.4.6.1 through 2.5.4.6.5 are added as a supplement to U.S. EPR FSAR.

2.5.4.6.1 Groundwater Conditions

Details of available groundwater conditions at the site are given in Section 2.4.12. The shallow (surficial) groundwater level in the CCNPP Unit 3 area ranges from approximately El. 68 to El. 85.7 ft, or an average El. of 80 ft. This elevation is considered as the in-situ, current condition groundwater elevation. Similarly, the groundwater level associated with the deeper hydrostatic surface was found to range from approximately El. 16 ft to El. 42 ft, with an average El. of 34 ft. Available observation well data indicate the groundwater table in the Intake Area is at about El. 3 ft.

The shallow groundwater should have little to no impact on the stability of foundations, as the site grading and excavation plans will implement measures to divert these flows away from excavations, i.e., through runoff prevention measures and/or ditches. There are no Seismic Category I foundations planned within the upper water-bearing soils. Groundwater in the powerblock after construction is expected to be at El. 55. Additional detail is provided in Section 2.4.12.

2.5.4.6.2 Dewatering During Construction

Temporary dewatering is required for groundwater management during construction. On the basis of defined groundwater conditions, groundwater control/construction dewatering is needed at the site during excavations for the Powerblock Area foundations. Groundwater associated with seepage in the shallow (upper) zones (Surficial aquifer) is controlled through site grading and/or a system of drains and ditches, as previously discussed. This may also consist of more positive control, including a series of sumps and pumps strategically located in

the excavation area to effectively collect and discharge the seepage that enters the excavation, in addition to ditches, drains, or other conveyance systems.

The drainage ditches are installed below grade level, at the peripheries, as the excavation progresses. These ditches are oriented in approximately north-south and east-west directions, i.e., at excavation corners or more frequently as warranted during construction. Once at the final subgrade, stone-filled drains are installed in the excavation interior for control of upward seepage, if any. These drains are in turn connected to exterior ditches and sumps. Each sump is equipped with a pump of sufficient capacity for efficient groundwater removal. Based on the estimated lateral groundwater flow rate derived in Section 2.4.12.5, a total of four pumps with capacity of 100 gpm each will be used for the dewatering.

Temporary dewatering is required for the excavation of the Ultimate Heat Sink Makeup Water Intake Structure and other neighboring structures. A sheetpile cofferdam, designed to aid with dewatering, needs to be extended into low permeability soils; however, some level of groundwater control is still required to maintain a relatively "dry" excavation during construction. As a minimum, pumps are installed to control and/or lower the groundwater level inside the cofferdam. Given the limited excavation size, one 100 gpm pump is sufficient for control of groundwater in this excavation.

Additional auxiliary pumps are available for removal of water from excavations during periods of unexpected storm events. The groundwater level in excavations will be maintained at a minimum of 3 ft below the final excavation level.

2.5.4.6.3 Analysis and Interpretation of Seepage

Analysis of the groundwater conditions at the site is ongoing at this time, given continued groundwater monitoring that is still in progress, as addressed in Section 2.4.12. A groundwater model, based on information currently available, has been prepared for the overall groundwater conditions at the site and is addressed in detail in Section 2.4.15. The groundwater program and milestones are provided in Section 2.4.12.

2.5.4.6.4 Permeability Testing

Testing for permeability of the site soils was performed using Slug tests, as discussed in Section 2.5.4.2.3. A detailed description of the tests and the results is provided in Section 2.4.12. A summary of the hydraulic conductivity values is presented in Table 2.5-33.

2.5.4.6.5 History of Groundwater Fluctuations

A detailed treatment of the ground water conditions is provided in Section 2.4.12.

2.5.4.7 Response of Soil and Rock to Dynamic Loading

The spectra developed in Section 2.5.2.6 and its specific location at a free ground surface reflect the seismic hazard in terms of PSHA and geologic characteristics of the site and represent the site-specific ground motion response spectrum. These spectra are modified to develop ground motion for design considerations. Detailed descriptions on response of site soils and rocks to dynamic loading are addressed in Section 2.5.2, a Site SSE for design is developed in Section 3.7.1.

2.5.4.8 Liquefaction Potential

The potential for soil liquefaction at the CCNPP Unit 3 site was evaluated following NRC Regulatory Guide 1.198 (USNRC, 2003c). The soil properties and profiles utilized are those described in Section 2.5.4.2.

Sections 2.5.4.8.1 through 2.5.4.8.6 are added as a supplement to the U.S. EPR FSAR.

2.5.4.8.1 Previous Liquefaction Studies

Two liquefaction studies are cited in the CCNPP Units 1 and 2 UFSAR (BGE, 1982), as follows. The same reference cites a horizontal ground acceleration of 0.08 g and a Richter magnitude of 4 to 5 for the OBE case, and a horizontal ground acceleration of 0.15 g and a Richter magnitude of 5 to 5.5 for the SSE case.

CCNPP Units 1 and 2 UFSAR (BGE, 1982) reports that the liquefaction potential at the site was evaluated using data from standard penetration test borings, laboratory test results, in-place density determinations, and geologic origin of the site soils. The results showed that the site soils did not possess the potential to liquefy. Quantitative values for the factor of safety against liquefaction were not given.

CCNPP Units 1 and 2 UFSAR (BGE, 1982) also reports on results of a liquefaction study for the siting of the Diesel Generator Building in the North Parking area as a part of CCNPP Units 1 and 2 development. This liquefaction evaluation was performed on data from standard penetration test borings, resulting in computed factors of safety from 1.3 to 2.4, with a median value of 1.8. On this basis, it was determined that the site of the Diesel Generator Building had adequate factor of safety against liquefaction (Bechtel, 1992).

2.5.4.8.2 Soil and Seismic Conditions for CCNPP Unit 3 Liquefaction Analysis

Preliminary assessments of liquefaction for the CCNPP Unit 3 soils were based on observations and conclusions contained within CCNPP Units 1 and 2 UFSAR (BGE, 1982). The site soils that were investigated for the design and construction of CCNPP Units 1 and 2 did not possess the potential to liquefy. Given the relative uniformity in geologic conditions between existing and planned units, the soils at CCNPP Unit 3 were preliminarily assessed as not being potentially liquefiable for similar ground motions, and were further evaluated for confirmation, as will be described later in this subsection. Based on this assessment, it was determined that aerial photography as outlined in Regulatory Guide 1.198 (USNRC, 2003c) would not add additional information to the planning and conduct of the subsurface investigation; therefore, was not conducted.

A common stratigraphy was adopted for the purpose of establishing soil boundaries for liquefaction evaluation. The adopted stratigraphy was that shown generically in Figure 2.5-106 and also by the velocity profiles shown in Figure 2.5-167 and Figure 2.5-169. Only soils in the upper 400 ft of the site were evaluated for liquefaction, based on available results from the CCNPP Unit 3 subsurface investigation. Soils below a depth of 400 ft are considered geologically old and sufficiently consolidated. These soils are not expected to liquefy, as will be further discussed in Section 2.5.4.8.4.

The liquefaction analysis was performed using a peak ground acceleration (PGA) of 0.15 g from the Site Safe Shutdown Earthquake (SSE) developed in Section 3.7.1. A sensitivity calculation was developed to study the impact that a distant, higher magnitude event, with lower acceleration would have in the Factor of Safety against liquefaction. The controlling distant event with magnitude 6.9 was used along with a maximum ground acceleration of

0.1g. The sensitivity analysis indicates that the Factor of Safety against liquefaction is about 14% larger for such scenario.

2.5.4.8.3 Liquefaction Evaluation Methodology

Liquefaction is defined as the transformation of a granular material from a solid to a liquefied state as a consequence of increased pore water pressure and reduced effective stress (Youd, et al., 2001). The prerequisite for soil liquefaction occurrence (or lack thereof) are the state of soil saturation, density, gradation and plasticity, and earthquake intensity. The present liquefaction analysis employs state-of-the-art methods (Youd, et al., 2001) for evaluating the liquefaction potential of soils at the CCNPP Unit 3 site. Given the adequacy of these methods in assessing liquefaction of the site soils, and the resulting factors of safety which will be discussed later in this subsection, probabilistic methods were not used.

In brief, the present state-of-the-art method considers evaluation of data from SPT, V_s, and CPT data. Initially, a measure of stress imparted to the soils by the ground motion is calculated, referred to as the cyclic stress ratio (CSR). Then, a measure of resistance of soils to the ground motion is calculated, referred to as the cyclic resistance ratio (CRR). Finally, a factor of safety (FOS) against liquefaction is calculated as a ratio of cyclic resistance ratio and cyclic stress ratio. Details of the liquefaction methodology and the relationships for calculating CSR, CRR, FOS, and other intermediate parameters such as the stress reduction coefficient, magnitude scaling factor, accounting for non-linearity in stress increase, and a host of other correction factors, can be found in Youd (Youd, et al., 2001). A magnitude scaling factor (MSF) of 1.93 was used in the calculations based on the adopted earthquake magnitude and guidelines in Youd (Youd, et al., 2001). Below are examples of liquefaction resistance calculations using the available SPT, V_s, and CPT data in the Powerblock Area and Intake Area. Calculations were performed mainly using spreadsheets, supported by spot hand-calculations for verification.

2.5.4.8.4 FOS Against Liquefaction Based on SPT Data

The equivalent clean-sand $CRR_{7.5}$ value, based on SPT measurements, was calculated following recommendations in Youd (Youd, et al., 2001), based on corrected SPT N-values $(N_1)_{60}$, including corrections based on hammer-rod combination energy measurements at the site. The soils at CCNPP site include clean granular soils with $(N_1)_{60}30$ that are considered too dense to liquefy and are classified as non-liquefiable (Youd, et al., 2001). Similarly, corrections were made for the soils fines contents, based on average fines contents and the procedure recommended in Youd (Youd, et al., 2001).

The collected raw (uncorrected) SPT N-values are shown in Figure 2.5-113 and Figure 2.5-114. SPT data from the figures were used for the liquefaction FOS calculations for over 2000 SPT N-value data points. The results are shown in Figure 2.5-176for the Powerblock Area and Figure 2.5-177 for the Intake Area.

For completeness, all data points, including data for clay soils and data above the groundwater level, were included in the FOS calculation, despite their known high resistance to liquefaction. The SPT N-values shown in Figure 2.5-113 and Figure 2.5-114 were mostly taken at 5-ft intervals. SPT in the deepest borings (B-301 and B-401) extended to about 400 ft below the ground surface.

Of the over 2,000 SPT N-value data points for which FOS values were calculated, no points resulted with FOS<1.1 below foundation grade.

Soils indicating FOS<1.1 are either at elevations that will eventually be lowered during construction which would result in the removal of these soils, or are at locations where no structures are planned. Hence, the low FOSs are not a concern for these samples. Based on SPT data, there is no potential for liquefaction for the CCNPP3 Unit 3 Powerblock and Intake Areas.

2.5.4.8.5 FOS Against Liquefaction Based on Shear Wave Velocity Data

Similar to the FOS calculations for the SPT values, equivalent clean-sand $CRR_{7.5}$ values, based on V_s measurements, were calculated following recommendations in Youd (Youd, et al., 2001). Soils at the CCNPP site include soils with normalized shear wave velocity (VS_1) exceeding a value of 215 m/s (705 fps). Clean granular soils with V_{S1} larger than 215 m/s (705 fps) are considered too dense to liquefy and are classified as non-liquefiable (Youd, et al., 2001). The limiting upper value of V_{S1} for liquefaction resistance is referred to as V_{S1}*; the latter varies with fines content and is 215 m/s (705 fps) and 200 m/s (656 fps) for fines contents of less than 5 percent and larger than 35 percent, respectively. As such, when values of V_{S1} are larger than V_{S1}*, the soils were considered too dense to liquefy, and therefore, the maximum CRR value of 0.5 was used in the FOS calculations.

Shear wave velocity data from the P-S logging measurements were used for the FOS calculations. The collected raw (uncorrected) V_s data are shown in Figure 2.5-118 and Figure 2.5-119 for the Powerblock and Intake Areas respectively. Suspension P-S velocity logging measurements were made at 0.5-m intervals (~1.6-ft). The two deepest measurements (at borings B-301 and B-401) extended to about 400 ft below the ground surface. Approximately 1,400 V_s data points were used for the FOS calculations. The results showing FOS against liquefaction using the shear wave velocity data are provided in Figure 2.5-178 and Figure 2.5-179.

The results show that all calculated FOSs exceeded 1.1 with significant margin; almost all are at least 4.0, with a few scattered values at about 2.0. The high calculated FOS values are the result of V_{S1} values typically exceeding the limiting V_{S1}* values, indicating no potential for liquefaction. Based on shear wave velocity data, there is no potential for liquefaction for the CCNPP Unit 3 Powerblock and Intake Areas.

2.5.4.8.6 FOS Against Liquefaction Based on CPT Data

The CPT testing at the CCNPP Unit 3 site included the measurement of both commonly measured cone parameters (tip resistance, friction, and pore pressure) and shear wave velocity. The evaluation of liquefaction based on both the commonly measured parameters and shear wave velocity is addressed herein. The CCNPP Powerblock CPT data was reviewed and correlated with the applicable SPT data and compared with guidelines in Robertson (Robertson, et al., 1988). This review process verified the CPT data by correlation to the CCNPP Unit 3 site-determined SPT values.

The equivalent clean-sand $CRR_{7.5}$ value, based on CPT tip measurements, was calculated following recommendations in Youd (Youd, et al., 2001), based on normalized clean sand cone penetration resistance $(q_{c1N})_{cs}$ and other parameters such as the soil behavior type index, Ic.

Cone tip resistance values from CPT soundings are shown in Figure 2.5-115 and Figure 2.5-116for the Powerblock and Intake Areas respectively. The CPT soundings encountered repeated refusal in the cemented sand layer, and could only be advanced deeper after pre-drilling through these soils, indicative of their high level of resistance to liquefaction. The deepest CPT sounding (C-407) penetrated 142 ft below the ground surface, encountering refusal at that depth, terminating at approximately El. -80 ft. Tip resistance measurements

were made at 5-cm intervals (~2-in). The results showing FOS against liquefaction using the CPT data are provided in Figure 2.5-180 and Figure 2.5-181 for the Powerblock and Intake Areas, respectively. For completeness, all data points, including data for clay soils, were included in the calculation, despite their known high resistance to liquefaction.

Only data points in the upper layers resulted in FOS < 1.1. CPT-based CRR relationship was intended to be conservative, not necessarily to encompass every data point; therefore, the presence of a few data points beyond the CRR base curve is acceptable (Youd, et al., 2001). The soils in Stratums I and IIa will be removed during construction. In addition an extremely conservative margin is adopted by using a PGA value of 0.15 g. Based on CPT data, there is no potential for liquefaction for the CCNPP3 Powerblock and Intake Areas.

2.5.4.8.7 Liquefaction Resistance of Soils Deeper Than 400 Feet

Liquefaction evaluation of soils at the CCNPP Unit 3 site was focused on soils in the upper 400 ft. The site soils, however, are much deeper, extending to approximately 2,500 ft below the ground surface. Geologic information on soils below a depth of 400 ft was gathered from the available literature, indicating that these soils are from about 50 to over 100 million years old. Liquefaction resistance increases markedly with geologic age, therefore, the deeper soils are geologically too old to be prone to liquefaction. Additionally, their compactness and strength are only anticipated to increase with depth, compared with the overlying soils. The Pleistocene soils have more resistance than Recent or Holocene soils and pre-Pleistocene sediments are generally immune to liquefaction (Youd, et al., 2001). Additionally, liquefaction analyses using shear wave velocity values of about 2,000 ft/sec near the 400-ft depth did not indicate any potential liquefaction at that depth, with the FOSs exceeding 5.0. With shear wave velocities increasing below the 400-ft depth, in the range of about 2,200 ft/sec to 2,800 ft/sec as indicated in Figure 2.5-166 through Figure 2.5-169, high resistance to liquefaction would be expected from these deeper soils. On this basis, liquefaction of soils at the CCNPP Unit 3 site below a depth of 400 ft is not considered possible.

2.5.4.8.8 Potential for Liquefaction of Backfill

Section 2.5.4.5 describes material specifications and compaction for structural fill. For foundation backfill, compaction will be done to 95 percent of Modified Proctor optimum dry density. The fill will be compacted to within 3 percent of its optimum moisture content.

Liquefaction in an engineered fill is not an issue if the recommended compaction practices are followed. Liquefaction occurs in loose sands and/or silts with poor gradation. An engineered fill is a compacted and well graded soil structure. Compaction practices need to be monitored during construction. Liquefaction of granular engineered fills will be prevented by assuring that the fill specifications are met during the implementation stages. Particular attention will be placed on the grain size and compaction requirements to ensure the specifications are fully met. Specifications for fill will include requirements for an on-site testing laboratory for quality control, especially material gradation and plasticity characteristics, the achievement of specified moisture-density criteria, fill placement/compaction, and other requirements to ensure that the fill operations conform to the earthwork specification for CCNPP Unit 3.

Regardless of the non-liquefiable nature of engineered fills, the liquefaction potential was also evaluated with the shear wave velocity approach. Figure 2.5-167 indicates that the values for the backfill are 790, 900, and 1080 fps. The 790 fps backfill will not be exposed to saturated conditions since it only corresponds to the first six ft from the surface. The results of the analysis are shown in Figure 2.5-182. Based on shear wave velocity data, there is no potential for liquefaction for the CCNPP3 backfill.

2.5.4.8.9 Concluding Remarks on Liquefaction Analysis

It is evident, from the collective results, that soils at the CCNPP Unit 3 site are overly-consolidated, geologically old, and sometimes even cemented. They are not susceptible to liquefaction due to acceleration levels from the anticipated earthquakes. A very limited portion of the data at isolated locations indicated potentially liquefiable soils, however, this indication cannot be supported by the overwhelming percentage of the data that represent these soils. Moreover, the state-of-the-art methodology used for the liquefaction evaluation was intended to be conservative, not necessarily to encompass every data point; therefore, the presence of a few data points beyond the CRR base curve is acceptable (Youd, et al., 2001). Additionally, in the liquefaction evaluation, the effects of age, overconsolidation, and cementation were ignored. These factors tend to increase resistance to liquefaction. Finally, the earthquake acceleration and magnitude levels adopted for the liquefaction analysis are conservative. More importantly, there is no documented liquefaction case for soils in the State of Maryland (USGS, 2000). Therefore, liquefaction is not a concern. A similar conclusion was arrived at for the original CCNPP Units 1 and 2 (BGE, 1982).

A significant level of site grading is anticipated at the CCNPP Unit 3 site during construction. This primarily results in the removal of geologically younger materials (the upper soils) from the higher elevations, and the placement of dense compacted fill in lower elevations. Limited man-made fill may be already present at the CCNPP Unit 3 site at isolated locations. These soils will be removed during construction.These activities, further improve the liquefaction resistance of soils at the site.

2.5.4.8.10 Regulatory Guide 1.198

Before and during the liquefaction evaluation, guidance contained in NRC Regulatory Guide 1.198 (USNRC, 2003c) was used. The liquefaction evaluation conforms closely to the NRC Regulatory Guide 1.198 guidelines.

Under "Screening Techniques for Evaluation of Liquefaction Potential," NRC Regulatory Guide 1.198 (USNRC, 2003c) lists the most commonly observed liquefiable soils as fluvial-alluvial deposits, eolian sands and silts, beach sands, reclaimed land, and uncompacted hydraulic fills. The geology at the CCNPP site includes fluvial soils and man-made fill at isolated locations. The liquefaction evaluation included all soils at the CCNPP site. The man-made fill, which is suspected only at isolated locations, will be removed during the site grading operations. In the same section, NRC Regulatory Guide 1.198 (USNRC, 2003c) indicates that clay to silt, silty clay to clayey sand, or silty gravel to clayey gravel soils can be considered potentially liquefiable. This calculation treated all soils at the CCNPP Unit 3 site as potentially liquefiable, including the fine-grained soils. The finer-grained soils at the CCNPP Unit 3 site contain large percentages of fines and/or are plastic and are, therefore, considered non-liquefiable, as also indicated by the calculated FOSs for these soils. In fact, all soils at the CCNPP Unit 3 site contain some percentage of fines and exhibit some plasticity, which tends to increase their liquefaction resistance. The same section of NRC Regulatory Guide 1.198 (USNRC, 2003c) confirms that potentially liquefiable soils that are currently above the groundwater table, are above the historic high groundwater table, and cannot reasonably be expected to become saturated, pose no potential liquefaction hazard. In the liquefaction analyses, the groundwater level was taken at elevation 80 ft. This water level may be a "perched" condition, situated above Stratum IIa Chesapeake Clay/Silt, with the actual groundwater level near the bottom of the same stratum in the Chesapeake Cemented Sand, or at about an average El. 39 ft. Despite the adopted higher groundwater level (a higher piezometric head of more than 40 ft), the calculated FOS overwhelmingly exceeded 1.1. The site historic groundwater level is not known, however, it is postulated that the groundwater level at the site has experienced some

fluctuation due to pumping from wells in the area and climatic changes. Groundwater levels at the site are not expected to rise beyond El. 55 ft in the future given the relief and topography of the site, promoting drainage. Similarly, NRC Regulatory Guide 1.198 (USNRC, 2003c) indicates that potentially liquefiable soils may not pose a liquefaction risk to the facility if they are insufficiently thick and of limited lateral extent. At the CCNPP Unit 3 site, the soil layers are reasonably thick and uniformly extend across the site, except where they have been eroded, yet the FOSs overwhelmingly exceeded 1.1. Soils identified as having FOS<1.1, regardless of the thickness, will be removed during grading operations or are located where no structures are planned.

Under "Factor of Safety Against Liquefaction," NRC Regulatory Guide 1.198 (USNRC, 2003c) indicates that FOS=1.1 is considered low, FOS=1.1 to 1.4 is considered moderate, and FOS = 1.4 is considered high. A FOS = 1.1 appears to be the lowest acceptable value. On the same issue, the Committee on Earthquake Engineering of the National Research Council (CEE, 1985) states that "There is no general agreement on the appropriate margin (factor) of safety, primarily because the degree of conservatism thought desirable at this point depends upon the extent of the conservatism already introduced in assigning the design earthquake. If the design earthquake ground motion is regarded as reasonable, a safety factor of 1.33 to 1.35... is suggested as adequate. However, when the design ground motion is excessively conservative, engineers are content with a safety factor only slightly in excess of unity." This, and a minimum FOS = 1.1 in NRC Regulatory Guide 1.198 (USNRC, 2003c), are consistent with the FOS = 1.1 adopted for the assessment of FOSs for the CCNPP Unit 3 site soils, considering the conservatism adopted in ignoring the cementation, age, and overconsolidation of the deposits, as well as the seismic acceleration and magnitude levels. Such level of conservatism in the evaluation, in conjunction with ignoring the geologic factors discussed above, justifies the use of FOS = 1.1 for liquefaction assessment of the CCNPP site soils.

2.5.4.9 Earthquake Site Characteristics

Section 2.5.2.6 describes the development of the horizontal ground motion response spectra (GMRS) for the CCNPP Unit 3 site. The selected ground motion is based on the risk-consistent/ performance-based approach of NRC Regulatory Guide 1.208, "A Performance-Based Approach to Define the Site-Specific Earthquake Ground Motion" (USNRC, 2007b) with reference to NUREG/CR-6728 (REI, 2001) and ASCE/SEI 43-05 (ASCE, 2005). Any deviation from the guidance provided in Regulatory Guide 1.208 is discussed in Section 2.5.2. Horizontal ground motion amplification factors are developed in Section 2.5.2.5 using site-specific data and estimates of near-surface soil and rock properties presented in Section 2.5.4. These amplification factors are then used to scale the hard rock spectra, presented in Section 2.5.2.4, to develop a soil Uniform Hazard Spectra (UHS), accounting for site-specific conditions using Approach 2A of NUREG/CR-6769 (USNRC, 2002). Horizontal spectra are developed from these soil UHS, using the performance-based approach of ASCE/SEI 43-05, accepted by Regulatory Guide 1.208. The motion is defined at the free ground surface of a hypothetical outcrop at the base of the foundation. Section 2.5.2.6 also describes vertical ground motion, which was developed by scaling the horizontal ground motion by a frequency-dependent vertical-to-horizontal (V:H) factor, presented in Section 2.5.2.6. Section 3.7.1 develops a Site Safe Shutdown Earthquake (Site SSE) that satisfies the minimum Safe Shutdown Earthquake Ground Motion for design identified in paragraph (d)(1) of 10 CFR 100.23 (CFR, 2007).

2.5.4.10 Static Stability

The CCNPP Powerblock Area is graded to establish the final site elevation, which will range from about El. 81 ft to 85 ft. An average grade elevation of 83 ft is assumed. The Reactor, Safeguards, and Fuel Buildings are seismic Category I structures and are supported on a

common basemat. For a basemat thickness of 10 ft and top of basemat about 31.5 ft below grade, the bottom of the basemat would be 41.5 ft below the final site grade, or El. 41.5 ft. The common basemat has an irregular shape, approximately 80,000 square feet (sq ft) in plan area, with outline dimensions of about 363 ft x 345 ft. For bearing capacity and settlement estimation, a representative foundation is used. Table 2.5-64 presents the values for elevation, depth, area, and loads of the seismic Category I structures and the main structures in the Powerblock area. This information is also shown in Figure 2.5-183.

Construction of the common basemat requires an excavation of about 41 to 42 ft (from approximately El. 83 ft). The resulting rebound (heave) in the ground due to the removal of the soils is expected to primarily take place in Stratum IIc Chesapeake Clay/Silt soils. A rebound of about 4 in is estimated due to excavation for the common basemat, and is expected to take place concurrent with the excavation. Ground rebound is monitored during excavation. The heave estimate is made based on the elastic properties of the CCNPP site soils and the response to the unloading of the ground by the excavation. The magnitude and rate of ground heave is a function of, among other factors, excavation speed and duration that the excavation remains open. Other factors remaining unchanged, shorter durations culminate in smaller values of ground heave.}

2.5.4.10.1 Bearing Capacity

The U.S. EPR FSAR includes the following COL Item in Section 2.5.4.10.1:

> A COL applicant that references the U.S. EPR design certification will verify that site-specific foundation soils beneath the foundation basemats of Seismic Category I structures have the capacity to support the bearing pressure with a factor of safety of 3.0 under static conditions.

This COL Item is addressed as follows:

{The ultimate bearing capacity of safety-related buildings for the Powerblock and Intake Areas is estimated using the closed form solutions proposed by Vesic (Vesic, et al., 1975) and Meyerhof (Meyerhof, et al., 1978). Factors of safety are obtained for different soil profile cases and compared with standard practice allowable values.

The soil profiles of CCNPP Unit 3 and Intake Areas are used in the analysis in order to determine the corresponding layer thickness and material properties. Stratum thicknesses and elevations are presented in Table 2.5-25.

Weighted average values of soil parameters are used in the analysis; weight factors are based on the relative thickness of each stratum within a specific depth (i.e. depth equal to the least lateral dimension of the building).

The water table in the Powerblock Area is conservatively considered to be at El. 83 ft, which corresponds to the average grade surface elevation. For the Intake Area, the water table is considered to be at El. 10 ft, which also corresponds to the average grade surface elevation. With the higher groundwater level, the bearing capacity estimate will be more conservative since overburden resistance is diminished by increased buoyant effect.

Average values of the soil strength parameters (c', Φ', s_u, γ) are considered in the analysis. Average unit weights are calculated using data from the entire CCNPP Unit 3 area (limited number of samples were available for strength parameters in the Powerblock Area, therefore

data from the Construction Laydown Area (CLA) area are included in the calculation of the average values). Sand layers present a relatively low cohesion due to the presence of fine particles, based on laboratory tests results. However, for this analysis the cohesion for sand layers is conservatively not considered (c′ = 0).

The ultimate static bearing capacity of a footing supported on homogeneous soils can be estimated using the following equation (Vesic, et al., 1975):

$$q_{ult} = cN_c s_c d_c i_c g_c b_c + \frac{1}{2}\gamma' B' N_\gamma s_\gamma d_\gamma i_\gamma g_\gamma b_\gamma r_\gamma + qN_q s_q d_q i_q g_q b_q$$

Where:

q_{ult}	→	Ultimate bearing capacity;
c	→	Cohesion;
N_c , N_γ , N_q	→	Bearing capacity factors;
		$N_q = e^{\pi \tan\Phi}\tan^2(45 + \Phi/2)$; $N_c = (N_q - 1)\cot\Phi$; $N_\gamma = 2(N_q + 1)\tan\Phi$;
Φ	→	Friction angle;
s_c , s_γ , s_q	→	Foundation shape correction factors;
d, i, g, b	→	Shape, depth, and inclination factors;
r_γ	→	Foundation size correction factor;
γ′	→	Effective unit weight of foundation media;
B′	→	Effective foundation width;

Three different cases are considered in the analysis:

a. Soil subsurface including all strata: For this case, weighted average values of the strength parameters are used based on relative thickness of each stratum in the zone between the bottom of the footing and a depth B below this point, where B is the least lateral dimension of the building. For this case, effective soil parameters are used (drained conditions). (Vesic, et al. 1975)

b. Soil subsurface considering only stratum IIb Chesapeake Cemented Sand. Soil parameters of this layer are used for the entire depth. For this case, effective soil parameters are used (drained conditions). (Vesic, et al. 1975)

c. The ultimate static bearing capacity of a footing supported on a dense sand stratum over a soft clay stratum can be estimated using the punching shear failure with a circular slip path (Meyerhof, et al., 1978):

$$q_{ult} = q_{u,b} + \frac{2\gamma_1 1 H_t^2}{B}\left(1 + \frac{2D}{H_t}\right)K_{ps}\tan\Phi_1 - \gamma_1 H_t \leq q_{ut}$$

$$q_{u,b} = c_2 N_{c_2}\,\zeta_{c_2} + \frac{1}{2}\gamma'_2 B' N_{\gamma_2}\,\zeta_{\gamma} 2r\gamma + \gamma'_1(H_t + D)N_{q_2}\,\zeta_{q_2}$$

$$q_{ut} = c_1 N_{c_1} \zeta_{c_1} + \frac{1}{2}\gamma'_1 B' N_{\gamma_1} \zeta_{\gamma_1} r_\gamma + \gamma'_b D N_{q_1} \zeta_{q_1}$$

Where:

q_{ult}	→	Ultimate bearing capacity;
$q_{u,b}$	→	Ultimate bearing capacity of a very thick bed of the bottom soft clay layer;
q_{ut}	→	Ultimate bearing capacity of upper dense sand layer;
γ'_1	→	Effective unit weight of the upper sand layer;
γ'_2	→	Effective unit weight of the lower clay layer;
γ'_β	→	Effective unit weight of backfill;
Φ_1	→	Friction angle of upper sand layer;
Φ_2	→	Friction angle of lower clay layer;
c_1	→	Cohesion of upper sand layer;
c_2	→	Cohesion of lower clay layer;
H_t	→	Depth from footing base to soft clay;
D	→	Depth from of footing base below ground surface;
K_{ps}	→	Punching shear coefficient;
B′	→	Effective foundation width;
ζ_q , ζ_c , ζ_γ	→	Geometry Factors;
N_c , N_γ , N_q	→	Bearing capacity factors;

Buildings are considered to have an equivalent rectangular foundation with the same area and moment of inertia as the original footprint shape. The analysis is preformed using uniformly distributed loads in all buildings. For the NI Common Mat, an average uniform load is used including the loads from the Reactor, Safeguard and Fuel Buildings. The vertical load imposed by adjacent structures is conservatively not included in the calculation of bearing capacity of each building, only the surcharge imposed by the backfill is considered.

The vertical loads and dimensions of the buildings that comprise the NI common mat are not symmetrical. This will result in overturning moments around the centroid of the common mat that will reduce the contact area of the foundation and hence the bearing capacity. To account for this reduction in the contact area, an effective area is used in the bearing capacity equations. The length (L) and width (B) of the foundation's footprint are reduced in proportion to the eccentricity of the resultant vertical force. For the CCNPP3 NI common mat the asymmetry in dimensions and static loads is not significant; the effective area is approximately 98% of the total area.

The Meyerhof model represents a more realistic approach to calculate the bearing capacity of the soil subsurface at CCNPP 3, by considering a dense sand layer overlying a softer clay layer. This model considers a punching shear failure mechanism between both layers.

A summary of the calculated allowable static and dynamic bearing capacities using both the layered and the homogeneous soil conditions are presented in Table 2.5-65. A factor of safety of 3.0 for static loads (dead plus live loads) and 2.0 for dynamic loading are typically considered to be acceptable.

A dynamic bearing capacity analysis was performed to assess the impact of seismic forces that produce overturning moments in the foundation. During overturning, the effective supporting area is reduced, resulting in a decrease in the bearing capacity of the subsurface. To take into account this effect and simulate the potential for higher edge pressures during dynamic loading, the seismic bearing capacity is calculated for three different foundation widths: B1 = 270 ft , B2 = 203 ft, and B3 = 135 ft, which correspond to the original foundation width, and two reduced values. The reduction for B2 and B3 is 25% and 50% are considered as a sensitivity analysis of the effective bearing area. The results of the analysis are provided in Table 2.5-74.

Even if the foundation width is reduced by half (B3 = 135 ft), the allowable dynamic bearing capacity (58.5 ksf) is larger than the AREVA design certification requirement of 26 ksf. For the case with average soil strength parameters and the original foundation width (B1=270 ft), the allowable dynamic bearing capacity is 72.9 ksf.

The dynamic bearing capacity of 72.9 ksf is lower than the allowable static bearing capacity of 87.8 ksf (Vesic method). The deduction due to seismic forces in this case is around 17%. For the same case, the deduction of ultimate static bearing capacity is approximately 45%. Lower deductions are expected for allowable bearing capacities since a smaller factor of safety is considered for the dynamic case. The factors of safety are FOS = 3 for static loading and FOS = 2 for dynamic loading.

Table 2.0-1 compares CCNPP Unit 3 site Characteristic Values with U.S. EPR FSAR design Parameters. The static and dynamic bearing capacity exceed the requirements established for the NI, EPGB and ESWB as shown in Table 2.0-1.

For static and dynamic loading conditions, and based on a factor of safety of 3.0 (static) and 2.0 (dynamic), the site provides adequate allowable bearing capacity.}

2.5.4.10.2 Settlement

The U.S. EPR FSAR includes the following COL Item in Section 2.5.4.10.2:

> A COL applicant that references the U.S. EPR design certification will verify that the differential settlement value of ½ inch per 50 ft in any direction across the foundation basemat of a Seismic Category I structure is not exceeded. Settlement values larger than this may be demonstrated acceptable by performing additional site specific evaluations.

This COL Item is addressed as follows:

{The surface topography and subsurface conditions of the CCNPP Unit 3 Powerblock Area make the estimation of settlement and building tilt complex. The objective of the settlement analysis of the CCNPP Powerblock Area is to provide an estimate of the time dependant settlement and heave distribution throughout the footprint of the Powerblock Area, including maximum settlement and tilt estimated for each of the facilities.

The settlement analysis of the CCNPP Powerblock Area was carried out under the following premises:

- Develop a three-dimensional model capable of capturing irregular subsurface conditions, realistic foundation footprint shapes, and asymmetric building loads;

- Perform a time-dependant simulation, that provides settlement and tilt estimates as a function of time through and after construction;
- Incorporate a construction sequence and examine the behavior of settlement and tilt as buildings are erected;
- Account for asymmetric topography, by recognizing that reloading time to original consolidation pressure after excavation will be variable throughout the foundation footprint;
- Perform the settlement analysis simultaneously for the NI and adjacent facilities, including the detached safety related structures (EPBG and ESWB);

2.5.4.10.2.1 Settlement Calculation Methodology

In order to address the issues described above, a Finite Element Method (FEM) model of the subsurface and structural interfaces was developed. The FEM has the capability of providing a numerical solution to the general equations of elasticity in continuous media. The settlement analysis of the CCNPP Powerblock Area is performed with the computer application PLAXIS 3D Foundation v2 (PLAXIS3D) (DUTP, 2007). The application has been validated and verified under the Paul C. Rizzo Associates, Inc. (RIZZO) Quality Assurance Program. The settlement computations have also been performed under RIZZO QA Program.

PLAXIS3D provides a FEM solution of the virtual work equation defining equilibrium conditions and natural boundary conditions in a differential equation form. The program calculates displacements with the use of numerical integration methods. In addition to the typical capabilities of a general FEM application for elastic solids, PLAXIS incorporates advanced constitutive models, (stress vs. strain relationships) that are capable of simulating the response of soils to external loading. Such response includes both elastic/elastoplastic displacement and consolidation. This feature makes PLAXIS3D a unique application for the analysis of foundation systems and its applicability to the CCNPP Powerblock settlement problem is ideal. The application allows for the elaboration of a three-dimensional representation of the subsurface conditions and the building geometries. The model is capable of capturing variation of soil properties below the footprints of the foundation and therefore it is possible to better assess differential settlement. All structures in the Powerblock Area are modeled simultaneously and load increments are applied in different steps in time.

The Mohr-Coulomb constitutive model is selected for the analysis. Other soil hardening constitutive models introduce further sophistication to account for the stress-dependency of the stiffness, but are slightly less conservative when compared to the Mohr-Coulomb model. This analysis accounted for increased unload and reload elastic moduli with the use of conservative ratios applied at different time steps during the unloading and loading sequence. This approach provided a better understanding of the effect that irregular topographic conditions had in settlement and tilt. Further details are provided in the following sections.

2.5.4.10.2.2 Settlement and Heave Analysis in the CCNPP Powerblock Area

The settlement analysis of the Powerblock Area is based on an FEM model of approximately 2500 ft x 2500 ft x 840 ft (Length x Width x Depth). The area occupied by the buildings is

approximately 1100 ft by 1100 ft. There are 42,130 nodes in the model. The boundary conditions for the sides of the model included allowing the vertical displacement, and restraining the two horizontal displacement components. The bottom of the model was restrained in vertical and horizontal directions. The free drainage conditions for consolidation were adapted on the model boundaries. Since the model boundaries were far enough from the loaded areas, the primary direction for the water flow is the vertical direction. In other words, the sides of the model are far enough from the loaded areas so that the consolidation behavior is not impacted by the free-drainage conditions implemented on the sides of the model.

Soil profiles, such as those shown by Figure 2.5-107, were taken as the basis for the geotechnical input of the FEM model. In addition, data from boreholes B-311, B-313, B-334, B-335, B-344, and B-357A were included to adequately represent the three-dimensional nature of the model. PLAXIS3D interpolates information between borehole locations to obtain the three-dimensional representation of the subsurface conditions, as shown in Figure 2.5-184. The figure presents a reduced version of one of the excavation profiles to illustrate how the FEM geometry conforms to the subsurface conditions. The CCNPP Powerblock Area model is a comprehensive mathematical representation of the physical conditions at the site.

The analysis depth is approximately twice the width of the NI foundation footprint. Therefore, given the dimensions of the NI common basemat, the model depth was extended to El. -760 ft. This was achieved by extending the Nanjemoy sand (the continuous soil layer deeper than -208 ft elevation) to the bottom of the model.

Two separate models were developed for the CCNPP Powerblock Area:

1. An Excavation and Dewatering Model (ED Model).

2. Construction and Post-Construction Model (CPC Model).

Heave Analysis: Excavation and Dewatering (ED Model)

On saturated soils, prior to excavation, it is necessary to dewater the excavation area. As water is extracted from the voids, soils will consolidate and settlement due to dewatering will take place. In addition, soils beneath dewatered areas will experience increased loading as consolidation of upper layers takes place. The effect that dewatering has on settlement depends on the soil properties, the hydrogeologic conditions, and to some extent on the pumping rates.

At the CCNPP Powerblock Area, the Stratum IIa Chesapeake Clay/Silt isolates the upper surficial aquifer from the layers beneath. The surficial aquifer is confined by the first clay layer and it does not influence the soils at and beneath foundation elevation. Therefore, dewatering will not produce settlement at the foundation level. In consequence soils will not experience increased stress due to dewatering and such increase need not be accounted for as an excess consolidation pressure as it is typically done if the surficial aquifer was not confined.

Heave will be experienced after excavation and the ED FEM model was used to estimate its magnitude. For this model, the Powerblock Area was divided in three zones considering different average ground elevations for each zone. The subdivision was performed based on the site topography information, as shown in Figure 2.5-185. The zones are:

- Zone I: low areas North East (Plant Local Coordinate System) with an average ground elevation of 60 ft;
- Zone II: South areas (Plant Local Coordinate System) with an average ground elevation of 80 ft;
- Zone III: high areas with an average ground elevation of 105 ft.

The division was done to capture the difference in heave resulting from different depths of excavation. As shown by the resulting variable heave distribution in Figure 2.5-186, the effect of topography is adequately captured. As expected, the magnitude of heave is directly related to the surface topography. Between the end of excavation and the beginning of construction, the maximum reported heave at the center of containment (Point C) is 4.7 in. Most of the heave is elastic and is experienced immediately after excavation. Table 2.5-66 provides heave results for the four locations shown in Figure 2.5-186.

Once excavation is completed, the foundation surface will be prepared for the placement of foundations. Settlement in the following sections will be reported from the beginning of construction or the initial reloading of the soil.

Settlement Analysis: Construction and Post-Construction (CPC Model)

The CPC model was designed to evaluate the settlements during and after construction. This model is not a continuation of the ED model. The excavation and dewatering stages included in ED model were assumed to be completed, and the excess pore pressure generated due to excavation and dewatering fully dissipated. As previously stated, settlement will be reported from the beginning of construction and beyond. The analysis also assumes that the ground surface was re-leveled after the immediate heave. As previously stated, long term heave is a small fraction of the total displacement when compared to the immediate elastic value.

The initial effective stress condition for the CPC model was in accordance with the post-excavation overburden geometry. The model assumes an average surface Elevation of 83 ft. The effect of asymmetric topography is evaluated by performing sensitivity analysis on the value of the initial ground surface elevation (i.e., initial overburden stress). A detailed discussion is provided later in this Section.

The building loads were applied in eight sequential steps as specified by Table 2.5-67. The table corresponds to the construction schedule. The loading sequence is also shown in Figure 2.5-187. Settlement analysis is conducted at the application of each step, accounting for both immediate and consolidation settlements. After the application of the last loading sequence and finalization of construction, partial rewatering occurs in the construction area. The final groundwater elevation is El. 55 ft. The construction schedule affects the timing of the settlement and tilt during construction. However, end values will be similar if variations that are typical during construction take place.

Backfill between El. 41.5 ft and El. 83 ft was placed in the first five steps indicated by Table 2.5-67 as follows:

1. During Step 1, backfill is placed between El. 41.5 ft and El. 48 ft.
2. During Step 2, additional backfill is placed between El. 48 ft and El. 61 ft.
3. During Step 3, additional backfill is placed between El. 61 ft and El. 66 ft.

4. During Step 4, additional backfill is placed between El. 66 ft and El. 76 ft.

5. During Step 5, additional and final backfill is placed between El. 76 ft and El. 83 ft.

The groundwater elevation in the Powerblock Area was modeled at El. 38 ft during construction to account for dewatering. Around the Powerblock Area, the groundwater elevation was maintained at El. 69 ft. For the post-construction conditions, groundwater elevation in the Powerblock Area was increased up to El. 55 ft and remained constant at that level, while the groundwater elevation around the Powerblock Area remained at El. 69 ft. Post construction groundwater levels will have little impact on the construction settlement.

The stiffness of the foundation mats is also accounted for in the analysis. As the construction proceeds, the deflection pattern of the foundations is expected to be closer to the rigid body motion due to the additional stiffness introduced into the foundation by the structure itself. The stiffness of the foundation mat was transitioned from an initial value based on a 10 ft thick concrete mat to a stiff, rigid-body like condition at the end of construction.

The soil properties used in the settlement analysis are provided in Section 2.5.4.2.5. The soil properties that directly impact the settlement analysis are:

- Unit Weight,
- Permeability and Coefficient of Consolidation,
- Strength parameters, used in the Mohr-Coulomb constitutive model,
- Elastic Modulus and Poisson Ratio,
- Ratio of Unload/Reload Modulus to Elastic Modulus.

The elastic modulus in the deeper Nanjemoy Sand was increased linearly, as a function of depth from its estimated value of 3,170 ksf at the interface with Layer IIC. The value of E at the lower boundary of the FEM model is 4,600 ksf, which corresponds to a rate increase of 2.6 ksf/ ft. The increase was performed according to the following relationship (DUTP, 2007) (Schanz, et al., 1999) applicable to a sand with no cohesion:

$$E = E_{ref}\sqrt{\frac{(1-\sin\Phi)\sigma'_1}{p_{ref}}}$$

Where:

E	→	Elastic modulus at desired depth (El. -760 ft, end of FEM model);
E_{ref}	→	Reference elastic modulus, calculated with effective vertical stress at El. -207.5 (Nanjemoy Sand top horizon elevation);
Φ	→	Friction angle (40°);
p_{ref}	→	Reference pressure (100 pressure units);
σ'_1	→	Effective vertical stress;

During the analysis, it was required to account for the asymmetric distribution of surface topography throughout the Powerblock Area. This condition is especially important for the NI

common basemat. Figure 2.5-175 clearly shows that the existing surface grade at the NI changes up to 50 ft in elevation. At the lower portions, the construction of the plant will reach the original pre-consolidation pressure relatively soon. On the contrary, for high elevation points, this condition will be reached at later stages into the construction. During the first six steps of construction, some points throughout the foundation footprint will be experiencing reloading, while others are subject to loads that are higher than the original overburden pressure. This fact will have direct influence in the estimation of tilt. The topographic conditions suggest that there is potential for the NI common basemat to present additional tilt towards the North or North East (Local Coordinates) direction along the cross section indicated in Figure 2.5-175.

In order to incorporate the influence of surface topography into the settlement estimates, sensitivity on the initial average surface elevation was performed according to the following cases:

1. *Settlement Representative of Low Surface Elevation Zones:* The unloading/reloading modulus was used until the end of the second loading step, when the reloading for the North East part of the Powerblock Area is expected to be completed. For Step three the elastic modulus value was reverted to its lower counterpart (loading Elastic modulus). This case represents the stress-stiffness correspondence for the parts of the Powerblock Area with an initial pre-excavation ground surface of about El. 60 ft.

2. *Settlement Representative of Medium Surface Elevation Zones:* The unloading/reloading modulus was used until the end of the third and fourth loading steps. These cases represent the stress-stiffness correspondence for the parts of the Powerblock Area with an initial pre-excavation ground surface of about El. 80 ft. These two cases cover the elevation range of most of the Powerblock Area.

3. *Settlement Representative of High Surface Elevation Zones:* The unloading/reloading modulus was used until the end of the fifth loading step, when reloading is expected to be completed for the totality of the footprint area. This case represents the stress-stiffness correspondence for the parts of the Powerblock Area with an initial pre-excavation ground surface of about El. 105 ft.

By performing the settlement analysis under multiple scenarios, it is possible to assign the most representative case for each point throughout the foundation footprint, and obtain a reliable estimate of the increase of tilt for each structure, specifically the NI. Figure 2.5-188 provides a conceptual representation of the three cases previously described. Depending on the original surface elevation with respect to plant grade, each zone throughout the footprint will be best represented by one of the three cases.

Settlement Analysis Results

The following plots and tables are provided for the purposes of presenting settlement and tilt estimates:

- Figure 2.5-190: Settlement vs. Time for center point of NI;

  This figure presents the calculation of settlement for cases that consider different initial elevations of surface topography. As previously discussed, revert from reloading

to loading modulus occurs sooner for low elevation points and therefore the low elevation case indicates larger settlement. Using conservatism, the case that best represents settlement at center point of containment is the case denominated "Medium Elevation E Revert (2)". According to this case, total settlement at centerline of the reactor building is estimated at 12.7 in.

Tilt across the NI, especially running West to East and South West to North East (Local Plant coordinates) will be heavily influenced by the variation of surface topography throughout the NI footprint. The relevance of such influence is directly related to the difference in settlement reported by the analysis cases shown in Figure 2.5-190.

- Figure 2.5-189: Settlement contour plot from FEM model (Medium Elevation Topography);

  The contour plots provide the incremental settlement from the Medium Elevation E Revert(2) case, reported after the application of each loading sequence. The maximum settlement for the NI footprint is estimated at 12.7 in. The plots shows the influence that the Nuclear Island has over the rest of the buildings. In general, the Powerblock Area will present a tilt tendency from the perimeter to the center of the footprint. Long term settlement beyond construction will be influenced by secondary consolidation and rewatering.

- Table 2.5-68: Settlement vs. Time for center point of each foundation (Medium Elevation Topography) and Figure 2.5-191, Settlement at the Center Point of Safety Related Buildings;

- Table 2.5-68 presents the tabular data of settlement under the footprint of each facility from the Medium Elevation E Revert(2) case. As expected, the Fuel Building and NI present the highest settlement. Figure 2.5-191 is the graphical representation of the settlement data provided by Table 2.5-68;

- Figure 2.5-192: Settlement tracking cross-sections;

  Tilt was recorded for several cross sections, as indicated by Figure 2.5-192. The selection of the cross-sections was done to assure that maximum tilt is captured.

- Figure 2.5-193: Foundation base settlement for four sections of the NI and Turbine Building;

  The figure indicates how the foundation settles after each step of the construction sequence. The results in the figure correspond to data resulting from the topography case that conservatively provides settlement at the centerline of the reactor ("Medium Elevation E Revert (2)").

- Table 2.5-73 presents differential settlements between the NI and adjacent buildings. The differential settlements are also shown in Table 2.5-73. Figure 2.5-192 shows the location of points considered for differential settlements.

  Differential settlements between the NI and each adjacent building are determined for pairs of points at the center of the NI and each surrounding building, and also for pairs of points at the edges of the NI and each surrounding building. For the edge to edge case, the closest points for the selected building pairs are considered. Also considered is the differential settlement between RWPB and NAB.

While calculating the differential settlement, the effect of the construction sequence is considered. The output from the model consists of settlements at the end of each one of 8 loading steps. The construction sequence indicates that construction of different buildings start at different loading steps. For example, EPGB construction starts at the 6th loading step, and any deformation obtained from the model prior to 6th loading step should be subtracted from the total deformation obtained at the end of 8th loading step. This correction aims to address the fact that construction for each building is expected to start on a level ground.

Differential settlements (Δu_y) for the pairs were computed by using the definition below:

$$(\Delta u_y) = (u_y)_{Adj.Bldg.} - (u_y)_{NI}$$

where $(u_y)_{Adj.Bldg.}$ and $(u_y)_{NI}$ are the settlements at the end of 8^{th} loading step and at the base of the adjacent building and NI, respectively.

The U.S. EPR standard design does not include specific requirements for the differential settlements between buildings. As shown in Table 2.5-73, the largest inter-building differential settlement was close to 9.8 inches between the center of the NI and the center of EPGB2. This difference will be minimized by the time interval in construction, much of the NI settlement will have occurred prior to connection being made between the buildings. The side-by-side Seismic Category I Buildings have edge-to-edge differential settlements of less than an inch. Thus, differential settlements expected between Cat I buildings do not pose a construction concern.

- Table 2.5-69: Maximum recorded tilt for the structures in the Powerblock Area.
- Figure 2.5-194: provides the settlement underneath each facility corresponding to the cases that analyze the sensitivity on surface topography. Low elevation points will have an increase in settlement after adjustment and high elevation points will see their settlement estimates reduced.

Long Term Settlement (Creep and Rewatering)

Long term settlements related to secondary consolidation or rewatering are estimated to be very small and both aspects will counteract each other. The stress increase induced by loading are consistently lower than the pre-consolidation condition. At CCNPP the ratio of final applied stress to the preconsolidation pressure always remains below 0.7 for the Stratum IIc Chesapeake Clay layer. The effective stress is always in the recompression range and secondary settlement is not significant (Terzaghi, et al., 1995).

Settlement Monitoring

A settlement monitoring program will be enforced to record heave of the excavation bottom, the effect of dewatering and the effect of Nuclear Island Basemat loading during and after construction. This is necessary to confirm that the estimated rate of heave and settlement is consistent with the field observations. The purpose of this monitoring program is to assess and document the actual settlements in comparison with the predicted and the acceptable limits. The settlement monitoring program consists of three primary elements:

- Piezometers to measure effects of dewatering and pore pressures in a soil layer prone to consolidation type settlement. Vibrating wire piezometers are preferred for this purpose as they are adequately sensitive and responsive and easily record positive

and negative changes on a real time basis. Piezometers should be screened in Stratum II-B (Chesapeake Cemented Sand) and Stratum II-C (Chesapeake Clay/Silt).

- Settlement monuments placed directly on concrete, preferably on the Mud Mat and on the corners of the structures at grade that are accessible with conventional surveying equipment.

- Settlement sensors and extensometers if monuments are not practical or if fills are used over consolidation type soils and it is necessary to monitor settlement of the consolidation type soils independent of the consolidation of the fill.

The instrumentation plan for the Powerblock Area of the site will consist of horizontal settlement sensors, Vibrating Wire (VW) piezometers, surface monuments, concrete anchored monuments, extensometers and one accelerometer. The definitive number of instruments needs to be established during design stages of the monitoring system. The tentative locations of the instruments are shown on Figure 2.5-239.

Tested and calibrated settlement sensors will be used to monitor settlement and heave within the excavation footprint. Settlement sensors will be installed at the bottom of the proposed foundation (bench mark El. 40) before the excavation of the Powerblock Area is started. The sensors will be placed at the approximate locations shown on Figure 2.5-239 and the required cables will be routed away from the fill area.

The settlement sensors have two important components, the sensor and the reservoir. The sensor will be located inside the limits of the structural backfill while the reservoir is located outside the fill limits in a borehole attached by a Borros anchor (Dunnicliff, 1988). The reservoir needs to be located on stable ground because it reads difference in settlement between the reservoir and sensor. The wires connecting the sensor to the reservoir are suited for direct burial. The wires shall be buried below the frost line for protection and to minimize temperature differentials that could result in erroneous settlement or heave measurements.

Figure 2.5-239 shows a tentative distribution and placement of VW piezometers to be installed around the Perimeter of the Powerblock Area. The VW piezometers will be used to measure ground water elevations and associated changes in pore pressure during dewatering, excavation, structural backfill placement, and plant construction.

Extensometers shall be installed in the Powerblock Area. These will be installed adjacent to the Reactor building, bench mark elevation 41.5, adjacent to the Turbine building, adjacent to the Essential Service Water Building (ESWB) Nos. 1, 2, and adjacent to ESWB Nos. 3 and 4. At least one extensometer will be installed adjacent to the Radioactive Waste Processing Building. The bench mark for the Turbine Building, ESWB and Radioactive Processing Building is El. 59.5. The extensometers shall be calibrated rod type borehole extensometers. The extensometers will either be protected by raising the standpipe out of the ground approximately one foot or by placing the extensometer approximately 10 to 12 inches below top of the ground surface.

After the structural backfill has been placed to the final grade, Surface Monuments (SM), bench mark El. 80 shall be placed on the surface of the backfill at approximate locations shown on Figure 2.5-239. The monuments shall consist of a one foot diameter concrete cylinders placed a minimum of three feet below final grade and be fitted with a brass dome cap with a point for survey use.

On the side of foundation mats, no later than 28 days after construction, National Geodetic Survey (NGS) (USDC, 1978) survey disks will be placed by drilling a cavity on the side of foundation mats. The cavity will be backfilled with a mortar mix and the survey disk will be anchored into the foundation mat. The disk needs to be located at strategic points of the mat and have a direct view to a benchmark or to other survey points that can relate to a benchmark.

One accelerometer shall be installed to record any seismic events that occur during or after construction. The accelerometer shall be placed within the mat foundation of the Reactor Building.

The Instrumentation Plan for the Makeup Water Intake Structure (MWIS) will consist of settlement sensors, extensometers and one accelerometer. Tentative location of these instruments is shown on Figure 2.5-240. Calibrated settlement sensors will be used to monitor settlement and heave within the excavation footprint of the UHS. Extensometers will be installed adjacent to the Circulating Water Makeup Intake Structure and adjacent to the UHS Makeup Water Intake Structure. The bench mark for the extensometers is El. -26.5. The extensometers shall be calibrated rod type borehole extensometers. The extensometers will either be protected by raising the standpipe out of the ground approximately one foot or placing the extensometer approximately 10 to 12 inches below top of the ground surface. Finally, one accelerometer shall be installed to record any seismic events that occur during or after construction. The accelerometer shall be placed within the foundation of the MWIS.

Each instrument will be read to determine baseline conditions after installation. For the settlement sensors, the baseline readings will be taken before any site earthwork has been performed. The baseline survey should be completed with a minimum of three different readings taken over several days to verify that the readings have stabilized.

Each instrument should be read at least twice a day in the initial stages of this project. During later stages of the project, the reading frequency may be adjusted to once per day and longer at the discretion of the Engineer.

Plots showing movement (settlement or heave) versus time should be maintained during construction, along with estimated load versus time curves. The site should remain dewatered until the curves go asymptotic, at which time connections between buildings can be made. Monitoring should continue after these connections are made in order to assure asymptotic conditions. After construction is completed, all instruments will be monitored for at least one year. At that time, the Engineer will define frequency and instruments to maintain a long-term monitoring program.

Conclusions – Settlement Analysis

The analysis and careful examination of the settlement results provide the following conclusions apply.

- Total average settlement at the end of construction beneath the Reactor Building footprint is estimated at 12.7 in. Settlement for other facilities is provided in Table 2.5-68 and Figure 2.5-194 for the medium topography case.
- Long term settlements related to secondary consolidation or rewatering are estimated to be very small and both aspects will counteract each other.

- Maximum tilt for each building is provided in Table 2.5-69. Maximum tilt is highest for Section CC' of the NI running from south west to north east (Local Coordinates), and Section BB' running west to east.

  Differential settlement or tilt depends on (1) the asymmetric nature of loads, (2) the irregular thickness of the subsurface strata, and (3) the asymmetry in surface topography. The first two are naturally captured by the FEM simulation. The third, influence of asymmetric topography, is captured by means of sensitivity analyses.

- The differential settlement between the NI and TB is provided after each loading step. Since both facilities are founded on different basemats, a discontinuity shows the magnitude of the differential settlement. The same condition applies between the NI and the NAB. The differential settlement between the NI and these two adjacent facilities is estimated to be in the order of one to two inches. Tilt between NAB and RB occurs in opposite directions, and both facilities tilt towards each other. This condition needs to be accounted for in the final design and construction.

- Groundwater is below foundation grade during construction. After construction, groundwater is expected to rise to El. 55. The settlement estimates are not sensitive to variations in the groundwater rebound level, if such variations are in the order of plus or minus ten feet.

The U.S. EPR FSAR Section 2.5.4.10.2 identifies differential settlement as a required parameter to be enveloped, defined as "½ inch per 50 ft in any direction across the foundation basemat of a Seismic Category I structure" and that "values larger than this may be demonstrated acceptable by performing additional site specific evaluations."

The estimated differential settlements do not meet the U.S. EPR FSAR requirement of ½ inch per 50 ft (or 1/1,200); however, additional site specific evaluations will be performed to demonstrate their acceptability, as follows.

To verify that foundations perform according to estimates, and to provide an ability to make corrections, if needed, major structure foundations are monitored for rate of movement during and after construction.

Foundations are designed to safely tolerate the anticipated total and differential settlements. Additionally, engineering measures are incorporated into design for control of differential movements between adjacent structures, piping, and appurtenances sensitive to movement, consistent with settlement estimates. This includes the development and implementation of a monitoring plan that supplies and requires evaluation of information throughout construction and post-construction on ground heave, settlement, pore water pressure, foundation pressure, building tilt, and other necessary data. This information provides a basis for comparison with design conditions and for projections of future performance.

The estimated differential settlements represent departures from the U.S. EPR FSAR requirements. Additional discussion of the acceptability of these estimated differential settlements is provided in Section 3.8.5.

2.5.4.10.2.3 Settlement in the Intake Area

The settlement model in the Intake Area is developed in a similar form. The model is much simpler and the influence of neighboring structures is negligible. The size of the foundation is very small compared to the variability in layer thickness throughout the footprint. Soil layers,

as shown in Figure 2.5-165 are horizontal. There is no additional complication introduced by asymmetric topography. The loading sequence for the Intake Area facilities is applied in a single step. Figure 2.5-195 provides the FEM model for the UHS MWIS.

The total settlement at the end of construction for the facilities in the Intake Area is provided in Table 2.5-70. The maximum total settlement is 3.6 in and the maximum estimated tilt is 0.4 in/50 ft.}

2.5.4.10.3 Uniformity and Variability of Foundation Support Media

The U.S. EPR FSAR includes the following COL Item in Section 2.5.4.10.3:

> A COL applicant that references the U.S. EPR design certification will investigate and determine the uniformity of the underlying layers of site specific soil conditions beneath the foundation basemats. The classification of uniformity or non-uniformity will be established by a geotechnical engineer.

This COL Item is addressed as follows:

{Three criteria are identified in the U.S. EPR FSAR for establishing uniformity in foundation support media, namely, 1) presence of soil and rock, 2) dip angle of soil layers, and 3) shear wave velocity. Each is addressed below:

1. Foundations of all Seismic Category I structures at the CCNPP Unit 3 site are supported on compacted structural fill which is in turn supported on natural soils. Bedrock at the site is very deep, at about 2,500 ft below ground surface. Given the considerable depth to bedrock, non-uniform foundation conditions resulting from combined soil-rock support are not applicable to foundations at the CCNPP Unit 3 site.

2. Detailed subsurface information is presented in Section 2.5.4. Stratigraphic profiles indicate that the stratigraphic lines delineating various soil units have gentle slopes, mostly sloping about 1 to 2 degrees. This is consistent with the regional dip of 1 to 2 degrees in Coastal Plain deposits (refer to Section 2.5.1 for more details). However, at isolated CCNPP Unit 3 locations, stratigraphic units dip steeper, up to about 10 degrees which may be due to inherent assumptions in developing the stratigraphic lines or paleochannels and/or irregular erosional surfaces. Regardless, these steeper angles are less than the dip angle of 20 degrees from the horizontal identified in the U.S. EPR FSAR as the criterion for determining levelness of layers. On this basis, the soil layers at the CCNPP Unit 3 site are considered horizontal. However, the settlement analysis accounts for the variability in the soil media with the implementation of a FEM model as discussed in Section 2.5.4.10.4.

3. Classification of uniformity (or non-uniformity) in foundation support media resides with the geotechnical engineer, per the U.S. EPR FSAR. Shear wave velocity (V_s) measurements are used for this determination because they are a) in-situ measurements reflecting the natural ground conditions and b) important input to the safety evaluation of structures such as in soil-structure interaction and seismic analyses. The V_s values were evaluated to a depth of 344 ft below the Nuclear Island (NI) foundation basemat, corresponding to El. -300 ft. The 344 ft value was selected based

on the three U.S. EPR FSAR criteria of: 1) 1.5 times an equivalent radius of foundation basemat, 2) 1.0 times the maximum foundation basemat dimension, or 3) no less than 200 ft below the bottom of the foundation basemat; with criterion (2) selected as the governing condition for the CCNPP Unit 3 NI basemat for its greater dimension. Minor appendages and protrusions in the irregularly-shaped U.S. EPR NI foundation were ignored in selecting the 344 ft value. The variations in shear wave velocity have been properly accounted for in the dynamic analysis by means of a best estimate soil profile.

Based upon the above, CCNPP Unit 3 is considered a Uniform Site.

2.5.4.10.4 Site Investigation for Uniform Sites

No departures or supplements.

2.5.4.10.5 Site Investigations for Non-uniform Sites

No departures or supplements.

2.5.4.10.6 Earth Pressure

Section 2.5.4.10.6 is added as a supplement to the U.S. EPR FSAR.

Static and seismic lateral earth pressures are addressed for below-grade walls. Seismic earth pressure diagrams are structure-specific. They are only addressed generically herein. Specific earth pressure diagrams are developed for specific structures based upon each structure's final configuration. Passive earth pressures are not addressed; they are excluded for conservatism for general purpose applications. Engineering properties for structural fill are used to estimate earth pressures. The properties of backfill are provided in Section 2.5.4.2.5.9. Structural backfill material is verified to meet the design requirements prior to use during construction. A surcharge pressure of 500 psf applied at the ground surface is assumed. The validity of this assumption will be confirmed during detailed design. In addition to earth pressures associated with the effective pressure distribution of the backfill materials, subsurface structures and walls may also be subjected to surcharge loads caused by heavy equipment operating close to the structure and by increased permanent lateral earth pressures caused by compaction of backfill material with heavy equipment. Compaction-induced earth pressures can cause a significant increase in the permanent lateral earth pressures acting on a vertical wall of a structure. The magnitude of the increase in lateral pressure is dependent, among other factors, on the effective weight of the compaction equipment and the weight, earth pressure coefficient, and Poisson's ratio of the backfill material.

The lateral pressure that will be generated due to the compaction of the backfill is calculated based on the assumption that the equipment can operate to within 6 inches of the wall. Significant reductions in lateral pressures occur as the closest allowable distance to the wall is increased. A 3.2-ton vibratory roller compactor is used to estimate lateral pressures due to compaction. The critical lateral pressure in excess of active and at-rest pressure associated with this equipment is considered to be 400 psf; the critical depth at which this critical pressure is reached, Dc, is 1.7 ft. However, the critical depth is conservatively considered as Dc = 0.

In developing the earth pressure diagrams, the following are assumed:

- Ground surface behind walls is horizontal,
- The side of the wall in contact with the backfill is vertical and there is no friction between the backfill and the wall,
- Retaining walls designed for the active earth pressure are allowed to move laterally, and building walls designed for the at-rest condition are prevented from moving laterally;
- Properties of backfill relevant to the earth pressure calculations are unit weight and angle of shearing resistance. These are provided in Table 2.5-51 and Table 2.5-54 respectively. The values are obtained from laboratory testing of backfill bulk samples and these are 145 pcf and 40°;
- Active and at rest earth pressure coefficients are provided in Table 2.5-58. These values are: $k_A = 0.22$, and $k_0 = 0.36$;
- For active and surcharge pressures, earthquake-induced horizontal ground accelerations are addressed by the application of $k_h g$. Vertical ground accelerations ($k_v g$) are considered negligible and are ignored (Seed, et al., 1970). A seismic horizontal acceleration of 0.15 g is conservatively assumed (consistent with the plant SSE).

2.5.4.10.6.1 Static Lateral Earth Pressures

The static active earth pressure is estimated with the following equation (Lambe, et al., 1969):

$$p_{AS} = K_{AS}\gamma z$$

Where:

p_{AS} → Static active earth pressure;
K_{AS} → Active earth pressure coefficient from Table 2.5-58;
γ → Unit Weight of backfill;
z → Depth below ground surface;

The static at-rest earth pressure is estimated with the following equation (Lambe, et al., 1969):

$$p_{0S} = K_{0S}\gamma z$$

Where:

p_{AS} → At rest earth pressure;
K_{AS} → At rest earth pressure coefficient from Table 2.5-58;
γ → Unit Weight of backfill;
z → Depth below ground surface;

Hydrostatic pressure is accounted for by assuming Groundwater Level at El. 55 ft, which is 13.5 ft above foundation level of the NI.

2.5.4.10.6.2 Seismic Lateral Earth Pressure

The active seismic pressure, p_{AE}, is given by the Mononobe-Okabe equation (Whitman, 1991), represented by:

$$p_{AE} = \Delta K_{AE} \gamma (H - z)$$

Where:

- p_{AE} → Active seismic pressure;
- ΔK_{AE} → Coefficient of active seismic earth pressure ($K_{AE} - K_{AS}$);
- K_{AE} → Mononobe-Okabe coefficient of active seismic earth thrust

$$K_{AE} = \frac{\cos^2(\Phi' - \theta)}{\cos^2\theta \left(\sqrt{\frac{\sin\Phi' \sin(\Phi' - \theta)}{\cos\theta}} \right)^2}$$

- θ → $\theta = \tan^{-1}(k_h)$

- k_h → Seismic coefficient (0.15 g)
- γ → Unit Weight of backfill;
- H → Below-grade height of wall;
- z → Depth below the top of the backfill;

The value ΔK_{AE} can be estimated as 0.75 k_h for k_h values less than about 0.25 g, regardless of the angle of shearing resistance of the backfill (Seed, et al., 1970).

The seismic at-rest pressure ΔK_{0E}, for below-grade walls for Category I structures is evaluated using a method that recognizes the frequency content of the design motion, limited building wall movements due to the presence of floor diaphragms, and uses the soil shear wave velocity and damping as input (Ostadan, 2004). To predict lateral seismic soil pressures for below-grade structural walls resting on firm foundations and assuming non-yielding walls, the method involves the following steps:

1. For conservatism, define the ground motion as the CCNPP Unit 3 Safe Shutdown Earthquake (SSE) peak ground acceleration. This value is the maximum spectral acceleration of the site specific spectra (See Section 3.7).

2. Compute the total mass for a representative Single Degree of Freedom (SDOF) system using Poisson's ratio and the mass density of the soil, m:

$$m = \frac{1}{2} \frac{\gamma}{g} H^2 \psi_v$$

Where:

γ/g → Total mass density of the structural backfill;

H → Height of wall

ψ_v → Factor to account for Poisson's ratio (ν), with | ν | = 0.3 adopted for structural backfill for unsaturated conditions, and 0.45 was considered for saturated conditions

$$\psi_v = \frac{2}{\sqrt{(1-\nu)(2-\nu)}}$$

3. Obtain the lateral seismic force as the product of the total mass obtained from Step 2, and 0.15 g.

4. Obtain the maximum lateral seismic soil pressure at the ground surface by dividing the lateral force obtained from Step 3 by the area under the normalized seismic soil pressure, or 0.744 H.

5. Obtain the soil pressure profile by multiplying the maximum pressure from Step 4 by the following pressure distribution relationship:

$$p(y) = -0.0015 + 5.05y - 15.84y^2 + 28.25y^3 - 24.59y^4 + 8.14y^5$$

Where:

y → Normalized height ratio (y/H). "y" is measured from bottom of the wall and y/H ranges from a value of zero at the bottom of the wall to a value of 1.0 at the top of the wall.

For well-drained backfills, seismic groundwater pressures need not be considered (Ostadan, 2004). Since granular backfill is used for the project, only hydrostatic pressures are taken into consideration. Seismic groundwater thrust greater than 35 percent of the hydrostatic thrust can develop for cases when k_h>0.3g (Whitman, 1990). Given the relatively low seismicity at the CCNPP Unit 3 site (k_h<0.1g), seismic groundwater considerations can be ignored.

Representative earth pressure diagrams are provided in Figure 2.5-196.

2.5.4.11 Design Criteria

No departures or supplements.

2.5.4.12 Techniques to Improve Subsurface Conditions

Major structures derive support from the very dense cemented soils or compacted structural backfill. Given the planned foundation depths and soil conditions at these depths, no special ground improvement measures are warranted. Ground improvement is limited to excavation of unsuitable soils, such as existing fill or loose/soft soils, and their replacement with structural backfill or lean concrete. It also includes proof-rolling of foundation subgrade for the purpose of identifying any unsuitable soils for further excavation and replacement, which further densifies the upper portions of the subgrade. In absence of subsurface conditions at the site that require ground improvement, ground control, i.e., maintaining the integrity of existing dense or stiff foundation soils, is the primary focus of earthworks during foundation

preparation. These measures include groundwater control, use of appropriate measures and equipment for excavation and compaction, subgrade protection, and other similar measures.

2.5.4.13 References

This section is added as a supplement to the U.S. EPR FSAR.

ACI, 1994. ACI, 1994. Manual of Concrete Practice, Part 1, Materials and General Properties of Concrete, American Concrete Institute [Report] - 1994.

API, 2007. Cathodic Protection of Aboveground Petroleum Storage Tanks, API Recommended Practice Number 651, American Petroleum Institute [Report] - 2007.

ASCE, 2005. American Society of Civil Engineers, "Seismic Design Criteria for Structures, Systems, and Components in Nuclear Facilities," American Society for Civil Engineers/ Structural Engineering Institute, Report ASCE/SEI 43-05 [Report] - 2005.

ASTM, 1999. Standard Test Method for Penetration Test and Split-Barrel Sampling of Soils, American Society for Testing and Materials, ASTM D1586-99. [Report] - 1999.

ASTM, 2000a. Standard Practices for Preserving and Transporting Soil Samples, American Society for Testing and Materials, ASTM D4220-95(2000) [Report] - 2000.

ASTM, 2000b. Standard Test Method for Performing Electronic Friction Cone and Piezocone Penetration Testing of Soils, American Society for Testing and Materials, ASTM D5778-95 (reapproved 2000), [Report] - 2000.

ASTM, 2000c. Standard Practice for Thin-Walled Tube Sampling of Soils for Geotechnical Purposes, American Society for Testing and Materials, ASTM D1587-00. [Report] - 2000.

ASTM, 2001a. Standard Test Method for Field Measurement of Soil Resistivity Using the Wenner Four-Electrode Method, American Society for Testing and Materials, ASTM G57-95 (reapproved 2001). [Report] - 2001.

ASTM, 2002a. Standard Test Methods for Laboratory Compaction Characteristics of Soil Using Modified Effort (56,000 ft-lbf/ft^3 (2,700 kN-m/m^3)), American Society for Testing and Materials, ASTM D1557-02 [Report] - 2002.

ASTM, 2002b. Standard Test Method (Field Procedure) for Instantaneous Change in Head (Slug) Tests for Determining Hydraulic Properties of Aquifers, American Society for Testing and Materials, ASTM D4044-96 (reapproved 2002). [Report] - 2002.

ASTM, 2004a. Standard Practice for Design and Installation of Ground Water Monitoring Wells, American Society for Testing and Materials, ASTM D5092-04. [Report] - 2004.

ASTM, 2004b. Standard Practice for Determining the Normalized Penetration Resistance of Sands for Evaluation of Liquefaction Potential, ASTM D6066 - 96(2004) [Report] - 2004.

ASTM, 2005a. Standard Test Method for Energy Measurement for Dynamic Penetrometers, American Society for Testing and Materials, ASTM D4633-05. [Report] - 2005.

ASTM, 2005b. Standard Specification for Portland Cement, American Society for Testing and Materials, ASTM C150-05. [Report] - 2005.

ASTM, 2005c. Standard Test Methods for Laboratory Determination of Water (Moisture) Content of Soil and Rock by Mass, American Society for Testing and Materials, ASTM 2216-05 [Report], 2009.

ASTM, 2006. Standard Practice for Description and Identification of Soils (Visual-Manual Procedure), American Society for Testing and Materials, ASTM D2488-06. [Report] - 2006.

ASTM, 2007a. Standard Test Method for Prebored Pressuremeter Testing in Soils, American Society for Testing and Materials, ASTM D4719-07 [Report] - 2007.

ASTM, 2007b. Standard Test Method for Density and Unit Weight of Soil in Place by Sand-Cone Method, American Society for Testing and Materials, ASTM 1556-07 [Report], 2009.

ASTM, 2008a. Standard Test Method for Soil Compaction Determination at Shallow Depths Using 5-lb (2.3 kg) Dynamic Cone Penetrometer, ASTM D7380-08 [Report], 2009.

ASTM, 2008b. Standard Test Method for In-Place Density and Water Content of Soil and Soil-Aggregate by Nuclear Methods (Shallow Depth), American Society for Testing and Materials, ASTM 6938-08a, [Report], 2009.

ASTM, 2009. Standard Test Methods for Laboratory Compaction Characteristics of Soil Using Modified Effort (56,000 ft-lbf/ft3(2700 kN-m/m3)), American Society for Testing and Materials, ASTM 1557-09 [Report], 2009.

Bechtel, 1992. Subsurface Investigation and Foundation Report for Calvert Cliffs Nuclear Plant Diesel Generator Project, Prepared for Baltimore Gas and Electric Company, Bechtel Power Corporation [Report] - 1992.

Bechtel, 2007. Reconciliation of EPRI and RCTS Results, Calvert Cliffs Nuclear Power Plant Unit 3, Bechtel Power Corporation, December 2007. [Report] - 2007.

BGE, 1982. Updated Final Safety Analysis Report, Calvert Cliffs Nuclear Power Plant (Units 1 and 2), Docket 50-317 and 50-318, Calvert County, Maryland, Baltimore Gas and Electric Company, Baltimore, Maryland [Report] - 1982.

CEE, 1985. Liquefaction of Soils During Earthquakes, National Research Council, Committee on Earthquake Engineering, National Academy Press [Report] - 1985.

CFR, 2007. Geologic and Seismic Siting Criteria, Title 10 Code of Federal Regulations, part 100.23, 2007.

Coduto, 2001. Coduto D.P., Foundation Design, Second Edition, p. 233 [Book] - 2001.

Davie, et al., 1988. Davie L. and Lewis M., Settlement of Two Tall Chimney Foundations [Conference] // Proceedings 2nd International Conference on Case Histories in Geotechnical Engineering. - pp 1309-1313 - 1988.

Deere, et al., 1996. Deere D. and Miller R. Engineering Classification and Index Properties of Intact Rock, University of Illinois, Prepared for Air Force Weapons Laboratory, Technical Report Number AFWL-TR-65-116 [Report] - 1996.

Dominion, 2006. North Anna Early Site Permit Application, Revision 9 Docket Number. 05200008, Dominion Nuclear North Anna LLC [Report] - 2006.

Dunnicliff, 1988. Geotechnical Instrumentation for Monitoring Field Performance, John Dunnicliff, John Wiley & Sons, Inc., 1988.

DUTP, 2007. PLAXIS 3D Foundation Version 2, Delft University of Technology & PLAXIS [Report] - 2007.

EPRI, 1990. Manual on Estimating Soil Properties for Foundation Design, F. Kulhawy and P. Mayne, Electric Power Research Institute, Report EL-6800 [Report] - 1990.

EPRI, 1993. Guidelines for Determining Design Basis Ground Motions, Electric Power Research Institute, Report Number TR-102293. [Report] - 1993.

FHWA, 1990. Reinforced Soil Structures, Vol. 1, Design and Construction Guidelines, Federal Highway Administration, Federal Highway Administration Report Number FHWA-RD-89-043 [Report] - 1990.

Hansen, 1996. Hansen H., Hydrostratigraphic Framework of the Piney Point-Nanjemoy Aquifer and Aquia Aquifer in Calvert and St. Mary's Counties, Maryland, Open-File Report No. 96-02-8, 1996. [Report] - [s.l.] : Maryland Geological Survey - 1996.

IBC 2006. International Building Code, International Code Council, Inc., Country Club Hills, IL, Table 1804.2 [Report] - 2006.

IEEE, 1983. Guide for Measuring Earth Resistivity, Ground Impedance, and Earth Surface Potentials of a Ground System Part 1: Normal Measurements, Institute of Electrical and Electronics Engineers, IEEE 81 [Report] - 1983.

Lambe, et al., 1969. Lambe T. and Whitman R. Soil Mechanics [Book] - New York : John Wiley and Sons Inc. -1969.

MACTEC, 2009a. Revised Laboratory Testing Results, Rev 2, Calvert Cliffs Nuclear Power Plant Unit 3, Report by MACTEC Engineering and Consulting, Inc., Charlotte, North Carolina [Report] - 2009.

MACTEC, 2009b. Structural Fill Static Laboratory Testing Results, Rev. 1, Report by MACTEC Engineering and Consulting, Inc., Charlotte, North Carolina [Report] - 2009.

MACTEC, 2009c. Structural Fill Dynamic Laboratory Testing Results, Rev. 1, Report by MACTEC Engineering and Consulting, Inc., Charlotte, North Carolina [Report] - 2009.

MACTEC, 2009d. Intake Samples Laboratory Test Data Report, Report by MACTEC Engineering and Consulting, Inc., Charlotte, North Carolina [Report] - 2009.

Meyerhof, et al., 1978. Ultimate Bearing Capacity of Foundation on Layered Soil Under Inclined Load, G. Meyerhof and A. Hanna, Canadian Geotechnical Journal, Volume 15, Number 4, pp 565-572 [Journal] - 1978.

NFEC, 1986. Foundations and Earth Structures, Design Manual 7.02, Naval Facilities Engineering Command, pp 7.02-63, Table 1 [Report] - 1986.

Ohya, 1986. In-Situ P and S Wave Velocity Measurement, Proceedings of In Situ '86, American Society of Civil Engineers -1986.

Ostadan, 2004. Seismic Soil Pressure for Building Walls-An Updated Approach, F. Ostadan, 11th International Conference on Soil Dynamics and Earthquake Engineering and 3rd International Conference on Earthquake Geotechnical Engineering, University of California, Berkeley [Conference] - 2004.

REI, 2001. Technical Basis for Revision of Regulatory Guidance on Design Ground Motions: Hazard- and Risk-consistent Ground Motion Spectra Guidelines: NUREG/CR 6728", Risk Engineering Inc., U.S. Nuclear Regulatory Commission [Report] - 2001.

Robertson, et al., 1988. Guidelines for Geotechnical Design Using CPT and CPTU, P. K. Robertson, and R. G. Campanella, Soil Mechanics Series No. 120, University of British Columbia [Journal] - 1988.

Rosen, et al., 1986. Rosen M. and Holdren G., Origin of Dolomite Cement in Chesapeake Group (Miocene) Siliciclastic Sediments: An Alternative Model to Burial Dolomatization [Journal] // Journal of Sedimentary Petrology. - Volume 56, Number 6, pp 788-798 -1986.

Salgado, 2008. The Engineering of Foundations, Salgado R. [Book] - 2008.

Schantz, et al., 1999. Schanz T., Vermeer P.A. and Bonnier P.G. The hardening soil model: Formulation and verification, Beyond 200 in Computational Geotechnics - 10 Years of PLAXIS [Conference] - 1999.

Schnabel, 2007a. Geotechnical Subsurface Investigation Data Report (Revision No. 1), CGG Combined Operating License Application (COLA) Project, Calvert Cliffs Nuclear Power Plant (CCNPP), Calvert County, Maryland, Schnabel Engineering North, LL [Report] - 2007.

Schnabel, 2007b. Geotechnical Subsurface Investigation Data Report Addendum No. 3 (RCTS Test Results), Revision 2, CGG Combined Operating License Application (COLA) Project, Calvert Cliffs Nuclear Power Plant (CCNPP), Report by Schnabel Engineering North, LLC [Report]. - Calvert County, Maryland : [s.n.] - 2007.

Schnabel, 2009. Geotechnical Subsurface Investigation Data Report, CGG Combined Operating License (COL) Project - Phase 2, Calvert Cliffs Nuclear Power Plant, Calvert County, Maryland, Report by Schnabel Engineering North, LLC [Report] - 2009.

Seed, et al., 1970. Seed H.B. and Whitman R.V., Design of Earth Retaining Structures for Dynamic Loads, Proc. Speciality Conference on Lateral Stresses in the Ground and Design of Earth-Retaining Structures, ASCE, New York, pp 103-147 [Conference] - 1970.

Senapathy, et al., 2001. Senapathy H., Clemente J. and Davie J. Estimating Dynamic Shear Modulus in Cohesive Soils, [Conference] // XVth International Conference on Soil Mechanics and Geotechnical Engineering - 2001.

SGS, 1993. Swedish Geotechnical Society, Recommended Standard for Cone Penetration Tests, Report SGF 1:93E, Stockholm, Sweden, 1993 [Report] - 1993.

SNOC, 2006. Vogtle Early Site Permit Application, Revision 1, Docket No. 052011, Southern Nuclear Operating Company, Inc. [Report] - 2006.

Terzaghi, et al., 1995. Terzaghi K., Peck R.B. and Mesri G., Soil Mechanics in Engineering Practice, Terzaghi, K., Peck, R.B., Mesri, G., John Wiley & Sons, Inc, New York, NY. [Book] - 1995.

USDC, 1978. National Oceanic and Atmospheric Administration (NOAA) Manual NOS NGS 1, Geodetic Benchmarks, U.S. Department of Commerce, 1978.

USGS, 1983. Preliminary Analysis of Geohydrologic Data from Test Wells Drilled Near Chester, on Kent Island, Queen Anne's County, MD, Open File Report 82-854, Mack F. [Report]. - [s.l.] : U.S. Geological Survey - 1983.

USGS, 1984. Summary of Hydrogeologic Data from a Deep (2,678 ft) Well at Lexington Park, St. Mary's County, Maryland, U.S. Geological Survey, Open File Report 84-02-1, Maryland Geological Survey, H. Hansen and J. Wilson [Report] - 1984.

USGS, 2000. Data for Quaternary Faults, Liquefaction Features, and Possible Tectonic Features in the Central and Eastern United States, East of the Rocky Mountain Front, U.S. Geological Survey, Open File Report 00-260, J. Crone and R. Wheeler [Report] - 2000.

USNRC, 2002. Technical Basis for Revision of Regulatory Guidance on Design Ground Motions: Development of Hazard- & Risk-Consistent Seismic Spectra for Two Sites, NUREG/CR-6769, U.S. Nuclear Regulatory Commission [Report] - 2002.

USNRC, 2003a. Site Investigations for Foundations of Nuclear Power Plants, Regulatory Guide 1.132, U.S. Nuclear Regulatory Commission [Report] - 2003.

USNRC, 2003b. Laboratory Investigations of Soils for Engineering Analysis and Design of Nuclear Power Plants, Regulatory Guide 1.138, Revision 2, U.S. Nuclear Regulatory Commission [Report] - 2003.

USNRC, 2003c. Procedures and Criteria for Assessing Seismic Soil Liquefaction at Nuclear Power Plant Sites, Regulatory Guide 1.198, U.S. Nuclear Regulatory Commission [Report] - 2003.

USNRC, 2007a. Combined License Applications For Nuclear Power Plants (LWR Edition), Regulatory Guide 1.206 [Report]. - [s.l.] : U.S. Nuclear Regulatory Commission -2007.

USNRC, 2007b. Regulatory Guide 1.208, A Performance-Based Approach to Define the Site-Specific Earthquake Ground Motion [Report] - 2007.

Vesic, et al., 1975. Bearing Capacity of Shallow Foundations, Foundation Engineering Handbook, A. Vesic, H. Winterkorn and H. Fang, Editors, Van Nostrand Reinhold Co [Journal] - 1975.

Whitman, 1990. Seismic Design and Behavior of Gravity Walls, Proceedings, Specialty Conference on Design and Performance of Earth-Retaining Structures, R. Whitman, ASCE, NY, pp 817-842 [Conference] - 1990.

Whitman, 1991. Seismic Design of Earth Retaining Structures, R. Whitman, Proceedings 2nd International Conference on Recent Advances in Geotechnical Earthquake Engineering and Soil Dynamics, pp 1767-1778 [Journal] - 1991.

Youd, et al, 2001. Youd T. L. [et al.] Liquefaction Resistance of Soils: Summary Report from the 1996 NCEER and 1998 NCEER/NSF Worrkshops on Evaluation of Liquefaction of Soils, ASCE Journal of Geotechnical and Geoenvironmental Engineering, Volume 127, Number 10, pp 817-833 [Journal] - 2001.}

2.5.5 Stability of Slopes

The U.S. EPR FSAR includes the following COL Item for Section 2.5.5:

> A COL applicant that references the U.S. EPR design certification will evaluate site-specific information concerning the stability of earth and rock slopes, both natural and manmade (e.g., cuts, fill, embankments, dams, etc.), of which failure could adversely affect the safety of the plant.

This COL Item is addressed as follows:

{This section addresses the stability of constructed and natural slopes. It was prepared based on the guidance in relevant sections of NRC Regulatory Guide 1.206, "Combined License Applications for Nuclear Power Plants (LWR Edition)" (NRC, 2007). Constructed slopes evolve as part of the overall site development.

The site of the Calvert Cliffs Nuclear Power Plant (CCNPP) Unit 3 is comprised of rolling topography. The site is planned to be graded in order to establish the final grade for the project, resulting in cuts and fills, as well as slopes. The stability of these slopes and their potential impact on safety-related structures are evaluated herein. Natural slopes at the site consist of the Calvert Cliffs; they are steep slopes undergoing continuous erosion. The impact of naturally-occurring erosion on these cliffs and their potential impact on safety-related structures are also evaluated.

Information on site conditions and geologic features is provided in Section 2.5.1. Section 2.5.4 presents a discussion of the properties of the underlying soil and the backfill.

All elevations referenced in this section are based on National Geodetic Vertical Datum of 1929 (NGVD 29).

Sections 2.5.5.1 through 2.5.5.5 are added as a supplement to the U.S. EPR FSAR.

2.5.5.1 Slope Characteristics

The characteristics of constructed and natural slopes are described below.

2.5.5.1.1 Characteristics of Constructed Slopes

Site grading for CCNPP Unit 3 structures will include such areas as the powerblock, switchyard, cooling tower (collectively identified as the CCNPP Unit 3 area), the intake area and the utility corridor between the CCNPP Unit 3 area and the intake area. The powerblock includes the

Reactor Building, Fuel Building, Safeguard Buildings, Emergency Power Generating Building (EPGB), Essential Service Water Building (ESWB), Nuclear Auxiliary Building (NAB), Access Building, Radioactive Waste Building, Turbine Building, Fire Protection Building and Switchgear Building. The intake area includes the Ultimate Heat Sink Makeup Water Intake Structure (UHS MWIS), Circulating Makeup Water Intake Structure (CW MWIS), Forebay and Fish Return. All the safety related structures are in these two areas. Natural ground surface elevations within the powerblock range from approximately Elevation 47 ft to Elevation 121 ft, and approximately Elevation 8 ft to Elevation 11 ft within the intake area, as shown in Figure 2.5-103. The centerline of the CCNPP Unit 3 powerblock is graded to approximately Elevation 85 ft. The finished grade in each major area will be approximately:

- Powerblock: Elevation 80 ft to Elevation 85 ft.
- Intake Area: Elevation 10 ft.
- Switchyard: Elevation 90 ft to 98 ft.
- Cooling Tower: Elevation 94 ft to 100 ft.
- Utility Corridor: Elevation 80 ft near proposed CCNPP Unit 3 to Elevation 8 ft near the Barge Slip.

Locations of these areas and associated structures, and a schematic of the overall grading configuration, are shown in Figure 2.5-197. The site grading within the powerblock will require both cut and fill, currently estimated at approximately 40 ft and 45 ft, respectively. The cut and fill operations will result in permanent slopes around the powerblock and Category I structures in the powerblock area. The maximum height of new slopes in the area of CCNPP Unit 3 powerblock is approximately 50 ft, located on the eastern side of the powerblock, sloping down from the powerblock.

The hill to the west of the intake area is approximately 90 ft high with a slope towards the east. The intake slope is constructed such that its toe is at least 100 ft from the intake structure.

An access road connects the CCNPP Unit 3 area and the Intake area. The cooling-water pipes and electrical duct banks are routed along the same alignment. This area is referred to as the 'Utility Corridor'. The maximum height of the slopes along the Utility Corridor is about 45 ft (from the road elevation 30 ft to top of slope elevation 75 ft).

Permanent slopes, whether cut or fill, will have an inclination of approximately 3:1 (horizontal to vertical). Earthworks for slope construction, including fill control, compaction, testing, etc. are addressed in Section 2.5.4.5.

Seven cross-sections that represent the typical site grading configuration were selected for evaluation based on location (e.g., proximity to Category I structures), slope geometry (e.g., height), and soil conditions. These cross-sections and their locations are shown in Figure 2.5-197 through Figure 2.5-199. Sections A, C, D and E are located in the powerblock area, Section B in the Construction Layout Area (CLA), Section F extends across the Utility Corridor, and Section G extends across the Intake Slope and Intake area. Slope stability calculations were made for these cross-sections; the results are discussed in Section 2.5.5.2.

2.5.5.1.2 Characteristics of Natural Calvert Cliffs

The CCNPP Unit 3 site area is located about 1,000 ft west of the steep cliffs known as the Calvert Cliffs, as shown in Figure 2.5-197. These cliffs make up the Chesapeake Bay shoreline

and reach elevations as high as 100 ft at their closest point to the CCNPP Unit 3 powerblock area. Stability of the Calvert Cliffs is discussed in Section 2.5.5.2.

2.5.5.1.3 Exploration Program and Geotechnical Conditions

The geotechnical exploration program, groundwater conditions, sampling, materials and properties, liquefaction potential, and other geotechnical parameters are addressed in Section 2.5.4. A summary relevant to the slope stability evaluation is presented below.

A geotechnical subsurface investigation was performed to characterize the upper 400 ft of soil at the CCNPP Unit 3 site. The site geology, based on geotechnical borings beneath the CCNPP Unit 3 site is comprised of fluvial and marine deposits that are about 2500 ft thick. Only the deposits in the upper 150 ft are of interest for the slope stability analyses. The subsurface, in the upper 150 ft, is divided into the following stratigraphic units:

- Stratum I: Terrace Sand
- Stratum IIa: Chesapeake Clay/Silt
- Stratum IIb: Chesapeake Cemented Sand
- Stratum IIc: Chesapeake Clay/Silt

Identification of soil layers was based on their physical and engineering characteristics. The characterization of the subsurface materials was based on a suite of tests consisting of standard penetration tests (SPT), in-soil borings including auto-hammer energy measurements, geophysical testing, and laboratory testing. Figure 2.5-106 provides an idealized profile for CCNPP Unit 3. Overall, the subsurface conditions encountered throughout the site are relatively uniform, as presented in detail in Section 2.5.4.

The first two soil layers, Terrace Sand and Chesapeake Clay/Silt IIa are not adequate foundation strata for safety related structures or facilities that will impose high contact pressures. These soils are susceptible to unacceptable levels of both elastic and long-term settlements. These soils will be removed in the powerblock area and replaced with Category I structural fill.

Based on the information provided in Section 2.4.12, in the powerblock area, shallow and deep groundwater regimes are present. For conservatism, the average groundwater level of Elevation 80 ft was chosen for slope stability evaluation in the powerblock, where in-situ soils were present. In locations where Category I structural fill replaced in-situ soils, the groundwater level was chosen as 55 ft. In the Intake Area, Intake Slope and Utility Corridor, the groundwater conditions are also based on the subsurface investigation and monitoring of observation wells. For conservatism, the groundwater levels in the Intake Area, Intake Slope and Utility Corridor were chosen as Elevations 10 ft, 37 ft and 24 ft, respectively. In naturally low-lying areas, that is, in area with ground surface elevations lower than groundwater level, the ground may be saturated. These areas will be inspected during construction for groundwater condition. Should these areas appear saturated and if they are to receive fill during construction, a layer of highly permeable drainage material will be placed between the natural soils and the fill to preclude saturation of the fill and to maintain the groundwater level near the bottom of the fill.

The geotechnical parameters for the purpose of slope stability evaluation are based on material properties derived from the data collected during the exploration program. For the

evaluation of the Utility Corridor, material properties based on data from the powerblock area were conservatively selected.

2.5.5.2 Design Criteria and Analysis

The stability of constructed slopes was assessed using limit equilibrium methods, which generally consider moment or force equilibrium of a potential sliding mass by discretizing the mass into vertical slices. This approach results in a Factor of Safety (FOS) that can be defined as (Duncan, 1996):

$$\text{FOS} = \frac{\text{Shear Strength of Soil}}{\text{Shear Stress Required for Equilibrium}}$$

Various limit equilibrium methods are available for slope stability evaluation, including the Ordinary method (Fellenius, 1936), Bishop's simplified method (Bishop, 1955), Janbu's simplified method, (Janbu, 1968), and Morgenstern-Price method (Morgenstern, 1965). These methods are routinely used for the evaluation of slopes, and their limitations and advantages are well documented. The main differences are:

1. Static equilibrium equations.
2. Interslice forces that are included in the analysis.
3. Assumed relationship between the interslice shear and normal forces.

The Ordinary method (Fellenius, 1936) is one of the earliest methods developed. It ignores all interslice forces and satisfies only moment equilibrium. Bishop's (Bishop, 1955) and Janbu's (Janbu, 1968) simplified methods satisfy only moment equilibrium and horizontal force equilibrium, respectively. Both Bishop's simplified method (Bishop, 1955) and Janbu's (Janbu, 1968) include the interslice normal force, but ignore the interslice shear force. The Morgenstern-Price method (Morgenstern, 1965) considers both shear and normal interslice forces, and it satisfies both moment and force equilibrium. The Ordinary method (Fellenius, 1936), Bishop's simplified method (Bishop, 1955) and Morgenstern-Price method (Morgenstern, 1965) were used to calculate FOSs for constructed slopes at the CCNPP Unit 3 site.

Dynamic analysis of the slopes can be performed using a pseudo-static approach, which represents the effects of seismic vibration by accelerations that induce inertial forces. These forces act in the horizontal and vertical directions at the centroid of each slice, and are defined as:

$$F_h = \left(\frac{a_h}{g}\right) W = k_h \, W$$

$$F_v = \left(\frac{a_v}{g}\right) W = k_v \, W$$

Where a_h and a_v are horizontal and vertical ground accelerations, respectively, W is the slice weight, and g is the gravitational acceleration constant. The inertial effect is specified by k_h and k_v coefficients, based on site seismic considerations.

Typical minimum acceptable values of FOS are 1.5 for normal long-term loading conditions and 1.0 to 1.2 for infrequent loading conditions (Duncan, 1996), e.g., during earthquakes.

2.5.5.2.1 Stability of Constructed Slopes

The slope stability analysis was performed using SLOPE/W (GEO-SLOPE, 2007). SLOPE/W 2007 has been independently validated and verified using the Ordinary (Fellenius, 1936), Bishop's (Bishop, 1955) and Morgenstern-Price methods. The software searches for a critical slip surface by attempting several hundred combinations of surfaces of different shapes. Both static and pseudo-static analyses were performed for the selected cross-sections, allowing the program to select the critical surface.

The initial code for SLOPE/W was developed by Professor D. G. Fredlund at the University of Saskatchewan in Canada. During the 1980s, the PC version became available. SLOPE/W contains formulation for 10 different methods for evaluating the stability of slopes, each with various assumptions in its development of the respective mathematical model. Some of these assumptions were described earlier in Section 2.5.5.2, with the main difference being in the treatment of interslice forces. SLOPE/W contains a variety of options for the shape of trial surfaces, e.g., circular, planar, composite, or block type, and locates the critical surface with the lowest possible FOS. The reasonableness of the surface, however, should be determined by the user as SLOPE/W, or other similar applications, cannot be expected to make these judgments. SLOPE/W also allows for the incorporation of forces due to water, as well as negative porewater (suction) and externally applied forces, when needed. Material properties may simply be defined in terms of unit weight, friction and/or cohesion, or made a function of other parameters, e.g., change in stress. SLOPE/W has two options for evaluating slopes subjected to rapid loading; namely, pseudo-statically or using results from other dynamic analyses such as a companion program that obtains dynamic stresses and porewater pressure. A complete description of SLOPE/W and slope stability formulations is given in SLOPE/W user manual (GEO-SLOPE, 2007).

The effect of surcharge loading was excluded from the analyses. Planned structures are sufficiently set back from edges of slopes so that they do not impose surcharge loading on the slope. The location and relative positions of safety-related structures to slopes in Sections A′, G′ and G″ for the powerblock and intake area are shown in Figure 2.5-200 and Figure 2.5-201. The site soils are not considered liquefiable for the seismic conditions of the site; therefore, liquefaction is not applicable to stability of slopes at the site. Liquefaction potential is addressed in detail in Section 2.5.4.8.

For the pseudo-static analysis in the CCNPP Unit 3 site, the inertial effect coefficient $k_h = 0.15$ was used, based on $a_h = 0.15g$, from the Site Safe Shutdown Earthquake (Site SSE) developed in Section 3.7.1. The vertical component, k_v, was chosen as 0.075.

In the static analysis, a Mohr-Coulomb failure criterion based on effective stress conditions was used. For the sand layers, it is assumed that the effective cohesion, c′, is equal to zero. This is a conservative approach which yields a lower factor of safety (FOS). The sand layers at the site contain varying amounts of clay and silt as shown in the boring logs provided in COLA Part 11J: Geotechnical Subsurface Investigation Data Report. The effective friction angle (Φ′) for the sand layers is based on standard penetration and cone penetration tests correlations, direct

shear and CIU-bar triaxial compression tests. For the clay/silt layers, c′ and Φ′ were obtained from the CIU-bar triaxial compression and direct shear tests.

Two cases were considered for the dynamic analysis:

- A Mohr-Coulomb failure criterion based on total stress conditions was used, to account for the hydrostatic pressure buildup. For the sand layers, total strength parameters (cohesion, c, and friction angle, Φ) were obtained from CIU triaxial compression and direct shear tests. For the clay/silt layers, the undrained shear strength, s_u, obtained from Unconsolidated Undrained (UU) and Unconfined Compression (UC) tests was used (Table 2.5-54).
- A Mohr-Coulomb failure criterion based on effective stress conditions, using the same parameters as in the static analysis.

Material properties for the slope stability analysis are presented for the powerblock, utility corridor, and the intake slope and intake area in Table 2.5-71.

Result of the static and pseudo-static slope stability analyses for critical surfaces, that is, surfaces with the lowest FOS, are shown in Figure 2.5-202 through Figure 2.5-210. In these figures, TSA and ESA represent total stress analysis and effective stress analysis, respectively. The computed FOSs shown on these figures are based on the Morgenstern-Price method (Morgenstern, 1965). Various runs were conducted on each slope to determine the lowest FOS. Sloughing or surficial failures that appeared during analyses were evaluated and disregarded when appropriate. For Sections A and B in the CCNPP Unit 3 area, two cases were considered: a) groundwater at the boundary between structural backfill and Chesapeake Sand, and b) groundwater located at Elevation 55 ft within structural backfill. In addition to the Morgenstern-Price method (Morgenstern, 1965), FOSs were also calculated using the Ordinary method and Bishop's simplified method (Bishop, 1955) for comparison. All three methods are implemented in SLOPE/W. The FOSs for these methods are summarized in Table 2.5-72, for effective stress and total stress conditions. The Ordinary method errs on the conservative side and yields lower FOSs because all interslice forces are ignored and only moment equilibrium is satisfied. The Bishop's method considers moment equilibrium and the normal interslice force. The Morgenstern-Price method considers moment and force equilibrium, and the interslice normal and shear forces. Both Bishop's and Morgenstern-Price methods yield higher FOSs.

An examination of the FOSs in Table 2.5-72 indicates that for the pseudo-static analyses (dynamic), the effective stress conditions yields lower FOSs. However, total stress conditions are more representative of dynamic conditions at the site since porewater pressures do not have time to dissipate. Results reported hereafter for pseudo-static analyses are based on total stress conditions.

In the powerblock and adjacent areas (Cross-sections A through E in Figure 2.5-198), all slopes show FOSs greater than 1.8 for the static case and greater than 1.6 for the pseudo-static case, based on the Morgenstern-Price method (Morgenstern, 1965), as shown in Figure 2.5-202 through Figure 2.5-208.

Along the Utility Corridor, at Cross-section F shown in Figure 2.5-199, a static FOS of 2.34 and a pseudo-static FOS of 2.82 was obtained with the Morgenstern-Price method, as shown in Figure 2.5-209.

In the intake area, at Cross-section G shown in Figure 2.5-199, a static FOS of 2.05 and a pseudo-static FOS of 1.93 were obtained using the Morgenstern-Price method, as shown in Figure 2.5-210.

As stated previously, typical minimum acceptable values of FOS are 1.5 for normal long-term loading conditions and 1.0 to 1.2 for infrequent loading conditions. The calculated FOSs for all slopes exceed the minimum acceptable values. Therefore, the slopes in the powerblock, intake area and utility corridor have sufficient static and dynamic stability against slope failure.

There are no dams or embankments that would affect the CCNPP Unit 3. Probable Maximum Flood (PMF) at the CCNPP Unit 3 area is accounted for by assuming a high groundwater level of 37 ft at the Intake Slope. A maximum flood level of 33.9 ft is postulated, this would only affect the Intake Slope.

2.5.5.2.2 Stability of Natural Calvert Cliffs

The Calvert Cliffs are steep, near-vertical slopes, formed by erosion processes over the last several thousand years. These processes are addressed in more detail in Section 2.4.9. The on-going erosion results in the cliffs failing along irregular, near-vertical surfaces. The failures are the result of shoreline erosion undermining the cliffs at the beach line. With sufficient undermining, the weight of the overlying deposits that make up the cliffs exceeds their shear strength, resulting in the undermined portion falling to the shoreline. Long-term and short-term processes, e.g., waves, tidal fluctuations, and extreme weather conditions, affect the Calvert Cliffs. The cliffs are estimated to undergo erosion near the CCNPP Unit 3 site area of about 2 ft to 4 ft per year, as described in Section 2.4.9.

In the proximity of CCNPP Unit 3, the cliffs rise to elevations in the range of about Elevation 30 ft to Elevation 100 ft, with a major portion maintaining about Elevation 90 ft, as shown in Figure 2.5-197. Given the past performance of the high cliffs, there is no reason to expect their future performance would appreciably differ; therefore, these cliffs are anticipated to continue to be globally stable, owing to the relatively high strength of the soil deposits that make up the cliffs (refer to Section 2.5.4.2 for strength data for these soils). Consistent with the results of the preconstruction exploration, all soils that make up the cliffs also include some level of plasticity, as well as a moderate amount of fines, resulting in moderate capillary forces and, therefore, enhanced stability and resistance to erosion.

The easternmost boundary of the CCNPP Unit 3 powerblock is set back a distance of about 1,000 ft from the cliffs, with at least 1,200 ft to the nearest Category I structure, as shown in Figure 2.5-197. This set back area will be free from any major construction, surcharge, re-grading, or other activities that could modify the ground or the loading conditions which would adversely impact the cliffs or their stability. Therefore, they are anticipated to remain unaffected by construction factors.

Although not expected, should the global stability of the cliffs, due to unforeseen conditions, be adversely impacted such that a major cliff failure could ensue, hypothesized failure scenarios may be in the form of (1) a wedge (or a plane) portion of the cliffs sliding into the Chesapeake Bay at an inclined angle, or (2) a portion of the cliffs separate and topple into the Chesapeake Bay. For the wedge-shaped hypothesis, conservatively assuming that an inclined angle of 45 degrees from the base of the cliffs could form a wedge that daylights at the top of the cliffs, only an area of approximately 100 ft from the cliffs' edge would be impacted by such an unexpected scenario, and the remaining 900-plus ft setback area would still be intact to provide sufficient global stability to CCNPP Unit 3. For the toppling hypothesis, except for

cases associated with erosion that will be discussed below, the hydrogeologic conditions that are prerequisite to this failure situation are not known to exist at the site, such as fractured bedrock or soils with planes of weakness due to fissures, slickensides, faults, or discontinuities; excessive seepage forces that could promote such failures; or prior failure history of the type hypothesized. Therefore, massive toppling failure of the Calvert Cliffs that could have an immediate, adverse impact on CCNPP Unit 3 is not kinematically possible.

The Calvert Cliffs, however, are expected to continue to erode, as they have in the past. Based on the estimated rate of erosion of 2 ft to 4 ft annually, at a constant rate, it will take approximately 25 to 50 years to erode about 100 ft of the cliffs. Or, it would take approximately 125 to 250 years for the cliffs to erode to within a distance of 500 ft from CCNPP Unit 3 outline (or 700 ft from any Category I structure). The estimated period of 125 to 250 years is appreciably more than the anticipated operating life of CCNPP Unit 3; therefore, stability of Calvert Cliffs due to erosion should not pose any immediate risk to the stability of soils supporting CCNPP Unit 3 in its lifetime.

2.5.5.2.3 Concluding Remarks

Based on analyses provided in this Section, the constructed and natural slopes at the site are sufficiently stable and present no failure potential that would adversely affect the safety of the proposed CCNPP Unit 3.

2.5.5.3 Logs of Borings

Logs of borings, and associated references, are provided in COLA Part 11J: Geotech Data Report.

2.5.5.4 Compacted Fill

Compacted fill, and associated references, are addressed in Section 2.5.4.5.

2.5.5.5 References

BGE, 1992. Updated Final Safety Analysis Report, Calvert Cliffs Nuclear Power Plant (Units 1 and 2), Calvert County, Maryland, Docket Numbers 50-317 and 50-318, Baltimore Gas and Electric Company, 1992.

Bishop, 1955. The Use of the Slip Circle in the Stability Analysis of Slopes, A. W. Bishop, Geotechnique, Vol. 5 (1), 7-17, 1955.

Duncan, 1996. State of the art: Limit equilibrium and finite-element analysis of slopes, J. M. Duncan, Journal of Geotechnical Engineering, ASCE, Vol. 122 (7), 577-596, 1996.

Fellenius, 1936. Calculation of Stability of Dams, W. Fellenius, Second Congress on Large Dams Transactions, Vol. 4, 445-462, 1936.

GEO-SLOPE, 2007. Stability Modeling with SLOPE/W 2007, An Engineering Methodology, Second Edition, Geo-Slope/W International Ltd., 2007.

Janbu, 1968. Slope Stability Computations. N. Janbu, Soil Mechanics and Foundation Engineering, The Technical University of Norway, 1968.

Morgenstern, 1965. The Analysis of the Stability of General Slip Surfaces, N.R. Morgenstern and V. E. Price, Geotechnique, Vol. 15(1), 79-93, 1965.

NRC, 2007. Combined License Applications for Nuclear Power Plants (LWR Edition), Regulatory Guide 1.206, Revision 0, U.S. Nuclear Regulatory Commission, March 2007.}

2.5.6 References

No departures or supplements.

Table 2.5-1— {Definitions of Classes Used in the Compilation of Quaternary Faults, Liquefaction Features, and Deformation in the Central and Eastern United States}

Class Category	Definition
Class A	Geologic evidence demonstrates the existence of a Quaternary fault of tectonic origin, whether the fault is exposed for mapping or inferred from liquefaction to other deformational features.
Class B	Geologic evidence demonstrates the existence of a fault or suggests Quaternary deformation, but either (1) the fault might not extend deeply enough to be a potential source of significant earthquakes, or (2) the currently available geologic evidence is too strong to confidently assign the feature to Class C but not strong enough to assign it to Class A.
Class C	Geologic evidence is insufficient to demonstrate (1) the existence of tectonic fault, or (2) Quaternary slip or deformation associated with the feature.
Class D	Geologic evidence demonstrates that the feature is not a tectonic fault or feature; this category includes features such as demonstrated joints or joint zones, landslides, erosional or fluvial scarps, or landforms resembling fault scarps, but of demonstrable non-tectonic origin.

Table 2.5-2— {Earthquakes 1985–2005, Update to the EPRI (NP-4726-A 1988) Seismicity Catalog with Emb ≥ 2.8, Within a 35° to 43° N, 71° to 89° W Latitude-Longitude Window, Incorporating the 200 mi (320 km) Radius Site Region}

(Page 1 of 4)

Catalog reference	Year	Month	Day	Hour	Minute	Second	Lat °N	Lon °W	Depth (km)	Dist. (km) [1]	Int	Emb	Smb	Rmb
Canada	1985	4	14	3	44	39.00	42.950	80.040	18	584		3.10	0.10	3.11
Canada	1985	4	14	11	39	54.00	41.580	80.400	18	484		3.20	0.10	3.21
SEUSSN	1985	6	10	12	22	38.30	37.248	80.485	11.1	378	4	3.30	0.10	3.31
ANSS	1985	10	15	20	0	39.30	42.493	71.502	2	612		2.97	0.30	3.08
ANSS	1985	10	19	10	7	40.30	40.980	73.830	6	359		3.90	0.41	4.10
ANSS	1985	10	21	10	37	15.00	40.990	73.840	5	359		3.30	0.10	3.31
ANSS	1986	1	31	16	46	43.33	41.650	81.162	10	536		5.00	0.10	5.01
SEUSSN	1986	3	26	16	36	23.90	37.245	80.494	11.9	379	4	3.30	0.25	3.37
SEUSSN	1986	12	3	9	44	21.20	37.580	77.458	1.6	129	4	3.30	0.25	3.37
SEUSSN	1986	12	10	11	30	6.10	37.585	77.468	1.2	130	5	3.50	0.10	3.51
SEUSSN	1986	12	24	17	58	38.30	37.583	77.458	1	129	4	3.30	0.25	3.37
SEUSSN	1987	1	13	14	50	40.90	37.584	77.465	2.5	129	4	3.30	0.25	3.37
ANSS	1987	7	13	5	49	17.43	41.896	80.767	5	530		3.80	0.10	3.81
ANSS	1987	7	13	7	52	12.00	41.900	80.800	5	533		3.00	0.10	3.01
ANSS	1987	7	13	13	5	22.00	41.900	80.800	5	533		2.90	0.10	2.91
Ohio	1987	7	13	18	25	11.98	41.880	80.750	0	528		2.80	0.10	2.81
ANSS	1987	7	14	14	51	10.00	41.900	80.800	5	533		2.80	0.10	2.81
Canada	1987	8	13	7	52	13.00	41.930	80.710	5	530		3.30	0.10	3.31
SEUSSN	1988	2	16	15	26	54.80	36.595	82.274	4	552	4	3.30	0.10	3.31
Ohio	1988	3	31	16	30	3.87	41.313	81.046	0	505		2.80	0.10	2.81
ANSS	1988	4	14	23	37	31.10	37.238	81.987	0	503		4.10	0.10	4.11
ANSS	1988	5	28	16	18	28.12	39.753	81.613	0	469		3.40	0.10	3.41
SEUSSN	1988	8	27	16	52	29.50	37.718	77.775	14.3	141	4	3.30	0.25	3.37
Canada	1988	12	28	23	28	24.00	41.640	81.170	5	536		2.80	0.10	2.81
ANSS	1989	4	10	18	12	16.00	37.136	82.068	0	514		4.30	0.10	4.31
SEUSSN	1989	6	4	9	49	28.20	37.224	78.293	8.8	210	3	2.80	0.10	2.81
Ohio	1989	8	1	16	12	48.75	41.898	80.758	0	530		2.80	0.10	2.81
Ohio	1989	8	1	16	50	30.74	41.893	80.752	0	529		2.90	0.10	2.91
SEUSSN	1990	1	13	20	47	56.20	39.366	76.851	4.1	110	5	3.50	0.10	3.51
ANSS	1990	5	5	20	48	56.18	36.035	71.674	10	497		3.70	0.10	3.71
ANSS	1990	10	23	1	34	48.27	39.512	75.506	10	144		3.16	0.30	3.26
Canada	1990	12	14	19	38	7.00	41.840	77.480	18	387		3.00	0.10	3.01
ANSS	1991	1	26	3	21	22.61	41.536	81.453	5	547		3.40	0.10	3.41
Ohio	1991	1	27	3	21	24.23	41.610	81.594	9.7	561		3.50	0.10	3.51
SEUSSN	1991	3	15	6	54	8.30	37.746	77.909	15.5	149	5	3.80	0.10	3.81
SEUSSN	1991	4	22	1	1	20.20	37.942	80.205	14.8	333	4	3.50	0.10	3.51
ANSS	1991	6	17	8	53	16.74	42.630	74.678	5	488		4.10	0.10	4.11

Table 2.5-2— {Earthquakes 1985–2005, Update to the EPRI (NP-4726-A 1988) Seismicity Catalog with Emb ≥ 2.8, Within a 35° to 43° N, 71° to 89° W Latitude-Longitude Window, Incorporating the 200 mi (320 km) Radius Site Region}

(Page 2 of 4)

Catalog reference	Year	Month	Day	Hour	Minute	Second	Lat °N	Lon °W	Depth (km)	Dist. (km) [1]	Int	Emb	Smb	Rmb
SEUSSN	1991	6	28	18	34	55.50	38.231	81.335	7	427		3.00	0.10	3.01
ANSS	1991	8	15	7	16	7.15	40.786	77.657	1	281		3.00	0.10	3.01
ANSS	1991	10	28	20	58	26.10	41.070	73.578	10	380		3.00	0.10	3.01
ANSS	1992	1	9	8	50	45.22	40.363	74.341	7.9	279		3.06	0.30	3.17
ANSS	1992	3	10	23	50	46.90	40.991	72.086	10	467		2.80	0.10	2.81
ANSS	1992	3	15	6	13	55.22	41.911	81.245	5	560		3.50	0.10	3.51
Canada	1992	3	26	3	43	20.00	42.110	80.850	2	552		2.90	0.10	2.91
Canada	1992	3	28	8	22	46.00	41.920	80.810	5	535		3.10	0.10	3.11
Canada	1992	3	31	1	54	55.00	42.010	80.790	18	541		2.80	0.10	2.81
SEUSSN	1993	1	1	5	8	5.20	35.878	82.086	2.3	573		2.97	0.30	3.08
SEUSSN	1993	3	10	14	32	21.60	39.233	76.882	5	97	4	3.30	0.25	3.37
SEUSSN	1993	3	15	4	29	54.70	39.197	76.870	0.9	93	5	3.50	0.10	3.51
ANSS	1993	5	10	9	15	8.60	40.347	76.018	5	215		2.80	0.10	2.81
SEUSSN	1993	7	12	4	48	20.80	36.035	79.823	5	399	4	3.30	0.10	3.31
ANSS	1993	10	16	6	30	5.32	41.698	81.012	5	530		3.60	0.10	3.61
SEUSSN	1993	10	28	6	0	0.00	39.250	76.770	0	95	4	3.30	0.25	3.37
SEUSSN	1993	10	28	6	1	0.00	39.250	76.770	0	95	4	3.30	0.25	3.37
Canada	1993	11	1	0	14	16.00	42.690	81.170	8.5	617		2.80	0.10	2.81
ANSS	1994	1	16	0	42	43.20	40.327	76.007	5	213		4.20	0.10	4.21
ANSS	1994	1	16	1	49	16.21	40.330	76.037	5	213		4.60	0.10	4.61
ANSS	1994	1	16	5	14	32.30	40.321	76.007	5	212		2.90	0.10	2.91
ANSS	1994	2	12	2	40	24.50	36.800	82.000	5	521		3.42	0.41	3.61
ANSS	1994	3	12	10	43	15.74	42.782	77.876	1	496		3.60	0.10	3.61
SEUSSN	1994	8	6	19	54	11.80	35.101	76.786	0	369	5	3.70	0.10	3.71
ANSS	1994	10	2	11	27	22.58	42.347	72.277	10	558		3.70	0.10	3.71
ANSS	1994	10	2	14	36	36.73	42.360	72.218	10	562		3.30	0.10	3.31
Ohio	1995	1	12	21	25	51.00	40.800	82.680	0	594		3.30	0.10	3.31
SEUSSN	1995	1	22	8	24	48.80	37.050	80.789	9.3	411	4	2.90	0.10	2.91
ANSS	1995	2	23	9	32	13.00	41.870	80.830	5	532		2.90	0.10	2.91
ANSS	1995	5	25	14	22	32.69	42.995	78.831	5	543		3.00	0.10	3.01
SEUSSN	1995	6	26	0	36	17.10	36.752	81.481	1.8	480	5	3.40	0.10	3.41
SEUSSN	1995	7	7	21	1	3.00	36.493	81.833	10	521	4	3.06	0.10	3.08
SEUSSN	1995	8	3	13	7	5.60	37.393	76.693	1	116	4	2.90	0.10	2.91
Canada	1995	10	21	17	4	24.00	42.800	77.880	1	498		2.90	0.10	2.91
ANSS	1996	3	22	20	22	12.58	41.690	71.242	11.9	569		3.17	0.41	3.37
Canada	1996	6	8	20	14	0.00	42.940	74.050	10.4	538		2.80	0.10	2.81
ANSS	1996	6	29	19	30	42.67	37.187	81.950	1	502		4.10	0.10	4.11

Table 2.5-2— {Earthquakes 1985–2005, Update to the EPRI (NP-4726-A 1988) Seismicity Catalog with Emb ≥ 2.8, Within a 35° to 43° N, 71° to 89° W Latitude-Longitude Window, Incorporating the 200 mi (320 km) Radius Site Region}

(Page 3 of 4)

Catalog reference	Year	Month	Day	Hour	Minute	Second	Lat °N	Lon °W	Depth (km)	Dist. (km) [1]	Int	Emb	Smb	Rmb
ANSS	1997	4	3	18	32	15.39	42.922	75.708	10.53	501		3.43	0.30	3.53
ANSS	1997	10	28	10	36	46.56	37.162	82.025	1	509		3.42	0.41	3.61
SEUSSN	1997	11	14	3	44	11.70	40.741	76.549	0	256		2.97	0.30	3.08
Canada	1998	1	27	0	38	30.00	42.030	80.990	18	554		3.00	0. 10	3.01
SEUSSN	1998	4	21	23	28	26.60	38.171	78.569	2	188	3	2.80	0.10	2.81
SEUSSN	1998	6	5	2	31	3.90	35.554	80.785	9.4	499		3.34	0.10	3.35
ANSS	1998	9	25	19	52	52.07	41.495	80.388	5	477		5.20	0.10	5.21
SEUSSN	1998	10	21	5	56	46.90	37.422	78.439	12.6	207	3	3.80	0.10	3.81
ANSS	1998	11	25	2	55	6.07	41.071	82.405	5	586		2.85	0.41	3.04
Canada	1998	12	25	21	22	3.00	41.120	81.750	18	542		2.80	0.10	2.81
ANSS	1999	1	25	20	12	30.00	42.730	77.850	3	490		2.85	0.41	3.04
ANSS	1999	9	22	10	2	22.29	41.826	81.476	18	569		2.93	0.41	3.12
ANSS	2000	1	27	14	49	40.00	43.000	71.180	1.4	671		3.09	0.41	3.28
ANSS	2000	6	16	4	2	53.00	42.100	72.820	9.8	508		3.33	0.41	3.53
ANSS	2000	8	7	2	2	30.40	40.958	81.151	5	490		3.01	0.41	3.20
ANSS	2001	1	26	3	3	20.06	41.942	80.802	5	536		4.23	0.41	4.42
Canada	2001	1	26	5	36	53.00	41.980	80.700	5	533		3.20	0.10	3.21
ANSS	2001	2	3	20	15	15.00	42.345	77.394	0	440		3.25	0.41	3.45
ANSS	2001	6	3	22	36	46.46	41.905	80.767	5	531		3.42	0.41	3.61
Canada	2001	7	26	10	46	55.00	41.200	82.510	5	601		3.10	0.10	3.11
SEUSSN	2001	9	22	16	1	20.60	38.026	78.396	0.4	176	3	3.20	0.10	3.21
SEUSSN	2001	12	4	21	15	13.90	37.726	80.752	8.5	384		3.10	0.10	3.11
ANSS	2002	4	28	0	7	20.90	41.850	81.370	5	564		2.85	0.41	3.04
ANSS	2002	7	11	21	53	45.96	40.386	71.332	0	488		3.07	0.41	3.27
ANSS	2002	9	28	23	47	27.00	42.870	71.730	5	631		2.93	0.41	3.12
SEUSSN	2003	5	5	16	32	33.90	37.655	78.055	2.8	165	5	3.90	0.10	3.91
ANSS	2003	6	30	19	21	17.20	41.800	81.200	4.6	549		3.58	0.41	3.77
ANSS	2003	8	26	18	24	18.40	40.606	75.106	3	266		3.74	0.41	3.93
ANSS	2003	11	4	13	37	31.80	40.251	75.877	1	207		2.85	0.41	3.04
SEUSSN	2003	12	9	20	59	18.70	37.774	78.100	10	162	6	4.50	0.10	4.51
Canada	2004	6	16	6	31	26.00	42.790	79.010	7	529		3.10	0.10	3.11
ANSS	2004	6	30	4	3	14.58	41.780	81.080	5	541		3.33	0.41	3.53
ANSS	2005	2	8	11	42	53.00	37.220	81.930	9.4	499		2.85	0.41	3.04
ANSS	2005	2	15	2	36	55.00	37.190	81.920	11.2	499		2.93	0.41	3.12
ANSS	2005	8	25	3	9	42.00	35.880	82.800	7.9	629		3.66	0.41	3.85
ANSS	2005	12	7	19	29	45.83	35.862	82.380	5	597		2.93	0.41	3.12
ANSS	2006	3	7	10	28	2.00	35.910	82.340	3.7	591		2.93	0.41	3.12

Table 2.5-2— {Earthquakes 1985–2005, Update to the EPRI (NP-4726-A 1988) Seismicity Catalog with Emb ≥ 2.8, Within a 35° to 43° N, 71° to 89° W Latitude-Longitude Window, Incorporating the 200 mi (320 km) Radius Site Region}

(Page 4 of 4)

Catalog reference	Year	Month	Day	Hour	Minute	Second	Lat °N	Lon °W	Depth (km)	Dist. (km) [1]	Int	Emb	Smb	Rmb
ANSS	2006	3	11	12	27	15.60	41.780	81.390	5	560		3.17	0.41	3.37
ANSS	2006	6	20	20	11	18.54	41.840	81.230	5	554		3.80	0.10	3.81

Note: Information included in Int column when reference material provided the information.

[1] Epicental distance to site location taken as 38.4272°N, 76.4370°W

Table 2.5-3— {Conversion Between Body-Wave (m_b) and Moment (M) Magnitudes}
(Page 1 of 2)

Convert	To	Convert	To
m_b	M	M	m_b
4.00	3.77	4.00	4.28
4.10	3.84	4.10	4.41
4.20	3.92	4.20	4.54
4.30	4.00	4.30	4.66
4.40	4.08	4.40	4.78
4.50	4.16	4.50	4.90
4.60	4.24	4.60	5.01
4.70	4.33	4.70	5.12
4.80	4.42	4.80	5.23
4.90	4.50	4.90	5.33
5.00	4.59	5.00	5.43
5.10	4.69	5.10	5.52
5.20	4.78	5.20	5.61
5.30	4.88	5.30	5.70
5.40	4.97	5.40	5.78
5.50	5.08	5.50	5.87
5.60	5.19	5.60	5.95
5.70	5.31	5.70	6.03
5.80	5.42	5.80	6.11
5.90	5.54	5.90	6.18
6.00	5.66	6.00	6.26
6.10	5.79	6.10	6.33
6.20	5.92	6.20	6.40
6.30	6.06	6.30	6.47
6.40	6.20	6.40	6.53
6.50	6.34	6.50	6.60
6.60	6.49	6.60	6.66
6.70	6.65	6.70	6.73
6.80	6.82	6.80	6.79
6.90	6.98	6.90	6.85
7.00	7.16	7.00	6.91
7.10	7.33	7.10	6.97
7.20	7.51	7.20	7.03
7.30	7.69	7.30	7.09
7.40	7.87	7.40	7.15
7.50	8.04	7.50	7.20
		7.60	7.26
		7.70	7.32

Table 2.5-3— {Conversion Between Body-Wave (m_b) and Moment (M) Magnitudes}
(Page 2 of 2)

Convert	To	Convert	To
m_b	M	M	m_b
		7.80	7.37
		7.90	7.43
		8.00	7.49

Table 2.5-4— {Summary of Bechtel Group Seismic Sources}

Source	Description	Distance[1] (km)	Distance[1] (mi)	Pa [2]	M_{max} (m_b) and Wts[3]	Smoothing Options and Wts[4]	Contributed to 99% of EPRI Hazard[5]	New Information to Suggest Change in Source: Geometry?[6]	New Information to Suggest Change in Source: M_{max}?[7]	New Information to Suggest Change in Source: RI?[8]
Sources within 200 mi (320 km)										
BZ5	S. Appalachians	0	0	1.00	5.7(0.10) 6.0 (0.40) 6.3 (0.40) 6.6 (0.10)	1 (0.33) 2 (0.34) 3 (0.33)	Yes	No	No	No
E	Central Virginia	79	49	0.35	5.4 (0.10) 5.7 (0.40) 6.0 (0.40) 6.6 (0.10)	1 (0.33) 2 (0.34) 4 (0.33)	Yes	No	No	No
BZ4	Atlantic Coastal Region	104	65	1.00	6.6 (0.10) 6.8 (0.10) 7.1 (0.40) 7.4 (0.40)	1 (0.33) 2 (0.34) 3 (0.33)	Yes	No	No	No
17	Stafford fault zone	70	43	0.10	5.4 (0.10) 5.7 (0.40) 6.0 (0.40) 6.6 (0.10)	1 (0.33) 2 (0.34) 4 (0.33)	No	No	No	No
13	Eastern Mesozoic Basins	99	62	0.10	5.4 (0.10) 5.7 (0.40) 6.0 (0.40) 6.6 (0.10)	1 (0.33) 2 (0.34) 4 (0.33)	No	No	No	No
24	Bristol Trends	135	84	0.25	5.7 (0.10) 6.0 (0.40) 6.3 (0.40) 6.6 (0.10)	1 (0.33) 2 (0.34) 4 (0.33)	No	No	No	No
23	Lebanon Trend	177	110	0.05	5.4 (0.10) 5.7 (0.40) 6.0 (0.40) 6.6 (0.10)	1 (0.33) 2 (0.34) 4 (0.33)	No	No	No	No
25	NY-Alabama Lineament	240	149	0.30	5.4 (0.10) 5.7 (0.40) 6.0 (0.40) 6.6 (0.10)	1 (0.33) 2 (0.34) 4 (0.33)	No	No	No	No

Notes:

1. Closest Distance betweensite and source measured in WLA GIS system using EPRI source files
2. Pa = probability of activity
3. Maximum Magnitude (M_{max}) and weights (wts.)
4. Smoothing options are defined as follows:
   1 = constant a, constant b (no prior b)
   2 = low smoothing on a, high smoothing on b (no prior b)
   3 = low smoothing on a, low smoothing on b (no prior b)
   4 = low smoothing on a, low smoothing on b (weak prior of 1.05)
   Weights on magnitude intervals are (1.0, 1.0, 1.0, 1.0, 1.0, 1.0, 1.0)
5. Did the source contribute to 99% of EPRI hazard calculated at CCNPP?
6. No, unless new geometry proposed in literature
7. No, unless EPRI M_{max} exceeded in literature
8. RI = recurrence interval; assumed no change if no new paleoseismic data or rate of seismicity has not significantly changed.

Table 2.5-5— {Summary of Dames & Moore Seismic Sources}

(Page 1 of 2)

Source	Description	Distance[1]		Pa[2]	M_{max} (m_b) and Wts.[3]	Smoothing Options and Wts.[4]	Contributed to 99% of EPRI Hazard[5]	New Information to Suggest Change in Source:		
		(km)	(mi)					Geometry?[6]	M_{max}?[7]	RI?[8]
Sources within 200 mi (320 km)										
47	Connecticut Basin	0	0	0.28	6.0 (0.75) 7.2 (0.25)	3 (0.75) 4 (0.25)	Yes	No	No	No
53	S. Appalachian Mobile Belt (Default Zone)	0	0	0.26	5.6 (0.80) 7.2 (0.20)	1 (0.75) 2 (0.25)	Yes	No	No	No
41	S. Cratonic Margin (Default Zone)	65	40	0.12	6.1 (0.80) 7.2 (0.20)	1 (0.75) 2 (0.25)	Yes	No	No	No
42	Newark-Gettysburg Basin	92	57	0.40	6.3 (0.75) 7.2 (0.25)	3 (0.75) 4 (0.25)	Yes	No	No	No
40	Central VA Seismic Zone	110	68	1.00	6.6 (0.80) 7.2 (0.20)	1 (0.75) 2 (0.25)	Yes	No	No	No
4	Appalachian Fold Belts	138	86	0.35	6.0 (0.80) 7.2 (0.20)	1 (0.75) 2 (0.25)	Yes	No	No	No
4A	Kink in Fold Belts	669	416	0.65	6.8(0.75) 7.2 (0.25)	3 (0.75) 4 (0.25)	Yes	No[9]	No	No
44	Stafford Fault Zone	64	40	1.00	5.0(0.80) 7.2 (0.20)	1 (0.69) 2 (0.23) 3 (0.06) 4 (0.02)	No	No	No	No
C01	Combination zone 4-4A-4B-4C-4D	138	86	NA	6.0(0.80) 7.2 (0.20)	1 (0.75) 2 (0.25)	No	No	No	No
4C	Kink in Fold Belt	164	102	0.65	5.0 (0.75) 7.2 (0.25)	3(0.75) 4 (0.25)	No	No	No	No
45	Hopewell Fault Zone	181	112	1.00	5.0 (0.80) 7.2 (0.20)	1 (0.69) 2 (0.23) 3 (0.06) 4 (0.02)	No	No	No	No
48	Buried Triassic Basins	197	122	0.28	6.0 (0.75) 7.2 (0.25)	3 (0.75) 4 (0.25)	No	No	No	No

Table 2.5-5— {Summary of Dames & Moore Seismic Sources}

(Page 2 of 2)

Source	Description	Distance[1]		Pa[2]	M_{max} (m_b) and Wts.[3]	Smoothing Options and Wts.[4]	Contributed to 99% of EPRI Hazard[5]	New Information to Suggest Change in Source:		
		(km)	(mi)					Geometry?[6]	M_{max}?[7]	RI?[8]
Sources within 200 mi (320 km)										
46	Dan River Basin	241	150	0.28	6.0 (0.75) 7.2 (0.25)	3 (0.75) 4 (0.25)	No	No	No	No
8	E. Marginal Basin	272	169	0.08	5.6 (0.80) 7.2 (0.20)	1 (0.75) 2 (0.25)	No	No	No	No
C02	Combination zone 8-9	272	169	NA	5.6 (0.80) 7.2 (0.20)	1 (0.75) 2 (0.25)	No	No	No	No
4B	Kink in Fold Belt(Giles Co. Area)	273	170	0.65	6.2 (0.75) 7.2 (0.25)	3 (0.75) 4 (0.25)	No	No	No	No
4D	Kink in Fold Belt	279	173	0.65	5.6 (0.75) 7.2 (0.25)	3 (0.75) 4 (0.25)	No	No	No	No
49	Jonesboro Basin	302	188	0.28	6.0 (0.75) 7.2 (0.25)	3 (0.75) 4 (0.25)	No	No	No	No
43	Ramapo Fault	319	198	0.20	6.1 (0.75) 7.2 (0.25)	3 (0.75) 4 (0.25)	No	No	No	No

1.Closest Distance between site and source measured in WLA GIS system using EPRI source files
2.Pa = probability of activity
3. Maximum Magnitude (M_{max})and weights (wts.)
4.Smoothing options are defined as follows:
1 = No smoothing on a, no smoothing on b (strong prior of 1.04)
2 = No smoothing on a, no smoothing on b (weak prior of 1.04)
3 = Constant a, constant b (strong prior of 1.04)
4 = Constant a, constant b (weak prior of 1.04)
Weights on magnitude intervals are (0.1, 0.2, 0.4, 1.0, 1.0, 1.0, 1.0)
5. Did the source contribute to 99% of EPRI hazard calculated at CCNPP?
6. No, unless new geometry proposed in literature
7. No, unless EPRI M_{max} exceeded in literature
8. RI = recurrence interval; assumed no change if no new paleoseismic data or rate of seismicity has not significantly changed.
9. This source zone falls outside the project area and was not covered by the post-EPRI earthquake catalog discussed in 2.5.2.1.

Table 2.5-6— {Summary of Law Engineering Seismic Sources}

(Page 1 of 3)

Source	Description	Distance[1]			M_{max} (m_b)and Wts.[3]	Smoothing Options and Wts.[4]	Contributed to 99% of EPRI Hazard[5]	New Information to Suggest Change in Source:		
		(km)	(mi)	Pa[2]				Geometry?[6]	M_{max}?[7]	RI?[8]
Sources within 200 mi (320 km)										
C11	Combination Zone 22-35	0	0	NA	6.8 (1.00)	2a (1.00)	Yes	No	No	No
22	Reactivated E. Seaboard Normal	0	0	0.27	6.8 (1.00)	2a (1.00)	Yes	No	No	No
C10	Combination Zone 8-35	7.5	5	NA	6.8 (1.00)	2a (1.00)	Yes	No	No	No
C09	Mesozoic Basins (8-bridged)	7.5	5	NA	6.8 (1.00)	2a (1.00)	Yes	No	No	No
107	Eastern Piedmont	8	5	1.00	4.9 (0.30) 5.5 (0.40) 5.7 (0.30)	1a (1.00)	Yes	No	No	No
17	Eastern Basement	71	44	0.62	5.7 (0.20) 6.8 (0.80)	1b (1.00)	Yes	No	No	No
M21	Mafic Pluton	83	52	0.43	6.8 (1.00)	5 (1.00) (a = 0.65, b = 0.99)	Yes	No	No	No
M20	Mafic Pluton	90	56	0.43	6.8 (1.00)	5 (1.00) (a = 0.57, b = 0.99)	Yes	No	No	No
M19	Mafic Pluton	100	62	0.43	6.8 (1.00)	5 (1.00) (a = 0.35, b = 0.99)	Yes	No	No	No
M18	Mafic Pluton	128	80	0.43	6.8 (1.00)	5 (1.00) (a = 0.22, b = 1.04)	Yes	No	No	No
M17	Mafic Pluton	169	105	0.43	6.8 (1.00)	5 (1.00) (a = 0.5, b = 1.04)	Yes	No	No	No
M16	Mafic Pluton	186	116	0.43	6.8 (1.00)	5 (1.00) (a = 0.87,b = 1.04)	Yes	No	No	No
C13	Combination Zone 22 - 24 - 35	0	0	NA	6.8 (1.00)	2a (1.00)	No	No	No	No
8-16	Mesozoic Basins – 16	7.5	5	0.27	6.8 (1.00)	a and b values calculated for C09	No	No	No	No
217	Eastern Basement Background	71	44	1.00	4.9 (0.50) 5.7 (0.50)	1b (1.00)	No	No	No	No

Table 2.5-6— {Summary of Law Engineering Seismic Sources}

(Page 2 of 3)

Source	Description	Distance[1]			M_{max} (m_b)and Wts.[3]	Smoothing Options and Wts.[4]	Contributed to 99% of EPRI Hazard[5]	New Information to Suggest Change in Source:		
		(km)	(mi)	Pa[2]				Geometry?[6]	M_{max}?[7]	RI?[8]
Sources within 200 mi (320 km)										
M25	Mafic Pluton	124	77	0.43	6.8 (1.00)	5 (1.00) (a = -0.48, b = 1.05)	No	No	No	No
M22	Mafic Pluton	148	92	0.43	6.8 (1.00)	5 (1.00) (a = 0.66, b = 0.99)	No	No	No	No
M26	Mafic Pluton	158	98	0.43	6.8 (1.00)	5 (1.00) (a = -0.32, b = 1.05)	No	No	No	No
M23	Mafic Pluton	198	123	0.43	6.8 (1.00)	5 (1.00) (a = 1.26, b = 0.99)	No	No	No	No
M24	Mafic Pluton	204	127	0.43	6.8 (1.00)	5 (1.00) (a = 1.27, b = 0.99)	No	No	No	No
8-12	Mesozoic Basins – 12	207	129	0.27	6.8(1.00)	a and b values calculated for C09	No	No	No	No
101	Western New England	214	133	1.00	4.5 (0.15) 5.5 (0.85)	1c (1.00)	No	No	No	No
M30	Mafic Pluton	243	151	0.43	6.8 (1.00)	5 (1.00) (a = -1.23, b = 1.05)	No	No	No	No
M29	Mafic Pluton	257	160	0.43	6.8 (1.00)	5 (1.00) (a = -0.38, b = 1.05)	No	No	No	No
M27	Mafic Pluton	259	161	0.43	6.8 (1.00)	5 (1.00) (a = 0.41, b = 1.04)	No	No	No	No
112	Ohio-Pennsylvania Block	269	167	1.00	4.6 (0.20) 5.1 (0.50) 5.5 (0.30)	1a (1.00)	No	No	No	No
M28	Mafic Pluton	273	170	0.43	6.8(1.00)	5 (1.00) (a = 0.38, b = 1.04)	No	No	No	No

Table 2.5-6— {Summary of Law Engineering Seismic Sources}

(Page 3 of 3)

Source	Description	Distance[1]			M_{max} (m_b)and Wts.[3]	Smoothing Options and Wts.[4]	Contributed to 99% of EPRI Hazard[5]	New Information to Suggest Change in Source:		
		(km)	(mi)	Pa[2]				Geometry?[6]	M_{max}?[7]	RI?[8]
Sources within 200 mi (320 km)										

1. Closest Distance between site and source measured in WLA GIS system using EPRI source files
2. Pa = probability of activity
3. Maximum Magnitude (M_{max})and weights (wts.)
4. Smoothing options are defined as follows:
   1a = High smoothing on a, constant b (strong prior of 1.05)
   1b = High smoothing on b, constant b (strong prior of 1.00)
   1c = High smoothing on a, constant b (strong prior of 0.95)
   2a = Constant a, constant b (strong prior of 1.05)
   5 = a,b values as listed above, with weights shown
5. Did the source contributeto 99% of EPRI hazard calculated at CCNPP?
6. No, unless new geometry proposed in literature
7. No, unless EPRI M_{max} exceeded in literature
8. RI = recurrence interval; assumed no change if no new paleoseismic data or rate of seismicity has not significantly changed.

Table 2.5-7— {Summary of Rondout Seismic Sources}

(Page 1 of 2)

Source	Description	Distance[1]		Pa[2]	M_{max} (m_b) and Wts.[3]	Smoothing Options and Wts.[4]	Contributed to 99% of EPRI Hazard[5]	New Information to Suggest Change in Source:		
		(km)	(mi)					Geometry?[6]	M_{max}?[7]	RI?[8]
Sources within 200 mi (320 km)										
C01	Background 49	0	0	NA	4.8 (0.20) 5.5 (0.60) 5.8 (0.20)	3 (1.00)	Yes	No	No	No
30	Shenandoah	21	13	0.96	5.2 (0.30) 6.3 (0.55) 6.5 (0.15)	1 (1.00) (a = -1.710, b = 1.010)	Yes	No	No	No
29	Central VA	88	55	1.00	6.6 (0.30) 6.8 (0.60) 7.0 (0.10)	1 (1.00) (a = -0.900, b = 0.930)	Yes	No	No	No
31	Quakers	112	70	1.00	5.8 (0.15) 6.5 (0.60) 6.8 (0.25)	1 (1.00) (a = -1.200, b = 0.960)	Yes	No	No	No
C09	49+32	0	0	NA	4.8 (0.20) 5.5 (0.60) 5.8 (0.20)	3 (1.00)	No	No	No	No
49-03	Appalachian Basement 3	0	0	1.00	4.8 (0.20) 5.5 (0.60) 5.8 (0.20)	2 (1.00)	No	No	No	No
32	Norfolk Fracture Zone	116	72	0.67	5.8 (0.15) 6.5 (0.60) 6.8 (0.25)	1 (1.00) (a = -2.110, b = 1.040)	No	No	No	No
49-04	Appalachian Basement 4	198	123	1.00	4.8 (0.20) 5.5 (0.60) 5.8 (0.20)	2 (1.00)	No	No	No	No
C07	50 (02) + 12	213	132	NA	4.8 (0.20) 5.5 (0.60) 5.8 (0.20)	3 (1.00)	No	No	No	No
50-02	Grenville Province 2	213	132	1.00	4.8 (0.20) 5.5 (0.60) 5.8 (0.20)	2 (1.00)	No	No	No	No

Table 2.5-7— {Summary of Rondout Seismic Sources}

(Page 2 of 2)

Source	Description	Distance[1]		Pa[2]	M_{max} (m_b) and Wts.[3]	Smoothing Options and Wts.[4]	Contributed to 99% of EPRI Hazard[5]	New Information to Suggest Change in Source:		
		(km)	(mi)					Geometry?[6]	M_{max}?[7]	RI?[8]
Sources within 200 mi (320 km)										
28	Giles County	316	196	1.00	6.6 (0.30) 6.8 (0.60) 7.0 (0.10)	1 (1.00) (a = -1.130, b = 0.900)	No	No	No	No

1.Closest Distance between site and source measured in WLA GIS system using EPRI source files
2.Pa = probability of activity;
3. Maximum Magnitude (M_{max})and weights (wts.)
4. Smoothing options are defined as follows:
1, 6, 7, 8 = a, b values as listed above, with weights shown
2 = Not listed in EQHAZARD Primer
3 = Low smoothing on a, constant b (strong prior of 1.0)
5 = a, b values aslisted above, with weights shown
5. Did the source contribute to 99% of EPRI hazard calculated at CCNPP?
6. No, unless new geometry proposed in literature
7. No, unless EPRI M_{max} exceeded in literature
8. RI = recurrence interval; assumed no change if no new paleoseismic data or rate of seismicity has not significantly changed.

Table 2.5-8— {Summary of Weston Seismic Sources}

(Page 1 of 4)

Source	Description	Distance[1]		Pa[2]	M_{max} (m_b) and Wts.[3]	Smoothing Options and Wts.[4]	Contributed to 99% of EPRI Hazard[5]	New Information to Suggest Change in Source:		
		(km)	(mi)					Geometry?[6]	M_{max}?[7]	RI?[8]
Sources within 200 mi (320 km)										
C21	Combination Zone 104-25	0	0	NA	5.4 (0.24) 6.0 (0.61) 6.6 (0.15)	1a (0.30) 2a (0.70)	Yes	No	No	No
C23	Combination Zone 104-22-26	0	0	NA	5.4 (0.80) 6.0 (0.14) 6.6 (0.06)	1a (0.50) 2a (0.50)	Yes	No	No	No
C24	Combination Zone 104-22-25	0	0	NA	5.4 (0.80) 6.0 (0.14) 6.6 (0.06)	1a (0.50) 2a (0.50)	Yes	No	No	No
C27	Combination Zone 104-28BCDE-22-25	0	0	NA	5.4 (0.30) 6.0 (0.70)	1a (0.70) 2a (0.30)	Yes	No	No	No
C28	Combination Zone 104-28BCDE-22-26	0	0	NA	5.4 (0.30) 6.0 (0.70)	1a (0.70) 2a (0.30)	Yes	No	No	No
C34	Combination Zone 104-28BE-26	0	0	NA	5.4 (0.24) 6.0 (0.61) 6.6 (0.15)	1a (0.20) 1b (0.80)	Yes	No	No	No
C35	Combination Zone 104-28BE-25	0	0	NA	5.4 (0.24) 6.0 (0.61) 6.6 (0.15)	1a (0.20) 1b (0.80)	Yes	No	No	No
28E	Zone of Mesozoic Basin	7	4	0.26	5.4 (0.65) 6.0 (0.25) 6.6 (0.10)	1b (1.00)	Yes	No	No	No
22	Central VA Seismic Zone	72	45	0.82	5.4 (0.19) 6.0 (0.65) 6.6 (0.16)	1b (1.00)	Yes	No	No	No
C19	Combination Zone 103-23-24	118	73	NA	5.4 (0.26) 6.0 (0.58) 6.6 (0.16)	1a (1.00)	Yes	No	No	No

Table 2.5-8— {Summary of Weston Seismic Sources}

(Page 2 of 4)

Source	Description	Distance[1]		Pa[2]	M_{max} (m_b) and Wts.[3]	Smoothing Options and Wts.[4]	Contributed to 99% of EPRI Hazard[5]	New Information to Suggest Change in Source:		
		(km)	(mi)					Geometry?[6]	M_{max}?[7]	RI?[8]
Sources within 200 mi (320 km)										
C07	Combination Zone 21-19	182	113	NA	5.4 (0.62) 6.0 (0.29) 6.6 (0.09)	1b (0.70) 2b (0.30)	Yes	No	No	No
C22	Combination Zone 104-26	0	0	NA	5.4 (0.24) 6.0 (0.61) 6.6 (0.15)	1a (0.30) 1b (0.70)	No	No	No	No
C25	Combination Zone 104-28BCDE	0	0	NA	5.4 (0.24) 6.0 (0.61) 6.6 (0.15)	1a (0.30) 2a (0.70)	No	No	No	No
C26	Combination Zone 104-28BCDE-22	0	0	NA	5.4 (0.24) 6.0 (0.61) 6.6 (0.15)	1a (0.30) 2a (0.70)	No	No	No	No
104	Southern Coastal Plain	0	0	1.00	5.4 (0.24) 6.0 (0.61) 6.6 (0.15)	1a (0.20) 2a (0.80)	No	No	No	No
C01	Combination Zone 28A thru E	7	4	NA	5.4 (0.65) 6.0 (0.25) 6.6 (0.10)	1b (1.00)	No	No	No	No
28B	Zone of Mesozoic Basin	92	57	0.26	5.4 (0.65) 6.0 (0.25) 6.6 (0.10)	1b (1.00)	No	No	No	No
103	Southern Appalachians	118	73	1.00	5.4 (0.26) 6.0 (0.58) 6.6 (0.16)	1a (0.20) 2a (0.80)	No	No	No	No
C17	Combination Zone 103-23	118	73	NA	5.4 (0.26) 6.0 (0.58) 6.6 (0.16)	1a (0.70) 2a (0.30)	No	No	No	No
C18	Combination Zone 103-24	118	73	NA	5.4 (0.26) 6.0 (0.58) 6.6 (0.16)	1a (0.70) 1b (0.30)	No	No	No	No

Table 2.5-8— {Summary of Weston Seismic Sources}

(Page 3 of 4)

Source	Description	Distance[1]		Pa[2]	M_{max} (m_b) and Wts.[3]	Smoothing Options and Wts.[4]	Contributed to 99% of EPRI Hazard[5]	New Information to Suggest Change in Source:		
		(km)	(mi)					Geometry?[6]	M_{max}?[7]	RI?[8]
Sources within 200 mi (320 km)										
21	New York Nexus	182	113	1.00	5.4 (0.62) 6.0 (0.29) 6.6 (0.09)	1b (1.00)	No	No	No	No
C08	Combination Zone 21-19-10A	182	113	NA	5.4 (0.62) 6.0 (0.29) 6.6 (0.09)	1b (0.70) 2b (0.30)	No	No	No	No
28A	Mesozoic Basin (or Intersection of sources 28 and 21)	182	113	0.26	5.4 (0.65) 6.0 (0.25) 6.6 (0.10)	1b (1.00)	No	No	No	No
28D	Zone of Mesozoic Basin	205	127	0.26	5.4 (0.65) 6.0 (0.25) 6.6 (0.10)	1b (1.00)	No	No	No	No
C09	Combination Zone 21-19-10A-28A	213	132	NA	5.4 (0.62) 6.0 (0.29) 6.6 (0.09)	1b(1.00)	No	No	No	No
C10	Combination Zone 21-19-28A	213	132	NA	5.4 (0.62) 6.0 (0.29) 6.6 (0.09)	1b (1.00)	No	No	No	No
28C	Zone of Mesozoic Basin	263	163	0.26	5.4 (0.65) 6.0 (0.25) 6.6 (0.10)	1b (1.00)	No	No	No	No
102	Appalachian Plateau	290	180	1.00	5.4 (0.62) 6.0 (0.29) 6.6 (0.09)	1a (0.20) 2a (0.80)	No	No	No	No

Table 2.5-8— {Summary of Weston Seismic Sources}

(Page 4 of 4)

Source	Description	Distance[1]		Pa[2]	M_{max} (m_b) and Wts.[3]	Smoothing Options and Wts.[4]	Contributed to 99% of EPRI Hazard[5]	New Information to Suggest Change in Source:		
		(km)	(mi)					Geometry?[6]	M_{max}?[7]	RI?[8]
Sources within 200 mi (320 km)										

1. Closest Distance between site and source measured in WLA GIS system using EPRI source files
2. Pa = probability of activity
3. Maximum Magnitude (M_{max})and weights (wts.)
4. Smoothing options are defined as follows:
   1a = Constant a, constant b (medium prior of 1.0)
   1b = Constant a, constant b (medium prior of 0.9)
   2a = Medium smoothing on a, medium smoothing on b (medium prior of 1.0)
   2b = Medium smoothing on a, medium smoothing on b (medium prior of 0.9)
5. Did the source contribute to 99% of EPRI hazard calculated at CCNPP?
6. No, unless new geometry proposed in literature
7. No, unless EPRI M_{max} exceeded in literature
8. RI = recurrence interval; assumed no change if no new paleoseismic data or rate of seismicity has not significantly changed.

Table 2.5-9— {Summary of Woodward-Clyde Seismic Sources}

(Page 1 of 2)

Source	Description	Distance[1]		Pa[2]	M_{max} (m_b) and Wts.[3]	Smoothing Options and Wts.[4]	Contributed to 99% of EPRI Hazard[5]	New Information to Suggest Change in Source:		
		(km)	(mi)					Geometry?[6]	M_{max}?[7]	RI?8
Sources within 200 mi (320 km)										
B20	Calvert Cliffs Background	0	0	NA	5.8 (0.33) 6.2 (0.34) 6.6 (0.33)	1(0.25) 6 (0.25) 7 (0.25) 8 (0.25)	Yes	No	No	No
61	Tyrone-Mt.Union Lineament	0	0	0.048	5.4 (0.33) 6.5 (0.34) 7.1 (0.33)	3 (0.33) 4 (0.34) 5 (0.33)	Yes	No	No	No
21	New Jersey Isostatic Gravity Saddle	77	48	0.135	5.3 (0.33) 6.5 (0.34) 6.9 (0.33)	2 (0.10) 3 (0.10) 4 (0.10) 5(0.10) 9 (0.60) (a = -1.406, b = 1.020)	Yes	No	No	No
63	Pittsburg-Washington Lineament	84	52	0.050	5.4 (0.33) 6.3 (0.34) 7.1 (0.33)	3 (0.33) 4 (0.34) 5 (0.33)	Yes	No	No	No
26	Central VA Gravity Saddle	108	67	0.434	5.4 (0.33) 6.5 (0.34) 7.0 (0.33)	2 (0.25) 3 (0.25) 4 (0.25) 5 (0.25)	Yes	No	No	No
27	State Farm Complex	111	69	0.474	5.6 (0.33) 6.3 (0.34) 6.9 (0.33)	2 (0.25) 3 (0.25) 4 (0.25) 5 (0.25)	Yes	No	No	No
23	Newark Basin Perimeter	166	103	0.374	5.5 (0.33) 6.3 (0.34) 6.8 (0.33)	2 (0.10) 3 (0.10) 4 (0.10) 5 (0.10) 9 (0.60) (a = 1.415, b = 0.900)	Yes	No	No	No
21A	New Jersey Isostatic Gravity Saddle No. 2 (Combo C2)	77	48	0.045	5.5 (0.33) 6.3 (0.34) 7.1 (0.33)	2 (0.10) 3 (0.10) 4 (0.10) 5 (0.10) 9 (0.60) (a = -1.406, b = 1.020)	No	No	No	No
28	Richmond Basin	135	84	0.092	5.3 (0.33) 6.0 (0.34) 7.2 (0.33)	3 (0.33) 4 (0.34) 5 (0.33)	No	No	No	No
02	Cont. ShelfInt	147	91	0.129	5.3 (0.33) 6.5 (0.34) 6.8 (0.33)	3(0.33) 4 (0.34) 5 (0.33)	No	No	No	No

Table 2.5-9— {Summary of Woodward-Clyde Seismic Sources}

(Page 2 of 2)

Source	Description	Distance[1]		Pa[2]	M_{max} (m_b) and Wts.[3]	Smoothing Options and Wts.[4]	Contributed to 99% of EPRI Hazard[5]	New Information to Suggest Change in Source:		
		(km)	(mi)					Geometry?[6]	M_{max}?[7]	RI?8
Sources within 200 mi (320 km)										
53	SE NY/NJ/PA NOTA Zone	154	96	0.100	5.5 (0.33) 6.3 (0.34) 6.8 (0.33)	2 (0.10) 3 (0.10) 4 (0.10) 5 (0.10) 9 (0.60) (a = -1.406, b = 1.020)	No	No	No	No
01	Cont. Shelf	171	106	0.158	5.4 (0.33) 5.5 (0.34) 7.0 (0.33)	3 (0.33) 4 (0.34) 5 (0.33)	No	No	No	No
22	Newark Basin	194	121	0.078	5.5 (0.33) 6.5 (0.34) 7.1 (0.33)	2 (0.10) 3 (0.10) 4 (0.10) 5 (0.10) 9 (0.60) (a = -1.503, b = 0.776)	No	No	No	No
24	Ramapo Fault	315	196	0.128	5.8 (0.33) 6.8 (0.34) 7.1 (0.33)	3 (0.33) 4 (0.34) 5 (0.33)	No	No	No	No
25	Hudson Valley	315	196	0.140	5.5 (0.33) 6.3 (0.34) 6.8 (0.33)	2 (0.20) 3 (0.20) 4 (0.20) 5 (0.20) 9 (0.20) (a = -0.929, b = 0.857)	No	No	No	No

1. Closest Distance between site and source measured in WLA GIS system using EPRI source files
2. Pa = probability of activity
3. Maximum Magnitude (M_{max}) and weights (wts.)
4. Smoothing options are defined as follows:
   1 = Low smoothing on a, high smoothing on b (no prior)
   2 = High smoothing on a, high smoothing on b (no prior)
   3 = High smoothing on a, high smoothing on b (moderate prior of 1.0)
   4 = High smoothing on a, high smoothing on b (moderate prior of 0.9)
   5 = High smoothing on a, high smoothing on b (moderate prior of 0.8)
   6 = Low smoothing on a, high smoothing on b (moderate prior of 1.0)
   7 = Low smoothing on a, high smoothing on b (moderate prior of 0.9)
   8 = Low smoothing on a, high smoothing on b (moderate prior of 0.8)
   Weights on magnitude intervals are all 1.0
   9 = a and b values as listed
5. Did the source contribute to 99% of EPRI hazard calculated at CCNPP?
6. No, unless new geometry proposed in literature
7. No, unless EPRI M_{max} exceeded in literature.
8. RI = recurrence interval; assumed no change if no new paleoseismic data or rate of seismicity has not significantly changed.

Table 2.5-10— {Comparison of EPRI Characterizations of the Central Virginia Seismic Zone}

EPRI Team	Source	Description	Distance[1] (km)	Distance[1] (mi)	Pa[2]	M_{max} (m_b) and Wts.[3]	Largest M_{max} Value Considered by EPRI Team: mb	Largest M_{max} Value Considered by EPRI Team: Mw[4]	Contributed to 99% of EPRI Hazard[5]
Bechtel Group	E	CentralVirginia	79	49	0.35	5.4(0.10) 5.7 (0.40) 6.0 (0.40) 6.6 (0.10)	6.6	6.49	Yes
Dames& Moore	40	Central VA Seismic Zone	110	68	1.00	6.6(0.80) 7.2 (0.20)	7.2	7.51	Yes
Law Engineering[6]	na	na	na	na	na	na	na	na	na
Rondout	29	Central VA	85	55	1.00	6.6(0.30) 6.8 (0.60) 7.0 (0.10)	7.0	7.16	Yes
Weston	22	CentralVA Seismic Zone	72	45	0.82	5.4(0.19) 6.0 (0.65) 6.6 (0.16)	6.6	6.49	Yes
Woodward-Clyde Consultants	26	Central VA Gravity Saddle	108	67	0.434	5.4(0.33) 6.5 (0.34) 7.0 (0.33)	7.0	7.16	Yes
Range of Largest M_{max} Value Considered by EPRI Teams =							m_b 6.6- 7.2 **M 6.5 - 7.5**		
Average of Largest M_{max} Values for 5 EPRI Teams (m_b) =							6.9		
Average of Largest M_{max} Values for 5 EPRI Teams (**M**) =							7.0		

1. Closest distance between site and source measured in WLA GIS system using EPRI source files
2. Pa = probability of activity
3. Maximum Magnitude (M_{max}) and weights (wts.)
4. mb converted from Mw using relations as presented in Microsoft Excel spreadsheet and included in Table 2.5-3
5. Source contribution to 99% ofEPRI hazard at Calvert Cliffs
6. Law Engineering team didnot define a Central VA seismic zone, but did define several mafic pluton sources in the central Virginia area. The seismicity parameters for the pluton sources were calculated from a large region surrounding each pluton, which effectively captured a majority of seismicity from the CVSZ

Table 2.5-11— {Bollinger (1992) Seismic Source Zone Parameters}

Source	Description	Approx. Distance[1] (km)	(mi)	a	b	M_{max} mbLg[2]	Ms[2]	Mw[3]	Focal Depth Distribution (km) Upper Bound (D_U) 10% Quantile	Lower Bound (D_L) 90% Quantile
RZ6	Central VA	80	50	1.18	0.64	6.40	7.10	6.20	4.5	13.4
RZ3	Giles County,VA	356	221	1.07	0.64	6.30	6.80	6.06	4.4	15.1
CZ1	Complementary(Background)	0	0	2.70	0.84	5.75	5.80	5.36	3.3	18.5
LZ1	Charleston, SC	665	413	1.69	0.77	6.90	8.10	6.98	5.0	10.2
RZ4A	Eastern TN	613	380	2.72	0.90	7.35	8.75	7.78	7.6	20.8
RZ4	Eastern TN	613	380	2.72	0.90	6.45	7.15	6.27	7.6	20.8
RZ5	NW S.C.and SW N.C.	534	331	2.14	0.82	6.00	6.20	5.66	2.3	11.2
LZ3	South Carolina Piedmont and Coastal Plain	520	323	1.86	0.80	6.00	6.20	5.66	0.8	7.4
LZ4	SC Fall Line	779	484	1.58	0.81	6.25	6.50	5.99	0.9	6.1
LZ2	Bowman,S.C.	654	406	1.34	0.78	6.00	6.20	5.66	2.4	5.8
LZ5	Area of LZ3 minus Area of LZ4	534	331	1.70	0.80	6.00	6.20	5.66	0.9	6.5
LZ6	Savannah River Site	715	444	1.34	0.80	6.50	7.20	6.34	0.8	7.4
RZ1	New Madrid, MO (small)	1129	701	3.32	0.91	7.35	8.75	7.78	3.0	11.6
RZ2	New Madrid, MO (large)	988	613	3.43	0.88	6.70	7.65	6.65	2.8	12.4

Note:

1 Closest Distance between site and source estimated (approximately)

2 m_b and Ms values presented in Bollinger (1992).

3 **M** converted from mbLg using average relations as presented in Table 2.5-3

Table 2.5-12— {Chapman Seismic Source Zone Parameters}

Source	Description	Approx. Distance[1]		Area		M_{max}[4,5]	M_{max}[6]	M_{max}[6]
		(km)	(mi)	(sq. km)	Reference[3]	(mbLg)	(M_w)	(m_b)
1	Giles County, VA	350	217	5.1×10^3	A	7.25	7.53	7.22
2	Central VA	73	45	2.0×10^4	A	7.25	7.53	7.22
3	Eastern TN	660	410	3.7×10^4	A	7.25	7.53	7.22
4	Southern Appalachians (VA, NC, SC, TN)	290	180	7.6×10^4	C	7.25	7.53	7.22
5	Northern VA, MD	40	25	4.3×10^4	C	7.25	7.53	7.22
6	Central Appalachians (PA, NJ, NY)	100	60	6.8×10^4	C	7.25	7.53	7.22
7	Piedmont - Coastal Plain	0	0	4.4×10^5	C	7.25	7.53	7.22
8	Charleston, SC	680	420	1.2×10^3	A	7.25	7.53	7.22
9	Appalachian Foreland (TN, KY, OH, WVA, PA)	100	60	6.5×10^5	A	7.25	7.53	7.22
10	New Madrid, MO	1165	725	6.1×10^3	B	7.70	8.28	7.32

Notes:

1 Closest Distance between site and source estimated (approximately) from Figure 1 in Chapman (Chapman, 1994).

3 Reference cited:

A Bollinger (Bollinger, 1989)

B Johnston (Johnson, 1985)

C Chapman (Chapman, 1994)

4 Values listed in Chapman (Chapman, 1994). With the exception of New Madrid, they assumed all sources would have the same M_{max} as the largest EQ to have occurred in the southeastern U.S. region, the 1886 Charleston, SC event. The Johnston (1992) Mw 7.5 was used and converted to mbLg by Chapman (Chapman,1994) using Atkinson (Atkinson, 1987) relation.

5 Note that more recent estimates of Charleston EQ magnitude are lower than Mw 7.53 of Johnston (1992):

Mw = 7.3 +0.26/-0.26 (Johnston, 1996)

Mw = 6.8 +0.3/-0.4 (Bakun, 2004)

6 mb to Mw conversion done using average of relations as presented in Microsoft Excel spreadsheet and in Table 2.5-3.

Table 2.5-13— {Summary of Selected USGS Seismic Sources}

Source	Description	M_{max} (M_w) and Wts.	Largest M_{max} Value Considered by USGS	
			M_w	m_b [1]
Sources within 200 mi (320 km)				
	Extended Margin Background	7.5(1.00)	7.5	7.20
Selected Sources Beyond 200 mi (320km)				
	Charleston	6.8 (0.20) 7.1 (0.20) 7.3 (0.45) 7.5 (0.15)	7.5	7.20
	Stable Craton Background	7.0 (1.00)	7.0	6.91

Note:

(1) mb converted from **M** using average relations, as presented in Table 2.5-3.

Table 2.5-14— {Chapman and Talwani (2002) Seismic Source Zone Parameters}

Charleston Characteristic Sources		Mean Recurrence		M_{max} [2]	
				mbLg	M
Charleston Area Source		550 years		nr	7.1 (.2) 7.3 (.6) 7.5 (.2)
ZRA Fault Source (Zone of River Anomalies)		550 years		nr	7.1 (.2) 7.3 (.6) 7.5 (.2)
Ashley River-Woodstock Fault Source (modeled as 3 parallel faults)		550 years		nr	7.1 (.2) 7.3 (.6) 7.5 (.2)
Non-Characteristic Background Sources		**a[1]**	**b[1]**	**mbLg**	**M**
1.	Zone1	0.242	0.84	6.84	7.00
2.	Zone2	-0.270	0.84	6.84	7.00
3.	Central Virginia	1.184	0.64	6.84	7.00
4.	Zone4	0.319	0.84	6.84	7.00
5.	Zone5	0.596	0.84	6.84	7.00
6.	Piedmont and Coastal Plain	1.537	0.84	6.84	7.00
6a.	Pied&CP NE	0.604	0.84	6.84	7.00
6b.	Pied&CP SW	1.312	0.84	6.84	7.00
7.	South Carolina Piedmont	2.220	0.84	6.84	7.00
8.	Middleton Place	1.690	0.77	6.84	7.00
9.	Florida and continental margin	1.371	0.84	6.84	7.00
10.	Alabama	1.800	0.84	6.84	7.00
11.	Eastern Tennessee	2.720	0.90	6.84	7.00
12.	Southern Appalachian	2.420	0.84	6.84	7.00
12a.	Southern Appalachian North	2.185	0.84	6.84	7.00
13.	Giles County, VA	1.070	0.84	6.84	7.00
14.	Central Appalachians	1.630	0.84	6.84	7.00
15.	Western Tennessee	2.431	1.00	6.84	7.00
16.	Central Tennessee	2.273	1.00	6.84	7.00
17.	Ohio-Kentucky	2.726	1.00	6.84	7.00
18.	West VA-Pennsylvania	2.491	1.00	6.84	7.00
19.	USGS (1996) gridded seismicity rates and b value	nr[3]	0.95	6.84	7.00

Notes:

1 a and b values in terms of mbLg magnitude

2 M_{max} range for characteristic events was designed to "represent the range of magnitude estimates of the 1886 Charleston shock. Square brackets indicate weights assigned to characteristic magnitudes. For non-characteristic background events, a truncated form of the exponential probability density function was used.

3 nr = not reported

Table 2.5-15— {Summary of Charleston Seismic Sources Changed in New UCSS Model (Bechtel, 2006)}

(Page 1 of 2)

ESTs	Source	Description	Distance		Pa[1]	M_{max} (m_b) and Wts.[2]	Smoothing Options and Wts.[3]	Interdependencies[4]	New Information to Suggest Change in Source:		
			(km)	(mi)					Geometry?[5]	M_{max}?[6]	RI?[7]
Bechtel Group	H	Charleston Area	644	400	0.50	6.8 (0.20) 7.1 (0.40) 7.4 (0.40)	1 (0.33) 2 (0.34) 4 (0.33)	P(H|N3) = 0.15	Yes[8]	Yes[8]	Yes[8]
Bechtel Group	N3	Charleston Faults	673	418	0.53	6.8 (0.20) 7.1 (0.40) 7.4 (0.40)	1 (0.33) 2 (0.34) 4 (0.33)	P(N3|H) = 0.16	Yes[8]	Yes[8]	Yes[8]
Dames & Moore	54	Charleston Seismic Zone	637	395	1.00	6.6 (0.75) 7.2 (0.25)	1 (0.22) 2 (0.08) 3 (0.52) 4 (0.18)	none	Yes[8]	Yes[8]	Yes[8]
Law Engineering	35	Charleston Seismic Zone	648	403	0.45	6.8(1.00)	2a(1.00)	Overlaps 8 and 22	Yes[8]	Yes[8]	Yes[8]
Rondout	24	Charleston	631	392	1.00	6.6 (0.20) 6.8 (0.60) 7.0 (0.20)	1 (1.00) (a = -0.710, b = 1.020)	none	Yes[8]	Yes[8]	Yes[8]
Weston	25	Charleston Seismic Zone	619	384	0.99	6.6 (0.90) 7.2 (0.10)	1b (1.00)	none	Yes[8]	Yes[8]	Yes[8]
Woodward-Clyde	30	Charleston (includes NOTA)	646	401	0.573	6.8 (0.33) 7.3 (0.34) 7.5 (0.33)	2 (0.10) 3 (0.10) 4 (0.10) 5 (0.10) 9 (0.60) (a = -1.005, b = 0.852)	ME with 29, 29A	Yes[8]	Yes[8]	Yes[8]
Woodward-Clyde	29	S.Carolina Gravity Saddle (Extended)	534	332	0.122	6.7 (0.33) 7.0 (0.34) 7.4 (0.33)	2(0.25) 3 (0.25)4 (0.25)5 (0.25)	ME with 29A, 29B, and 30	Yes[8]	Yes[8]	Yes[8]
Woodward-Clyde	29A	SC Gravity Saddle No. 2 (Combo C3)	577	359	0.305	6.7 (0.33) 7.0 (0.34) 7.4 (0.33)	2 (0.25) 3 (0.25) 4 (0.25) 5 (0.25)	ME with 29, 29B, and 30	Yes[8]	Yes[8]	Yes[8]
Notes:											

Table 2.5-15— {Summary of Charleston Seismic Sources Changed in New UCSS Model (Bechtel, 2006)}

(Page 2 of 2)

ESTs	Source	Description	Distance		Pa[1]	M_{max} (m_b) and Wts.[2]	Smoothing Options and Wts.[3]	Interdependencies[4]	New Information to Suggest Change in Source:		
			(km)	(mi)					Geometry?[5]	M_{max}?[6]	RI?[7]
1	Pa = probability of activity										
2	Maximum Magnitude (M_{max}) and weights (wts.)										
3	Smoothing options are defined as follows: SeeTable 2.5-3 thru Table 2.5-8 for details.										
4	ME = mutually exclusive; PD = perfectly dependent;										
5	No,unless (1) new geometry proposed in literature or (2) new seismicity pattern										

Table 2.5-16— {Geographic Coordinates (Latitude and Longitude) of Corner Points of Updated Charleston Seismic Source (UCSS) Geometries (Bechtel, 2006)}

Source Geometry	Longitude, West (decimal degrees)	Latitude, North (decimal degrees)
A	80.707	32.811
A	79.840	33.354
A	79.527	32.997
A	80.392	32.455
B	81.216	32.485
B	78.965	33.891
B	78.3432	33.168
B	80.587	31.775
B'	78.965	33.891
B'	78.654	33.531
B'	80.900	32.131
B'	81.216	32.485
C	80.397	32.687
C	79.776	34.425
C	79.483	34.351
C	80.109	32.614

Table 2.5-17— {Local Charleston-Area Tectonic Features}

Name of Feature	Evidence	Key References
Adams Run fault	**subsurface stratigraphy**	**(Weems, 2007)**
Ashley River fault	microseismicity	Talwani (1982, 2000) **(Weems, 2007)**
Appalachian detachment (decollement)	gravity & magnetic data seismic reflection & refraction	Cook (1979, 1981) Behrendt (1981, 1983) (Seeber, 1981)
Blake Spur fracture zone	oceanic transform postulated to extend westward to Charleston area	(Fletcher, 1978) (Sykes, 1978) (Seeber, 1981)
Bowman seismic zone	microseismicity	Smith and Talwani (1985)
Charleston fault	subsurface stratigraphy	(Lennon, 1986) (Talwani, 2000) **(Weems, 2007)**
Cooke fault	seismic reflection	Behrendt (1981, 1983) (USGS, 1983a) (USGS, 1983c) Behrendt and Yuan (1987)
Drayton fault	seismic reflection	(USGS, 1983a) (Behrendt, 1983) (Behrendt, 1987)
East Coast fault system/ Zone of river anomalies (ZRA)	geomorphology seismic reflection microseismicity	(Marple ,1993) Marple (2000, 2004)
Gants fault	seismic reflection	(Hamilton, 1983) (Behrendt, 1987)
Helena Banks fault zone	seismic reflection	Behrendt (1981, 1983) (Behrendt, 1987)
Middleton Place-Summerville seismic zone	microseismicity	(SSA, 1981) (SSA, 1993)
Sawmill Branch fault	**microseimicity**	**(Talwani, 2004)**
Summerville fault	**microseimicity**	**USGS, 1997**
Woodstock fault	geomorphology microseismicity	Talwani (1982, 1999, 2000) Marple (1990, 2000)

Note: Those tectonic features identified following publication of the EPRI teams' reports (post-1986) are highlighted by **bold-face** type.

Table 2.5-18— {Comparison of Post-EPRI NP-6395-D 1989 Magnitude Estimates for the 1886 Charleston Earthquake}

Study	Magnitude Estimation Method	Reported Magnitude Estimate	Assigned Weights	Mean Magnitude (M)
EPRI (1994)	worldwide survey of passive-margin, extended-crust earthquakes	**M 7.56 ± 0.35**	--	7.56
Martin (1994)	geotechnical assessment of 1886 liquefaction data	**M 7 - 7.5**	--	7.25
Johnston (1996)	isoseismal area regression, accounting for eastern North America anelastic attenuation	**M 7.3 ± 0.26**	--	7.3
Chapman (2002) (South Carolina Department of Transportation)	consideration of available magnitude estimates	**M 7.1** **M 7.3** **M 7.5**	0.2 0.6 0.2	7.3
Frankel et al**.** (2002) (USGS National seismic hazard mapping project)	consideration of available magnitude estimates	**M 6.8** **M 7.1** **M 7.3** **M 7.5**	0.20 0.20 0.45 0.15	7.2
Bakun (2004)	isoseismal area regression, including empirical site corrections	MI 6.4 - 7.2	--	6.9
Note:				
95% confidence interval estimate; MI (intensity magnitude) is considered equivalent to **M** (Bakun and Hopper 2004).				

Table 2.5-19— {Comparison of Talwani and Schaeffer (2001) and UCSS Age Constraints on Charleston-Area Paleoliquefaction Events}

Liquefaction Event	Event Age (YBP) [2]	Talwani (2001) [1]				(Bechtel 2006)
		Scenario 1		Scenario 2		
		Source	M	Source	M	Event Age(YBP) [2, 3, 4]
1886A.D.	64	Charleston	7.3	Charleston	7.3	64
A	546± 17	Charleston	7+	Charleston	7+	600± 70
B	1,021± 30	Charleston	7+	Charleston	7+	1,025± 25
C	1,648± 74	Northern	6+	--	--	--
C′	1,683± 70	--	--	Charleston	7+	1,695± 175
D	1,966± 212	Southern	6+	--	--	--
E	3,548± 66	Charleston	7+	Charleston	7+	3,585± 115
F	5,038± 166	Northern	6+	Charleston	7+	--
F′	--	--	--	--	--	5,075± 215
G	5,800± 500	Charleston	7+	Charleston	7+	--
Notes:						

1 Modified after Talwani, 2001 Table 2.

2 Years before present, relative to 1950 A.D.

3 Event ages based upon recalibration of radiocarbon (to 2-sigma using OxCal 3.8 (Bronk Ramsey, 1995; 2001) data presented in Talwani 2001 Table 2.

4 See Table B-1 for recalibrated 2-sigma sample ages and Table B-2 for 2 sigma age contrainsts on paleoliquefaction events.

Table 2.5-20— {Comparison of EPRI-SOG Seismic Hazard Results and Replication Calculated in 2006, for PGA, 10 Hz, and 1 Hz Spectral Velocity}

PGA comparison			
Ampl, cm/sˆ2	2006 mean	EPRI-SOG mean	% difference
50	4.43E-04	4.30E-04	3.1%
100	1.07E-04	1.03E-04	3.8%
250	1.17E-05	1.13E-05	3.5%
500	1.42E-06	1.37E-06	3.7%
10 Hz comparison			
Ampl, cm/s	2006 mean	EPRI-SOG mean	% difference
1	7.92E-04	7.74E-04	2.3%
5	2.39E-05	2.32E-05	2.9%
10	3.41E-06	3.33E-06	2.5%
20	3.32E-07	3.26E-07	1.7%
1 Hz comparison			
Ampl, cm/s	2006 mean	EPRI-SOG mean	% difference
1	1.59E-03	1.56E-03	1.9%
5	1.35E-04	1.33E-04	1.3%
10	3.64E-05	3.58E-05	1.6%
20	7.68E-06	7.53E-06	1.9%

Table 2.5-21— {Mean Magnitudes and Distances from Deaggregations}

Struct. frequency	Annual Freq. Exceed.	Overall hazard		Hazard from R<100 km		Hazard from R>100 km	
		M	R, km	M	R, km	M	R, km
1 & 2.5 Hz	1.00E-04	6.3	300	5.6	39	6.8	430
5 & 10 Hz	1.00E-04	5.5	97	5.5	35	6.2	220
1 & 2.5 Hz	1.00E-05	6.3	220	5.8	27	6.9	450
5 & 10 Hz	1.00E-05	5.4	35	5.5	18	6.5	190
1 & 2.5 Hz	1.00E-06	6.2	120	5.9	18	7.1	460
5 & 10 Hz	1.00E-06	5.5	17	5.6	11	6.8	160

Table 2.5-22— {Horizontal and Vertical GMRS Amplitudes and Common V/H Ratios}

Freq	Horizontal GMRS (g)	Vertical GMRS (g)	V/H
0.1	2.70E-03	2.03E-03	0.75
0.125	4.70E-03	3.52E-03	0.75
0.15	7.85E-03	5.89E-03	0.75
0.2	2.02E-02	1.52E-02	0.75
0.3	3.35E-02	2.51E-02	0.75
0.4	3.57E-02	2.68E-02	0.75
0.5	4.25E-02	3.19E-02	0.75
0.6	6.73E-02	5.04E-02	0.75
0.7	8.19E-02	6.14E-02	0.75
0.8	9.14E-02	6.85E-02	0.75
0.9	9.55E-02	7.16E-02	0.75
1	1.03E-01	7.69E-02	0.75
1.25	1.23E-01	9.23E-02	0.75
1.5	1.28E-01	9.64E-02	0.75
2	1.23E-01	9.26E-02	0.75
2.5	1.29E-01	9.70E-02	0.75
3	1.51E-01	1.14E-01	0.75
4	1.69E-01	1.27E-01	0.75
5	1.72E-01	1.29E-01	0.75
6	1.80E-01	1.40E-01	0.778
7	1.72E-01	1.38E-01	0.802
8	1.64E-01	1.35E-01	0.823
9	1.57E-01	1.32E-01	0.841
10	1.50E-01	1.28E-01	0.858
12.5	1.38E-01	1.23E-01	0.892
15	1.28E-01	1.18E-01	0.921
20	1.09E-01	1.05E-01	0.965
25	9.80E-02	9.80E-02	1
30	8.77E-02	8.77E-02	1
35	8.27E-02	8.27E-02	1
40	7.97E-02	7.97E-02	1
45	7.81E-02	7.81E-02	1
50	7.73E-02	7.73E-02	1
60	7. 63E-02	7.63E-02	1
70	7.59E-02	7.59E-02	1
80	7.57E-02	7.57E-02	1
90	7.56E-02	7.56E-02	1
100	7.55E-02	7.55E-02	1

Table 2.5-23— {Calvert Cliffs Site Amplification Factors for 10^{-4} and 10^{-5} Input Motions and HF and LF Rock Spectra}

Freq. (Hz)	10^{-4} HF	10^{-4} LF	10^{-5} HF	10^{-5} LF
0.1	2.36	1.45	2.52	1.45
0.125	2.22	1.66	2.31	1.68
0.15	2.32	1.99	2.38	2.05
0.2	3.25	3.21	3.24	3.27
0.3	3.06	3.03	2.99	2.89
0.4	1.94	1.86	1.92	1.78
0.5	1.92	1.79	1.95	1.81
0.6	2.65	2.52	2.67	2.49
0.7	2.94	2.84	2.89	2.73
0.8	3.01	2.94	2.96	2.82
0.9	2.99	2.92	2.92	2.77
1	3.10	3.03	3.02	2.85
1.25	3.21	3.16	3.07	2.94
1.5	2.64	2.61	2.50	2.40
2	1.86	1.85	1.76	1.70
2.5	1.63	1.61	1.53	1.47
3	1.71	1.67	1.59	1.51
4	1.66	1.61	1.48	1.39
5	1.29	1.25	1.13	1.06
6	1.21	1.18	1.03	0.97
7	1.06	1.03	0.88	0.83
8	0.94	0.92	0.77	0.73
9	0.85	0.83	0.69	0.66
10	0.77	0.77	0.62	0.60
12.5	0.62	0.64	0.48	0.50
15	0.53	0.56	0.40	0.44
20	0.40	0.47	0.30	0.37
25	0.34	0.42	0.26	0.35
30	0.31	0.39	0.23	0.33
35	0.29	0.38	0.23	0.33
40	0.29	0.38	0.23	0.33
45	0.30	0.39	0.24	0.34
50	0.32	0.41	0.25	0.36
60	0.37	0.46	0.30	0.41
70	0.46	0.55	0.36	0.49
80	0.56	0.65	0.44	0.58
90	0.65	0.74	0.51	0.66
100	0.73	0.81	0.57	0.72

Table 2.5-24— {Values of UHS (Hard Rock Conditions)}

Frequency, Hz	10^{-4} SA, g	10^{-4} SA, g	10^{-5} SA, g	10^{-5} SA, g	10^{-6} SA, g	10^{-6} SA, g
	Mean	Median	Mean	Median	Mean	Median
100	0.0766	0.0579	0.271	0.198	0.845	0.546
25	0.228	0.155	0.767	0.529	2.39	1.46
10	0.149	0.121	0.493	0.389	1.42	1.04
5	0.102	0.0839	0.309	0.246	0.846	0.599
2.5	0.0577	0.0459	0.158	0.123	0.402	0.274
1	0.0269	0.0191	0.0722	0.0450	0.166	0.0989
0.5	0.0164	0.00938	0.0488	0.0224	0.114	0.0476

Table 2.5-25— {Summary Thickness and Termination Elevation}

ENTIRE SITE		Thickness [feet]			Termination Elevation [feet]		
		Min	Max	Avg	Min	Max	Avg
Stratum I - Terrace Sand		1	68	28	32	82	61
Stratum IIa - Chesapeake Clay/Silt		4	36	19	5	67	43
Stratum IIb - Chesapeake Cemented Sand	Layer 1	3	69	24	-2	46	22
	Layer 2	3	55	23	-17	30	0
	Layer 3	4	39	16	-31	-9	-22
Stratum IIc - Chesapeake Clay/Silt		190	195	193	-215	-208	-211
Stratum III - Nanjemoy Sand		>101*	>115*	>108*	-	-	-
** Data based on borings B-301 and B-401*							
POWERBLOCK AREA		**Thickness [feet]**			**Termination Elevation [feet]**		
		Min	**Max**	**Avg**	**Min**	**Max**	**Avg**
Stratum I - Terrace Sand		1	52	21	45	79	62
Stratum IIa - Chesapeake Clay/Silt		4	30	18	34	55	45
Stratum IIb - Chesapeake Cemented Sand	Layer 1	8	45	26	3	43	20
	Layer 2	4	55	23	-17	28	-3
	Layer 3	5	39	16	-31	-9	-23
Stratum IIc - Chesapeake Clay/Silt		190	190	190	-208	-208	-208
Stratum III - Nanjemoy Sand		>101*	>101*	>101*	-	-	-
** Data based on borings B-301*							
INTAKE AREA		**Thickness [feet]**			**Termination Elevation [feet]**		
		Min	**Max**	**Avg**	**Min**	**Max**	**Avg**
Stratum I - Terrace Sand (NP)		-	-	-	-	-	-
Stratum IIa - Chesapeake Clay/Silt (NP)		-	-	-	-	-	-
Stratum IIb - Chesapeake Cemented Sand	Layer 1	5	5	5	3	3	3
	Layer 2	3	31	15	-12	-1	-8
	Layer 3	9	24	15	-28	-17	-22
Stratum IIc - Chesapeake Clay/Silt		>13	>141	>57	-	-	-
Stratum III - Nanjemoy Sand		-	-	-	-	-	-
** Data based on borings B-775 (NP) Not Present*							

Table 2.5-26— {Summary of Field Tests}

Field	Test Standard	Number of Tests
Test Borings	ASTM D1586/1587	200
Observation Wells	ASTM D5092	47
CPT Soundings(1)	ASTM D5778	74*
Suspension P-S Velocity Logging	EPRI TR-102293	13
Test Pits	N/A	20
Field Electrical Resistivity Arrays	ASTM G57/IEEE 81	4
SPT Hammer Energy Measurements	ASTM D4633	10
Pressuremeter	ASTM D4719	2
Dilatometer	ASTM D6635	2
Notes: - (1) Includes additional off-set soundings		

Table 2.5-27— {Summary of As-Conducted Boring Information}

(Page 1 of 5)

Location	Depth [ft]	Termination Elevation (Bottom) [ft]	Coordinates [ft], Maryland State Plane (NAD 1927)		Surface Elevation [ft] (NGVD 1929)	Date of As Built Survey
			North	East		
B-301	403.0	-308.5	217024.1	960815.1	94.5	9/15/2006
B-301A	350.0	-253.3	217011.1	960816.8	96.7	11/21/2008
B-301B	120.0	-23.2	217002.6	960819.2	96.8	11/21/2008
B-302	200.0	-123.6	217122.2	960767.0	76.4	9/15/2006
B-303	200.0	-112.6	217016.9	960867.7	87.4	9/15/2006
B-304	200.0	-132.0	217188.6	960896.9	68.0	9/15/2006
B-305	151.5	-79.5	217166.3	960686.7	72.0	9/15/2006
B-306	150.0	-31.4	217024.3	960681.8	118.6	9/15/2006
B-307	201.5	-82.2	216955.3	960690.1	119.3	9/15/2006
B-308	150.0	-42.9	216906.7	960771.3	107.1	9/15/2006
B-309	150.0	-49.9	216949.2	960890.7	100.1	9/15/2006
B-310	100.0	-8.4	217081.4	960616.6	91.6	5/15/2006
B-311	150.0	-91.6	217268.6	960771.8	58.4	9/15/2006
B-312	99.5	-44.2	217293.0	960740.0	55.3	5/15/2006
B-313	150.0	-99.3	217372.3	960713.7	50.7	9/15/2006
B-314	100.0	-47.2	217321.9	960654.5	52.8	9/15/2006
B-315	100.0	-34.5	217184.7	960559.4	65.5	9/15/2006
B-316	100.0	8.1	216767.2	960864.4	108.1	9/15/2006
B-317	100.0	-5.6	217094.7	961249.2	94.4	5/15/2007
B-318	200.0	-102.2	217019.3	961227.2	97.8	5/15/2006
B-319	100.0	2.9	216963.6	961123.0	102.9	9/15/2006
B-320	150.0	-43.6	216943.5	961044.1	106.4	5/15/2006
B-321	150.0	-79.3	217152.5	960333.2	70.7	5/25/2006
B-322	100.0	-10.1	217170.0	960202.7	89.9	9/15/2006
B-323	200.0	-92.5	217028.0	960060.9	107.5	9/15/2006
B-324	101.5	3.7	216906.4	960114.4	105.2	9/15/2006
B-325	100.0	-15.0	216949.0	960549.7	85.0	9/15/2006
B-326	100.0	3.1	216859.2	960652.3	103.1	9/15/2006
B-327	150.0	-63.1	216865.7	960573.4	86.9	9/15/2006
B-328	150.0	-73.7	216828.9	960493.2	76.3	9/19/2006
B-329	100.0	-25.2	216800.4	960379.4	74.8	9/19/2006
B-330	100.0	-14.5	216715.4	960523.7	85.5	9/15/2006
B-331	100.0	-31.7	216970.6	960481.8	68.3	9/15/2006
B-332	100.0	-34.6	217127.4	960400.5	65.4	9/15/2006
B-333	98.8	-9.3	216657.0	960386.2	89.5	9/15/2006
B-334	100.0	-13.3	216515.5	960556.6	86.8	9/15/2006
B-335	100.0	-0.5	216732.7	960703.3	99.5	5/15/2006
B-336	100.0	-3.1	216632.9	960750.3	96.9	9/15/2006
B-337	100.0	-28.2	217257.9	960264.4	71.8	9/15/2006
B-338	99.6	-1.6	217121.1	960150.1	98.0	5/25/2006
B-339	100.0	-8.0	217095.2	960212.0	92.0	9/15/2006
B-340	100.0	-15.4	217171.3	961225.2	84.6	9/15/2006
B-341	100.5	-2.3	217036.4	961104.5	98.2	9/15/2006
B-342	250.0	-174.3	217217.6	960272.9	75.7	11/21/2008
B-343	250.0	-166.9	217037.8	960306.8	83.1	11/21/2008

Table 2.5-27— {Summary of As-Conducted Boring Information}
(Page 2 of 5)

Location	Depth [ft]	Termination Elevation (Bottom) [ft]	Coordinates [ft], Maryland State Plane (NAD 1927)		Surface Elevation [ft] (NGVD 1929)	Date of As Built Survey
			North	East		
B-344	250.0	-177.7	216976.8	960358.0	72.3	5/14/2008
B-345	250.0	-180.4	217097.3	960392.9	69.6	11/21/2008
B-346	100.0	-38.2	217206.4	960400.4	61.8	5/14/2008
B-347	200.0	-139.8	217214.2	960531.8	60.2	5/14/2008
B-348	200.0	-131.6	217148.9	960567.4	68.4	11/21/2008
B-349	100.0	-45.6	217396.4	960537.5	54.4	5/15/2008
B-350	100.0	-53.4	217516.2	960789.0	46.6	5/14/2008
B-351	100.0	-29.9	217072.1	960538.3	70.1	11/21/2008
B-352	200.0	-90.7	216829.4	960893.9	109.3	11/21/2008
B-353	200.0	-89.1	216772.7	960972.2	110.9	5/13/2008
B-354	251.5	-159.1	217131.1	961098.9	92.4	11/20/2008
B-355	250.0	-161.8	217052.6	960993.5	88.2	5/13/2008
B-356	250.0	-129.0	216965.3	961264.9	121.0	11/20/2008
B-357	105.0	-1.9	216923.1	961175.4	103.1	11/20/2008
B-357A	250.0	-147.0	216928.8	961167.0	103.0	11/20/2008
B-401	401.5	-329.4	216344.1	961516.8	72.1	9/15/2006
B-402	200.0	-117.8	216405.1	961463.5	82.2	5/15/2006
B-403	200.0	-136.6	216305.8	961562.9	63.4	5/15/2006
B-404	200.0	-132.1	216441.3	961596.5	67.9	9/21/2006
B-405	150.0	-28.0	216487.4	961408.7	122.0	9/15/2006
B-406	150.0	-31.6	216315.6	961352.0	118.4	9/15/2006
B-407	200.0	-118.4	216239.0	961412.5	81.6	9/15/2006
B-408	150.0	-81.6	216261.7	961482.0	68.4	9/15/2006
B-409	150.0	-88.5	216253.8	961614.8	61.6	4/20/2006
B-410	55.0	64.1	216374.3	961323.7	119.1	4/20/2006
B-410A*	98.7	20.4	216381.3	961323.7	119.1	4/20/2006
B-411	150.0	-68.6	216556.3	961517.2	81.5	9/15/2006
B-412	98.9	-6.7	216589.2	961495.4	92.2	9/15/2006
B-413	150.0	-27.1	216694.9	961413.3	122.9	9/15/2006
B-414	100.0	21.2	216630.2	961354.5	121.2	9/15/2006
B-415	98.7	20.6	216480.9	961264.2	119.3	4/20/2006
B-416	100.0	-13.8	216084. 5	961596.3	86.2	9/15/2006
B-417	101.5	-52.3	216435.8	961901.1	49.2	9/15/2006
B-418	200.0	-156.3	216340.3	961976.7	43.7	9/22/2006
B-419	100.0	-44.7	216267.8	961895.6	55.3	9/21/2006
B-420	150.0	-87.4	216213.5	961670.4	62.6	9/15/2006
B-421	150.0	-34.4	216497.6	961019.8	115.6	9/15/2006
B-422	100.0	4.0	216478.2	960915.0	104.0	9/15/2006
B-423	201.5	-91.4	216331.8	960850.2	110.1	9/15/2006
B-424	100.0	18.9	216263.3	960818.6	118.9	4/26/2006
B-425	101.5	16.9	216247.5	961274.7	118.4	4/20/2006
B-426	100.0	-16.3	216193.0	961386.6	83.7	9/21/2006
B-427	150.0	-33.7	216164.1	961272.7	116.3	9/19/2006
B-428	150.0	-35.9	216109.2	961210.1	114.1	9/19/2006
B-429	100.0	3.7	216087.9	961119.3	103.7	9/19/2006

Table 2.5-27— {Summary of As-Conducted Boring Information}
(Page 3 of 5)

Location	Depth [ft]	Termination Elevation (Bottom) [ft]	Coordinates [ft], Maryland State Plane (NAD 1927)		Surface Elevation [ft] (NGVD 1929)	Date of As Built Survey
			North	East		
B-430	100.0	2.5	216006.9	961193.1	102.5	9/19/2006
B-431	101.5	16.9	216271.1	961177.3	118.4	4/20/2006
B-432	100.0	18.6	216399.0	961139.1	118.6	4/20/2006
B-433	100.0	-2.5	215963.8	961107.5	97.5	4/27/2006
B-434	100.0	5.2	215827.1	961244.3	105.2	5/2/2006
B-435	100.0	7.7	216020.1	961404.7	107.7	9/15/2006
B-436	100.0	8.3	215923.9	961441.6	108.3	9/22/2006
B-437	100.5	10.1	216521.8	960968.8	110.6	9/15/2006
B-438	6.5	99.5	216414.9	960848.9	106.0	9/28/2006
B-438A	100.0	6.6	216412.0	960867.3	106.6	9/28/2006
B-439	100.0	13.8	216340.5	960948.7	113.8	9/15/2006
B-440	100.0	-43.7	216349.5	961813.7	56.3	9/21/2006
B-701	75.0	-66.3	219485.5	960507.6	8.7	9/21/2006
B-702	50.0	-39.7	218980.6	961183.2	10.3	9/21/2006
B-703	100.0	-54.6	218171.0	960957.0	45.4	9/21/2006
B-704	50.0	-10.4	217991.1	960926.1	39.6	9/21/2006
B-705	50.0	-3.3	217581.3	960917.9	46.8	4/19/2006
B-706	50.0	27.4	217140.1	961339.7	77.4	9/21/2006
B-707	50.0	17.4	217397.0	961481.8	67.4	9/21/2006
B-708	100.0	-62.7	217585.8	961810.6	37.4	9/28/2006
B-709	50.0	-18.8	217642.8	961978.2	31.3	9/28/2006
B-710	75.0	-27.0	217542.5	962136.9	48.0	9/28/2006
B-711	50.0	3.0	216755.7	961743.5	53.0	4/19/2006
B-712	50.0	-7.6	216506.2	961997.6	42.4	9/22/2006
B-713	50.0	8.0	216117.7	962283.2	58.0	9/28/2006
B-714	50. 0	66.0	215705.7	962034.4	116.0	10/16/2006
B-715	50.0	36.3	214951.8	962639.6	86.3	10/17/2006
B-716	49.5	32.9	215003.2	961364.6	82.4	10/16/2006
B-717	50.0	40.7	214302.5	962349.3	90.7	10/17/2006
B-718	50.0	67.5	214130.5	961929.1	117.5	10/18/2006
B-719	49.4	25.8	213978.7	961500.2	75.2	10/18/2006
B-720	75.0	-1.5	215674.5	962378.5	73.5	9/28/2006
B-721	100.0	1.3	215545.8	962462.1	101.3	5/4/2006
B-722	73.9	25.9	215386.1	962467.0	99.8	5/4/2006
B-723	75.0	15.0	215108.0	963000.8	90.0	4/28/2006
B-724	100.0	-3.0	214780.0	963106.2	97.0	4/28/2006
B-725	75.0	-16.0	214664.3	963219.4	59.0	4/28/2006
B-726	75.0	3.3	215564.7	961709.6	78.3	10/16/2006
B-727	100.0	4.9	215300.9	961885.0	104.9	10/16/2006
B-728	75.0	37.3	215163.6	961910.1	112.3	10/16/2006
B-729	75.0	42.3	214861.9	962454.6	117.3	10/17/2006
B-730	75.0	40.4	214728.5	962523.8	115.4	10/17/2006
B-731	99.3	16.4	214546.5	962547.9	115.7	10/17/2006
B-732	75.0	15.7	215034.1	961594.7	90.7	5/11/2006
B-733	100.0	-12.1	214866.8	961697.7	87.9	5/11/2006

Table 2.5-27— {Summary of As-Conducted Boring Information}
(Page 4 of 5)

Location	Depth [ft]	Termination Elevation (Bottom) [ft]	Coordinates [ft], Maryland State Plane (NAD 1927)		Surface Elevation [ft] (NGVD 1929)	Date of As Built Survey
			North	East		
B-734	75.0	30.7	214589.6	961812.5	105.7	5/9/2006
B-735	75.0	16.2	214805.5	961021.8	91.2	10/16/2006
B-736	75.0	23.3	214681.7	961154.3	98.3	10/16/2006
B-737	100.0	-36.5	214511.9	961147.4	63.5	10/16/2006
B-738	75.0	12.3	213826.3	961679.6	87.3	10/19/2006
B-739	99.8	0.5	213719.6	961793.3	100.4	10/19/2006
B-740	75.0	-0.7	213605.1	961781.1	74.3	10/19/2006
B-741	75.0	6.4	213760.5	961029.8	81.4	10/18/2006
B-742	100.0	2.4	213472.8	961217.2	102.4	10/18/2006
B-743	75.0	28.6	213315.7	961232.0	103.6	5/9/2006
B-744	100.0	13.3	216377.3	959963.4	113.3	9/29/2006
B-745	75.0	36.7	215971.2	960529.0	111.7	9/29/2006
B-746	75.0	7.8	215743.4	960721.4	82.8	9/29/2006
B-747	75.0	15.3	216176.3	959945.0	90.3	9/29/2006
B-748	100.0	-17.6	216039.7	960288.7	82.4	9/29/2006
B-749	75.0	27.5	215775.1	960332.2	102.5	9/29/2006
B-750	73.9	-1.6	215849.2	959930.1	72.4	9/29/2006
B-751	73.9	18.3	215588.9	960146.2	92.2	9/29/2006
B-752	100.0	-4.2	215489.2	960257.6	95.8	9/29/2006
B-753	40.0	8.8	217831.2	960648.9	48.8	9/21/2006
B-754	50.0	17.0	217369.8	960290.4	67.0	9/21/2006
B-755	40.0	55.0	215923.7	961637.9	95.0	9/22/2006
B-756	50.0	56.9	215504.6	961215.1	106.9	4/21/2006
B-757	40.0	66.9	215135.1	960760.6	106.9	10/16/2006
B-758	40.0	42.6	215133.3	960332.7	82.6	10/16/2006
B-759	100.0	-1.7	214526.3	960025.3	98.4	10/19/2006
B-765	102.0	-4.6	216424.5	959701.2	97.4	9/29/2006
B-766	50.0	58.9	216932.9	959791.5	108.9	9/19/2006
B-768	100.0	-51.6	217116.0	962243.0	48.4	9/28/2006
B-769	50.0	4.2	216589.8	962559.5	54.2	9/28/2006
B-770	50.0	71.6	215466.6	962827.0	121.6	10/18/2006
B-771	100.0	-89.4	219268.2	960931.9	10.6	7/1/2008
B-772	100.0	-89.4	219323.9	960876.1	10.6	7/1/2008
B-773	165.0	-157.1	219241.3	961045.9	7.9	7/1/2008
B-773A	150.0	-141.7	219233.1	961052.9	8.3	11/25/2008
B-773B	150.0	-142.0	219248.1	961039.9	8.0	11/25/2008
B-774	150.0	-139.9	219196.0	961000.5	10.1	7/1/2008
B-775	100.0	-90.3	219105.3	961091.5	9.7	7/1/2008
B-776	51.5	-41.9	219143.0	961053.7	9.6	7/14/2008
B-778	121.5	-7.9	219075.0	960739.6	113.6	11/25/2008
B-779	102.0	-1.2	218941.1	960604.8	100.8	7/2/2008
B-780	6.0	3.7	219546.2	960610.0	9.7	11/25/2008
B-780A	8.0	1.2	219542.4	960604.1	9.2	11/25/2008
B-780B	50.0	-40.8	219532.9	960625.2	9.2	11/25/2008
B-781	50.0	-39.6	219400.9	960780.8	10.4	7/14/2008

Table 2.5-27— {Summary of As-Conducted Boring Information}
(Page 5 of 5)

Location	Depth [ft]	Termination Elevation (Bottom) [ft]	Coordinates [ft], Maryland State Plane (NAD 1927)		Surface Elevation [ft] (NGVD 1929)	Date of As Built Survey
			North	East		
B-782	51.5	-41.6	218936.5	961232.1	9.9	7/1/2008
B-785	70.0	28.1	218155.9	960637.4	98.1	11/25/2008
B-786	11.5	50.5	217943.5	960500.5	62.0	11/25/2008
B-786A	80.0	-17.9	217943.2	960496.4	62.1	11/25/2008
B-786B	115.0	-60.8	217914.6	960460.7	54.2	11/25/2008
B-787	100.0	-50.6	217780.9	960598.1	49.4	11/25/2008
B-788	50.0	2.1	217495.9	960896.1	52.1	11/21/2008
B-789	100.0	-42.7	217401.7	960986.9	57.3	11/21/2008
B-790	49.7	23.0	217278.1	961110.5	72.7	5/13/2008
B-791	100.0	-12.5	217143.5	961245.1	87.5	5/13/2008
B-821	50.0	-41.1	218736.3	961124.6	8.9	7/1/2008
B-821A	115.0	-89.6	218571.3	960962.8	25.4	11/25/2008
B-821B	7.6	-1.3	218727.2	961275.2	6.3	11/25/2008
B-821C	30.0	-22.6	218739.5	961258.1	7.4	11/25/2008
B-822	50.0	-11.2	218440.2	960840.8	38.8	7/2/2008

Table 2.5-28— {Summary of Standard Penetration Test Data}

ENTIRE SITE		SPT N VALUE [Blows/ft]			SPT N CORRECTED [Blows/ft]		
		Min	Max	Avg	Min	Max	Avg
Stratum I - Terrace Sand		0	70	11	0	91	16
Stratum IIa - Chesapeake Clay/Silt		3	100	10	4	100	14
Stratum IIb - Chesapeake Cemented Sand	Layer 1	4	100	59	6	100	82
	Layer 2	0	100	16	0	100	22
	Layer 3	10	100	43	14	100	60
Stratum IIc - Chesapeake Clay/Silt		5	100	20	7	100	28
Stratum III - Nanjemoy Sand		28	100	56	36	100	72
POWERBLOCK AREA		**SPT N VALUE [Blows/ft]**			**SPT N CORRECTED [Blows/ft]**		
		Min	Max	Avg	Min	Max	Avg
Stratum I - Terrace Sand		0	70	10	0	91	14
Stratum IIa - Chesapeake Clay/Silt		3	50	11	4	70	15
Stratum IIb - Chesapeake Cemented Sand	Layer 1	6	100	63	9	100	89
	Layer 2	1	100	17	1	100	24
	Layer 3	12	100	45	16	100	63
Stratum IIc - Chesapeake Clay/Silt		9	100	21	14	100	30
Stratum III - Nanjemoy Sand		34	100	58	44	100	75
INTAKE AREA		**SPT N VALUE [Blows/ft]**			**SPT N CORRECTED [Blows/ft]**		
		Min	Max	Avg	Min	Max	Avg
Stratum I - Terrace Sand		-	-	-	-	-	-
Stratum IIa - Chesapeake Clay/Silt		-	-	-	-	-	-
Stratum IIb - Chesapeake Cemented Sand	Layer 1	26	26	26	35	35	35
	Layer 2	1	100	12	1	100	17
	Layer 3	12	100	39	16	100	54
Stratum IIc - Chesapeake Clay/Silt		5	44	16	7	59	22
Stratum III - Nanjemoy Sand		-	-	-	-	-	-

Notes:
- A cut-off value of 100 blows/ft is used

Table 2.5-29— {Summary Undisturbed Tube Samples}
(Page 1 of 9)

Boring	Drill Rig	Date	Sample No.	Depth [ft]	Rec [in]	Field Remarks
B-301	U. TRUCK	5/25/2006	UD-1	33.5 - 35.5	24	MH
			UD-2	43.5 - 45.3	21	MH
			UD-3	88.5 - 90.5	0	
			UD-4	98.5 - 99.8	6	SM
			UD-5	138.5 - 140.5	4	SC / SM
		5/30/2006	UD-6	158.5 - 159.6	13	13" push, CL with fine sand
			UD-7	168.5 - 170.5	9	CL / MH
			UD-8	183.5 - 184.3	10	MH
B-301A	U. TRUCK	8/18/2008	UD-1	58.0 - 58.8	9	SP
			UD-2	60.0 - 61.9	23	SC
			UD-3	68.0 - 69.8	22	SM
			UD-4	198.0 - 199.9	23	MH
			UD-5	218.0 - 219.9	23	SM
			UD-6	238.0 - 239.9	23	MH
			UD-7	258.0 - 260.0	24	MH
			UD-8	268.0 - 269.8	22	MH
			UD-9	278.0 - 279.9	23	MH
			UD-10	288.0 - 290.0	24	MH
			UD-11	298.0 - 300.0	24	MH
			UD-12	308.0 - 309.9	23	SC
			UD-13	318.0 - 319.9	23	SC
			UD-14	328.0 - 330.0	24	SC
			UD-15	338.0 - 339.8	22	SC
			UD-16	348.0 -350.0	24	SM
B-301B	U. TRUCK	8/25/2008	UD-1	78.0 - 80.0	24	SM
			UD-2	88.0 - 89.9	23	SM
			UD-3	98.0 - 100.0	24	SM
			UD-4	108.0 -110.0	24	SM
			UD-5	118.0 -120.0	24	SM
B-302	C. ATV	5/30/2006	UD-1	83.5 - 84.9	16	16" push SM with fine sand, shell
			UD-2	128.5 - 130.5	12	MH
B-303	U. TRUCK	5/9/2006	UD-1	28 - 30	24	CL
				38 - 39.6	19	19" push, SC
B-304	U. ATV	5/30/2006	UD-1	73.5 - 75.5	22	SM
			UD-2	98.5 - 99.5	12	12" push, SC
			UD-3	138.5 - 139.3	10	MH
B-305	C.ATV	7/17/2006	UD-1	12.5 - 14.3	22	CH
			UD-2	19.5 - 21.2	16	MH
			P-3	35 - 37	5	pitcher, cemented sand
			P-4	39.5 - 41.5	22	pitcher, SM
			UD-5	52.5 - 53.5	7	f. sandy silt, shell
			P-6	89.5 - 91.5	8	pitcher, sand
B-306	U. TRUCK	5/5/2006	UD-1	58 - 60	24	CL
			UD-2	68 - 70	24	CL

Table 2.5-29— {Summary Undisturbed Tube Samples}
(Page 2 of 9)

Boring	Drill Rig	Date	Sample No.	Depth [ft]	Rec [in]	Field Remarks
B-307	U. TRUCK	5/15/2006	UD-1	123.5 - 124.7	14	SM
			UD-2	178.5 - 180.4	23	MH
B-308	U. TRUCK	5/3/2006	UD-1	43 - 45	24	CL
		5/4/2006	UD-2	53 - 55	16	CL
		5/4/2006	UD-3	63 - 65	0	sand
B-309	C. TRUCK	5/11/2006	UD-1	33.5 - 35.5	23	CL
		5/11/2006	UD-2	43.5 - 45.5	24	CL
		5/11/2006	UD-3	53.5 - 55.5	23	SC
B-310	C. ATV	6/15/2006	UD-1	78.5 - 79.8	15	SC
B-312	C. ATV	5/18/2006	UD-1	10.5 - 12.3	17	21" push, CH
		5/18/2006	UD-2	38.5 - 38.6	0	0.5" push
		5/18/2006	UD-3	98.5 - 99.5	12	12" push, MH
B-313	U. ATV	5/22/2006	UD-1	93.5 - 94.7		CL
			UD-2	123.5 - 124.3		ML
B-314	U. ATV	5/22/2006	UD-1	13.5 - 15.5	12	CH
B-315	C. ATV	5/22/2006	UD-1	23.5 - 25.5	14	CH
B-316	C. TRUCK	5/4/2006	UD-1	43.5 - 45.5	24	CL
		5/4/2006	UD-2	53.5 - 55.5	24	CL
B-317	C. TRUCK	5/5/2006	UD-1	28.5 - 30.5	24	CL
		5/5/2006	UD-2	38.5 - 40.5	24	CH
		5/5/2006	UD-3	48.5 - 50.3	21	SC
B-318	U. ATV	6/3/2006	UD-1	148.5 - 149.1	3	7" push, f. sandy SILT
B-319	U. ATV	5/5/2006	UD-1	33.5 - 35.5	24	MH
		5/5/2006	UD-2	43.5 - 45.5	27	MH
		5/5/2006	UD-3	53.5 - 54.3	10	MH
B-320	C. TRUCK	5/8/2006	UD-1	38.5 - 40.5	24	MH
		5/9/2006	UD-2	48.5 - 50	18	18" push, clayey sand
B-321	C. ATV	6/5/2006	UD-1	23.5 - 25	18	CH
		6/6/2006	UD-2	73.5 - 75.5	24	SM
B-322	U. ATV	5/18/2006	UD-1	28.5 - 30.5	28	CL
			UD-2	38.5 - 39.9	27	SM
			UD-3	48.5 - 49.3	9	SC
B-323	U. ATV	6/7/2006	UD-1	83.5 - 84.8	15	MH
			UD-2	178.5 - 179.1	0	MH
B-324	U. ATV	6/7/2006	UD-1	60 - 62	24	CH
			P-2	69 - 71	22	SM
			P-3	85.5 - 87.5	5	SM
B-326	U. ATV	5/4/2006	UD-1	33.5 - 35.5	28	CL
		5/4/2006	UD-2	43.5 - 45.5	28	MH
		5/4/2006	UD-3	53.5 - 55.5	27	sandy lean clay, bottom 2" bent
B-327	C. ATV	5/25/2006	UD-1	113.5 - 114.2	9	ML
			UD-2	138.5 - 140.5	10	SM
B-328	C.ATV	6/19/2006	UD-1	63.5 - 65.5	24	SM
			UD-2	93.5 - 94.6	12	SC
			UD-3	123.5 - 124.4	11	ML, shell

Table 2.5-29— {Summary Undisturbed Tube Samples}
(Page 3 of 9)

Boring	Drill Rig	Date	Sample No.	Depth [ft]	Rec [in]	Field Remarks
B-329	C.ATV	6/13/2006	UD-1	63.5 - 65.3	22	SM
			UD-2	73.5 - 75.5	24	SM
B-330	U. ATV	5/25/2006	UD-1	28.5 - 29.2	0	
B-331	C. ATV	5/24/2006	UD-1	18.5 - 20.5	24	MH
B-332	C. ATV	6/2/2006	UD-1	73.5 - 74.6	13	SM
B-333	U. ATV	5/17/2006	UD-1	28.5 - 30.5	24	MH
			UD-2	38.5 - 40.5	24	CL
			UD-3	48.5 - 48.8	4	SM
B-334	U. TRUCK	5/24/2006	UD-1	23 - 25	24	CL
			UD-2	33 - 35	13	CL
B-335	U. ATV	5/3/2006	UD-1	31 - 33	24	CL
			UD-2	38.5 - 40.5	24	CH
			UD-3	48.5 - 50.5	24	CL
			UD-4	58.5 - 58.8	3	tube deformed, SPT @ bottom, sand with shell
B-336	U. ATV	5/15/2006	UD-1	33.5 - 35.5	24	CH
			UD-2	43.5 - 45.5	24	CH
			UD-3	53.5 - 55.5	15	SC
B-337	C. ATV	6/7/2006	UD-1	53.5 - 54.6	13	ML
B-338	C.ATV	6/13/2006	UD-1	48.5 - 50.5	24	MH / ML
			UD-2	94.5 - 95.0	?	not on boring log
			UD-3	95 - 97	?	not on boring log
			UD-4	98.5 - 99.6	7	SM
B-340	C.TRACK	8/4/2006	P-1	66 - 68	12	SC, cemented
B-341	C.TRACK	8/4/2006	UD-1	88.5 - 90.5	24	SM
			UD-2	98.5 - 100.5	24	SP-SM
B-344	C. ATV	7/24/2008	UD-1	181.5 - 182.8	16	SM
			UD-2	191.5 - 193.4	23	SM
			UD-3	201.5 - 202.5	12	SM
			UD-4	204.0 - 206.0	24	SM
			UD-5	211.5 - 213.5	24	SM
			UD-6	221.5 - 223.5	24	ML
			UD-7	231.5 - 233.5	24	ML
			UD-8	241.5 - 243.5	24	ML
B-354	C. ATV	7/3/2008	UD-1	196.5 - 197.3	10	SM
			UD-2	197.3 - 199.3	24	SM
			UD-3	206.5 - 208.5	24	SM
			UD-4	216.5 - 218.5	24	SP-SM
			UD-5	226.5 - 228.5	24	SM
			UD-6	236.5 - 238.5	24	SM
			UD-7	246.5 - 248.1	19	SM
B-355	C. ATV	7/15/2008	UD-1	191.5 - 193.4	23	ML
			UD-2	201.5 - 203.4	23	SM

Table 2.5-29— {Summary Undisturbed Tube Samples}
(Page 4 of 9)

Boring	Drill Rig	Date	Sample No.	Depth [ft]	Rec [in]	Field Remarks
B-356	C-TRUCK	7/16/2008	UD-1	221.5 - 222.6	13	ML
			UD-2	223.0 - 224.5	18	ML
			UD-3	231.5 - 233.5	24	SM
			UD-4	241.5 - 243.5	24	SM
B-401	U.TRUCK	6/20/2006	UD-1	68.5 - 70.5	23	SM
			UD-2	98.5 - 99.8	15	ML
			UD-3	123.5 - 124.8	16	CL
			UD-4	138.5 - 140.5	23	MH
		6/21/2006	UD-5	158.5 -159.3	10	MH
		6/21/2006	UD-6	173.5 - 174.4	11	MH
		6/22/2006	UD-7	198.5 - 200.5	21	ML
		6/22/2006	UD-8	213.5 - 214.6	13	ML
			UD-9	228.5 - 229.6	13	ML
			UD-10	243.5 - 244.4	8	ML
			UD-11	348.5 - 350.5	7	
B-403	C.ATV	6/21/2006	UD-1	63.5 - 64.9	20	SM
			UD-2	98.5 - 99.5	12	ML
			UD-3	123.5 - 124.5	12	ML
B-404	U.ATV	6/23/2006	UD-1	52 - 53.6	18	SP-SM
			UD-2	66 - 67.5	18	SC
			UD-3	83.5 - 85.1	17	SC
B-405	C. TRUCK	5/16/2006	UD-1	58.5 - 60.5	22	CL
			UD-2	68.5 - 70.5	24	CL
B-406	U. TRUCK	5/17/2006	UD-1	63.5 - 65.5	24	CH
			UD-2	73.5 - 75.2	12	21" push, SC
B-407	U. ATV	5/14/2006	UD-1	53.5 - 54.5	11	12" push, SM with shell
		5/15/2006	UD-2	78.5 - 79	4	tube bent, SM
		5/15/2006	UD-3	128.5 - 129	6	ML with sand
		5/15/2006	UD-4	153.5 - 153.9	5	tube bent, MH
B-409	C.TRUCK	6/22/2006	P-1	35	13	Pitcher, SP
			UD-2	17.5 - 19	24	SC
			UD-3	50 - 52	24	SM
			UD-4	62.5 - 64.5	24	SM
			UD-5	95 - 96.6	19	ML, sandy SILT
		6/27/2006	UD-6	137.5 - 139	18	MH
B-410	C. TRUCK	5/1/2006	UD-1	53.5 - 55.5	0	shelby tube lost in hole, not accepted
		5/1/2006	UD-2	60.5 - 62.5	15.5	remnant tube recovered, not accepted
B-410A	C. TRUCK	5/1/2006		53.5 - 55.5	24	CH, not on log
		5/1/2006	UD-2	63.5 - 65.5	7	CH
		5/2/2006	UD-3	73.5 - 75	18	CH, f. sand at bottom
B-411	C.ATV	7/26/2006	UD-1	23 - 25	16	CH
B-413	U. TRUCK	5/15/2006	UD-1	73 - 75	24	CL
B-414	U. TRUCK	5/11/2006	UD-1	58 - 60	24	CL
		5/11/2006	UD-2	68 - 70	24	CL

Table 2.5-29— {Summary Undisturbed Tube Samples}
(Page 5 of 9)

Boring	Drill Rig	Date	Sample No.	Depth [ft]	Rec [in]	Field Remarks
B-420	U. TRUCK	6/6/2006	UD-1	63.5 - 65.5	24	SM
		6/7/2006	UD-2	128.5 - 130.3	22	CL
B-421	C. TRUCK	5/10/2006	UD-1	48.5 - 50.5	24	ML
		5/10/2006	UD-2	58.5 - 60.5	24	CL
B-422	C. ATV	5/4/2006	UD-1	38.5 - 40.5	24	CL
		5/4/2006	UD-2	48.5 - 50.5	23	CH
		5/4/2006	UD-3	58.5 - 59.3	8	CH / SC
B-423	C. ATV	5/4/2006	UD-1	103.5 - 105.3	21	SM
			UD-	113.5 - 113.8	0	
			UD-2	158.5 - 160.1	19	CL
			UD-3	178.5 - 179.8	16	MH
			UD-4	188.5 - 189.2	8	MH
B-425	U. TRUCK	5/1/2006	UD-1	57 - 59	24	CH
		5/1/2006	UD-2	65 - 67	24	CH
		5/1/2006	UD-3	75 - 77	24	CH
B-427	C. TRUCK	5/2/2006	UD-1	63.5 - 65.5	24	CH
		5/2/2006	UD-2	73.5 - 74.8	15	SC
B-428	U. TRUCK	5/2/2006	UD-1	57 - 59	21	CH, bottom 10" bent
		5/2/2006	UD-2	60 - 62	24	CL, bent
		5/2/2006	UD-3	63 - 65	20	CL, bottom 10" bent
		5/2/2006	UD-4	66 - 68	24	CL, bottom 5" bent
		5/2/2006	UD-5	69 - 71	7	CL, bottom 3" bent
B-429	U. ATV	5/1/2006	UD-1	45 - 47	24	CH
		5/1/2006	UD-2	53.5 - 55.5	0	
		5/1/2006	UD-3	58.5 - 60	18	SC
B-430	C. ATV	5/1/2006	UD-1	30 - 32	10	ML
		5/1/2006	UD-2	38.5 - 39.2	5	SC
		5/1/2006	UD-3	48.5 - 50.1	18	MH
		5/1/2006	UD-4	58.5 - 59.3	18	ML
B-433	C. TRUCK	5/17/2006		28.5 - 30.5	24	not on log
		5/17/2006	UD-2	38.5 - 40.5	24	CL
		5/17/2006	UD-3	48.5 - 48.8	4	CL from log
B-434	C. ATV	5/9/2006	UD-1	43.5 - 45.5	6.5	CL
		5/9/2006	UD-2	53.5 - 55	18	CH
		5/10/2006	UD-3	63.5 - 64.3	14	CH
B-436	C. ATV	5/9/2006	UD-1	48.5 - 50.5	18	CL
B-437	U.TRUCK	7/10/2006	UD-1	13.5 - 15.5	23	SM
			UD-2	98.5 - 100.5	22	SM
B-438a	U.TRUCK	7/10/2006	UD-1	93.5 - 95.5	14	SM
B-440	U. ATV	6/6/2006	UD-1	51 - 53	24	SM
			UD-2	58.5 - 58.6	0	
B-701	C.TRUCK	6/28/2006	UD-1	43.5 - 44.9	17	ML
B-703	C.TRUCK	6/28/2006	UD-1	18.5 - 20.5	19	CH
			UD-2	73.5 - 75.5	10	SM
B-708	U. ATV	5/9/2006	UD-1	78.5 - 79.5	12	12" push, sand
B-714	U. ATV	5/9/2006	UD-1	48 - 50	24	SC

Table 2.5-29— {Summary Undisturbed Tube Samples}
(Page 6 of 9)

Boring	Drill Rig	Date	Sample No.	Depth [ft]	Rec [in]	Field Remarks
B-722	U.ATV	7/18/2006	UD-1	13 - 15	24	SM
B-723	C.TRACK	6/1/2006	UD-1	28.5 - 30.2	20	SP-SC
			UD-2	38.5 - 40.5	24	CL
B-724	C. TRACK	6/5/2006	UD-1	73.5 - 75.5	21	SM
B-725	C. TRACK	6/6/2006	UD-1	63.5 - 65.5	24	SM
B-726	C.TRACK	8/1/2006	UD-1	10.5 - 12.5	0	No Recovery
		8/1/2006	UD-2	23.5 - 25.5	19.5	CH
B-727	C. ATV	5/10/2006	UD-1	48.5 - 50.5	22	
		5/11/2006	UD-2	63.5 - 65.5	20	24" push
B-728	C. ATV	5/11/2006	UD-1	53.5 - 55.5	23	CH
B-729	C. TRUCK	5/19/2006	UD-1	68.5 - 70.5	24	CH
B-730	C. TRUCK	5/18/2006	UD-1	53.5 - 55.5	0	No Recovery
			UD-2	68.5 - 70.5	24	CH
B-731	C. TRACK	5/31/2006	UD-1	58.5 - 60.5	24	SM
B-732	C.TRACK	6/8/2006	UD-1	15 - 17	24	SM
B-733	C. TRACK	6/8/2006	UD-1	23.5 - 25.5	24	CL
			UD-2	88.5 - 90.5		CH/MH
B-734	C. TRACK	6/7/2006	UD-1	48.5 - 50.5	24	CL
B-735	C.TRACK	6/28/2006	UD-1	28 - 30	24	sand
B-737	C.TRACK	7/19/2006	UD-1	10.5 - 12.5	24	SC / CL
B-739	C. TRACK	6/15/2006	UD-1	51- 52	12	SC
			UD-2	83.5 - 84	5	CL
			UD-3	96 - 96.8	9	SP-SM
B-742	C. TRACK	6/15/2006	UD-1	78.5 - 78.6	0	
			UD-2	88.5 - 88.8	3	SM, sample placed in jar
B-743	U.ATV	7/10/2006	UD-1	23.5 - 25.5	21	SM
			UD-2	38 - 40	0	
B-746	C. TRACK	7/18/2006	UD-1	13.5 -15.5	24	SM
B-748	C.TRACK	7/17/2006	UD-1	13.5 - 15.5	24	ML
B-749	C. TRUCK	5/23/2006	UD-1	43.5 - 45.5		
B-750	C.TRACK	7/10/2006	UD-1	28.5 - 30.5	0	
			UD-2	48.5 - 49.5	11	clayey sand, shells
B-751	C. TRUCK	5/22/2006	UD-1	33.5 - 35.5		
			UD-2	43.5 - 45.5		
B-752	C.TRACK	7/5/2006	UD-1	58 - 59.5	18	clay
B-759	C.TRACK	7/5/2006	UD-1	56.5 - 57	0	
			UD-2	66 - 68	24	CH
			UD-3	98 - 98.5	5	SC, tube bent
B-765	C. TRACK	7/12/2006	P-1	70 - 72	8	cemented fine sandy silt, trace clay, trace shells
			P-2	100 - 102	20	clayey fine sandy silt
B-768	C.TRUCK	6/20/2006	UD-1	43.5 - 45.3	20	SM
			UD-2	73.5 - 75.5	24	SM

Table 2.5-29— {Summary Undisturbed Tube Samples}
(Page 7 of 9)

Boring	Drill Rig	Date	Sample No.	Depth [ft]	Rec [in]	Field Remarks
B-771	C. TRACK	7/24/2008	UD-1	31.5 -33.5	24	SM
			UD-2	41.5 - 43.5	24	SM
			UD-3	51.5 - 53.5	24	SP-SM
			UD-4	61.5 - 63.5	24	SM
			UD-5	71.5 - 73.5	24	ML
			UD-6	81.5 - 83.5	24	ML
			UD-7	91.5 - 93.5	24	ML
B-772	C. TRACK	7/29/2008	UD-1	41.5 - 43.5	24	SM
			UD-2	51.5 - 52.6	13.5	SM
			UD-3	56.5 - 58.5	24	ML
B-773A	C. TRUCK	8/7/2008	UD-1	13.0 - 15.0	24	SM
			UD-2	23.0 - 24.3	15.5	SC
			UD-3	33.0 - 34.6	9	ML
			UD-4	43.0 - 45.0	24	SM
			UD-5	53.0 - 55.0	24	SM
			UD-6	63.0- 65.0	24	SM
			UD-7	73.0 - 75.0	24	MH
			UD-8	83.0 - 84.6	19	MH
			UD-9	93.0 - 94.8	21	SC
			UD-10	103.0 - 105.0	24	MH
			UD-11	113.0 - 114.8	22	SM
			UD-12	123.0 - 124.9	23	SM
			UD-13	136.0 - 137.8	22	SM
			UD-14	148.0 - 150.0	24	MH
B-773B	U. TRUCK	10/16/2008	UD-1	5.0 - 7.0	24	SM
			UD-2	15.0 - 16.8	22	SM
			UD-3	25.0 - 26.8	21	SC
			UD-4	35.0 - 37.0	24	ML
			UD-5	45.0 - 46.9	23	SM
			UD-6	55.0 - 57.0	24	SM
			UD-7	65.0 - 67.0	24	SM
			UD-8	75.0 - 77.0	24	MH
			UD-9	85.0 - 87.0	24	MH
			UD-10	95.0 - 97.0	24	SC
			UD-11	105.0 - 107.0	24	MH
			UD-12	115.0 - 116.5	18	SM
			UD-13	125.0 - 127.0	24	SM
			UD-14	135.0 - 137.0	24	SM
			UD-15	145.0 - 147.0	24	MH

Table 2.5-29— {Summary Undisturbed Tube Samples}
(Page 8 of 9)

Boring	Drill Rig	Date	Sample No.	Depth [ft]	Rec [in]	Field Remarks
B-774	U.ATV	7/30/2008	UD-1	11.5 - 13.1	19	SP-SM
			UD-2	16.5 -17.9	16.5	SM
			UD-3	21.5 - 23.4	23	SM
			UD-4	31.5 - 33.4	23	SM
			UD-5	41.5 - 43.5	24	SM
			UD-6	51.5 - 53.5	24	SM
			UD-7	81.5 - 83.3	22	MH
			UD-8	101.5 - 103.5	24	SM
			UD-9	111.5 - 113.4	23	SM
			UD-10	121.5 - 123.0	18	SM
			UD-11	131.5 - 133.4	22.5	SM
			UD-12	141.5 - 143.2	20	MH
B-776	C. TRACK	7/22/2008	UD-1	36.5 - 38.2	20	ML
			UD-2	46.5 - 47.8	16	SM
B-778	C. TRACK	8/18/2008	UD-1	6.5 - 8.5	24	SM
			UD-2	11.5 - 13.5	24	SM
			UD-3	21.5 - 22.4	11	SM
			UD-4	23.5 - 24.5	12	SP-SM
			UD-5	31.5 - 32.5	12	SP-SM
			UD-6	33.5 - 34.4	10.5	SP-SM
			UD-7	41.5 - 43.1	19	CL
			UD-8	51.5 - 53.5	24	ML
			UD-9	61.5 - 63.5	24	GP
			UD-10	71.5 - 73.5	24	ML
			UD-11	81.5 - 83.5	24	ML
			UD-12	91.5 - 92.5	12	GP
			UD-13	93.5 - 94.7	14	SP
			UD-14	101.5 - 103.2	20	SP
			UD-15	111.5 - 113.5	24	SM
B-779	C. TRACK	8/13/2008	UD-1	6.5 - 8.3	21	SP
			UD-2	11.5 -13.5	24	SM
			UD-3	21.5 - 23.5	24	CL
			UD-4	31.5 - 33.5	24	SP
			UD-5	41.5 - 43.5	24	SM
			UD-6	51.5 - 52.5	12	ML
			UD-7	53.5 - 55.5	24	ML
			UD-8	61.5 - 63.5	24	ML
			UD-9	71.5 - 73.3	22	SM
			UD-10	81.5 - 82.8	16	SP-SM
			UD-11	96.5 - 97.7	14	SP-SM
			UD-12	100.0 - 102.0	24	SP-SM
B-782	C. TRACK	7/23/2008	UD-2	46.5 - 47.3	9	SM

Table 2.5-29— {Summary Undisturbed Tube Samples}
(Page 9 of 9)

Boring	Drill Rig	Date	Sample No.	Depth [ft]	Rec [in]	Field Remarks
B-786B	C. TRACK	11/6/2008	UD-1	5.0 - 7.0	24	SP-SM
			UD-2	15.0 -16.5	18	SM
			UD-3	25.0 - 26.0	12	SP
			UD-4	27.0 - 28.8	21	CH
			UD-5	35.0 - 36.7	20	CL
			UD-6	45.0 - 46.5	18	SM
			UD-7	55.0 - 57.0	24	SP-SM
			UD-8	65.0 - 66.8	22	SP-SM
			UD-9	75.0 - 76.8	21	SP-SM
			UD-10	85.0 -87.0	24	ML
			UD-11	95.0 - 97.0	24	SM
B-821A	C. TRACK	11/11/2008	UD-1	10.0 - 11.2	14	SP-SM
			UD-2	12.0 - 13.0	12	SP-SM
			UD-3	20.0 - 22.0	24	SP-SM
			UD-4	30.0 - 32.0	24	SM
			UD-5	40.0 - 41.5	18	SM
			UD-6	50.0 - 52.0	24	ML
			UD-7	60.0 - 62.0	24	ML
			UD-8	70.0 - 71.0	12	SM
			UD-9	72.0 - 73.0	12	SM
			UD-10	80.0 - 82.0	24	ML
			UD-11	90.0 - 90.9	11	ML
			UD-12	92.0 - 93.6	19	SM
			UD-13	100.0 - 101.8	21	ML

Table 2.5-30— {Summary of Hammer Rod Energy Measurements}

Drill Rig	Boring	ETR Range [%]	Average ETR [%]	Adjustment [ETR%/60%]
Failing 1500 Truck	B-401	67-88	78	1.3
CME 550X ATV	B-403	73-92	84	1.4
CME 750 ATV	B-404	78-90	87	1.45
CME 75 Truck	B-409	69-90	84	1.4
Diedrich D50 ATV	B-744	73-84	81	1.35
CME 75 ATV (Phase II)	B-348 & B-357	77-95	90	1.5
CME 550X ATV (Phase II)	B-354	79-90	83	1.38
Diedrich D50 ATV (Phase II)	B-791	74-85	81	1.35
CME 75 Truck (Phase II)	B-356	86-92	90	1.5

Table 2.5-31— {Summary As-Conducted CPT Information}

(Page 1 of 2)

Location	Depth [ft]	Bottom Elevation [ft]	Coordinates [ft], Maryland State Plane (NAD 1927)		Ground Surface Elevation [ft] (NGVD 1929)	Date of As Built Survey	Remarks PD: Pre-Drill S: Seismic D: Dissipation		
			North	East			PD	S	D
C-301	52.3	42.5	217041.78	960820.13	94.84	9/15/2006		×	·
C-302	61.7	29.2	217088.9	960833.77	90.94	9/15/2006		·	×
C-302-2*	55.3	39.2	217026.56	960817.55	94.51	7/26/2006		·	·
C-302-2a*	138	-43.5	217026.56	960817.55	94.51	7/26/2006	×85 ft	·	×
C-303	25.4	36.2	217230.6	960804	61.58	4/24/2006		·	
C-303a*	47.1	14.5	217230.6	960804	61.58	7/25/2006	×45 ft	·	·
C-303a-1*	71.4	-9.8	217230.6	960804	61.58	7/25/2006	×50 ft	·	·
C-303b*	123.4	-61.8	217230.6	960804	61.58	7/25/2006	×80 ft	·	×
C-304	26.7	34.3	217235.29	960606.73	60.95	9/15/2006		×	×
C-305	74.3	41.6	216876.5	960961.5	115.91	4/24/2006		·	·
C-306	56.9	40.4	217042.12	961184.89	97.31	9/15/2006		·	×
C-306a*	102.5	-5.2	217038.92	961181.69	97.31	7/27/2006	×80 ft	·	·
C-307	75.3	42.3	216853.68	961079.64	117.64	9/15/2006		×	·
C-308	48.2	36.1	217129.9	960263.7	84.33	5/1/2006		×	·
C-309	70.1	35.9	217045.62	960110.76	106.04	9/15/2006		·	×
C-311	34.9	39.1	216869.75	960488.16	73.97	9/15/2006		·	·
C-312	56.4	43.4	216799.2	960596.36	99.75	9/15/2006		·	·
C-313	37.2	42.7	216757.92	960336.75	79.93	9/15/2006		·	·
C-314	39.5	40.6	216531.4	960493.83	80.09	9/15/2006		·	·
C-401	28.1	39.4	216384.26	961574.09	67.46	9/15/2006		×	·
C-401-2a*	81.9	-14.4	216381.06	961570.89	67.46	7/27/2006	×55 ft	×	·
C-401-2b*	131.2	-63.7	216381.06	961570.89	67.46	7/27/2006	×85 ft	×	×
C-402	34.5	38.6	216333.85	961494.18	73.13	9/15/2006		·	×
C-403	43.8	39.2	216517.33	961511.47	82.96	9/15/2006		·	·
C-404	80.1	39.1	216524.3	961308.9	119.21	4/20/2006		×	×
C-405	40	35.5	216163.49	961666.32	75.54	9/15/2006		·	·
C-406	15.6	28.3	216380.92	961901.51	43.89	9/28/2006		·	×
C-407	32.3	30.9	216159.2	961732.2	63.23	6/22/2006		×	×
C-407-2a*	96.3	-33.1	216161.5	961726.7	63.23	7/28/2006	×50 ft	·	×
C-407-b*	142.4	-79.2	216161.5	961726.7	63.23	7/31/2006	×95 ft	·	×
C-408	77.4	40.8	216396.64	961001.81	118.18	9/15/2006		×	·
C-408a*	98.3	19.9	216398.76	960999.69	118.18	7/24/2006	×98 ft	×	·
C-408-2a*	123.7	-5.5	216393.81	961004.64	118.18	7/31/2006	×105 ft	×	·
C-409	80.5	38.6	216288.45	960760.56	119.12	9/15/2006		·	×
C-411	80.4	36.2	216178.94	961178.21	116.6	9/19/2006		·	×
C-412	76.8	37.5	216093.75	961306.66	114.31	9/28/2006		·	·
C-413	13.6	86.3	216045.53	961037.78	99.9	9/28/2006		·	·
C-414	62.5	39.9	215893.42	961201.1	102.36	9/28/2006		·	×
C-415	20	36.6	216305.7	961857.4	56.63	5/26/2006			
C-701	29.5	-18.6	219262.19	960933.61	10.95	9/21/2006	·	·	×
C-701a*	28.1	-17.2	219265.39	960936.81	10.95	7/21/2006	·	·	·
C-702	20.3	-9	218720.05	961033.95	11.34	9/21/2006	·	·	·
C-703	32.6	35.2	217361.27	961165.03	67.82	10/17/2006	·	·	×

Table 2.5-31— {Summary As-Conducted CPT Information}
(Page 2 of 2)

Location	Depth [ft]	Bottom Elevation [ft]	Coordinates [ft], Maryland State Plane (NAD 1927)		Ground Surface Elevation [ft] (NGVD 1929)	Date of As Built Survey	Remarks PD: Pre-Drill S: Seismic D: Dissipation		
			North	East			PD	S	D
C-704	48.2	-2.8	217500.74	961710.02	45.36	9/28/2006	·	·	·
C-705	34	-2.9	217637.26	961983.1	31.08	9/28/2006	·	·	·
C-706	50	55.3	216958.95	961494.86	105.28	9/21/2006	·	·	·
C-707	19.5	20.9	216308.12	962079.42	40.35	9/22/2006	·	·	·
C-708	50	63	215658.28	961962.86	112.97	10/16/2006	·	·	·
C-709	50	61.7	215027.59	962824.89	111.73	10/18/2006	·	·	·
C-710	21.2	85	214875.83	961187.31	106.15	10/16/2006	·	·	·
C-711	34.9	65.6	214222.13	962176.75	100.54	10/17/2006	·	·	·
C-712	29.7	29.4	213909.83	961370.06	59.05	10/18/2006	·	·	×
C-713	41.8	21.3	215855.86	962296.57	63.11	9/28/2006	·	·	·
C-714	85.1	24.2	214920.3	963057.62	109.32	10/18/2006	·	·	×
C-715	57.3	33.6	215445.62	961798.99	90.85	10/16/2006	·	·	·
C-716	20.5	75.7	214432.49	962659.44	96.21	10/17/2006	·	·	·
C-717	66.6	35.8	214698.14	961692.58	102.35	10/16/2006	·	·	×
C-718	34.1	33.6	214343.71	961205.59	67.67	10/16/2006	·	·	·
C-719	12	78.2	214025.3	961636.9	90.21	10/18/2006	·	·	·
C-720	70.7	28	213593.77	961134.09	98.66	10/18/2006	·	·	×
C-721	52	35.6	216157.88	960330.47	87.62	9/29/2006	·	·	·
C-722	38.4	36.1	215478.76	960648.26	74.52	10/16/2006	·	·	·
C-723	68.7	28.9	215988.18	959760.36	97.6	9/29/2006	·	·	×
C-724	152.2	-144.3	219309.8	960973.5	7.9	8/6/2008	×	×	·
C-724A	13.3	-5.4	219309.3	960973.9	7.9	8/6/2008		×	·
C-725	152.4	-144.2	219157.7	961143.9	8.2	8/7/2008	×	×	·
C-726	52.5	-43.3	219479.9	960691.8	9.2	8/6/2008		·	·
C-727	101.1	-92.9	219368.3	960914.9	8.2	8/6/2008	×	·	×
C-728	52.8	-42.8	218975.5	961193	10	8/5/2008	·	·	·
C-747	52.8	-43.7	218860.2	961248.5	9.1	8/4/2008	×	·	·
C-748	41.3	-8.9	218521.4	960909.8	32.4	8/20/2008	·	·	·
C-748A	52	-19.7	218518.9	960908.7	32.3	8/21/2008	·	·	·
C-749	18.4	43.9	218344.5	960737.8	62.3	8/20/2008	·	·	·
C-749A	41.2	21.1	218346.4	960740	62.3	8/21/2008	×	·	·

Notes:
- (*) Location and elevation approximated based on offset observed in the field and recorded on Field Checklist

Table 2.5-32— {Summary of As-Conducted Observation Well Information}

(Page 1 of 2)

Location	Depth [ft]	Termination Elevation (Bottom) [ft]	Coordinates [ft], Maryland State Plane (NAD 1927)		Surface Elevation [ft] (NGVD 1929)	Elevation (Top of Concrete at Base of Well Head Protector) [ft]	Elevation GW Level Measuring Point (V-Notch) [ft]	Date of As Built Survey
			North	East				
OW-301	80	14.5	217048.02	960814.47	94.51	94.78	96.27	9/15/2006
OW-313A	57.5	-6.5	217367.31	960705.3	51.03	51.31	53.2	9/15/2006
OW-313B	110	-59.3	217372.34	960713.67	50.73	51.16	53.54	9/15/2006
OW-319A	35	68.1	216962.56	961116.12	103.13	103.31	104.91	9/15/2006
OW-319B	85	18.5	216957.32	961125.02	103.53	103.85	105.35	9/19/2006
OW-323A	43.5	63.5	217034.46	960057.07	106.96	107.55	109.69	9/19/2006
OW-328	72	4.3	216828.86	960493.21	76.29	76.55	77.85	9/19/2006
OW-336	74	23.1	216643.18	960746.61	97.11	97.5	99.07	9/16/2006
OW-401	77.5	-6.1	216348.86	961530.99	71.38	71.91	73.49	9/21/2006
OW-413A	50	73.2	216703.14	961418.81	123.15	123.51	125.04	9/15/2006
OW-413B	125	-2.1	216694.88	961413.25	122.9	123.25	124.85	9/15/2006
OW-418A	40	3.7	216340.41	961966.46	43.66	44.31	45.83	9/22/2006
OW-418B	92	-48.3	216340.25	961976.71	43.67	44.13	45.77	9/22/2006
OW-423	43	68.1	216339.99	960882.24	111.12	111.67	113.16	9/15/2006
OW-428	50	63.9	216105.21	961212.38	113.92	114.32	115.92	9/19/2006
OW-436	50	58.1	215922.47	961446.87	108.13	108.53	110.39	9/22/2006
OW-703A	49	-5	218171.23	960967.72	44.02	44.44	45.65	9/21/2006
OW-703B	80	-34.4	218171.67	960958.91	45.57	45.97	47.53	9/21/2006
OW-705	52	-4.3	217566.62	960917.18	47.71	47.77	50.22	9/15/2006
OW-708A	34	3.4	217586.23	961803.52	37.44	37.82	39.61	9/28/2006
OW-711	50	2.9	216748.48	961741.61	52.92	53.26	55.31	9/22/2006
OW-714	50	66	215705.73	962034.37	116.02	116.32	117.98	10/16/2006
OW-718	43	75.5	214133.58	961924.87	118.53	118.96	120.41	10/18/2006
OW-725	60	-2	214649.3	963212.73	58.04	58.38	59.94	10/18/2006
OW-729	42	76.9	214872.58	962445.93	118.88	119.44	121.11	10/17/2006
OW-735	72	19.2	214805.48	961021.83	91.2	91.81	93.44	10/16/2006
OW-743	55	48.7	213320.62	961234.01	103.65	104.05	105.89	10/18/2006
OW-744	50	47.5	216405.37	960089.41	97.5	97.96	99.81	9/29/2006
OW-752A	37	58.3	215482.18	960250.12	95.3	95.73	97	9/29/2006
OW-752B	97	-1.2	215489.21	960257.57	95.79	96.09	97. 41	9/29/2006
OW-754	44	23	217369.78	960290.37	67	67.21	68.85	9/15/2006
OW-756	42	64.6	215497.07	961212.39	106.56	107.07	108.77	10/16/2006
OW-759A	35	62.8	214536.47	960055.02	97.78	98.05	99.69	10/19/2006
OW-759B	90	8.4	214526.25	960056.32	98.35	98.72	100.14	10/19/2006
OW-765A	29	68.4	216424.51	959701.22	97.37	97.92	99.6	9/29/2006
OW-765B	102	-5.8	216420.42	959693.64	96.82	97.19	98.47	9/29/2006
OW-766	37	71.9	216932.89	959791.5	108.89	109.32	110.72	9/19/2006
OW-768A	42	6.5	217106.06	962238.98	48.48	48.96	49.84	9/28/2006
OW-769	42	12.2	216589.75	962559.47	54.23	54.39	56.43	9/28/2006
OW-770	42	79.6	215466.6	962826.95	121.59	121.79	123.08	10/18/2006
OW-304	72.8	-4	217158.1	960920.8	68.8	69.28	71.01	7/17/2008
OW-308	103	8.4	216928	960750	111.4	111.95	113.62	7/17/2008

Table 2.5-32— {Summary of As-Conducted Observation Well Information}
(Page 2 of 2)

Location	Depth [ft]	Termination Elevation (Bottom) [ft]	Coordinates [ft], Maryland State Plane (NAD 1927)		Surface Elevation [ft] (NGVD 1929)	Elevation (Top of Concrete at Base of Well Head Protector) [ft]	Elevation GW Level Measuring Point (V-Notch) [ft]	Date of As Built Survey
			North	East				
OW-774A	23	-13.3	219187.3	961030.5	9.7	10.2	12.2	7/31/2008
OW-774B	52.8	-42.7	219176.7	961020.2	10.1	10.5	12.55	7/31/2008
OW-778	52	61.3	219100.6	960728.6	113.3	113.7	115.45	8/27/2008
OW-779	52.5	48.4	218958.7	960587.3	100.9	101.3	102.94	8/27/2008
OW-781	53	-42.7	219421.3	960764.4	10.3	10.8	12.87	7/29/2008

Table 2.5-33— {In-Situ Hydraulic Conductivity (Slug) Test Results}

Location	Screened Interval Depth [ft]	USCS Soil Classification	Hydraulic Conductivity [fps]
OW-301	65 - 75	SP	$1.58X10^{-4}$
OW-313A	40 - 50	SM, ML	$7.50X10^{-6}$
OW-313B	95 - 105	CL, ML, MH	$2.74X10^{-7}$
OW-319A	20 - 30	SP-SM, SC, CH, CL	$2.89X10^{-6}$
OW-319B	70 - 80	SM	$3.42X10^{-5}$
OW-323A	30 - 40	SP, SP-SM	$6.24X10^{-5}$
OW-328	60 - 70	SM, OH	$3.79X10^{-6}$
OW-336	60 - 70	SP-SM, SM	$2.10X10^{-5}$
OW-401	63 - 73	SM	$6.77X10^{-6}$
OW-413A	35 - 45	SP-SM	$1.21X10^{-5}$
OW-413B	110 - 120	SP-SM, SM	$2.78X10^{-6}$
OW-418A	25 - 35	SP-SM	$4.41X10^{-6}$
OW-418B	75 - 85	SC, SM	$2.16X10^{-7}$
OW-423	28 - 38	SP-SM, SM, SC	$6.86X10^{-5}$
OW-428	35 - 45	SM, SC	$1.19X10^{-5}$
OW-436	29 - 39	SC, SM	$2.80X10^{-6}$
OW-703A	35 - 45	SM	$1.34X10^{-5}$
OW-703B	68 - 78	SM, ML	$1.08X10^{-6}$
OW-705	40 - 50	SC, SM	$4.99X10^{-6}$
OW-708A	22 - 32	SM	$2.56X10^{-5}$
OW-711	35 - 45	SM	$6.04X10^{-6}$
OW-714	38 - 48	SP-SM, SC	$2.81X10^{-6}$
OW-718	30 - 40	SP-SM	$4.44X10^{-6}$
OW-725	48 - 58	SM	$7.54X10^{-6}$
OW-735	60 - 70	SP-SM, SM	$5.48X10^{-5}$
OW-743	40 - 50	SP-SM, SM	$6.23X10^{-7}$
OW-744	38 - 48	CL, SC, SM	$1.07X10^{-6}$
OW-752A	25 - 35	CH, SM	$7.03X10^{-5}$
OW-752B	85 - 95	SP-SM	$3.35X10^{-6}$
OW-754	32 - 42	CL, SM	$5.29X10^{-6}$
OW-756	30 - 40	SP-SM, SP-SC	$2.01X10^{-4}$
OW-759A	20 - 30	SM, SC, MH	$4.64X10^{-7}$
OW-759B	75 - 85	SM, SP, SP-SM	$1.17X10^{-6}$
OW-765A	17 - 27	SP-SM	$1.00X10^{-5}$
OW-765B	82 - 92	SM	$1.36X10^{-6}$
OW-766	20 - 30	SP-SM	$1.10X10^{-6}$
OW-768A	30 - 40	SM	$5.29X10^{-6}$
OW-769	32 - 42	SM, SC	$1.74X10^{-6}$
OW-304	60 - 70	SM	$4.31X10^{-6}$
OW-308	90 - 100	SP-SM	$1.87X10^{-5}$
OW-774A	20-Oct	SM	$2.72X10^{-5}$
OW-774B	40 - 50	SC	$1.44X10^{-7}$
OW-778	40 - 50	ML,CH	Dry
OW-779	40 - 50	CH	Dry
OW-781	40 - 50	SM,ML	$4.01X10^{-7}$

Table 2.5-34— {Summary As-Conducted Test Pit Information}

Location	Depth [ft]	Termination Elevation (Bottom) [ft]	Coordinates [ft], Maryland State Plane (NAD 1927)		Surface Elevation [ft] (NGVD 1929)	Date of As Built Survey
			North	East		
TP-B307	6.7	112.7	216957.53	960690.62	119.35	9/19/2006
TP-B314	9	43.8	217320.35	960658.25	52.78	9/15/2006
TP-B315	8.5	57.3	217182.5	960563.12	65.8	9/15/2006
TP-B334	10	77	216515.64	960560.94	87.03	9/19/2006
TP-B335	8	91.6	216730.79	960706.97	99.64	9/19/2006
TP-B407	7	74.3	216391.76	961465.02	81.25	9/21/2006
TP-B414	6.5	114.3	216631.18	961530.95	120.83	9/15/2006
TP-B415	6.5	112.4	216490.91	961298.37	118.92	9/15/2006
TP-B423	8	97.9	216414.95	960849.03	105.86	9/19/2006
TP-B434	8.5	96.7	215825.9	961244.18	105.24	9/22/2006
TP-B435	10	97.7	216020.06	961404.74	107.71	9/19/2006
TP-B715	8.5	79.7	214964.18	962637.77	88.16	10/17/2006
TP-B716	8.8	88.3	214983.83	961289.79	97.13	10/16/2006
TP-B717	8	82.5	214297.68	962346.36	90.53	10/17/2006
TP-B719	8	64.3	213966.93	961493.94	72.28	10/18/2006
TP-B727	7	97.3	215299.14	961883.13	104.33	10/16/2006
TP-B744	6.5	106.8	316377.3	959963.38	113.28	9/29/2006
TP-B758	9	73.6	215133.29	960332.67	82.63	10/16/2006
TP-C309	8	100.5	217020.05	960105.24	108.45	9/19/2006
TP-C723	7	89.8	215989.07	959754.78	96.75	9/29/2006

Table 2.5-35— {Summary of Field Electrical Resistivity Information}

Location	Depth [ft]	Coordinates [ft], Maryland State Plane (NAD 1927)		Surface Elevation [ft] (NGVD 1929)	Date of As Built Survey
		North	East		
R-1	6.7	215837.3	960255.8	85.45	5/3/2006
R-2	9	215837.3	960255.8	85.45	5/3/2006
R-3	8.5	216622.5	960406.8	89.12	5/2/2006
R-4	10	215915.4	961114	99.4	4/27/2006

Table 2.5-36— {Field Electrical Resistivity}

Spacing [ft]	Location				Min [ohm -m]	Max [ohm -m]	Avg [ohm -m]
	R1 El. 85.5	R2 El. 85.5	R3 El. 89.1	R4 El. 99.4			
	Measured Resistivity [ohm -m]						
1.5	1210	1520	3070	471	471	3070	1568
3.0	2480	2410	3750	640	640	3750	2320
5.0	3220	2780	4550	660	660	4550	2803
7.5	3110	2890	5440	806	806	5440	3062
10.0	2490	2700	6240	1130	1130	6240	3140
15.0	1870	2780	5370	1340	1340	5370	2840
20.0	1570	1960	4100	1790	1570	4100	2355
30.0	1310	2060	1960	1640	1310	2060	1743
40.0	739	1590	1010	1280	739	1590	1155
50.0	314	1080	415	975	314	1080	696
100.0	45	487	69	463	45	487	266
200.0	37	116	38	57	37	116	62
300.0	48	76	31	41	31	76	49

Table 2.5-37— {Geophysical Data from CCNPP Units 1 and 2 UFSAR}

STATION	Compressional Velocities							
	Surficial Sediments (Pleistocene)		Unconsolidated Sediments (Tertiary)		Intermediate Sediments (Cretaceous)		Basement Rock	
	Wave Velocity [fps]	Thickness [ft]	Wave Velocity [fps]	Thickness [ft]	Wave Velocity [fps]	Thickness [ft]	Wave Velocity [fps]	Thickness [ft]
Solomons Shoal	-	-	5900	3080	-	-	15,170	3130
Solomons Deed	-	-	6080	1070	6980	1900	18,100	3080
Site	2200	40	5500	-	-	-	-	-
Site	-	-	5900	-	-	-	-	-

Table 2.5-38— {Pressuremeter Test Results, PM-301}

(Page 1 of 2)

Test	Depth [ft]	El. [ft]	Layer/Material		G [ksf]	$G_{u/r}$ [ksf]	*v*	E [ksf]	$E_{u/r}$ [ksf]	$E_{u/r}$ / E
CC30	9.0	85.5	I	sand, some gravels	38	63	0.30	99	164	1.6
CC31	18.0	76.5	I	sand, some gravels	148	993	0.30	386	2581	6.7
CC32	29.5	65.0	I	clayey sand, silt	80	787	0.30	209	2045	9.8
CC33	28.0	66.5	I	clayey sand, silt	104	993	0.30	271	2581	9.5
CC34	41.0	53.5	IIa	sandy clay, lean clay	219	619	0.45	635	1795	2.8
CC35	39.5	55.0	IIa	sandy clay, lean clay	230	583	0.45	668	1690	2.5
CC36	51.0	43.5	IIb-1	interbedded fat clay with silty sand	508	1758	0.30	1322	4571	3.5
CC37	49.5	45.0	IIb-1	interbedded fat clay with silty sand	454	999	0.30	1179	2598	2.2
CC38	60.8	33.7	IIb-1	clayey sand, some cementation	859	3517	0.30	2232	9143	4.1
CC39	59.3	35.2	IIb-1	clayey sand to sand	572	1985	0.30	1488	5162	3.5
CC40	70.4	24.1	IIb-1	interbedded cemented sand, silt	963	9600	0.30	2504	24960	10.0
CC41	68.9	25.6	IIb-1	interbedded cemented sand, silt	637	6600	0.30	1656	17160	10.4
CC42	80.9	13.6	IIb-2	interbedded sand and clay	644	4705	0.30	1674	12232	7.3
CC43	79.4	15.1	IIb-2	interbedded sand and clay	255	3136	0.30	663	8155	12.3
CC44	91.0	3.5	IIb-2	interbedded cemented sand, silt	625	5280	0.30	1625	13728	8.4
CC45	89.5	5.0	IIb-2	interbedded cemented sand, silt	731	9827	0.30	1900	25551	13.4
CC46	101.0	-6.5	IIb-2	silty sand, some cementation	510	3517	0.30	1326	9143	6.9
CC47	99.5	-5.0	IIb-2	silty sand	508	2271	0.30	1322	5904	4.5
CC48	111.0	-16.5	IIb-3	silty sand, trace clay, cementation	1017	6273	0.30	2643	16310	6.2
CC49	109.5	-15.0	IIb-3	silty sand, trace clay	731	2839	0.30	1900	7382	3.9
CC50	120.8	-26.3	IIb-3	interbedded silty sand, sandy clay	731	3517	0.30	1900	9143	4.8
CC51	119.3	-24.8	IIb-3	interbedded cemented sand, silt	907	6273	0.30	2359	16310	6.9
CC52	131.0	-36.5	IIc	sandy clay, clayey sand, silt	510	2358	0.45	1479	6839	4.6
CC53	129.5	-35.0	IIc	sandy clay, clayey sand, silt	454	1985	0.45	1315	5757	4.4
CC54	141.0	-46.5	IIc	clayey sand, sandy clay	417	2580	0.45	1208	7482	6.2
CC55	139.5	-45.0	IIc	clayey sand, sandy clay	510	1999	0.45	1479	5797	3.9
CC56	151.0	-56.5	IIc	sandy clay	564	2580	0.45	1637	7482	4.6
CC57	149.5	-55.0	IIc	sandy clay	461	1999	0.45	1337	5797	4.3
CC58	161.0	-66.5	IIc	interbedded silty sand, sandy clay	740	2271	0.45	2145	6585	3.1
CC59	159.5	-65.0	IIc	interbedded silty sand, sandy clay	740	1758	0.45	2145	5099	2.4
CC60	171.0	-76.5	IIc	clayey sand, sandy clay	510	2358	0.45	1479	6839	4.6
CC61	169.5	-75.0	IIc	clayey sand, sandy clay	625	2166	0.45	1813	6283	3.5
CC62	181.0	-86.5	IIc	sandy elastic silt, trace clay	770	2358	0.45	2234	6839	3.1
CC63	179.5	-85.0	IIc	sandy elastic silt, trace clay	693	2278	0.45	2010	6607	3.3
CC64	191.0	-96.5	IIc	sandy elastic silt	907	2580	0.45	2631	7482	2.8
CC65	189.5	-95.0	IIc	sandy elastic silt	693	1999	0.45	2010	5797	2.9
CC66	201.0	-106.5	IIc	sandy elastic silt, clay	693	1999	0.45	2010	5797	2.9
CC67	199.5	-105.0	IIc	sandy elastic silt, clay	731	2166	0.45	2119	6283	3.0
CC68	210.9	-116.4	IIc	interbedded clayey sand, silty sand	731	1851	0.45	2119	5369	2.5

Table 2.5-38— {Pressuremeter Test Results, PM-301}
(Page 2 of 2)

Test	Depth [ft]	El. [ft]	Layer/Material		G [ksf]	$G_{u/r}$ [ksf]	*v*	E [ksf]	$E_{u/r}$ [ksf]	$E_{u/r}$ / E
CC69	209.4	-114.9	IIc	interbedded clayey sand, silty sand	770	1999	0.45	2234	5797	2.6
CC70	221.0	-126.5	IIc	clayey sand to sandy clay	417	3147	0.45	1208	9125	7.6
CC71	219.5	-125.0	IIc	clayey sand to sandy clay	376	2166	0.45	1091	6283	5.8
CC72	231.0	-136.5	IIc	clayey sand to sandy clay	357	1851	0.45	1036	5369	5.2
CC73	229.5	-135.0	IIc	clayey sand to sandy clay	357	1999	0.45	1036	5797	5.6
CC74	241.0	-146.5	IIc	clayey sand	461	1851	0.45	1337	5369	4.0
CC75	239.5	-145.0	IIc	clayey sand	417	1720	0.45	1208	4989	4.1
CC76	251.0	-156.5	IIc	clay to sandy clay	510	1851	0.45	1479	5369	3.6
CC77	249.5	-155.0	IIc	clay to sandy clay	693	1999	0.45	2010	5797	2.9
CC78	261.0	-166.5	IIc	interbedded clay and sandy silt	396	2166	0.45	1148	6283	5.5
CC79	259.5	-165.0	IIc	interbedded clay and sandy silt	396	1720	0. 45	1148	4989	4.3
CC80	271.0	-176.5	IIc	interbedded clay and sandy silt	417	1603	0.45	1208	4650	3.8
CC81	269.5	-175.0	IIc	interbedded clay and sandy silt	693	2358	0.45	2010	6839	3.4
CC82	281.0	-186.5	IIc	elastic silt, trace sand	510	1720	0.45	1479	4989	3.4
CC83	279.5	-185.0	IIc	elastic silt, trace sand	625	1851	0.45	1813	5369	3.0
CC84	291.0	-196.5	IIc	interbedded elastic silt and clay	461	1720	0.45	1337	4989	3.7
CC85	289.5	-195.0	IIc	interbedded elastic silt and clay	536	1498	0.45	1556	4345	2.8
CC86	301.0	-206.5	IIc	interbedded elastic silt and clay	594	2580	0.45	1722	7482	4.3
CC87	299.5	-205.0	IIc	interbedded elastic silt and clay	461	2358	0.45	1337	6839	5.1
CC88	310.7	-216.2	III	cemented sand, behaved like rock	Unsuccessful Test					
CC89	321.0	-226.5	III	interbedded clayey sand, clay	1096	3870	0.30	2850	10062	3.5
CC90	319.5	-225.0	III	interbedded clayey sand, clay	1220	4720	0.30	3171	12272	3.9
CC91	328.5	-234.0	III	cemented sand, behaved like rock	Unsuccessful Test					
CC92	338.5	-244.0	III	clayey sand	1156	3537	0.30	3005	9197	3.1
CC93	350.0	-255.5	III	clayey sand	807	3568	0.30	2098	9278	4.4
CC94	348.5	-254.0	III	clayey sand	768	3969	0.30	1996	10320	5.2
CC95	361.0	-266.5	III	clayey sand	990	3232	0.30	2573	8404	3.3
CC96	359.5	-265.0	III	clayey sand	695	3568	0.30	1808	9278	5.1

Notes:
- G - Shear Modulus; $G_{u/r}$ - Unload/Reload Shear Modulus
- v - Poisson Ratio
- E - Elastic Modulus; $E_{u/r}$ - Unload/Reload Elastic Modulus

Table 2.5-39— {Pressuremeter Test Results, PM-701}

Test	Depth [ft]	El. [ft]	Layer/Material		G [ksf]	$G_{u/r}$ [ksf]	*v*	E [ksf]	$E_{u/r}$ [ksf]	$E_{u/r}$ / E
CC03	23.5	-14.8	IIc	interbedded silts, sand, some gravel	578	3960	0.45	1676	11484	6.9
CC04	30.7	-22.0	IIc	silty sand, trace clay, shell fragments	494	3960	0.45	1432	11484	8.0
CC05	29.2	-20.5	IIc	silty sand, trace clay, shell fragments	382	2360	0.45	1109	6844	6.2
CC06	40.9	-32.2	IIc	sandy clay, silt	382	1625	0.45	1109	4712	4.2
CC07	39.3	-30.6	IIc	sandy clay, silt	610	2638	0.45	1768	7649	4.3
CC08	51.0	-42.3	IIc	silty sand, shell fragments	346	1935	0.45	1002	5611	5.6
CC09	49.5	-40.8	IIc	silty sand, shell fragments	346	3406	0.45	1002	9877	9.9
CC10	60.5	-51.8	IIc	elastic silt, clay + sand	762	2129	0.45	2211	6175	2.8
CC11	59.0	-50.3	IIc	elastic silt, clay + sand	913	3406	0.45	2647	9877	3.7
CC12	70.5	-61.8	IIc	silty sand, trace clay, shell fragments	329	1832	0.45	953	5313	5.6
CC13	69.0	-60.3	IIc	silty sand, trace clay, shell fragments	364	2360	0.45	1054	6844	6.5
CC14	80.7	-72.0	IIc	sandy silt, some clay	402	1625	0.45	1167	4712	4.0
CC15	79.2	-70.5	IIc	sandy silt, some clay	762	1769	0.45	2211	5129	2.3
CC16	90.6	-81.9	IIc	elastic silt, clay + sand	382	1290	0.45	1109	3742	3.4
CC17	89.1	-80.4	IIc	elastic silt, clay + sand	808	1625	0.45	2344	4712	2.0
CC18	100.5	-91.8	IIc	silty sand, trace clay, shell fragments	282	1935	0.45	818	5611	6.9
CC19	99.0	-90.3	IIc	silty sand, trace clay, shell fragments	913	2638	0.45	2647	7649	2.9
CC20	110.7	-102.0	IIc	sandy elastic silt, clay	644	1935	0.45	1867	5611	3.0
CC21	109.2	-100.5	IIc	sandy elastic silt, clay	469	1625	0.45	1359	4712	3.5
CC22	120.1	-111.4	IIc	silty sand, some clay	610	1499	0.45	1768	4348	2.5
CC23	118.6	-109.9	IIc	silty sand, some clay	382	1769	0.45	1109	5129	4.6
CC24	130.8	-122.1	IIc	silty sand	297	2129	0.45	861	6175	7.2
CC25	129.3	-120.6	IIc	silty sand	329	2129	0.45	953	6175	6.5
CC26	140.8	-132.1	IIc	silty sand to sandy silt, some clay	297	1499	0.45	861	4348	5.0
CC27	139.3	-130.6	IIc	silty sand to sandy silt, some clay	578	1935	0.45	1676	5611	3.3
CC28	150.9	-142.2	IIc	sandy elastic silt	494	2048	0.45	1432	5939	4.1
CC29	149.4	-140.7	IIc	sandy elastic silt	423	2129	0.45	1227	6175	5.0

Notes:
- G - Shear Modulus; $G_{u/r}$ - Unload/Reload Shear Modulus
- v - Poisson Ratio
- E - Elastic Modulus; $E_{u/r}$ - Unload/Reload Elastic Modulus

Table 2.5-40— {Summary of Laboratory Tests and Quantities}

Test		Standard/Method	Number of Tests (1)		
			PB	IA	BF
Index	Unified Soil Classification System (USCS)	ASTM D2488	591	10	3
	Natural moisture content	ASTM D2216	1048	10	18
	Grain size analysis (sieve)	ASTM D422	546	10	9
	Grain size analysis (hydrometer)	ASTM D6913	546	10	6
	Atterberg limits	ASTM D4318	423	10	3
	Organic content	ASTM D2974	79	10	3
	Specific gravity	ASTM D854	126	10	3
	Unit Weight	Not Specified	126	10	-
Chemical	pH	ASTM D4972	116	-	3
	Chloride	EPA 300.0	116	-	3
	Sulfate	EPA 300.0	116	-	3
	Resistivity	ASTM G187	-	-	14
Static Performance/Strength	Consolidation	ASTM D2435	79	-	3
	Permeability(2)	AST 2434	-	-	3
	Unconfined compression (UC)	ASTM D2166	25	-	-
	Unconsolidated-Undrained Triaxial (UU)	ASTM D2850	110	-	-
	Consolidated-Undrained Triaxial (CU-)	ASTM D4767	10	-	3
	Consolidated-Drained Triaxial (CD)	Unspecified	-	-	3
	Direct Shear (DS)	ASTM D3080	43	-	-
	Modified Proctor (Moisture-Density)	ASTM D1557)	-	-	4
	California Bearing Ratio	ASTM D1883	12	-	2
Dynamic Resonant Column Torsional Shear		Not Specified	13	10	8

Notes:
- (1) PB: Powerbolck Area (Includes Construction Laydown, Cooling and Transmission Corridor)
  IA: Intake Area
  BF: Backfill
- (2) Description of slug tests and the results are provided in Section 2.4.12.

Table 2.5-41— {Index Properties, Powerblock Area}

POWERBLOCK AREA		USCS	Stat	γ_{moist} [%]	w [%]	LL [%]	PL [%]	PI [%]	Fines [%]
Stratum I - Terrace Sand		SM, SP-SMC	Min	120.0	4.5	NV	NP	NP	4.6
			Max	124.0	36.2	55.0	20.0	37.0	72.0
			Avg	121.3	15.8	19.7	8.0	11.7	21.8
Stratum IIa - Chesapeake Clay/ Silt		CH MH	Min	103.0	15.1	27.0	11.0	8.0	50.0
			Max	122.3	42.5	79.0	36.0	54.0	99.7
			Avg	115.4	31.2	57.4	20.7	36.6	79.5
Stratum IIb - Chesapeake Cemented Sand	Layer 1	SM SP	Min	117.0	13.5	NV	NP	NP	2.1
			Max	128.4	36.2	72.0	32.0	50.0	72.7
			Avg	122.2	24.1	24.8	12.0	12.8	26.2
	Layer 2	SM SP-SM	Min	120.5	25.0	NV	NP	NP	10.6
			Max	126.0	44.2	72.0	41.0	40.0	87.0
			Avg	122.5	30.5	19.7	10.6	9.1	23.3
	Layer 3	SM	Min	123.0	16.1	NV	NP	NP	9.8
			Max	123.0	38.7	49.0	28.0	28.0	35.9
			Avg	123.0	26.0	17.3	9.5	7.8	23.7
Stratum IIc - Chesapeake Clay/ Silt		MH SM	Min	86.5	27.5	39.0	20.0	9.0	19.6
			Max	117.0	109.8	199.0	119.0	133.0	99.5
			Avg	103.9	51.2	95.4	42.9	52.5	59.9
Stratum III - Nanjemoy Sand		SC SM	Min	123.5	13.4	36.0	14.0	18.0	13.9
			Max	132.0	44.5	79.0	36.0	59.0	44.6
			Avg	127.0	29.1	57.1	22.6	34.5	23.3
Backfill		GP GM	Min	136.8	7.1	NV	NP	NP	7.2
			Max	150.4	5.6	NV	NP	NP	11.4
			Avg	146.2	6.3	NV	NP	NP	9.3

Notes:
- γ_{moist}: Moist Unit Weight
- w: Water Content
- LL: Liquid Limit
- PL: Plastic Limit
- NP: Non Plastic
- NV: Non Viscous
- NA: Not Available

Table 2.5-42— {Index Properties, Intake Area}

INTAKE AREA		USCS	Stat	γ_{moist} [%]	w [%]	LL [%]	PL [%]	PI [%]	Fines [%]
Stratum I - Terrace Sand		SM, SP-SM	Min	NA	NA	NA	NA	NA	NA
			Max	NA	NA	NA	NA	NA	NA
			Avg	NA	NA	NA	NA	NA	NA
Stratum IIa - Chesapeake Clay/ Silt		CH MH	Min	NA	NA	NA	NA	NA	NA
			Max	NA	NA	NA	NA	NA	NA
			Avg	NA	NA	NA	NA	NA	NA
Stratum IIb - Chesapeake Cemented Sand	Layer 1	SM SP	Min	NA	7.9	NA	NA	NA	16.5
			Max	NA	7.9	NA	NA	NA	16.5
			Avg	NA	7.9	NA	NA	NA	16.5
	Layer 2	SM SP-SM	Min	NA	9.4	NV	NP	NP	6.3
			Max	NA	36.0	27.0	17.0	10.0	44.2
			Avg	NA	24.4	5.4	3.4	2.0	18.9
	Layer 3	SM	Min	118.2	15.4	NV	NP	NP	8.4
			Max	123.4	37.4	42.0	23.0	22.0	37.9
			Avg	120.4	25.5	13.3	9.2	4.1	25.9
Stratum IIc - Chesapeake Clay/ Silt		SM MH	Min	93.6	22.4	NV	NP	NP	11.0
			Max	118.4	94.5	143.0	79.0	110.0	98.3
			Avg	108.2	48.5	72.5	32.6	39.9	49.0
Stratum III - Nanjemoy Sand		SC SM	Min	Not Encountered					
			Max						
			Avg						
Backfill		GP GM	Min	136.8	7.1	NV	NP	NP	7.2
			Max	150.4	5.6	NV	NP	NP	11.4
			Avg	146.2	6.3	NV	NP	NP	9.3

Notes: -γ_{moist}: Moist Unit Weight
- w: Water Content
- LL: Liquid Limit
- PL: Plastic Limit
- NP: Non Plastic
- NV: Non Viscous
- NA: Not Available

Table 2.5-43— {Summary of Soils Chemical Testing Data}

CCNPP Unit 3		USCS	Stat	pH [CaCl2]	pH [H2O]	Sulfate (1)	Chloride (2)
Stratum I - Terrace Sand		SM, SP-SM	Min	2.6	2.7	0.0	<10
			Max	6.7	7.6	2.6	48.6
			Avg	4.6	5.5	0.2	<12
Stratum IIa - Chesapeake Clay/Silt		CH MH	Min	2.6	2.5	0.0	<10
			Max	4.9	5.8	2.6	10.7
			Avg	3.1	3.6	0.7	<10
Stratum IIb - Chesapeake Cemented Sand	Layer 1	SM SP	Min	2.4	2.5	0.0	<10
			Max	7.4	8.0	3.1	145.0
			Avg	5.7	5.8	0.6	<22
	Layer 2	SM SP-SM	Min	2.4	2.5	0.0	<10
			Max	7.4	8.0	3.1	145.0
			Avg	5.7	5.8	0.6	<22
	Layer 3	SM	Min	2.4	2.5	0.0	<10
			Max	7.4	8.0	3.1	145.0
			Avg	5.7	5.8	0.6	<22
Stratum IIc - Chesapeake Clay/Silt		SM MH	Min	6.6	7.0	0.2	<10
			Max	6.6	7.0	0.2	<10
			Avg	6.6	7.0	0.2	<10
Stratum III - Nanjemoy Sand		SC SM	Min	NA	NA	NA	NA
			Max	NA	NA	NA	NA
			Avg	NA	NA	NA	NA
Backfill		GP GM	Min	8.3	-	204.0	<2.1
			Max	8.5	-	446.0	2.2
			Avg	8.4	-	325.0	2.1

Notes:
(1) Expressed as [%] for in-situ soils and as [mg/Kg] for backfill
(2) Expressed as [ppm] for in-situ soils and as [mg/Kg] for backfill
- NA: Not Available

Table 2.5-44— {Consolidation Test Results, Powerblock Area}

POWERBLOCK AREA		USCS	Stat	C_r	C_c	e_o	p'_c [ksf]	OCR
Stratum I - Terrace Sand		SM, SP-SM	Min	0.009	0.37	0.85	11.40	4.26
			Max	0.009	0.37	0.85	11.40	4.26
			Avg	0.009	0.37	0.85	11.40	4.26
Stratum IIa - Chesapeake Clay/ Silt		CH MH	Min	0.013	0.46	0.82	11.20	4.91
			Max	0.043	0.68	1.15	35.00	15.40
			Avg	0.026	0.54	1.03	21.66	8.10
Stratum IIb - Chesapeake Cemented Sand	Layer 1	SM SP	Min	0.006	0.04	0.63	20.20	2.82
			Max	0.012	0.32	0.92	30.00	22.61
			Avg	0.010	0.19	0.80	24.40	9.99
	Layer 2	SM SP-SM	Min	0.003	0.11	0.71	4.20	1.00
			Max	0.003	0.11	0.90	23.80	4.68
			Avg	0.003	0.11	0.80	14.00	2.84
	Layer 3	SM	Min	NA	NA	NA	NA	NA
			Max	NA	NA	NA	NA	NA
			Avg	NA	NA	NA	NA	NA
Stratum IIc - Chesapeake Clay/ Silt(1)		SM MH	Min	0.007	0.35	1.01	21.40	2.14
			Max	0.169	1.73	2.41	42.30	5.66
			Avg	0.060	0.95	1.61	33.30	3.21
Stratum III - Nanjemoy Sand		SC SM	Min	0.021	0.26	0.73	29.20	1.76
			Max	0.092	0.91	1.42	32.80	1.90
			Avg	0.045	0.53	1.00	30.40	1.85
Backfill		GP GM	Min	Large preconsolidation pressure of 54 ksf reported in one instance. It was not possible to define the virgin compression slope and the preconsolidation pressure.				
			Max					
			Avg					

Notes: -
C_r: Recompression index
- C_c: Compression index
- e_o: Initial void ratio
- p'_c: Preconsolidation pressure
- (1) Properties given for clay portions of layer

Table 2.5-45— {Consolidation Test Results, Intake Area}

INTAKE AREA		USCS	Stat	C_r	C_c	e_o	p'_c [ksf]	OCR
Stratum I - Terrace Sand		SM, SP-SM	Min	NA				
			Max					
			Avg					
Stratum IIa - Chesapeake Clay/ Silt		CH MH	Min					
			Max					
			Avg					
Stratum IIb - Chesapeake Cemented Sand	Layer 1	SM SP	Min					
			Max					
			Avg					
	Layer 2	SM SP-SM	Min					
			Max					
			Avg					
	Layer 3	SM	Min	0.006	0.135	0.635	32.5	17.7
			Max	0.006	0.135	0.635	32.5	17.7
			Avg	0.006	0.135	0.635	32.5	17.7
Stratum IIc - Chesapeake Clay/Silt		SM MH	Min	0.020	0.371	0.97	25.7	3.7
			Max	0.155	1.641	1.95	40.8	9.2
			Avg	0.085	1.036	1.47	32.4	7.1
Stratum III - Nanjemoy Sand		SC SM	Min	Not Encountered				
			Max					
			Avg					
Backfill		GP GM	Min	Large preconsolidation pressure of 54 ksf reported in one instance. It was not possible to define the virgin compression slope and the preconsolidation pressure.				
			Max					
			Avg					

Notes:
- C_r: Recompression index
- C_c: Compression index
- e_o: Initial void ratio
- p'_c: Preconsolidation pressure
- NA: Not Available

Table 2.5-46— {Shear Strength Laboratory Testing Data, Powerblock Area}

POWERBLOCK AREA		USCS	Stat	Triaxial Test				Direct Shear		s_u [ksf]	
				c' [ksf]	φ' [°]	c [ksf]	φ' [°]	c [ksf]	φ' [°]	UC	UU
Stratum I - Terrace Sand		SM, SP-SM S	Min	0.55	27.9	1.16	13.3	0.42	24.9	1.72	1.20
			Max	0.55	27.9	1.16	13.3	0.89	26.0	1.72	1.46
			Avg	0.55	27.9	1.16	13.3	0.66	25.5	1.72	1.33
Stratum IIa - Chesapeake Clay/Silt		CH MH	Min	0.44	31.0	0.72	12.5	0.64	19.0	1.14	1.42
			Max	0.98	32.1	2.06	17.0	1.38	30.1	4.06	4.60
			Avg	0.71	31.6	1.39	14.8	1.01	22.9	2.50	2.38
Stratum IIb - Chesapeake Cemented Sand	Layer 1	SM SP	Min	0.30	33.5	0.59	19.5	NA	NA	NA	0.80
			Max	0.30	33.5	0.59	19.5	NA	NA	NA	2.44
			Avg	0.30	33.5	0.59	19.5	NA	NA	NA	5.76
	Layer 2	SM SP-SM M	Min	0.04	30.0	1.94	13.4	NA	NA	NA	0.90
			Max	1.00	34.6	3.36	20.0	NA	NA	NA	0.90
			Avg	0.52	32.3	2.65	16.7	NA	NA	NA	0.90
	Layer 3	SM	Min	NA	NA	NA	NA	NA	NA	NA	NA
			Max	NA	NA	NA	NA	NA	NA	NA	NA
			Avg	NA	NA	NA	NA	NA	NA	NA	NA
Stratum IIc - Chesapeake Clay/Silt		SM MH	Min	NA	NA	NA	NA	0.00	29.0	3.74	1.80
			Max	NA	NA	NA	NA	1.58	35.0	5.24	9.58
			Avg	NA	NA	NA	NA	0.79	32.0	4.49	6.37
Stratum III - Nanjemoy Sand		SC SM	Min	NA	NA	NA	NA	NA	NA	NA	4.56
			Max	NA	NA	NA	NA	NA	NA	NA	7.66
			Avg	NA	NA	NA	NA	NA	NA	NA	5.78
Backfill		GP GM	Min	0.00	42.5	-	-	NA	NA	-	-
			Max	0.00	43.5	-	-	NA	NA	-	-
			Avg	0.00	43.0	-	-	NA	NA	-	-

Notes:
- NA: Not Available
- UC: Unconfined compression
- UU: Unconsolidated undrained triaxial test

Table 2.5-47— {Shear Strength Laboratory Testing Data, Intake Area}

INTAKE AREA		USCS	Stat	Triaxial Test c' [ksf]	Triaxial Test φ' [°]	Triaxial Test c [ksf]	Triaxial Test φ' [°]	Direct Shear c [ksf]	Direct Shear φ' [°]	s_u [ksf] UC	s_u [ksf] UU
Stratum I - Terrace Sand		SM, SP-SM	Min	NA							
			Max								
			Avg								
Stratum IIa - Chesapeake Clay/Silt		CH MH	Min								
			Max								
			Avg								
Stratum IIb - Chesapeake Cemented Sand	Layer 1	SM SP	Min								
			Max								
			Avg								
	Layer 2	SM SP-SM	Min								
			Max								
			Avg								
	Layer 3	SM	Min	0.00	38.0	NA	NA	0.46	28.2	NA	NA
			Max	0.00	38.0	NA	NA	0.46	28.2	NA	NA
			Avg	0.00	38.0	NA	NA	0.46	28.2	NA	NA
Stratum IIc - Chesapeake Clay/Silt		SM MH	Min	0.00	19.4	2.69	0.0	0.00	24.4	NA	1.92
			Max	3.63	37.3	7.68	18.7	2.10	38.7	NA	8.32
			Avg	1.52	31.9	4.35	11.9	0.73	30.8	NA	4.83
Stratum III - Nanjemoy Sand		SC SM	Min	Not Encountered							
			Max								
			Avg								
Backfill		GP GM	Min	0.00	42.5	-	-	NA	NA	-	-
			Max	0.00	43.5	-	-	NA	NA	-	-
			Avg	0.00	43.0	-	-	NA	NA	-	-

Notes:
- NA: Not Available
- UC: Unconfined compression
- UU: Unconsolidated undrained triaxial test

Table 2.5-48— {Modified Proctor Tests on Backfill Samples}

Sample	Modified Proctor						98% MP		90% MP	
	Uncorrected			Corrected						
	w [%]	γ_{dry} [pcf]	γ_{moist} [pcf]	w [%]	γ_{dry} [pcf]	γ_{moist} [pcf]	γ_{dry} [pcf]	γ_{moist} [pcf]	γ_{dry} [pcf]	γ_{moist} [pcf]
CR6 Composite FUGRO	6.9	145.2	155.2	6.0	148.0	156.9	145.0	153.7	133.2	141.2
CR6 Composite MACTEC	6.4	144.0	153.2	6.0	145.3	154.0	142.4	150.9	130.8	138.6
GAB Composite MACTEC	6.4	145.9	155.2	5.7	148.6	157.1	145.6	153.9	133.7	141.4
GAB Composite FUGRO	7.1	145.3	155.6	6.5	148.5	158.2	145.5	155.0	133.7	142.3
Min	6.4	144.0	153.2	5.7	145.3	154.0	142.4	150.9	130.8	138.6
Max	7.1	145.9	155.6	6.5	148.6	158.2	145.6	155.0	133.7	142.3
Avg	6.7	145.1	154.8	6.1	147.6	156.5	144.6	153.4	132.8	140.9
Notes: *- USCS: GP-GM*										

Table 2.5-49— {RCTS Testing Samples}

Sample		Depth [ft]	USCS	Type	γ_{dry} [pcf]	w [%]
POWERBLOCK AREA	B-437-6	13.5	SP-SM	UD	124.1	7.2
	B-301-10	33.5	CH	UD	117.5	31.1
	B-305-17	39.5	SC	UD	117.2	34.7
	B-404-14	52.0	SP-SM	UD	117.6	27.7
	B-401-31	138.5	CH	UD	104.1	44.1
	B-401-67	348.5	SM	UD	116.4	35.6
	B-401-48	228.5	MH	UD	98.2	58.6
	B-301-78	383.5	SM	Jar	116.4	34.4
	B-306-17	68.0	CH	UD	115.8	30.7
	B-409-15	35.0	SP-SM	UD	124.8	23.3
	B-404-22	83.5	SM	UD	115.4	32.2
	B-401-42	198.5	SM	UD	101.2	48.8
	B-409-39	95.0	SM	UD	109.3	33.1
INTAKE AREA	B-773-2	15.9	SM	UD	125.7	23.3
	B-773-3	27.0	SC	UD	111.6	35.0
	B-773-4	37.0	CH	UD	103.0	53.6
	B-773-5	47.0	SC	UD	110.9	34.1
	B-773-6	57.0	CH	UD	106.4	44.5
	B-773-7	66.1	CH	UD	110.1	33.5
	B-773-9	87.0	CH	UD	99.1	59.2
	B-773-11	107.0	CH	UD	102.5	55.1
	B-773-13	127.0	SC	UD	108.3	45.2
	B-773-15	147.0	CH	UD	101.5	52.3
BACKFILL	CR6 Composite(1)	-	GP-GM	Bulk	145.4	6.4
	GAB Composite(1)	-	GP-GM	Bulk	147.3	5.8
	CR6 Vulcan Average(1)	-	GP-GM	Bulk	143.1	5.5

Notes:
(1) Test results reported for target unit weight of 95% Modified Proctor

Table 2.5-50— {Low Strain Results for Backfill Samples}

Source	γ_{dry} [pcf]	Moisture Content [%]	Confining Pressure [ksf]	G_{max} [ksf]	V_s [fps]	D [%]
CR-6 Composite	145.4	6.4	1.08	2680	770	4.61
			2.16	3851	922	4.1
			4.32	5846	1133	3.41
CR-6 Vulcan Avg	143.1	5.5	1.08	3741	917	2.31
			2.16	5196	1080	1.96
			4.32	7054	1257	1.88
GAB Composite	147.3	5.8	1.08	3904	923	3.91
			2.16	5444	1089	3.33
			4.32	7427	1270	2.99

Table 2.5-51— {USCS Classification and Index Properties}

STRATUM			USCS	γ_{moist} [pcf]	w [%]	LL [%]	PL [%]	PI [%]	Fines [%]
POWERBLOCK AREA	I - Terrace Sand		SM, SP-SM	120.0	16.0	20.0	8.0	12.0	21.8
	IIa - Chesapeake Clay/Silt		CH MH	115.0	31.0	57.0	21.0	36.0	79.5
	IIb - Chesapeake Cemented Sand	L1	SM SP	120.0	24.0	26.0	13.0	13.0	26.2
		L2	SM SP-SM	120.0	31.0	20.0	11.0	9.0	23.3
		L3	SM	120.0	26.0	17.0	9.0	8.0	23.7
	IIc - Chesapeake Clay/Silt		MH SM	105.0	51.0	95.0	42.0	53.0	59.9
	III - Nanjemoy Sand		SC SM	125.0	29.0	57.0	22.0	35.0	23.3
INTAKE AREA	I - Terrace Sand		SM, SP-SM	NA	NA	NA	NA	NA	NA
	IIa - Chesapeake Clay/Silt		CH MH	NA	NA	NA	NA	NA	NA
	IIb - Chesapeake Cemented Sand	L1	SM SP	NA	8.0	NA	NA	NA	16.5
		L2	SM SP-SM	NA	24.0	5.0	3.0	2.0	18.9
		L3	SM	120.0	26.0	13.0	9.0	4.0	25.9
	IIc - Chesapeake Clay/Silt		SM MH	110.0	49.0	73.0	33.0	40.0	49.0
	III - Nanjemoy Sand		SC SM	125.0	29.0	57.0	22.0	35.0	23.3
BACKFILL			GP GM	145.0	6.0	NV	NP	NP	9.0

Notes:
- NP: Non Plastic
- NV: Non Viscous
- NA: Not Available

Table 2.5-52— {Guidelines for Soil Chemistry Evaluation}

Soil Corrosiveness					
Property	**Range for Steel Corrosiveness**				
	Little Corrosive	**Mildly Corrosive**	**Moderately Corrosive**	**Corrosive**	**Very Corrosive**
Resistivity [ohm-m]	>100[A], [B]	20-100[A] 50-100[B] >30[C]	10-20[A] 20-50[B]	5-10[A] 7-20[B]	<5[A] <7[B]
pH		>5.0 and <10[B]		5.0-6.5[A]	<5.0[A]
Chlorides (ppm)		<200[B]		300-1,000[A]	>1,000[A]
Soil Aggressiveness Recommendations for Normal Weight Concrete Subject to Sulfate Attack					
Concrete Exposure	**Water Soluble Sulfate (SO_4) in Soil, Percent**		**Cement Type**		**Max W/C Ratio**
Mild	0.00-0.10		---		---
Moderate	0.10-0.20		II, IP(MS), IS(MS)		0.5
Severe	0.20-2.0		V[1]		0.45
Very Severe	Over 2.0		V with pozzolan		0.45

Notes:
- (A) API, 2007
- (B) FHWA, 1990
- (C) ACI, 1994
- (1) Or a blend of Type II cement and a ground granulated blast furnace slag or a pozzolan that gives equivalent sulfate resistance

Table 2.5-53— {Performance Properties under Static Loading}

STRATUM			C_r	C_c	e_o	p'_c [ksf]	OCR	c_v [ft^2/year]	k_h [ft/s]	k_v [ft/s]
POWERBLOCK AREA	I - Terrace Sand		0.009	0.37	0.85	11.40	4.26	NA	NA	NA
	IIa - Chesapeake Clay/Silt		0.026	0.54	1.03	21.66	8.10	316.0	1.62E-09	1.62E-09
	IIb - Chesapeake Cemented Sand	L1	0.010	0.19	0.80	24.40	9.99	2018.0	9.84E-06	9.84E-07
		L2	0.003	0.11	0.80	14.00	2.84	2018.0	9.84E-06	9.84E-07
		L3	0.010	0.19	0.80	24.40	9.99	2018.0	9.84E-06	9.84E-07
	IIc - Chesapeake Clay/Silt		0.06	0.95	1.61	33.30	3.21	1913.0	1.62E-09	1.62E-09
	III - Nanjemoy Sand		0.05	0.53	1.00	30.40	1.85	2018.0	9.84E-07	9.84E-08
INTAKE AREA	I - Terrace Sand		NP	NP	NP	NP	NP	NP	NP	NP
	IIa - Chesapeake Clay/Silt		NP	NP	NP	NP	NP	NP	NP	NP
	IIb - Chesapeake Cemented Sand	L1	NP	NP	NP	NP	NP	NP	NP	NP
		L2	NA	NA	NA	NA	NA	NA	NA	NA
		L3	0.01	0.14	0.64	32.50	17.69	2018.0	9.84E-06	9.84E-07
	IIc - Chesapeake Clay/Silt		0.09	1.04	1.47	32.44	7.11	1913.0	1.62E-09	1.62E-09
	III - Nanjemoy Sand		0.05	0.53	1.00	30.40	1.85	2018.0	9.84E-07	9.84E-08
BACKFILL			Consolidation in backfill material will not be significant						9.50E-03	9.50E-04

Notes:
- NP: Not Present
- NA: Not Available
- c_v Values correspond to an applied pressure of 8 ksf for IIA, 32 ksf for IIb, and 64 ksf for IIc
- k_h is horizontal hydraulic conductivity; k_v is vertical hydraulic conductivity
- Intake area values for deeper strata are obtained from Powerblock recommendation

Table 2.5-54— {Strength Properties of Soils}

STRATUM			c' [ksf]	φ' [°]	c [ksf]	φ [°]	S_u [ksf]
POWERBLOCK AREA	I - Terrace Sand		0.0	27.9	1.2	13.3	1.5
	IIa - Chesapeake Clay/Silt		0.7	31.6	1.4	14.8	2.4
	IIb - Chesapeake Cemented Sand	L1	0.0	33.5	1.2	19.5	5.8
		L2	0.0	32.3	2.7	16.7	0.9
		L3	0.0	31.7	1.2	19.5	5.8
	IIc - Chesapeake Clay/Silt		0.8	32.0	1.4	14.8	5.4
	III - Nanjemoy Sand(1)		0.0	40.0	1.2	19.5	5.8
INTAKE AREA	I - Terrace Sand		NP	NP	NP	NP	NP
	IIa - Chesapeake Clay/Silt		NP	NP	NP	NP	NP
	IIb - Chesapeake Cemented Sand	L1	NP	NP	NP	NP	NP
		L2	NP	NP	NP	NP	NP
		L3	0.0	33.1	NA	NA	5.8
	IIc - Chesapeake Clay/Silt		1.5	31.1	4.3	11.9	4.8
	III - Nanjemoy Sand(1)		0.0	40.0	1.2	19.5	2.9
BACKFILL			0.0	40.0	-	-	-

Notes:
(1) Friction of 40 degrees assumed, recommendation at Intake taken from Powerblock
NA: Not Available
NP: Not Present

Table 2.5-55— {Estimation of Elastic Modulus}

STRATUM			E [ksf] from various methods						
			Vs (1)	PM	SPT		s_u		Avg
					(2)	(3)	(4)	(5)	
POWERBLOCK AREA	I - Terrace Sand		729	241	504	268	-	-	436
	IIa - Chesapeake Clay/Silt		1210	652	-	-	1098	1415	1094
	IIb - Chesapeake Cemented Sand	L1	4090	1575	3204	1226	-	-	2525
		L2	1300	1573	864	375	-	-	1028
		L3	5120	2200	2268	914	-	-	2625
	IIc - Chesapeake Clay/Silt		1560	1555	-	-	2772	3573	2365
	III - Nanjemoy Sand		4300	2500	2700	-	-	-	3166
INTAKE AREA	I - Terrace Sand		NP	NP	NP	NP	NP	NP	NP
	IIa - Chesapeake Clay/Silt		NP	NP	NP	NP	NP	NP	NP
	IIb - Chesapeake Cemented Sand	L1	NP	NP	NP	NP	NP	NP	NP
		L2	941	-	612	308	-	-	620
		L3	1840	-	1944	752	-	-	1512
	IIc - Chesapeake Clay/Silt		1290	-	-	-	2169	1928	1796
	III - Nanjemoy Sand(6)		4300	2500	2700	-	-	-	3166
BACKFILL			1920		-	-	-	-	1920

Notes:
- (1) Calculated from $G_{dyn}/G_{static} = 10$;
- (2) $E = 18N_{60}$ (Davie, 1988); [tsf]
- (3) $E = \beta_0$ sqrt(OCR) + $\beta_1 N_{60}$; [psf]
- (4) $E = 450\ s_u$ (Davie, 1988); [tsf]
- (5) $E = 2G(1+\nu)$; $G = 200\ s_u$ (Senapathy, 2001); [tsf]
- (6) Values adopted from Powerblock Area
- NP: Not Present

Table 2.5-56— {Basis for Recommendation of $E_{u/r}/E$ Ratio}

STRATUM			$E_{u/r}/E$			
			Min	Max	Avg	Rec
POWERBLOCK AREA	I - Terrace Sand		1.6	9.8	6.9	3.0
	IIa - Chesapeake Clay/Silt		2.5	2.8	2.7	3.0
	IIb - Chesapeake Cemented Sand	L1	2.2	10.4	5.6	3.0
		L2	4.5	13.4	8.8	4.5
		L3	3.9	6.9	5.4	3.9
	IIc - Chesapeake Clay/Silt		2.4	7.6	4.0	3.0
	III - Nanjemoy Sand(1)		3.1	5.2	4.1	3.1
INTAKE AREA	I - Terrace Sand		NP	NP	NP	NP
	IIa - Chesapeake Clay/Silt		NP	NP	NP	NP
	IIb - Chesapeake Cemented Sand	L1	NP	NP	NP	NP
		L2	NA	NA	NA	4.5
		L3	-	-	-	3.0
	IIc - Chesapeake Clay/Silt		2.0	9.9	4.8	3.0
	III - Nanjemoy Sand		-	-	-	3.0
BACKFILL			-	-	-	-

Notes:
- Values from pressuremeter tests at B-301 (Powerblock Area) and B-701 (Intake Area)
- NP: Not Present
- NA: Not Available

Table 2.5-57— {Elastic Properties Under Static Conditions}

STRATUM			E [ksf]	$\nu^{(1)}$	G [ksf]	$E_{u/r}/E$
POWERBLOCK AREA	I - Terrace Sand		436	0.30	168	3.0
	IIa - Chesapeake Clay/Silt		1094	0.45	377	3.0
	IIb - Chesapeake Cemented Sand	L1	2525	0.30	971	3.0
		L2	1028	0.30	395	4.5
		L3	2625	0.30	1010	3.9
	IIc - Chesapeake Clay/Silt		2365	0.45	815	3.0
	III - Nanjemoy Sand		3166	0.30	1218	3.1
INTAKE AREA	I - Terrace Sand		NP	NP	NP	NP
	IIa - Chesapeake Clay/Silt		NP	NP	NP	NP
	IIb - Chesapeake Cemented Sand	L1	NP	NP	NP	NP
		L2	620	0.30	239	4.5
		L3	1512	0.30	581	3.0
	IIc - Chesapeake Clay/Silt		1796	0.45	619	3.0
	III - Nanjemoy Sand[(2)]		3166	0.30	1218	3.0
BACKFILL			1920	0.35	711	not used

Notes:
- (1) Adopted from typical values reported in the literature (Salgado, 2008).
- (2) Adopted from Powerblock Area
- NP: Not Present

Table 2.5-58— {Earth Pressure Coefficients}

STRATUM			K_a	K_P	K_0	tan δ[(1)]	FOS against Sliding[(2)]
POWERBLOCK AREA	I - Terrace Sand		0.36	2.76	0.53	0.40	2.7
	IIa - Chesapeake Clay/Silt		0.31	3.20	0.48	0.35	2.3
	IIb - Chesapeake Cemented Sand	L1	0.29	3.46	0.45	0.45	3.0
		L2	0.30	3.30	0.47	0.45	3.0
		L3	0.31	3.21	0.47	0.45	3.0
	IIc - Chesapeake Clay/Silt		0.31	3.25	0.47	0.40	2.7
	III - Nanjemoy Sand		Not Required				
INTAKE AREA	I - Terrace Sand		NP	NP	NP	NP	
	IIa - Chesapeake Clay/Silt		NP	NP	NP	NP	
	IIb - Chesapeake Cemented Sand	L1	NP	NP	NP	NP	
		L2	NA	NA	NA	NA	
		L3	0.29	3.41	0.45	0.45	3.0
	IIc - Chesapeake Clay/Silt		0.32	3.14	0.48	0.40	2.7
	III - Nanjemoy Sand		Not Required				
BACKFILL			0.22	4.60	0.36	0.40	2.7

Notes:
- (1) tan δ is sliding resistance
- values of φ are used to determine K coefficients
$Ka = \tan^2(45-\varphi'/2)$; $K_p = \tan^2(45+\varphi'/2)$; $K_0 = 1 - \sin(\varphi')$
- (2) Factor of Safety is tan δ divided by SSE acceleration, 0.15 g.
The FOS does not account for passive earth pressure on the sides of the buildings.

Table 2.5-59— {Dynamic Properties for Powerblock Area}

POWERBLOCK AREA	El [ft msl]	D [ft]	γ [pcf]	G_o [ksf]	V_s [fps]	V_p [fps]	ν	Damping [%]	
								$S^{(1)}$	$P^{(2)}$
Backfill 1	85.0	0.0	145.0	2810	790	1645	0.35	1.50	0.50
Backfill 2	79.0	6.0	145.0	3650	900	1915	0.36	1.50	0.50
Backfill 3	63.0	22.0	145.0	5250	1080	2260	0.35	1.50	0.50
I, Terrace Sand	85.0	0.0	120.0	2330	790	2903	0.46	1.40	0.47
IIA, Chesapeake Clay/Silt	60.0	25.0	115.0	4320	1100	4623	0.47	1.30	0.43
IIB-1, Che. Cem. Sand	45.0	40.0	120.0	7840	1450	4800	0.45	1.30	0.43
IIB-2, Che. Cem. Sand	30.0	55.0	120.0	12070	1800	5970	0.45	1.30	0.43
IIB-3, Che. Cem. Sand	15.0	70.0	120.0	4760	1130	5762	0.48	1.30	0.43
IIB-4, Che. Cem. Sand	0.0	85.0	120.0	11280	1740	5771	0.45	1.30	0.43
IIc, Chesapeake Clay/Silt	-15.0	100.0	105.0	5100	1250	5254	0.47	1.10	0.37
III, Nanjemoy Sand (NS1)	-200.0	285.0	125.0	12440	1790	5937	0.45	1.30	0.43
III, Nanjemoy Sand (NS2)	-220.0	305.0	125.0	21070	2330	6274	0.42	1.30	0.43
III, Nanjemoy Sand (NS3)	-230.0	315.0	125.0	16000	2030	5793	0.43	1.30	0.43
III, Nanjemoy Sand (NS4)	-270.0	355.0	125.0	14460	1930	5896	0.44	1.30	0.43
I1, Deep Soil	-317.0	402.0	115.0	17290	2200	5389	0.40	1.30	0.43
I2, Deep Soil	-1000.0	1085.0	115.0	19390	2330	5707	0.40	1.30	0.43
I3, Deep Soil	-1500.0	1585.0	115.0	23220	2550	6246	0.40	1.30	0.43
I4, Deep Soil	-2000.0	2085.0	115.0	28000	2800	6859	0.40	1.30	0.43
I5, Bedrock	-2446.0	2531.0	162.0	125780	5000	9354	0.30	1.30	0.43
I6, Bedrock	-2456.0	2541.0	162.0	246520	7000	13096	0.30	1.30	0.43
I7, Bedrock	-2466.0	2551.0	162.0	425830	9200	17212	0.30	1.30	0.43
Base	-3000.0	3085.0	162.0	425830	9200	17212	0.30	1.30	0.43

Notes:
- (1) Shear damping based on RCTS test results
- (2) P damping assumed as 1/3 of S damping

Table 2.5-60— {Dynamic Properties for Intake Area}

INTAKE AREA	El [ft msl]	D [ft]	γ [pcf]	G_o [ksf]	V_s [fps]	V_p [fps]	ν	Damping [%]	
								$S^{(1)}$	$P^{(2)}$
Backfill 1	10.0	0.0	145.0	2810	790	1645	0.35	1.50	0.50
Backfill 2	4.0	6.0	145.0	3650	900	1915	0.36	1.50	0.50
Backfill 3	-12.0	22.0	145.0	5250	1080	2260	0.35	1.50	0.50
IIB-3, C. Cemented Sand	-0.3	8.2	120.0	2270	780	1610	0.35	1.30	0.43
IIB-4, C. Cemented Sand	-2.3	10.2	120.0	6890	1360	5580	0.47	1.30	0.43
IIC-1, C. Clay/Silt	-18.7	26.6	115.0	4720	1150	5250	0.47	1.30	0.43
IIC-2, C. Clay/Silt	-43.0	50.9	105.0	4310	1150	5250	0.47	1.30	0.43
IIC-3, C. Clay/Silt	-105.0	112.9	115.0	4720	1150	5250	0.47	1.30	0.43
IIC-4, C. Clay/Silt	-131.0	138.9	105.0	4310	1150	5250	0.47	1.30	0.43
III, Nanjemoy Sand (NS1)	-200.0	207.9	125.0	12440	1790	5937	0.45	1.10	0.37
III, Nanjemoy Sand (NS2)	-220.0	227.9	125.0	21070	2330	6274	0.42	1.30	0.43
III, Nanjemoy Sand (NS3)	-230.0	237.9	125.0	16000	2030	5793	0.43	1.30	0.43
III, Nanjemoy Sand (NS4)	-270.0	277.9	125.0	14460	1930	5896	0.44	1.30	0.43
I1, Deep Soil	-317.0	324.9	115.0	17290	2200	5389	0.40	1.30	0.43
I2, Deep Soil	-1000.0	1007.9	115.0	19390	2330	5707	0.40	1.30	0.43
I3, Deep Soil	-1500.0	1507.9	115.0	23220	2550	6246	0.40	1.30	0.43
I4, Deep Soil	-2000.0	2007.9	115.0	28000	2800	6859	0.40	1.30	0.43
I5, Bedrock	-2446.0	2453.9	162.0	125780	5000	9354	0.30	1.30	0.43
I6, Bedrock	-2456.0	2463.9	162.0	246520	7000	13096	0.30	1.30	0.43
I7, Bedrock	-2466.0	2473.9	162.0	425830	9200	17212	0.30	1.30	0.43
Base	-3000.0	3007.9	162.0	425830	9200	17212	0.30	1.30	0.43

Notes:
- (1) Shear damping based on RCTS test results
- (2) P damping assumed as 1/3 of S damping

Table 2.5-61— {Strain Dependant Properties for Powerblock Area}

Strata	Strain	G/G_{max}	Damping [%]
I-Terrace Sand	0.0001	1.0000	1.40
	0.0003	1.0000	1.50
	0.0010	0.9800	1.80
	0.0030	0.9150	2.30
	0.0100	0.7600	3.80
	0.0300	0.5600	6.50
	0.1000	0.3400	10.50
	0.3000	0.2000	14.80
	1.0000	0.1000	-
IIC-Chesapeake Clay/Silt	0.0001	1.0000	1.10
	0.0003	1.0000	1.10
	0.0010	1.0000	1.10
	0.0030	1.0000	1.13
	0.0100	0.9900	1.20
	0.0300	0.9400	1.50
	0.1000	0.8000	2.40
	0.3000	0.6300	4.10
	0.6000	0.5000	5.80
	1.0000	0.4000	7.40
All Other Natural Soils	0.0001	1.0000	1.30
	0.0003	1.0000	1.30
	0.0010	1.0000	1.40
	0.0030	0.9900	1.60
	0.0100	0.9400	2.20
	0.0300	0.8200	3.20
	0.1000	0.6200	5.40
	0.3000	0.4200	8.40
	0.6000	0.3100	10.60
	1.0000	0.2500	12.60

Table 2.5-62— {Strain Dependant Properties for Intake Area}

Strata	Strain	G/G_{max}	Damping [%]		Strata	Strain	G/G_{max}	Damping [%]
IIB, IIC-1 & III	0.0001	1.0000	1.30		IIC-3	0.0001	1.0000	1.10
	0.0003	1.0000	1.30			0.0003	1.0000	1.10
	0.0010	1.0000	1.40			0.0010	1.0000	1.10
	0.0030	0.9900	1.60			0.0030	0.9700	1.13
	0.0100	0.9400	2.20			0.0100	0.8600	1.20
	0.0300	0.8200	3.20			0.0300	0.7400	1.50
	0.0548	0.7200	4.30			0.0548	0.6500	1.95
	0.1000	0.6200	5.40			0.1000	0.5600	2.40
	0.1732	0.5200	6.90			0.1732	0.4700	3.25
	0.3000	0.4200	8.40			0.3000	0.3900	4.10
	0.4243	0.3650	9.50			0.4243	0.3400	4.95
	0.6000	0.3100	10.60			0.6000	0.3000	5.80
	1.0000	0.2500	12.60			1.0000	0.2400	7.40
IIC-2	0.0001	1.0000	1.10		IIC-4	0.0001	1.0000	0.80
	0.0003	1.0000	1.10			0.0003	1.0000	0.80
	0.0010	1.0000	1.10			0.0010	1.0000	0.80
	0.0030	0.9900	1.13			0.0030	0.9900	0.90
	0.0100	0.9400	1.70			0.0100	0.9400	1.12
	0.0300	0.8200	3.20			0.0300	0.8200	1.50
	0.0548	0.7200	4.30			0.0548	0.7200	1.95
	0.1000	0.6200	5.40			0.1000	0.6200	2.40
	0.1732	0.5200	6.90			0.1732	0.5200	3.25
	0.3000	0.4200	8.40			0.3000	0.4200	4.10
	0.4243	0.3650	9.50			0.4243	0.3650	4.95
	0.6000	0.3100	10.60			0.6000	0.3100	5.80
	1.0000	0.2500	12.60			1.0000	0.2500	7.40

Table 2.5-63— {Strain Dependant Properties for Backfill}

Strata	Strain	G/G_{max}	Damping [%]
BACKFILL	0.0001	1.0000	1.49
	0.0003	0.9700	1.57
	0.0010	0.8900	1.84
	0.0032	0.7400	2.71
	0.0100	0.5300	5.02
	0.0316	0.3000	9.38
	0.1000	0.1300	15.00
	0.3160	0.0600	-
	1.0000	0.0382	-

Table 2.5-64— {Building Elevation, Depth, Area, and Load}

	Building	El. [ft]	Depth [ft]	Area [ft^2]	Load [kips]	Pressure [ksf]	Eq. Shape [ft] (1)
Nuclear Island	Reactor Building (RB)	41.5	41.5	26268	313477	11.9	270 x 300
	Fuel Building (FB)	41.5	41.5	14545	216806	14.9	
	Safeguard Building 1 (SGB1)	41.5	41.5	9198	108064	11.7	
	Safeguard 2&3 Buildings (SGB23)	41.5	41.5	20952	200814	9.6	
	Safeguard Building 4 (SGB4)	41.5	41.5	9247	104079	11.3	
Other Buildings	Nuclear Auxiliary Building (NAB)	48.0	35.0	12559	122000	9.7	105 x 120
	Access Building (AB)	48.0	35.0	7620	49300	6.5	95 x 80
	Rad. Waste Building (RWPB)	47.0	36.0	16970	109700	6.5	130 x 130
	E. Power Gen. Buildings (EPGB)	76.0	7.0	12611	40200	3.2	84 x 150
	E. Service Water Building (ESWB)	61.0	22.0	16284	88700	5.4	105 x 155
	Turbine Building (TB)	60.5	22.5	101305	446600	4.4	270 x 380
Intake Area	UHS Makeup Water Intake Structure (UHS MWIS)	-27.5	37.5	5162	34146	7.1	58 x 89
	Notes: *- (1) Equivalent Rectangular shape* *Depth is based on average site grade elevation of 83 ft*						

Table 2.5-65— {Bearing Capacity}

Building	Bulding Load [ksf]	Ultimate Bearing Capacity q_{ult} [ksf]			Allowable Bearing Capacity q_a [ksf] (1)	
		VESIC		MEYERHOF	STATIC	DYNAMIC
		Case a	Case b	Case c (2)		
NI Common Mat	11.8	192.7	228.9	70.5	23.5	35.2
NAB	9.7	170.7	179.1	105.8	35.3	52.9
EPGB	3.2	113.6	102.2	115.0	34.1	51.1
ESWB	5.4	145.7	153.8	118.0	39.3	59.0
UHS MWIS (3)	7.1	NA	35.2	NA	11.7	17.6

Notes:
- (1) With FS = 3.0 for static conditions and FS = 2.0 for dynamic condition (minimum q_{ult} used)
- (2) Case c, Dense sand over soft clay
- (3) Case b with Stratum II-C used for UHS, other scenarios are not applicable (NA).

Table 2.5-66— {Heave after Excavation}
Measured at NI Foundation Level

Location	Vertical Displacement after Excavation [in]	
	Immediate	1 Year
A	-2.2	-2.4
B	-3.0	-3.5
C	-4.7	-5.3
D	-3.1	-3.5

Table 2.5-67— {Foundation Loading Sequence}

Building Name		Loads [ksf]								
	Step	0	1	2	3	4	5	6	7	8
	Day	0	60	140	300	500	800	1000	1400	2000
	Month	0	2	4	10	16	26	33	46	66
	Year	0	1	1	1	2	3	3	4	6
Reactor (RB)		0.0	0.1	0.2	2.1	3.8	7.5	9.6	9.8	11.9
Fuel (FB)		0.0	0.0	1.0	1.7	2.0	5.7	9.0	14.9	14.9
Safeguard 1 (SGB1)		0.0	0.0	0.8	3.8	5.9	8.6	11.8	11.8	11.8
Safeguard 2&3 (SGB23)		0.0	0.0	1.0	1.7	2.6	5.4	8.2	9.6	9.6
Safeguard (SGB4)		0.0	0.0	0.8	3.6	5.6	8.2	11.3	11.3	11.3
Nuclear Auxiliary (NAB)		0.0	0.0	0.9	1.8	3.5	5.3	7.1	9.7	9.7
Access (AB)		0.0	0.0	0.9	1.9	2.8	4.6	5.6	6.5	6.5
Radioactive Waste (RWPB)		0.0	0.0	0.0	0.0	0.0	0.7	2.2	6.5	6.5
Emergency Power Gen. (EPGB)		0.0	0.0	0.0	0.0	0.0	0.0	0.5	3.2	3.2
Emergency Service Water (ESWB)		0.0	0.0	0.0	0.0	0.0	1.6	5.5	5.5	5.5
Turbine (TB)		0.0	0.0	0.0	0.6	1.8	3.2	4.4	4.4	4.4
Turbine Extension (TBE)		0.0	0.0	0.0	0.6	1.8	3.2	4.4	4.4	4.4

Table 2.5-68— {Building Center Point Settlement Estimates}

Building Name		Settlement [in] (Medium Elevation Surface Topography)(1)							
	Step	1	2	3	4	5	6	7	8
	Day	60	140	300	500	800	1000	1400	2000
	Month	2	4	10	16	26	33	46	66
	Year	1	1	1	2	3	3	4	6
Reactor (RB)		0.3	1.1	2.0	3.1	7.1	10.2	12.1	12.7
Fuel (FB)		0.3	1.3	2.0	3.0	6.8	9.8	12.4	13.0
Safeguard 1 (SGB1)		0.3	1.4	2.3	3.3	7.1	10.1	11.4	12.0
Safeguard 2&3 (SGB23)		0.3	1.4	2.2	3.2	7.0	9.9	11.1	11.6
Safeguard (SGB4)		0.3	1.3	2.2	3.2	6.9	9.8	12.1	12.5
Nuclear Auxiliary (NAB)		0.4	1.4	2.2	3.2	6.5	9.1	12.0	12.3
Access (AB)		0.4	1.6	2.4	3.5	7.0	9.8	11.4	11.7
Radioactive Waste (RWPB)		0.5	1.3	1.9	2.7	5.1	6.9	9.4	9.6
E. Service Water 1 (ESWB1)		0.0	1.6	2.0	2.6	4.7	7.0	7.4	7.4
E. Service Water 2 (ESWB2)		0.0	1.7	2.2	2.9	5.5	8.3	8.9	9.1
E. Service Water 3 (ESWB3)		0.0	2.0	2.5	3.3	6.0	8.8	9.1	9.2
E. Service Water 4 (ESWB4)		0.0	1.9	2.3	3.0	5.3	7.9	8.1	8.2
E. Power Generating (EPBG1)		0.0	0.0	0.0	3.8	5.9	7.6	9.5	9.6
E. Power Generating (EPBG2)		0.0	0.0	0.0	3.7	5.7	7.1	8.5	8.7

Notes:
- (1) Settlement estimates correspond to Medium Elevation Surface Topography 2, Revert after 4th Step

Table 2.5-69— {Maximum Tilt at End of Construction}

Building	Section	Tilt Direction (1)	Tilt [in/50 ft]	
			Tilt Average Elevation Case(2)	Construction Baseline(3)
NI	AA	N	-0.10	-0.10
	BB	E	0.27	0.27
	CC	SW	-0.21	-0.21
	DD	SE	0.32	0.32
ESWB1	EE	NW	-0.80	-0.59
	FF	NE	-0.17	-0.18
ESWB2	GG	SW	0.29	0.23
	HH	NW	-0.88	-0.72
ESWB3	II	NE	0.13	-0.17
	JJ	SE	0.19	0.13
ESWB4	KK	SW	0.36	0.28
	LL	SE	0.53	0.42
EPBG1	MM	SW	0.35	0.16
	NN	SE	0.68	0.49
EPBG2	OO	NE	0.72	-0.42
	PP	NW	0.37	-0.14

Notes
- (1) Local Plant Coordinates
- (2) Tilt recorded with calculation for Medium Elevation Surface Topography Revert 2
Sign is positive for clockwise tilt and negative for counter-clockwise
- (3) Correction to subtract the observed tilt before the construction of the building

Table 2.5-70— {Settlement and Tilt for UHS Facilities}

Building	Δ Center [in]	Maximum Tilt (1) [in/50 ft]
Ultimate Heat Sink Makeup Water Intake Structure (UHS MWIS)	3.5	0.1
Forebay	3.4	0.1
Cooling Water Makeup Intake Structure (CW MIS)	3.6	0.4
Notes *- (1) Adjustment for construction not incorporated.*		

Table 2.5-71— {Material Properties for Slope Stability}

Stratum	Material Property	Powerblock(1)	Intake Area & Intake Slope	Utility Corridor
Structural Backfill	Unit Weight (pcf)	145	-	-
	c (psf)	0	-	-
	φ (degrees)	40	-	-
	c′ (psf)	0	-	-
	φ′ (degrees)	40	-	-
Stratum I: Terrace Sand	Unit Weight (pcf)	120	120	120
	c (psf)	1100	1100	1100
	φ (degrees)	13	13	13
	c′ (psf)	0	0	0
	φ′ (degrees)	32	32	32
Stratum IIa: Chesapeake Clay/ Silt	Unit Weight (pcf)	115	115	115
	c (psf)	2500	3400	2500
	φ (degrees)	0	0	0
	c′ (psf)	900	1400	900
	φ′ (degrees)	25	28	25
Stratum IIb: Chesapeake Cemented Sand	Unit Weight (pcf)	120	120	120
	c (psf)	2800	2800	2800
	φ (degrees)	17	17	17
	c′ (psf)	0	0	0
	φ′ (degrees)	34	34	34
Stratum IIc: Chesapeake Clay/ Silt	Unit Weight (pcf)	105	110	105
	c (psf)	5000	4800	5000
	φ (degrees)	0	0	0
	c′ (psf)	2300	1000	2300
	φ′ (degrees)	26	26	26

Notes:
(1) Powerblock includes the Construction Laydown Area CCNPP

Table 2.5-72— {Computed Factors of Safety for Critical Slip Surface}

Slope Section	Affected Area	Effective Stress Conditions						Total Stress Conditions[1]		
		Static Analysis			Pseudo-static (Dynamic)Analysis			Pseudo-static (Dynamic) Analysis		
		Ordinary	Bishop	M-P	Ordinary	Bishop	M-P	Ordinary	Bishop	M-P
A - Case a	Powerblock	1.92	2.19	2.18	1.32	1.47	1.47	1.73	1.76	1.76
A - Case b		1.63	1.89	1.89	1.14	1.27	1.28	1.61	1.68	1.68
B - Case a		1.95	2.22	2.22	1.35	1.49	1.49	1.76	1.81	1.81
B - Case b		1.85	2.12	2.12	1.23	1.40	1.41	1.74	1.78	1.79
C		1.96	2.02	2.02	1.31	1.36	1.36	3.15	3.24	3.24
D		1.93	1.97	1.97	1.32	1.38	1.38	4.09	4.14	4.14
E		1.98	2.05	2.05	1.34	1.41	1.41	3.15	3.15	3.15
F	Intake Area	2.20	2.34	2.34	1.57	1.68	1.69	2.73	2.81	2.82
G	Utility Corridor	1.87	2.04	2.05	1.24	1.34	1.35	1.86	1.92	1.93

Notes:
Ordinary = Ordinary method
Bishop = Bishop's simplified method
M-P = Morgenstern-Price method
Typical minimum acceptable values of FOS are 1.5 for static conditions and 1.0 to 1.2 for pseudo-static (e.g., earthquake) conditions (Duncan, 1996)
(1) Total stress conditions are more representative of dynamic conditions are not used in the discussion.

Table 2.5-73— {Building Points with Associated Differential Settlements}

(Page 1 of 2)

Building Name		Pair of Point No.		u_y (in.)		Δu_y (in.)
		NI	Adj. Bldg.	NI	Adj. Bldg.	
Emergency Power Generating Building 1 (EPBG1)	Center	1	54	12.7	3.7	9.1
	Edge	21	57	10.7	3.9	6.8
	Edge	22	56	12.1	4.4	7.7
	Edge	26	56	11.6	4.4	7.2
Emergency Power Generating Building 2 (EPBG2)	Center	1	59	12.7	3.0	9.8
	Edge	12	60	11.4	3.5	7.8
	Edge	14	60	10.9	3.5	7.4
	Edge	19	63	10.4	3.1	7.2
Emergency Service Water Building 2 (ESWB2)	Center	1	74	12.7	6.2	6.6
	Edge	12	77	11.4	6.5	4.8
	Edge	12	78	11.4	7.4	3.9
	Edge	30	75	12.4	5.8	6.6
	Edge	30	78	12.4	7.4	4.9
	Edge	31	77	12.3	6.5	5.7
	Edge	31	78	12.3	7.4	4.8
Emergency Service Water Building 3 (ESWB3)	Center	1	69	12.7	5.9	6.8
	Edge	21	70	10.7	6.1	4.6
	Edge	21	71	10.7	6.1	4.6
	Edge	21	72	10.7	5.5	5.1
	Edge	26	70	11.6	6.1	5.4
	Edge	26	71	11.6	6.1	5.5
Turbine Building (TB)	Center	1	84	12.7	8.9	3.9
	Edge	19	86	10.4	10.3	0.0
	Edge	20	85	10.7	10.3	0.4
	Edge	20	86	10.7	10.3	0.3
	Edge	21	85	10.7	10.3	0.4
Nuclear Auxiliary Building (NAB)	Center	1	42	12.7	11.9	0.8
	Edge	22	40	12.1	11.4	0.7
	Edge	23	39	12.6	13.3	0.7
	Edge	28	36	12.3	12.3	0.0
	Edge	33	38	12.7	13.3	0.6
	Edge	34	37	12.7	13.3	0.6
	Edge	36	28	12.3	12.3	0.0
Acess Building (AB)	Center	1	45	12.7	11.3	1.4
	Edge	16	46	12.1	12.3	0.2
	Edge	21	47	10.7	11.2	0.5
	Edge	25	44	12.1	12.6	0.4
	Edge	26	43	11.6	11.6	0.1

Table 2.5-73— {Building Points with Associated Differential Settlements}

(Page 2 of 2)

Building Name		Pair of Point No.		u_y (in.)		Δu_y (in.)
		NI	Adj. Bldg.	NI	Adj. Bldg.	
		RWPB	NAB	RWPB	NAB	
Radwaste Building (RWPB) - Nuclear Auxiliary Building (NAB)		51	41	7.3	10.1	2.7
		52	40	8.7	11.4	2.6
u_y (NI) - Settlements at the end of the 8th loading step at the base of the N						
u_y (Adj. Bldg) - Settlements at the end of the 8th loading step at the base of the adjacent building						
Δu_y - Differential Settlements						

Table 2.5-74— {Seismic Bearing Capacity Results}

Dynamic Bearing Capacity	Foundation Width (ft)		
	$B_1 = 270$	$B_2 = 203$	$B_3 = 135$
Ultimate, q_{ult} (ksf)	145.8	131.9	117.0
Allowable, q_a (ksf) (1)	72.9	66.0	58.5
Notes: (1) Factor of Safety for dynamic forces is FOS = 2.0. i.e., $q_a = q_{ult}/FOS$			

Figure 2.5-1— {Map of Physiographic Province}

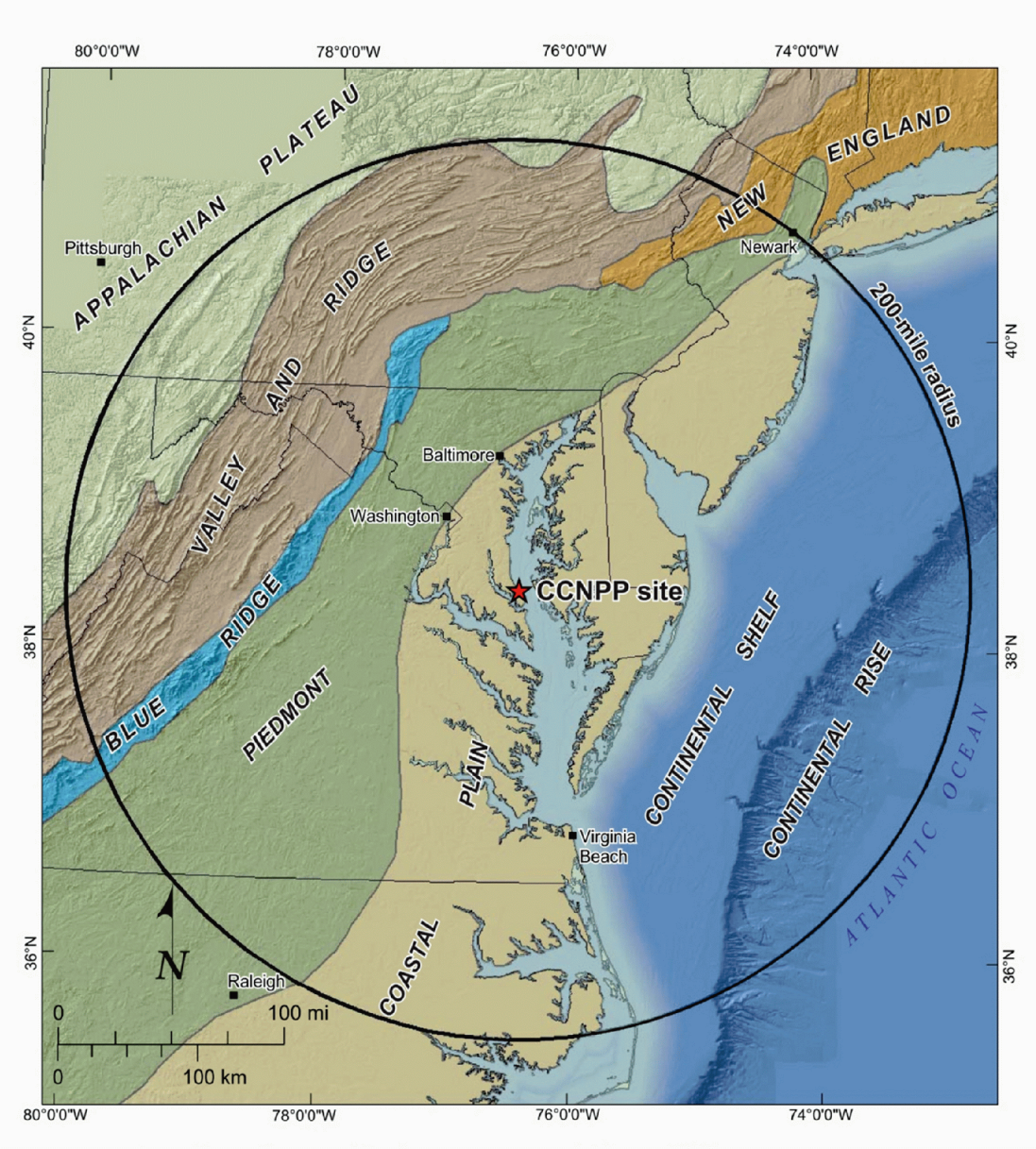

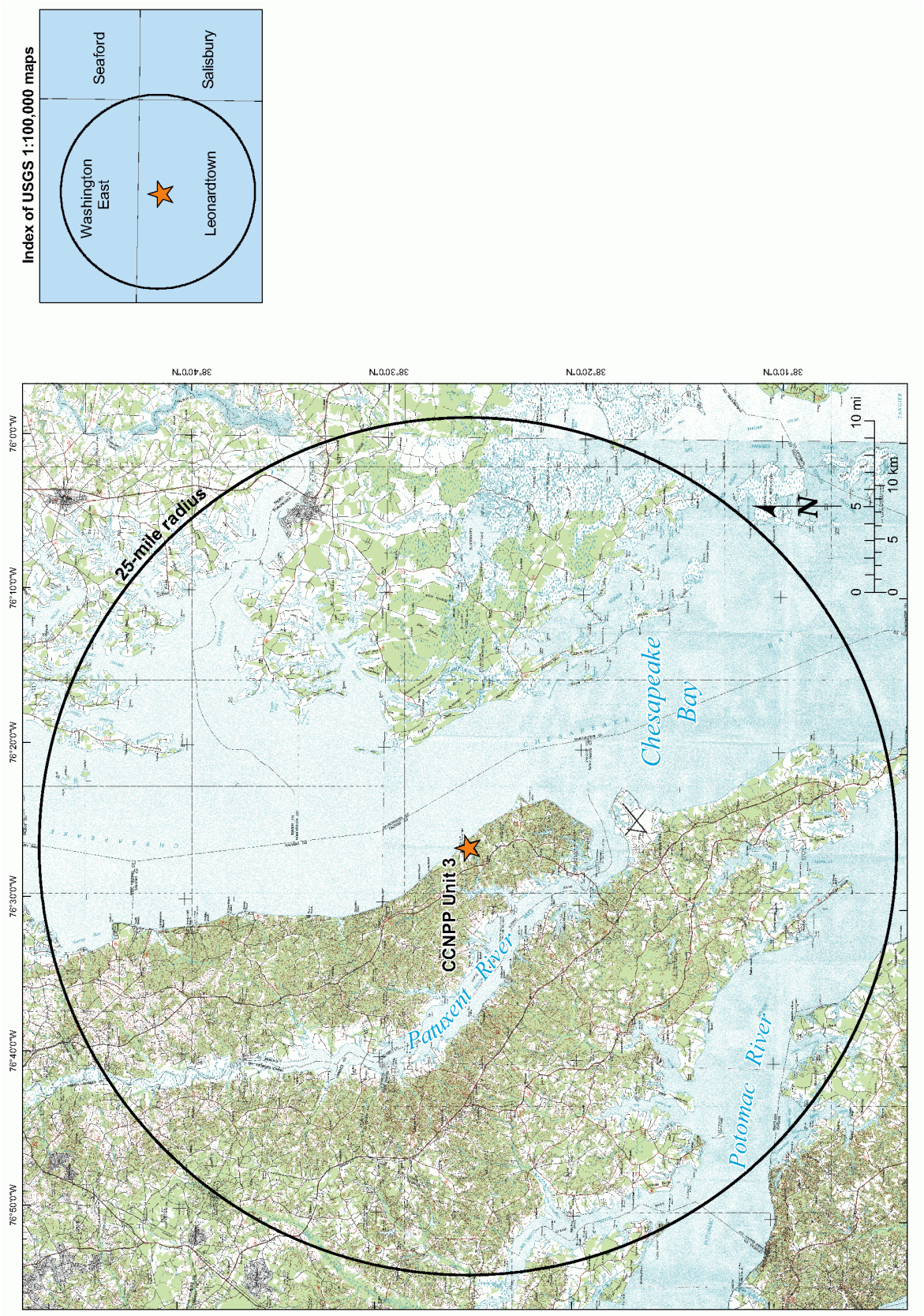

Figure 2.5-2— {Site Vicinity Topographic Map 25-Mile (40-Km) Radius}

Figure 2.5-3— {Site Area Topographic Map 5-Mile (8-Km) Radius}

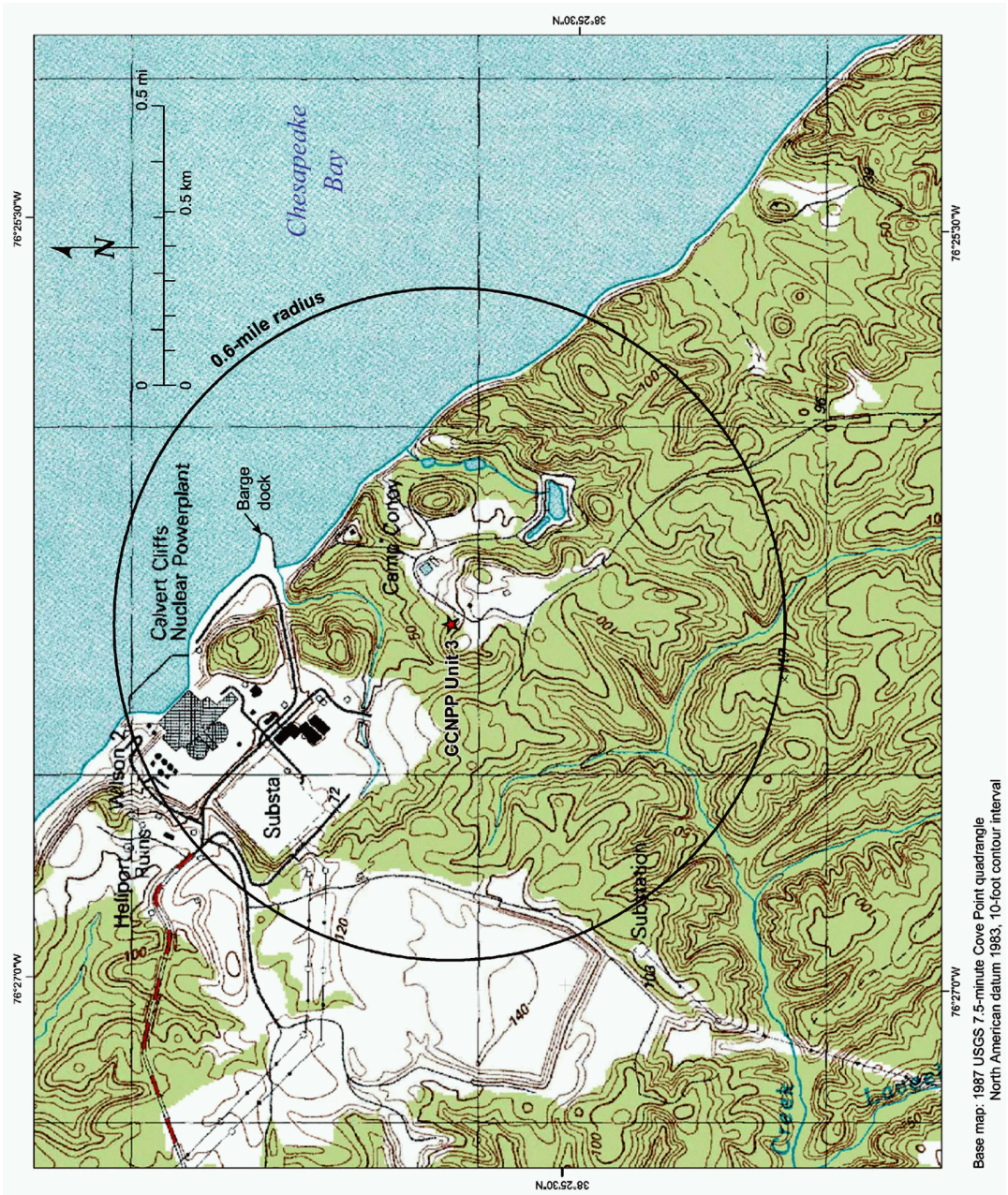

Figure 2.5-4— {Site Topographic Map 0.6-Mile (1-Km) Radius}

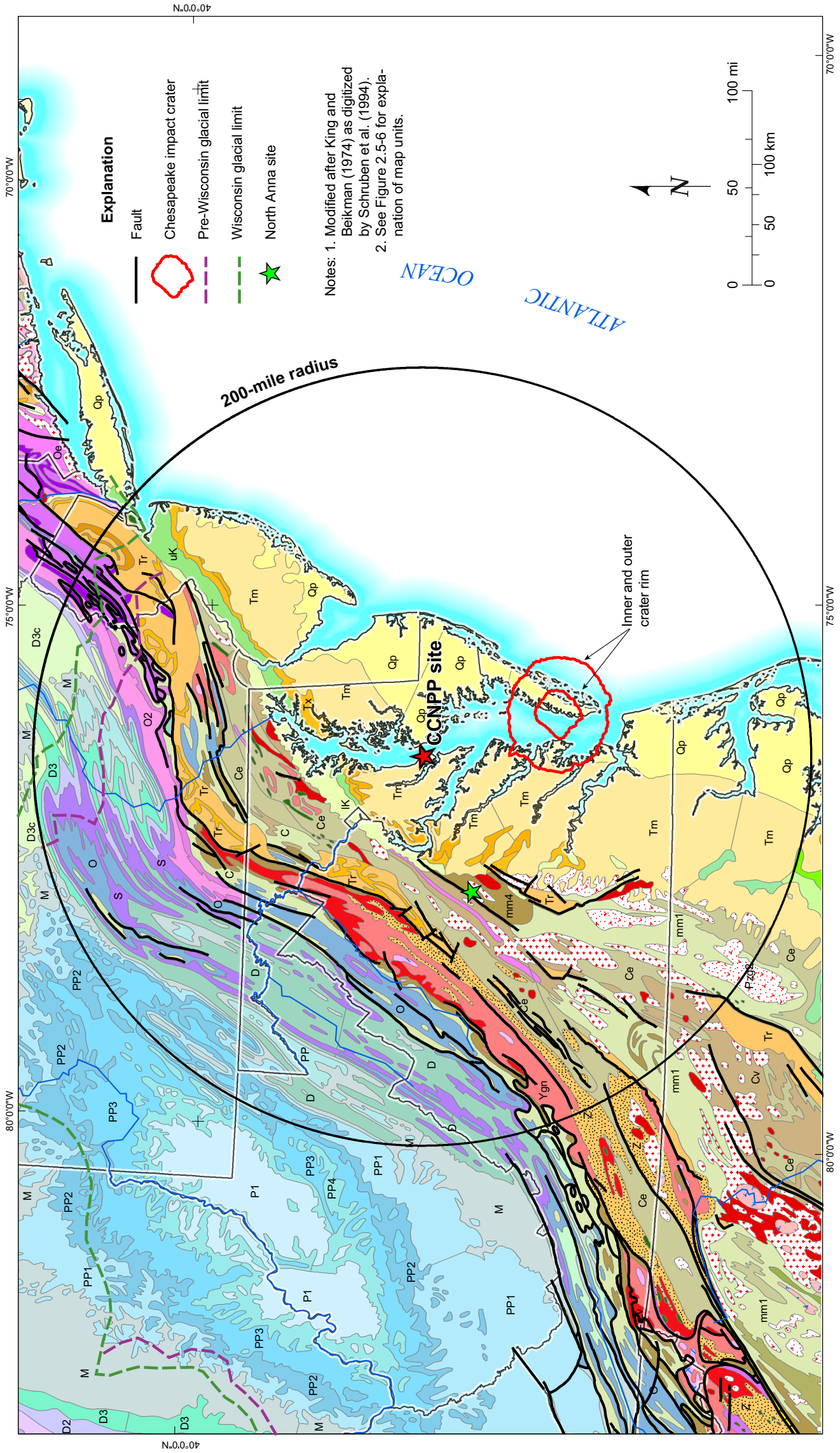

Figure 2.5-5— {Regional Geologic Map 200-Mile (320-Km) Radius}

Figure 2.5-6— {Regional Geologic Map 200-Mile (320-Km) Radius Explanation}

Stratified Sequence

Cenozoic

- Quaternary (Q): Qp Pleistocene
- Tertiary (T): Tm Miocene; Te Eocene; Tx Paleocene

Mesozoic

- Cretaceous (K): uK Upper Cretaceous — uK4 Navarro Group; uK1 Woodbine and Tuscalossa Group
- Cretaceous (K): lK Lower Cretaceous — lK3 Washita Group
- Triassic (Tr): Tr Triassic

Paleozoic

- Permian (P): P1 Wolfcampian Series
- Pennsylvanian (PP): Upper — PP4 Virgilian Series; PP3 Missourian Series
- Pennsylvanian (PP): Middle — PP2 Des Moinesian Series
- Pennsylvanian (PP): Lower — PP1 Atokan and Morrowan Series
- Mississippian (M): M Mississippian
- Devonian (D): D3 Upper Devonian; D2 Middle Devonian; D1 Lower Devonian
- Silurian (S): S Silurian
- DS Devonian and Silurian
- Ordovician (O): O2 Middle Ordovician-Mohawkian; O1 Lower Ordovician-Canadian
- OC Lower Ordovician and Cambrian-carbonate rocks
- lPz Lower Paleozoic
- Cambrian (C): C Cambrian

Precambrian

- Precambrian: Z; Y
- Z Z sedimentary rocks

Continental Deposits

- D3c Upper Devonian continental
- Cq Basal Lower Cambrian clastic rocks

Eugeosynclinal Deposits

- De Devonian eugeosynclinal
- Oe Ordovician eugeosynclinal
- Ce Cambrian eugeosynclinal

Volcanic Rocks

- Trv Mafic Lava interbedded in Triassic Newark Group
- Ov Ordovician volcanic rocks
- Cv Cambrian volcanics
- Zv Z volcanic rocks

Plutonic and Intrusive Rocks

- Tri Triassic mafic intrusives
- um Ultramafic rocks
- Pzg3 Upper Paleozoic granitic rocks
- Pzmi Paleozoic mafic intrusives
- Pzg2 Middle Paleozoic granitic rocks
- Pzg1 Lower Paleozoic granitic rocks
- Zg Z granitic rocks
- Ya Anorthosite

Metamorphic Rocks

- cat Cataclastic rocks
- Metamorphic Complexes:
  - mm1 Felsic paragneis and schist
  - mm2 Mafic paragneiss (= hornblende, amphibolite)
  - mm3 Migmatite
  - mm4 Felsic orthogneiss (= granite gneiss)
- Ym Paragneiss and schist
- Ygn Orthogneiss

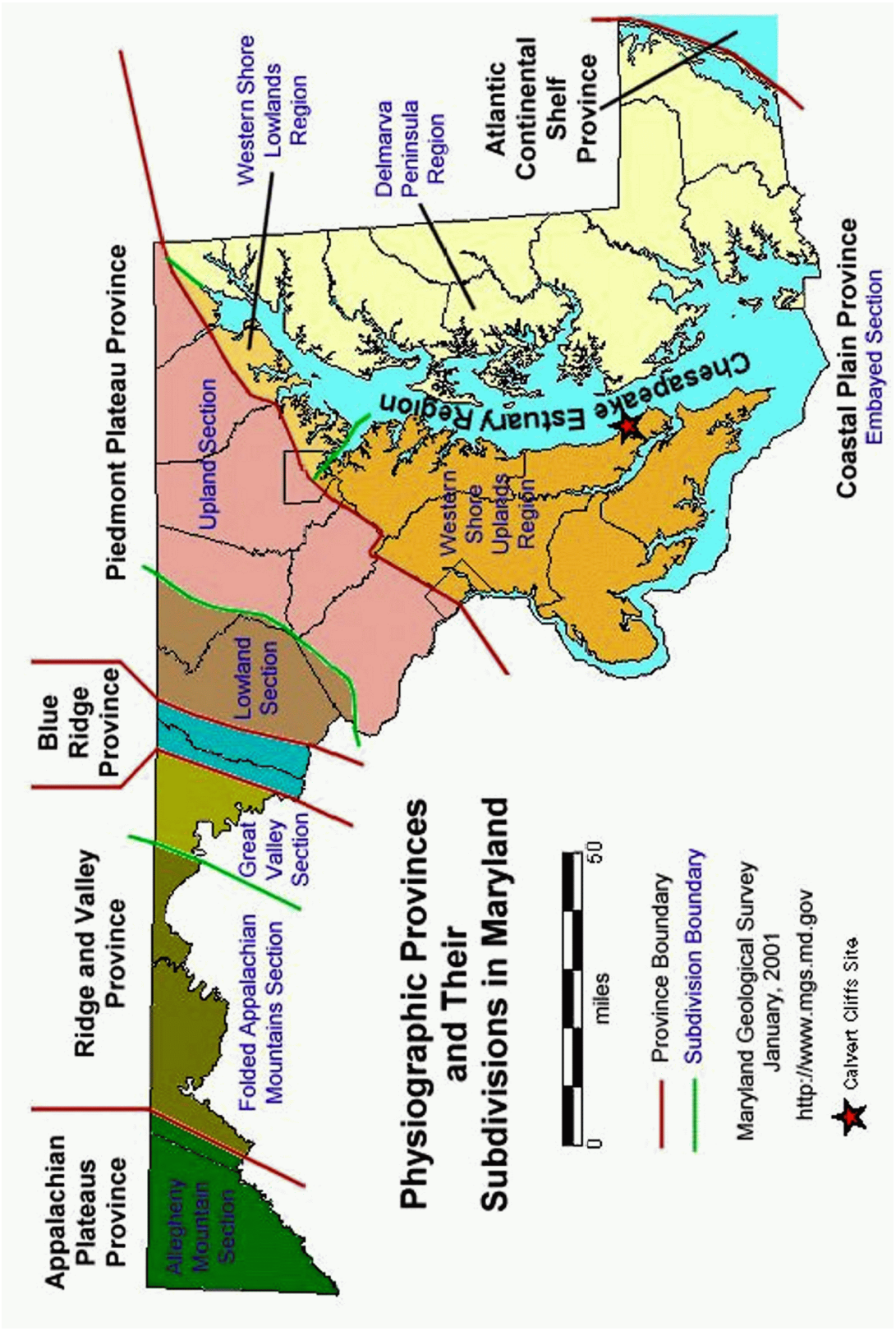

Figure 2.5-7— {Physiographic Map of Maryland}

Figure 2.5-8— {Evolution of the Applachian Orogen}

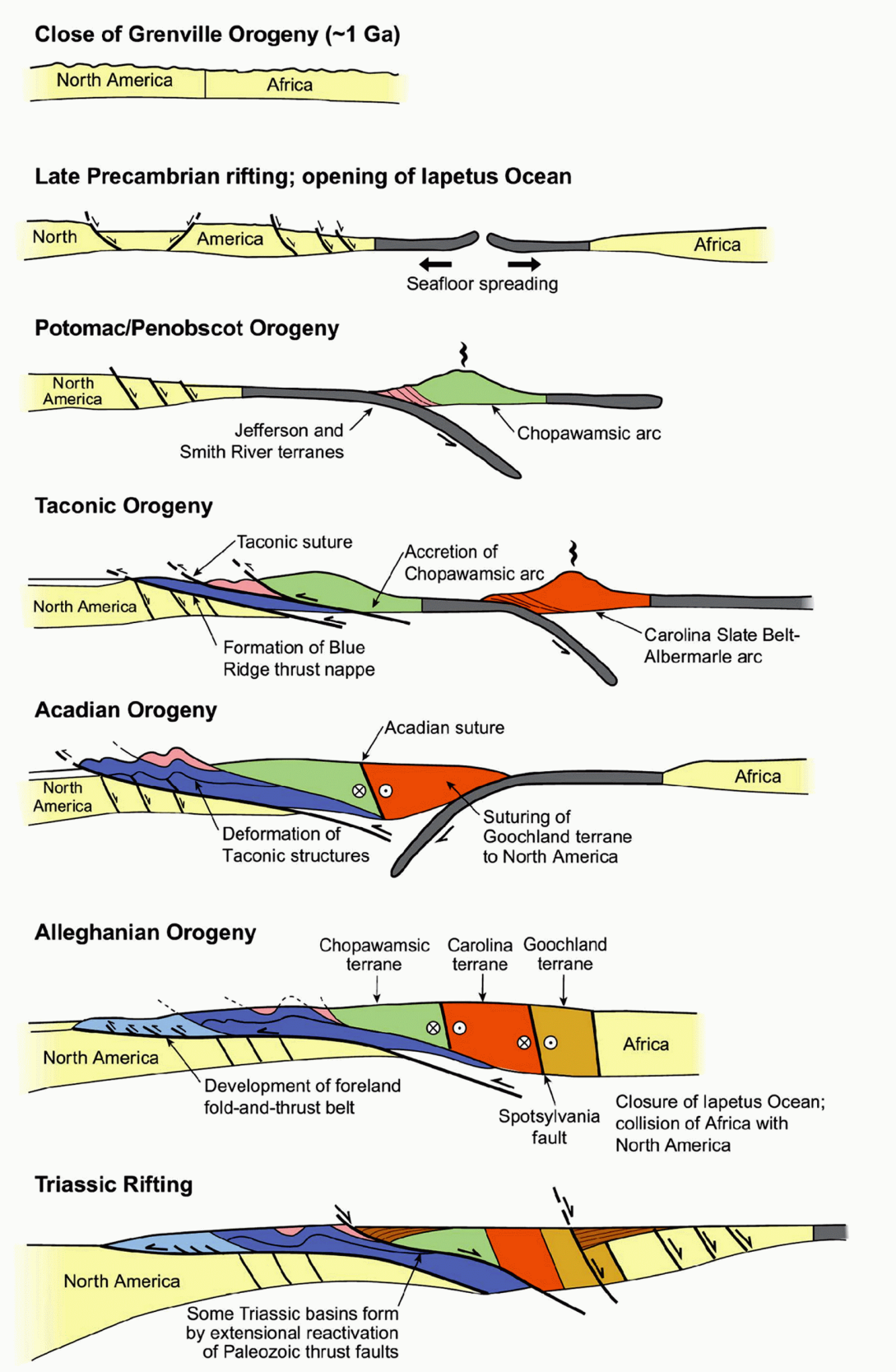

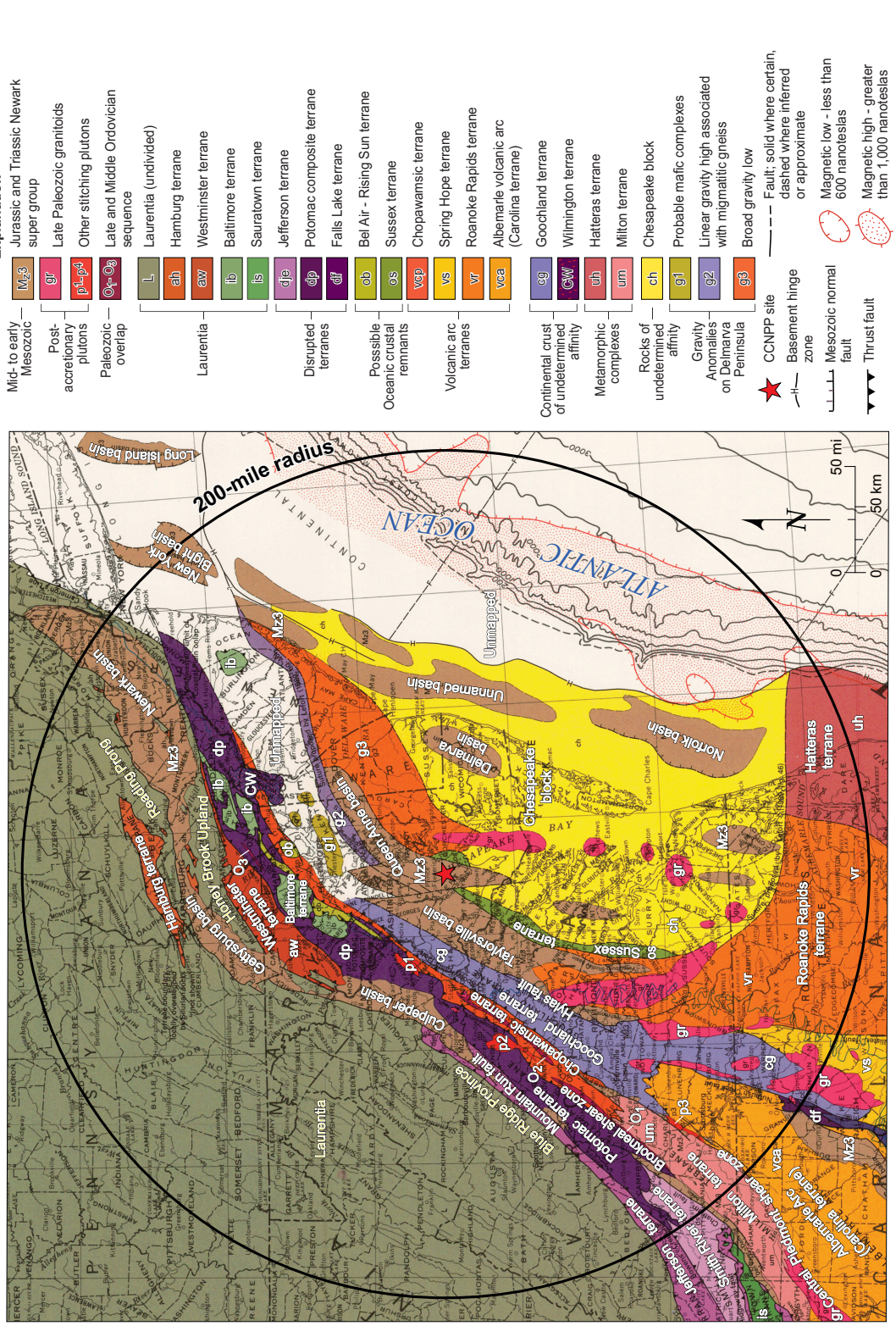

Figure 2.5-9— {General Technostatigraphic Terrane Map 200-mile (320 km) Radius (modified from Horton 1991)}

Figure 2.5-10— {Map of Mesozoic Basins}

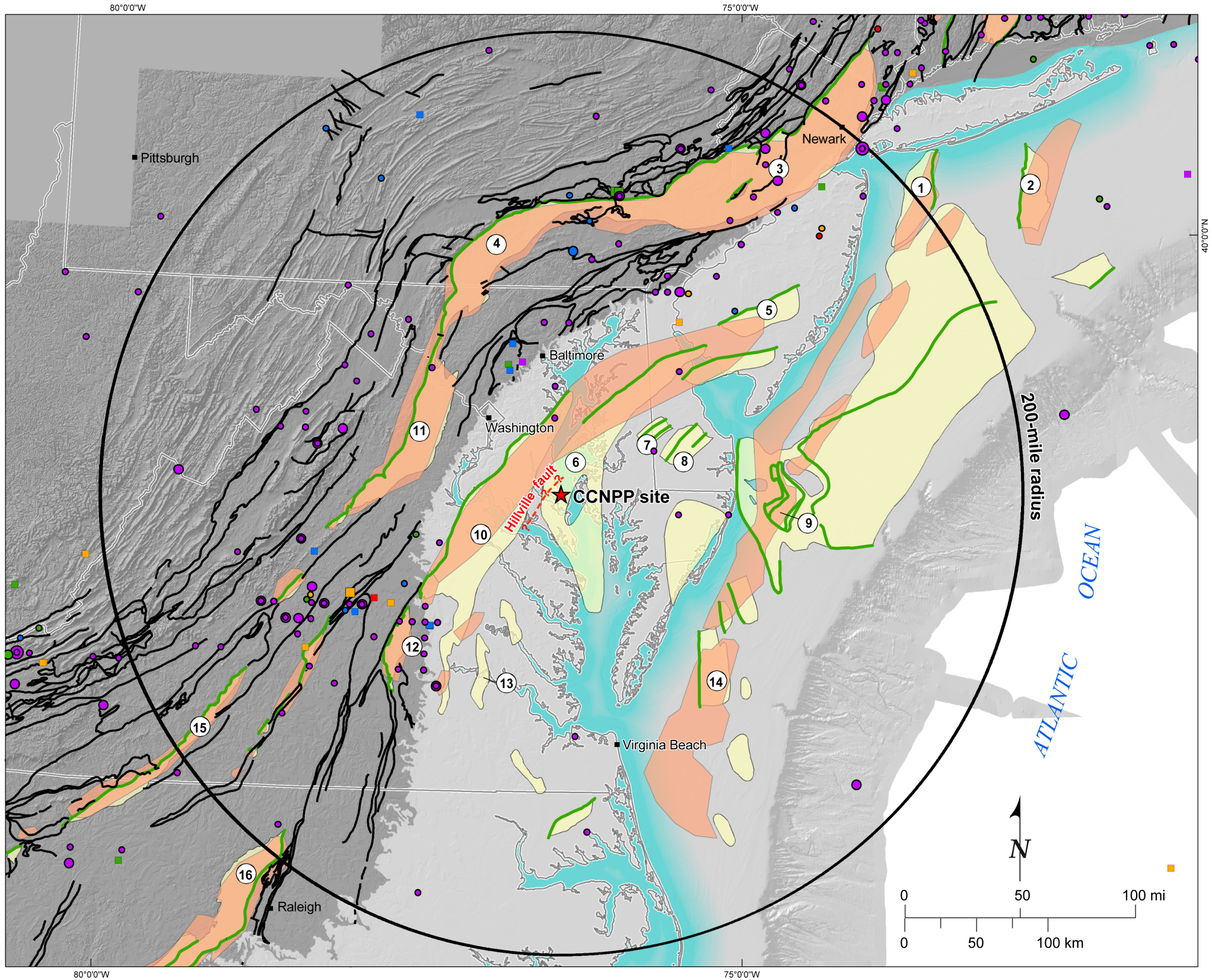

Explanation

Faults

- Paleozoic (Hibbard et al., 2006)
- Mesozoic (Benson, 1992)

Mesozoic Basins:

- Benson (1992)
- Schlische and Olsen (1990)

*Mesozoic Basins**

1. New York Bight basin
2. Long Island basin
3. Newark basin
4. Gettysburg basin
5. Buena basin
6. Queen Anne basin
7. Greenwood basin
8. Bridgeville basin
9. Fenwick basin
10. Taylorsville basin
11. Culpeper basin
12. Richmond basin
13. Toano basin
14. Norfolk basin
15. Dan River-Danville basin
16. Deep River basin

*Basin names from Benson (1992)

Earthquake Epicenters (by magnitude, Emb)

EPRI Catalog (1627 - 1984)	*Eastern U.S. Seismicity (1985 - 2006)*
3.00 - 3.99	3.00 - 3.99
4.00 - 4.99	4.00 - 4.99
5.00 - 5.99	5.00 - 5.20
6.00 - 6.99	
7.00 - 7.35	

Depth (km)	*Depth (km)*
0	0
0.1 - 4	0.1 - 4
5 - 9	5 - 9
10 - 14	10 - 14
15 - 19	15 - 19

Note: Emb is an equivalent body wave magnitude explained in Section 2.5.2.1.

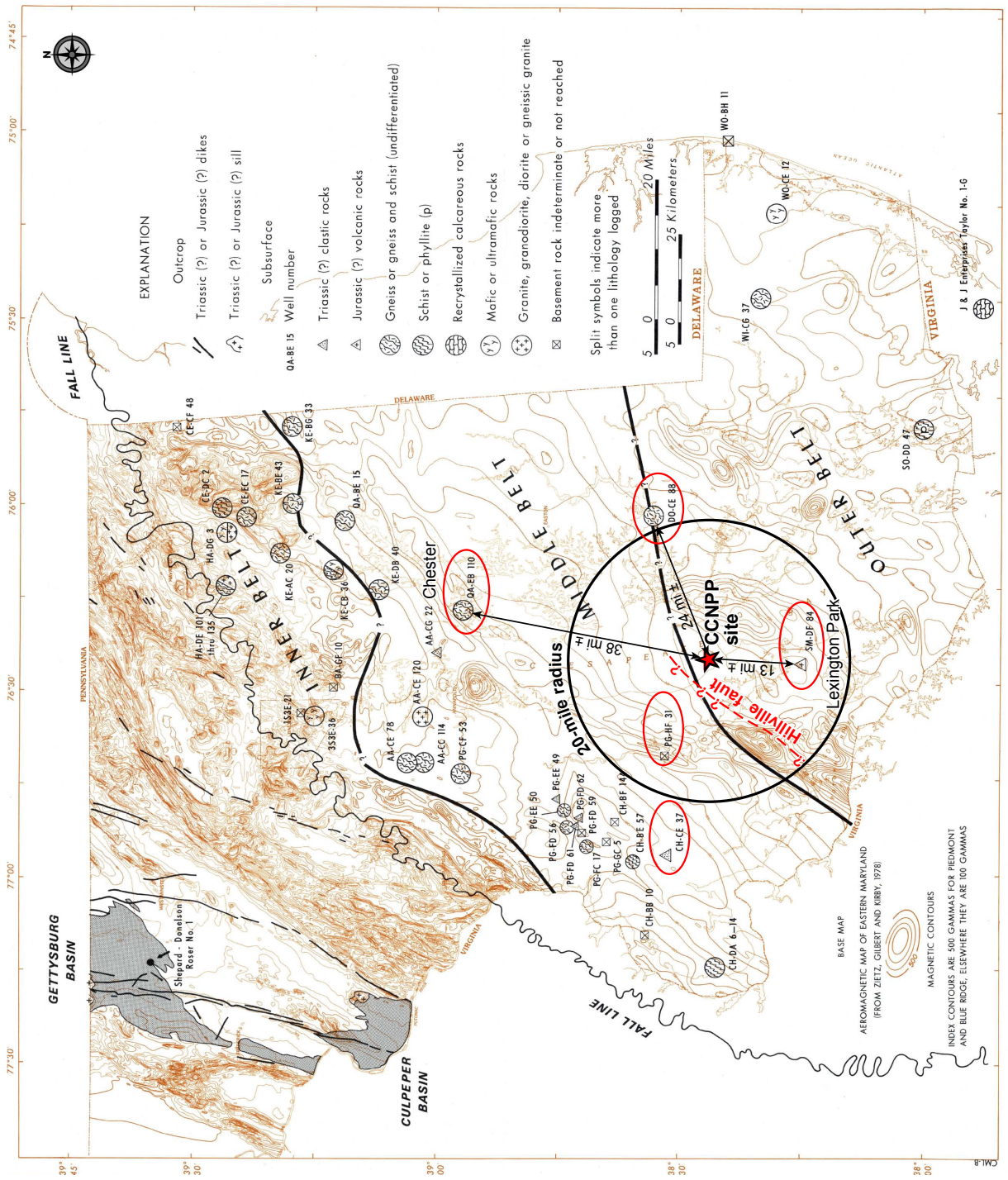

Figure 2.5-11— {Lithologies of Basement Rocks from Coastal Plain Wells}

Figure 2.5-12— {Tectonic Features of the Mid-Atlantic Passive Margin}

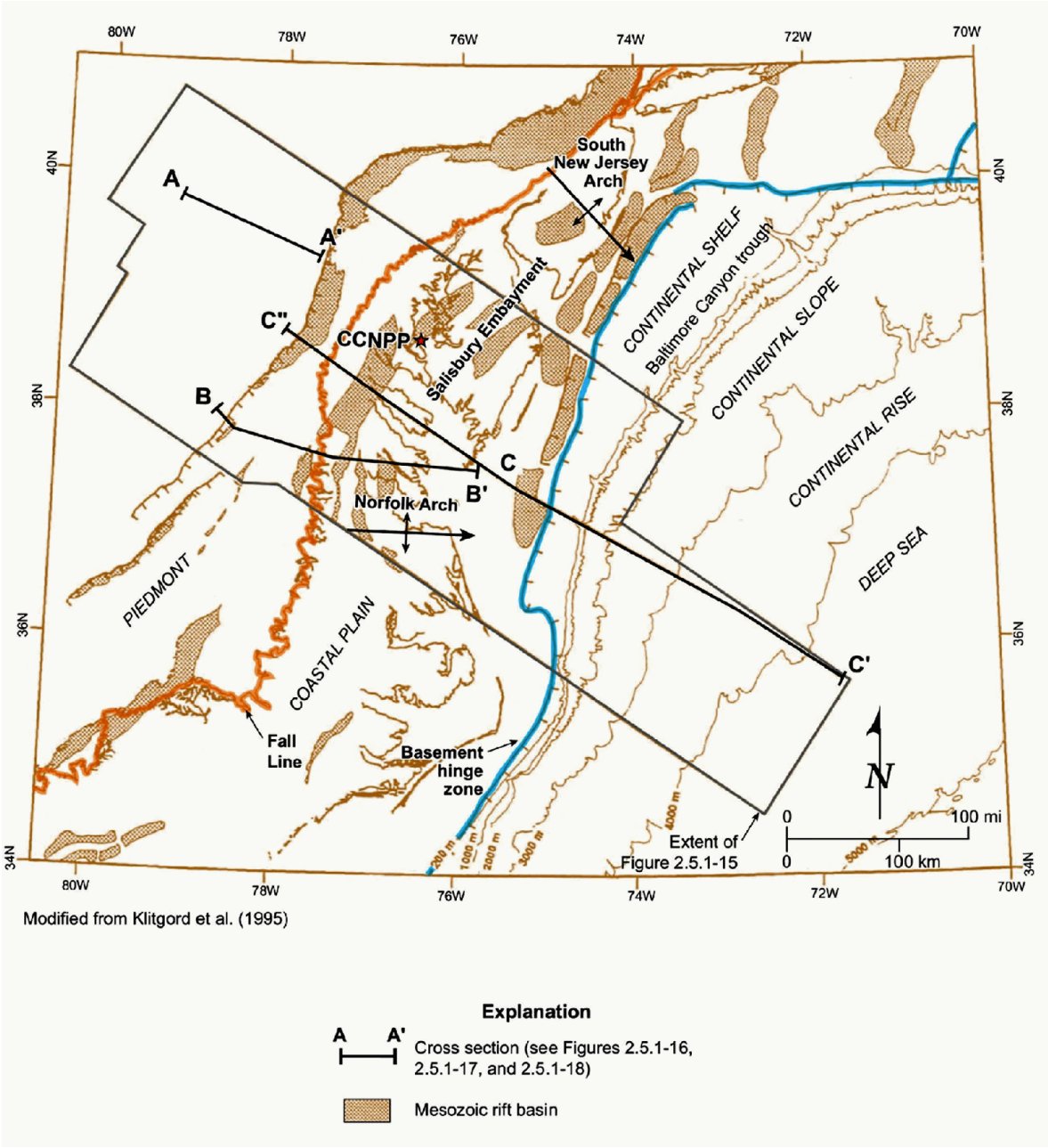

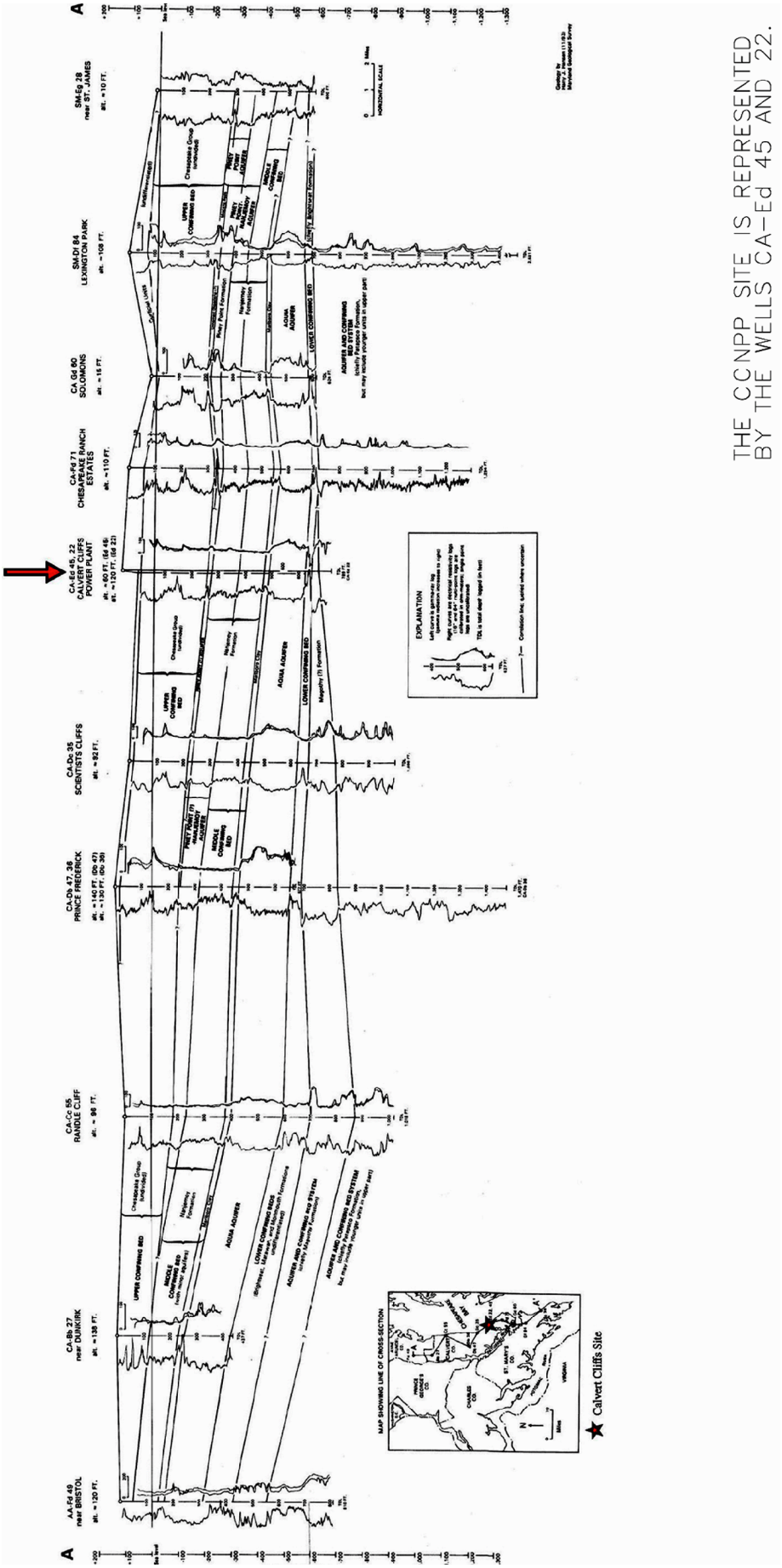

Figure 2.5-13— {Stratigraphic Cross-Section Through Anne Arundel, Calvert and St. Mary's Counties}

Figure 2.5-14— {Structure-Contour Map of the Top of the Piney Point-Nanjemoy Aquifer}

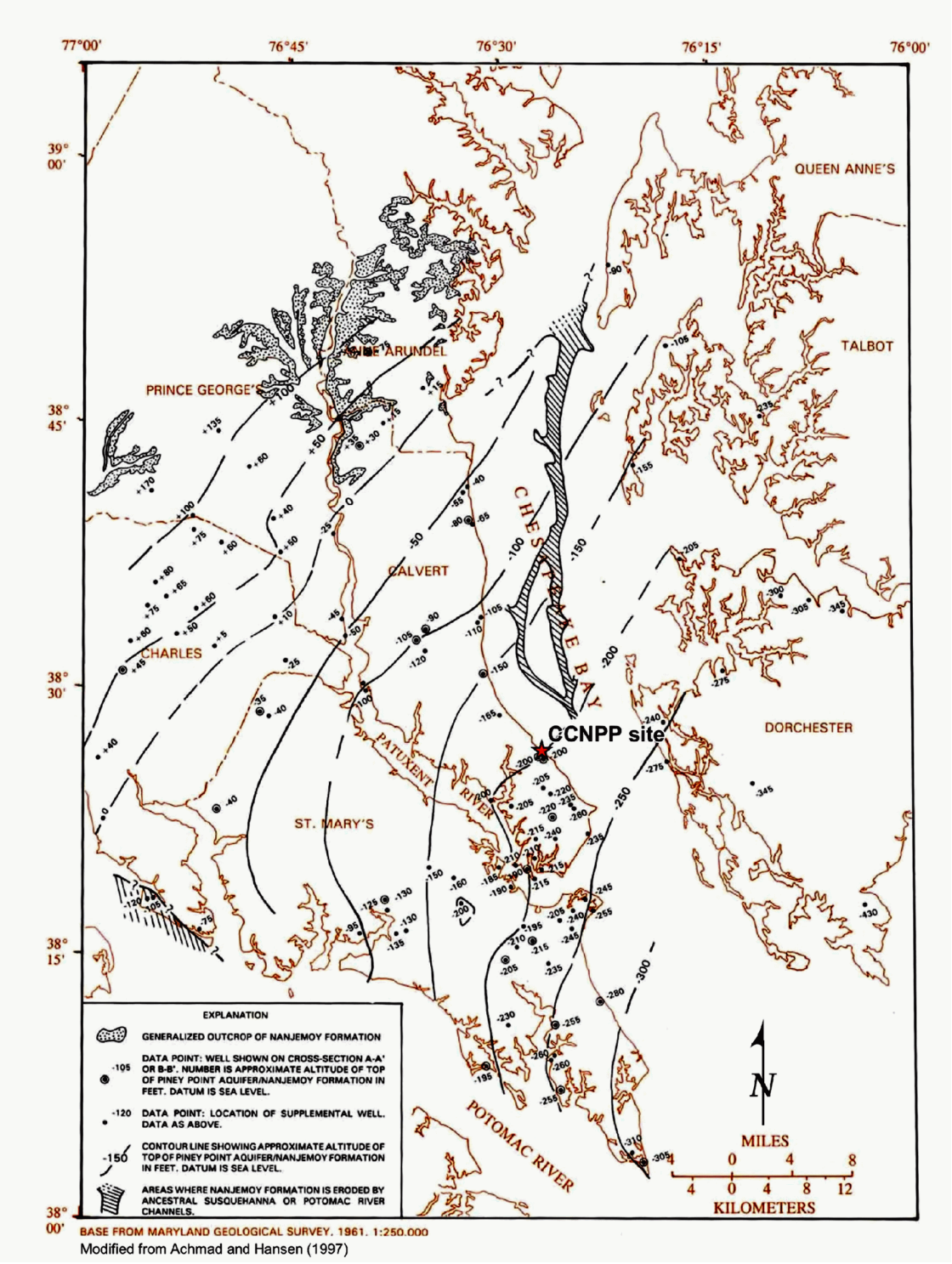

Modified from Achmad and Hansen (1997)

Figure 2.5-15— {Tectonic Age of Crust}

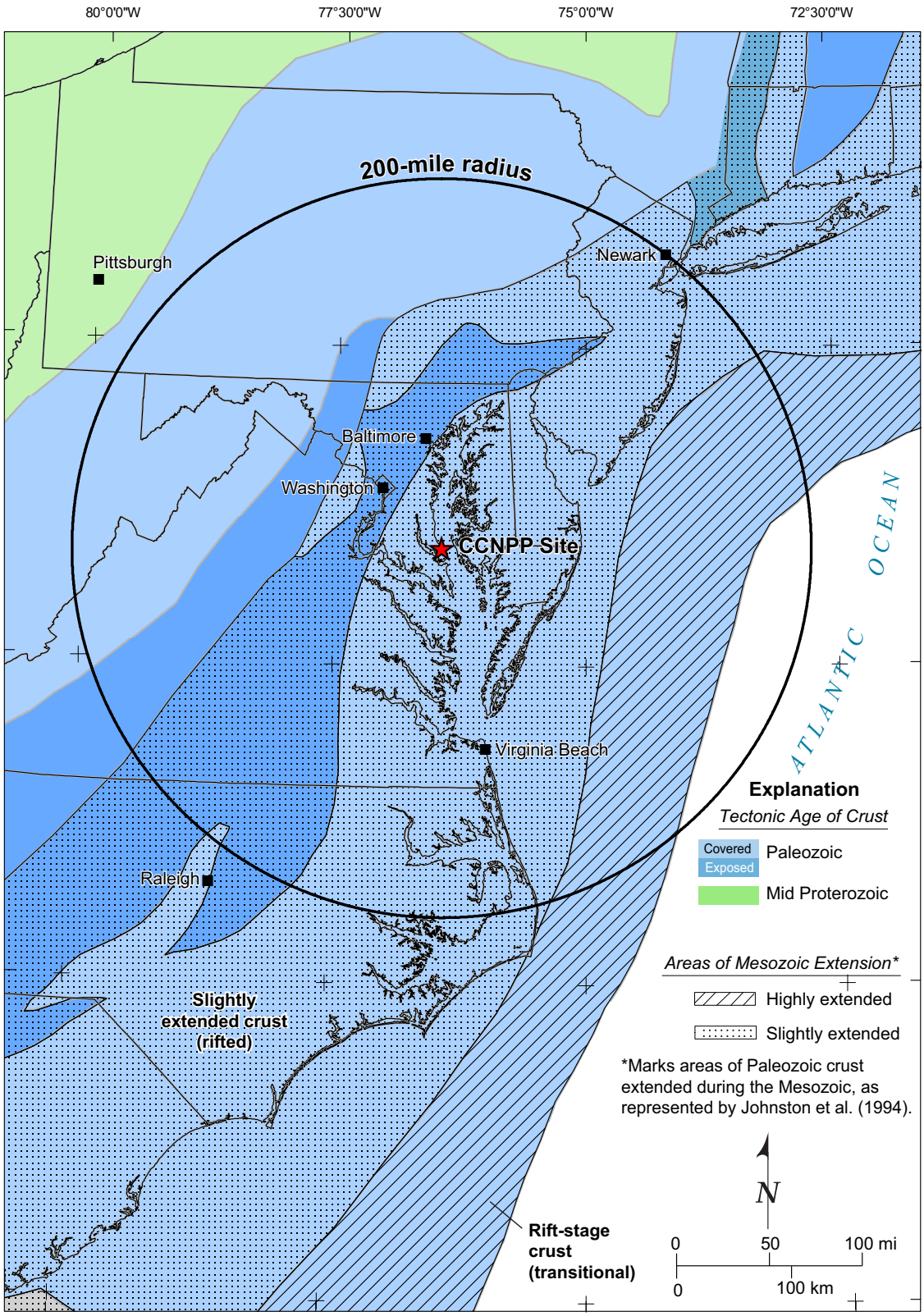

Johnston et al. (1994)